Tailor-Made Polymers

Edited by
John R. Severn and
John C. Chadwick

Related Titles

Matyjaszewski, K., Gnanou, Y., Leibler, L. (eds.)

Macromolecular Engineering

Precise Synthesis, Materials Properties, Applications

2007

ISBN: 978-3-527-31446-1

Barner-Kowollik, C. (ed.)

Handbook of RAFT Polymerization

2007

ISBN: 978-3-527-31924-4

Ghosh, S. K. (ed.)

Functional Coatings

by Polymer Microencapsulation

2006

ISBN: 978-3-527-31296-2

Meyer, T., Keurentjes, J. (eds.)

Handbook of Polymer Reaction Engineering

2005

ISBN: 978-3-527-31014-2

Advincula, R. C., Brittain, W. J., Caster, K. C., Rühe, J. (eds.)

Polymer Brushes

Synthesis, Characterization, Applications

2004

ISBN: 978-3-527-31033-3

Tailor-Made Polymers

Via Immobilization of Alpha-Olefin Polymerization Catalysts

Edited by
John R. Severn and John C. Chadwick

WILEY-VCH Verlag GmbH & Co. KGaA

The Editors

Dr. John R. Severn
Borealis Polymers Oy
P.O. Box 330
06101 Porvoo
Finnland

Dr. John C. Chadwick
Laboratory of Polymer Chem.
Eindhoven Univ. of Techn.
Postbus 513
5600 MB Eindhoven
Niederlande

Library of Congress Card No.:
applied for

British Library Cataloguing-in-Publication Data
A catalogue record for this book is available from the British Library.

Bibliographic information published by the Deutsche Nationalbibliothek
Die Deutsche Nationalbibliothek lists this publication in the Deutsche Nationalbibliografie; detailed bibliographic data are available on the Internet at <http://dnb.d-nb.de>.

Composition SNP Best-set Typesetter Ltd., Hong Kong

Printing Strauss GmbH, Mörlenbach

Bookbinding Litges & Dopf GmbH, Heppenheim

Cover Design

Printed in the Federal Republic of Germany
Printed on acid-free paper

ISBN: 978-3-527-31782-0

Preface

Polyolefins represent approximately 50% by weight of all commodity and commodity-plus polymers, which in turn amounts to about 90% by weight of the global polymer production. Today, literally hundreds of polyolefin grades are available commercially, with an incredible variety of properties and applications, ranging from ultra-rigid thermosets (stiffer than steel, but with the premium of a much lower density) to high-performance elastomers, via all conceivable thermoplastic and elastoplastic materials in between. Yet, if one looks at their chemical composition, polyolefins are surprisingly limited: polyethylene, polypropylene, a few copolymers of ethene with propene or another alpha-olefin, and little else. The key reason for this apparent contradiction is the unique and thorough molecular control of the polymerization process that modern transition metal-based catalysts are able to provide. With the correct choice of catalyst system and reaction conditions, it is possible to produce polyolefin materials with precisely defined and tunable chain microstructures and molecular mass distributions; this translates into a correspondingly fine control in the way such chains crystallize (when they are able to) and flow. In addition, a rich toolbox for supramolecular material design provides almost unlimited possibilities for further tailoring and diversification by means of intelligent processing, blending and additives formulations and technologies.

The result has been an unprecedented success story, as demonstrated by the exponential growth curve of the annual world consumption of polyolefins, from less than 10^5 tonnes during the mid-1950s to the present-day 10^8 tonnes. It might be worthy to add here that polyolefins should be regarded as a metastable state of the light fractions of refined oil. Rather than flaring them – as has happened in the past – they may be temporarily solidified, used for all sorts of smart applications at a nominal cost, and then burned to produce energy (the most logical way of recycling/disposing). If this point were to be understood by politicians, environmentalists and opinion-makers, polyolefins would be recognized for what they are – the greenest and most environmentally friendly materials ever invented.

For almost three decades, the industrial production of high-density polyethylene (HDPE) and isotactic polypropylene (iPP) was based exclusively on heterogeneous catalysts (of the Ziegler–Natta- or Phillips type), and characterized by many differ-

Tailor-Made Polymers. Via Immobilization of Alpha-Olefin Polymerization Catalysts.
Edited by John R. Severn and John C. Chadwick

ISBN: 978-3-527-31782-0

ent and ill-defined active species. However, a massive research effort resulted in major improvements of catalytic performance, although it is fair to admit that the approach was purely empirical.

It was only during the early 1980s that the serendipitous discovery of methylalumoxane as an effective activator of metallocene precatalysts made it possible to derive the first industrially appealing homogeneous ethene polymerization catalysts. Soon after that, with the implementation of stereorigid *ansa*-metallocenes with chirotopic sites, it was demonstrated that stereoregular polypropylenes could also be obtained in solution, and this opened the era of "single-site" catalysts. The strong point of a homogeneous catalyst is its well-defined structure, which translates into a single active species and a corresponding microstructural uniformity of the polymerization products. Although the active species can be designed, at least in principle, in order to achieve better/different catalytic properties, the drawback is that, for most industrial olefin polymerization process technologies, a heterogeneous catalyst is needed. Unfortunately, changing a homogeneous single-site catalyst into a heterogeneous (supported) one is a logical but by no means simple solution; in fact, the process forms the subject of this whole book.

Homogeneous "Single-site" Olefin Polymerization Catalysts: A Brief Mechanistic Introduction

In spite of the popularity of the definition, no transition metal-based olefin polymerization catalyst can be "single-site". In fact, the reaction mechanism inherently involves two *cis* coordination sites of the metal: one for the σ-bound growing polymeryl (i.e., the active site), and one for the incoming monomer. The chain migratory insertion path ensuring the least nuclear motion results in an exchange of polymeryl and monomer coordination sites, which means that both are (or at least can be) active sites. What is important to realize is that in most cases the two sites are *not* equivalent; therefore, defining a homogeneous catalyst as "single-center" would, in our opinion, be more appropriate.

The catalytic cycle of olefin polymerization in homogeneous phase is fairly simple. The active species is usually a coordinatively unsaturated $[L_yMR]^+$ cation, generated from a $L_yM(X)(Y)$ precursor (M = transition metal; L_y = ancillary ligand(s); X and Y = monodentate anionic ligands, such as halide or amide) by alkylation and reaction with a strong Lewis acid. In the case where X and Y are alkyl groups, alkylation may be unnecessary and the coordination vacancy can also be produced by reaction with a Brønsted acid. A key point here is that the counteranion needs to be poorly coordinating, so as not to prevent/slow-down monomer access to the transition metal.

Chain propagation is believed to involve olefin π-coordination at the metal, followed by the formation of a four-center transition state and migratory insertion. A regular alternation of insertions at the two coordination sites is expected under a kinetic quench regime; at the other limit, a Curtin–Hammett regime can be

observed in case of a rapid (relative to insertion) relocation of the growing polymeryl between the two metal coordination sites (e.g., under conditions of monomer starvation).

Chain transfer can occur, for example via β-H elimination (to the monomer and/or to the metal), or by trans-alkylation with main group metal alkyl cocatalysts. Molecular hydrogen can be added deliberately to decrease the polymer molecular weight via σ-bond metathesis. In all cases, the newly formed M—H or M—R bond is an active site, and can initiate the growth of a new polymeryl.

In the homopolymerization of ethene, the above is expected to result in perfectly linear polyethylene chains, which is indeed the norm. However, with some catalysts, and under certain conditions, a vinyl-terminated polyethylene chain may be released into the reaction medium where it acts as a macromonomer and inserts into a different M–Polyethylenyl bond; this leads to the formation of a "long-chain-branched" polyethylene. A different type of branched polyethylene, on the other hand, has been obtained with a number of sterically hindered late transition metal catalysts showing a high propensity to intramolecular β-H elimination; repeated steps of β-H elimination and macro-olefin reinsertion into the M—H bond (a process often referred to as "chain walking") can result in extensively branched polyethylenes resembling those produced by radical polymerization.

The case of alpha-olefins in general – and of propene in particular – is more complicated. A prochiral alpha-olefin molecule can insert into a M—R bond in four different ways, depending on the regiochemistry (1,2 or 2,1) and on the choice of enantioface (*re* or *si*). In most cases, a strong preference is observed for one insertion regiochemistry (usually the 1,2); compared with heterogeneous Ziegler–Natta catalysts, however, most homogeneous single-site catalysts (and particularly metallocenes) are remarkably less regioselective, and occasional regiodefects are detected in the polymer by ^{13}C NMR, typically in the form of head-to-head/tail-to-tail enchainments. For a catalyst to be stereoselective, on the other hand, a second element of chirality must combine with that arising from monomer coordination. In principle, this can be the configuration of the growing chain, and in particular of the stereogenic C in the last-inserted monomeric unit (chain end control); occasional cases of 1,3-*like* or 1,3-*unlike* asymmetric induction have indeed been reported in propene polymerizations mediated by single-site catalysts, but always at low temperatures and with modest entity. Much more important – and also industrially relevant – on the other hand, is the case of catalysts with chirotopic active sites, in which the selection of monomer enantioface results from non-bonded contacts in the active pocket shaped by the ancillary ligand(s) (site control). Notably, in practically all known cases the chiral recognition is not due to direct steric interactions between the incoming monomer and the ancillary ligand(s); rather, the latter constrains the growing polymer chain into a chiral conformation, which in turn favors monomer insertion with the enantioface pointing the alkyl substituent *anti* to the first chain C—C bond (a mechanism of stereocontrol known as "growing chain orientation"). The stereoregularity of the resulting polymer depends on the symmetry of the catalytic species: for propene polymerization, in particular, an isotactic polymer is expected out of C_2-symmetric species with

homotopic active sites, whereas a syndiotactic polymer will form at C_S-symmetric species with enantiotopic sites, provided that chain propagation occurs under a kinetic quench regime. Far less predictable is the case of C_1-symmetric species with diastereotopic sites, which can yield practically all microstructures (e.g., isotactic, syndiotactic, hemi-isotactic) depending on the enantioselectivity of the individual sites and on the kinetic regime of chain propagation.

Relative to ethene, propene and higher alpha-olefins usually have a (much) lower insertion rate, which makes the concurrent processes of chain transfer and isomerizations (much) more competitive. In particular, in many cases β-H elimination to the monomer is only slightly slower than (poly-)insertion, particularly at high temperature, which is obviously undesired and must be contrasted with a proper ancillary ligand design. Intramolecular β-H elimination, in turn, can also be significant; at odds with the polyethylene case, poly(alpha-olefin) chains are too bulky to undergo chain walking, and tend to be isomerized locally (e.g., 2,1-to-3,1 isomerization, chain-end epimerization).

Immobilizing "Single-site" Olefin Polymerization Catalysts: The Basic Problems

A single-site olefin polymerization catalyst is a well-defined molecular entity which is intolerant to virtually everything; moreover, its performance is critically dependent on the precise ligand environment of the transition metal center. Therefore, immobilizing one such catalyst on a suitable solid or glassy inorganic or organic matrix is a formidably complicated task. Apart from the requirements on the support, which must be harmless to the catalyst (and also to the polymer end-user!) and also amenable to morphology control (with the related delicate issues of shape replication, fragmentation and heat/mass-transfer properties, etc.), the main difficulty is how to introduce a strong non-labile binding between the support and the active species without altering (deteriorating) the performance of the latter.

In the various chapters of this book, the possible strategies (e.g., physical or chemical adsorption, tethering, etc.) will be introduced and discussed in detail. Here, we would like to mention a few basic problems of general relevance.

- *Catalyst productivity*. For an efficient catalytic action it is mandatory that the monomer has an easy access to the active sites. Selective catalysts have an active pocket which fits tightly to the incoming monomer. We have already commented on the crucial importance of a poorly coordinating counteranion for cationic catalysts. In view of all this, it can be understood that introducing a strong link between the catalyst and the support, without limiting the accessibility of the active sites, is extremely complicated. As a matter of fact, the productivity of most immobilized catalysts is one or more orders of magnitude lower than that of the same catalysts in solution. However, there are exceptions, as we shall see. One advantage of immobilized

catalysts, on the other hand, is that intermolecular catalyst deactivation processes that can be highly detrimental in solution are usually frozen on surfaces; therefore, provided that a good productivity can be achieved, this tends to be maintained for a longer reaction time.

- *Catalyst selectivity*. The proximity to a surface inevitably represents a perturbation to the catalyst active pocket, not only in terms of accessibility, but also of symmetry. In particular, the stereoselectivity of C_S-symmetric and C_1-symmetric catalysts can be altered by the immobilization, because this may change the relative monomer insertion frequency at the two sites. A limiting case which has been reported is that of propene polymerization at certain C_S-symmetric *ansa*-zirconocene catalysts, which is syndiotactic-selective in solution and can be isotactic-selective on a surface because one side of the catalyst would be obstructed by the support. C_2-symmetric catalysts with homotopic sites are expected to be relatively insensitive to this problem; however, in case of severe decrease of insertion rate, a loss in stereoselectivity can result here due to an increased impact of growing chain epimerization (*vide infra*).
- *Competing reaction processes*. Immobilizing a single-site catalyst affects the kinetics of *all* reactions occurring at that catalyst – that is, (poly-)insertion, chain-transfer and isomerization processes. It is very unlikely that the effect is proportional for all such processes (some of which are intramolecular). Therefore, it is to be expected that some microstructural features of the polymer produced (e.g., long and/or short branches, terminal unsaturations, average molecular mass and molecular mass distribution, regiodefects, etc.) change upon catalyst immobilization. Of course, this also holds true for copolymerization statistics.

December 2007 *John R. Severn and John C. Chadwick*

Contents

Tailor-Made Polymers. Via Immobilization of Alpha-Olefin Polymerization Catalysts.
Edited by John R. Severn and John C. Chadwick

ISBN: 978-3-527-31782-0

List of Contributors

Helmut G. Alt
Universität Bayreuth
Lehrstuhl für Anorganische Chemie II
Universitätsstr. 30
95447 Bayreuth
Germany

Michael Bartke
Fraunhofer Polymer Pilot Plant Center
Value Park A 74
06258 Schkopau
Germany

Elizabeth A. Benham
Chevron Phillips
Bartesville Technology Center
Highways 60 & 123
Research & Technology
83-E Bartlesville, OK 74004-0001
USA

John C. Chadwick
Laboratory of Polymer Chemistry
Eindhoven University of Technology
P.O. Box 513
5600 MB Eindhoven
The Netherlands
and
Dutch Polymer Institute (DPI)
P.O. Box 902
5600 AX Eindhoven
The Netherlands

Kathy S. Collins
Chevron Phillips
Bartesville Technology Center
Highways 60 & 123
Research & Technology
83-E Bartlesville, OK 74004-0001
USA

P.K. Das
Science Complex, Room 225L
Cameron University
2800 West Gore Boulevard
Lawton, OK 73505-6377
USA

Tailor-Made Polymers. Via Immobilization of Alpha-Olefin Polymerization Catalysts.
Edited by John R. Severn and John C. Chadwick

ISBN: 978-3-527-31782-0

Gerhard Fink
Max-Planck-Institut für Kohlenforschung
Kaiser-Wilhelm-Platz 1
45470 Mülheim a.d. Ruhr
Germany

Nic Friederichs
SABIC Europe
Research and Development
P.O. Box 319
6160 AH Geleen
The Netherlands

Markus Gahleitner
Borealis Polyolefine GmbH
St.-Peter-Str.25
4021 Linz
Austria

Thomas Garoff
Borealis Polymers Oy
P.O. Box 330
FI-06101 Porvoo
Finland

Nourdin Ghalit
SABIC Europe
Research and Development
P.O. Box 319
6160 AH Geleen
The Netherlands

Christian Gäl
Universität Bayreuth
Lehrstuhl für Anorganische Chemie II
Universitätsstr. 30
95447 Bayreuth
Germany

Jason C. Hicks
School of Chemical & Biomolecular Engineering
Georgia Institute of Technology
311 Ferst Drive
Atlanta, GA 30332-0100
USA

Gregory G. Hlatky
Lyondell Chemical Company
Catalyst Development
11530 Northlake Drive
Cincinnati, OH 45249
USA

Kumindini Jayaratne
Groningen
The Netherlands

Michael D. Jensen
Grace Davison Specialty Catalysts
7500 Grace Drive
Columbia, MD 21044
USA

Christopher W. Jones
School of Chemical & Biomolecular Engineering
Georgia Institute of Technology
311 Ferst Drive
Atlanta, GA 30332-0100
USA

Markus Klapper
Max-Planck-Institut für Kohlenforschung
Ackermannweg 10
55128 Mainz
Germany

Hilkka Knuuttila
Materials Research
Department of Chemistry
University of Joensuu
P.O. Box 111
80101
Finland

Young Soo Ko
Deparment of Chemical Engineering
Kongju National University
275 Budae-dong, Cheonan
Chungnam
330-717
Korea

Arja Lehtinen
Borealis AS
3960 Stathelle
Norway

Michael W. Lynch
Lyondell Chemical Company
Catalyst Development
11530 Northlake Drive
Cincinnati, OH 45249
USA

Joel L. Martin
Chevron Phillips
Bartesville Technology Center
Highways 60 & 123
Research & Technology
83-E Bartlesville, OK 74004-0001
USA

Albert P. Masino
Chevron Phillips
Bartesville Technology Center
Highways 60 & 123
Research & Technology
83-E Bartlesville, OK 74004-0001
USA

Max P. McDaniel
Chevron Phillips
Bartesville Technology Center
Highways 60 & 123
Research & Technology
83-E Bartlesville, OK 74004-0001
USA

Neal D. McDaniel
7 Lawrence Dr., Apt. 104
Princeton, NJ 08540
USA

John R. Severn
Borealis Polymers Oy
P.O. Box 330
06101 Porvoo
Finland

Mathew G. Thorn
Novolen Technology
Cincinnati Technical Center
11530 Northlake Drive
Cincinnati, OH 45249
USA

Seong Ihl Woo
Department of Chemical and Biomolecular Engineering
Korea Advanced Institute of Science and Technology
373-1 Kusong-dong
Yusong-gu
305-701, Taejon
Korea

Wei Xu
Saudi Basic Industries Corp. Research & Technology Center
P.O. Box 42503
Riyadh 11551
Kingdom of Saudi Arabia

Qing Yang
Chevron Phillips
Bartesville Technology Center
Highways 60 & 123
Research & Technology
83-E Bartlesville, OK 74004-0001
USA

1
Designing Polymer Properties

Markus Gahleitner and John R. Severn

1.1
Polyolefins

Polyolefins represent approximately 50% by weight of all commodity and commodity-plus polymers, which in turn amount to about 90% by weight of the global polymer production. Literally hundreds of polyolefin grades are available commercially with an incredible variety of properties and applications, ranging from ultra-rigid thermosets (stiffer than steel, but with the premium of a much lower density) to high-performance elastomers via all conceivable thermoplastic and elastoplastic materials in between. Yet, if one looks at the chemical composition, polyolefins are surprisingly limited: polyethylene, polypropylene, a few copolymers of ethene with propene or another alpha-olefin, and little else. The key reason for this apparent contradiction is the unique and thorough molecular control of the polymerization process that modern transition metal-based catalysts are able to provide. With a proper choice of catalyst system and reaction conditions, it is possible to produce polyolefin materials with precisely defined and tunable chain microstructures and molecular mass distributions; this translates into a correspondingly fine control of the way in which such chains crystallize (when they are able to) and flow. In addition, a rich "toolbox" for supramolecular material design provides almost unlimited possibilities of further tailoring and diversification by means of intelligent processing, blending and additives formulations and technologies.

The result is an unprecedented success story, demonstrated by the exponential growth curve of polyolefin world consumption from less than 100 KT per annum during the mid-1950s to the current 100 Mt. It is worthy to add here that polyolefins should be considered as a metastable state of the light fractions of refined oil. Rather than flaring them, as has happened in the past, these are temporarily solidified, used for all forms of smart applications at a nominal cost, and burned afterwards to produce energy (the most logical way of recycling/disposing). If this was understood by politicians, environmentalists and opinion-makers, polyolefins would be recognized for what they are, namely the greenest and most environmentally friendly materials ever invented.

Tailor-Made Polymers. Via Immobilization of Alpha-Olefin Polymerization Catalysts.
Edited by John R. Severn and John C. Chadwick

ISBN: 978-3-527-31782-0

For almost three decades, the industrial production of high-density polyethylene (HDPE) and isotactic polypropylene (iPP) was based exclusively on heterogeneous catalysts (of the Ziegler–Natta or Phillips type) characterized by many different and ill-defined active species. Although massive research effort resulted in major improvements of catalytic performance, it is fair to admit that the approach was purely empirical.

It was only during the early 1980s that the serendipitous discovery of methylalumoxane as an effective activator of metallocene precatalysts made it possible to develop the first industrially appealing homogeneous ethene polymerization catalysts. Soon after that, with the implementation of stereorigid *ansa*-metallocenes with chirotopic sites, it could be demonstrated that stereoregular polypropylenes could also be obtained in solution. This opened the era of "single-site" catalysts.

The strong point of a homogeneous catalyst is its well-defined structure, which translates into a single active species and a corresponding microstructural uniformity of the polymerization products. Moreover, the active species can be designed – at least in principle – in order to achieve better/different catalytic properties. The drawback is that, for most industrial olefin polymerization process technologies, a heterogeneous catalyst is needed. Unfortunately, changing a homogeneous single-site catalyst into a heterogeneous (supported) one is a logical, but by no means simple, solution; in fact, it is the subject of this whole book.

1.2
Levels and Scales of Polymer Structure and Modification

Thermoplastic polyolefin polymers have reached a wide application range since their original introduction during the latter half of the 20th century. The adaptation to often quite difficult requirements to processability, mechanics, optics and long-term behavior has been achieved by a number of structural modifications, starting at the chain chemistry level and ending in the component design and processing step [1]. From a dimensional point of view this can be translated into a diagram for different (length) scales of polymer design (Figure 1.1). The following section of this chapter will deal with these levels as seen from the chemistry, the morphology, and the property sides of material design.

1.2.1
Chain Structure: Chemistry, Interaction, Regularity, and Disturbance

Polymer design starts at the level of the molecule, at the chain structure defining the basic characteristics of the material, such as being crystalline or amorphous, and thus determining application properties to a large extent. Polarity, ranging from apolar pure polyolefins to polycondensates with intensive hydrogen bridge formation between the chains, is one major factor here. While both polyamide-6 (PA-6, nylon) and HDPE have similar levels of crystallinity (~60%), their melting points are, at 220 and 135 °C, quite different. At the same time the reaction to

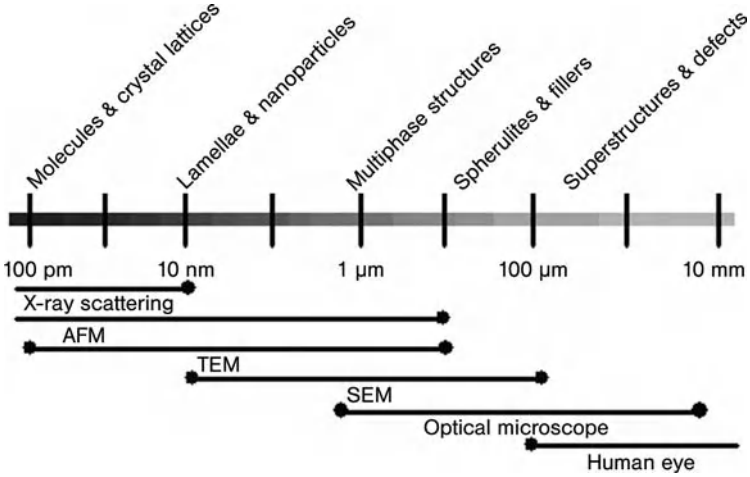

Figure 1.1 Structural levels and respective dimensions for the systematic modification of polymeric materials with appropriate investigation tools for characterization.

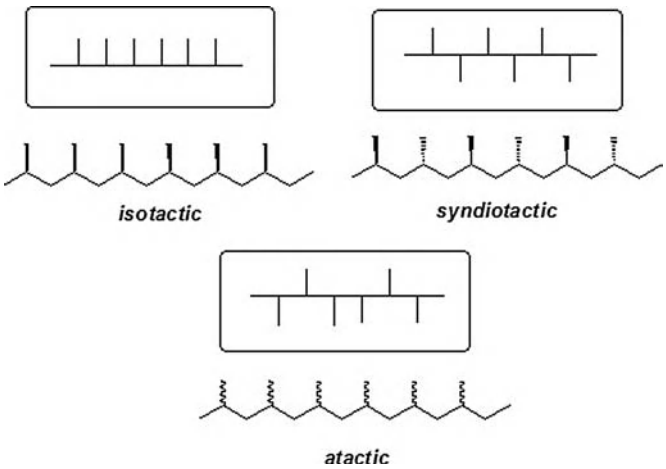

Figure 1.2 Tacticity.

environmental effects such as humidity and ultraviolet (UV) radiation will already be predetermined here. At a given level of polarity, stereochemistry and bulkiness of side groups has a decisive effect, separating crystallizable from amorphous subspecies of the same polymer; examples are the difference between atactic and isotactic polystyrene (aPS/iPS) or members of the polypropylene family – atactic (aPP), syndiotactic (sPP) and isotactic (iPP) [2] (Figure 1.2). Basically, the same effect – namely a disturbance of the chain structure first reducing and finally disrupting the ability to crystallize – can be achieved by copolymerization. One well-known point here is the crystallinity and density control of polyethylene (PE) by incorporating higher α-olefins such as 1-butene, 1-hexene or 1-octene, although

similar effects can also be achieved for aromatic polyesters with aliphatic diesters [3]. Further consequences of this modification, such as effects on melting temperature (i.e., sealing properties), crystal size (i.e., transparency), modulus (i.e., stiffness) and free volume (i.e., gas and vapor permeability) will be discussed below.

1.2.1.1 Chain Topology: SCB, LCB, and Special Structures

While stereostructure and chemistry suffice to describe the polymer chain at a local level of a few monomeric units, the chain topology is required to differentiate between purely linear and various branched polymers. The rheology and processability, but ultimately also the mechanical properties, of a polymer are decisively affected by the branching structure, which can be roughly split into short-chain branched (SCB) and long-chain branched (LCB) polymers [4]. The usual parameter serving as distinction here is the branch length or branch molecular weight, where LCB represents a branch molecular weight above the critical molecular weight (M_C) of the respective polymer. In detail, star-, H-, and comb structures must be differentiated, while the existence of "branches on branches" (also called "multi-branching", typical for low-density polyethylene, LDPE, from a high-pressure process [5]) adds a further dimension to the system's complexity (Figure 1.3).

1.2.1.1 Molecular Weight Distribution (MWD)

Technical polymers are polydisperse, showing a more or less broad MWD as result of a number of factors. Multi-site catalysts, kinetics and residence time distribution are among the main factors contributing to polydispersity, which can be related again to both processing and end-use properties, either directly or via the characteristic parameters of averages and moments (in the most simple case the number average, M_N, and weight average, M_W, molecular weight) [3, 6]. Two important distinctions must be made here: (i) the mechanical consequences of an MWD fraction are significantly higher (and the rheological ones lower) if the fraction is below M_C; and (ii) all changes are much more critical for glassy polymers, where

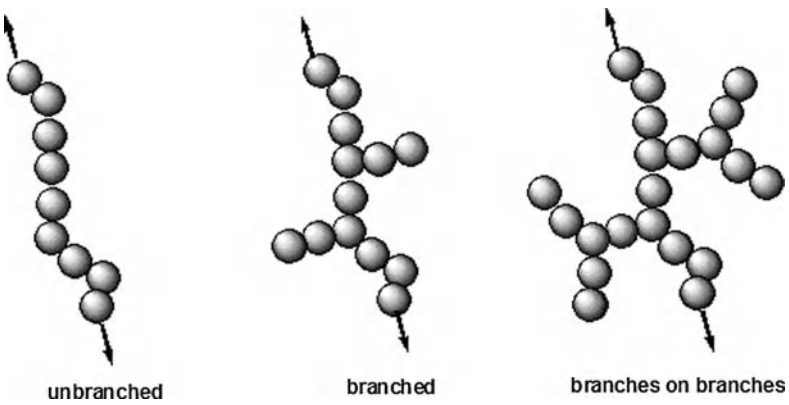

Figure 1.3 Schematic representation of chain topology.

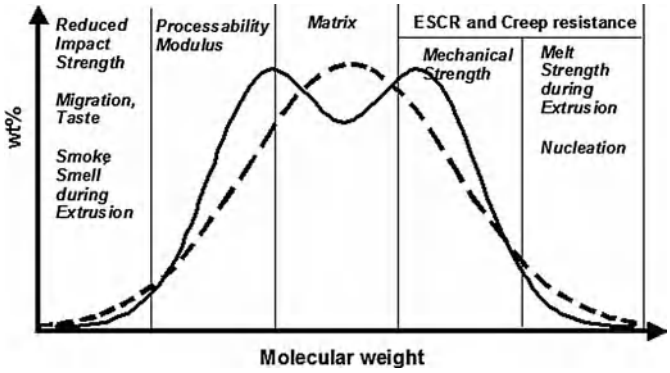

Figure 1.4 Contributions of various molecular-weight fractions to the property profile of polyethylenes with monomodal (dashed line) and bimodal (full line) molecular weight distribution.

the mechanics are defined by entanglements rather than by crystalline structures.

Modern polyolefin materials mostly have a rather elaborate designed MWD, in which the various fractions contribute to the different target properties (or problems) of the overall system. Figure 1.4 provides a rough outline of this property design for the case of bimodal polyethylenes, where this development is already well advanced, partly resulting from the very wide MWDs and possibly even with conventional Ziegler or chromium catalyst systems.

In reality, complete control of the produced MWD is limited by the characteristics of the catalyst and residence time distribution of the polymerization process. Chromium catalysts are unsuitable because of their inherently broad MWD, and even in the case of titanium-(Ziegler-)-catalysts limits are frequently reached in controlling the low-molecular-weight fraction (critical below M_C because of a lack of integration into the crystalline structure and entanglements) and extremely high-molecular-weight fractions (critical in film grades in which "gels" consisting of higher-molecular-weight or crosslinked material deteriorate the performance). A further limitation in broadening the MWD is the need to homogenize such materials, which also makes special extruder constructions necessary.

1.2.1.3 Blends and Other Multiphase Structures

As alloys are decisive for the wide application range of metals, blends and composites have further expanded the accessible property range of polymers. The underlying idea is to combine the advantages of different components, the base being a thermoplastic polymer, while the second (disperse) component can be inorganic (filler, fiber), elastomeric (and even crosslinked), or also thermoplastic [7, 8]. Details for these materials, which can be produced in multi-stage copolymerization, melt compounding or a combination of both processes, are provided below.

1.2.2
Semi-crystalline Polymers: From Lattices to Superstructures

Focusing the discussion on semicrystalline systems from now on is justified as this is the main area of catalytic and stereoselective polymerization. Even within this range of materials the variation in crystallinity, melting point and modulus is very wide and closely related to structural factors, as mentioned above.

1.2.2.1 Chain Structure and Crystallization Speed

The crystallization of polymers is a slow process in comparison to other materials such as metals. This results on the one hand from the high molecular weight and the related long characteristic times of the materials, and on the other hand from the low heat conductivity. It also limits the maximum degree of crystallinity, which for polyolefins rarely exceeds 60%. The process of solidification can therefore be separated into nucleation and crystal growth, which have been shown to be defined by different molecular characteristics of the polymer.

Crystal growth rate is defined mainly by the "smoothness" and regularity of the chain; consequently, among polyolefins the highest values are found for HDPE, which also has the most simple crystal structure based on chain folding (zig-zag structure in the lattice) only. Increased bulkiness will reduce the growth rate, as shown for a number of different polymers in Figure 1.5 [2, 9]. The maximum of the $G_C(T)$ function will normally be found approximately halfway between the melting point T_M and the glass transition point T_G, with PE being a notable exception. Polypropylene (PP) is one of the best investigated polymers in this respect, with both the contributions of stereoregularity and comonomer content being well documented [10]. A clear correlation to both processing speed and modulus can be recognized.

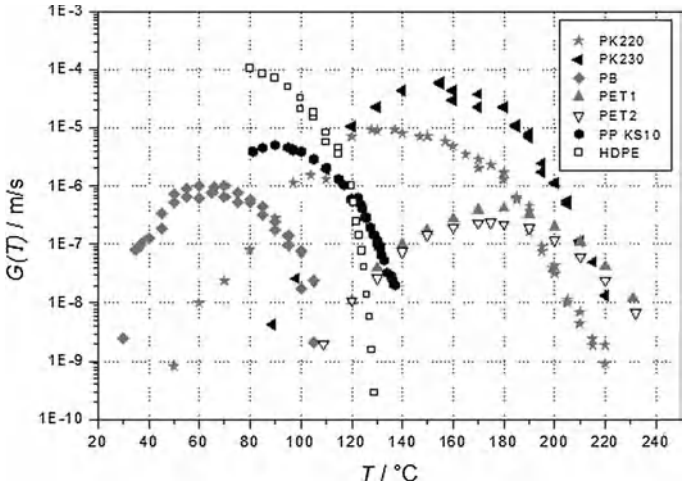

Figure 1.5 Temperature-dependence of crystal growth rate for polymers with different chain structure. (Data from Ref. [11].)

1.2.2.2 Lamellar Thickness and Modulus

A rather important contribution to the mechanical performance of polyolefins is the correlation of modulus to not only the overall crystallinity but also the lamellar thickness in the system. The latter is correlated to the crystallization temperature according to the Gibbs–Thompson equation (demonstrated for example for ethylene–octene copolymers by Rabiej et al. [12]), resulting in a general correlation also for the case of PP, as shown in Figure 1.6, where for three types of polymer-independent but parallel dependences were achieved. As shown in the report by Pukánszky et al. [13], although nucleation contributes significantly to the performance via this relationship, isotacticity effects [14] and also the isotactic sequence length are highly relevant.

1.2.2.3 Nucleation and Polymorphism

For the pure polymer the MWD and especially the high-molecular-weight fraction – that is, the part of the composition having the highest relaxation time and therefore acting as self-nucleants [15, 16] have been found to be decisive for the nucleation density ($N_C(T)$), which is the second decisive factor for mechanics and optics, but also shrinkage and warpage of injection-molded parts. The maximum of the temperature dependence of $N_C(T)$ is, however, located always at lower temperatures than $G_C(T)$, allowing the use of other highly efficient external nucleating agents as further design instruments. These are even more important for rather slowly crystallizing polymers such as syndiotactic PP. However, to be efficient, and especially to improve transparency, the efficiency must be rather high.

Special considerations must be taken in the case of polymorphic polymers such as isotactic and syndiotactic PP or poly-1-butene (PB-1). Normally, one of the

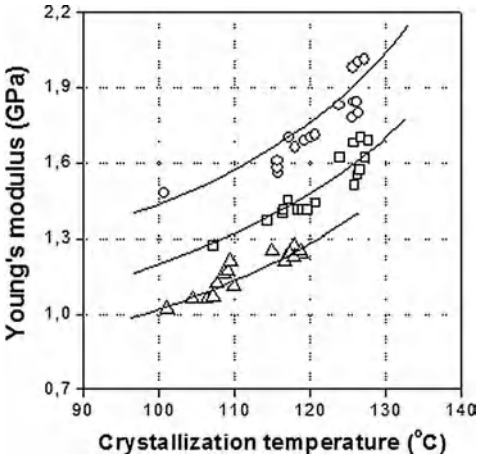

Figure 1.6 Dependence of the tensile modulus (Young's modulus) and crystallization temperature of non-nucleated and differently nucleated versions of three different polypropylene (PP) types: ○, homopolymer; □, impact copolymer; △, random copolymer. (Data from Ref. [13].)

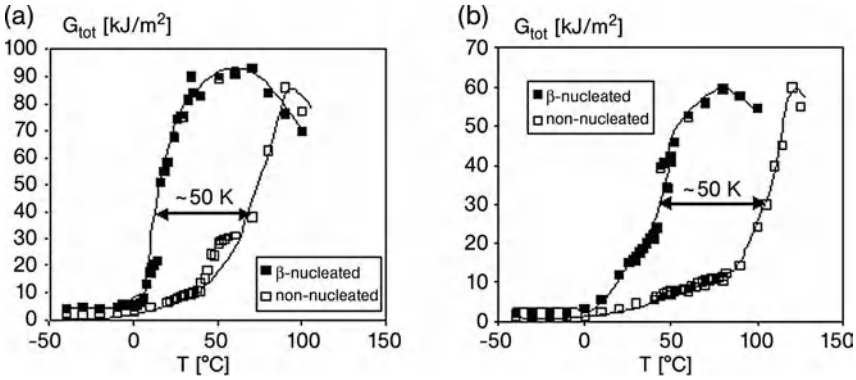

Figure 1.7 Evolution of the fracture energy, G_{tot}, with the temperature, T, for non-nucleated and β-nucleated resins with different flowabilities (melt flow ratios, MFR). (a) MFR 0.3 °C min^{-1}; (b) MFR 2 °C min^{-1}; a ductile-brittle transition temperature chosen as the temperature corresponding to half of the maximum of G_{tot} in the considered MFR range (this reflects the transition from a semi-ductile to a fully ductile behavior, without breaking the tested specimen). Test speed 1.5 m s^{-1} on injection-molded specimens. (Data from ref. [17].)

possible crystal modifications will be the most stable, being the α-modification for iPP. With selective nucleating agents the β-modification can be promoted in processing, resulting in materials with a significantly higher impact strength and allowing stretching into microporous films. The wide potential of these specifically nucleated iPP materials which also have a lower ductile–brittle transition temperature (see Figure 1.7) has been recently outlined in a review by Grein [17].

1.2.2.4 **Flow-induced Structures and Processing Effects**

Especially components and articles produced in conversion processes involving high deformation (shear or extension), such as injection molding, stretch-blow molding, mono- or biaxially oriented films or fibers, derive their morphology and application properties largely from flow-induced crystallization phenomena. These are well investigated for iPP, PB-1 and PE, and also demonstrate the strong influence of the MWD here. Notably, the group of Kornfield [18] has demonstrated the consequences of very small fractions of long molecules being related to the stronger orientation of these by flow stresses. Highly oriented skin layers with a far higher modulus than the less-oriented core of injection-molded specimens [19], as well as the enormous strength of highly oriented PE fibers, result from these mechanisms.

A similarly important role is played when quenching the normally semicrystalline polymers by very high cooling rates into materials with limited or even no crystallinity. Very drastic examples of this are poly(ethylene-terephthalate) (PET) and poly(lactic acid) (PLA), both of which can be quenched into a fully amorphous state. In the case of iPP, another crystal modification – the mesomorphic or smectic form – is achieved by quenching with cooling rates of more than 100 K s^{-1} [20]; this finding is of great practical relevance in the production of PP cast films.

1.2.3 Multiphase Structures

Blends and composites are considered whenever the highest mechanical requirements or seemingly conflicting property demands are confronted for a specific application. These need not be limited to mechanics, but can also involve dimensional stability or processability.

1.2.3.1 General Concepts of Impact Modification

Originally developed for the naturally more brittle amorphous polymers, the concept of elastomer-based impact modification is also applicable for semicrystalline polymers [21, 22]. The relevance is highest for polymers with a glass transition within the application temperature range, such as iPP ($T_G \sim 0\,°C$), adding mobility with elastomeric components having a far lower T_G, which is the case for ethylene-propylene-"rubbers" (EPR) in the range from –60 to –40 °C. Alternative concepts such as hard-phase impact modification with inorganic micro- or nanoparticles [23] have not yet gained widespread application, while crosslinked elastomer phases have a solid position for special areas.

1.2.3.2 Multi-stage Copolymers (PP)

While the addition of elastomeric impact modifiers such as EPR, ethylene propylene diene monomer (EPDM), styrene elastomers or ethylene-based plastomers in extrusion mixing allows for maximum flexibility in property design [7]; it also involves high cost, and the compatibility is often limited. The multi-stage copolymerization of propylene with ethylene (or higher α-olefins), where the elastomer is produced directly in the reactor, represents a much more economical way of producing materials with high impact strength. Products from the latter process are generally still called "block-copolymers", though a more correct name would be "heterophasic copolymers". In Figure 1.8, it can be seen that the polymer contains not only crystalline PP and essentially amorphous EPR, but also crystalline PE in the "core" of the EPR particles. The properties of these materials are defined by the quantity, size and internal structure of these soft particles, where the primary design parameter is the quantity of disperse elastomer phase. The linear effect on the modulus as compared to the step function in toughness is demonstrated graphically in Figure 1.6.

Further composition parameters such as molecular weight and comonomer distribution of the EPR phase allow reactor design [24], while the further addition of PE and other elastomer or filler components are used for post-polymerization modification.

1.2.3.3 Polymer Blends and Reactive Modification

Blends between polymers of different chemical nature, such as PP/PA-6 or PE/PS, almost always require compatibilization, for which either graft- or block-copolymers are applied [25]. Both, the combination of polar and non-polar property aspects (e.g., paintability with limited water uptake) and the possibility of reaching highest

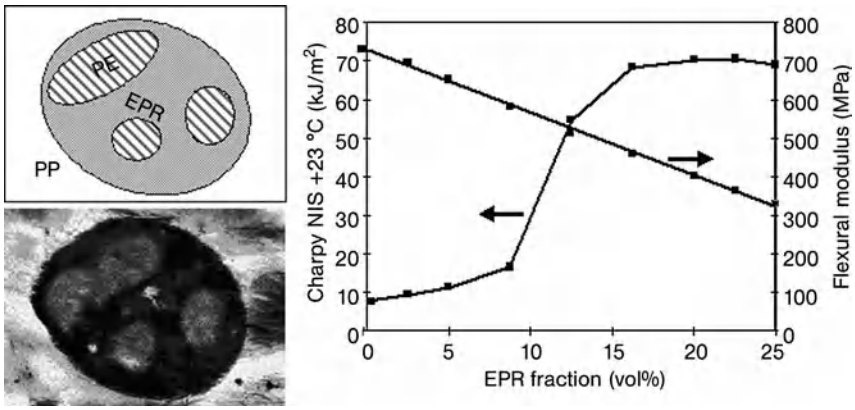

Figure 1.8 General structure of heterophasic EP-copolymers. Left: PP and PE crystalline, EPR amorphous; image from RuO_4-stained transmission electron microscopy image). Right: influence of the amount of elastomer phase (EPR) on stiffness and impact strength of such polymer systems.

temperature resistance by three-dimensional (3-D) network structures, as in glass fiber-reinforced PP/PA-6.

Special property combinations can be reached by reactive modification, which in the case of polyolefins is practically always based on radical grafting reactions [26]. The potential applications of this technology range from the production of long-chain branched PP with high melt strength offering advantages in foaming, and other processes with strong extensional flow, via the stabilization or partial crosslinking of phase structures (up to thermoplastic vulcanizates, TPVs) up to polar modifiers and compatibilizers (e.g., by grafting with maleic anhydride). In the case of PE the process is even more flexible because the inherent risk of degradation is lower.

1.2.3.4 **Compounds and (Nano)Composites**

Further modifications are possible, for example through the addition of fillers and reinforcements of mostly mineral nature. The possible mechanical profiles are determined by the properties of the base polymer, as well as by the quantity and nature of the filler [27]. Especially when using glass fibers, which open the highest strength level, further improvements are possible by modifying the fiber surface (sizing) and using compatibilizers (adhesives). Parts of this category are also organic reinforcing fibers from natural (regenerative) sources such as hemp, flax, or wood fibers. The strength of glass-fiber-reinforced materials is not achieved with such additions, and the lot-to-lot variations of natural fibers are problematic; however, the full combustibility of such composites is seen as an advantage.

The new generation of nanofillers promised even better opportunities for property profile optimization [28]. Very small and highly anisotropic particles resulting from an exfoliation of organically modified clay have a strong reinforcing potential

in polycondensates such as PA-6, whilst in polyolefins the problems of dispersion and exfoliation are much greater. *In-situ* methods are considered as a viable alternative here, as they avoid the problems of melt phase dispersion; however, they are still in the early stages of development for catalyst-based systems.

1.2.4
Property Optimization in Processing

One final possibility for optimizing part properties is the application of special processing (conversion) technologies. As mentioned above, the ultimate mechanical properties of semi-crystalline polymers depend heavily on not only the crystallinity but also the morphology of the formed crystalline structures. In this way, a massive increase in strength can be achieved through the targeted production of oriented structures; examples include the SCORIM (shear-controlled injection molding) process [29] or the "Push-Pull" injection-molding process. Even larger increases in the elastic modulus, and also in breaking strength, can be achieved in fiber-spinning processes by post-drawing in either the solid or semi-solid state. A combination of this process, with weaving and sintering of these high-strength PP-fibers to plates for later thermoforming, was developed by the group of Ward in the United Kingdom [30], and is presently marketed under the product name "curv". By using this technique, modulus values of up to 5000 MPa can be achieved.

1.3
Polymer Design: The Catalyst's Point of View

As illustrated above, designing polymer properties can be achieved at various scales. The following section concentrates on polymer design from a catalyst point of view. The primary role of a single-site catalyst is its ability to influence the molecular architecture of a polymer chain (molecular weight, MWD, comonomer incorporation and distribution, stereoselectivity, regioselectivity and block structure). Emphasis will be placed in this section on single-site α-olefin polymerization catalysts and their prodigious ability to tailor the molecular architecture of a polymer, through rational design of the steric and electronic environment of the active site. That said, however, it should be noted that the "true" rational design of a catalyst system is not commonplace, and the vast majority of reports of single-site catalysts have been more "pot-luck" than precision. Put in a nutshell, the art of single-site catalyst tailoring is the ability to encourage or discourage certain competing reactions, by tailoring the catalyst system, polymerization conditions (or both) to produce a polymer resin with a desired molecular architecture. The success of this approach has seen this fascinating area of catalysis and polymer science grow, in less than three decades, to truly gargantuan proportions. It has greatly benefited from the understanding of the kinetic mechanisms at play during polymerization, rational tailoring of the steric and electronic properties of the catalyst, activation, and the advent of powerful computational modeling. In addition,

the development of detailed physical measurements and rheological testing of the resultant polymer resins, facilitated by their narrowly dispersed nature that has allowed a synergistic combination of one or more of the above.

Due to the great volume of material, only the basic tools and concepts will be discussed here, along with illustrative "case studies". For a more detailed discussion, the reader is directed elsewhere [31–100].

1.3.1 Mechanisms and Kinetics: A "Tailors Toolbox"

At this point it is worth recapping on some of the basic developments in the understanding of metal-catalyzed polymerization processes. During a typical polymerization, numerous competing reactions are occurring with different rates and orders. Consequently, understanding the mechanisms and how their kinetic rates are affected by polymerization conditions – for example, are the rates monomer-dependent or independent? – can provide considerable help. Equally, an understanding of the steric and electronic requirements of a mechanism are important if the aim is to (potentially) raise or lower the energy of a transition state in order to promote or discourage a desired reaction, or to control how a monomer is enchained (stereo- or regioselectivity, etc).

1.3.1.1 Activation, Initiation, Propagation: On your Marks, Get Set, . . . Go!!

Activation The "activation" of a single-site precatalyst complex is typically achieved via contact with an appropriate cocatalyst species. It is crucially important to select the correct combination for the particular polymer process or target. It is also an area that is typically overlooked, with focus being paid to altering the complex rather than to the activation process. In terms of activity, major improvements can be achieved merely by altering the activation package.

Common procedures for generating "primary" ion-pairs start from metal chloride or alkyl precursors (Figure 1.9). For dichloride precatalysts (L-MCl_2), the generation of the species requires the initial conversion of one (L-M(R)Cl) or both of the chlorides (L-MR_2) into alkyls species. Subsequent abstraction of either the remaining chloride or the alkyl moiety forms a "primary" ion pair (cationic 14*e* metal center). Typically, although MAO fulfils all of the above criteria, they can also be achieved via a combination of alkylating agent and an abstracting agent (Cl or R). For dialkyl precatalysts, alkyl abstraction is typically achieved via two routes. Abstraction via Lewis acids such as $B(C_6F_5)_3$ or MAO is commonplace; however, ability of the resultant anions ($[RB(C_6F_5)_3]^-$ or [R-MAO]$^-$] to coordinate to the cationic metal center is heavily dependent on the nature of R and the ability to delocalize the negative charge in the cation. Alternate alkyl abstractors are Brønsted ($[HNMe_2Ph]^+$) or Lewis acidic ($[CPh_3]^+$) cations which contain a weakly coordinating counterion (e.g., $[B(C_6F_5)_4]^-$) [40–44].

It is important to highlight that formation of the "primary" ion pair is governed by kinetic considerations, and its chemistry is dominated by equilibria reactions,

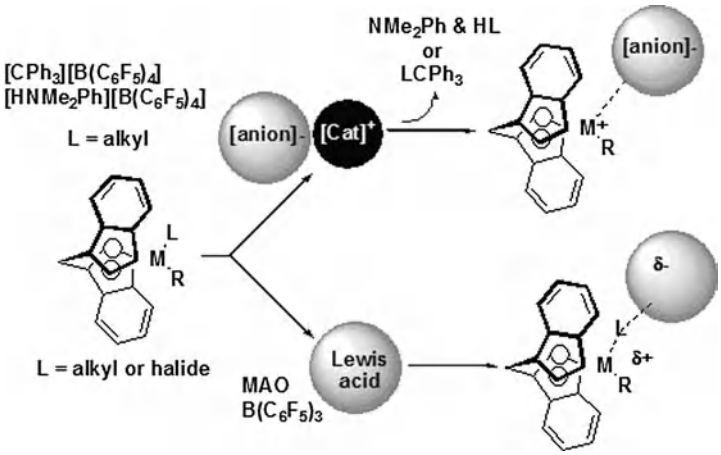

Figure 1.9 Schematic representation of precatalyst "activation" via archetypal Lewis and Brønsted acidic cocatalyst/activators.

for example the coordination of basic metal alkyls such as trimethylaluminum or even a dialkyl precatalyst complex to the cationic center.

Initiation The initiation of the polymerization process is believed to occur as a result of the displacement of the anion and coordination of the monomer in the "primary" complex. Whether the monomer binding is an associative or dissociative mechanism remains a matter of debate (Figure 1.10). Briefly, the anion dissociation mechanism generates an available coordination site on the metal center, which grabs a monomer for subsequent enchainment. Anion dissociation is an equilibrium reaction, and therefore the tendency for anion re-association would also arise. This begs the question of how fast the re-association reaction is, relative to the rate of propagation (does it interrupt the growth of a chain, or not?). The energetics of anion dissociation (charge separation) is also questionable in the non-polar environments that normally exist in industrial processes.

In the associative mechanism, monomer coordination and anion displacement is a concerted process. Therefore, how and in what direction the monomer approaches the metal center, and the steric influence of the anion may have important consequences for microstructure control [40–48].

As mentioned above, displacement of the anion and the coordination of the monomer are believed to result in the initiation of the active species, heralding the start of propagation. However, this still may not tell the whole picture, as interesting findings from the groups of Fink [49] and Landis [50] seem to suggest that the catalyst initiation step (active site formation) follows the irreversible insertion of the first monomer.

Propagation Once the active species is formed, the commonly accepted mechanism for chain propagation is based on the migratory insertion mechanism of

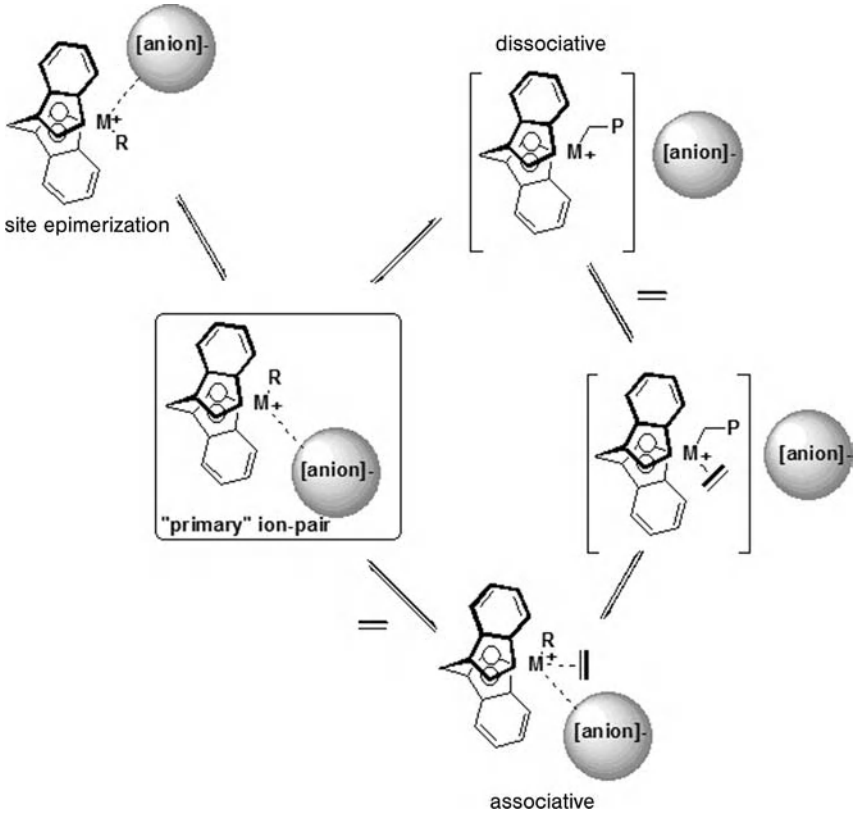

Figure 1.10 Schematic representations of associative and dissociative mechanisms for the coordination of an olefin.

Cosse–Arlman and further refinements [51]. The mechanism is basically a two-step process in which the olefin coordinates to the available coordination site metal center and is inserted via *cis* opening of the double bond, leading to chain migration (Figure 1.11; Site A to Site B). A regular alternation of insertions at the two coordination sites is expected under a kinetic quench regime; at the other limit, a Curtin–Hammett regime can be observed in case of fast (relative to insertion) relocation of the growing polymeryl between the two metal coordination sites (e.g., under conditions of monomer starvation). In addition, the mechanisms indicate that an olefin must be face-on to the metal, with the double bond parallel to the metal alkyl bond. The presence of α-agostic interaction "conformationally locks" the growing polymer chain and/or assists in stabilizing the transition state and secondary insertions, which may occur in α-olefins higher than ethylene; these are also illustrated in Figure 1.11 [52].

In very basic terms, the whole process up to this point is akin to a Formula 1 race. In the activation step, the driver (precatalyst) enters the car (cocatalyst) and switches the engine on. However, the race cannot start until the driver engages

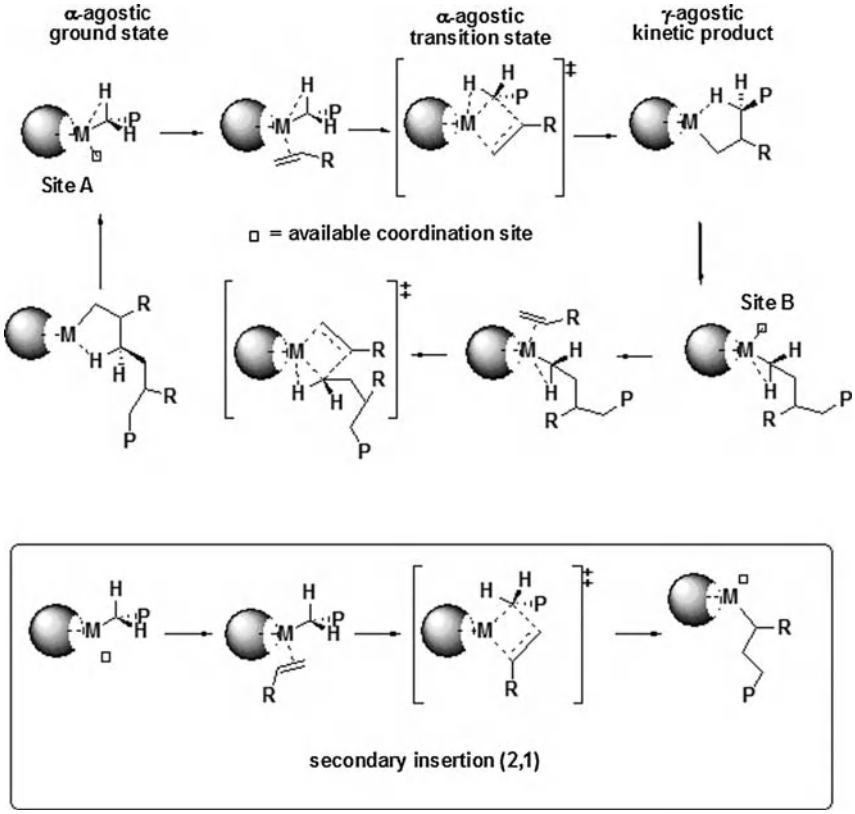

Figure 1.11 α-Agostic-assisted Cosse–Arlman mechanism (after Refs. [52a,b]).

the gear (coordinates olefin), drops the clutch (displaces the anion), and accelerates away (chain propagation).

1.3.1.2 Chain Transfer

Chain transfer is a statistical chain event in the life of a growing polymer chain. It is not necessarily the termination of the final polymer chain, as many chain-transferred products are subsequently reinserted. This is exemplified by the appearance of ethyl and methyl branches in the homo-polymerization of ethylene with metallocenes [53, 54], branch formation by the ubiquitous Brookhart systems [55], the formation of LCB polymers (vinyl released end-group macro-monomer re-insertion) [56], and reversible transmetallation ("chain shuttling") [57].

Understanding chain transfer can help in tailoring a catalyst's performance to either promote or discourage one or more of the chain-transfer mechanisms. Typically, tailoring starts by an analysis of the end-groups in a polymer produced by a "first-generation" system. The analysis of end-groups then provides a "fingerprint" of what types of chain transfer have occurred, and which are the dominant. "Second-generation" systems can then be designed to address any short comings

and to attain the desired molecular weight capabilities. Typically, two routes are employed to tune the molecular weight capabilities of a system: the polymerization conditions and the metal precatalyst. Investigations conducted by Fink and coworkers on ethylene insertion rates, into differing Ti–R bonds (rate of insertion R = Pr^n >> Et >> Me) may also be interesting to consider in terms of what group is left on the metal following chain transfer, and how quickly can that center reinitiate chain-propagation [49].

The apex of controlled chain transfer allows the formation of interesting block copolymers or polyolefins with extremely narrow molecular weight distributions ($M_w/M_n \approx 1.1$) [58]. The control of chain transfer can also allow the synthesis of resins with increased amounts of end-groups that are beneficial for post modification (e.g., crosslinking).

β-Transfer Chain transfer via β-hydride transfer occurs via two distinct mechanisms that afford a polymer chain with the same end-group: (i) β-hydride transfer to the metal center, yielding a metal hydride; or (ii) β-hydride transfer to an incoming (co)monomer, yielding a metal alkyl (Figure 1.12) [59–62]. β-Hydride transfer to a (co)monomer after a secondary insertion is also shown in Figure 1.12. Such a chain-transfer mechanism can become important in terms of molecular weight for such centers where propagation after secondary insertion is slow [59, 60, 63]. Whilst both mechanisms yield the same product, it is important to understand the difference and possible implications towards molecular weight tailoring.

β-Hydride transfer to metal is a unimolecular process, and the transfer rate is independent of monomer concentration. For most systems, the propagation is dependent on monomer concentration, and therefore an increased monomer concentration can lead to high molecular weights. In contrast, β-hydride transfer to a (co)monomer is dependent on the monomer concentration, and therefore increases proportionally with the propagation rate; as a result, the molecular weight is often

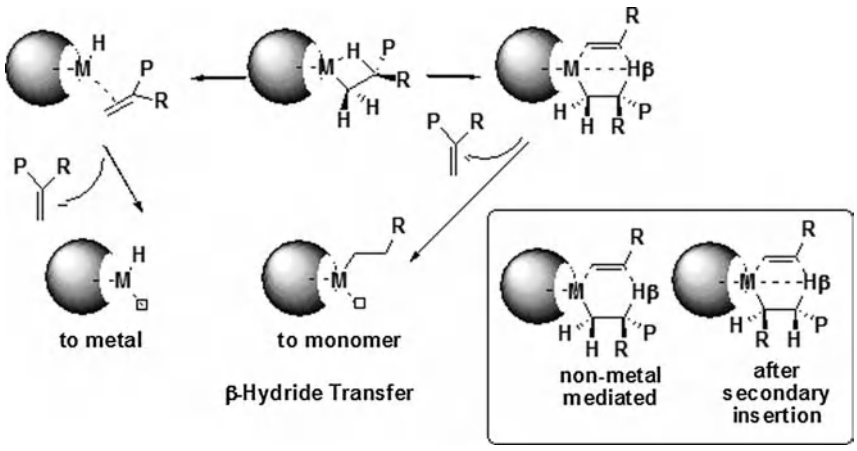

Figure 1.12 Schematic representations of β-hydride chain-transfer reactions.

independent of the monomer concentration. Generally, speaking β-hydride transfer to a (co)comonomer is the dominant termination mechanism.

A variety of end-groups results from β-hydride transfer to a (co)comonomer, and these are dictated by what and how the last (co)monomer was enchained (ethylene or 1-olefin; primary or secondary insertion). For primary insertion, β-hydride transfer leads to the formation of a vinyl (ethylene; CH_2=CH_2-polymeryl) or vinylidene (1-olefin; CH_2=CH(R)-polymeryl) polymer end-group. In contrast, *trans*-vinylene end-groups arise following β-hydride transfer following a secondary insertion of propylene or a higher α-olefin.

β-Me transfer to the metal center is an additional chain-transfer mechanism in propylene polymerizations. As shown in Figure 1.13, such a termination mechanism results in a vinyl end-group for propylene, forming a potential macromonomer (LCB) [64], unlike the vinylidene product from a β-hydride-transferred chain transfer [65].

Chain-transfer Agents: Transmetallation and Hydrogenolysis Chain transfer via transmetallation occurs through a metal alkyl-containing chain-transfer agent, via an exchange of the polymer chain and the chain transfer agent's alkyl group. Such chain-transfer agents are typically, but necessarily, aluminum alkyl compounds such as Al_2Me_3 or Al_2Et_3. Following termination and work-up of the resultant polymer resin, the reactive Al–carbon bonds are hydrolyzed to yield a saturated hydrocarbon (Figure 1.14). However, chains residing on aluminum can be

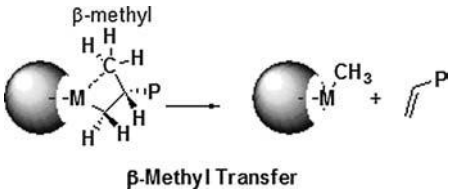

Figure 1.13 Schematic representations of the β-methyl chain-transfer reactions.

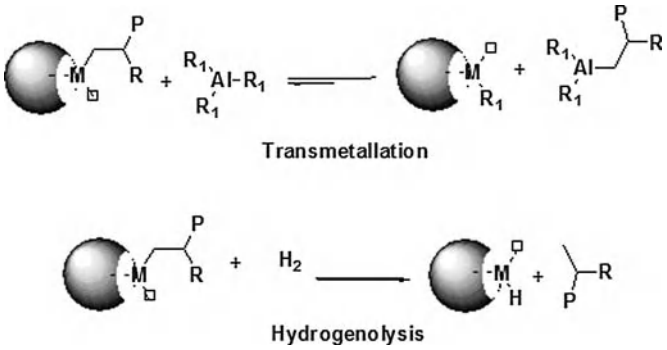

Figure 1.14 Schematic representations of transmetallation and hydrogenolysis chain-transfer reactions.

captured and converted into useful macromonomers [66]. It should be noted that this reaction is reversible – that is, the secondary metal can transfer this chain back to an active site. Mastering this reaction has resulted in a recent major breakthrough in polyolefin catalysis, and this will be discussed in more detail in a subsequent section [57].

Chain transfer via hydrogenolysis is achieved by the addition of hydrogen, which leads to saturated end-groups (Figure 1.14). As hydrogenolysis is the preferred means of controlling the molecular weight under industrial conditions, an understanding of how reactive a catalyst system is to hydrogen, and how it affects productivity, is extremely important in any catalyst system, particularly for the single-site catalysts which are commonly highly reactive towards hydrogen.

1.3.1.3 **Insertion Control**

Copolymerization Control Ethylene copolymers (e.g., ULDPE, VLDPE, LLDPE, MDPE) represent the most successful application area of single-site catalysts. The control of such copolymerization is primarily achieved through an understanding of the relative reactivity ratios of ethylene and comonomer(s) for a particular system (precatalyst + cocatalyst).

Ethylene is the most reactive olefin, with alpha-olefin reactivities decreasing as the length of the alkyl group increases. However, the rate of decrease in the reactivity diminishes as the length of the alkyl group increases. Linear α-olefins are more reactive than their branched counterparts, with a drastic decrease in reactivity seen for the branched molecules at the β-carbon (CH_2=CRR′). This effect is generally attributed to steric crowding in the vicinity of the reactive double bond.

Apart from the general reactivities of α-olefins, their reactivity is highly dependent on the catalyst structure [67]. In general, single-site catalyst are more reactive towards α-olefin comonomers than are traditional catalysts (e.g., Ziegler and Cr), although the reactivity of an α-olefin is highly dependent on the metal and the ligand structure. Electronic factors at the active site, as well as steric environment in the vicinity of the active site, determine the reactivity and structure of the copolymer (SCB, M_w). Although many general conclusions on the influence of ligand structure on polymer structure have been drawn, the details of how the combination of electronic and steric affects the relative reactivities remain unclear. Ligand substitution, active metal and the presence of some form of rigidity in the structure (e.g., *ansa*-bridges) each have distinct effects on the polymerization behavior [68].

Stereo-regio Control A prochiral α-olefin molecule can insert into a M–R bond in four different ways, depending on the regiochemistry (1,2 or 2,1), and on the choice of the enantioface (*re* or *si*). In most cases, a strong preference is observed for one insertion regiochemistry (usually the 1,2); compared with heterogeneous Ziegler–Natta catalysts, however, most homogeneous single-site catalysts (and particularly metallocenes) are remarkably less regioselective, and occasional regio-

defects are detected in the polymer by using ^{13}C NMR, these typically being in the form of head-to-head/tail-to-tail enchainments.

The stereochemistry of a polymerization reaction is governed by the symmetry and steric environment of the metal center (ancillary ligand and anion) and the growing polymer chain. In the latter case, the stereogenic center formed by the last monomer enchainment influences the stereochemistry of the subsequent monomer addition. If this influence is significant and overrides that of the ancillary ligand, then the stereochemical regulation of the process is referred to as "chain-end-controlled". The archetypal examples of this are isotactic enriched polypropylene from low-temperature polymerization with Cp_2TiPh_2 (primary insertion) [69] and syndiotactic polypropylene from vanadium-based Ziegler catalysts (secondary insertion) [70]. If the single-site catalyst contains a chiral ancillary ligand set that is able to induce a "chiral pocket" at the active site, and which overrides the influences of the polymer-chain end, then the stereochemical regulation of the process is referred to as "enantiomorphic-site-controlled". It is this process that is most amenable for the rational tailoring of a catalyst and, subsequently, the polymer microstructure that is formed.

Enantiomorphic Site Control In the majority of cases, enantiomorphic site control can be predicted by the symmetry of the metal center. Ewen was the first to link the symmetry at a metallocene center and the microstructure of the resultant polymer (Figure 1.15) [71]. Strictly speaking, the active species is asymmetric due to the presence of the growing polymer chain and the available coordination site; however, it is assumed that the polymerization rapidly equilibrates between the

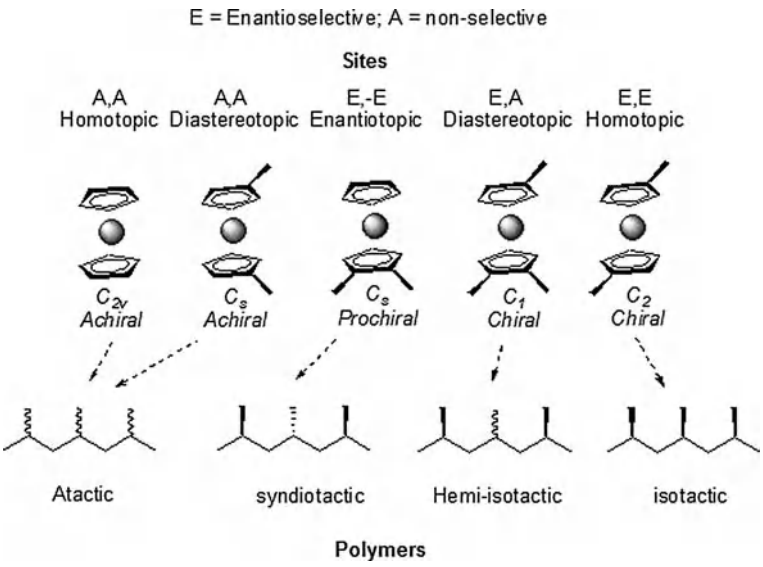

Figure 1.15 Ewen's symmetry rules.

two coordination sites. Based on Ewen's symmetry rules, the catalysts are divided into five main symmetry categories [71]:

- C_{2v} symmetric catalysts typically produce atactic or moderately stereoregular polymers (chain-end-controlled).
- C_s symmetric catalysts containing two distereotopic coordination sites typically produce atactic or moderately stereoregular polymers (chain-end-controlled).
- C_s symmetric catalysts containing two enantiomorphic coordination sites frequently produce syndiotactic polymers.
- C_1 symmetric catalysts are distereotopic and contain an enantioselective and non-selective coordination site. Ewen's symmetry rule predict a hemi-isotactic structure where alternating chiral–achiral insertion takes place. In practice, however, balancing the "steric excesses" is very important and makes prediction based only on symmetry very difficult.
- C_2 symmetric catalysts contain two homotopic sites and typically form isotactic polymers via enantiomorphic site control (both racemic and enantiomerically pure versions).

Although the Ewen symmetry rules are rather simplistic, they are typically the first starting point for catalyst design. Tailoring of the catalyst then revolves around the ability to dictate in which direction the growing chain is orientated, and how the incoming monomer is presented by the application of "steric pressure" (repulsive non-bonded interactions). Detailed mechanistic studies concerning enantiofacial selectivity, α-agostic-assisted olefin insertion and their relevance to stereocontrol, as well as the possible role that anions play, may be found elsewhere [59–62].

Defects The stereocontrol of a polymerization reaction, as with most things in life, is not perfect. Defects are enchained (stereo-error or regio-error) into a polymer during its lifetime, and occur, typically, via either the mis-insertion of a monomer or following an epimerization reaction (site or chain). As the frequency and distribution of defects plays a key role in dictating the polymer's properties, an understanding of how they arise and what they are dependent on has become a key feature in catalyst design.

In isotactic polypropylene polymerization there are two main types of chain defect, regio-error or stereo-error (Figure 1.16). The mechanism shown in Figure 1.17 is the idealized enantiomorphic site-controlled enchainment of propylene. As can be seen, the growing monomer chain is orientated in such a way as to minimize the non-bond interaction with the benzo-fragment of the indenyl moiety. In addition, the incoming ligand is enantiofacially presented in such a way as to minimize any interaction with the growing chain. The combination of homotopic sites, the controlled orientation of the growing chain, a consistent presentation of the correct enantioface of monomer, and an absence of chain-end epimerization, leads to the formation of pure isotactic polypropylene.

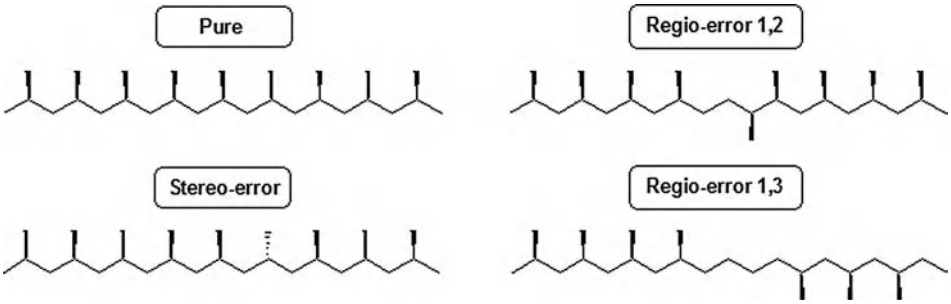

Figure 1.16 Stereo- and regio-defects in isotactic polypropylene.

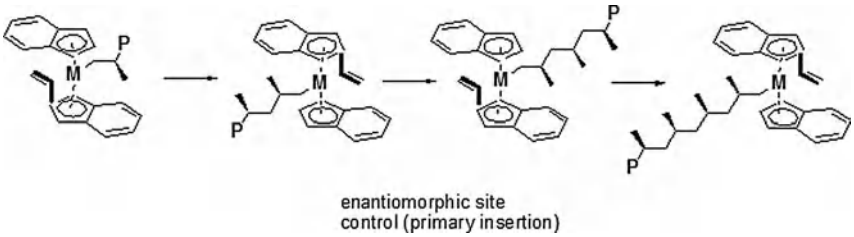

Figure 1.17 Schematic representation of chain propagation on a C_2 symmetric catalyst via enantiomorphic site control.

Figures 1.18 and 1.19 illustrate the various mechanisms that have been proposed to account for stereo-defects (Figure 1.18) and regio-defects (Figure 1.19) in isotactic polypropylene catalyzed via C_2-symmetric systems. Stereo-errors are thought to result from the enchainment of a propylene monomer with the "wrong" enantioface, or via a unimolecular chain-end epimerization mechanism. The latter mechanism is thought by some to be the dominant cause of stereo-defects due to the fact that such defects tend to increase with decreasing monomer concentration (lower propagation rates but the same chain-end epimerization rate). Regio-errors result from a secondary insertion of propylene; if this secondary insertion is propagated, then a 2,1-regio-defect is formed. However, if propagation after a secondary insertion is slow relative to a chain-end epimerization reaction from a secondary to a primary alkyl (alleviating steric hindrance), then a 1,3 regio-defect is formed.

Defects (stereo- or regio-errors) in the backbone of an isotactic polypropylene disrupt the chain in a similar way that the addition of comonomer does in polyethylene or polypropylene (EPR). As discussed above, chain disruption affects the crystallization parameters of the polymer and, in turn, some of its physical properties. Assigning the impact of one type of defect compared to another is a matter for debate; it would appear from Figure 1.16 that the 2,1 and 1,3 regio-error defects seem to have a larger defect foot-print (more disruption of the chain) than the stereo-error defects. Fischer and Mülhaupt, however, clearly proved that both regio- and stereo-error units are incompatible with the crystal lattice. Moreover,

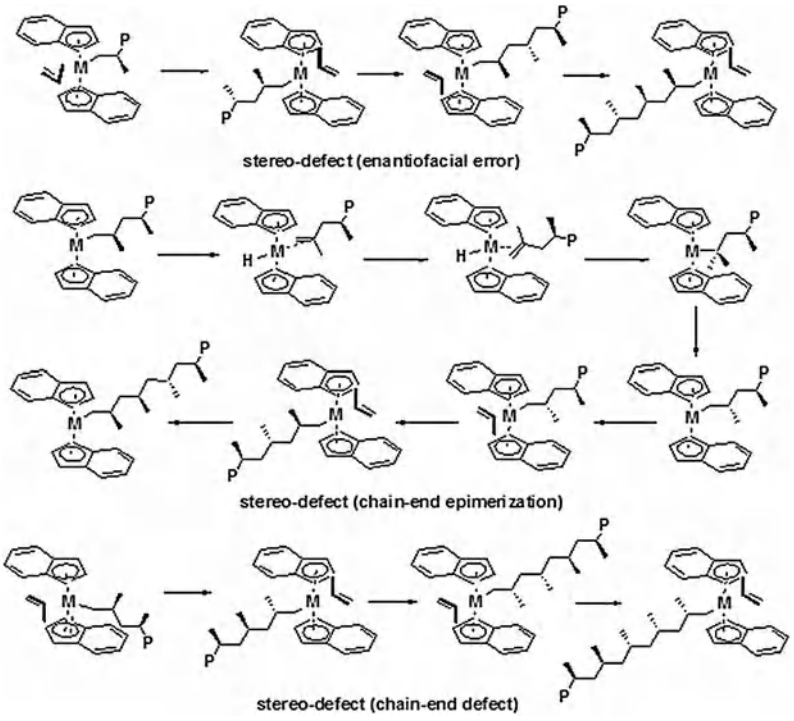

Figure 1.18 Stereo-defect formation.

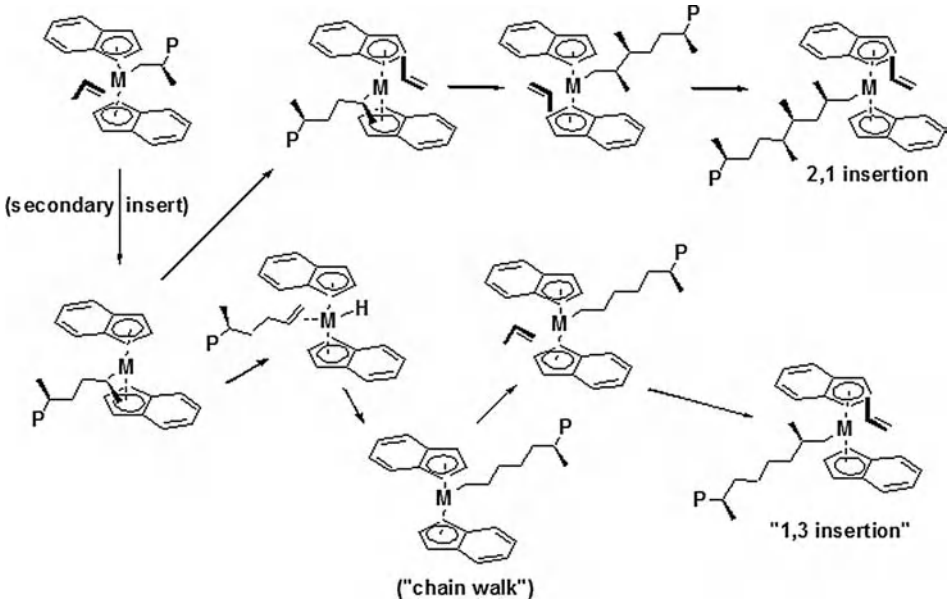

Figure 1.19 Regio-defect formation.

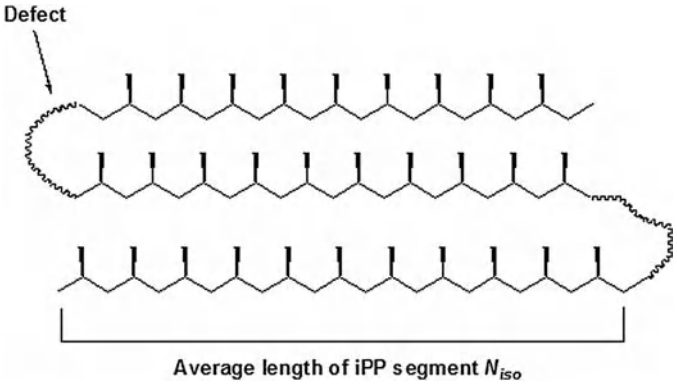

Figure 1.20 Schematic representation of the average length of iPP sequences.

the key to the situation is the distribution of defects and, more importantly, the average pure isotactic segment length (crystallizable sequence) between defects (n_{iso}) (Figure 1.20) [72a]. As might be imagined, the molecular weight of the polymer (M_w) and the number of defects need also to be taken into account.

Single-site catalysts typically distribute their defects homogeneously throughout the length of a polymer chain, unlike Ziegler–Natta catalysts which tend to "concentrate" defects in blocks with extremely long isotactic segment lengths. As a result, the more homogeneous a distribution, the more effective it is in segmenting the polymer (for the same molecular weight and defect content). Single-site catalysts typically have short isotactic segments (n_{iso}), and as a result they commonly crystallize in the γ-form (the γ-form modification of iPP is often achieved by the incorporation of low amounts of comonomer, typically ethylene), which has implications for certain, notably optical, properties (the γ-form does not form spherulites). The relevance of isotactic sequence length – especially for highly isotactic polypropylenes – to the achieved modulus level has been demonstrated by Viville et al., by utilizing a combination of analytical methods [72b]. It should always be remembered, however, that a variety of factors in combination play a role in defining the properties of microstructure, molecular weight, molecular weight distribution, and morphology of the crystalline domains. A more homogeneous distribution of regio-errors also has implications for propylene copolymers (in particular of ethylene copolymers), as ethylene is thought to be much more effective at insertion following a secondary insertion of propylene. This leads to a more random distribution of comonomer in the case of single-site catalysts.

Stereo-defects arise in syndiotactic polypropylene derived from the Ewen/Razavi family of C_s symmetrical metallocene (Figure 1.21) [73]. As described above, an enantioface error and a chain-end-epimerization lead to the propagation of a stereo-defect. However, as the C_s symmetric metallocene has a distereotropic site, a site-epimerization reaction ("back-skipping") can result in the formation of the same enantiomeric site. Hence, rather than alternating between the distereotropic sites, two consecutive insertions occur at the same enantioface, a process which

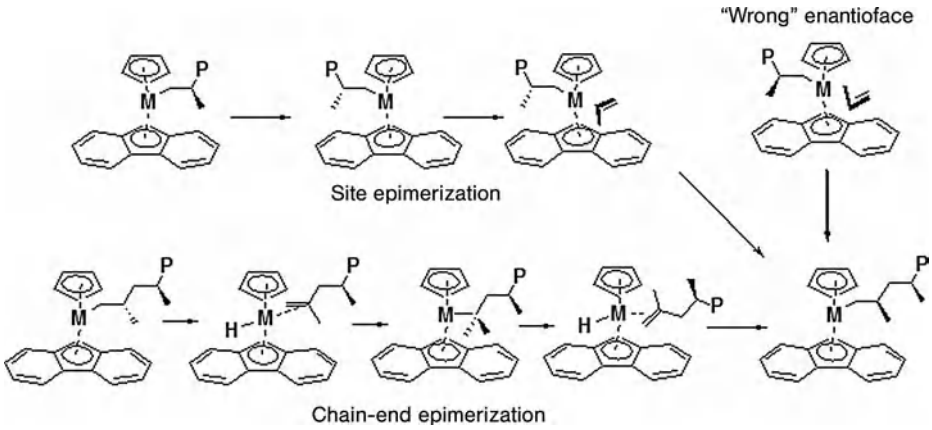

Figure 1.21 Schematic representation of stereo-defect formation on a C_s symmetric catalyst.

is possibly anion-assisted (Figure 1.22) [45]. Site epimerization does not result in stereo-defects in C_2-symmetric complexes, as their sites are homotopic and therefore site epimerization forms the same enantioface.

1.3.1.4 Summary

This section has hopefully illustrated the range of mechanistic tools that can be used to tailor the behavior of a precatalyst. One of the most important points to note is that migratory insertion requires the active metal center to possess at least two active sites. The nature of each active site is determined by the metal and the steric, electronic nature and symmetry that the ancillary ligand imparts to the metal, as well as the cocatalyst. It is also influenced the structure of the growing chain arising from various insertion (primary or secondary *re* or *si*). Therefore, a "single-site" catalyst can in fact possess numerous active sites with differing reactivity ratios to (co)monomer or chain-transfer agents, different regioselectivity and enantioface stereoselectivity. However, under set conditions the above processes behave, statistically, in the same way from one polymer chain to the next.

1.3.2 Case Study 1: Development of Commercially Relevant Single-Site iPP Catalysts

The development of commercially relevant single-site iPP catalysts is perhaps the archetypal elegant example of what the rational tailoring of a precatalyst can achieve, in terms of activity and the polymer resins that they produce.

The genesis of commercial single-site iPP catalysts and their development can be traced back to the stereo-rigid C_2-symmetric metallocenes of Brintzinger (*rac*-Et(Ind)MCl_2, M = Ti or Zr) [74]. It was Ewen, whilst employing the titanium catalyst above, who first correlated the C_2 symmetry of the metallocene to isotacticity [75]. However, the titanium complex proved too thermally unstable and had a low isotacticity. By using the zirconium analogue, Kaminsky and Brintzinger attained

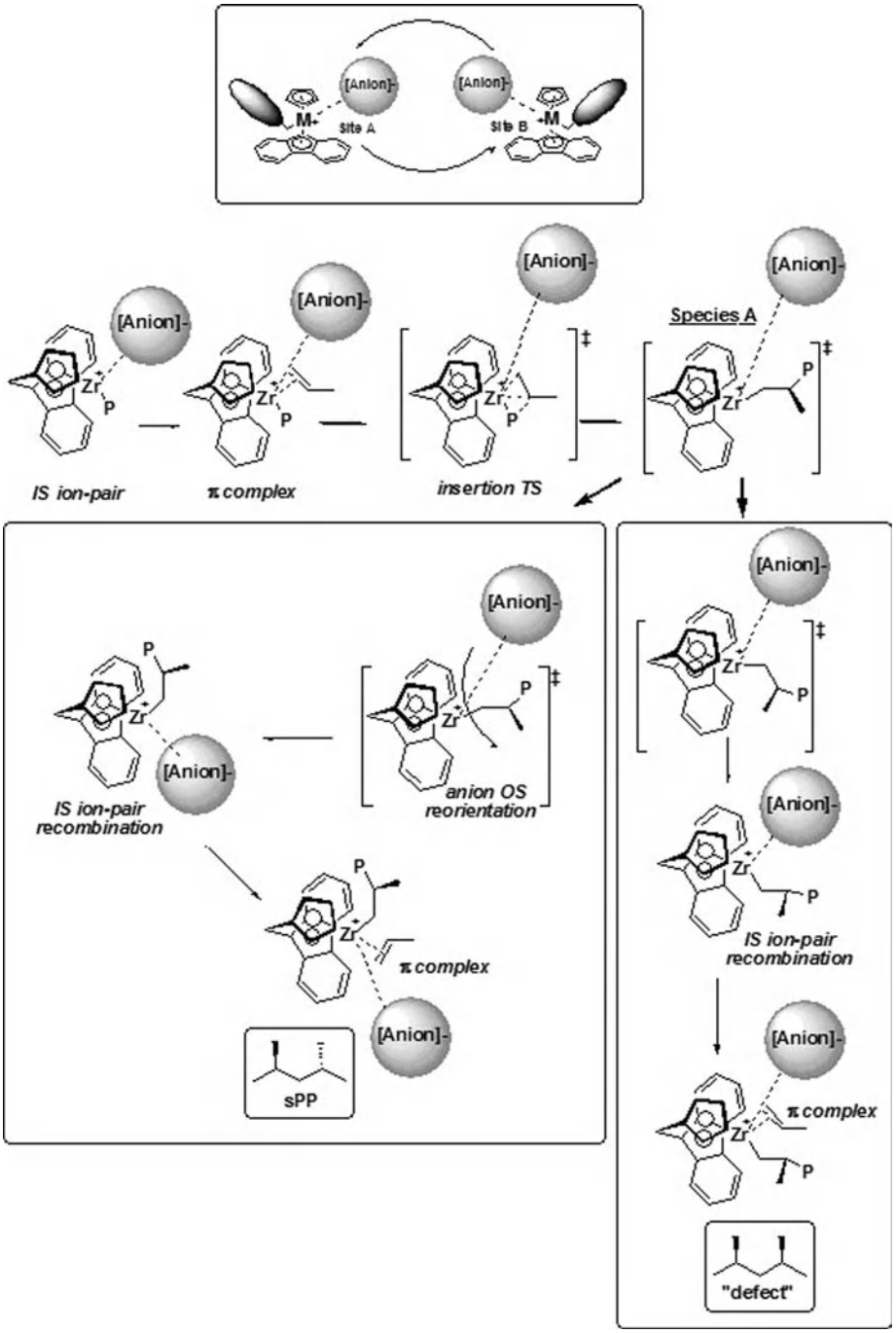

Figure 1.22 Site epimerization.

higher thermal stabilities and stereoselectivities [76]. Subsequent development of the bridged bis-indenyl zirconocenes indicated that the nature of the bridging atom could increase the stereoselectivity and molecular weight of a polypropylene ($H_2C < Me_2 < C_2H_4 < Me_2Si$) under industrially applicable conditions, although all of these systems were far from being commercially viable catalysts (Figure 1.23) [60].

Ultimately, it was the seminal studies of Spaleck and coworkers, with their rational tailoring of the basic C_2-symmetrical complex $Me_2Si(Ind)ZrCl_2$ (C_2-1) (Figure 1.24; Table 1.1) which truly illustrated the full potential [77]. As can be seen from Figure 1.24 and Table 1.1, the introduction of a methyl group in the 2 position of the indenyl moiety increased the molecular weight and stereoregularity, and was also found to reduce region-errors. The result was the production of polypropylenes with higher melting points, albeit with reduced activity. The introduction of an aryl ring in the 4-position of the indenyl moiety increased the polymer's stereoregularity, but once again a reduction in activity was observed. Finally,

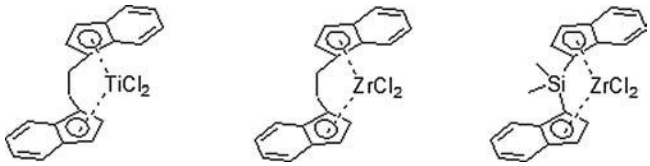

Figure 1.23 Evolution of C_2-symmetric complexes for the isotactic polymerization of propylene.

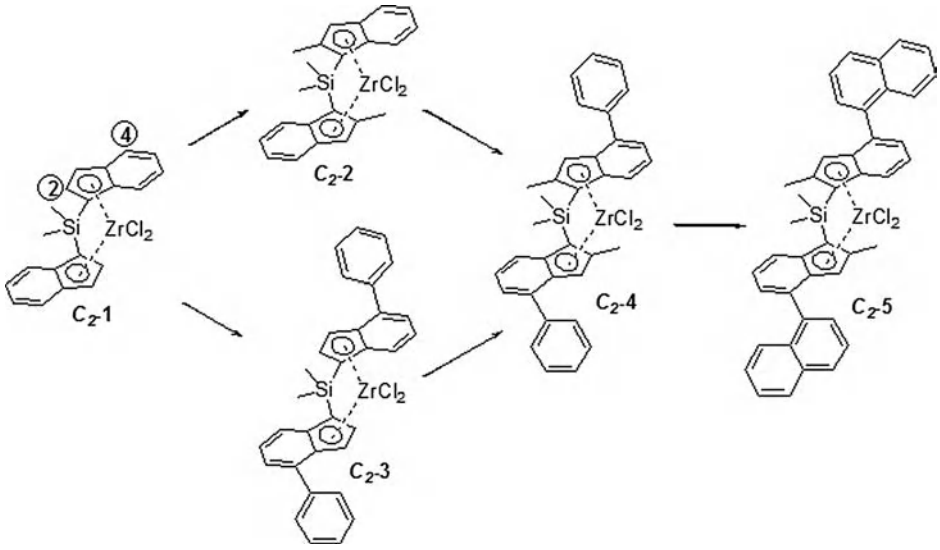

Figure 1.24 Evolution of a C_2-symmetric catalyst.

Table 1.1 Polymerization performances of Spaleck and coworkers C_2 symmetric complexes [77].

rac-Zirconocenes	C_2-1	C_2-2	C_2-3	C_2-4	C_2-5
Activity (kg PP $mmol_{Zr}^{-1} h^{-1}$)	190	99	48	755	875
% *mmmm*	81.7	88.5	86.5	95.2	99.1
T_m	137	145	148	157	161
M_v	36 000	195 000	42 000	729 000	920 000

a combination of substituents in the 2 and 4 positions of the indenyl moiety led to an order of magnitude increase in activity, along with increased stereoregularity, molecular weight and melting point of the final polymer resin.

Further evolutions of "Spaleck-type" polypropylene catalysis has led to catalysts with reportedly increased activities, molecular weights, and melting points. Such development has also further refined the structures [78], and highlighted the importance of the bridging atom and the substituents on it [79], as well as the active metal center [80]. In addition, it has heralded the development of the heterocene-based systems of Ewen, Jones and Elder, which have added yet another dimension to the "tailors toolbox" (not only for polypropylene) [81, 82]. Interestingly, similar structure–property relationships can be seen in ethylene-1-octene polymerization with C_2-1, C_2-2, C_2-4, C_2-5. Mülhaupt and coworkers reported that substitution in the 2 position of the indenyl moiety leads to increased molecular weights, while the addition of an aryl functionality in the 4 position increased the ability to incorporate comonomer [83]. Once again, the combination of these two changes led to a considerable increase in molecular weight and activity for a given comonomer incorporation (density).

The effect of the steric influence on molecular weight capability and stereoselectivity is easily understood. From a stereoselectivity point of view, the introduction of aryl and methyl groups allows for a better orientation of the growing polymer chain. As for molecular weight, if we consider the steric requirements for the transition states for chain propagation and chain transfer via β-hydride transfer to monomer (see Figure 1.11), a rather compact, four-centered transition state is seen to be required for chain propagation, and this can be accommodated in a relatively small space. Chain transfer to the (co)monomer, on the other hand, requires a six-centered transition state (see Figure 1.12) which utilizes more space and is more likely to be destabilized by the steric hindrance of the ligand framework. The increase in activity can be rationalized by the effective separation of the electrophilic active center and the counterion induced by the steric environment induced by the ligand, which in addition may hinder dinuclear deactivation mechanisms. The substitution pattern potentially enhances the degree of unsaturation associated with the active cationic center, thus increasing the reactivity towards propylene. The culmination of these studies led to the first single-site polypropylene catalysts with commercially viable performances.

1.3.3
Case Study 2: One Monomer, Many Microstructures

1.3.3.1 Propylene

The impact of what may seem like "subtle" changes in the stereochemistry and steric environment of the catalyst may have a considerable impact on the microstructure of the polymer [73, 84–87]. The different polypropylene microstructures, ranging from syndio, isotactic to atactic, that can be obtained by slight variations in the ligand environment are highlighted in Figure 1.25. The figures also illustrates how finely balanced some systems are; like a modern-day fighter aircraft, they are extremely agile and capable of an extraordinary range of "maneuvers" but more often than not this agility is based on an inherent "instability".

Although complex *Cs*-2 possesses all the symmetry and structural requirements of a syndio-specific catalyst, when activated this catalyst produces perfectly atactic polypropylene. The dynamic interchange between pseudo-axial/equatorial C–H (boat/chair confirmation on either side) geometries is presumed to disrupt the balance of steric forces and stereorigidity (Figure 1.26) [87].

The delicacy required when balancing steric control is highlighted by the C_1-symmetric family of metallocenes. From Ewen's symmetry rules, the predicted microstructure should be hemi-isotactic, but a range of polymer microstructures can be obtained depending on the "steric excess" of the substituent on the 3-position of the cyclopentadienyl moiety. Complex C_1-1 [84] is capable of producing hemi-isotactic polypropylene, whilst C_1-2 [85] and C_1-3 [86] have been used to prepare iPP or hemi-isotactic stereo-block polypropylene, respectively.

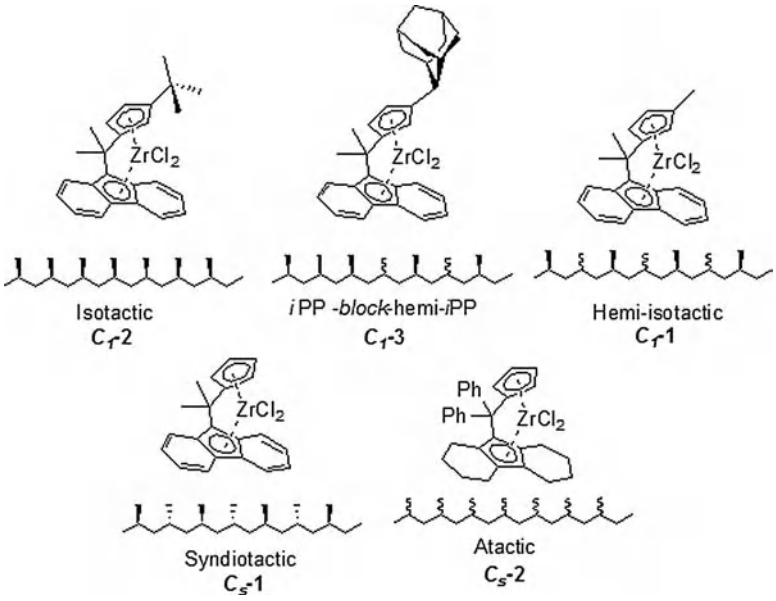

Figure 1.25 Symmetry is just part of the puzzle.

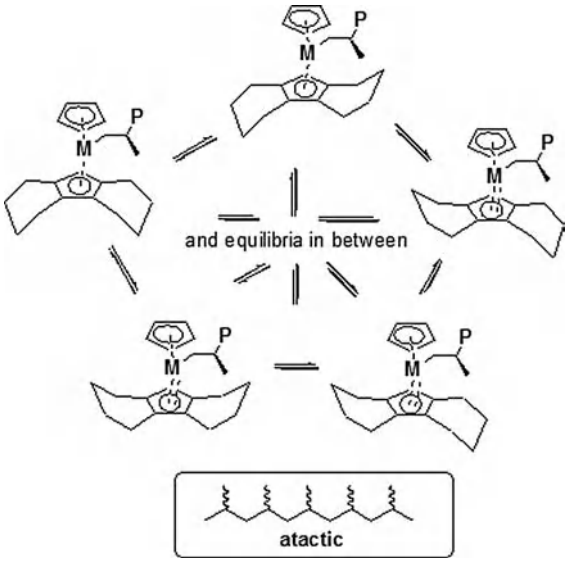

Figure 1.26 A mechanism for the formation of atactic polypropylene from a C_s symmetric catalyst.

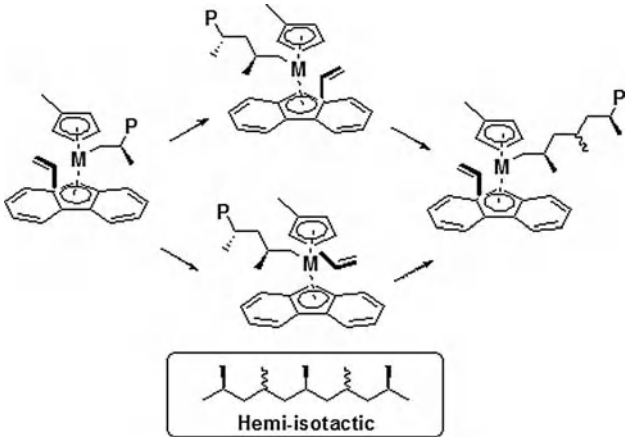

Figure 1.27 Formation of hemi-isotactic polypropylene.

The formation of hemi-isotactic PP is best explained via typical migratory insertion with distereotopic sites, one of which is enantioselective and the other aselective (Figure 1.27). The formation of isotactic or hemi-isotactic stereo-block polypropylene remains a topic for debate. At present, two limiting mechanisms are proposed for the formation of isotactic polypropylene. These are "site epimerization" or "alternating" mechanisms (Figure 1.28). The prevailing literature has invoked the "site epimerization" mechanism to explain the formation whereby, following migratory insertion at the enantioselective site (Site B in Figure 1.28),

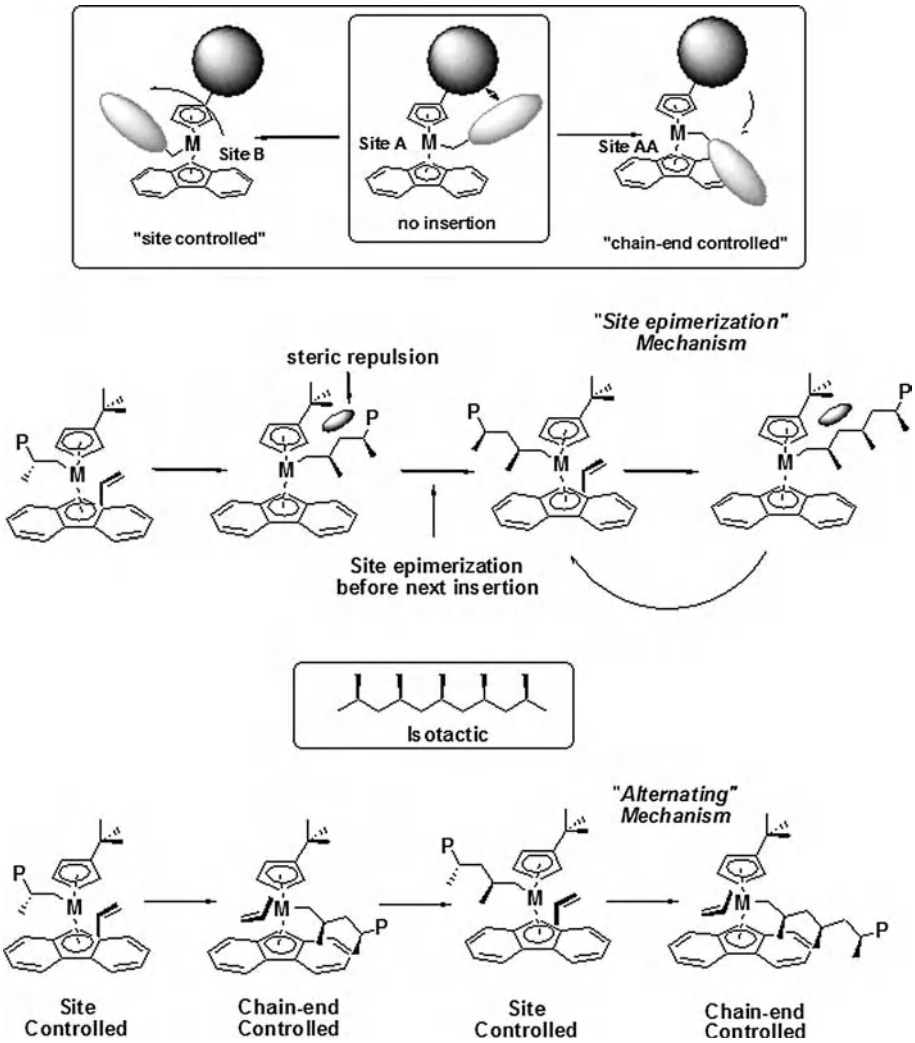

Figure 1.28 Formation of isotactic polypropylene (iPP) from a C_1 symmetric metallocene.

the growing polymer chain is located on the crowded (*tert*-butyl) side of the metallocene. Steric repulsion forbids subsequent insertion, and so forces a site epimerization to occur (Site A to B). This leads to an inversion of the stereochemistry at the metal center and a re-formation of the initial enantioselective site. Propagation then continues via this two step process (insertion–"back-skip"–insertion, etc.) to form isotactic polypropylene.

In the "alternating" mechanism, insertion occurs at the enantioselective and aselective sites of the metallocene. Insertion occurs at the enantioselective site (Site B, Figure 1.28), after which an available site becomes open due to a redirection of the growing polymer chain away from the steric bulk of the *tert*-butyl moiety and

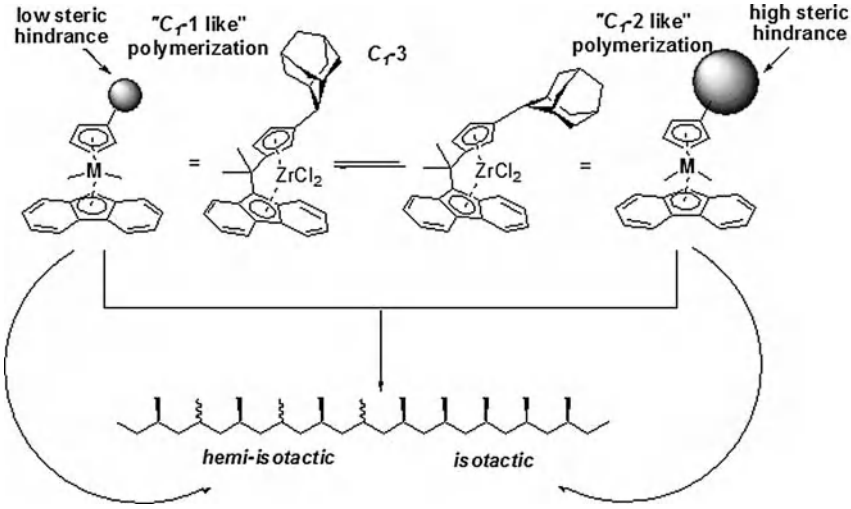

Figure 1.29 Formation of hemi-isotactic-*co*-isotactic stereoblock copolymers.

towards the fluorenyl group (Site A to AA). Insertion of the next monomer occurs with a *trans* arrangement between the polymer chain and the methyl group of the propylene monomer. Isotactic enchainment of propylene then continues via an *alternating* enantiomorphic site-controlled and chain-end-controlled mechanism [88].

The formation of hemi-isotactic-*co-isotactic* stereo-block polypropylene from C_2-2 can then be rationalized in terms of the adamantly ligand "oscillating" between positions that exert high or low steric hindrance of the growing polymer chain, within the time frame of polymer growth (Figure 1.29) [87].

The copolymerization of ethylene and propylene with bridged metallocenes $Me_2E(3\text{-}RCp)(Flu)X_2$/MAO (E = C, X = Me; E = Si, X = Cl; R = H or alkyl) have also been investigated [89]. Ethylene/propylene copolymerization with metallocenes having heterotopic active sites (R = Me, *i*-Pr) yield alternating, isotactic ethylene/propylene copolymers. Both, the nature of the substituent R and the bridging atom (E) influenced the copolymerization behavior, including copolymerization activity, copolymer sequence distribution, molecular weight, and stereochemistry.

1.3.3.2 Ethylene

Iron 2,6-bis(arylimino)pyridyl Complexes The Brookhart–Gibson family of 2,6-bis(arylimino)pyridyl iron complexes are effective catalysts for the conversion of ethylene either to highly-linear HDPE or to linear α-olefins with Schulz–Flory distribution, depending on the aryl group on the imine moiety [90]. For linear HDPE, the conditions are that the aryl rings bear either alkyl/aryl groups on both *ortho*-positions or a large alkyl group, such as *tert*-butyl, on an *ortho*-position. The presence of *ortho*-substituents locks the aryl groups orthogonal to the N–N–N plane (Figure 1.30), and also on the timescale of polymerization, which induces a

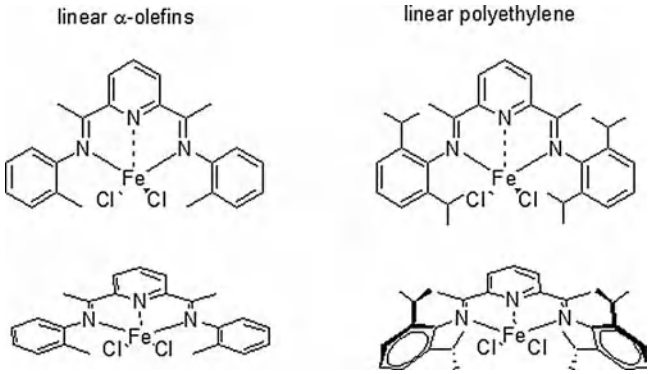

Figure 1.30 Ligand bonding patterns and its affects on the molecular weight capabilities of 2,6-bis(arylimino)pyridyl iron complexes.

retarding effect on the chain-transfer rate. Typically, the steric bulk of the aryl *ortho*-substituents affects the productivity and the polymer's molecular weight. A general rule of thumb is that an increased steric bulk increases the molecular weight by (retarded chain transfer, as discussed above), but decreases productivity. The HDPEs produced by 2,6-bis(arylimino)pyridyl Fe(II) catalysis exhibit high melting points (133–139 °C) accompanied by remarkably high heats of fusion (ΔH = 220–230 J g^{-1}); improved stiffness, high densities and gas permeability are also claimed. The absence of branches on the polymer chains indicates that the Fe(II) polymerization catalysts are unable to isomerize the produced alkyl via a "chain-walking" mechanism, nor to incorporate early-produced α-olefins into the growing polymer chain (SCB or LCB) [91].

Iron 2,6-bis(arylimino)pyridyl complexes in combination with MAO and $ZnEt_2$ (>500 equiv.) have been shown by Gibson and coworkers to catalyze polyethylene chain growth on zinc [92]. The catalyzed chain growth process is characterized by an exceptionally fast and reversible exchange of the growing polymer chains between the iron and zinc centers. Upon hydrolysis of the resultant ZnR_2 product, a Poisson distribution of linear alkanes is obtained; linear α-olefins with a Poisson distribution can be generated via a nickel-catalyzed displacement reaction. The remarkably efficient iron-catalyzed chain growth reaction for $ZnEt_2$ compared to other metal alkyls can be rationalized on the basis of: (i) relatively low steric hindrance around the zinc center; (ii) their monomeric nature in solution; (iii) the relatively weak Zn–C bond; and (iv) a reasonably close match in Zn–C and Fe–C bond strengths.

Nickel α-Diimine The physical properties of the homopolyethylenes produced by these catalyst systems vary widely depending on the type and extent of branching and polymer molecular weight. It is clear from various studies that structural variations of the α-diimine ligand coupled with the conditions of polymerization (temperature and ethylene pressure) can be used to control branching and molecu-

lar weight in a "predictable" way (Figure 1.31). Thus, variably branched polyethylenes can be produced without the use of an additional α-olefin comonomer (as is required for early metal catalysts) with properties that not only span the range of HDPE to LLDPE to LDPE but also include amorphous, elastomeric homopolymers [55, 93, 94].

In the chain-walking mechanism, the active center moves along the growing polymer chain (Figure 1.32). The process commences when a β-hydride transfer is followed by reinsertion, instead of a monomer addition. In this process the active site moves from the terminal carbon in the polymer chain to the next carbon in the backbone. This chain-walking step can be repeated several times before a monomer is added to the chain or the chain is terminated. A monomer insertion after a chain-walking step produces a branch. Figure 1.32 illustrates a simplified scheme of this mechanism. Chain walking is believed to occur in both directions – that is, from the terminal carbon towards the center of the backbone, and from any internal carbon backward to the terminal carbon. For nickel-diimine systems there is no evidence of branches on branches or branches separated by only one carbon, whilst a different behavior has been observed for palladium-α-diimine-catalyzed polyethylene, which does possess branches on branches.

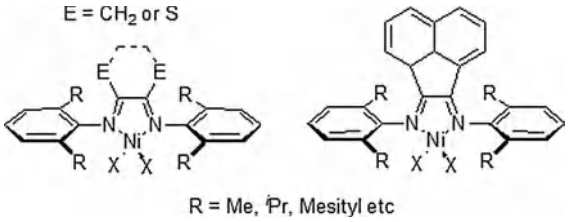

Figure 1.31 Nickel α-diimine.

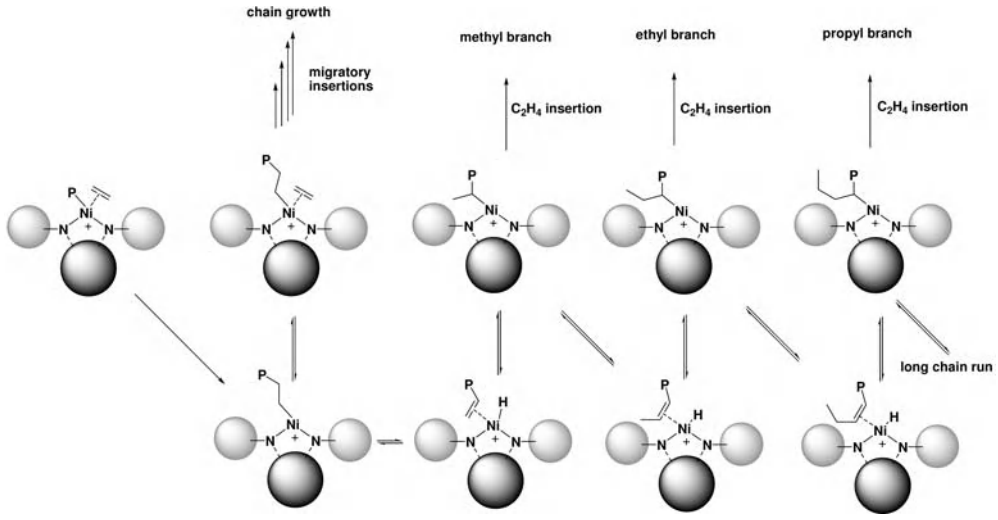

Figure 1.32 Chain-walking mechanism.

Due to the kinetics of chain transfer, several generalized trends can be used for tailoring the polymer. Increasing the steric bulk of the *ortho* aryl substituents on the α-diimine ligand increases the molecular weights of the polyethylenes. It also increases the extent of branching, as well as the turnover frequency (TOF). The electron-withdrawing substituents, such as *o*-CF_3, appear to increase the TOF more than expected, based simply on steric effects. Catalysts bearing alkyl substituents on the backbone carbon atoms tend to produce higher-molecular-weight polymers with narrower molecular weight distributions than do catalysts bearing the planar aromatic (acenaphthyl) backbone. Increases in ethylene pressure lead to dramatic reductions in the extent of branching in the polymer, presumably due to an increased rate of trapping and insertion relative to the rate of chain isomerization, which is independent of C_2H_4.

Increases in polymerization temperatures result in increased branching and decreased molecular weights.

1.3.4
Case Study 3: FI Catalysts; From Lazy to Hyperactive, and Beyond

The metallocene systems described above are exceptionally versatile in terms of ancillary ligand modification. However, such modification typically require numerous synthetic steps with varying degrees of selectivities and yields. The phenoxy-imine systems, as developed by Fujita and coworkers, illustrate the tremendous diversity that can be achieved in tuning the electronic and steric environment via a combination of two base component libraries [95].

The basic ligand system can be divided into two base reagents; salicylaldehydes (FI-A) and primary amines (FI-B) (Figure 1.33). The condensation of the two typically results in high selectivity and yields (hence its versatility in high-throughput developments). In addition, both reagents have a rich commercial inventory or a straightforward synthetic route. With this basic toolbox, Fujita and coworkers elegantly demonstrated the range of radically different activities, thermal stabilities, molecular weight capabilities and molecular weight distributions that could be achieved by varying combination of R_1, R_2 and R_3 groups on the final ligand.

An extraordinary increase in activity – by four to five orders of magnitude – was achieved via a relatively simple ligand modification (see Figure 1.34), whereby it

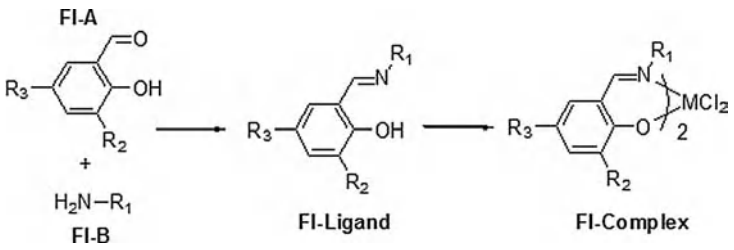

Figure 1.33 Modular synthesis of a phenoxy-imine precatalyst complex.

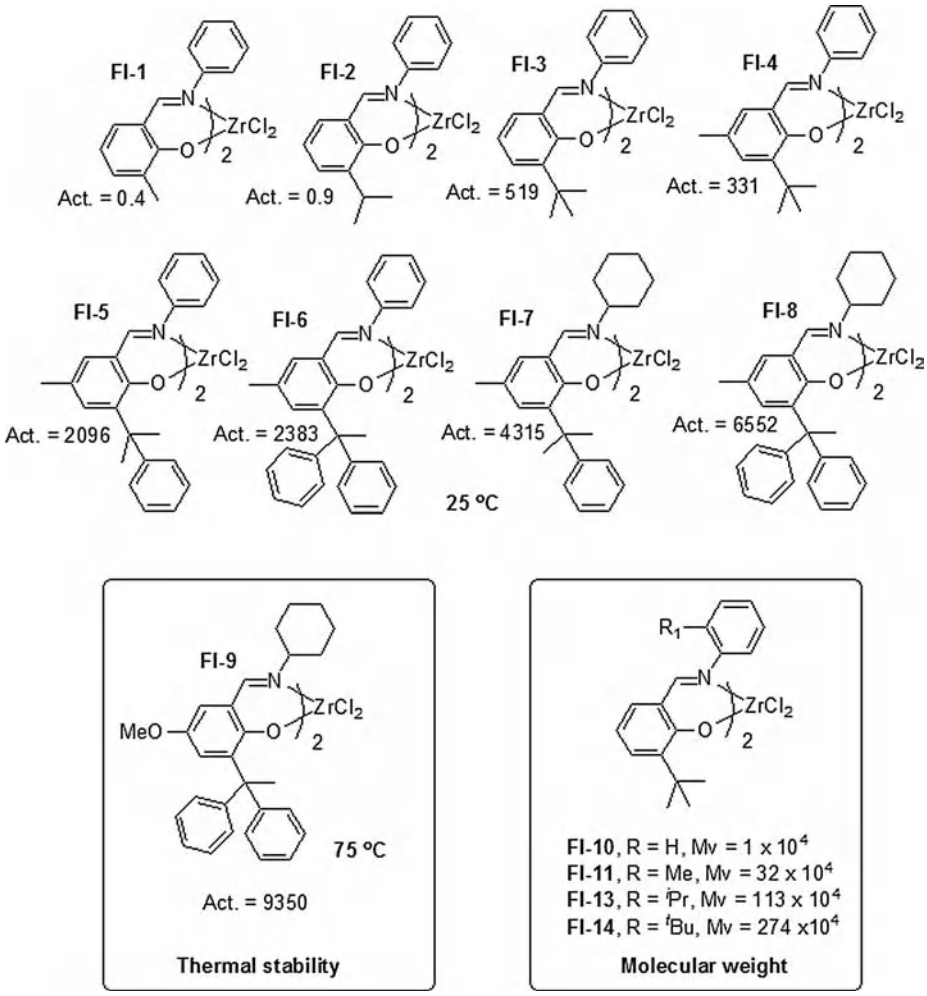

Figure 1.34 Rational design of the phenoxy-imine ligand and it affect on activity, thermal stability and molecular weight capabilities.

was demonstrated that the activity correlated directly to the steric hindrance of the R_2 substituent on the phenoxy-imine ligand (FI-ligand).

Fujita's group proposed that steric hindrance in this position protects the oxygen atom from either the coordination of Lewis acids (TMA, MAO), or the active center from typical di-nuclear deactivation processes. Improving ion-pair separation was also proposed. However, the thermal stabilities peaked at relatively low polymerization temperatures (40–50 °C) and declined rapidly at typical temperatures used in industry (above 70 °C). Poor thermal stability and activity loss was attributed to a decomposition of the active species due to a loss of the ligand(s). Once again, the group designed the ligand framework by the addition of an electron-donating

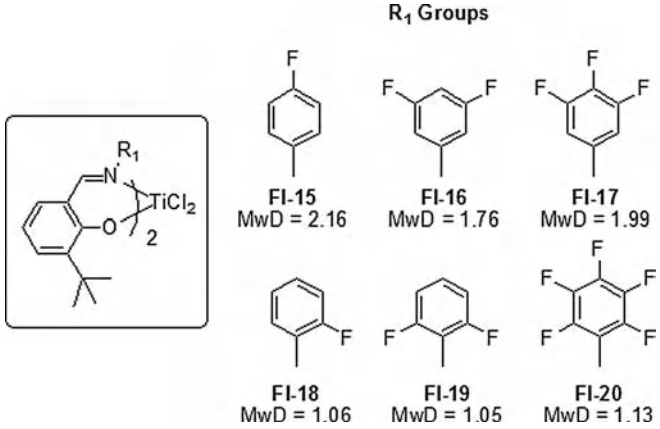

Figure 1.35 Rational design of the phenoxy-imine ligand framework to attain highly controlled ("living") polymerization of ethylene.

group in the R_3 position, thereby imparting a large electronic influence on the zirconium and strengthening the metal–ligand interactions. The synergistic benefits of fine-tuning the electronic and steric nature of the catalyst were clearly demonstrated in the performance of FI-9, which is both highly active and thermally stable.

In the process of tailoring the structure, Fujita's group also clearly demonstrated the effect of steric hindrance in the R_1 position, which increased considerably (by three orders of magnitude from FI-10 to F14) as the steric hindrance at the *ortho* position increased. The "*ortho*" effect has also been used to obtain a highly controlled polymerization. The crucial role of an *ortho*-fluorine in this process is illustrated in Figure 1.35. It has been postulated, based on computational calculations, that the *ortho*-fluorine forms an attractive interaction with the β-hydride of the growing polymer chain, making it less prone to transfer to metal and or monomer. However, recent studies by Busico have shown that the fluorine groups is not sterically benign, and that a controlled status is achieved via a "traditional" repulsive interaction, rather than via an atypical attractive interaction [96]. Whatever the reason, controlled status has been achieved and subsequently been successfully exploited by the groups of Coates and Fujita to produce mono-disperse *s*PP (via an unusual 2,1 chain-end-controlled process) and well-defined di-block copolymers of the type *s*PP-*block*-PE and *s*PP-*block*-EPR [58, 95].

1.3.5
Case Study 4: "Chain-shuttling"

Reversible transmetallation and the formation of "blocky" polyolefins are not new to the world of science [97–99]. However, until recently most tailored block structures were generated with either one type of monomer (propylene) or via a living polymerization. Although the process is extremely precise, by definition each cata-

lyst molecule produces only one polymer chain, and it is not therefore particularly economic from a "technical" polymer point of view, other than as a potential compatibilizer [58, 95].

Arriola and coworkers recently disclosed a breakthrough in polyolefin catalyst that allows the large-scale manufacture of block copolymers [57]. At the heart of the technology is a continuous solution process and a three-part catalytic system (Figure 1.36). The latter consists of a combination of two single-site catalysts (preferably post-metallocenes) which have substantially different monomer selectivities, and a reversible chain-transfer agent (CSA). For example, a zirconium

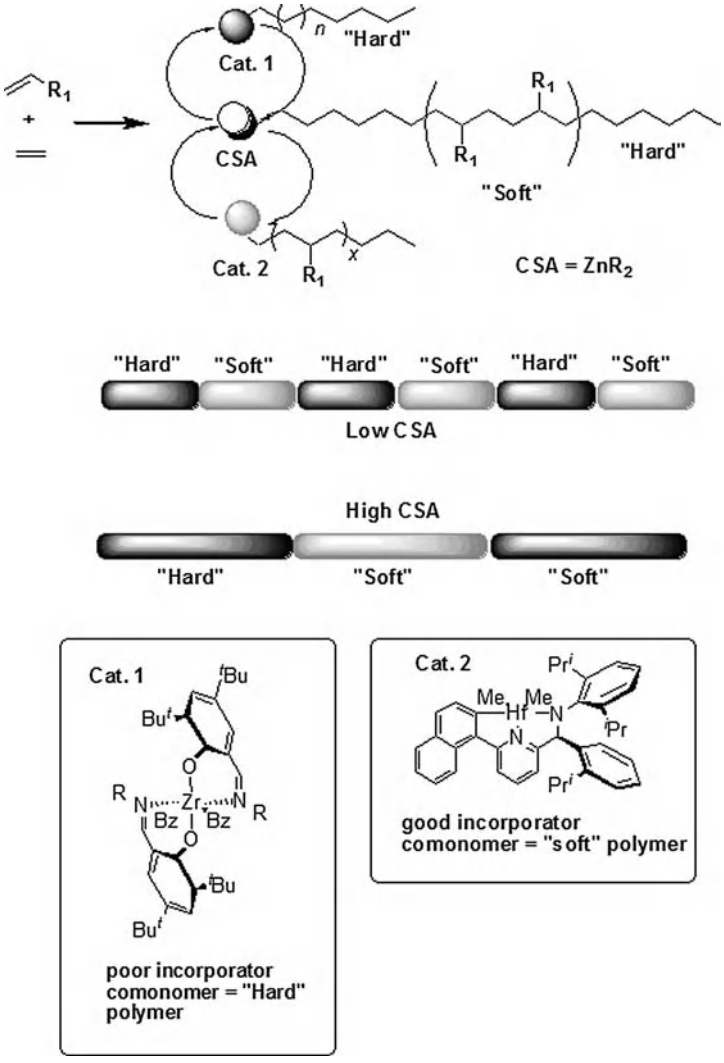

Figure 1.36 "Chain shuttling".

bis(phenoxyimine) (FI) Cat.1, which is a poor incorporator of comonomer, produces a "hard" (rigid) comonomer-lean polymer, whereas the hafnium pyridylamide (Versify™ catalyst) Cat.2 is a good incorporator of comonomer, producing a "soft" (elastomeric) comonomer-rich polymer. The diethyl zinc then intermittently "shuttles" the growing polymer chain between Cat.1 and Cat.2. The conditions and amount of chain-shuttling can be controlled so as to form block structures with longer or strong block lengths, whilst an absence of chain shuttling results in a bimodal composition. As might be imagined, a considerable amount of experimentation and tailoring was needed to optimize this reaction, and it is unsurprising that such an innovation resulted from the application of well planned high-throughput techniques.

The impressive results of catalyst tailoring are the polymeric resins that are produced with alternating blocks of the two "hard" and "soft" polymers. As mentioned above, the rate of "chain-shuttling" – and thus the "blockiness" of the product – can be controlled by the concentration of the monomers, and diethyl zinc and the resultant block-copolymer on its face offer "new-to-the-world" combinations of property performance for olefin-based elastomers. A clear example of this is the ability to "decouple" the modulus from the melting point. Compared to statistical ethylene–octene copolymers, the blocky architecture imparts a substantially higher crystallization temperature, a higher melting temperature, and a better-organized crystalline morphology, while maintaining a lower glass transition temperature. The differences between blocky and statistical copolymers become progressively more apparent as the total comonomer content increases. The high melting point versus mono-modal metallocene grade PE at the same density (120 °C versus *m*PE 60 °C at density 870 g dm^{-3}) results in an enhanced balance between flexibility and heat resistance. Additional improved properties are higher abrasion resistance, a higher recovery after elongation, a strong compression performance, and faster set-up times [100].

1.4 Immobilizing "Single-site" Olefin Polymerization Catalysts: The Basic Problems

A single-site olefin polymerization catalyst is a well-defined molecular entity which is intolerant to virtually everything, and which has a performance that is critically dependent on the precise ligand environment of the transition metal center. Therefore, immobilizing one such catalyst on a suitable solid or glassy inorganic or organic matrix is a formidably complicated task. Apart from the requirements for the support, which must be harmless to the catalyst (and also to the polymer end-user!) and amenable to morphology control (with the related delicate issues of shape replication, fragmentation and heat/mass transfer properties, etc.), the main difficulty is how to introduce a strong, non-labile binding between the support and the active species without altering (deteriorating) the performance of the latter.

Although the possible strategies (e.g., physical or chemical adsorption, tethering, etc.) will be introduced and discussed in detail in various chapters of this book, at this point it is worth mentioning a few basic problems of general relevance.

Catalyst Productivity For an efficient catalytic action, it is mandatory that the monomer has an easy access to the active sites. Selective catalysts have an active pocket which fits tightly to the incoming monomer. The crucial importance of a poorly coordinating counter-anion for cationic catalysts was mentioned previously. In view of all this, it can be understood that the introduction of a strong link between the catalyst and support, without limiting the accessibility of the active sites, is extremely complicated. In fact, the productivity of most immobilized catalysts is one or more orders of magnitude lower than that of the same catalysts in solution, though there are some exceptions. One advantage of immobilized catalysts, on the other hand, is that intermolecular catalyst deactivation processes which may be highly detrimental in solution are usually frozen on surfaces; therefore, if a good productivity can be achieved it tends to be maintained for a longer reaction time.

Catalyst Selectivity The proximity to a surface inevitably represents a perturbation to the catalyst active pocket, not only in terms of accessibility but also of symmetry. In particular, the stereoselectivity of C_s-symmetric and C_1-symmetric catalysts can be altered by the immobilization, because this may change the relative monomer insertion frequency at the two sites. One limiting case which has been reported is that of propene polymerization at certain C_s-symmetric *ansa*-zirconocene catalysts, which is syndiotactic-selective in solution but may be isotactic-selective on a surface because one side of the catalyst would be obstructed by the support. C_2-symmetric catalysts with homotopic sites are expected to be relatively insensitive to this problem; however, in case of a severe decrease of insertion rate, a loss in stereoselectivity may result due to an increased impact of growing chain epimerization (*vide infra*).

Competing Reaction Processes Immobilizing a single-site catalyst affects the kinetics of *all* reactions occurring at that catalyst, including (poly-)insertion, chain transfer, and isomerization processes. It is very unlikely that such an effect would be proportional for all such processes (some of which are intramolecular), and therefore it is to be expected that some microstructural features of the polymer produced (e.g., long and/or short branches, terminal unsaturations, average molecular mass and molecular mass distribution, regiodefects, etc.) will change upon catalyst immobilization. Of course, this also holds true for copolymerization statistics.

References

1 W. Neißl, M. Gahleitner, *Macromol. Symp.* 2002, *181*, 177.
2 V. Busico, R. Cipullo, *Prog. Polym. Sci.* 2001, *26*, 443.
3 D.M. Connor, S.D. Allen, D.M. Collard, C.L. Liotta, D.A. Schiraldi, *J. Appl. Polym. Sci.* 2001, *80*, 2696.
4 M. Gahleitner, *Prog. Polym. Sci.* 2001, *26*, 895.
5 N.J. Inkson, T.C.B. McLeish, O.G. Harlen, D.J. Groves, *J. Rheol.* 1999, *43*, 873.
6 J.A. Pople, G.R. Mitchell, S.J. Sutton, A.S. Vaughan, C.K. Chai, *Polymer* 1999, *40*, 2769.

7 G.H. Michler, *Polym. Adv. Technol.* 1998, *9*, 812.

8 M. Slouf, G. Radonjic, D. Hlavata, A. Sikora, *J. Appl. Polym. Sci.* 2006, *101*, 2236.

9 G. Eder, H. Janeschitz-Kriegl, *Structure development during processing. 5. Crystallization. Materials and Technology Series*, Verlag Chemie-Wiley, Weinheim, 1997, pp. 269–342.

10 M. Gahleitner, P. Jääskeläinen, E. Ratajski, C. Paulik, J. Reussner, J. Wolfschwenger, W. Neißl, *J. Appl. Polym. Sci.* 2005, *95*, 1073.

11 G. Eder, *Non-isothermal Polymer Crystallization*, in: A.J. Ryan (Ed.), *Polymers and Materials Chemistry, Encyclopedia of Materials: Science and Technology*, Vol. *V*, 2002, pp. 6213–6218.

12 S. Rabiej, B. Goderis, J. Janicki, V.B.F. Mathot, M.H.J. Koch, G. Groeninckx, H. Reynaers, J. Geland, A. Włochowicz, *Polymer* 2004, *45*, 8761.

13 B. Pukánszky, I. Mudra, P. Staniek, *J. Vinyl. Addit. Technol.* 1997, *3*, 53.

14 R. Phillips, G. Herbert, J. News, M. Wolkowicz, *Polym. Eng. Sci.* 1994, *34*, 1731.

15 B. Fillon, B. Lotz, A. Thierry, J.C. Wittmann, *J. Polym. Sci. B: Polym. Phys.* 1993, *31*, 1407.

16 M. Gahleitner, J. Wolfschwenger, K. Bernreitner, W. Neißl, C. Bachner, *J. Appl. Polym. Sci.* 1996, *61*, 649.

17 C. Grein, *Adv. Polym. Sci.* 2005, *188*, 43.

18 M. Seki, D.W. Thurman, J.P. Oberhauser, J.A. Kornfield, *Macromolecules* 2002, *35*, 2583.

19 R. Phillips, G. Herbert, J. News, M. Wolkowicz, *Polym. Eng. Sci.* 1994, *34*, 1731.

20 V. Brucato, S. Piccarolo, V. La Carrubba, *Chem. Eng. Sci.* 2002, *57*, 4129.

21 A. Van der Wal, R. Nijhof, R.J. Gaymans, *Polymer* 1998, *39*, 6781.

22 B. Pukanszky, F.H.J. Maurer, *Polymer* 1995, *36*, 1617.

23 Z. Bartczak, A.S. Argon, R.E. Cohen, M. Weinberg, *Polymer* 1999, *40*, 2331, 2347, 2367.

24 C. Grein, K. Bernreitner, A. Hauer, M. Gahleitner, W. Neißl, *J. Appl. Polym. Sci.* 2003, *87*, 1702.

25 L.A. Utracki, M.R. Kamal, *Polym. Eng. Sci.* 1982, *22*, 96.

26 M. Rätzsch, M. Arnold, E. Borsig, H. Bucka, N. Reichelt, *Prog. Polym. Sci.* 2002, *27*, 1195.

27 J. Kolařík, J. Jančář, *Polymer* 1992, *33*, 4961.

28 S.S. Ray, M. Okamato, *Prog. Polym. Sci.* 2003, *28*, 1539.

29 G. Kalay, R.A. Sousa, R.L. Reis, A.M. Cunha, M.J. Bevis, *J. Appl. Polym. Sci.* 1999, *73*, 2473.

30 I.M. Ward, P.J. Hine, *Polymer* 2004, *45*, 1423.

31 L. Resconi, J.C. Chadwick, L. Cavallo, in: D.M.P. Mingos, R. Crabtree, R. (Eds.), *Comprehensive, Organometallic Chemistry III*, Elsevier, New York, 2007.

32 J. Scheirs, W. Kaminsky (Eds.), *Metallocene-Based Polyolefins, Preparation, Properties and Techniques*, Wiley, New York, 1999.

33 G.M. Benedikt, B.L. Goodall (Eds.), *Metallocene Catalyzed Polymers*, William Andrew Publishing, New York, 1998.

34 G.M. Benedikt (Ed.), *Metallocene Technology and Modern Methods in Commercial Applications Catalyzed Polymers*, William Andrew Publishing, New York, 1998.

35 B. Reiger, L. Saunders-Bauch, S. Kacker, S. Striegler (Eds.), *Late Transition Metal Polymerization Catalysts*, Wiley-VCH, Weinheim, 2003.

36 K. Soga, M. Terano (Eds.), *Catalyst Design for Taylor-made Polyolefins, Studies in Surface Science and Catalysis*, Elsevier, Amsterdam, 1994, Vol. *89*, p. 277.

37 A.O. Patil, G. Hlatky (Eds.), *Beyond Metallocenes: Next-Generation Polymerization Catalysts*, ACS Symposium Series 857, Oxford University Press, 2004.

38 G.G. Hlatky, *Coord. Chem. Rev.* 1999, *181*, 243.

39 P.J. Shapiro, *Coord. Chem. Rev.* 2002, *231*, 67.

40 M. Bochmann, *J. Organomet. Chem.* 2004, *689*, 3982.

41 J.-N. Pédeutour, K. Radhakrisknan, H. Cramail, A. Deffieux, *Macromol. Rapid Commun.* 2001, *22*, 1095.

42 E.Y.-X. Chen, T. Marks, *Chem. Rev.* 2000, *100*, 1391.

43 E. Zurek, T. Ziegler, *Prog. Polym. Sci.* 2004, *29*, 107.

44 F. Focante, P. Mercandelli, A. Sironi, L. Resconi, *Coord. Chem. Rev.* 2006, *250*, 170.

45 S. Tomasi, A. Razavi, T. Ziegler, *Organometallics* 2007, *26*, 2024.

46 M.-C. Chen, J.A.S. Roberts, T.J. Marks, *J. Am. Chem. Soc.* 2004, *126*, 4605.

47 P.A. Wilson, M.H. Hannant, J.A. Wright, R.D. Cannon, M. Bochmann, *Macromol. Symp.* 2006, *236*, 100.

48 V. Busico, V. van Axel Castelli, P. Aprea, R. Cipullo, A. Segre, G. Malarico, M. Vacatello, *J. Am. Chem. Soc.* 2003, *125*, 5451.

49 G. Fink, R. Rottler, R. Mynott, W. Fenzel, *Angew. Makromol. Chem.* 1987, *154*, 1.

50 Z. Liu, E. Somsook, C.B. White, K.A. Rosaaen, C.R. Landis, *J. Am. Chem. Soc.* 2001, *123*, 11193.

51 E.J. Arlman, P. Cosse, *J. Catal.* 1964, *3*, 99.

52 (a) M. Brookhart, M.L.H. Green, *J. Organomet. Chem.* 1983, *250*, 395; (b) D. T. Laverty, J.J. Rooney, *J. Chem. Soc., Faraday Trans. I* 1983, *79*, 869.

53 L. Izzo, L. Caporaso, G. Senatore, L. Olivia, *Macromolecules* 1999, *33*, 6913.

54 R. Schubbe, K. Angermund, G. Fink, R. Gooddard, *Macromol. Chem. Phys.* 1995, *196*, 478.

55 S.D. Ittel, L.K. Johnson, M. Brookhart, *Chem. Rev.* 2000, *100*, 1169.

56 A.L. McKnight, R.M. Waymouth, *Chem. Rev.* 1998, *98*, 2587.

57 D.J. Arriola, E.M. Carnahan, P.D. Hustad, R.L. Kuhlman, T.T. Wenzel, *Science* 2006, *312*, 714.

58 (a) G.J. Domski, J.M. Rose, G.W. Coates, A.D. Bolig, M. Brookhart, *Prog. Polym. Sci.* 2007, *32*, 30; (b) G.W. Coates, P.D. Hustad, S. Reinartz, *Angew. Chem. Int. Ed.* 2002, *41*, 2236.

59 V. Busico, R. Cipullo, *Prog. Poly. Sci.* 2001, *26*, 443.

60 L. Resconi, L. Cavallo, A. Fait, F. Piemontesi, *Chem. Rev.* 2000, *100*, 1253.

61 G.W. Coates, *Chem. Rev.* 2000, *100*, 1223.

62 K. Angermund, G. Fink, V.R. Jensen, R. Kleinschmidt, *Chem. Rev.* 2000, *100*, 1457.

63 (a) C.L. Landis, D.R. Sillars, J. Batterton, *J. Am. Chem. Soc.* 2004, *126*, 8890; (b) V. Busico, R. Cipullo, V. Romanelli, S. Ronca, M. Togrou, *J. Am. Chem. Soc.* 2005 *127*, 1608. Further reading on "dormant site" generation follow secondary insertion.

64 (a) T. Shiono, S.M. Azad, T. Ikeda, *Macromolecules* 1999, *32*, 5723; (b) W. Weng, E.J. Markel, A.H. Dekmezian, *Macromol. Chem. Phys.* 2001, *22*, 1488.

65 (a) Y. Suzuki, T. Yasumoto, K. Mashima, J. Okuda, *J. Am. Chem. Soc.* 2006, *128*, 13017; (b) P. Yang, M.C. Baird, *Organometallics* 2005, *24*, 6013; (c) P.J. Chirik, N.F. Dalleska, L.M. Henling, J.E. Bercaw, *Organometallics* 2005, *24*, 2789. Interesting additional reading on β-Me transfer.

66 For examples, see: (a) K.K. Kang, T. Shiono, T. Ikeda, *Macromolecules* 1997, *30*, 1231; (b) A.-L. Mogstad, R.M. Waymouth, *Macromolecules* 1994, *27*, 2313.

67 (a) B.A. Krenstel, Y.V. Kissin, V.J. Kleiner, L.L. Stotskaya, *Polymer and co-polymers of higher α-olefins*, Hanser Publishers, Munich, 1997; (b) J.A. Ewen, in: J. Scheirs, W. Kaminsky (Eds.), *Metallocene-Based Polyolefins, Preparation, Properties and Techniques*, Wiley, New York, 1999.

68 J. Shum, M.J. Schneider, R. Mülhaupt, *J. Mol. Catal.* 1998, *128*, 215.

69 J.A. Ewen, *J. Am. Chem. Soc.* 1984, *106*, 6355.

70 G. Natta, I. Pasquon, A. Zimbelli, *J. Am. Chem. Soc.* 1962, *82*, 1488.

71 J.A. Ewen, *J. Mol. Catal. A: Chemistry* 1998, *128*, 103.

72 (a) D. Fischer, R. Mulhaupt, *Makromol. Chem. Phys.* 1994, *195*, 1143; (b) P. Viville, D. Daoust, A.M. Jonas, B. Nysten, R. Legras, M. Dupire, J. Michel, G. Debras, *Polymer* 2001, *42*, 1953.

73 J.A. Ewen, R.L. Jones, A. Razavi, J.D. Ferrara, *J. Am. Chem. Soc.* 1998, *110*, 6255.

74 F.R.W.P. Wild, L. Zsolani, G. Huttner, H.-H. Brintzinger, *J. Organomet. Chem.* 1982, *232*, 233.

75 J.A. Ewen, *J. Am. Chem. Soc.* 1984, *106*, 6355.

76 W. Kaminsky, K. Külper, H.-H. Brintzinger, *Angew. Chem., Int. Ed.* 1985, *24*, 507.

77 W. Spaleck, F. Küber, A. Winter, J. Rohrmann, B. Bachmann, M. Antberg, V. Dolle, E. Paulus, *Organometallics* 1994, *13*, 954.

78 N. Kashiwa, S. Nojoh, J. Imuta, T. Tsutsui, in: W. Kaminsky (Ed.), *Metalorganic Catalysts for Synthesis and Polymerization*, Springer-Verlag, Berlin, 1999, p. 30.

79 A. Winter, Maack Polypropylene Conference, Zurich, 2006. Congress papers available online from Maack Business Services (http://www.mbspolymer.com/).

80 J.A. Ewen, A. Zambelli, P. Longo, J.M. Sullivan, *Macromol. Rapid Commun.* 1998, *19*, 71.

81 J.A. Ewen, M.J. Elder, R.L. Jones, A.L. Rheingold, L.M Liable-Sands, R.D. Sommer, *J. Am. Chem. Soc.* 2001, *123*, 4763.

82 C. De Rosa, F. Auriemma, A. Di Capua, L. Resconi, S. Guidotti, I. Camurati, I.E. Nifant'ev, P. Laishevtsev, *J. Am. Chem. Soc.* 2004, *126*, 17040.

83 P. Walter, J. Heinemann, H. Ebeling, D. Mäder, S. Trinkle, R. Mülhaupt, in: R. Blom, A. Follestad, E. Rytter, M. Tilset, M. Ystenes (Eds.), *Organometallic Catalysts and Olefin Polymerisation*, Springer-Verlag, Berlin, 2001, p. 319.

84 J.A. Ewen, M.J. Elder, R.L. Jones, L. Haspeslagh, J.L. Atwood, S.G. Bott, K. Robinson, *Makromol. Chem. Makromol Symp.* 1991, *48–49*, 235.

85 (a) S. Miyake, Y. Okumura, S. Inazawa, *Macromolecules* 1995, *28*, 3074; (b) A. Razavi, D. Vereecke, L. Peters, K. Den Dauw, L. Nafpliotis, J.L. Atwood, in: G. Fink, R. Mülhaupt, H.-H. Brintzinger (Eds.,) Ziegler Catalysts, Springer-Verlag, Berlin, 1995, p. 111; (c) A. Razavi, U. Thewalt, *Coord. Chem. Rev.* 2006, *250*, 155.

86 S.A. Miller, J.E. Bercaw, *Organometallics* 2002, *21*, 934.

87 A. Razavi, J.L. Atwood, *J. Organomet. Chem.* 1993, *459*, 117.

88 S.A. Miller, J.E. Bercaw, *Organometallics* 2006, *25*, 3576.

89 W. Fan, M.K. Leclerc, R.M. Waymouth, *J. Am. Chem. Soc.* 2001, *123*, 9555.

90 V.C. Gibson, S.K. Spitzmesser, *Chem. Rev.* 2003, *103*, 283.

91 C. Bianchini, G. Giambastiani, I.G. Rios, G. Mantovani, A. Meli, A.M. Segarra, *Coord. Chem. Rev.* 2006, *250*, 1391.

92 G.J.P. Britovsek, S.A. Cohen, V.C. Gibson, M. van Meurs, *J. Am. Chem. Soc.* 2004, *126*, 10701.

93 D.P. Gates, S.A. Svejda, E. Oñate, C.M. Killian, L.K. Johnson, P.S. White, M. Brookhart, *Macromolecules* 2000, *33*, 2320.

94 D. Meinhard, M. Wegner, G. Kipiani, A. Hearley, P. Reuter, S. Fischer, O. Marti, B. Rieger, *J. Am. Chem. Soc.* 2007, *129*, 918.

95 H. Makio, N. Kashiwa, T. Fujita, *Adv. Synth. Catal.* 2002, *344*, 477.

96 V. Busico, G. Talarico, R. Cipullo, *Macromol. Symp.* 2005, *226*, 1.

97 J.C.W. Chien, Y. Iwamoto, M.D. Rausch, W. Wedler, H.H. Winter, *Macromolecules* 1997, *30*, 3447.

98 S. Lieber, H.-H. Brintzinger, *Macromolecules* 2000, *33*, 9192.

99 C. Pryzbyla, G. Fink, *Acta Polym.* 1999, *50*, 77.

100 H.P. Wang, D.U. Khariwala, W. Cheung, S.P. Chum, A. Hiltner, E. Baer, *Macromolecules* 2007, *40*, 2852.

2
Traditional Heterogeneous Catalysts

2.1
Ziegler–Natta Catalysts in Polyolefin Synthesis

John C. Chadwick, Thomas Garoff, and John R. Severn

2.1.1
Introduction

The continual evolution of the ubiquitous Ziegler catalysts, in either the Ziegler polyethylene (PE) or Ziegler-Natta polypropylene (PP) form, has ensured their dominance in the commercial production of PE and polypropylene PP for the past 50 years [1–6]. Modern Ziegler catalysts with ferocious productivity (in excess of 100 kg PO g^{-1} catalyst, depending on the target resin) and a relatively inexpensive manufacturing cost (tens of € per kg catalyst) are commonplace [1]. In an industry where small savings can make or break a new polymer technology, it is understandably difficult to compete with the economics of such catalysts, particularly for commodity-based resins.

The industrious heart of the Ziegler system is an organometallic catalyst formed via the reaction and interaction of an alkyl aluminum compound and a Group 3 (V), or more commonly Group 4, transition metal chloride. The $TiCl_3$ catalysts used in the early industrial processes for PE and PP (first and second generations) were typically prepared by the reduction of $TiCl_4$ with an aluminum alkyl or aluminum metal, generating a solid of composition $TiCl_3 \cdot 0.33AlCl_3$. The reaction of $TiCl_4$ and $AlEt_3$ (molar ratio 3 : 1) at low temperatures in hydrocarbon solution resulted in the controlled precipitation of catalysts having spheroidal particle morphology. The β-$TiCl_3 \cdot 0.33AlCl_3$ formed was converted to the more stereoselective γ-form by heating to 160–200 °C [7]. This catalyst was used, together with $AlEt_2Cl$ as cocatalyst, in slurry processes, with typical PP yields being around 1–4 kg g^{-1} catalyst. The very low catalyst activity (by today's standards) meant that the removal (de-ashing) of catalyst residues from the polymer was necessary. In many cases, limited catalyst stereoselectivity meant that it was also necessary to remove "atactic" polymer from the product, leading to complicated and expensive manufacturing processes.

Tailor-Made Polymers. Via Immobilization of Alpha-Olefin Polymerization Catalysts.
Edited by John R. Severn and John C. Chadwick

ISBN: 978-3-527-31782-0

During the early 1970s, an improved (second-generation) $TiCl_3$ catalyst was developed by Solvay [8]. The catalyst preparation procedure involved the treatment of $TiCl_3/AlCl_3/AlEtCl_2$, produced by reaction of $TiCl_4$ with $AlEt_2Cl$, with diisoamyl ether to remove aluminum from the solid. Subsequent treatment with $TiCl_4$ catalyzed the transformation from the β- to the δ-form of $TiCl_3$ at a relatively mild temperature (<100 °C) [9]. By using catalysts of this type, it was possible to obtain PP yields in the range 5 to 20 $kg\,g^{-1}$ catalyst in 1 to 4 hours polymerization in liquid monomer [10].

For PE, $TiCl_3$ catalysts are reported give a broad molecular weight distribution (MWD = 4–12), and a very inhomogeneous chemical composition distribution (CCD) for linear low-density polyethylene (LLDPE). However, δ-$(TiCl_3)\cdot 0.33AlCl_3$ has been reported to give a low level of hydrocarbon-soluble material [11].

2.1.2 Ziegler–Natta Catalysts for Polypropylene

Since the first discoveries by Karl Ziegler and Giulio Natta in 1953/1954, Ziegler–Natta catalysts for the production of PP have evolved from the $TiCl_3$-based systems described above, having limited activity and selectivity, to the highly active and stereoselective $MgCl_2$-supported catalysts which now dominate PP manufacture. The application of different Lewis bases (electron donors) in catalyst preparation and polymerization has led to a range of $MgCl_2$-supported catalyst systems giving ever-increasing control over polymer tacticity, molecular weight and MWD, enabling the production of polymers with processability and properties suited to very different end-use applications.

Ziegler–Natta catalysts are generally described in terms of generations, corresponding to the chronological order of their development [2]. The first and second generations refer to the $TiCl_3$ catalysts described above, which were developed up until the 1970s. The basis for the $MgCl_2$-supported catalysts lay in the discovery, during the late 1960s, of "activated" $MgCl_2$ able to support $TiCl_4$ and give high catalyst activity, and the subsequent discovery of electron donors capable of increasing the stereospecificity of the catalyst so that (highly) isotactic PP could be obtained. Dependent on the type of electron donor used, these catalysts are termed third, fourth, or fifth generation, as described in Table 2.1.

2.1.2.1 Third-Generation $MgCl_2$-supported Catalysts

The first steps in the development of third-generation catalysts took place with the discovery, during the late 1960s, of "activated" $MgCl_2$ as a support for $TiCl_4$, followed by the incorporation into the catalyst system of electron donors giving high catalyst stereospecificity [3, 12–14]. Initially, activated $MgCl_2$ was prepared by ball-milling a mixture of magnesium chloride and ethyl benzoate, which led to the formation of very small (≤3 nm-thick) primary crystallites of $MgCl_2$ [9]. Subsequent X-ray diffraction studies have revealed that activated $MgCl_2$ also has a disordered structure, with rotational disorder in the stacking of the Cl–Mg–Cl triple layers [15, 16]. The combination of small crystallite size and large rotational disorder

Table 2.1 $MgCl_2$-based Ziegler–Natta catalysts for polypropylene. Data indicate catalyst performance for different internal and external donors.

Internal donor	*Year of discovery*	*External donor*	*Productivity (kg PP g^{-1} cat.)*	*Amorphous fraction (wt.%)*	*MWD (M_w/M_n)*
Benzoate	1971	Benzoate	15–30	4–7	8–10
Phthalate	1980	Alkoxysilane	40–70	1–5	6–8
Diether	1988	–	100–130	2–5	4–5
Diether	1988	Alkoxysilane	70–100	1–2	4–5
Succinate	1999	Alkoxysilane	40–70	1–5	10–15

MWD, molecular weight distribution.

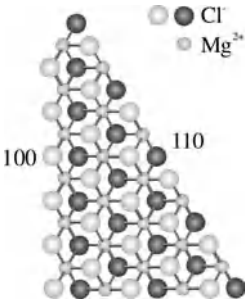

Figure 2.1 Model for a monolayer of a $MgCl_2$ crystal, showing the most probable 100 and 110 cleavage cuts. (Figure provided courtesy of Dr. F. Piemontesi, Basell Polyolefins.)

appears to lead to a high catalyst activity [17]. Giannini [12] has indicated that, on preferential lateral cleavage surfaces, the magnesium atoms are coordinated with four or five chlorine atoms, as opposed to six chlorine atoms in the bulk of the crystal. These lateral cuts correspond to (110) and (100) faces of $MgCl_2$, as illustrated in Figure 2.1. It was suggested by Corradini [18, 19] that bridged, dinuclear Ti_2Cl_8 species can coordinate to the (100) cut of $MgCl_2$ and give rise to the formation of chiral, isospecific active species. Preferential coordination of the donor (in this case ethyl benzoate) on the more acidic (110) cut would therefore lead to the (100) cut being prevailingly occupied by Ti_2Cl_8 dimers. It is certainly so that the function of the donor is to control the amount and distribution of $TiCl_4$ on the support surface, as well as stabilizing small crystallites of $MgCl_2$, but recent mechanistic and modeling studies have provided strong evidence for the formation of active species on the (110) cut of $MgCl_2$. This is discussed in more depth later in the chapter.

Ziegler–Natta catalysts comprising $MgCl_2$, $TiCl_4$ and an "internal" electron donor are typically used in combination with an aluminum alkyl cocatalyst such as $AlEt_3$ and an "external" electron donor added in polymerization. Third-generation catalysts in which the internal donor is ethyl benzoate are used in combination with a second aromatic ester, such as methyl *p*-toluate or ethyl *p*-ethoxybenzoate, as external donor. The requirement for the external donor is due to the fact that, when the catalyst is brought into contact with the cocatalyst, a large proportion of the internal donor is lost as a result of alkylation and/or complexation reactions. The external donor replaces, to a large extent, the internal donor in the solid catalyst, thereby maintaining high catalyst stereospecificity. It has been demonstrated that the most active and stereospecific catalyst systems are those which allow the highest incorporation of external donor [20], the effectiveness of a catalyst system depending more on the combination of donors than on the individual internal or external donor.

2.1.2.2 Fourth-Generation $MgCl_2$-supported Catalysts

During the early 1980s, a new generation of catalysts was developed in which the internal donor is a phthalate ester such as diisobutyl phthalate and the external donor is an alkoxysilane of type $RR'Si(OMe)_2$ or $RSi(OMe)_3$ [21]. This became the most widely used catalyst system in PP production. A further feature which contributed greatly to the commercial success of $MgCl_2$-supported catalysts was the development of spherical catalysts with controlled particle size and porosity, prepared via chemical rather than mechanical activation of magnesium chloride. Many different approaches have been followed, such as reaction of a magnesium alkyl or alkoxide with a chlorinating agent or $TiCl_4$, or by complexation of $MgCl_2$ with an alcohol. For example, the cooling of emulsions of molten $MgCl_2 \cdot n$EtOH in paraffin oil gives almost perfectly spherical supports, which are then converted into the catalysts by reaction with $TiCl_4$ in the presence of the appropriate donor [2]. Temperatures of at least 80 °C and at least two $TiCl_4$ treatment steps are normally used, in order to obtain high-performance catalysts in which the titanium is mainly present as $TiCl_4$ rather than the $TiCl_3OEt$ generated in the initial reaction with the support. Catalysts obtained via chemical routes generally have a BET surface area of around $300\,m^2\,g^{-1}$ and pore volumes in the range 0.3 to $0.4\,cm^3\,g^{-1}$ [2]. An exception is the recent development of a low-porosity catalyst, prepared via solidification from emulsion [22], which nevertheless undergoes rapid fragmentation and particle growth during polymerization [23]. A single Ziegler–Natta catalyst particle contains millions of primary crystallites, often in the form of quasi-hexagonal thin platelets [24, 25], which agglomerate to form clusters of subparticles [26]. The particular internal particle morphology depends on the catalyst preparation route. A catalyst prepared via precipitation of a support from solution by reacting $TiCl_4$ with a complex of $MgCl_2$, epichlorohydrin and tributyl phosphate has been shown to contain primary particles in which long rods of $MgCl_2$ crystallites emanate from a central (nucleation) point [27].

The most effective alkoxysilane external donors for high catalyst stereospecificity are methoxysilanes containing relatively bulky groups alpha to the silicon atom

[28–30]. Typical examples include cyclohexyl(methyl)dimethoxysilane and dicyclopentyldimethoxysilane [31]. Of these, the latter gives particularly high stereospecificity [32] and a broader MWD [33]. High PP stereoregularity and broad MWD has also been obtained by the use of dimethoxysilanes containing polycyclic amino groups [34, 35].

A particular advantage of the fourth-generation catalysts over the third-generation systems is their greater stability during polymerization. The ethyl benzoate-based catalysts exhibit very high initial activity but then decay rapidly, losing around 90% of their activity during the course of a 1-hour polymerization. This limits their productivity to around 30 kg PP g^{-1} catalyst under typical polymerization conditions (bulk liquid monomer, ca. 70 °C). In contrast, productivities up to around 70 kg PP g^{-1} catalyst are achievable with the fourth-generation, phthalate-based systems.

2.1.2.3 Fifth-Generation $MgCl_2$-supported Catalysts

The discovery and development of the fourth-generation phthalate/alkoxysilane-based catalyst systems was based on the consideration that bidentate donors should be able to form strong chelating complexes with tetracoordinate Mg atoms on the (110) face of $MgCl_2$, or binuclear complexes with two pentacoordinate Mg atoms on the (100) face. As was the case for the third-generation catalysts, the function of the external donor is to replace the internal donor lost by alkylation and complexation reactions with the Al alkyl cocatalyst.

The search for further catalyst improvements led to the development of internal donors which not only had the correct oxygen–oxygen distance for effective coordination with $MgCl_2$ but which, unlike phthalate esters, were not removed from the support on contact with $AlEt_3$. Thus, certain 2,2-disubstituted-1,3-dimethoxypropanes were found to meet these criteria [36–39]. The best performance was obtained when bulky substituents in the 2-position led to the diether having a most probable conformation [40] with an oxygen–oxygen distance in the range of 2.8 to 3.2 Å.

The fact that the diether internal donor is not extracted when the catalyst is brought into contact with the $AlEt_3$ cocatalyst means that high stereospecificity can be obtained even in the absence of external donor. Furthermore, fifth-generation catalyst systems of type $MgCl_2/TiCl_4$/diether-AlR_3 show particularly high polymerization activity and good stability (low decay), typically giving yields exceeding 100 kg PP g^{-1} catalyst. They also give a relatively narrow MWD and show high sensitivity to chain transfer with hydrogen. In other words, relatively low concentrations of hydrogen are sufficient to give effective control over the PP molecular weight, so that a wide range of polymer grades can be produced.

The high hydrogen response of fifth-generation, diether-based catalysts arises from chain transfer after the occasional secondary (2,1-) rather than the usual primary (1,2-) monomer insertion [41]. The reactivation of "dormant" (2,1-inserted) species via chain transfer with hydrogen also explains the frequently observed activating effect of hydrogen in propylene polymerization, giving yields which may be around three times those observed in the absence of hydrogen [42]. These con-

clusions have been based on ^{13}C NMR determination of the relative proportions of *i*Bu- and *n*Bu-terminated chains, resulting from chain transfer with hydrogen after primary and secondary insertion, respectively:

$$\text{Ti-CH}_2\text{CH(CH}_3\text{)[CH}_2\text{CH(CH}_3\text{)]}_n\text{Pr} + \text{H}_2 \rightarrow \text{Ti-H} + i\text{BuCH(CH}_3\text{)[CH}_2\text{CH(CH}_3\text{)]}_{n-1}\text{Pr}$$

$$\text{Ti-CH(CH}_3\text{)CH}_2\text{[CH}_2\text{CH(CH}_3\text{)]}_n\text{Pr} + \text{H}_2 \rightarrow \text{Ti-H} + n\text{BuCH(CH}_3\text{)[CH}_2\text{CH(CH}_3\text{)]}_{n-1}\text{Pr}$$

Not only the high hydrogen response but also the relatively narrow PP MWDs obtained with diether-based catalysts can be attributed to chain transfer after 2,1-insertion. In these systems, even the most highly stereospecific active sites are not totally regiospecific; a proportion of approximately one secondary insertion for every 2000 primary insertions at highly isospecific sites has been noted [41]. The probability of chain transfer with hydrogen after a secondary insertion is such that this is sufficient to prevent the formation of very high-molecular-weight chains, taking into account that the highest molecular weight fraction of the polymer is formed on the active species having the highest isospecificity. The broader MWDs obtained with catalysts containing ester internal donors are likely to be due to the presence of (some) isospecific active sites having very high regiospecificity and therefore lower hydrogen sensitivity [43].

2.1.2.4 **New Developments**

Recently, a further family of $MgCl_2$-supported catalysts has been developed in which the internal donor is a succinate ester [44, 45]. As is the case with phthalate-based catalysts, an alkoxysilane is used as external donor. The essential difference between these catalysts is that the succinate-based systems produce PP having a much broader MWD.

The desired MWD of a PP depends on the end-use application of the polymer. A narrow value, and relatively low molecular weight, is advantageous in fiber-spinning applications. In contrast, the extrusion of pipes and thick sheets requires a high melt strength, and therefore a relatively high molecular weight and broad MWD. A broad MWD, along with high isotactic stereoregularity, is also beneficial for high crystallinity and therefore high rigidity. The new succinate-based catalysts enable very broad MWD PP homopolymers to be produced in a single reactor, and also produce heterophasic copolymers having an improved balance of stiffness and impact strength, taking into account that the incorporation of a rubbery (ethylene/propylene) copolymer phase into a PP homopolymer matrix increases impact strength but leads at the same time to decreased stiffness.

The characteristics of the various families of $MgCl_2$-supported catalysts, along with the chronological order of their development, are summarized in Table 2.1.

2.1.2.5 **Mechanistic Aspects**

It is generally assumed that the active species in propylene polymerization with $MgCl_2$-supported catalysts comprises trivalent titanium, but only a limited propor-

tion of the titanium in the catalyst is actually catalytically active. Estimates of the concentrations of active centers (C*, expressed as a proportion of the total Ti present) have ranged from less than 1% to more than 20%, depending on the particular catalyst and the method used for the determination of C* [46–48]. The proportions of isospecific and weakly-specific active species are of course dependent on catalyst composition, and in particular on the internal and external donors present in the system. The propagation rate constant (k_p) is around an order of magnitude higher for isospecific sites than for weakly-specific sites and the value of k_p increases significantly in the presence of hydrogen [49], in accordance with the reactivation of "dormant" (2,1-inserted) centers by chain transfer with hydrogen. Stopped-flow polymerization studies have shown that hydrogen is only effective as chain-transfer agent when the catalyst and cocatalyst have been precontacted, indicating that effective chain transfer with hydrogen requires the presence of species able to promote the dissociation of hydrogen [50, 51].

It is well established that the nature of the active species in $MgCl_2$-supported Ziegler–Natta catalysts is strongly dependent on the nature of the internal and external donors. Effective external donors not only increase the isotactic index of PP (the proportion of polymer insoluble in boiling heptane or in xylene at 25 °C), but can also increase in absolute terms the amount of isotactic polymer formed [52, 53]. The external donor not only decreases "atactics" formation but can also increase the degree of steric control at isospecific sites [54]. A powerful technique to study the effects of electron donors on site selectivity in Ziegler–Natta catalysts is the determination of the stereoregularity of the first insertion step in propylene polymerization. First-step stereoregularity is particularly sensitive to the steric environment of the active center, due to the fact that the stereospecificity of the first monomer insertion is always lower than that of the following propagation steps. Investigation of the effect of Lewis bases on the first-step stereoregularity resulting from propylene insertion into a Ti–Et bond formed via chain transfer with ^{13}C-enriched $AlEt_3$, using a $MgCl_2/TiCl_4$/diisobutyl phthalate catalyst, showed that the mole fraction of erythro (isotactic) placement in the isotactic polymer fraction was 0.67 with no external donor, 0.82 with $MeSi(OEt)_3$, and 0.92 with $PhSi(OEt)_3$ [55]. It could be concluded that the alkoxysilane external donor was present in the environment of at least part of the isospecific centers. Subsequent studies indicated that similar considerations apply to diether donors [56, 57].

The presence of a donor molecule in the vicinity of isospecific active species is an important feature of a mechanistic model recently proposed by Busico, based on detailed ^{13}C NMR analysis of the PP chain microstructure [58]. This model is based on the fact that defects arising from stereoirregular insertions are not randomly distributed along the chain but are clustered. The chain can therefore contain, in addition to highly isotactic blocks, sequences which can be attributed to weakly isotactic (isotactoid) and to syndiotactic blocks. This implies that the active site can isomerize very rapidly (during the growth time of a single polymer chain, i.e., in less than 1 second) between three different propagating species. The same sequences are present, but in different amounts, in both the soluble and insoluble fractions. The polymer can therefore be considered to have a stereoblock

structure in which highly isotactic sequences alternate with defective isotactic (isotactoid) and with syndiotactoid sequences. The relative contributions of these sequences can be related to site transformations involving the presence or absence of steric hindrance in the vicinity of the active species. ^{13}C NMR studies have indicated [59] the presence of C_1-symmetric active species in $MgCl_2$-supported catalysts, with a mechanism of isotactic propagation which is analogous to that for certain C_1-symmetric metallocenes, in the sense that propylene insertion at a highly enantioselective site tends to be followed by chain "back-skip" rather than a less regio- and stereoselective insertion when the chain is in the coordination position previously occupied by the monomer. It is proposed that a (temporary) loss of steric hindrance from one side of an active species with local C_2-symmetry, giving a C_1-symmetric species, may result in a transition from highly isospecific to moderately isospecific propagation. The loss of steric hindrance on both sides can lead to syndiospecific propagation in which chain-end control becomes operative. This model is illustrated in Figure 2.2.

If it is considered that the steric hindrance in the vicinity of the active species can result from the presence of a donor molecule, and that the coordination of such a donor is reversible, the above model provides us with an explanation for the fact that strongly-coordinating, stereorigid donors typically give stereoregular polymers in which the highly isotactic sequences predominate [60]. It has been suggested [61] that the high stereospecificity obtained using silanes having one or more bulky hydrocarbyl groups is due to the silane stabilizing "fluctuating" isospecific sites, with the bulky hydrocarbyl groups protecting the silane from removal from the catalyst surface via complexation with aluminum alkyl. Stereospecific active species involving the coordination of $AlEt_3$ or $AlEt_2Cl$ in the vicinity of the titanium atom have also been proposed [62].

The fundamental question remains as to whether the active species are situated on the (100) or the (110) face of $MgCl_2$. Possible modes of coordination of $TiCl_4$ on $MgCl_2$ are illustrated in Figure 2.3. After many years of uncertainty and debate, experimental and modeling studies now appear to be resolving this issue. A recent

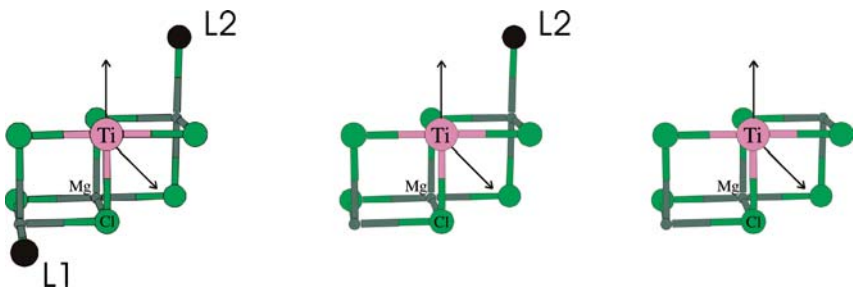

Figure 2.2 Model of possible active species for highly isotactic, isotactoid and syndiotactic propagation. (Reproduced with permission from *Macromelcules* **2003**, *26*, 2616–2622; © American Chemical Society.)

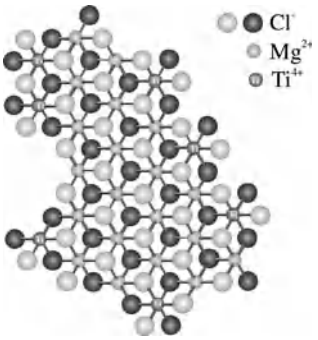

Figure 2.3 Proposed coordination modes of $TiCl_4$ species on $MgCl_2$ lateral cuts, showing dimeric and monomeric species on the 100 cut, and monomeric species on the 110 cut. (Figure provided courtesy of Dr. F. Piemontesi, Basell Polyolefins.)

investigation of the Raman spectra of the products of co-milling mixtures of $MgCl_2$ and $TiCl_4$ led to the conclusion, supported by *ab-initio* calculations, that the adsorption of $TiCl_4$ gave a species with octahedrally coordinated titanium, on the (110) lateral cut of $MgCl_2$ [63, 64]. This stable complex was not removed by washing with solvent, whereas dimeric species (Ti_2Cl_8) on the (100) cut were easily removed. The monomeric species was therefore concluded to be the active site precursor in $MgCl_2$-supported catalysts. There is also strong evidence from modeling studies that the dominant coordination mode of diether donors to $MgCl_2$ is via bidentate coordination on the (110) cut [65, 66]. Taking into account the evidence for the presence of a donor molecule in the vicinity of stereospecific active species, these results indicate that it is likely that both the active titanium and the diether donor are located on the (110) lateral cut. It has also been shown [67, 68] that the use of a diether as external donor in combination with a $MgCl_2/TiCl_4$/phthalate ester catalyst gives active species which are very similar to those present when the diether is used as internal donor. This could therefore imply that the active species in phthalate-based catalysts are similarly located on the (110) cut.

Recent molecular modeling studies conducted by Cavallo [69] have revealed that, in contrast to the strong preference of diethers and alkoxysilanes for coordination on the (110) cut of $MgCl_2$, succinate donors show much less preference for a single coordination mode. In this case, the energies of coordination on the (110) and (100) cuts are much closer and, in addition to bidentate coordination to a single Mg atom on the (110) cut, bridging coordination to Mg atoms on the same or adjacent (110) monolayers is possible. The ability of succinates to assume a number of different coordination modes on the (110) cut, adjacent to adsorbed $TiCl_4$, would be expected to lead to the formation of different active sites and is in line with the broad MWD of PP produced by catalysts containing a succinate as internal donor.

2.1.3 Ziegler Catalysts in Polyethylene

The development of Ziegler PE catalysts containing $MgCl_2$, along with the Union Carbide Corporation (UCC) gas-phase process, marked a step change in PE manufacturing [70]. As a result, Ziegler PE catalysts grew to become the most dominant family of catalysts for the manufacture of linear PE. As with the PP catalyst, $MgCl_2$ functions not only as a support material but also as a part of the active complex. These catalysts have shown very high activities and are also reported to give narrower molecular weight and chemical composition distributions, compared to $TiCl_3$-based catalysts. Three main groups of $MgCl_2$-supported catalysts have been described: (i) catalysts prepared by ball milling; (ii) those impregnated on silica carrier; and (iii) those prepared by precipitation.

2.1.3.1 Ideal Catalysts?

Before entering further discussions, it is important to note that there is no one ideal catalyst for the full range of PE densities and polymerization processes. The ideal catalyst for a particular product often depends on whose perspective (the PE manufacturer, the converter or the consumer) one takes, although the best product for the lowest cost is the common defining motive. A PE manufacturer for example may be interested in maximizing the throughput of the reactor, increasing the productivity to reduce catalyst cost, and reducing losses to flare or recycling. These considerations will depend heavily on the process technology employed [slurry continuous stirred-tank reactor (CSTR) or loop, gas-phase or cascaded combinations], often placing unique requirements on the catalyst for a particular product target. Polyethylene converters may be interested in the processability of a product (e.g., reduced energy consumption in extrusion) or increased throughput (an ability to increase line speed). A reduction in extractable components or catalyst residue may also be important for taste and odor, optical properties and end-use applications (e.g., wire and cable, food and medical applications or water pipes). Finally, the customer may want the ideal catalyst for a product property performance which could be, for example, high-strength films with high machine direction tear (MD tear) or dart impact strength, or pipe applications where high pressure ratings and environmental stress crack resistance are important. Finding common ground and addressing the needs throughout the full value chain from manufacturer to converter to customer is therefore needed to develop the ideal catalyst for a particular combination.

2.1.3.2 Ball-milled $MgCl_2$-based Ziegler Catalysts

Magnesium dichloride, as mentioned above, cannot be used as such as support material for the preparation of a Ziegler catalyst without some form of conditioning. The crystal structure must be changed from the α-$MgCl_2$ to the δ-$MgCl_2$ form, where the closely packed layered structure is strongly interrupted by stacking defects [71–78]. $TiCl_4$ or $TiCl_3$ are often co-milled with $MgCl_2$, melding together to form a solid solution. In general, higher productivities have been achieved with

high titanium loadings, but it has also been shown that the specific activity per g-Ti is higher, the lower the titanium loading. In this activation process the specific surface area of the catalyst increases from 1–2 to 100–200 g m^{-2}. Productivities have been reported to be around 10 kg PE g^{-1} catalyst per hour, and the optimum amount of Ti in these catalysts is believed to be around 3 wt.%, coordinating to the unsaturated 100 and 110 faces of $MgCl_2$. As a result of the variety of coordination possibilities for the active $TiCl_4$, the catalysts provide a rather broad MWD of between 4 and 6. Today, however, ball-milling of $MgCl_2$ is no longer commonplace.

2.1.3.3 $MgCl_2$-Titanium Catalysts on Silica

Silica-based catalysts have found wide use, especially in gas-phase processes where a controlled particle size and distribution is needed in order to keep the bed in position. The silica support acts as a carrier material, imparting morphology control to the catalyst. In theory, it is not considered as a part of the active center, but it offers a large pore volume and surface area. The silica is impregnated with the catalyst components, which can either be added together or in differing order. The resulting supported catalysts may consist of up to 50 wt.% of the catalyst component. The data in Table 2.2 illustrate how the order in which the reagents are added affects the catalyst productivity, along with the molecular weight and density of the resultant resins. Kelly and coworkers impregnated silica with butyl(ethyl)magnesium and then added four catalyst components. The order of addition was found to have a significant effect on productivity [79a].

A wide variety of catalysts can also be achieved by altering the physical properties of the silica support material (particle size and distribution, pore volume, surface area, etc.). In addition, the calcination conditions for the support can be altered, thereby altering the proportions of isolated and hydrogen-bonded hydroxyl or siloxane bridge groups. The activities of these catalysts depend to some degree on the amount of titanium that is chemically bound and the amount of "free" $TiCl_4$ (the more "free" titanium, the higher the activity). Typically, silica-based catalysts

Table 2.2 The effect of the order of chemical addition on a Ziegler catalyst.

Catalyst	*Addition order*				*Product (g)*	*MI (g 10 min^{-1})*	*Density (g cm^{-3})*
	1st	*2nd*	*3rd*	*4th*			
1	^{t}BuCl	THF	$TiCl_4$	TNOAl	14.8	0.79	0.928
2	^{t}BuCl	THF	TNOAl	$TiCl_4$	7.7	0.74	0.93
3	^{t}BuCl	TNOAl	THF	$TiCl_4$	22.5	1.07	0.927
4	^{t}BuCl	$TiCl_4$	THF	TNOAl	17.5	0.74	0.926
5	TNOAl	THF	^{t}BuCl	$TiCl_4$	9.1	0.63	0.931
6	TNOAl	^{t}BuCl	THF	$TiCl_4$	37.9	0.78	0.922
7	THF	TNOAl	^{t}BuCl	$TiCl_4$	12	0.69	0.929
8	THF	^{t}BuCl	$TiCl_4$	TNOAl	11.7	0.65	0.93
9	THF	^{t}BuCl	TNOAl	$TiCl_4$	8.4	0.93	0.933

possess improved chemical composition distributions (CCD) in ethylene copolymerization [79–94].

2.1.3.4 Precipitated and Supported $MgCl_2$-based Catalysts

Precipitated and $MgCl_2$-supported catalysts, along with silica-based catalysts, represent the majority of all Ziegler catalysts used in PE production. Precipitated Ziegler catalysts are prepared by first bringing into a dissolved state as many of the catalyst components as possible. $MgCl_2$ is then precipitated as an amorphous material, imparting high catalytic activity to the system. Usually, this is done by adding highly soluble magnesium and or aluminum alcoholates or alkyl to the reaction solution, and then precipitating the catalyst by the addition of a suitable chlorination agent. Titanium can be added either as a soluble complex or used as one of the chlorination agents. By using different "tricks" during precipitation, and by adding suitable donor compounds, particle size and particle size distribution can be directed to a certain extent. Supported systems are typically prepared via the titanation of a prepared support derived from magnesium dichloride and ethanol (emulsified or spray-dried).

A large number of investigations have been carried out to measure the number of active sites on these catalysts – that is, the mole fraction of the total amount of Ti that takes part in the polymerization. Values ranging from 0.1 to 100% have been reported, with between 1% and 4% being the most common result. This wide discrepancy in the results is not only due to differences in the chemical composition of the catalysts, but also depends on the method used in the measurement [95–114].

2.1.3.5 Spray-dried $MgCl_2$-Titanium Catalysts

Spray-drying techniques are commonly used to prepare $MgCl_2$-based Ziegler PE systems. In spray-drying, droplets containing a solution or slurry of the catalyst components are sprayed into a chamber under drying conditions to remove the solvent or slurry diluent, leaving behind a solid residue. The characteristics of the droplets formed can be used to tailor the particle size of the final catalyst. Structural reorganization of the particle can be influenced by volume and size changes. In addition, spray-drying conditions can be used to form substantially spheroidal catalyst particles (large or small) or aggregated particles, with a homogeneous composition or porosity. Typically, spray-drying techniques employ a "filler" component to aid control of the shape and composition of the catalyst. Common fillers are hydrophobic fumed silicas, which impart a relatively high viscosity to the slurry to be spray-dried and also improve the mechanical strength of the final catalyst. The filler may also generate increased porosity in the final catalyst [115–117].

2.1.3.6 General Polymerization Behavior of the $MgCl_2$-Titanium-based Ziegler Catalysts

The most common features of the Ziegler PE catalysts in homo and copolymerization conditions can be summarized as follows:

- Hydrogen decreases activity but is the most common reagent to adjust molecular weight. The effect on activity is opposite to what is seen in propylene polymerization.
- The amount of ethane gas produced increases with the amount of hydrogen added.
- Activity increases if a comonomer (α-olefin) is added.
- Molecular weight often drops when a comonomer is incorporated.
- Incorporation of the comonomer is better, the shorter is the chain length of the α-olefin, but density decreases with increasing α-olefin chain length.
- Donor addition (compounds that form complexes but do not react, such as R–O–R or R–CO–O–R) decreases activity, regardless of whether the donor is added during catalyst synthesis, during pre-contacting, or during polymerization.
- The molecular weight increases when donors are added, and the MWD becomes narrower.
- Comonomer incorporation typically increases if donors are added.
- Deactivation is seen predominantly in copolymerization, whereas homopolymerization can often be quite stable.
- The ability to incorporate a comonomer typically drops during polymerization, whilst at the same time molecular weight increases and the MWD becomes broader.
- The cocatalyst, AlR_3, activates the Ziegler catalyst, but can also have a deactivating effect, depending on the concentration of AlR_3 or the alkyl group.
- The molecular weight falls with increased amounts of AlR_3.
- Donor compounds, and support materials in general, decrease the effect of AlR_3.
- Comonomer incorporation and molecular weight increase when the cocatalyst is in chlorinated form (Al-R → Al-Cl).

When synthesizing LLDPE, there is first a harmonic drop in density with increasing comonomer content, until a density of approximately 920 kg m^{-3} has been reached, after which the density falls slowly. A similar situation occurs with regard to the melting point of the material; an initial harmonic drop in melting point down to about 120 °C with increasing comonomer incorporation, after which the melting point decreases at a substantially slower rate. In addition, the hexane-soluble fraction in the material, while not of concern at lower comonomer levels, typically starts to increase at the same tipping point as density and melting temperature. Above a critical point in comonomer content, there is a rapid drop in the consistency of the comonomer distribution. The highly soluble fraction at lower densities makes the material sticky and soluble, which limits its processability.

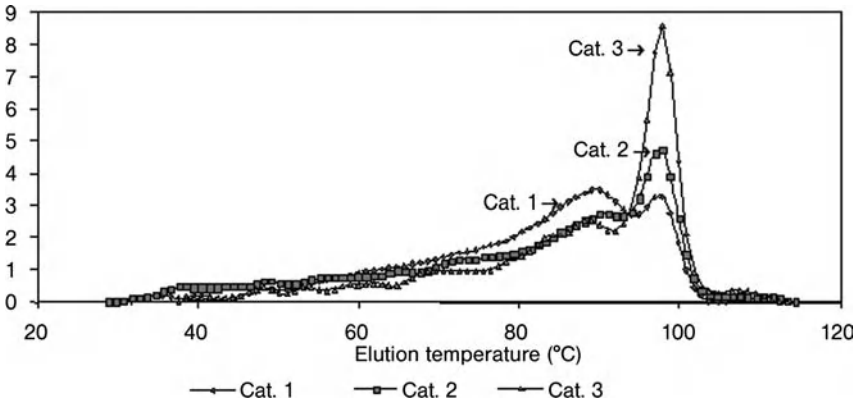

Figure 2.4 Temperature-rising elution fractionation (TREF) curves for polymer samples produced with three different catalyst systems under identical conditions.

This behavior of the Ziegler catalysts is the practical reason why typically there is a limit to the density of the PE produced in a particular process. The general belief is that most of the mechanical properties of PE are a function of MWD and CCD. To take full advantage of these materials, control over CCD and MWD is needed, and this one of the greatest challenges and areas of research in Ziegler PE industrial research and development.

A temperature-rising elution fractionation (TREF) curve of LLDPE illustrates the above traits (Figure 2.4). A sharp fraction of high-density polyethylene (HDPE) material can always be seen at higher elution temperatures, indicating the presence of a fraction with negligible comonomer content and having a high melting temperature. In approximate terms, the LLDPE material is dominated by 15- to 20-nm-thick backbone lamellae, containing little or no comonomer and representing the HDPE fraction. From these central lamellae there are branches of thinner lamellae containing the comonomer and representing the ideal copolymer. Together with the thick lamellae, these form the spherulites that have a diameter of 10 to 50 μm. In between the branches is the amorphous fraction containing an excess of comonomer. The branches can also be interconnected by tie-molecules that form bridges between the lamellae, thereby increasing the strength of the material [118–134].

2.1.3.7 Models for Chemical Composition Distribution and Comonomer Drift

Several models have been developed to describe the heterogeneous chemical composition distribution and the phenomenon of comonomer drift during Ziegler catalyzed copolymerization experiments.

The "multi-site, isolated-site and selective poisoning" model for Ziegler PE catalysts consists of three different types of active titanium, located in clusters or isolated sites. For clustered titanium the model proposes that these types of site are very comonomer sensitive, being able to produce even block copolymer [135, 136].

These sites are believed to produce low-molecular-weight and hydrocarbon-soluble material. At the other extreme are isolated titanium sites, with very low to no comonomer sensitivity, producing high-molecular-weight HDPE material. According to electron paramagnetic resonance (EPR) studies, about 20% of the sites would be in this state in a normal Ziegler PE catalyst [137, 138]. Several intermediate forms between the multi-site titanium and the isolated-site titanium could exist, producing copolymers having features between the extremes. Most important would be titanium species that form pairs, which are assumed to produce the ideal LLDPE material with an even CCD, and at the same time possess a high enough molecular weight capacity. The partition of titanium across different sites would explain the tendency of typical Ziegler PE catalysts to produce a broad MWD and CCD. The partitioning is further assumed to be mobile during polymerization. Electron donors could possibly either redistribute or "selectively" poison titanium species.

Changes in the Ziegler PE catalyst behavior with respect to polymerization time have been claimed to result from diffusion limitation [139–142]. This would be due to the high density of HDPE causing the formation of tight crystal packing, which may in turn influence the relative diffusion rates of the monomer, comonomer and hydrogen. This means that, when starting a polymerization, there is relatively little diffusion hindrance for the monomer and the hydrogen, but as the particle grows there is a gradually increasing diffusion limitation, which manifests as a gradual deactivation and a growing molecular weight, and a decrease in comonomer incorporation. Increased activity when adding comonomers can be explained by the diffusion model in that comonomer incorporation produces a less-crystalline material, thus facilitating diffusion of the monomer through the growing particle. This model could also explain why catalysts with a higher pore volume or surface area show a higher activity. Furthermore, an explanation as to why a lower activity is seen in the presence of hydrogen can also be provided. Hydrogen provides a lower molecular weight and therefore a higher crystallinity, which in turn creates a higher diffusion resistance. Finally, the model could be used to explain why there would be a change in behavior at a certain mol.% of comonomer, in that (co)monomer diffusion would occur most easily through areas in the polymer having high comonomer contents. Hence, whilst this model can explain both the drift in polymerization behavior and the change in such behavior at a certain mol.% of comonomer, it cannot explain the influence seen when using donors.

The oxidation state model is based on the drift in the oxidation state of titanium [93]. This model has been the prevailing discussion in Ziegler PE catalyst systems which, for LLDPE, tend to partition between two extremes of high and low comonomer incorporation during the course of a polymerization. The oxidation states in the catalyst have also been found to change with time (albeit in the absence of monomer). Consequently, the assumption drawn is first that titanium(IV) is comonomer-active and also hydrogen-sensitive, giving a relatively low-molecular-weight polymer with a high comonomer content. Second, titanium(III) is moderately comonomer-sensitive, giving a good CCD and a moderately high molecular weight. Finally, titanium(II) would be comonomer-insensitive and therefore

produce high-molecular-weight HDPE-type material. The difference in the polymerization behavior is proposed to explain the broad MWD and CCD seen when using typical Ziegler PE catalysts (Figures 2.5 and 2.6). The oxidation state distribution would also be subject to a continuous drift during polymerization, caused by the AlR_3. This would explain the decrease in activity, comonomer response and hydrogen response, and also the increase in MWD. The model has been used to improve the quality of LLDPE by manipulating the redox chemistry with nitrous oxide (:N–N=O) [143, 144], and by slowing down the reduction of Ti(III) to Ti(II) by the addition of donors or less-reducing cocatalyst components.

As noted from the discussion above, none of the existing models used to describe the behavior of a typical Ziegler–Natta PE catalyst is able to explain all of the typical polymerization features seen when using this type of catalyst. Additional factors such as the steric environment around the metal center and the coordination

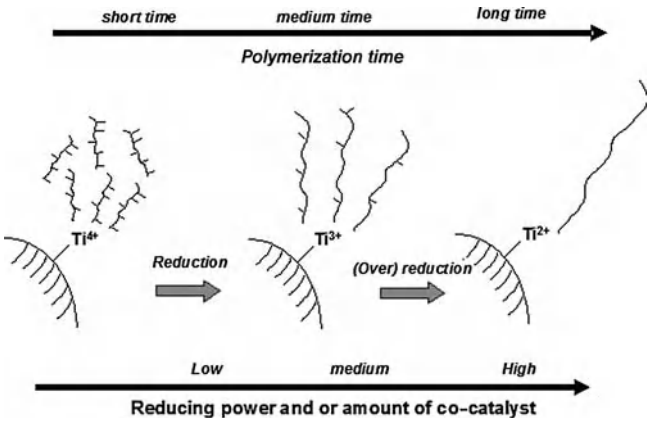

Figure 2.5 Titanium oxidation state drift, and its effect on comonomer response.

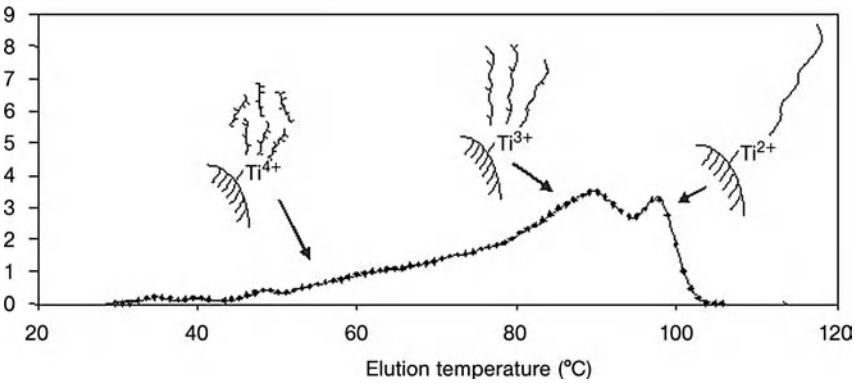

Figure 2.6 Temperature-rising elution fractionation (TREF) curve illustrating the types of polymers, proposed to be produced at active sites with differing titanium oxidation states.

number, along with the cumulative effect on the electronic properties (orbitals), can also be considered. Hence, a considerable amount of knowledge is required to fully describe these catalysts. As stated earlier, the development of a fundamental understanding of the catalyst, and more importantly the ability to direct the Ziegler PE catalyst behavior at higher comonomer contents, whilst retaining a more homogeneous CCD with the MWD and solubles contents held under control, represents the core challenge in the research and development of these catalysts.

2.1.3.8 **Vanadium-based Ziegler Catalysts**

Vanadium catalysts have also been classified as belonging to the Ziegler–Natta catalyst family. $(AcAc)_2VCl$, $OV(OEt)_3$, VCl_3, VCl_4 or Cl_3VO with or without SiO_2 or $MgCl_2$ carrier, and with and without –ClCF- promoters, have been used in this respect [145–149]. Cl_2VR, where vanadium is in the oxidation state of (III), is believed to be the active species in polymerization, and between 2 and 6 mol.% of the V is stated to be in the active, polymerizing form. Vanadium catalysts are reported to give a narrow MWD (2–3) and CCD in LLDPE polymerization. The vanadium-based catalysts are reported to rapidly deactivate (after 2–4 min, only 10% of activity remains), and to be very sensitive to hydrogen, losing most of their activity if even minute amounts of hydrogen are added. The rapid deactivation is believed to originate from a fast reduction of V(VI) and V(III) to V(II), and is probably why "weak" cocatalysts such as diethylaluminum chloride (DEAC) or triisobutylaluminum (TIBA) are recommended. Because of this rapid deactivation, these vanadium catalysts have found most use in solution processes (DOW, DSM and Mitsui) where ethylene/propylene (EP) elastomers are produced. Densities of 900 kg m^{-3} and less can be achieved using propene and/or 1-octene as comonomer, giving a very strong film material.

2.1.4 **Concluding Remarks**

Despite the advances in single-site-catalyzed polymerization that have been made during the past 20 years, the proportion of PE, and in particular PP, manufactured by single-site technology is still low compared to Ziegler–Natta-catalyzed polyolefins. The success of Ziegler–Natta catalysts for PP and PE production is the result of continual advances and improvements in catalyst composition and performance, leading to efficient polyolefin manufacturing processes and to an ever-increasing control over polymer structure and properties. As indicated above, different catalysts are required for different applications and, with the development and application of new types of electron donor or synthetic preparations, it is now possible to produce polymers ranging from narrow to broad molecular weight distributions. Nevertheless, single-site catalysts such as metallocenes can provide important advantages for certain applications. Ziegler–Natta and single-site catalysts should therefore be regarded as complementary rather than competitive systems, which together provide the basis for an expanding range of polymers with closely controlled molecular structures.

2.2
Chromium Polymerization Catalysts: Still Alive in Polyethylene Production

Hilkka Knuuttila and Arja Lehtinen

2.2.1
Introduction

During the early 1950s, at about the time when K. Ziegler first published the details of his transition metal catalyst (the Ti tetrachloride–triethylaluminum catalyst for ethylene polymerization), P. Hogan and R. Banks, who conducted research at Phillips Petroleum Company, discovered that inorganic chromium salts were able to polymerize olefins [152, 153]. Soon afterwards, Phillips developed the slurry loop process to utilize the catalyst, while 10 years later during the early 1960s Union Carbide adapted chromium catalysts for their fluidized-bed gas-phase process. Chromium-based Phillips catalysts (inorganic chromium supported on silica) have now been used industrially for 50 years, and have reserved their position in high-density polyethylene (HDPE) production, still accounting for approximately one-third of current global HDPE production. Today, however, strong competition has led to revolutionary improvements in polyethylene catalysts and process technologies, resulting in technically more sophisticated polyethylene resins. In particular, structurally tailored bimodal Ziegler–Natta polyethylene is increasingly replacing Cr HDPE in more demanding applications such as pipe and blow molding, and is already regarded as a property standard in film applications.

A traditional Phillips catalyst is based on chromium(VI) oxide, usually supported on silica or aluminosilicate. The raw catalyst is often referred to as a "precursor" as it is not active in polymerization before being undergoing further treatments such as activation by heat (calcination). Unlike Ziegler–Natta and single-site catalysts, a traditional chromium catalyst does not require a cocatalyst to be active in polymerization. In general, the behavior of CrO_x/SiO_2 catalysts in ethylene polymerization is quite different from that observed for Ziegler–Natta and single-site catalysts.

Even after so many years in commercial use, chromium catalysts remain a somewhat mysterious subject in both academic and industrial research. The precise nature of the active site at the molecular level is still debated today; neither is the polymerization mechanism fully understood, even though new spectroscopic techniques have been adapted to clarify the molecular structure and environment of the active chromium site [154–156].

2.2.2
The Chromium Catalyst System

Supported chromium catalysts can be classified in two main families: (i) those based on chromium oxide (Phillips type); and (ii) those using organochromium compounds. A possible third family may be considered if organosilylchromate

catalysts are considered as a group in their own right. All of these catalyst types can vary widely in composition, and are produced commercially by companies such as Basell, Grace Davison, Ineos Silicas, PQ Corporation, and Univation technologies.

The CrO_x/silica catalyst is typically prepared by impregnating an aqueous solution of a chromium(III) compound (e.g., acetate, acetyl acetonate), earlier also CrO_3, onto a porous support material with high surface area and large pore volume, usually amorphous silica. A typical catalyst loading is less than 1 wt.% Cr on the silica surface [157, 158]. Drying and calcination at temperatures of 500 to 900 °C are then followed by treatment in dry air or oxygen to activate the catalyst [159]. In the activation step, the Cr(III) compounds are oxidized to Cr(VI) compounds. Chromium(VI) itself is not active in polymerization reaction, and must be further activated by reduction to lower oxidation states, most probably to Cr(II). This occurs in the polymerization reactor when the activated catalyst comes in contact with the ethylene monomer. Typically, this route is applied for the industrial use of Phillips-type chromium catalysts.

The polymerization performance of a supported chromium catalyst is extremely sensitive towards its preparation method and the properties of the support material used. Therefore, numerous variations exist of the basic chromium catalyst in which either the chromium compound or its support is chemically modified before or during the catalyst preparation. This in turn provides the tools to tailor a material's properties suitable for different applications, for example molecular weight distribution (MWD). In this way, the polymer's properties may be influenced by changing the chemical surroundings and electron deficiency of the chromium atom, for example by using titanium, aluminum or fluorine compounds [160–162].

The bis-triphenylsilyl chromate catalyst (earlier known as S2 catalyst by Union Carbide) has been used successfully in the commercial production of HDPE resins for film and pipe applications, due mainly to its ability to polymerize material with broad MWD [163]. Typically, this catalyst is prepared by supporting the silyl chromate compound onto a precalcined silica carrier following the pre-reduction of chromium(VI) to chromium(III) by an aluminum alkyl compound such as diethyl aluminum ethoxide. Recently, a new synthesis route was presented for the conversion of a chromium oxide catalyst to the silyl chromate catalyst by introducing a silyl ligand from a corresponding silanol compound and performing synthesis on the chromate surface [164, 165].

The silica-supported chromocene catalyst developed by Union Carbide has not been generally accepted for industrial use due to material processing difficulties and issues about catalyst stability. In this catalyst, chromocene (Cp_2Cr, where $Cp = \eta^5\text{-}C_5H_5$, cyclopentadienyl) is attached onto the partially dehydroxylated silica surface. During supporting, one of the cyclopentadienyl ligands is released while the other remains bound to the chromium. The characteristics of a chromocene catalyst differ from those of other supported chromium catalysts, and include a relatively narrow MWD, high selectivity between ethylene and α-olefins (no copolymerization), and a good hydrogen response for molecular weight control [166].

Supported chromium-based catalysts are typically used in particle-forming polymerization processes, such as a slurry process in which dissolved ethylene is polymerized to form solid polymer particles suspended in a hydrocarbon diluent, and a gas-phase process where ethylene is polymerized to a solid polymer in a fluidized bed of polymer particles [167].

2.2.2.1 Activation of the Chromium Catalyst

When a chromium compound is deposited onto a fully hydrated porous silica support with silanol groups, the supported catalyst is calcined at high temperature in air or oxygen in order to activate it [154]. The catalyst may also be activated and reduced to lower oxidation states in catalyst preparation step by utilizing carbon monoxide or metal alkyl compounds as reducing agents [154, 159].

The surface of hydrated silica is heterogeneous due to the presence of different types of hydroxyl groups (isolated, geminal and vicinal), which play an important role in adsorption and chemical reactions. In the preactivation phase, dehydroxylation occurs by the first physisorbed H_2O being removed, followed by different silanol groups, depending on the calcination temperature. Examples of these reactions are shown in the schematic thermogravimetric curve of a chromium oxide catalyst (Figure 2.7). The removal of isolated silanol groups requires very high calcination temperatures [168], with chromium(III) being oxidized to chromium(VI) during the calcination step. The monodispersed surface monochromate or dichromate ester species are formed at 150 to 350 °C and anchored onto the silica surface (Figure 2.8), where at least the monochromate species serve as an active site. The catalyst activity is heavily dependent upon the activation temperature used for the catalyst preparation [159]. In general, only part (0–1%) of the chromium loading is active in polymerization, and probably not in excess of 10% [169–171].

At higher calcination temperatures (usually at ca. 900 °C) the amorphous silica begins to sinter and the pore structure starts to collapse. As a consequence, it loses

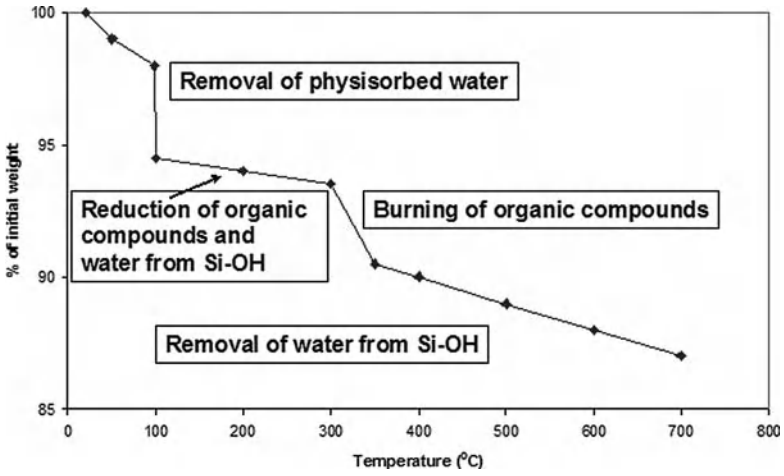

Figure 2.7 A schematic presentation of the thermogravimetric analysis of a CrO_x/SiO_2 catalyst.

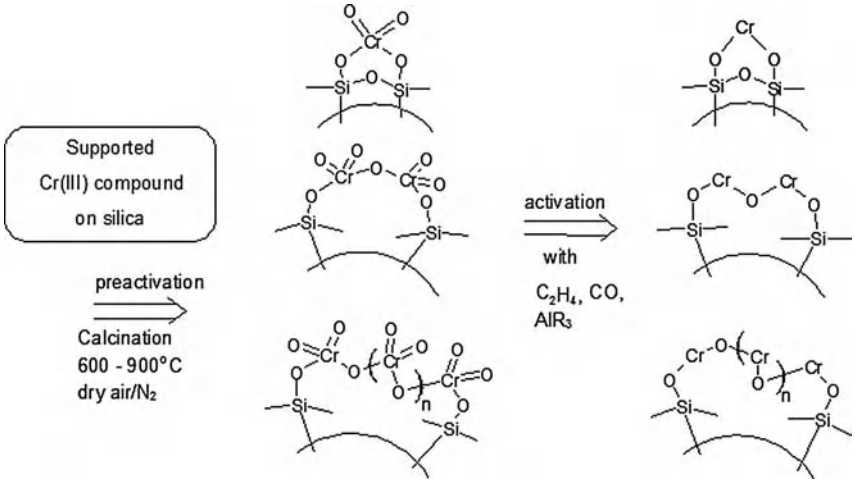

Figure 2.8 Anchoring and reduction reactions of chromate on silica surface.

its high surface area as the small pores begin to fuse together to form larger pores. It is a well-known phenomenon that alkali metals promote the sintering of silica while enhancing the formation and breakage of Si–O–Si bonds [172]. For example, it appears that sodium induces a much more drastic effect on sintering on the surface area than on the pore volume. Compared to sodium-induced sintering, normal sintering only slightly reduces the average pore radius [173]; therefore, in the specifications of commercial silica carriers the Na content must be held within confined limits.

Recently, further studies on the activation of CrO_x/SiO_2 catalysts by metal alkyls have begun to attract interest from a number of research groups. Metal alkyls, besides boron alkyls (triethylboron, TEB), are not widely used as cocatalysts in commercial processes. The introduction of a metal alkyl cocatalyst influences the active site formation, polymerization kinetics and structure of polymer chains. A metal alkyl may be introduced to the chromium catalyst system in: (i) the catalyst preparation phase; (ii) during catalyst aging or the pretreatment stage in a polymerization reactor, just before monomer feeding; or (iii) at the polymerization stage, with simultaneous interaction of the catalyst with a metal alkyl cocatalyst and monomer. According to the studies of Blom et al., the stage at which the metal alkyl is introduced to the system has a crucial effect on polymerization behaviour and polymer properties [174, 175].

Terano et al. have performed kinetic studies on the simultaneous interaction of catalyst with an Al-alkyl cocatalyst and monomer. The cocatalysts triethyl aluminum (TEA) and diethyl aluminum ethoxide (DEAE) each provided different polymerization kinetics. CrO_x/SiO_2(600 °C)/TEA was responsible for two types of basic polymerization kinetics: (i) rapid formation–rapid decay; and (ii) slow formation–slow decay. In the case of CrO_x/SiO_2(600 °C)/DEAE, the kinetics was of the single type [176]. Because aluminum alkyls are strong reducing agents, they may be used

during the catalyst preparation phase to pre-reduce Cr(VI) chromate to a lower oxidation state. Most likely, at the same time the metal alkyl is able to alkylate the chromium center [177, 178], as no induction time can be found and the polymerization rate is increased.

The reduction of CrO_x/SiO_2-Al_2O_3 catalysts with alkoxides (e.g., diethylaluminum ethoxide) and other reducing agents results in more productive, hydrogen-sensitive, polymerization catalysts which allow the use of hydrogen to control the molecular weight of the polyethylene. Such use of hydrogen appears also to have an effect on the chain-transfer reaction and the ratio of unsaturated to saturated end groups (this is changed from 1 : 1 to 3 : 2) [179]. With a conventional Phillips-type chromium catalysts, the termination reaction occurs by β-hydrogen elimination to produce an unsaturated double bond at the end of the polymer chain. The ratio of the $–CH=CH_2$ and $–CH_3$ end groups is then 1 : 1.

2.2.3 Polymerization Mechanism

During recent years the exact mechanisms for initiation, propagation and chain transfer have been widely debated, and in particular the initiation reaction has remained an open question for decades. Despite intensive research and the use of the latest spectroscopic methods and catalyst modeling to clarify the structural features of the precursor of the Cr active site, the polymerization mechanism of CrO_x/SiO_2 catalyst is still not fully understood [156].

A chromium oxide catalyst may not be immediately active for ethylene polymerization following its exposure to ethylene in the reactor, and the induction period (i.e., when there is no detectable activity) ranges typically between 10 and 60 minutes, or even longer, before the polymerization starts [154]. When the ethylene in the reactor reduces Cr(VI) to Cr(II) to initiate the polymerization, formaldehyde or acetaldehyde is formed simultaneously in a redox reaction. Formaldehyde (and acetaldehyde) is able to coordinate strongly to Cr(II). However, the reduction reaction of surface chromate is not the sole contributor to the induction period of the CrO_x/SiO_2 catalysts. Another contribution is made by ethylene metathesis through the formation of a chromium–carbene species. The gradual desorption of residual formaldehyde from the surface Cr(II) species is considered to cause an accelerating-type polymerization, with metathesis-active sites transforming to polymerization-active sites. The coexistence of metathesis sites with polymerization sites may be indicated by the *in-situ* formation of short olefin comonomers during ethylene homopolymerization with calcined chromium oxide catalysts. The existence of a metathesis initiation during the induction period was first proposed by Terano et al. [180, 181], and the first evidence of chromium–carbene complex formation was later obtained during the induction period using X-ray photoelectron spectroscopy (XPS) [182]. More recently, spectroscopic studies performed by Groppo and colleagues also shed some light on the polymerization mechanism and the initiation reaction. By using *in-situ* Fourier transform infra-red (FTIR) measurements, this group identified the first spectroscopic evidence of the creation of a metalla-

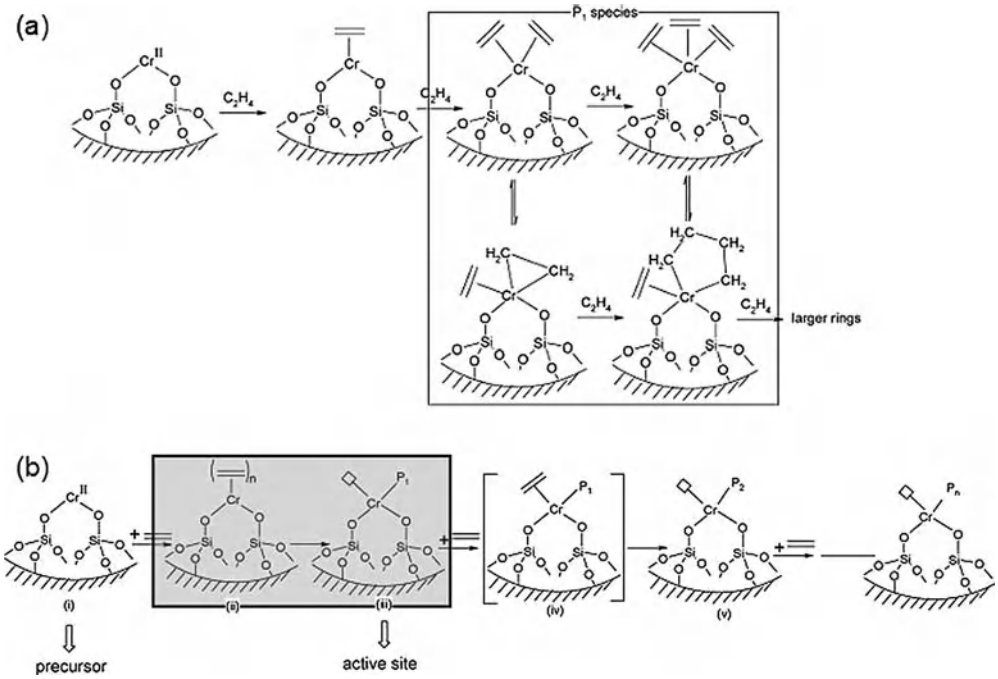

Figure 2.9 A schematic presentation of the initiation mechanism of a CrO_x/SiO_2 catalyst in ethylene polymerization. (a) The metallacyclo mechanism; (b) the mechanism according to a Ziegler–Natta-like behavior. (Reproduced with permission from Ref. [183]; © 2006, Elsevier.)

cycle intermediate species during ethylene polymerization on the $Cr(II)/SiO_2$ catalyst. This finding was considered to be key evidence that the initiation mechanism followed a metallacycle route, which was also found to occur for several ethylene trimerization and tetramerization catalysts [183]. The mechanism of metallacycle formation is shown in Figure 2.9. Previously, the $Cr(II)\cdots(C_2H_4)_n$ π-bonded complex had been identified by these authors [184].

Following the induction period, the polymerization rate with chromium oxide catalysts begins to increase with time until eventually it levels off. This time-related increase in polymerization rate suggests that the concentration of active catalytic species is not constant but rather increases with time, as proposed by the new reaction mechanism studies. The polymer chain length is determined by the rate of chain growth relative to chain transfer, with both reactions being highly sensitive to the surroundings of the active Cr center. Catalyst activity is heavily dependent on the activation temperature used in catalyst preparation, and the existence of different types of Cr active centers with different chain-termination rates has been proposed [159]. The chain-transfer rate is not only very sensitive to polymerization temperature [159], but is also accelerated by modifying agents such as Ti and F. The growth of the polymer chain is terminated by the β-hydrogen elimina-

tion reaction, which produces a vinyl group at one chain end and a methyl group at the other (Scheme 2.1).

Most likely, due to the diversity of active sites and time-varying polymerization rate, the supported chromium oxide catalysts typically produce a broader MWD than either Ziegler–Natta (M_w/M_n ~ 3–6) or metallocene catalysts (M_w/M_n ~ 2–3) (Figure 2.10).

During the polymerization reaction, CrO_x/SiO_2 catalysts are very sensitive to all polar compounds, such as oxygen, water, methanol, carbon monoxide, and acetylene. These compounds are able to act as strong catalyst poisons, coordinating to the active center and influencing the initiation reaction by extending the induction time rather than affecting the polymerization itself [186]. Due to the induction

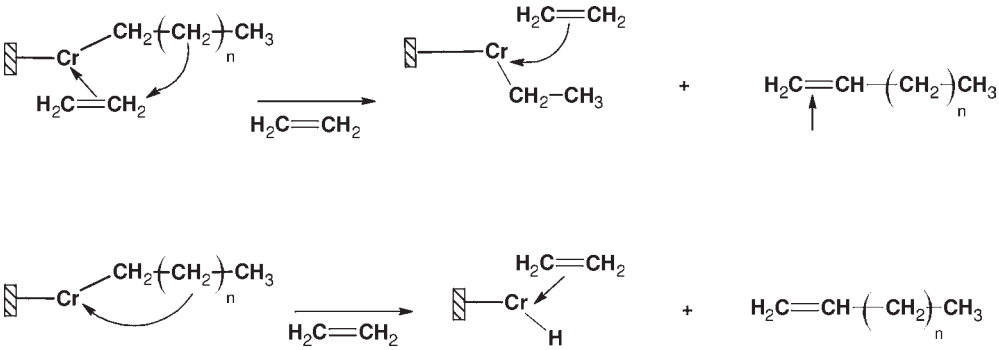

Scheme 2.1 Termination reactions of a CrO_x/SiO_2 catalyst.

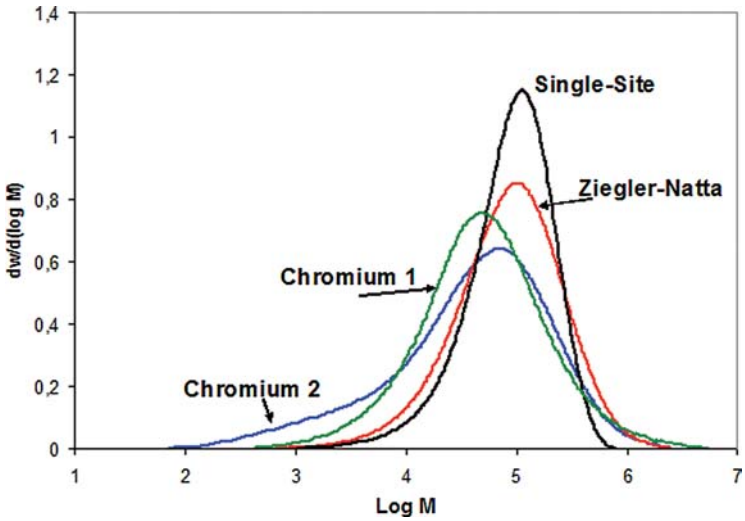

Figure 2.10 The influence of catalyst on the molecular weight distribution of unimodal polyethylene (PE) film material. Chromium 1 = high-density polyethylene (HDPE) film; Chromium 2 = linear low-density polyethylene (LLDPE).

period and reasonably short residence times used in continuous-slurry polymerizations, chromium catalysts may often leave the slurry loop reactor before reaching maximum activity. The average residence time in a gas-phase reactor is longer, from 3 to 6 hours [167]. The induction period can be reduced, for example by using carbon monoxide (CO) in the activation step [187], or by using a metal alkyl such as triethylaluminum (TEA) as a poison scavenger in the polymerization reactor. The use of poison scavengers also increases catalyst activity.

2.2.4 Chromium Catalyst Performance

2.2.4.1 The Effect of Carrier Material and Calcination Temperature

The carrier material plays a major role in chromium catalyst chemistry. In addition to being an inert carrier, the support material increases the effective surface area of the catalyst, stabilizes the valency of the transition metal centers, participates in catalyst site formation by chemically anchoring the chromium compound to the surface, isolates the chromium sites thereby preventing their destruction by mutual interaction, and also provides a template for polymer particle growth [188]. The most common support in commercial catalysts is silica, although porous silica-alumina (aluminosilicate), silica-titania, and aluminum phosphate may also be used as support material for a chromium catalyst.

As the type of carrier used (based on chemistry, total pore volume, average pore size, surface area) and its heat history influence the performance of a chromium oxide catalyst, its activity and what type of polymer it produces, the commercial chromium oxide catalysts may be divided in five groups: low pore volume; medium pore volume; high pore volume; aluminum-phosphated; and fluorided. These different catalyst versions behave differently in polymerization and provide different polymer properties. Therefore, by correctly choosing the catalyst type and activation profile, the polymer properties can be tailored for different end-use applications. For example, Cr/aluminophosphate catalysts produce polymers having a broader MWD than is obtained using a plain silica carrier [189]. However, if a narrower MWD but a still high molecular weight is needed, then a fluorinated Cr catalyst may be used. If a lowering of the molecular weight is desirable, then the catalyst should be supported on silica-titania [160].

Silica (silica gel) used as a carrier for chromium-based polymerization catalysts is a synthetic amorphous and porous material having a high pore volume (typically 1.0–2.5 $mL\,g^{-1}$ SiO_2) and a high surface area (typically 200–600 $m^2\,g^{-1}$ SiO_2). The size, shape, porosity and fragility of the silica also plays an important role in regulating the shape and morphology of the polymer particles in the particle-forming polymerization processes. In order to avoid problems in polymerization processes (e.g., fines, poor polymer flowability), an ideal silica support might be spherical and have a large surface area, good porosity and sufficient mechanical strength as the growing polymer particles replicate the shape of the catalyst particles. On the other hand, the silica particles should be fragile enough to fragment during polymerization, or otherwise the catalyst would have little or no activity. The catalyst

activity increases with increasing total pore volume. An odd feature noticed in practice is that even the molar mass of the polymer seems to depend on the pore radius. The use of a support material with larger pores leads to polyethylene with a lower molecular weight [154, 190]. The activity of the catalyst is also very sensitive to the temperature at which it was calcined, as increasing the calcination temperature also increases the activity. Surface hydroxyls are thought to interfere with the polymerization reaction by coordinating to active chromium centers. Dehydroxylation occurs during the calcination step, and a higher activation temperature leads to a more effective decrease in the surface hydroxyl population [159, 185]. However, the calcination temperature used affects not only the activity of the catalyst but also the polymer properties, such as the average molecular weight (melt flow rate) of the polymer, the higher calcination temperature resulting in a lower molecular weight (higher melt flow rate) [154, 159].

The data in Figure 2.11 show how the activation temperature influences not only the catalyst activity but also the molecular weight and MWD of the polymer produced [191].

2.2.4.2 **Effect of Polymerization Temperature**

The way in which the main variables of the chromium oxide catalyst, and also its activation and polymerization conditions, affect catalyst activity and the molecular weight and MWD of the polymer product are summarized in Table 2.3. Catalyst activity usually increases with increasing polymerization temperature; hence, present-day slurry loop reactors are operated over a temperature range of 80 to 110 °C, while reaction temperatures of 70 to 100 °C are common in gas-phase processes [167].

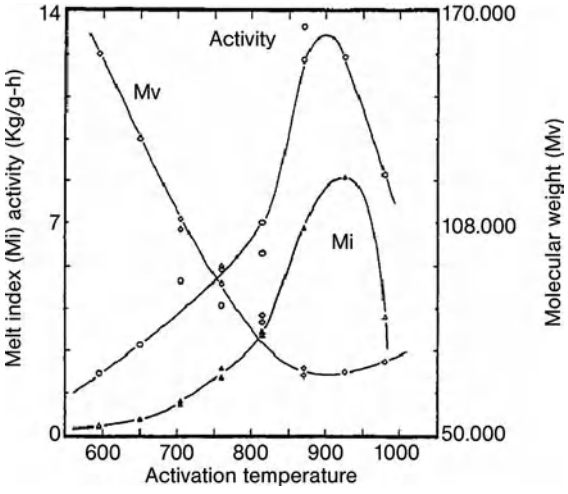

Figure 2.11 Performance of chromium-based catalysts as a function of the calcination temperature. (Reproduced with permission from Ref. [191]; © 1988, American Chemical Society.)

Table 2.3 Summary of the catalyst and process variables influencing catalyst performance.

Variable	*Responses*		
Catalyst	***Mw***	***MWD***	***Activity***
Chromium content ↑	0	0	+++ ↑
Pore volume ↑	++ ↓	+ ↓	+++ ↑
Added Ti ↑	++ ↓	+ ↑	+ ↑
Added Al ↑	+ ↑	+ ↑	
Added F ↑	+ ↑	++ ↓	0
Catalyst particle size ↑	0	0	+++ ↓
Activation			
Temperature ↑	++++ ↓	++ ↓	+++ ↑
Reduction vs. no reduction	+++ ↑	+ ↓	+++ ↑
Reactor conditions			
Temperature ↑	++ ↓	+ ↓	+++ ↑
C_2 = concentration ↑	++ ↑	+ ↑	+++ ↑
Co-monomer ($C_4^=$, $C_6^=$)	+++ ↓	++ ↓	++ ↑
Co-catalyt, TEB	++ ↓	++ ↑	+ (++) ↑
Scavenger, TEA	0	0	++ ↑
Hydrogen	+ ↓	+ ↓	+ ↓
Poisons O_2, CO, H_2O	++ ↓	+ ↑	+++ ↓

+ some effect; ++++ high effect; 0 no or neglectable effect.↑ increase; ↓ decrease.

Recently, Niemantsverdriet et al. have used silicon wafer (Si(100)) as a support to synthesize the model Phillips catalyst [192, 193]. The active component was impregnated onto the model support, which may be further calcined or treated in the correct manner. This model was used to study the effect of polymerization temperature on the performance of $CrO_x/SiO_2/Si(100)$. By combining the activity with the molecular weight data, a huge increase in activity could be confirmed with increasing polymerization temperature, although a visible decrease in molecular weight could not be identified for polymerization temperatures below 100 °C. Above 100 °C, however, the decrease in molecular weight was obvious. Flat model catalysts are also well suited also for surface spectroscopic studies.

2.2.4.3 Effect of Hydrogen/Hydrogen Sensitivity

Phillips-type chromium oxide catalysts show very little sensitivity to hydrogen, and behave quite differently compared to the Ziegler–Natta and metallocene catalysts, which are considered to be hydrogen-sensitive. That is, the hydrogen acts as a chain-transfer agent, terminating the growth of the polymer chain and yielding an saturated polymer [171]. Thus, as the hydrogen response of chromium oxide catalysts is poor, hydrogen has only a minor effect on the melt flow rate (molecular weight) of the polymer, even if it tends to narrow the MWD. Instead of hydrogen, the molecular weight of the polymer is usually controlled by the polymerization temperature [154, 189]. However, some members of the chromium-based polym-

erization catalyst family are more sensitive to hydrogen than is conventional chromium oxide on silica. One well-known hydrogen-sensitive catalyst is chromocene on silica, which has an even greater hydrogen response than the Ziegler–Natta catalysts and produces highly saturated material [166].

$$-Cr-CH_2-(CH_2)_n-CH_3 \rightarrow -Cr-H + CH_3-(CH_2)_n-CH_3$$

Both, CrO_3 alone and organochromium compounds on an aluminum phosphate carrier, are reported to be hydrogen-sensitive [189]. Although the chain-transfer reaction occurs by hydrogenation, the termination by β-elimination is favorable and therefore polyethylene with a high vinyl group content is produced.

Metal alkyls may also sometimes terminate polymer chains through alkyl exchange; aluminum, zinc and boron alkyls have each been reported to do this for some chromium catalysts [189, 194–196].

2.2.5 Summary

Over the years that chromium oxide catalysts have been in use, our understanding of the physico-chemical nature of the surface Cr species during preactivation and monomer activation processes has increased continuously. The result has been an improved catalyst preparation, a more controlled polymerization, and a continuous quest for new types of chromium catalyst, such as Cr single-site catalysts, non-Cr Phillips catalysts, and mixed catalysts [182].

The structural features and properties of a polymer are mainly defined by the catalyst and process used in its production (Figure 2.12). Polyethylene resins pro-

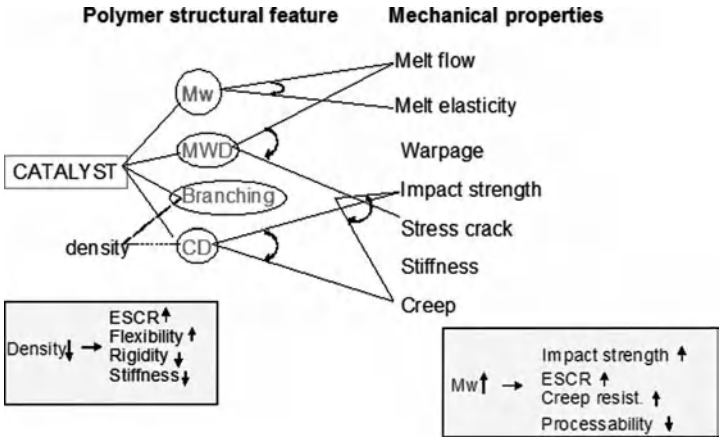

Figure 2.12 Structure–property relationship indicating the connection between polymer and catalyst. (Modified from the figure in Ref. [191].)

duced with chromium catalysts typically have a high molecular weight and form a broad to very broad MWD (see Figure 2.11). They often also contain very low levels of long-chain branching (LCB) whereas, through the incorporation of *in-situ*-formed short α-olefin comonomers, small amounts of short-chain branching may also be found in homopolymers [154]. The low- and high-molecular-weight tails associated with Cr polyethylene resins affect the processing and mechanical properties of the products made from them. Excessive amounts of low-molecular-weight material can decrease a material's environmental stress crack resistance (ESCR) and, in the worst case, migrate out of the material. Large amounts of very high-molecular-weight material can result in gel formation, processing difficulties, and warpage on cooling. Long-chain branching has a major effect on polymer flow behavior (rheology), and in some applications may be detrimental for the mechanical properties. Long-chain branching causes orientation in film and in blow-molding, decreases die swell and ESCR, but causes an increase in melt strength. Therefore, when basic chromium catalysts are modified, the ability to control LCB formation is of equal benefit to control over the polymer molecular weight and MWD.

Due to its high molecular weight and broad MWD, chromium-catalyzed high-density polyethylene is used in applications where good processability and certain mechanical strength is needed (e.g., blow-molding, films, pipes). For example, the typical performance criteria for HDPE films are stiffness, tensile strength, puncture resistance, tear strength and barrier properties. Improvements in all these properties, and a resultant reduction in film thickness, has led to the tailoring of MWD and especially comonomer/short-chain branching incorporation. This has been made possible in both bimodal and multimodal processes with Ziegler–Natta catalysts, and has resulted in an increasing replacement of Cr HDPE with bimodal Ziegler–Natta HDPE for different film applications. In high-molecular-weight (HMW) blow-molding, such as the production of drums and gasoline tanks, chromium materials have been better able to defend their position [197].

Linear low-density polyethylene (LLDPE) resins are also important materials in blown and cast film production. During the 1990s, Phillips Petroleum developed a range of chromium catalyst low-density linear polyethylene (LDLPE) grades, to compete first with conventional unimodal LLDPE produced with Ziegler–Natta catalysts and later with metallocene-catalyzed LLDPE. LDLPE has a much broader MWD and a lower melt flow rate (MFR) than the corresponding conventional Ziegler–Natta and metallocene materials, and contains a low level of LCB. Although LDLPE has good processability in film blowing, the film obtained is very hazy and has in general worse impact and tear properties than films produced from the other LLDPEs with a narrower MWD. Since their development, the LDLPE-type polymers have not gained any large market share, and seem – like Cr HDPE – to have lost in competition to bimodal Ziegler–Natta materials [198, 199].

In pipe applications, the move from PE80- to PE100-type materials has been in progress in Europe for more than 10 years, with the United States following far behind. A PE100 pipe classification means that the pipe must withstand hoop stress of 10 MPa for up to 50 years at 20 °C. Until now, the PE100 requirements

have been fulfilled only by the bimodal Ziegler–Natta polyethylenes [200, 201]. In order to solve this problem, the research team at Chevron Phillips, using modified chromium oxide catalysts and a Phillips slurry loop process, recently developed a multimodal high-density polyethylene, produced in a single reactor where the catalyst is supported on a modified aluminum phosphate carrier. The new PE100 pipe resin has an exceptionally high molecular weight and a broad MWD, a high degree of SCB in very long chains, and a reduced amount of LCB when compared to resins made using chromium catalysts on conventional supports. The new resin is said to exhibit greater toughness and resistance to sagging during pipe extrusion than the conventional bimodal pipe resins [202, 203].

As mentioned above, chromium catalyst technology has enjoyed a strong position in unimodal HDPE production for over 50 years, and competition, both with new catalysts that allow a better control of the polymer microstructure and with multireactor processes, will be difficult to overcome. However, the future will show whether polyethylene produced in a single reactor with novel chromium catalysts can compete with bimodal/multimodal Ziegler–Natta or single-site materials. Or, in other words, whether the new multimodal chromium polyethylene will become a commercial success and be accepted by pipe producers and further developed for film and molding applications in order to gain large market volumes.

References

1 L.L. Böhm, *Angew. Chem. Int. Ed.* 2003, *42*, 5010–5030.

2 E. Albizzati, G. Cecchin, J.C. Chadwick, G. Collina, U. Giannini, G. Morini, L. Noristi, in: N. Pasquini (Ed.), *Polypropylene Handbook*, 2nd edn., Hanser Publishers, Munich, 2005, pp. 15–106.

3 N. Kashiwa, *J. Polym. Sci.: Part A: Polym. Chem.* 2004, *42*, 1–8.

4 (a)W. Kuran, in: *Principles of Coordination Polymerisation*, John Wiley & Sons Ltd., 2001, pp. 43–243; (b) A. Peacock, in *Handbook of Polyethylene: Structures, Properties, and Applications*, Marcel Dekker, New York, 2000.

5 B.A. Krentsel, Y.V. Kissin, V.J. Kleiner, L.L. Stotskaya, *Polymers and Copolymers of Higher α-Olefins*, Carl Hanser Verlag, Munich, Vienna, New York, 1997.

6 H. Martin, Patent right aspects in connection with four decades of Ziegler catalysts, in: G. Fink, R. Mülhaupt, H.H. Brintzinger (Eds.), *Ziegler Catalysis*, Springer-Verlag, Berlin, Heidelberg, 1995, p. 15.

7 J. Boor, *Ziegler-Natta Catalysts and Polymerizations*, Academic Press, New York, 1979.

8 J.P. Hermans, P. Henrioulle, U.S. Patent 4,210,738, 1972.

9 B.L. Goodall, in: S. van der Ven (Ed.), *Polypropylene and other Polyolefins. Polymerization and Characterization*, Elsevier, Amsterdam, 1990, pp. 1–133.

10 A. Bernard, P. Fiasse, in: T. Keii, K. Soga (Eds.), *Catalytic Olefin Polymerization*, Elsevier, Amsterdam, 1990, pp. 405–423.

11 J.H. Kim, Y.T. Jeong, S.I. Woo, *J. Polym. Sci., Polym. Chem.* 1994, *32*, 2979–2987.

12 U. Giannini, *Makromol. Chem., Suppl.* 1981, *5*, 216–229.

13 P. Galli, L. Luciani, G. Cecchin, *Angew. Makromol. Chem.* 1981, *94*, 63–89.

14 P.C. Barbè, G. Cecchin, L. Noristi, *Adv. Polym. Sci.* 1987, *81*, 1–81.

15 P. Galli, P.C. Barbè, G.P. Guidetti, R. Zannetti, A. Martorana, A. Marigo, M. Bergozza, A. Fichera, *Eur. Polym. J.* 1983, *19*, 19–24.

16 R. Gerbasi, A. Marigo, A. Martorana, R. Zannetti, G.P. Guidetti, G. Baruzzi, *Eur. Polym. J.* 1984, *20*, 967–970.

17 A. Marigo, C. Marega, R. Zannetti, G. Morini, G. Ferrara, *Eur. Polym. J.* 2000, *36*, 1921–1926.

18 P. Corradini, V. Busico, G. Guerra, in: W. Kaminsky, H. Sinn (Eds.), *Transition Metals and Organometallics as Catalysts for Olefin Polymerization*, Springer-Verlag, Berlin, 1988, pp. 337–348.

19 V. Busico, P. Corradini, L. De Martino, A. Proto, V. Savino, E. Albizzati, *Makromol. Chem.* 1985, *186*, 1279–1288.

20 M.C. Sacchi, I. Tritto, C. Shan, R. Mendichi, L. Noristi, *Macromolecules* 1991, *24*, 6823–6826.

21 S. Parodi, R. Nocci, U. Giannini, P.C. Barbè, U. Scatà, European Patent 45977, 1981.

22 T. Leinonen, P. Denifl, European Patent 1273595, 2003.

23 M. Abboud, P. Denifl, K-H. Reichert, *Macromol. Mater. Eng.* 2005, *290*, 1220–1226.

24 L. Noristi, E. Marchetti, G. Baruzzi, P. Sgarzi, *J. Polym. Sci.: Part A: Polym. Chem.* 1994, *32*, 3047–3059.

25 H. Mori, M. Sawada, T. Higuchi, K. Hasebe, N. Otsuka, M. Terano, *Macromol. Rapid Commun.* 1999, *20*, 245–250.

26 G. Cecchin, E. Marchetti, G. Baruzzi, *Macromol. Chem. Phys.* 2001, *202*, 1987–1994.

27 M. Chang, X. Liu, P.J. Nelson, G.R. Munzing, T.A. Gegan, Y.V. Kissin, *J. Catal.* 2006, *239*, 347–353.

28 M. Härkönen, J.V. Seppälä, T. Väänänen, in: T. Keii, K. Soga (Eds.), *Catalytic Olefin Polymerization*, Elsevier, Amsterdam, 1990, pp. 87–105.

29 A. Proto, L. Oliva, C. Pellecchia, A.J. Sivak, L.A. Cullo, *Macromolecules* 1990, *23*, 2904–2907.

30 T. Okano, K. Chida, H. Furuhashi, A. Nakano, S. Ukei, in: T. Keii, K. Soga (Eds.), *Catalytic Olefin Polymerization*, Elsevier, Amsterdam, 1990, pp. 177–183.

31 N. Ishimaru, M. Kioka, A. Toyota, European Patent 350170, 1989.

32 J.C. Chadwick, G.M.M. van Kessel, O. Sudmeijer, *Macromol. Chem. Phys.* 1995, *196*, 1431–1437.

33 J.C. Chadwick, *Macromol. Symp.* 2001, *173*, 21–35.

34 S. Ikai, H. Ikeuchi, H. Satoh, T. Inoue, H. Sano, European Patent 841348, 1997.

35 S. Yao, Y. Tanaka, *Macromol. Theory Simul.* 2001, *10*, 850–854.

36 E. Albizzati, U. Giannini, G. Morini, C.A. Smith, R. Zeigler, in: G. Fink, R. Mülhaupt, H.H. Brintzinger (Eds.), *Ziegler Catalysts. Recent Scientific Innovations and Technological Improvements*, Springer-Verlag, Berlin, 1995, pp. 413–425.

37 E. Albizzati, P.C. Barbè, L. Noristi, R. Scordamaglia, L. Barino, U. Giannini, G. Morini, European Patent 361494, 1989.

38 G. Morini, A. Cristofori, European Patent 728724, 1996.

39 E. Albizzati, U. Giannini, G. Morini, M. Galimberti, L. Barino, R. Scordamaglia, *Macromol. Symp.* 1995, *89*, 73–89.

40 L. Barino, R. Scordamaglia, *Macromol. Symp.* 1995, *89*, 101–111.

41 J.C. Chadwick, G. Morini, E. Albizzati, G. Balbontin, I. Mingozzi, A. Cristofori, O. Sudmeijer, G.M.M. van Kessel, *Macromol. Chem. Phys.* 1996, *197*, 2501–2510.

42 G. Guastalla, U. Giannini, *Makromol. Chem., Rapid Commun.* 1983, *4*, 519–527.

43 J.C. Chadwick, F.P.T.J. van der Burgt, S. Rastogi, V. Busico, R. Cipullo, G. Talarico, J.J.R. Heere, *Macromolecules* 2004, *37*, 9722–9727.

44 G. Morini, G. Balbontin, Y. Gulevich, H. Duijghuisen, R. Kelder, P.A. Klusener, F. Korndorffer, International Patent WO 00/63261, 2000.

45 G. Cecchin, G. Morini, A. Pelliconi, *Macromol. Symp.* 2001, *173*, 195–209.

46 G.D. Bukatov, V.A. Zakharov, *Macromol. Chem. Phys.* 2001, *202*, 2003–2009.

47 P.J.T. Tait, G.H. Zohuri, A.M. Kells, I.D. McKenzie, in: G. Fink, R. Mülhaupt, H. H. Brintzinger (Eds.), *Ziegler Catalysts. Recent Scientific Innovations and Technological Improvements*, Springer-Verlag, Berlin, 1995, pp. 343–362.

48 A.K. Yaluma, P.J.T. Tait, J.C. Chadwick, *J. Polym. Sci.: Part A: Polym. Chem.* 2006, *44*, 1635–1647.

49 G.D. Bukatov, V.S. Goncharov, V.A. Zakharov, *Macromol. Chem. Phys.* 1995, *196*, 1751–1759.

50 H. Mori, K. Tashino, M. Terano, *Macromol. Rapid Commun.* 1995, *16*, 651–657.

51 B. Liu, N. Murayama, M. Terano, *Ind. Eng. Chem. Res.* 2005, *44*, 2382–2388.

52 N. Kashiwa, J. Yoshitake, A. Toyota, *Polym. Bull. (Berlin)* 1988, *19*, 333–338.

53 J.C. Chadwick, in: G. Fink, R. Mülhaupt, H.H. Brintzinger (Eds.), *Ziegler Catalysts. Recent Scientific Innovations and Technological Improvements*, Springer-Verlag, Berlin, 1995, pp. 427–440.

54 M. Kakugo, T. Miyatake, Y. Naito, K. Mizunuma, *Macromolecules* 1988, *21*, 314–319.

55 M.C. Sacchi, F. Forlini, I. Tritto, R. Mendichi, G. Zannoni, L. Noristi, *Macromolecules* 1992, *25*, 5914–5918.

56 M.C. Sacchi, F. Forlini, I. Tritto, P. Locatelli, G. Morini, G. Baruzzi, E. Albizzati, *Macromol. Symp.* 1995, *89*, 91–100.

57 G. Morini, E. Albizzati, G. Balbontin, I. Mingozzi, M.C. Sacchi, F. Forlini, I. Tritto, *Macromolecules* 1996, *29*, 5770–5776.

58 V. Busico, R. Cipullo, G. Monaco, G. Talarico, M. Vacatello, J.C. Chadwick, A.L. Segre, O. Sudmeijer, *Macromolecules* 1999, *32*, 4173–4182.

59 V. Busico, R. Cipullo, G. Talarico, A.L. Segre, J.C. Chadwick, *Macromolecules* 1997, *30*, 4786–4790.

60 J.C. Chadwick, G. Morini, G. Balbontin, I. Camurati, J.J.R. Heere, I. Mingozzi, F. Testoni, *Macromol. Chem. Phys.* 2001, *202*, 1995–2002.

61 M. Härkönen, J. Seppälä, R. Chûjô, Y. Kogure, *Polymer* 1995, *36*, 1499–1505.

62 B. Liu, T. Nitta, H. Nakatani, M. Terano, *Macromol. Chem. Phys.* 2002, *203*, 2412–2421.

63 L. Brambilla, G. Zerbi, S. Nascetti, F. Piemontesi, G. Morini, *Macromol. Symp.* 2004, *213*, 287–301.

64 L. Brambilla, G. Zerbi, F. Piemontesi, S. Nascetti, G. Morini, *J. Mol. Catal. A: Chem.* 2006, *263*, 103–111.

65 R. Scordamaglia, L. Barino, *Macromol. Theory Simul.* 1998, *7*, 399–405.

66 M. Toto, G. Morini, G. Guerra, P. Corradini, L. Cavallo, *Macromolecules* 2000, *33*, 1134–1140.

67 M.C. Sacchi, F. Forlini, I. Tritto, P. Locatelli, G. Morini, L. Noristi, E. Albizzati, *Macromolecules* 1996, *29*, 3341–3345.

68 J.C. Chadwick, G. Morini, G. Balbontin, I. Mingozzi, E. Albizzati, *Macromol. Chem. Phys.* 1997, *198*, 1181–1188.

69 G. Cecchin, G. Morini, F. Piemontesi, A. Ferraro, J. News, L. Cavallo, in: *EUPOC 2003. European Polymer Conference on Stereospecific Polymerization and Stereoregular Polymers*, Milan, Italy, 2003.

70 (a) A. Miller, U.S. Patent 4,003,712, 1977; (b) I.J. Levine, F.J. Karol, U.S. Patent 4,011,382, 1977; (c) F.J. Karol, G.L. Goeke, B.E. Wagner, W.A. Fraser, R.J. Jorgensen, U.S. Patent 4,302,566, 1981; (d) R.J. Jorgensen, G.L. Goeke, F.J. Karol, U.S. Patent 4,349,648, 1982.

71 N. Kashiwa, J. Yoshitake, *Makromol. Chem., Rapid Commun.* 1982, *3*, 211–214.

72 L. Sun, S. Lin, *J. Polym. Sci., Polym. Chem.* 1990, *28*, 1237–1254.

73 Q. Wu, H. Wang, S. Lin, *Makromol. Chem. Rapid Commun.* 1992, *13*, 357–361.

74 Y. Vermel, V.A. Zakharov, Z.K. Bukatova, G.P. Shkurina, L.G. Yechevskaya, E.M. Moroz, S.V. Sudakova, *Polymer Science U.S.S.R.* 1980, *22*, 23–30.

75 H. Mori, K. Hasebe, M. Terano, *Polymer* 1999, *40*, 1389–1394.

76 A.S.N. Al-Arifi, *J. Appl. Polym. Sci.* 2004, *93*, 56–62.

77 P. Galli, P. Barbè, G. Guidetti, R. Zannetti, A. Martorana, A. Marigo, *Eur. Polym. J.* 1983, *19*, 19–24.

78 C.W. Moberly, M.B. Welch, L.M. Fodor U.S. Patent 4,234,710, 1980.

79 (a) M. Kelly, S.K. Goyal, V. Ker, P.M. de Wit, B.S. Kimberley, P.P.M. Hoang, U.S. Patent 7,211,535, 2007; (b) M. Kelly, D. Jeremic, V. Ker, C. Russell, U.S. Patent 6,140,264, 2000; (c) S.K. Goyal, T.W. Wiwchar, V. Ker, M. Kelly, U.S. Patent 6,825,293, 2004.

80 R.O. Hagerty, R.O. Mohring, L.M. Allen, European Patent 0,231,102, 1995.

81 (a) T.E. Nowlin, R.I. Mink, European Patent 0,612,327, 1997; (b) T.E. Nowlin, R.I. Mink, European Patent 0,729,478, 1999; (c) T.E. Nowlin, R.I. Mink, European Patent 0,701,575, 1999: (d) R.I. Mink, T. Nowlin, PCT Patent Appl. 9513873, 1995.

82 M.A. Apecetche, P.A. Cao, M.D. Awe, A.D. Schoed-Wolters, R.W. Impleman, U.S. Pat. Appl. 200670281879, 2006.

83 L. Spencer, European Patent 0,775,163, 1998.

84 (a) H. Mavridis, M.K. Reinking, R.N. Shroff, J.A. Mutchler, C.S. Holland, K.M. Lindstrom, K.M. Gupte, M.H. Treptau, F.M. Mirabella, U.S. Patent 6,171,993, 2001; (b) M.K. Reinking U.S. Patent 7,151,145, 2006.

85 (a) L. Sillantaka, U. Plamqvist, E. Iiskola, S. Koavujäri, U.S. Patent 6,043,326, 2000; (b) S. Ala-Huikku, M. Lommi, European Patent 0,573,633, 1996.

86 (a) R.A. Dombro, U.S. Patent 4,335,016, 1982; (b) T.J. Pullukat, R.E. Hoff U.S. Patent 4,374,753, 1983.

87 C. Brun, A. Cheux, E. Barthel, European Patent 0,296,021, 1992.

88 (a) C. Lalange-Magne, C. Royer-Mladenov, European Patent 1,490,415, 2006; (b) BP Lavera SNC European Patent Appl. 1,502,924, 2005.

89 A.J. Hartshorn, E. Jones, U.S. Patent 4,324,691, 1982.

90 (a) M. Kioka, K. Kawakita, A. Toyota, European Patent 0,494,084, 1989; (b) M. Kioka, K. Kawakita, A. Toyota, European Patent Appl 408,750, 1991.

91 Z. Salajka, J. Kratochvíla, P. Hudec, P. Věčorek, *J. Polym. Sci., Polym. Chem.* 1993, *31*, 1493–1498.

92 F.J. Karol, S.-C. Kao, K.J. Cann, *J. Polym. Sci., Polym. Chem.* 1993, *31*, 2541–2553.

93 Y.V. Kissin, F.M. Mirabella, C.C. Meverden, *J. Polym. Sci., Polym. Chem.* 2005, *43*, 4351–4362.

94 K. Soga, R. Ohnishi, T. Sano, *Polym. Bull.* 1982, *7*, 547–552.

95 C.R. Wolf, M.M.C. Forte, J.H.Z. dos Santos, *Catal. Today* 2005, 107–108.

96 K.K. Kang, J.K. Oh, Y.I. Jeong, T. Shiono, T. Ikeda, *Macromol. Rapid Commun.* 1999, *20*, 308–311.

97 E. Pérez, R. Benavente, A. Bello, J.M. Pereña, *Polym. Eng. Sci.* 1991, *31*, 1189–1193.

98 V.B. Skomorokhov, V.A. Zakharov, V.A. Kirillov, *Macromol. Chem. Phys.* 1996, *197*, 1615–1631.

99 R. Quijada, A.M. Wanderlay, Studies on the copolymerization of ethylene and α-olefins with Ziegler-Natta catalyst supported on alumina or magnesium chloride, in: T. Keii, K. Soga (Eds.), *Catalytic Polymerizations of Olefins*, Kadansha, Tokyo, 1986, pp. 419–429.

100 V.A. Zakharov, S.I. Makhtarulin, V.A. Poluboyarov, V.F. Anufrienko, *Makromol. Chem.* 1984, *185*, 1781–1793.

101 A. Muñoz-Escalona, H. García, A. Albornoz, *J. Appl. Polym. Sci.* 1987, *34*, 977–988.

102 J.C.W. Chien, J.D. Capistran, L.C. Dickinson, F.E. Karasz, *Organic Coatings and Plastics Chemistry* 1980, *43*, 875–878.

103 V.A. Zakharov, S.I. Makhtarulin, Y.I. Yermakov, *React. Kinet. Catal. Lett.* 1978, *9*, 137–142.

104 (a) G. Govoni, G. Patroncini, European Patent 0,560,035, 1993; (b) M. Covezzi, P. Galli, G. Govoni, R. Rinaldi, European Patent 0,560,312, 1993; (c) P. Baita, M. Covezzi, G. Mei, G. Morini, J.T.M. Pater, PCT Int. Appl. 2005/058982, 2005.

105 K. Matsuura, N. Kuroda, M. Miyoshi, M. Matsuzaki, U.S. Patent 3,917,575, 1975.

106 Z. Zhu, M. Chang, C.J. Aarons, U.S. Patent 7,153,803, 2006.

107 K. Yamaguchi, N. Kanoh, T. Tanaka, N. Enokido, A. Murakami, S. Yoshida, U.S. Patent 3,989,881, 1976.

108 T. Iwao, H. Sasaki, A. Ito, M. Kono, U.S. Patent 4,187,385, 1980.

109 E. Gelus, European Patent 0,703,246, 1994.

110 R. Spitz, C. Brun, J.-F. Joly, U.S. Patent 5,055,535, 1991.

111 E. Berger, U.S. Patent 4,296,223, 1981.

112 J.-C. Bernard, C. Berruyer, L. Havas, European Patent 0,376,559, 1993.

113 S.I. Woo, I. Kim, U.S. Patent 5,192,729, 1993.

114 H. Chen, T.J. Coffy, E.S. Shamshoum, European Patent 0,855,409, 1998.

115 (a) R.J. Jorgensen, PCT Int. Appl. 2006/020623, 2006; (b) A.D. Hammer, F.J. Karol, European Patent 0,020,818, 1986; (c) F.J. Karol, G.L. Goeke, E.B. Wagner, W.A. Frazer, R.J. Jorgensen, European Patent 0,004,645, 1991.

116 B.E. Wagner, R.J. Jorgensen, U.S. Patent 6,982,237, 2006.

117 M.T. Zoeckler, B.E. Wagner, S.-C. Kao, U.S. Patent Appl. 2007/0060725, 2007.

118 F.M. Mirabella, B. Christ, *J. Polym. Sci., Polym. Phys.* 2004, *42*, 3416–3427.
119 T. Usami, Y. Gotoh, S. Takayama, *Macromolecules* 1986, *19*, 2722–22726.
120 L. Wild, T.R. Ryle, D.C. Knobeloch, *Am. Chem. Soc., Polym. Prep.* 1982, *23*, 133–134.
121 E.C. Kelusky, C.T. Elston, R.E. Murray, *Polym. Eng. Sci.* 1987, *27*, 1562–1571.
122 P. Smith, R.S.-J. Manley, *Macromolecules* 1979, *12*, 483–491.
123 R. Hingmann, J. Rieger, M. Kersting, *Macromolecules* 1995, *28*, 3801–3806.
124 E. Pérez, A. Bello, J.M. Pereña, R. Benavente, M.C. Martínez, C. Aguilar, *Polymer* 1989, *30*, 1508–1512.
125 Y.-M. Kim, J.-K. Park, *J. Appl. Polym. Sci.* 1996, *61*, 2315–2324.
126 R. Benavente, J.M. Pereña, A. Bello, C. Aguilar, M.C. Martinez, *J. Mater. Sci.* 1990, *25*, 4162–4168.
127 P. Galli, G. Vecellio, *Prog. Polym. Sci.* 2001, *26*, 1287–1336.
128 M. Cossar, J. Teh, A. Kivisto, J. Mackenzie, *Appl. Spectrosc.* 2005, *59*, 300–304.
129 S. Hosoda, K. Kojima, M. Furuta, *Makromol. Chem.* 1986, *187*, 1501–1514.
130 S. Hosoda, A. Uemura, Y. Shigematsu, I. Yamamoto, K. Kojima, *Stud. Surf. Sci. Catal.* 1994, *89*, 365–372.
131 T.-Y. Cho, E.J. Shin, W. Jeong, B. Heck, R. Graf, G. Strobl, H.W. Spiess, D.Y. Yoon, *Macromol. Rapid Commun.* 2006, *27*, 322–327.
132 N. Brown, I.M. Ward, *J. Mater. Sci.* 1983, *18*, 1405–1420.
133 B. Schneider, H. Pivcová, D. Doskočilová, *Macromolecules* 1972, *5*, 120–124.
134 S.-W. Tsui, R.A. Duchett, I.M. Ward, *J. Mater. Sci.* 1992, *27*, 2799–2806.
135 H.-S. Chang, W.-D. Song, K.-J. Chu, Son-Ki Ihm, *Macromolecules* 1992, *25*, 2086–2903.
136 K.-J. Chu, J.B.P. Soares, A. Penlidis, S.-K. Ihm, *Macromol. Chem. Phys.* 1999, *200*, 1298–1305.
137 N. Kashiwa, T. Shinozaki, *Plastics Eng.* 1997, *40*, 273–293.
138 J.J.A. Dusseault, C.C. Hsu, *J.M.S.-Rev. Macromol. Chem. Phys.* 1993, *C33*(2), 103–145.
139 J.V. Seppälä, M. Auer, *Prog. Polym. Sci.* 1990, *15*, 147–176.
140 A. Koivumäki, J. Seppälä, *Macromolecules* 1993, *26*, 5535–5538.
141 J.-G. Wang, W.-B. Zhang, B.-T. Huang, *Makromol Chem., Macromol. Symp.* 1992, *63*, 245–258.
142 V. Busico, P. Corradini, A. Ferraro, A. Proto, *Makromol. Chem.* 1986, *187*, 1125–1130.
143 R.R. Ford, R.K. Stuart, PCT. Int. Appl. 00/24790, 2000.
144 R.R. Ford, J.J. Vanderbilt, D.S. Williams, European Patent Appl. 1,187,857, 2004.
145 R. Spitz, V. Pasquet, M. Patin, A. Guyot, The activation of supported vanadium catalysts in ethylene polymerization, in: G. Fink, R. Mülhaupt, H.H. Brintzinger (Eds.), *Ziegler Catalysis*, Springer-Verlag, Berlin, Heidelberg, 1995, pp. 401–411.
146 L.G. Echevaskaya, V.A. Zakharov, G.D. Bukatov, *React. Kinet. Catal. Lett.* 1987, *34*, 99–104.
147 N. Kashiwa, T. Tsutsui, *Makromol. Chem., Rapid Commun.* 1983, *4*, 491–495.
148 D.R. Burfield, P.J. Tait, *Polymer* 1972, *13*, 315–320.
149 K. Soga, R. Ohnishi, T. Sano, *Polym. Bull.* 1982, *7*, 547–552.
150 C. Cozewith, G. Ver Strate, *Macromolecules* 1971, *4*, 482–489.
151 Y. Doi, S. Ueki, T. Keii, *Macromolecules* 1979, *12*, 814–819.
152 J.P. Hogan, R.L. Banks, U.S. Patent 2,825,721, 1958.
153 M.B. Welch, H. Hsieh, in: C. Vasiele, R.B. Seymour (Eds.), *Handbook of Polyolefins*, Marcel Dekker, New York, 1983, pp. 21–38.
154 M.P. McDaniel, *Adv. Catal.* 1985, *33*, 47.
155 P.C. Thüne, J. Loos, A.M. de Jong, P.J. Lemstra, J.W. Niemantsvendriet, *Top. Catal.* 2000, *13*, 67.
156 E. Groppo, C. Lamberti, S. Bordiga, G. Spoto, A. Zecchina, *Chem. Rev.* 2005, *105*, 115.
157 S.M. Augustine, J.P. Blitz, *J. Catal.* 1996, *161*, 641.
158 V.J. Ruddick, P.W. Dyer, G. Bell, V.C. Gibson, J.P.D. Badyall, *J. Phys. Chem.* 1996, *100*, 11062.
159 M.P. McDaniel, M.B. Welch, *J. Catal.* 1983, *82*, 98.

160 M.P. McDaniel, M.B. Welch, M.J. Dreiling, *J. Catal.* 1983, *82*, 118.
161 T. Pullukat, R.E. Hoff, M. Shida, *J. Polym. Sci., Polym. Chem.* 1980, *18*, 2857.
162 B. Rebenstorf, *J. Mol. Catal.* 1991, *66*, 59.
163 W.L. Carrick, R.J. Turbett, F.J. Karol, G.L. Karapinka, A.S. Fox, R.N. Johnson, *J. Polym. Sci.: Polym. Chem.* 1972, *10*, 2609.
164 K. Cann, M. Apecetche, M. Zhang, *Macromol. Symp.* 2004, *213*, 29.
165 Y. Fang, W. Xia, M. He, B. Liu, K. Hasebe, M. Terano, *J. Mol. Catal. A: Chemistry* 2006, *247*, 240.
166 F.J. Karol, G.L. Karapinka, C. Wu, A.W. Dow, R.N. Johnson, W.I. Garrick, *J. Polym. Sci., Part A-1* 1972, *10*, 2621.
167 H. Knuuttila, A. Lehtinen, A. Nummila-Pakarinen, Advanced polyethylene technologies – controlled material properties, in: A.-C. Albertsson (Ed.), *Long Term Properties of Polyethylene*, Springer, Berlin, Heidelberg, 2005, pp. 13–27.
168 S. Haukka, E. Lakomaa, A. Root, *J. Phys. Chem.* 1997, *97*, 5085.
169 E. Groppo, C. Lamberti, S. Bordiga, G. Spoto, A. Zecchina, *Chem. Rev.* 2005, *105*, 115.
170 B.M. Weckhuysen, R.A. Schoonheydt, *Catal. Today* 1999, *51*, 215.
171 J.P. Hogan, *J. Polym. Sci.* 1970, *8*, 2637.
172 R.K. Ihler, *The Chemistry of Silica, Solubility, Polymerization, Colloid and Surface Properties, and Biochemistry*, John Wiley & Sons, New York, 1979.
173 M.P. McDaniel, D.R. Witt, E.A. Benham, *J. Catal.* 1998, *176*, 344.
174 O. Bade, R. Blom, M. Ystenes, *J. Mol. Catal. A: Chemistry* 1997, *161*, 249.
175 O. Bade, R. Blom, M. Ystenes, *J. Mol. Catal. A: Chemistry* 1998, *163*, 135.
176 W. Xia, B. Liu, Y. Fang, K. Hasbe, M. Terano, *J. Mol. Catal. A: Chemistry* 2006, *256*, 301.
177 M.P. McDaniel, M.M. Johnson, *J. Catal.* 1986, *101*, 446.
178 T.W. Woo, S.I. Woo, *J. Catal.* 1990, *123*, 215.
179 H. Knuuttila, M.-R. Hakala, K. Kallio, Conference Proceedings, AIChE 1992, Spring National Meeting, Olefin Polymerization, I.
180 B. Liu, H. Nakatani, M. Terano, *J. Mol. Catal. A: Chemistry* 2003, *201*, 189.
181 B. Liu, H. Nakatani, M. Terano, *J. Mol. Catal. A: Chemistry* 2002, *184*, 387.
182 B. Liu, M. Terano, Advances in Polyolefins conference 7, Sept. 2005, Houston, USA.
183 E. Groppo, C. Lamberti, S. Bordiga, G. Spoto, A. Zecchina, *J. Catal.* 2006, *240*, 172.
184 E. Groppo, C. Lamberti, S. Bordiga, G. Spoto, A. Damin, A. Zecchina, *J. Phys. Chem. B* 2005, *109*, 15024.
185 M.P. McDaniel, M.B. Welch, *J. Catal.* 1983, *82*, 110.
186 M.P. McDaniel, S.J. Martin, *J. Phys. Chem.* 1991, *95*, 3289.
187 Y. Fang, B. Liu, K. Hasebe, M. Terano, *J. Polym. Sci., Polym. Chem.* 2005, *43*, 4632.
188 J. Scheirs, S.W. Bigger, N.C. Billingham, *J. Polym. Sci.,: Polym. Chem.* 1992, *30*, 1873.
189 M.P. McDaniel, M.M. Johnson, *Macromolecules* 1987, *20*, 773.
190 W.D. Niegisch, S.T. Crisafulli, T.S. Nagel, B.E. Wagner, *Macromolecules* 1992, *25*, 3910.
191 M.P. McDaniel, *Ind. Eng. Chem. Res.* 1988, *27*, 1559.
192 P.C. Thüne, R. Linke, W.J.H. van Genninp, A.M. de Jong, J.W.J. Niemantsverdriet, *J. Phys. Chem.* 2001, *B105*, 3073.
193 E.M.E. van Kimmenade, J. Loos, J.W. Niemantsverdriet, P.C. Thüne, *J. Catal.* 2006, *240*, 39.
194 J. Carven, U.S. Patent 3,639,381, 1972.
195 Y. Tafima, et al., European Patent Appl. 0364290, 1989.
196 K. Yamaguchi, M. Hasuo, I. Ito, U.S. Patent 3,759,918, 1973.
197 L.L. Böhm, W. Brevers, R. Kaps, W. Racky, Proceedings, PE 2001 World Conference, February 13–15, 2001, Zurich, Switzerland.
198 A. Sukhadia, SPE ANTEC Conference Proceedings, 1998, paper 31.
199 A. Sukhadia, SPE ANTEC Conference Proceedings, 1999, paper 107.
200 L.L. Böhm, H.F. Enderle, M. Fleissner, *Adv. Mater.* 1992, *4*, 223.

201 J. Scheirs, L.L. Böhm, J.C. Boot, P.S. Leevers, *Trends in Polymer Science* 1996, *4*, 408.

202 P.J. DesLauriers, M.P. McDaniel, D.C. Rohlfing, R.K. Krishnaswamy, S.J. Secora, E.A. Benham, P.L. Maeger, A.R. Wolfe, A.M. Sukhadia, B.B. Beaulieu, *Polym. Eng. Sci.* 2005, *45*, 1203.

203 P.J. DesLauriers, M.P. McDaniel, D.C. Rohlfing, R.K. Krishnaswamy, S.J. Secora, P.L. Maeger, E.A. Benham, A.R. Wolfe, A.M. Sukhadia, W.B. Beaulieu, SPE ANTEC Conference Proceedings, 2005, pp. 3168–3172.

3
Polymer Particle Growth and Process Engineering Aspects

Michael Bartke

3.1
Heterogeneous Polymerization with Supported Catalysts versus Polymerization in Homogeneous Phase

In homogeneous polymerization processes, the polymer formed is soluble in the solvent and forms a single-phase polymer solution. In polymer solutions, viscosity increases rapidly with increasing polymer content (up to several magnitudes), and depends heavily on the polymer properties, and especially the molecular weight of the polymer produced. With increasing viscosity, mixing and transport processes, heat removal in particular become more difficult.

In heterogeneous processes with supported catalysts, the polymer is not soluble in the continuous phase and forms a dispersion of solid polymer particles suspended in the surrounding bulk phase. Polymer dispersions have a significantly lower viscosity compared to polymer solutions of same polymer content. Thus, heat removal and mixing are much less problematic for heterogeneous processes compared to homogeneous processes.

The solution process for polyethylene is presently the only homogeneous process applied commercially for the production of polyolefins. Commercial heterogeneous processes for polyolefins include slurry polymerization, in which the catalyst is suspended in an inert suspension media, and bulk polymerization, in which the liquid monomer is used as continuous phase, and gas-phase polymerization, as well as combinations thereof.

Another difference between solution and slurry-, bulk- or gas-phase polymerization can be seen in the temperature window applied. Solution processes in general are operated well above the melting point of the polymer, typically around or above 160 °C, compared to slurry- or gas-phase polymerization which function at below 100 °C. Depending on the optimal temperature window of a given catalyst, either solution or slurry- (respectively gas-phase) polymerization may be favorable.

Tailor-Made Polymers. Via Immobilization of Alpha-Olefin Polymerization Catalysts.
Edited by John R. Severn and John C. Chadwick

ISBN: 978-3-527-31782-0

3.2
Phenomena in Polymerization with Heterogeneous Catalysts

Following a classification introduced by Ray [1], the phenomena of polymerization processes with supported catalysts can be grouped on the basis of three different levels of scale:

- In the macro-scale, phenomena on the reactor scale such as mixing, mass- and heat transfer to/from the continuous phase, residence time distribution, particle size distribution, control and stability of the reactor are investigated.
- In the meso-scale, phenomena on the particle scale such as catalyst fragmentation, morphology development and phase equilibria and mass- and heat transfer processes within the polymerizing particle are the focus of attention.
- In the micro-scale, the molecular processes at the active site, the reaction kinetics are the main topic.

The focal point of this chapter is the meso-scale, as catalyst heterogenization may have a major influence on meso-scale phenomena.

3.2.1
The Particle as Microreactor

In heterogeneous polymerization with supported catalysts, the reaction takes place in the polymer particles formed. Hence, these catalyst (polymer) particles must be considered as microreactors (or in fact as semi-batch microreactors) within the process.

The monomer and other reaction partners such as comonomers and chain-transfer agents must be transported from the bulk phase to the particle, and from the particle surface to the active sites of the catalyst. The heat of reaction [for polypropylene (PP), 84 kJ mol^{-1}; for polyethylene (PE), 101 kJ mol^{-1}] is released at the active site of the catalyst, and must be transported through the polymer particle to the particle surface, from there to the bulk phase, and finally from the bulk phase to the cooling system of the reactor.

Due to phase-equilibria and transport processes, the concentrations and temperatures at the active site may differ significantly from those in the bulk phase.

Polymer particles grow significantly during the course of polymerization. Productivities of, for example, 100 kg PP g^{-1} catalyst and more correspond to an increase in the particle diameter of a factor in the range of 50; this means that a catalyst particle of 20 μm yields a polymer particle of 1 mm diameter.

Not only mass and heat transfer but also other process characteristics are significantly affected by polymer particle morphology.

3.2.2
Polymer Particle Growth and Morphology Development

Polymer particle growth and has been the focus of intense scientific activities during the past decades. In fact, many different morphology models for polymerizing particles have been developed over the years, and reviews of the relevant literature may be found elsewhere [2–4]. Some underlying model assumptions of selected models, together with some of the main findings, are discussed briefly in the following sections.

Assuming that the catalyst particle does not break up during polymerization, a core-shell morphology for the polymer is the consequence (Figure 3.1). The catalyst particle serves as a core, around which a growing shell-like layer of polymer is formed. The reaction takes place only on the external surface of the catalyst particle, with the monomer being absorbed at the surface of the polymer layer and transported to the catalyst surface. The growing polymer layer resembles a severe mass-transfer resistance, and causes a significant decay in the rate of polymerization. Crabtree et al. [5] have described experimental results for reaction rate and molecular weight distribution (MWD) for a Ziegler–Natta catalyst in a slurry polymerization of ethylene by a core-shell model. It is due to these serious mass-transfer resistances that, in industrial processes, the core-shell morphology is avoided. However, the core-shell model represents a limiting case with maximum mass-transfer resistance, and consequently is of theoretical interest. Comparisons with other single-particle models can be found elsewhere [3–5].

The multigrain model is the most widely used particle model for describing particle growth in polyolefin polymerization. The basic concept was proposed by Yermakov et al., while the first detailed calculations were carried out by Ray and colleagues [6]. In fact, Ray's group has constantly improved and extended the multigrain model during the 1980s and 1990s [7–14].

The multigrain model presumes that the catalyst is instantly disintegrating into fragments at the very beginning of the polymerization process. It is also assumed that the reaction takes place on the surface of the catalyst fragments, and that the catalyst fragments or "micrograins" polymerize according to a core-shell morphology and together form a porous macroparticle (see Figure 3.1).

Heat and mass transfer are considered in the multigrain-model on two different scales: (i) mass transfer within the pores of the macroparticle (pore diffusion); and

Figure 3.1 The basic particle morphology as assumed in core-shell, multigrain, and polymeric flow models.

(ii) mass transfer through the polymer layer around the catalyst fragments within the micrograins. The model uses two diffusion coefficients for both macro- and microparticle diffusion.

According to parameter studies [6, 7], the main mass-transfer resistance – especially in the case of slurry polymerization – seems to be the mass-transfer resistance on the macroparticle scale due to the longer diffusion pathways. In general, mass-transfer resistances predicted by the multigrain-model are much less pronounced than those predicted by the core-shell model.

For catalyst systems with one type of active site, a polydispersity of about four can be explained by diffusion limitations [8]. The description of broader MWDs cannot be described solely by mass-transfer limitations, and requires the consideration of multiple sorts of active site [7, 8], as is generally accepted for Ziegler–Natta type catalysts.

The influence of external transport resistances at the interface of the particle and the continuous phase has been discussed [9]. For slurry polymerizations with highly active catalysts, the external mass transfer can become limiting, whilst limited heat removal in gas-phase polymerization may lead to overheating up to a point where particle melting occurs [10]. Recently, Hutchinson et al. have extended the multigrain model to copolymerizations [11].

During recent years, the description of particle morphology has been constantly improved. The original form of the multigrain-model implied constant porosity during the course of polymerization. However, constant porosity requires a continuous spatial rearrangement of the micrograins within the macroparticle, which is unlikely to be a realistic assumption. Hutchinson et al. [11] subsequently abandoned the assumption of constant porosity and instead assumed a constant spatial arrangement of the micrograins. The model modification predicted – as observed experimentally – that strong concentration gradients would increase the porosities up to hollow particles. In any case, the model predicted porosities that would be equal to or even larger than the catalyst porosity. However, with metallocene catalysts, very compact polymer particles with a lower porosity than the catalyst particle were observed. Debling [12] explained this finding by suggesting a lower melting point and thus a higher compressibility of the micrograin particles.

Naik et al. [13] studied the influence of leaching of the active compound from the catalyst support. Extraction of the active compound results in the reaction no longer occurring solely on the catalyst surface, but also in the polymer phase of the micrograins. For gas-phase polymerizations, this reduced the mass-transfer resistance and increased activity. In slurry polymerizations, the extracted active compound may also polymerize within the pores of the catalyst, the result being pore clogging and an increased mass-transfer resistance. A reduced rate and a potentially dramatic reduction in porosity may be the consequence of such effects. In this case, the multigrain morphology is deemed to be transferring into a polymeric-flow morphology [14].

With help from the multigrain-model, numerous observations of polyolefin polymerization may be explained, although the number of model parameters involved might become substantial.

One other, often used, particle model – namely, the polymeric flow model – has been proposed in two very similar reports by both Schmeal and Streen [15] and Singh and Merrill [16], the aim being to explain the experimentally observed broad MWDs. In analogy to the multigrain model, instant catalyst fragmentation during the very early stages of polymerization is assumed. In contrast to the multigrain-model, the polymeric flow model is a quasi-homogeneous model, where the polymer and catalyst fragments are treated as one compact phase (see Figure 3.1). As a consequence, only one effective diffusion coefficient is required in order to describe the transport processes occurring.

The polymer formed by reaction cannot be accumulated within the particle, and thus is transported outwards by convection. The catalyst fragments and all other species present are distributed within the particle by this internal convective polymer flux. In other investigations, Galvan and Tirell [17] have used a polymeric flow model with two active sites for simulation studies.

Hoel et al. [18] have applied a polymeric flow model for copolymerization, while Sun et al. [19] and Bartke and colleagues [20] have used polymeric flow models for the gas-phase polymerization of butadiene with supported catalysts based on neodymium.

Sakar and Gupta [21] have proposed a polymeric multigrain model, which is based on a discretized version of the polymeric flow model. In order to better take into account particle morphology, the effective diffusion coefficient is calculated depending on catalyst concentration as function of time and spatial position.

Catalyst fragmentation was studied experimentally during the early 1970s, when both Hock [22] and Buls and Higgins [23] proved, using electron microscopy, that during the early stages of polymerization the rapid fragmentation of heterogeneous Ziegler–Natta catalysts of approximate size 30 μm fragmented to approximately 10 to 100 nm, and thus became embedded in the polymer particle.

Although, both the polymeric flow model and the multigrain model assume instantaneous fragmentation of the catalyst, the fragmentation process itself has not been considered. The first quantitative studies on catalyst fragmentation were carried out during the early 1980s by Laurence and Chiovetta [24] and Ferrero and Chiovetta [25–28], the model developed being based on the multigrain-model. The catalyst particle was considered, as for the multigrain-model, to be an agglomeration of micrograins.

Polymerization begins in the pores of the catalyst, which clogs due to polymer formation such that the monomer concentrations inside the particle are very low. Initially, polymerization takes place in the outer regions of the particle, and the hydraulic forces induced by polymer formation lead to catalyst fragmentation. In the model, fragmentation is correlated to a critical growth factor whereby, if the micrograins increase their diameter by a specific degree, then fracture occurs and the micrograin is separated from the catalyst core. It then forms a second porous particle phase in which polymerization takes place according to the multigrain-model. The model describes fragmentation as a consecutive fragmentation from outside to the inside of the catalyst particle (Figure 3.2).

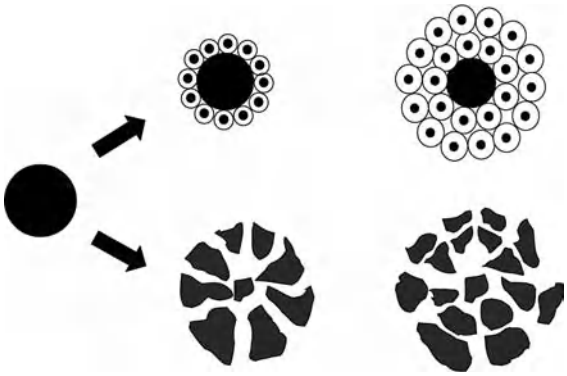

Figure 3.2 Catalyst fragmentation patterns (from outside to inside versus bisectional).

In one report [22], for a $MgCl_2$-based Ziegler–Natta catalyst, critical growth factors are described ranging from about 1.03 to 1.06, which means that fragmentation took place when the micrograins had grown by 3–6% in diameter. For the gas-phase polymerization of propylene [23], complete fragmentation of the catalyst was seen to occur within seconds. Consideration of the fragmentation process, compared to the multigrain model, leads to significantly lower predictions of temperature increases at the start of the polymerization. For polymerization in liquid propylene (bulk polymerization), the model predicts longer fragmentation periods, in the scale of minutes, and anticipates a less-pronounced temperature increase due to improved heat-removal conditions in the liquid phase [25, 26]. In 1995, Bonini and colleagues [29] presented a very similar model for the fragmentation of a metallocene catalyst supported on silica in slurry polymerization of propylene. The critical growth factors obtained for this catalyst indicated, with values between 1.4 and 2.1, that fragmentation for this silica-supported catalyst occurred significantly more slowly than for $MgCl_2$-supported catalysts.

A completely different approach was proposed by Estenoz and Chiovetta [30, 31]. Based on experimental observations with silica-supported chromium catalysts, these authors formulated a particle model in which the catalyst initially broke up into large fragments, which broke up further during the course of polymerization (see Figure 3.2). During the fragmentation process, new active surfaces of the catalyst were continuously released. Fragmentation was seen to begin in the larger pores, as these had the lowest hydraulic resistance towards polymer formation, and continued in the smaller pores until the hydraulic pressure built up by polymerization was insufficient to break up the support. For silica supports, fragment sizes in the range of 0.1 to 10 μm are indicated. This model was quasi-homogenous in nature, and no further morphology predictions were made, the fragmentation process being described solely by the surface/volume ratio of the catalyst fragments. Model parameters may also be obtained by morphology data of the catalyst support such as pore size, pore size distribution and BET surface.

In the tension-model proposed by Kittilsen and McKenna [32], the catalyst fragmentation was initially explained by the underlying physical phenomena, the build

up and relaxation of mechanical stresses. This model is based on the multigrain model, but in additionally to the mass- and heat balances, the mechanical stress in the particle, resulting from a build up by volume expansion due to polymerization, is calculated. When the stress exceeds a critical limit, the relaxation of stress in the form of fragmentation in a tangential direction occurs, such that the micrograins separate and continue their growth. In contrast to the other fragmentation models discussed above, apart from assuming spherical symmetry the tension model does not include any à priori assumptions on the location or direction of the fragmentation process. Fragmentation occurs where the build-up of tensions in the particle are highest. The formation of hollow particles has been explained by the presence of highly active catalysts [30]. The basic concept which has been further developed by Kosek et al. [33, 34]. In their model, the mechanical force interactions between the microelements of a particle (e.g., the micrograins of a porous macroparticle) are described by a viscoelastic Maxwell model. Depending on the particle growth, mechanical material properties, mass-transfer conditions, and the uniformity of catalyst loading, a variety of different polymer particle morphologies have been described, including compact particles, macrocavity formation, hollow particle formation, loss of sphericity and the formation of cauliflower-like structures, disintegration into fines, and the attrition of micrograins.

3.2.3
Mass Transfer in Polymerizing Particles

From the results of various particle modeling studies it can be concluded, that both mass- and heat-transfer resistances are most pronounced during the early stages of polymerization, when activity is high and the particles are still very small.

For the above-mentioned particle models, different mass-transfer mechanisms such as fickian diffusion, pore diffusion, multicomponent diffusion, diffusion and convection have been utilized.

For many of the present highly active catalyst systems, the outlined models would in general predict unrealistically high mass-transfer restrictions, which have not been observed experimentally. Hence, it may be concluded that mass-transfer parameters, and especially effective diffusion coefficients, are often severely underestimated or the corresponding diffusion length, often the micro- and macroparticle radii are used, are significantly overestimated [2].

Although convection may contribute to overall mass transfer, under industrial conditions the convective mass transfer will invariably decrease due to an accumulation of inerts within the particle and a corresponding reduction in pressure gradient as the driving force for convection [2].

One general problem in the quantification of mass transfer is a lack of experimental data. For gas-phase conditions, effective diffusion coefficients can be determined from sorption experiments [20, 35, 36]. However, these mass-transfer parameters have not been determined under reactive conditions. In fact, for slurry

or bulk polymerization even fewer experimental data are available concerning mass transfer in polymerizing particles.

3.2.4 Role of Catalyst Porosity

Within the generally accepted understanding of catalyst fragmentation and mass transfer, catalyst and polymer particle porosity plays an important role.

According to all fragmentation models available, catalyst fragmentation begins in the pores of the catalyst particle. Mass transfer in the pores, according to Knudsen diffusion, is assumed to be about one magnitude faster compared to molecular diffusion in (unporous-) polymer films. Kiparissides et al. predicted that, with decreasing porosity, there would be a decrease in the effective diffusion coefficient of factor of about four [37]. However, catalyst systems without any measurable porosity but with high activity in polymerization and complete and rapid fragmentation of the catalyst particle have been described [38–40].

Sorption studies carried out with PP particles prepared by catalysts with different porosities showed no significant differences in effective diffusion coefficients, depending on the particle morphology [39].

It is possible that the role of catalyst porosity might depend to a much greater extent on the nature of the catalyst support material and the catalyst preparation process:

- Porosity may be needed for a specific catalyst preparation process, such as the impregnation of a metallocene complex on a silica carrier.
- For particle fragmentation, the solubility of the monomer in the support material is an important factor; for support materials with *no* solubility for monomers (e.g., inorganic support material, silica), the pores are needed to facilitate catalyst fragmentation. For catalyst support materials *with* solubility for monomers (e.g., (partially-) organic compounds or polymeric carriers), porosity may not necessarily be needed to start catalyst particle fragmentation.
- For the effect of porosity on mass transfer, further experimental data regarding the effective length of diffusion are needed. The above-mentioned highly active unporous catalysts systems suggest that the role of porosity in mass transfer in polymerization is overestimated in the particle models presently available.

3.2.5 Particle Homogeneity/Videomicroscopy

The interparticle homogeneity of heterogeneous polymerization catalysts – or, more precisely, a uniform polymerization behavior of catalyst particles – is important from the points of view of both process and product.

Unactive catalyst particles will not disintegrate and ultimately locate in the polymer product, the result being reduced clarity in film products or fiber breakage during spinning processes in the case of fiber grades. An uneven loading of the catalyst particles might lead to the generation of fines in the case of low loading, or to particle overheating in the case of a too-high loading; both can lead to process problems. In the case of multi-step processes, differences in the kinetic profile might also lead to different polymer compositions on a particle scale.

One excellent technique by which to study the homogeneity of heterogeneous catalysts under reaction conditions is *videomicroscopy*. This was first applied to polymerization by Eberstein and Reichert [41], in the gas-phase polymerization of butadiene with a heterogeneous Ziegler–Natta ZN catalyst. Pater and Weickert [42, 43], as well as Fink et al. [44, 45] and Reichert and colleagues [46, 47] subsequently applied videomicroscopy to polyolefin polymerization.

In videomicroscopy, the resting catalyst particles are polymerized in a gas phase within a pressure cell equipped with a window. The polymerization is observed through the window, using a digital video camera mounted on top of a microscope with suitable magnification. Two-dimensional (2-D) pictures of the growing particles are then recorded during the course of polymerization, and from these the volume growth and hence catalyst activity can be calculated. The generally laborious analysis required may be conducted computationally, using by digital image processing.

Originally, videomicroscopy was used to study single-particle kinetics. However, it should be borne in mind that the reaction conditions – and especially the heat-removal conditions of resting particles – are incomparable to those of industrial reactor conditions. Indeed, temperature increases of several decades, as measured with infrared technology, have been reported by Pater and Weickert [43] in the case of ethylene polymerization. In virtually all videomicroscopic investigations, more or less pronounced inhomogeneities between different catalyst particles have been reported. This means, on the one hand, that for kinetic studies a statistical analysis of the data must be applied in order to obtain reliable kinetic information, although on the other hand it does mean that videomicroscopy may be used to study the homogeneity of catalyst polymerization behavior.

Both, Abboud et al. [47] and Bartke et al. [40], used videomicroscopy to study the homogeneity of different heterogenization techniques for supported metallocene catalysts. In both cases, depending on the heterogenization technique, significant differences in particle homogeneity could be detected.

3.2.6 Prepolymerization

As mentioned above, mass- and especially heat-transfer, limitations are likely to occur during the initial stages of the polymerization.

One useful approach to avoid overheating and its associated problems such as loss of morphology and thermal deactivation, is that of *prepolymerization* [48, 49]. With prepolymerization, an initial polymerization is conducted under mild conditions (lower temperature and/or monomer concentrations), such that a reduced

rate occurs. Consequently, heat production – and thus overheating – is obviously also reduced, and particle fragmentation and morphology development take place in a more homogeneous and controlled manner. Prepolymerization is usually run only up to very low yields, perhaps 10 to 500 g prepolymer per gram catalyst. Thus, although the contribution of prepolymerization to the final polymer product is, in terms of product properties, negligible, its influence on the polymerization process is significant.

Prepolymerizing under mild conditions to a polymerization degree of $5^3 = 125$ represents an increase in catalyst mass by a factor of 125. For highly active catalysts this would be less than 1% of the final productivity. For this prepolymerization degree, the particle diameter is increased roughly by a factor of 5, and the (external) particle surface by a factor of $5^2 = 25$. Thus, a prepolymer entering a main polymerization reactor that is polymerizing at high activity has a 25-fold larger heat-transfer area available for heat removal compared to the "virgin" catalyst. Although heat-transfer coefficients decrease with increasing particle size, the temperature difference between the particle and surrounding bulk phase that is needed in order to remove the heat of reaction is significantly lower for the prepolymer in comparison to the virgin catalyst polymerizing at the same rate.

Particle overheating during the main stage of polymerization can be avoided by correct prepolymerization. As a result of continuous improvements in catalyst productivity, prepolymerization is becoming increasingly important and more widely used.

3.3 Polymerization Processes and Reactors for Polymerization with Heterogeneous Catalysts

3.3.1 Slurry/Bulk Processes

In *slurry polymerization* the catalysts are suspended in an inert suspension medium, typically alkanes such as hexane, isobutane, or propane. The monomer, comonomer and chain-transfer agents must be dissolved in the suspension medium. The slurry process is used for the polymerization of polyethylene, predominantly to produce high-density polyethylene (HDPE). The slurry polymerization of ethylene is limited to higher densities, since linear low-density polyethylene (LLDPE) fractions with high a comonomer content and/or a low molecular weight would partially dissolve in the suspension medium and this would lead to reactor fouling.

In *bulk-* or *liquid pool polymerization*, the monomer is used as the suspension medium. In bulk polymerization, which is widely used for the production of PP, heat removal from the polymer particle to the liquid bulk-phase is superior to that seen with gas-phase polymerization.

When designing a catalyst for use in slurry- or bulk polymerization, the avoidance of leaching (i.e., the extraction of active components into the liquid phase) is

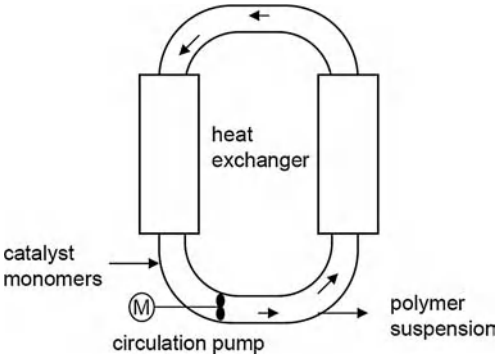

Figure 3.3 Schematic representation of a slurry loop reactor.

essential. Leaching can lead to uncontrolled homogeneous polymerization in the liquid phase and the formation of deposits on the reactor walls. This so-called "reactor fouling" significantly reduces the operability and hence the economy of a process.

Slurry- or bulk processes are usually carried out either in continuous stirred-tank reactors (CSTRs) or in loop reactors. *Loop reactors* (Figure 3.3) have the advantage of a higher specific heat-transfer surface area and thus better heat-removal conditions. In contrast to CSTRs, loop reactors do not have a gas phase present in the reactor, and consequently the pressure may increase much more rapidly in case of a malfunction; hence, such reactors must be equipped with an effective blow-down system. Loop reactors operate under industrial conditions, with high circulation rates. The high velocities inside the reactor improve the heat-removal conditions and also reduce the risk of deposit formation on the reactor walls. At high circulation rates, the residence time distribution of a loop reactor approaches that of a CSTR. However, the presence of size-selective reactor outlets such as settling legs or cyclones can significantly affect the residence time distribution, as demonstrated by Zacca et al. [50, 51].

3.3.2 Gas-Phase Polymerization

In gas-phase polymerization, a broad product window can be achieved. Due to the absence of a liquid phase, leaching or dissolution of low-density/low-molecular-weight fractions of the polymer is not an issue. Gas-phase processes have advantages in investment and operating costs, as no recycling of the solvent/suspension medium is required.

The gas-phase polymerization of PE on an industrial scale is carried out solely in fluidized-bed reactors (FBRs) (Figure 3.4). The typical reaction conditions include a temperature of 80–100 °C, a pressure of approximately 20 bar, and residence times of between 1.5 and 3 hours. Fluidization of the powder is achieved by superficial gas velocities in the cylindrical section of the FBR of typically 0.1 to 0.5 $m\,s^{-1}$. In the expansion zone of an FBR, the gas velocity is lowered below the

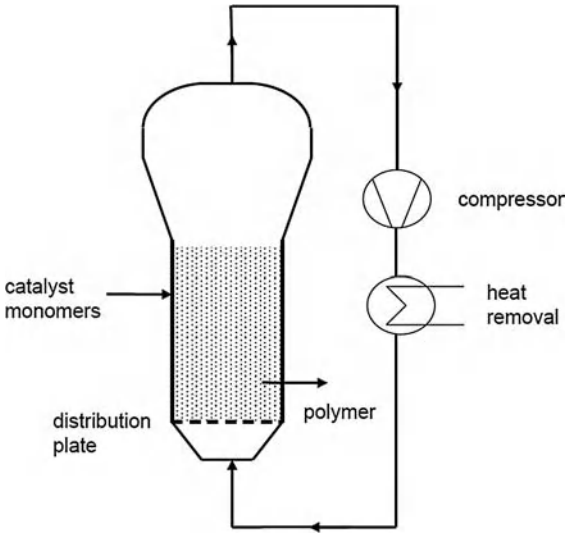

Figure 3.4 Schematic representation of a fluidized bed reactor.

fluidization velocity in order to avoid any carry-over of particles to the gas circulation. As the fluidization velocity is a function of particle size, a narrow catalyst particle size distribution and high bulk density of the polymer are desirable for the efficient operation of an FBR.

The heat of reaction is removed in the gas recycle loop, either by cooling or by the condensation of condensable components such as propane ("condensed mode operation"). The residence time distribution is usually described as being well mixed and CSTR-like, although sizing effects may play a significant role [50, 51].

The operability of FBRs is limited by agglomeration for sticky products, such as LLDPE with a very low density. Static electricity may also lead to operability problems, and consequently antistatic agents are normally used.

Compared to polymerization in the liquid phase, heat removal is more critical during the initial phase of polymerization. Prepolymerization represents a useful method of avoiding overheating and the formation of hot spots in the reactive bed.

The gas-phase polymerization of PP is carried out in either an FBR or a stirred-tank reactor. Both, horizontal and vertical stirred-bed reactors are used on an industrial scale. In stirred-bed reactors the fluidization is achieved by agitators, and consequently they are less sensitive towards broader particle size distribution than FBRs.

3.3.3
Cascaded Processes

Today, polyolefins are used in many application areas which previously required the use of more expensive engineering plastics. An important technique by which

to broaden property combinations and thus the application area of polyolefins, is multi-stage polymerization. In this process, different fractions of polymer with varying properties such as molecular weight and/or comonomer content are produced in a series of reactors operated under different conditions. In this way, multimodal polymers or multiphase polymers with new properties and property combinations may be obtained.

In the case of PE, multistage processes are used to produce multimodal polymers, for example by the combination of two types of reactors of same type (e.g., two slurry tank reactors in Mitsui's CX® process; or two FBRs in Basell's Spherilene® process) or a combination of two reactors of different types (e.g., a slurry loop reactor combined with a fluidized-bed, gas-phase reactor in the Borstar® process of Borealis). In this way, polymers with a bimodal MWD and/or polymer fractions with different comonomer contents may be produced (Figure 3.5).

Multistage processes are widely used for the production of PP, and in particular for the production of heterophasic PP copolymers. In the first stage of either bulk- or gas-phase polymerization, a homopolymer or random copolymer is produced as a matrix material. Subsequently, an ethylene-rich, rubber-like copolymer, which is immiscible with the matrix material, is produced in a gas-phase polymerization. If the matrix material is produced as a bimodal polymer, then reactor cascades of three or more reactors may be utilized.

For multistage processes the carry-over of critical reaction partners from one reactor to another must be taken into account. For example, if a reaction partner of the first reactor (e.g., hydrogen as chain-transfer agent, or comonomer) is not desired in the second reactor, then an appropriate separation unit may need to be positioned between the reactors, such as a flash tank to remove hydrogen.

Due to the inevitable residence time distribution of continuously operated reactors, a distribution of properties for the final polymer product is always obtained [50, 51]. For example, in the case of a two reactor-cascade with a split of 50 wt.% production in each reactor, certain fractions of polymer particles with a locally lower (or higher) fraction of polymer produced in the first reactor will be obtained. The catalyst homogeneity and kinetics may further influence this property distribution. These inhomogeneities may also have an influence not only on the final polymer properties but also on the operability of the process, and so should be taken into consideration during its design.

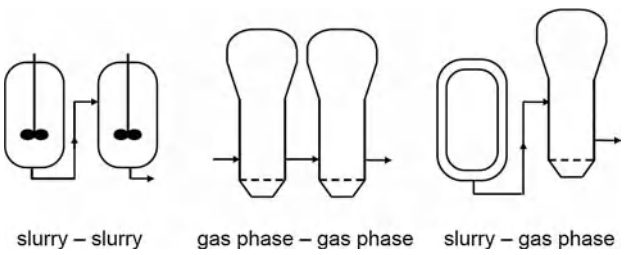

Figure 3.5 Cascaded processes.

Whilst it is clear that multimodal polymers offer more opportunities for product development, it is also clear that multistage polymerization plants are more complex and require higher investment costs.

Alternative concepts for the production of multimodal polymers include the use of multisite catalysts in single-stage processes (e.g., Univation's Prodigy™ catalysts for the gas-phase polymerization of ethylene). In this case, the investment costs are lower compared to a multistage process, but the controllability of the polymer properties is also much reduced, as only one set of reaction conditions is available in order to adjust for instance a bimodal MWD. New developments for the production of multimodal polymers include reactors with different reaction zones, such as the multizone circulation reactor in the Spherizone® [52] process by Basell. This gas-phase reactor for the production of bimodal PP matrix material is a combination of an expanded FBR section (riser) and a moving-bed reactor section (downer) (Figure 3.6). In the riser section, low-molecular-weight material may be produced at a higher hydrogen concentration, whereas in the downer section high-molecular-weight is produced at lower hydrogen concentrations. The carry-over of hydrogen from riser to downer is reduced by the use of a gas barrier, which involves spraying liquid propylene on the top of the downer section. The polymer circulates a couple of times through both reactor sections, such that a better particle homogeneity compared to a multireactor set-up can be achieved. In terms of investment costs, reactors with different reaction zones lie between single-reactor and multireactor set-ups.

Weickert [53] has proposed a multizone reactor on the basis of a FBR with an internal circulation.

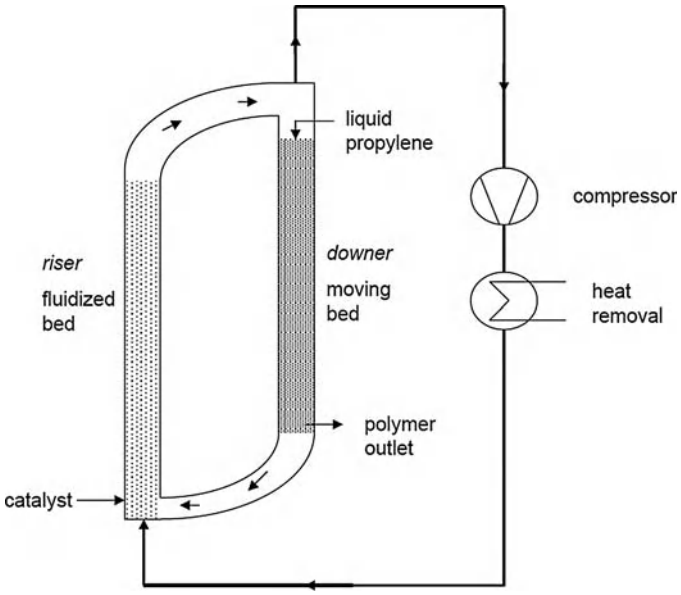

Figure 3.6 Schematic representation of Basell's multi-zone circulating reactor.

3.4
Requirements for Polymerization Catalysts

From a process engineering point of view, some general requirements for heterogeneous polymerization catalysts may be summarized:

- The kinetics (temperature window, catalyst life) must always fit the process.
- A uniform impregnation/activation of the catalyst particles, with homogeneous polymerization behavior
- Smooth and complete fragmentation of the carrier
- No break-up of catalyst particles
- A narrow particle size distribution
- High bulk density/compact particles
- No leaching of active compounds

References

1 W.H. Ray, *Bunsengesellschaft für Physikalische Chemie* 1986, *90*, 947.
2 T.F. McKenna, J.B.P. Soares, *Chem. Eng. Sci.* 2001, *56*, 3931.
3 W.R. Schmeal, J.R. Street, *AIChE J.* 1971, *17*, 1188.
4 D. Singh, R.P. Merill, *Macromolecules* 1971, *4*, 599.
5 J.R. Crabtree, F.N. Grimsby, A.J. Nummelin, J.M. Sketchley, *J. Appl. Polym. Sci.* 1973, *17*, 959.
6 E.J. Nagel, V.A. Kirillov, W.H. Ray, *Ind. Eng. Chem. Prod. Res. Dev.* 1980, *19*, 372.
7 S. Floyd, T. Heiskanen, T.W. Taylor, G.E., Mann, W.H. Ray, *J. Appl. Polym. Sci.* 1987, *33*, 1021.
8 S. Floyd, T. Heiskanen, W.H. Ray, *Chem. Eng. Prog.* 1988, *84*, 56.
9 S. Floyd, K.Y. Choi, T.W. Taylor, W.H., Ray, *J. Appl. Polym. Sci.* 1986, *31*, 2231.
10 R.A. Hutchinson, W.H. Ray, *J. Appl. Polym. Sci.* 1987, *34*, 657.
11 R.A. Hutchinson, C.M. Chen, W.H. Ray, *J. Appl. Polym. Sci.* 1992, *44*, 1389.
12 J.A. Debling, PhD thesis, University of Wisconsin-Madison, 1997.
13 S.D. Naik, W.H. Ray, *J. Appl. Polym. Sci.* 2001, *79*, 2565.
14 M. Hamba, G.C. Han-Adebekun, W.H. Ray, *J. Polym. Sci., Polym. Chem. 1997*, 35, 2075.
15 W.R. Schmeal, J.R. Street, *AIChE J.* 1971, *17*, 1188.
16 D. Singh, R.P. Merill, *Macromolecules* 1971, *4*, 599.
17 R. Galvan, M. Tirrell, *Chem. Eng. Sci.* 1986, *41*, 2385.
18 E.L. Hoel, C. Cozewith, G.D. Byrne, *AIChE J.* 1994, *40*, 1669.
19 J. Sun, C. Eberstein, K.-H., Reichert, *J. Appl. Polym. Sci.* 1997, *64*, 203.
20 M. Bartke, A. Wartmann, K.-H. Reichert, *J. Appl. Polym. Sci.* 2003, *87*, 270.
21 P. Sarkar, S.K. Gupta, *Polymer* 1992, *33*, 1477.
22 C.W. Hock, *J. Polym. Sci., Polym. Chem.* 1966, *4*, 3055.
23 V.W. Buls, T.L. Higgins, *J. Polym. Sci., Polym. Chem.* 1970, *8*, 1037.
24 R.L. Laurence, M.G. Chiovetta, in: K.-H. Reichert, W. Geiseler (Eds.), *Polymer Reaction Engineering*, Hauser-Verlag, München, 1983, pp. 74–112.
25 M.A. Ferrero, M.G. Chiovetta, *Polym. Eng.* 1987, *27*, 1436.
26 M.A. Ferrero, M.G. Chiovetta, *Polym. Eng. Sci.* 1987, *27*, 1448.
27 M.A. Ferrero, M.G. Chiovetta, *Polym. Eng. Sci.* 1991, *31*, 886.
28 M.A. Ferrero, M.G. Chiovetta, *Polym. Eng. Sci.* 1991, *31*, 904.

29 F. Bonini, V. Fraaije, G. Fink, *J. Polym. Sci., Polym. Chem.* 1995, *33*, 2393.

30 D.A. Estenoz, M.G. Chiovetta, *Polym. Eng. Sci.* 1996, *36*, 2208.

31 D.A. Estenoz, M.G. Chiovetta, *Polym. Eng. Sci.* 1996, *36*, 2229.

32 P. Kittilsen, T.F. McKenna, H. Svendsen, H.A. Jakobsen, S.B. Frederiksen, *Chem. Eng. Sci.* 2001, *56*, 4015.

33 Z. Grof, J. Kosek, M. Marek, *AIChE J.* 2005, *51*, 2048.

34 B. Horackova, J. Kosek, in: W. Marquardt, C. Pantelides (Eds.), *Morphogenesis of polyolefin particles in polymerization reactors*, 16th European Symposium on Computer-Aided Process Engineering, Elsevier B.V, 2006.

35 A. Sliepcevich, G. Storti, M. Morbidelli, M., *J. Appl. Polym. Sci.* 2000, *78*, 464.

36 M. Patzlaff, A. Wittebrock, K.-H. Reichert, *J. Appl. Polym. Sci.* 2006, *100*, 2642.

37 V. Kanellopoulos, G. Dompazis, B. Gustafsson, C. Kiparissides, *Ind. Eng. Chem. Res.* 2004, *43*, 5166.

38 M. Abboud, P. Denifl, K.-H. Reichert, *J. Appl. Polym. Sci.* 2005, *98*, 2191.

39 M. Abboud, P. Denifl, K.-H. Reichert, *Macromol. Mater. Eng.* 2005, *290*, 1220.

40 M. Bartke, M. Oksman, M. Mustonen, P. Denifl, *Macromol. Mater. Eng.* 2005, *290*, 250.

41 C. Eberstein, B. Garmatter, K.-H. Reichert, G. Sylvester, *Chem. Ing. Tech.* 1996, *68*, 820.

42 J.T.M. Pater, G. Weickert, W.P.M. van Swaaij, *Chimia* 2001, *55*, 231.

43 J.T.M. Pater, G. Weickert, W.P.M. van Swaaij, *AIChE J.* 2004, *49*, 450.

44 S. Knoke, D. Ferrari, B. Tesche, G. Fink, *Angew. Chem.* 2003, *115*, 5244.

45 D. Ferrari, G. Fink, *Macromol. Mater. Eng.* 2005, *290*, 1125.

46 K. Kallio, A. Wartmann, K.-H. Reichert, *Macromol. Rapid Commun.* 2001, *22*, 1330.

47 M. Abboud, K. Kallio, K.-H. Reichert, *Chem. Eng. Technol.* 2004, *27*, 694.

48 F.A.N. Fernandes, L.M.F. Lona, *Braz. J. Chem. Eng.* 2000, *47*, 163.

49 J.T.M. Pater, G. Weickert, W.P.M. van Swaaij, *AIChE J.* 2003, *49*, 180.

50 J.J. Zacca, J.A. Debling, W.H. Ray, *Chem. Eng. Sci.* 1996, *51*, 4859.

51 J.J. Zacca, J.A. Debling, W.H. Ray, *Chem. Eng. Sci.* 1997, *52*, 1941.

52 G. Mei, P. Herben, C. Cagnani, A. Mazzucco, *Macromol. Symp.* 2006, *245–246*, 667.

53 R.R. Tupe, G. Weickert, *Dechema Monogr.* 2004, *138*, 311.

4
Methylaluminoxane (MAO), Silica and a Complex: The "Holy Trinity" of Supported Single-site Catalyst

John R. Severn

4.1
Introduction

Methylaluminoxane (MAO), silica and a precatalyst complex–just like celery, onions and carrots (or bell peppers)–are the three key ingredients (French "*Mirepoix*" and Cajun "*Holy Trinity*") to many a successful recipe. This chapter focuses on how precatalyst complexes, methylaluminoxanes and silica support have been combined to produce supported single-site catalysts.

Silica and MAO are the most commonly employed support material and cocatalyst, respectively, in the immobilization of a single-site precatalyst. It is advantageous to have some basic knowledge of the reagents in question, how they can be tailored, and how they interact with each other. In addition, the chapter will provide examples of selected immobilization procedures and discuss the important factors and pitfalls that may affect the outcome of the polymerization experiment, focusing on the goal of a commercial catalyst.

4.1.1
Background

The development of single-site catalysts began when Cp_2TiCl_2 was combined with an alkyl aluminum complex to afford a catalyst that could polymerize ethylene [1, 2]. These systems were low in activity and relatively unstable, but were effective models for studying the mechanistic behavior of heterogeneous Ziegler–Natta catalysts. The activation effect of water in such systems was initially noted by the groups of Reichert [3], Breslow [4] and Kaminsky [5]; however, the major breakthrough came when Sinn and Kaminsky demonstrated that this activation was due to the formation of MAO from the partial hydrolysis of trimethylaluminum [6]. The MAO cocatalysts yielded an order of magnitude increase in activity and stability of metallocene-based catalysts and this, coupled with the unprecedented ability to tailor the polymer microstructure, resulted in considerable industrial interest and investment into the field. A true single-site catalyst produces polymers with a Schulz–Flory molecular weight distribution (MWD) ($M_w/M_n = 2$ and $M_z/M_w = 1.5$).

Tailor-Made Polymers. Via Immobilization of Alpha-Olefin Polymerization Catalysts.
Edited by John R. Severn and John C. Chadwick

ISBN: 978-3-527-31782-0

In addition, polymer chains with a uniform microstructure (comonomer incorporation, tacticity, etc.) are formed. One or a combination of these features can impart unique macroscopic properties to such polymer resins, the formation of which demands a catalyst with active sites that are identical and have all sites operating ideally under very homogeneous polymerization conditions.

However, the vast majority of polyolefin production capacity is based on particle-forming processes such as slurry/bulk, gas-phase, or cascaded-combinations [7, 8]. Such processes are extremely large-scale (150–800 kton $year^{-1}$) and operate continuously. They rely on solid heterogeneous catalyst particles that form discrete polymer particles to provide good reactor operability. It therefore became evident, during the development of single-site α-olefin polymerization catalysts, that the homogeneous catalysts required heterogenization in such a way as to avoid fouling, allow continuous operation, and retain the desired polymer properties in such processes. As might be imagined, it is quite a challenge to achieve "true" single-site behavior on a heterogeneous catalyst particle, and in practice supported single-site catalysts often provide somewhat broader MWDs as a result of generating multiple active sites or (co)monomer concentration gradients within the particle. However, there may be some tolerance to a deviation from true single-site behavior if it does not adversely affect the desired polymer properties. It is this wish to capture the unique polymer performance package offered by polymer resins derived from single-site catalysts that has led to the "art" of immobilizing or heterogenizing becoming an area of intense research [7, 8].

4.1.2 Commercial Catalysts

The reader is constantly reminded that single-site catalysts are only immobilized to allow operation in commercial particle-forming processes, to produce commercially viable products. It should also be stated that the particle-forming processes have certain limitations as to what type of polymer (density, melting point, etc.) they can produce. In addition, the immobilization of a single-site catalyst is not an absolute requirement to produce polymer resins with "tailored" single-site properties, as several commercial grades of polymer are derived from solution-based process technologies [7, 8].

At the outset of developing a commercial/industrial immobilization strategy for a single-site precatalyst, it is important to take into account and balance several different factors that could affect the success of the intended catalyst. The first consideration is the targeted polymer resin; it is important to consider that the polyolefin industry ultimately sells the property package of a plastic product, and not a particular polymer resin. If the property package of the targeted single-site catalytic resin can be achieved at a more economical cost by using a traditional Cr- or Ziegler–Natta-based resin, or by a blending/additive combination, then it will be. The targeted resin may also place requirements on the polymerization process in terms of density ranges or multimodal features. The target resin strongly dictates the choice of single-site precatalysts, particularly for resins with high

molecular weight and good comonomer incorporation (polyethylene, PE) or isotacticity (polypropylene, PP) demands. The volume sales of the target resin will also affect the economic viability from a process point of view, as grade transitions can be costly, particularly between traditional heterogeneous and single-site catalysts. In addition, the target resin needs, ideally, to be produced at close to the plant production capacity rate.

In all commercial particle-forming polyolefin processes the catalyst remains in the finished polymer product unless extracted, which is a costly process. Therefore, it is the catalyst productivity – that is, how much polymer is produced by how much solid catalyst (including complex, cocatalyst and carrier) – that is crucially important, and not the activity of the metal complex alone. Additionally, each polymer product may require a specific polymer stabilization package. As a consequence it is important to consider if the nature and/or quantity of the catalyst residues, additives or their byproducts, following melt-state shaping, are benign or detrimental to the quality or long-term stability of the final product.

The polymerization process is an equally important factor placing further requirements on a catalyst. Each proprietary process has its own limits in terms of monomer and comonomer concentrations, temperature, temperature control (ΔT), and residence time distribution. These factors place requirements on the catalyst in terms of its kinetic profile, which may have a strong effect on the polymer target capability and can be tailored to a certain extent by all the components in the final catalyst (support, precatalyst, cocatalyst, and synthetic strategy).

One of the main factors to affect process operability is *reactor fouling*. This typically occurs in a single-site catalyst polymerization when active species leach from the surface of the heterogeneous catalyst and begin to polymerize homogeneously. It results in the formation of polymer deposits on the surfaces of a reactor, its internal parts such as gas-distribution plates, heat exchangers, impeller blades and thermocouples and additional process hardware such as recycling lines and compressors. These polymer deposits build up over a period of time, contributing to a decrease in the ability to control the process (heat-transfer, catalyst efficiency, product throughput and split-control in cascaded processes), and hence the ability to produce the desired polymer resin to specification. This can spiral out of control to a point where the reactor needs to be shut down, cleaned, and restarted. Fouling is also detrimental to all parts of a polymerization process, including the reactor and its associated hardware (pumps, motor and gearboxes, etc.), which may need to be changed or maintained. The cleaning, maintenance and restart process can take several days, and is extremely costly and time-consuming. It should be borne in mind, however, that catalyst leaching is not the only cause of reactor fouling. Indeed, the build-up of static electricity, overheating of a catalyst/polymer particle through heat-transfer problems or poor control of the processes can also result in fouling [9].

If the catalyst has passed the requirements of the target resin and the process, then once again economics comes into the equation, and these may be quite complex. For example, catalyst A may be 50% more productive than catalyst B, but

if it costs three times as much to produce it is not as economical – unless the increased productivity allows the producer to include additional value to the resultant polymer resin (lower catalyst residues, enhanced film quality, etc.) or to reduce their costs (fill the production rate of the plant). It should be noted that catalyst quality and consistency are also crucial considerations in the commercial application of any polyolefin catalyst, and this is particularly important for single-site catalysts. The catalyst must perform consistently and produce material on-specification day in, day out and year in, year out in the plants. In order to achieve this, the producer requires relatively robust synthetic strategies, and the control of every step of the process (starting material, quality, handling and reaction equipment, process control, etc.), not forgetting the storage/shipping stability of the final catalyst.

Important factors intimately linked to "economics" are legal issues such as freedom to operate (FTO) and intellectual property rights (IPR). All steps in the process of producing a polymer resin from a single-site catalyst have been protected to some extent, and these can either be licensed (where possible) or must be circumvented. As might be imagined, the acquisition of a license for several of the steps may be very expensive and, especially if there is more than one licensor involved, this may prove uneconomic if the cost offsets the "added value" that has come from the tailored material in the first place. Consequently, legal issues have become one of the main reasons for the relatively slow penetration of single-site catalysts and resulting resins. Ultimately, the profitability – and hence the commercial viability of any polyolefin technology – is governed by the ability to save costs and or to "add value" to the final product that overcompensates for any increased costs.

4.1.3
Polymer Particle Growth

It is important to have some understanding of how the catalyst particle produces a polymer particle, and also how that polymer particle grows, before undertaking an immobilization strategy. Ideally, a single catalyst particle of a certain shape should result in a single polymer particle of the same shape. Various models describing particle growth during olefin polymerization have been developed. For further information, the reader is directed to a review by McKenna and Soares [10], in which the authors discuss single particle modeling for olefin polymerization catalysts, and the recent investigations of Kosek et al. [11] and McKenna et al. [12].

It is important that the mechanical strength of the catalyst particle is sufficiently high to prevent disintegration into smaller fragments (as this may lead to fines formation), but low enough to allow controlled progressive expansion during polymerization. As the polymerization proceeds, the initial catalyst support becomes fragmented and dispersed within the growing polymer matrix (Figure 4.1). The morphology of the starting support is replicated in the final polymer, so that a spherical support in the size range 10 to 100 μm will give spherical polymer

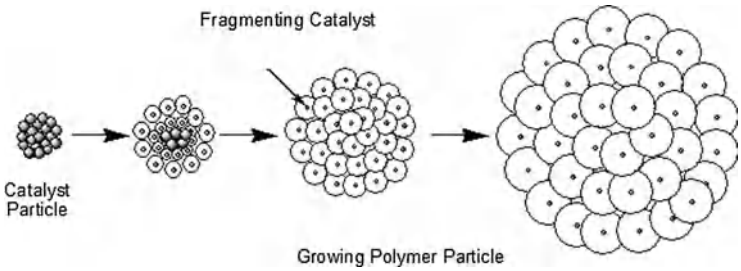

Figure 4.1 Schematic representation of a model for the growth of a single polymer particle.

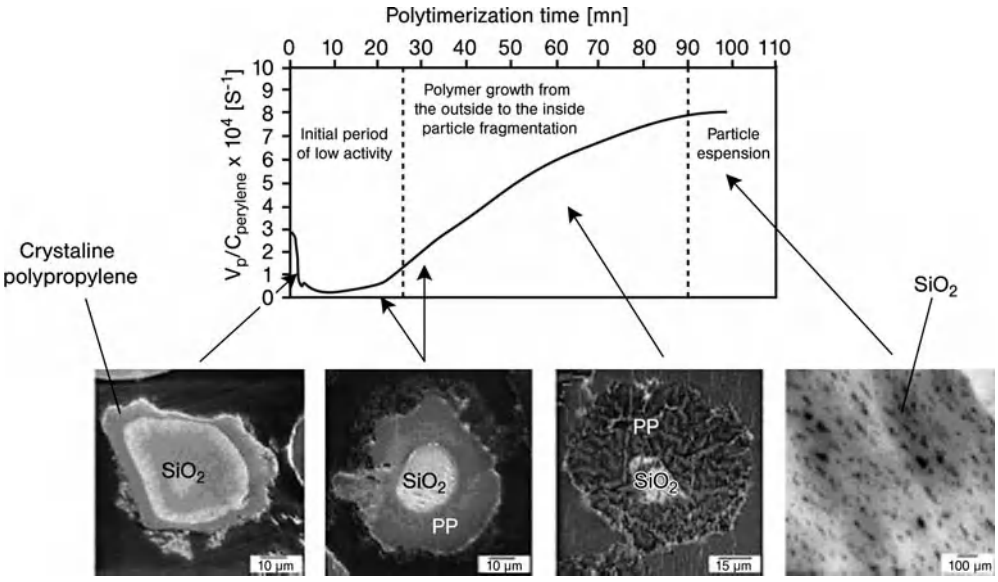

Figure 4.2 Schematic polymer growth and particle expansion from experimental analysis. (Reproduced with permission from Ref. [13b]; © 2004, Wiley-VCH.)

morphology with particle size generally in the range of 100 to 3000 µm, dependent on the catalyst productivity.

Extensive fragmentation and uniform particle growth are key features in the replication process, and are dependent on a high surface area, a homogeneous distribution of catalytically active centers throughout the particle, and free access of the monomer to the innermost zones of the particle. For silica-supported catalysts, it is frequently observed in the literature that polymer growth starts at and near the particle surface, leading to the formation of a shell of polyolefin around the catalyst particle. This imposes a diffusion limitation, preventing free access of the monomer to active sites within the particle. Fink and others have highlighted that this mechanism of particle growth is associated with a kinetic profile in which an initial induction period is followed by an acceleration after which, in the absence of chemical deactivation, a stationary rate is obtained [13]. Figure 4.2

represents such a profile. However, as the author states, this is for a low loading of active complex, so the actual time for each stage may be considerably compressed. Although a catalyst chemist may not require a deep knowledge of all the particle growth models, Böhm's visualization that each individual polymerizing particle should be considered as a microreactor with its own mass and heat balances is handy to keep in mind at all times [14].

4.2 Basic Ingredients

4.2.1 Silica Supports

Silica has been used as a support for α-olefin polymerization catalysts since the late 1950s. Although it is often referred to as an "inert" support, it is far from the "innocent bystander" that the term implies. In fact, it is one of the crucial components in a considerable number of heterogeneous single-site, chromium and Ziegler–Natta (PE) polymerization catalyst systems. Therefore, a deeper understanding of the physical properties of the silica supports, and how to tailor them, is of paramount importance in making a good industrial catalyst. The key properties, which can be altered to varying degrees during the manufacture of the silica and have a major influence on a heterogeneous single-site polyolefin catalyst, are:

- Chemical composition
- Surface chemistry (number and type of surface species such silanol, silyl-ether and Lewis and/or Brønsted acid sites)
- Particle size
- Particle morphology (granular, spheroidal, agglomerated, etc.)
- Silica manufacture
- Physical properties (surface area, pore volume, pore size distribution)
- Attrition/mechanical properties

4.2.1.1 Silica Synthesis

Silica is typically produced in a pipeline mixing process by reacting sodium silicate and a mineral acid, typically sulfuric acid, yielding silichydroxide and Na_2SO_4. The acidification of the sodium silicate solution promotes the condensation of the silichydroxide to form polysilic acid units, which continue to condense, yielding a polymer having the approximate composition of silica. The extent of polymerization increases in line with the concentration of the solution and, more importantly, with decreasing pH. A transparent hydrosol containing micelles in the range of 1 to 3 nm in diameter is formed. The size of micelles can be studied by using transmission electron microscopy (TEM), while the pH of the solution can be used to adjust the size of the micelles; at a higher pH the micelles are larger [15].

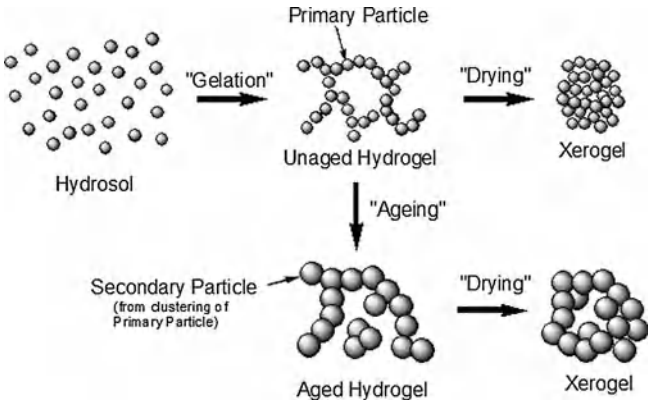

Figure 4.3 A schematic representation of silica support manufacture.

The next step in the preparation is gelation of the hydrosol (Figure 4.3). A three-dimensional (3-D) network is formed via hydrogen bridges between the hydroxyl groups on the surface of the micelles. This process is obviously affected by the pH; the starting pH of the hydrosol is around 10, and this is reduced by the addition of an acid. The pH, mixing and temperature of the reaction all influence how quickly the hydrogel is formed. To strengthen the material the gel is treated at appropriate temperatures and at the appropriate pH; in this process the mass fractional dimension is increased. In practice it is a question of crosslinking the silica material which provides the mass with increased strength. Smaller particles are dissolved and reprecipitated on the larger particles and between those, making them stronger and strengthening the whole construction. During the ageing process the surface area decreases (Ostwald-ripening). For a polyolefin catalyst, tailoring at this stage is extremely important as the catalyst needs to be strong enough to withstand synthesis and handling of the final catalyst, but weak enough to be easily friable during polymerization. The friability of a support can also considerably affect the polymer particle growth and kinetic profile of a polymerization.

After the ageing process the hydrogel is washed to remove the dissolved salts from the silica matrix. The salts remaining in the matrix and final silica can affect its thermal and electrical properties. The thermal stability of the silica depends heavily on the purity (i.e., the degree of washing); the more Na_2O that is left in the silica after neutralization and washing, the lower the melting point of the silica, and consequently the effects of sintering that may occur in high-temperature processes. The degree of static electricity that occurs in silica is affected by the amount of salts left in the silica following washing. This also affects the surface acidity of the material, which in turn influences the coordination capacity of the silica. This surface acidity can be greatly influenced by Al^{3+} doping of the silica surface. Sodium and sulfate residues typically arise from poor washing of the hydrogel, whilst calcium, magnesium and soda residues are commonly a result of the water supply. The sand used in the silicate manufacture commonly entrains salts of Fe,

Al, and Ti into the final silica. For polyolefin catalysts, extensive washing is employed to remove potential polyolefin catalyst poisons, although the extent of washing also greatly influences the price of the silica.

The final step in the preparation of the silica is drying, during which the pore volume decreases drastically due to shrinkage of the silica particle. Before drying, the pore volume is about 4–5 mL g^{-1} SiO_2, but after drying this is commonly about 1–2 mL g^{-1} SiO_2. The mean pore diameter is typically in the range of 10 to 30 nm. As a general rule, the faster the drying occurs, the larger the pore volume; therefore, if small pores or high porosity are demanded in the silica, the untreated silica can be rapidly dried. Drying can also be achieved through an emulsification step. Here, an aqueous solution of the hydrogel can be exchanged to a light hydrocarbon that has a much lower surface tension and thus causes much smaller internal pressures to occur in the interior of the silica, and the capillary forces are also smaller. Another possibility is to distil the solution off under supercritical conditions, thus avoiding surface tension effects (e.g., Aerogel) [15].

Spherical silica is typically created by spray-drying a slurry of milled particles. In this process, the small silica primary particles are agglomerated and "glued" together by what is believed to be remnant material, derived from the colloidal segment of the wet-milled material present in the slurry to form the final particle. The cross-section of such a particle is shown in Figure 4.4 [16]. The procedure creates a more or less spherical form in the material (microspheroids). The void space between the particles is known as the interstitial void space; this starts at the surface of the particle and penetrates into the interior of the agglomerate. Considerable care must be taken when tailoring the process to achieve the desired particle size and distribution, whilst controlling the interstitial void space between the particles, and avoiding the large or non-uniform distribution of void space in the particle. The physical strength of this "microspheroidal" material is less than

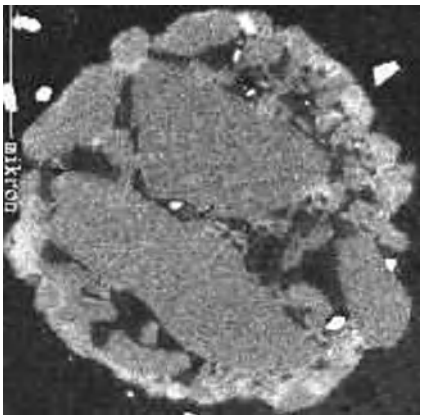

Figure 4.4 Cross-sectional scanning electron microscopy image of a spheroidal silica support. (Reproduced with permission from Borealis Polymers; Ref. [16].)

Table 4.1 Physical properties of a representative sample of spheroidal, polymerization-grade silica supports.

	Surface area ($m^2 g^{-1}$)	*Pore volume ($mL g^{-1}$)*	*Average pore diameter (Å)*	*Average particle size (μm)*
Grace Davison				
Sylopol® 948	~278	~1.68	~242	~58
Sylopol® 952	~272	~1.71	~253	~33
Sylopol® 955	~276	~1.76	~266	~31
INEOS				
ES-70X	~273	~1.54	~225	~39
ES-747JR	~263	~1.60	~244	~20
ES-757	~316	~1.59		~25
PQ Corp.				
MS-3040	~428	~3	~281	~63
MS-1732	~497	~1.5	~121	~60
MS-1733	~311	~1.79		~74
Fuji Silysia				
P10	~270	~1.5	~222	~20

that of granular-shaped material, and can be tailored to achieve the right balance of mechanical strength and friability during polymerization. The physical properties of a representative sample of polymerization-grade spheroidal silica supports are listed in Table 4.1 [17].

4.2.1.2 **Thermal Modification**

Typical "polymerization grades" of silica require some form of thermal treatment to remove H_2O from the surface and to adjust the relative ratios of the various species, whilst at the same time controlling the physical properties of the silica (pore volume and mechanical strength). Calcinations are normally conducted in processes that place low stress on the support material such as fixed or fluidized-bed ovens, multiple hearth furnaces, or rotary calcination ovens. The atmosphere of the calcination is typically air, an inert gas, or a combination of the two (air calcination, inert gas-cooled), and is conducted in such a way as to avoid sintering. It consists of three phases: heating; calcinations; and cooling, each of which may need to be controlled in terms of the rate of temperature increase/decrease, the hold time at calcination temperature and/or agitation, in order to obtain a consistent support material with the desired properties [15].

In its unmodified and fully hydroxylated form, the surface of silica is saturated in silanol groups. Three different hydroxyl groups can be distinguished: isolated (I); geminal (II); and vicinal (III) (Figure 4.5). Water molecules can easily adsorb onto this type of surface, either through hydrogen bonds to the silanol groups or through physical adsorption. Generally speaking, a physically adsorbed water molecule desorbs at 25–105 °C, and hydrogen-bonded water at 105–180 °C. At temperatures above 180 °C, the adjacent vicinal silanol groups begin to condense with each

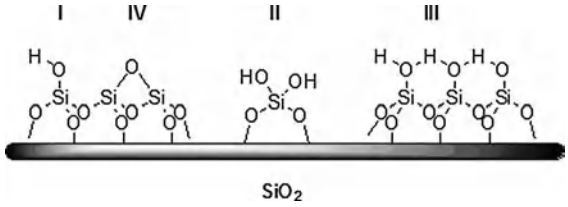

Figure 4.5 Various silica surface species.

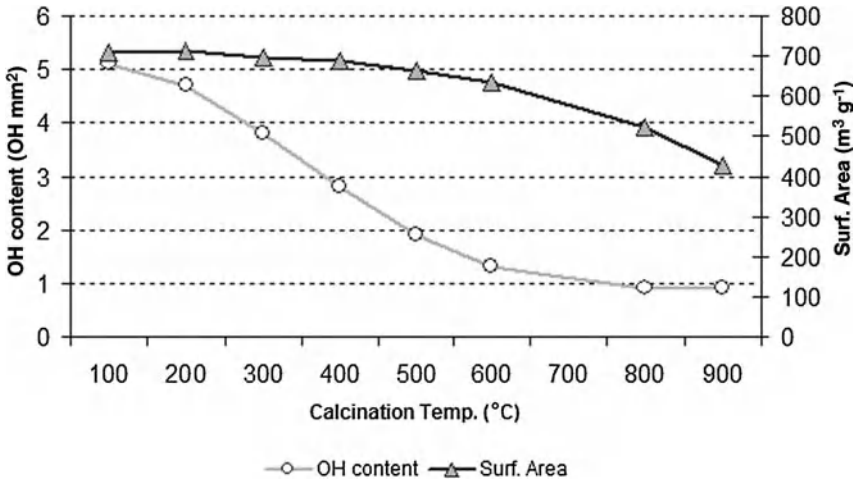

Figure 4.6 Effect of calcination temperature on silica OH content and surface area for a silica gel.

other to form a surface siloxane (silyl ether; Figure 4.5, IV). This process possibly continues to elevated temperatures, with Pruski et al. reporting that strong hydrogen-bonded silanol groups are still present even after calcinations to 350 °C *in vacuo* [18]. The final density of silanol groups depends on the calcination temperature (and time at that temperature), but usually ranges between one and five OH nm^{-2}. The calcination temperature also alters the pore-size distribution and pore volume of the support. An increased calcination temperature usually yields supports with reduced pore volumes and surface areas (see Figure 4.6) [15]. For microspheroidal supports, an increased calcination temperature typically leads to an increase in the strength of the particle, which may be above the desirable level. Therefore, a more friable precalcined support material may be needed. The tailoring of the surface species can also be performed via reaction with certain surface modifiers, such as chloro- or alkoxy-silanes or disilazanes. An analysis of the hydroxyl content on a silica surface may also facilitate patentable claims [19].

The full range of hydroxylated, dehydroxylated or partially-dehydroxylated silicas have been employed in the preparation of heterogeneous single-site α-olefin polymerization catalysts, and whilst some degree of thermal treatment is usually required, the exact calcination temperature and profile of the support may depend on several factors such as mechanical strength of support, polymerization process,

cocatalyst, and/or precatalyst combination and target properties of the polymer resins.

4.2.2 Methylaluminoxane

Methylaluminoxane (MAO) is a generic term, used to describe a cocktail of oligomeric and polymeric species containing Al–O–Al and Al–CH_3 bonds that coexist in multiple equilibria. MAO is mainly formed by the "controlled" hydrolysis of trimethylaluminum (TMAL). Apart from residual TMAL, no other structural components or specific molecules have been unambiguously isolated and identified, including the "active ingredient". However, a considerable number of thoughtful experimental and theoretical studies have been undertaken to highlight this area [20, 21]. Such studies remain crucial to understanding how different species and equilibria in MAO solutions affect its storage and shipment stability, the activity and stereoselectivity of the final catalyst system, and also the molecular weight and MWDs of the resultant polymer resins.

4.2.2.1 Synthesis of MAO

Methylaluminoxanes are predominantly formed by the partial hydrolysis of trimethylaluminum, or a combination of mostly trimethylaluminum and an additional trialkylaluminum. Several sources of water have been employed in the manufacture of MAO. Initially, the water of crystallization (inorganic salt hydrates) was utilized, and this allowed good control of the hydrolysis procedure. However, with the exception of lithium salt hydrates, the entrainment of inorganic salts into the final product may affect its quality and performance. Furthermore, the low yield in terms of converted TMAL found in the final solution affects the economics of the manufacturing process. Water on the surface of intensely cooled ice, or derived from emulsified water vapor in saturated nitrogen, are typical commercial routes for standard MAO production [20].

As might be imagined, studies of the reaction mechanism for the formation of unidentified components within MAO have proved extremely challenging, although the advent of powerful computational hardware and software has assisted such study to some degree. Recently, Hall and colleagues modeled the initial steps in the formation of MAO via a combination of *ab-initio* molecular dynamics and standard *ab-initio* methods [22]. In their study, the first step is the formation of TMAL-OH_2 (A in Figure 4.7), which is described as a bifunctional monomer. The monomer can then undergo further reaction to form the dimeric hydroxide (B in Figure 4.7). Hall's group then used a combination of species A and B, and TMAL to account for various structures proposed in their mechanism, which resembles a step polymerization, with termination by reaction with the free TMAL. Interestingly, the mechanism resulted in proposed structures with CH_3/Al ratios greater than 1, and within the range of experimental values.

Relatively recently, MAO derived from non-hydrolytic routes has become commercially available. The conversion of TMAL to MAO is achieved by treatment

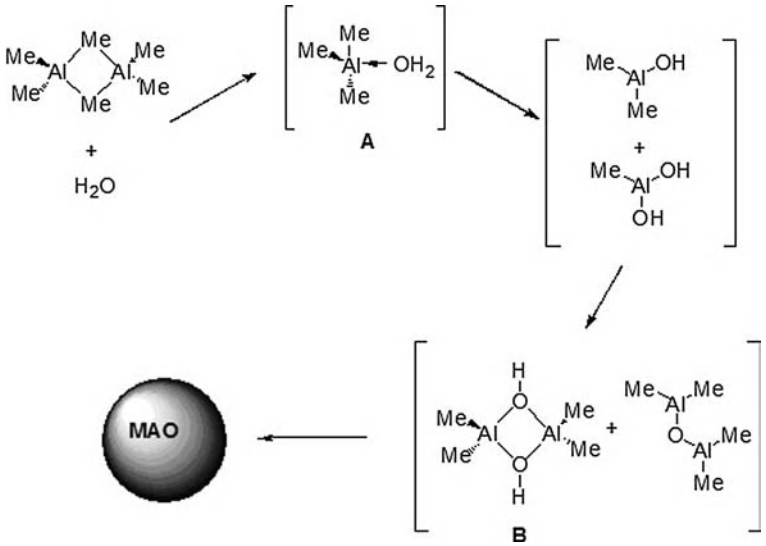

Figure 4.7 Proposed reaction scheme for the hydrolytic formation of methylaluminoxane (MAO).

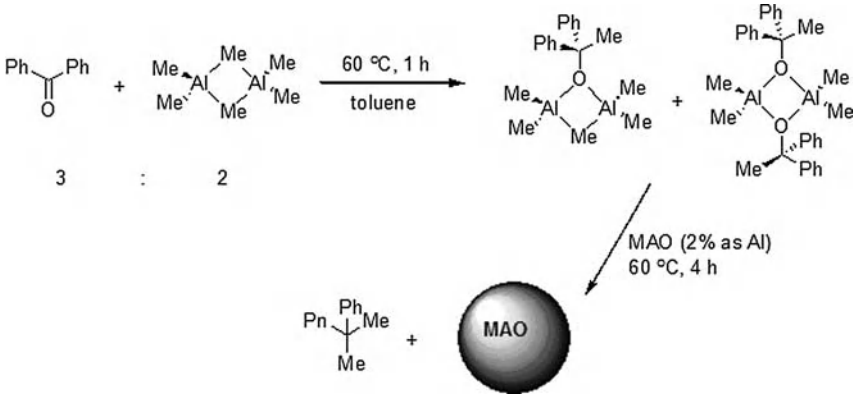

Figure 4.8 Proposed reaction scheme for the non-hydrolytic formation of methylaluminoxane (MAO).

with a carbonyl-containing organic compound [20]. An example of a non-hydrolytic route to MAO, via TMAL and benzaphenone, is illustrated in Figure 4.8. Deffieux et al. proposed that the synthesis proceeds via the initial formation of aluminum alcoholates, which form oligomeric Al–O compounds (MAO-like). However, shifting the reaction towards the formation of aluminoxane structures generally requires the presence of catalytic amounts of commercial MAO [23]. MAO derived from a non-hydrolytic process is claimed to have a longer storage stability and to cause less gel formation.

4.2.2.2 Characterization of MAO

The characterization of MAO solutions is of crucial importance for silica-supported systems, especially in understanding how the components of MAO interact with the various chemical species present on a silica surface, as well as the single-site precatalyst. In addition, the batch-to-batch consistency of a MAO solution may affect the final catalyst's preparation, quality and/or performance.

Typical commercial samples of MAO are assayed with regard to MAO content (wt.%), aluminum content (wt.%), amount of "free" (residual) trimethylaluminum, and the extent of hydrolysis. The MAO content is most often a measure of "solids" contents, and is nominally estimated by the amount of "solid" material obtained on stripping a sample to dryness. It should be noted, however, that such "solid" MAO typically contains remnants of solvent, trimethylaluminum, and also usually small amounts of higher hydrocarbons (process oil), entrained during the commercial manufacturing process. The aluminum contents of MAO solutions are measured by digesting a sample in an acid or base, followed by colorimetric or potentiometric analyses, or via inductively coupled plasma (ICP) spectroscopy. Typically, the aluminum concentrations for unmodified MAO synthesized via hydrolytic methods are 4–5 wt.% Al for 10 wt.% MAO solutions, and 13–14 wt.% Al for 30 wt.% MAO solutions.

Quantification of the amount of "free" TMAL in a sample of MAO is a vital part of the jigsaw puzzle. For example, TMAL has been shown to: (i) assist in the activation and polymerization process or encumber it (depending on the precatalyst or leaving group); (ii) alter the kinetic profile of a catalytic system; (iii) affect molecular weights, polydispersity and stereoselectivity; and (iv) promote catalyst leaching or restrict the amount of "active" aluminum on a silica-supported catalyst. Exact quantification of the free TMAL content of an MAO solution is relatively problematic, and various physical methods have been employed including distillation under set conditions and colorimetric or thermometric titrations with phenazine or a sterically hindered alcohol, respectively. However, spectroscopic methods – notably nuclear magnetic resonance (NMR) – are by far the most common and routine means of quantifying the free TMAL content, although great care and experience is needed in interpreting the results. Typically, the "free" TMAL content can be in the range of 10 to 50% of the total aluminum content, depending on the synthetic route.

The extent of hydrolysis of the sample is usually measured by the amount of methane gas generated when a sample is digested with an aqueous acid. This, in combination with the aluminum content, provides a measure of hydrolysis, and is typically expressed as the ratio of Me/Al. By combining these results it is possible to determine the chemical formula of the MAO repeat unit. Consequently, after analyzing numerous samples, Imhoff et al. reported that the average chemical formula of the repeat unit was $AlMe_{(1.4)}O_{(0.8)}$ for unmodified MAO synthesized hydrolytically [24].

Molar mass measurements of MAO have long been a disputed area. Reported values range from 250 to 3000 Da, and are typically determined from cryoscopic or ebullioscopic measurements. Cryoscopic measurements are undertaken on the

dry friable form of MAO. As with NMR analysis, great care should be taken in analyzing these samples, as the presence of residual solvent, TMAL and process oil must all be taken into consideration when determining the molecular weight, as does the complete solubility of the MAO in the cryoscopic medium. For example, toluene solutions of MAO typically display a Tyndall effect indicating incomplete solubility, and may be considered more as colloidal dispersions. Therefore, a combination of cryoscopy and NMR is used to determine the average molecular weight. Typical values for unmodified MAO synthesized via hydrolytic routes, resulting from a combination of cryoscopy and NMR, are between 700 and 1500 Da. Taking into account the average chemical formula for the repeat units, the average MAO molecule consists of between 10 to 20 Al [20].

For supported catalysts, an estimation of the size of MAO may prove to be important when discussing its ability to diffuse into the variously sized pores of a support (see Table 4.1). For example, Talsi et al. utilized ^{27}Al NMR [25], whilst Hansen et al. analyzed ^{1}H NMR spin-lattice relaxation time data to estimate the size of MAO [26]. The conclusion of Talsi's study was that MAO exists as oligomers that reversibly break into smaller MAO units on heating (120 °C). The sizes of these oligomers and smaller MAO units were estimated to be 13–15 Å or 9–11 Å in diameter, respectively. Hansen reported an estimated value of 19–20 Å for MAO at ambient temperature; however, when the model was applied to MAO at 120 °C a calculated value for the diameter of 8 Å was found, which was in good agreement with the value reported by Talsi at the same temperature. In a related study, Babushkin and Brintzinger reported data on the size of the [Me–MAO]- anion, determined from pulsed-field gradient NMR experiments [27]. An observed mean effective hydrodynamic radius of 12.2–12.5 Å was reported, from which the authors calculated that each MAO molecule consisted of 150 to 200 Al atoms, assuming a solid spherical shape and the volume occupied by a AlO(Me) unit, based on proposed small cage structures. Whilst the actual number of aluminum atoms present is highly debatable, given the assumption made, it is interesting to consider the results on the effective size of the [Me–MAO]- anion with regard to its possible mobility in the various pores of a silica support.

In the absence of precise crystallographic and spectroscopic characterization, several structural interpretations of the "real" or "active" components of MAO have been proposed. Although the initial models proposed linear chain or ring structures, these contain 2- and 3-coordinate oxygen and aluminum, respectively, which contradicts the multinuclear NMR measurements of 3- and 4-coordinate oxygen and aluminum atoms, and is much more in keeping with aluminum chemistry. As a result, linear ladder structures and 3-D structures such as nanotubes [28], and in particular cages, were proposed. At present, the favored structure for MAO is a cage [21], although nanotubes have also recently been suggested.

It should be noted, however, that the above studies have been carried out almost exclusively on MAO produced via the hydrolysis of TMAL, with very few investigations utilizing samples produced via non-hydrolytic means. Recently, Stellbrink and coworkers reported an extensive analysis of polymethylaluminoxane (PMAO-IP; Akzo Nobel) formed via a non-hydrolytic process [29]. The group utilized a

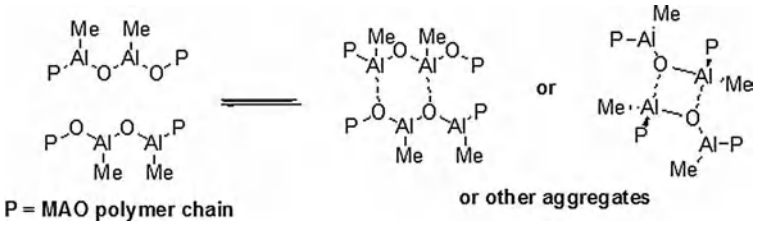

Figure 4.9 Proposed mechanism to account for chain branching in PMAO-IP.

combination of small-angle neutron scattering (SANS), fortified with static and dynamic light-scattering, ^{1}H NMR spectroscopy, and elemental analysis. As a result, it was proposed that most of the PMAO-IP existed in a linear polymeric form with [–Al(CH_3)O–] as a repeat unit (monomer), with methyl groups partially replaced by higher alkyl chains. The molecular weight for the polymer chains was estimated at 20 kg mol^{-1}, corresponding to an average degree of polymerization of ≈300 and a radius of gyration of ≈46 Å. An increased volume fraction of the MAO led to a proposed chain-branching mechanism seen in Figure 4.9. Finally, the group reported that only 0.8% of the PMAO-IP forms large-scale 3-D aggregate structures with a size ≥1000 Å, with a higher oxygen : aluminum ratio and lower alkyl content.

4.2.2.3 MAO Interaction with a Precatalyst Complex

One of the main goals in the development of single-site catalysts is to understand how such a precatalyst is activated and interacts with the various species in MAO. The hope is that, with a better understanding of the important species present in MAO, and which are surplus to requirements, it might be possible to design routes that selectively synthesize and/or immobilize such species. As a result, catalysts with dramatically improved activities (metal activity), productivities (increased metal loading capability) and selectivities may possibly be created. Unfortunately, at present a complete understanding of the interactions and various species formed between MAO and single-site catalysts is not available. However, it is known that the species present in MAO may have a considerable effect on catalyst activity, kinetic profile, stereoselectivity and molecular weight capability. These interaction depend upon a combination of the precatalyst complex, leaving group, the type of MAO, the metal : aluminum ratio, and the solvent and temperature.

It is generally believed that MAO first acts as a methylating agent for the precatalyst (where needed), and then generates an active cationic metal center, by abstraction of one of the leaving groups. However, while this is the most probable route to the active catalyst, it is in fact a rather simplistic view, even for the ubiquitous zirconocenes. In reality, and following many excellent spectroscopic investigations, several species have been identified and structures proposed, at differing aluminum : metal ratios (Figure 4.10) [20, 21, 30].

Recently, Brintzinger et al. utilized ultraviolet (UV)/visible [31] and NMR [32] spectroscopies to study MAO interaction with $Me_2Si(Ind)_2ZrCl_2$ and labeled

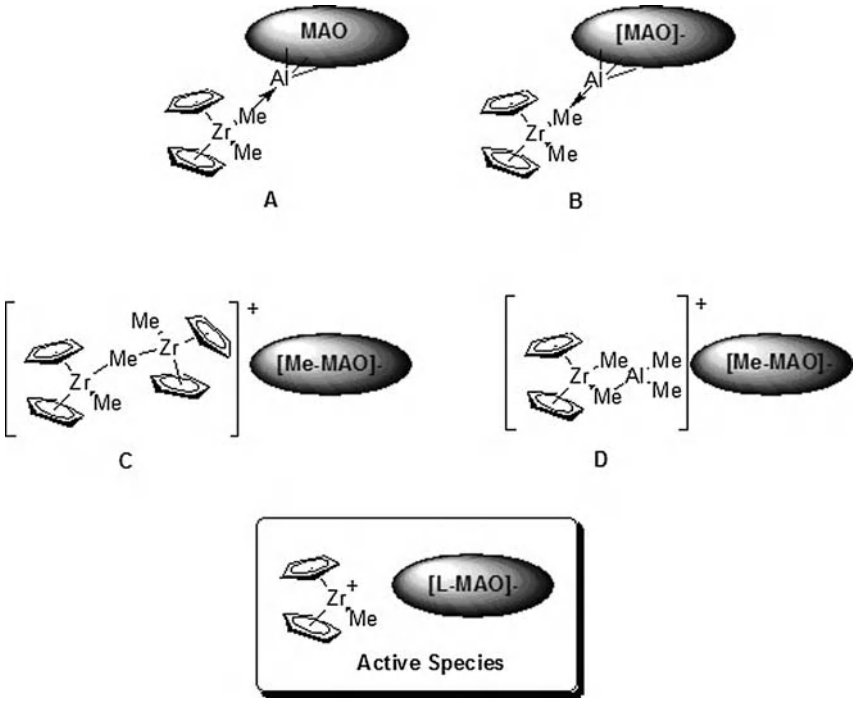

Figure 4.10 Some of the structures proposed to exist when MAO and Cp_2ZrMe_2 are contacted together under varying ratios (Al : Zr).

$(MeCp)_2ZrCl_2$, respectively. The results led this group to propose a highly interesting concept, namely that two forms of MAO existed, with two distinctly different forms of [Me–MAO]- anions being generated, with different equilibria. Apparently, strongly Lewis acidic forms of MAO, which comprise a small fraction of the total Al content of the MAO, are the key to obtaining highly activated systems. The group further postulated that a substantial reduction in the amount of excess MAO needed to fully activate a zirconocene could be achieved by a greater fraction of the strongly Lewis acid form of MAO.

4.2.2.4 MAO Interaction with a Silica Surface

The reactions of MAO and its component species (e.g., TMAL) with a silica surface have been studied by several groups employing a variety of analytical, spectroscopic and theoretical techniques, or a combination of these. As a result, numerous surface species have been proposed. For example, Bartam et al. proposed a chemisorption model for the interaction of MAO with a silica surface based on Si–Me and Al–Me population ratios [33]. In the surface model, a monomethyl–aluminum complex and methyl groups bound to silicon atom are proposed to be the predominant surface species at room temperature (Figure 4.11). It should be noted that the surface aluminum species are 3-coordinate, and should in principle

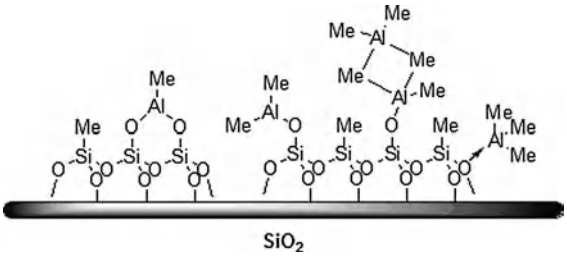

Figure 4.11 Proposed surface alkyl aluminum species.

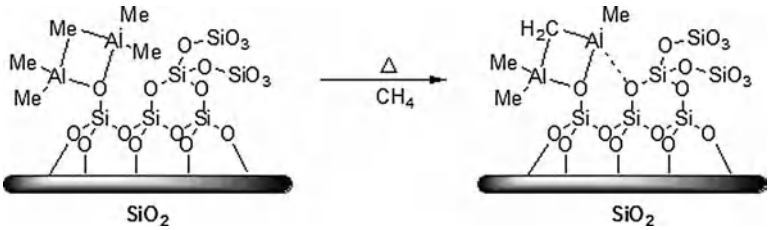

Figure 4.12 Generation of bridging methane species.

be highly reactive Lewis acids, with the potential to abstract a leaving group from a single-site catalyst and generate an active catalyst.

Scott and coworkers challenged many of the proposed structures formed when TMAL is contacted with a silica surface, in their case Aerosil 380 (calcined at 500 °C) [34]. This comprehensive study was not based on one particular analytical technique, but rather was built from the ground up, with quantitative (analysis of volatiles and surface organometallics) and spectroscopic (infrared, ^{13}C, and ^{29}Si solid-state cross-polarization/magic angle sample (CP/MAS) NMR analysis. The main product in their case was believed to result from the reaction of an isolated surface silanol and the dimeric form of TMAL (Figure 4.12). The proposed structures also contained 4-coordinate aluminum, which appeared to be much more realistic. Interestingly, the group also found that, at elevated temperatures, the surface alkylaluminum species could undergo C–H activation reactions to form a methylene-bridged complex (Figure 4.12).

Studies on the interaction of an alkyl aluminum with silica have included elegant NMR spectroscopic analyses. For example, Maciel and coworkers used multinuclear solid-state CP/MAS NMR to analyze the effect that methylating agents (MeLi, MeMgBr, and TMAL) have on a "dried" and $SiMe_3$-capped silica surface. The initial studies focused on the generation of Si–Me groups resulting from the cleavage of surface (Si)–O–(Si) or (Si)–$OSiMe_3$ linkages, rather than the actual alkyl aluminum species. The results indicated that TMAL cleavage of the (Si)–O–(Si) linkage occurred to only a minor extent, while the (Si)–O–$SiMe_3$ linkage remained significantly intact [35]. More recently, the group focused on the surface species formed by the reaction of TMAL with silica. Here, TMAL was contacted with a high-surface-area silica gel ($500\,m^2\,g^{-1}$), which had been dried

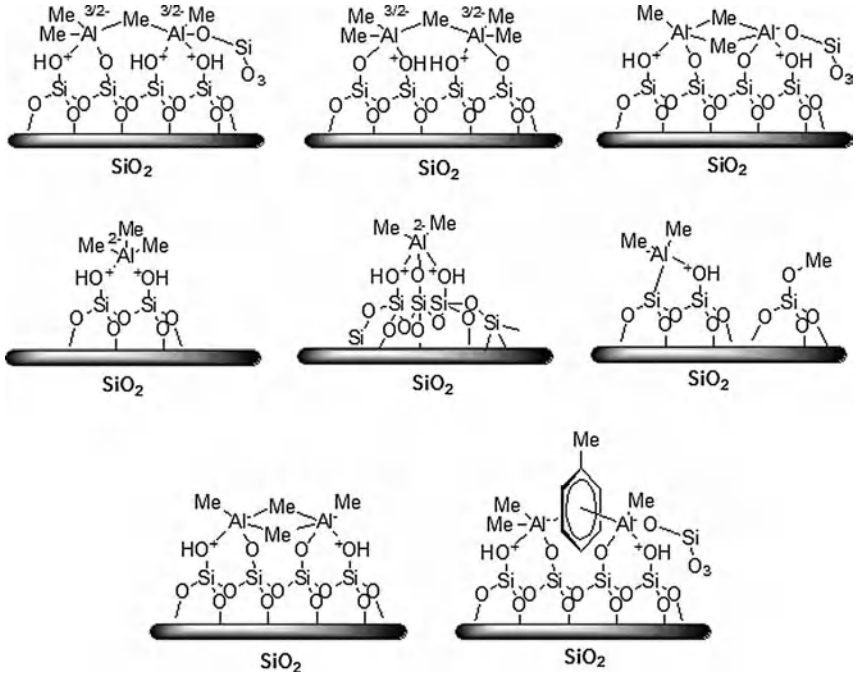

Figure 4.13 Proposed surface species as identified by Maciel et al. [34].

in vacuo at 150 °C. An analysis of results led the group to propose a considerable number of hypothetical surface species, some of which are illustrated in Figure 4.13 [36].

The results of infrared (IR) studies on TMAL/SiO_2 and MAO/SiO_2 interactions led Zakharov et al. to propose that the terminal surface silanol groups react rapidly with TMAL via protolysis to yield methane, with a slower reaction and chemisorption of the MAO to the surface [37]. The determination of adsorption isotherms for TMAL and MAO on silica, as well as *in-situ* monitoring of the interaction, via IR and diffuse reflectance IR spectroscopy (DRIFTS), have been employed by dos Santos et al. [38]. The DRIFT spectra taken from calcined Davison 948 (600 °C) before and after treatment with various levels of MAO are shown in Figure 4.14. The sharp peak at 3747 cm^{-1} was assigned to isolated silanol groups, and the broad band centered at 3692 cm^{-1} to silanol groups retained inside the pore (intraglobular). It can be seen that, at low MAO contents (1.0–6.0 wt.% Al), there is still a fraction of isolated silanol groups which are totally consumed at higher contents (8.0–24.0 wt.% Al). Zakharov's group also proposed that, for preparations above 12 wt.% Al, part of the MAO remained only physisorbed on a MAO-coated support, and might be at least partially removable (leachable). Aluminum levels below 12 wt.% correspond to typical industrial preparations involving such calcined silicas, where leaching is not observed. However, it should be noted that situation relates to only one type of silica calcined to one temperature, and the distribution of aluminum across the particle(s) was not disclosed.

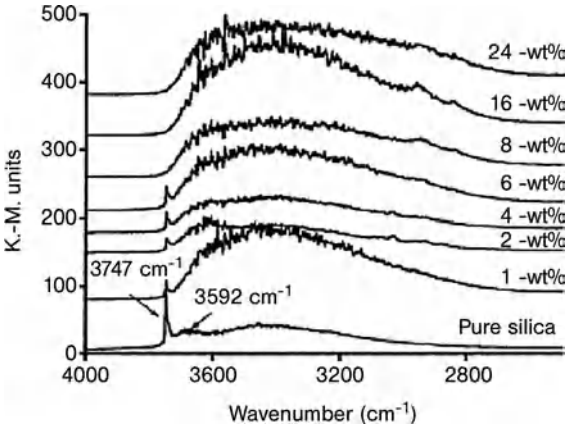

Figure 4.14 DRIFT spectra of MAO-modified silicas, with Al content ranging from 0 to 24 wt.% Al/SiO_2. (Reproduced with permission from Ref. [38]; © 2001 Elsevier.)

It is interesting to note that supported activators have been generated by the reaction of an alkyl aluminum compound with silica. However, this is achieved by the hydrolysis of TMAL, in the presence of a silica support that contains absorbed water, thus generating an aluminoxane cocatalyst *in situ* [7]. Chang prepared silica-supported aluminoxanes via the hydrolysis of TMAL and/or AlR_3 (R = Et or *i*Bu) with "undehydrated" or hydrated silica (ca. 5–35 wt.% H_2O) suspended in a hydrocarbon diluent [39]. Improvements in activity were noted when the supported aluminoxanes were either aged [40] or heat-treated [41].

It should be noted that all of these studies on the interaction of silica and alkyl aluminum are intimately related to the physical properties and calcination temperature of the silica, as well as to the alkyl aluminum used.

4.3 Catalyst Preparations

Although numerous individual synthetic strategies have been employed to produce a catalyst from a combination of MAO, silica, and a precatalyst complex, they fall into three basic routes (Figure 4.15). The MAO or alkyl aluminum source can first be contacted with the silica, whilst the precatalyst complex (or MAO-activated complex) is introduced in a subsequent step (Route A). Activation of the precatalyst with MAO prior to impregnation of the silica (Route B) is one of the simplest and most effective methods. The third approach (Route C) involves the introduction of the precatalyst to the silica support prior to contact with MAO.

It is not the goal of this chapter to provide a full review for each and every preparation that has been employed, but merely to provide selective illustrative examples of each synthetic strategy. In addition, it is difficult to predict which route to choose or start with for a particular precatalyst, to generate an industrially

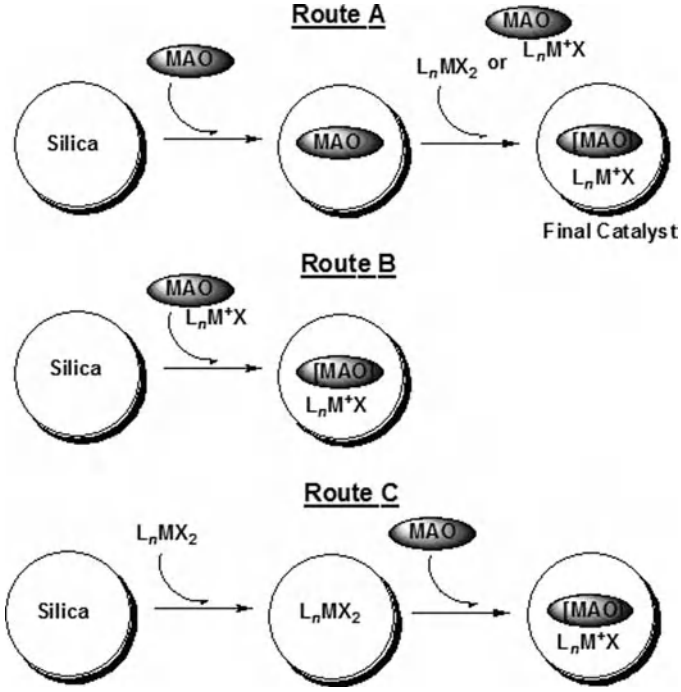

Figure 4.15 Schematic representation of the various synthetic strategies.

applicable catalyst. It should be borne in mind that there is no universally recommended route for all catalysts, and as a result a considerable amount of investigative research will be needed to identify the optimum preparation for a particular precatalyst family. That said, however, there are some general "rules of thumb".

Route C is usually avoided as it is difficult to predict how the tailored ancillary ligand system of a precatalyst will interact/react with the silica surface, particularly for ancillary ligand systems that are susceptible to protolysis. In addition, close contact to the support surface may affect the local steric environment. It is, therefore, hardly surprising that successful examples of grafted post-metallocene complexes are so rare. Typically, routes A or B are employed, particularly for industrial applications. If the precatalyst is stable towards prolonged contact with MAO, then routes A or B are available. However, should the precatalyst/MAO solution be unstable or susceptible to over-reduction or any other common deactivation mechanism [20, 30], then route A, avoiding any MAO-complex precontacting stage, would most likely be the best starting point.

4.3.1
Illustrative Examples of Route C

As mentioned previously, precontacting silica with a precatalyst, prior to the addition of MAO, is not a common procedure for immobilizing a catalyst. One of the

main reasons for this is to predict how the various surface hydroxyl groups would interact with the metal center, and how the resultant species would interact with MAO. The effects of silica calcination temperature and grafting reaction conditions on the performance of such systems have been studied extensively by dos Santos and coworkers [42]. This group dehydroxylated silica *in vacuo* at various temperatures between room temperature and 450 °C, and reacted these with solutions of $^{n\text{Bu}}Cp_2ZrCl_2$ at different contact temperatures and times. Silica pretreated at a higher temperature led to lower catalyst loadings, but when contacted with MAO it afforded catalyst systems with higher activities and produced resins of higher molecular weight and narrower MWDs. High grafting temperatures and long contact times led to higher metal contents, but reduced the activity of the system. The polarity of the metallocene solution seemed to have little effect on metal loading or final activity, whereas a coordinating solvent such as tetrahydrofuran led to a more active system, albeit with lower metal contents. An analysis of the supported zirconocenes indicated the presence of two different surface species, one of which was believed to be inactive, possibly due to a combination of steric and electronic considerations. Additionally, the amount of residual silanol groups on the support following contact with the zirconocene was believed to affect the catalytic performance of the system. dos Santos and colleagues also studied the grafting reaction of several other metallocenes on silica dehydroxylated at 450 °C *in vacuo*, in the hope of understanding how the steric bulk on the metallocene affected the grafting process. The metal contents were found to depend on the metal center (Ti < Hf < Zr), the coordination sphere, and the support. Alkyl substitution of the cyclopentadienyl ligand had no significant effect on the metal loadings of the catalyst, and the inductive effect of the substituent had a greatly reduced effect on the activity in ethylene-*co*-1-hexene polymerization, when compared to the corresponding homogeneous systems. Furthermore, the ethyl-bridged indenyl derivatives gave higher metal contents than the more bulky dimethylsilyl-bridged analogues [43].

4.3.2
Illustrative Examples of Route A

Precontacting a toluene or aliphatic hydrocarbon solution of MAO with a calcined silica, followed by washing, drying, and reaction with an appropriate precatalyst, is one of the earliest and most frequently used and commercially available means to facilitate the immobilization of single-site α-olefin polymerization catalysts. Welborn [44] and Takahashi [45] were among the first to disclose the contacting of silica with a toluene solution of MAO. In both cases, isolation and treatment of the silica-supported MAO with a dichloride or dialkylmetallocene yielded supported single-site catalysts that were effective in the homopolymerization and copolymerization of ethylene in a stirred-bed, gas-phase process. Similar procedures have been reported for a range of precatalysts [7].

Employing a heat-treatment regime in a particular step(s) of the supportation procedure has been reported to improve not only the fixation of MAO to the silica

surface but also the performance of the finished catalyst. Razavi, Gauthier and coworkers at Fina found that refluxing the silica/MAO toluene suspension prior to contact with a C_2- or C_1-symmetric metallocene improved the stereoselectivity and activity of the finished catalyst and yielded polymer resins with good bulk density and morphology [46, 47]. The catalyst efficiency was also strongly related to the temperature used in supporting the metallocene onto the MAO-treated silica. Higher catalytic activities of the finished catalysts were observed when low contact and washing temperatures (–20 to 0 °C) were employed during fixation of the metallocene.

The same group also showed that the silica support plays a crucial role in the final activity of the catalyst system. MAO/SiO_2 samples were prepared as above on three different types of silica (weight ratio of $MAO : SiO_2 = 0.61–0.65 : 1$) and contacted with $Me_2Si(2\text{-Me-4-PhInd})_2ZrCl_2$ at differing loadings. The productivities for catalysts derived from these systems are shown graphically in Figure 4.16. At a 1 wt.% loading of complex on the MAO/SiO_2, similar productivities were obtained with all three silicas. However, when the catalyst loading was doubled, a vast difference in performance became apparent among the silicas. Interestingly, it was proposed that a large "critical pore diameter" (CPD) – which is defined as the pore volume after contacting the silica pore with MAO and complex – is crucial to achieving high activity, and that the appropriate CPD is facilitated by a combination of heat fixation of MAO and an appropriate support.

A highly effective means of thoroughly fixing the MAO to a silica surface was reported by Jacobsen and coworkers at Dow [48]. The procedure involved the room-temperature treatment of calcined (250 °C) or hydrated silica with a toluene solution of MAO. The toluene was then removed *in vacuo*, rather than being filtered or decanted, to afford a dry solid silica/MAO mixture that was subjected to a heat treatment step (100–200 °C, ca. 2 h) prior to being washed with toluene (20 or 90 °C)

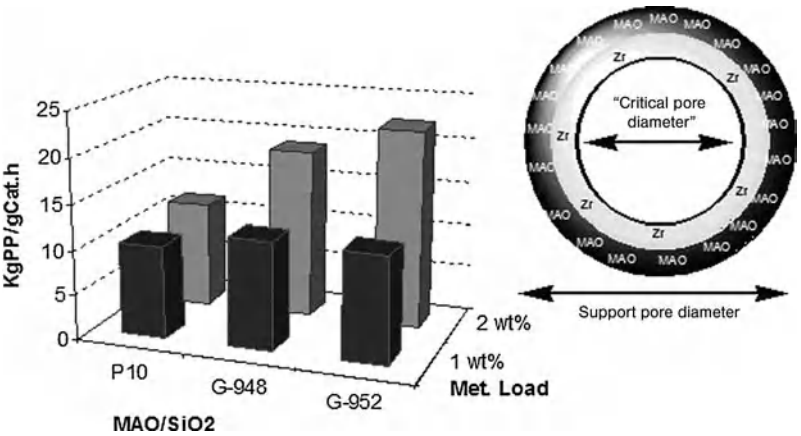

Figure 4.16 Effect of silica and complex loading plus schematic representation of the critical pore diameter (P10 from Fuji Sylsia; G-948 and G-952 from Grace Davison).

and dried *in vacuo* (100–120 °C, ca. 1 h). An analysis of the various supports showed that heating the dry solid silica/MAO led to a more thorough fixation of the aluminum and, presumably of MAO, to the surface of the support. The washing steps were needed to remove the "non-fixed" aluminoxanes, and additionally allow for a dispersion of any agglomerated particles that might have formed during the heating step, thus providing a particle size distribution similar to the starting support. The Dow group subsequently discovered that, for the constrained geometry catalyst, $Me_2Si(C_5Me_4)(^tBuN)TiMe_2$, a synthesis strategy which involved a combination of uncalcined silica treated with MAO, followed by a thermal heat treatment of the dried resultant mixture (silica-supported MAO, or SMAO), yielded a catalyst with higher activity than those derived from other combinations (Figure 4.17). The patent also contained claims for a supported single-site catalyst with an aluminum content of between 15 and 40 wt.%; once again, this places restriction on competitors wishing to utilize this or other methods to produce high-aluminum-loaded catalysts.

Heating a toluene solution of MAO (30 wt.%) at an elevated temperature (50–80 °C) for prolonged periods (1–7 h), prior to contact with vacuum-dried silica (200 °C), is also claimed to yield benefits. Diefenbach and coworkers at Albemarle compared such supported activators to samples prepared without heat treatment in the copolymerization of ethylene and 1-hexene, using *rac*-$Et(Ind)_2ZrCl_2$. The results showed that heat-treating the MAO solution prior to contact with silica led to appreciable improvements in catalytic activity (ca. 25%) and product morphology [49].

The chemical modification of MAO before or after supportation has been reported to lead to specific improvements in a supported catalyst performance. The isolation of solid MAO and its depletion of TMAL was utilized by Meijers et al. [50]. The group added solid MAO to a suspension of dried silica (150 °C, 10 h, N_2 flow) in toluene at room temperature. On completion of this reaction, a solution of the low-valent precatalyst complex, $Et(Cp'')(NMe_2)TiCl_2$ (Cp″ =

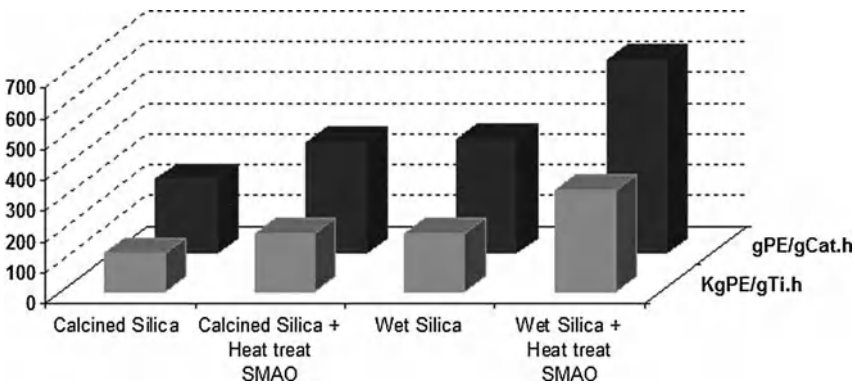

Figure 4.17 Effect of supporting strategy on the performance of $Me_2Si(C_5Me_4)(^tBuN)TiMe_2$-based catalysts.

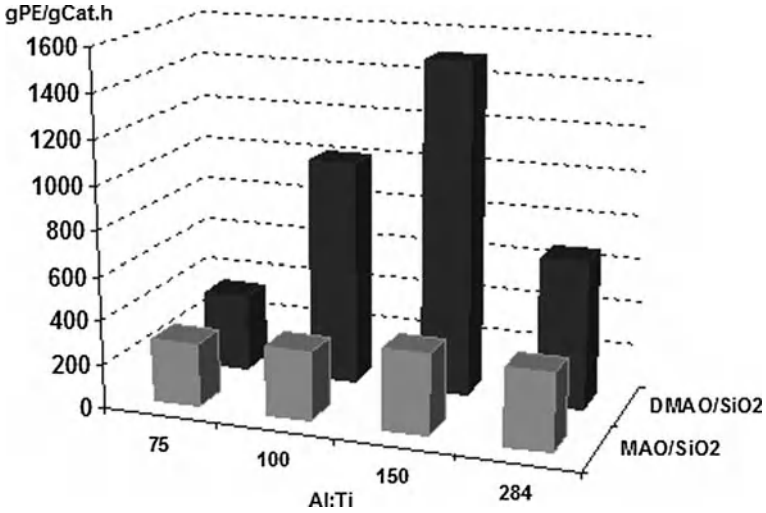

Figure 4.18 Polymerization performance of supported, low-valent geometry precatalyst, illustrating the benefits of employing depleted MAO (DMAO) in the catalyst preparation.

2,4-$(SiMe_3)_2Cp$) was added and allowed to react with the SiO_2/MAO prior to removal of the solvent *in vacuo*. The isolated catalyst, when used to homopolymerize ethylene at various pressures and Al/Ti ratios, was considerably more active than a comparative example synthesized using the commercial MAO (Figure 4.18).

Jeremic and coworkers at Nova Chemicals reported that the addition of cellulose to MAO afforded "sweet" MAO which, when contacted with calcined silica (600 °C) and used in conjunction with (Ind)(^{t}Bu$_3$P=N)TiCl$_2$, yielded a catalyst that was more active than the corresponding cellulose-free protocol in ethylene-*co*-1-hexene polymerization [51]. The cellulose presumably reacts with the free TMAL in MAO, which most likely has an adverse affect on the complex.

Alternatively, chemical modification of the inorganic oxide support with an organic, inorganic or organometallic complex has been used to: (i) remove the surface hydroxyl groups; (ii) produce a more uniform surface species; (iii) add an additional functionality; or (iv) alter the electronic properties such as the number and nature of Lewis and Brønsted acidic sites of the support. The most common organic surface modifiers have been chloro- or alkoxy-silanes [52–54]. Gao and coworkers disclosed an example of a fluorine-modified silica, by contacting the support with an aqueous solution of NaF. Drying the modified support in air, followed by calcination under N_2, afforded a fluorinated support which, when consecutively contacted with MAO and (Ind)(^{t}Bu$_3$P=N)TiCl$_2$, afforded supported catalysts with higher activities than the corresponding "un-fluorinated" support [55].

4.3.3
Illustrative Examples of Route B

The combination of a solution of the precatalyst with MAO, prior to contact with a silica support, has become a frequently utilized and successful technique for producing a supported, single-site α-olefin polymerization catalyst. The process has several advantages, notably from an industrial viewpoint. For example, it reduces the amounts of solvent used and byproducts produced, and also involves a limited number of steps, particularly the time- and energy-intensive steps such as drying. All of these benefits typically result in a lowering of manufacturing costs. In addition, precontacting allows MAO to solubilize a poorly soluble precatalyst prior to impregnation, and can also allow a more effective activation of the metal center (for certain complexes) to be carried out in a homogeneous solution rather than in a heterogeneous phase, where problems with diffusion or side reactions may occur.

An early and highly successful example of the above procedure was disclosed by Burkhardt and coworkers at Exxon [56]. In this protocol a metallocene precatalyst was initially contacted with a solution of MAO prior to contact with calcined silica. The slurry of metallocene/MAO/SiO_2 was then mixed together, whilst the temperature was gradually elevated (to ca. 50 °C). At about the same time, the research group at Hoechst were seeking an effective means of immobilizing some of the first commercially interesting C_2-symmetric metallocene precatalysts, such as $Me_2Si(2\text{-Me-4-PhInd})_2ZrCl_2$ and $Me_2Si(2\text{-Me-4-(1-Napth)Ind})_2ZrCl_2$ [57]. The precatalysts performed exceptionally well in the homogeneous solution polymerization of propylene, affording catalytic systems with MAO that possessed high activity, stereoselectivity, and molecular weight capability. However, the retention of all these features on immobilization had presented a much greater challenge, and a subsequent collaboration between Exxon and Hoechst led to a successful combination of the respective precatalyst and immobilization technologies. Modifications to the basic procedure of adding a MAO/precatalyst solution to a silica support have been reported to afford dramatic improvements in activity and/or morphological control. Allowing a solution of MAO and $Me_2Si(2\text{-Me,4-PhInd})_2ZrCl_2$ to stand in the dark overnight before addition to silica is also reported to lead to an almost doubling in activity when compared to catalysts derived from an immediate contact with the support [58].

The pacification of a silica surface with an alkyl aluminum complex prior to contact with a solution of MAO/precatalyst is commonly encountered, particularly for commercially applicable stereoselective complexes. Once again, this is most likely due to the fact that the highly tailored metal centers of such complexes can be easily perturbed by steric and/or electronic influences of the support material [7]. If the alkyl aluminum complex is MAO, this could be considered as a "hybrid" version of Routes A and B in Figure 4.15. However, whilst such a route may be beneficial, it may also add further complexity or flexibility, as consideration must be given as to what fraction of the total MAO should be added at the silica and precatalyst steps.

This delicate balance has been elegantly demonstrated by Winter and coworkers at NTH [59], who started with a set amount of silica, MAO and *rac*-Me_2Si(2-Me-Benz[*e*]Ind)$_2ZrCl_2$, but varied the fractions of the total MAO to be added to the silica and *rac*-Me_2Si(2-Me-Benz[*e*]Ind)$_2ZrCl_2$ stages to produce a number of catalysts. In addition, the group investigated the effects of heat treatment and washing of the MAO/silica. The representative results of these investigations are listed in Table 4.2. Once again, heat treatment of the MAO/SiO_2 was extremely beneficial in terms of catalyst productivity when compared with preparations **1** and **2** and also the "route A-type" preparations **6** and **7**. However, the percentage of total MAO added to the silica or complex before heat treatment was also clearly critical (Table 4.2, c.f. preparations **1**, **3**, and **7**). The catalyst with the highest productivity demonstrates the potential cumulative benefits of such a route, and this is achieved by a combination of a high percentage of the total MAO contacted with silica, followed by heat treatment and washing of the resultant product, before the addition of the complex previously contacted with a low percentage of the total MAO. Those skilled in the art will understand that there might be considerable variation in the SiO_2 : MAO:Complex ratios found in each of the final catalysts, despite the set ratio used in the total synthesis. However, this example clearly demonstrates the complexity/flexibility available by combining a set amount of one complex, one type of MAO (manufacturer, wt.%, degree of hydrolysis and residual TMAL) on one type of silica (average pore volume and particle size, surface area and calcination temperature) in various ways.

Much effort has been made to support metallocene/MAO catalysts on silica which has been chemically modified by an inorganic complex. Speca, for example, reported the chemical treatment of silica by solid $[NH_4][X]$ (X = F, SiF_6, PF_6 or BF_4), to produce a fluorine-modified silica. The modified silica, when treated with a metallocene/MAO solution, afforded catalysts that were up to three times more active than comparative "unmodified" examples, in the bulk polymerization of propylene [60].

It is important, for a number of reasons, to ensure that a substantial proportion of the active sites are present in the inner volume of the catalyst particle, and to reduce waste and byproduct formation. To this end, a major commercial advance has been the development of controlled pore-filling or "incipient wetness" tech-

Table 4.2 Effect of supporting strategy on the performance of *rac*-Me_2Si(2-Me-Benz[*e*]Ind)$_2ZrCl_2$-based catalysts.

Catalyst preparation/Steps	**1**	**2**	**3**	**4**	**5**	**6**	**7**
MAO + SiO_2 (% total MAO)	83	83	33	33	33	100	100
Heat treatment of MAO/SiO_2 (reflux 4 h)	Yes	No	Yes	No	No	No	Yes
Washing of MAO/SiO_2	Yes	No	Yes	No	Yes	Yes	Yes
MAO + Complex (% total MAO)	17	17	67	67	67	0	0
Productivity (kg PP g^{-1} Cat h^{-1}) (PP)	8.7	3.8	4.2	4.5	4.4	3.3	7.4
Productivity (kg PP g^{-1} Cat h^{-1}) (PP with H_2)	18	6.1	7.2	8.1	8	5.9	11.9

niques for the impregnation of silica with a solution of MAO or complex/MAO, or MAO/SiO_2 with a solution of complex. In these procedures, the volume of the desired active ingredient solution may be less than (60–95%) [61], equal to (100%), or slightly higher (125–150%) than the pore volume of the support. The desired active ingredient solution, in the majority of cases, is added slowly or incrementally to a stirred sample of support (calcined silica or dried MAO/SiO_2) [62]. In such preparations, capillary forces draw the active ingredient solution into the pores of the support, thus aiding impregnation of the complex to the inner surfaces of the support. However, it should be noted that the final distribution of the active ingredients across the whole support material is non-equilibrium-driven, and sometimes passing the mud-point and entering a slurry (typically >150% pore volume support) state is beneficial to reach a more equilibrium-driven environment (for example, see Figure 4.19) [16]. It should be noted that with all preparations the amount of energy needed to mix the components in the dry, mud or slurry states,

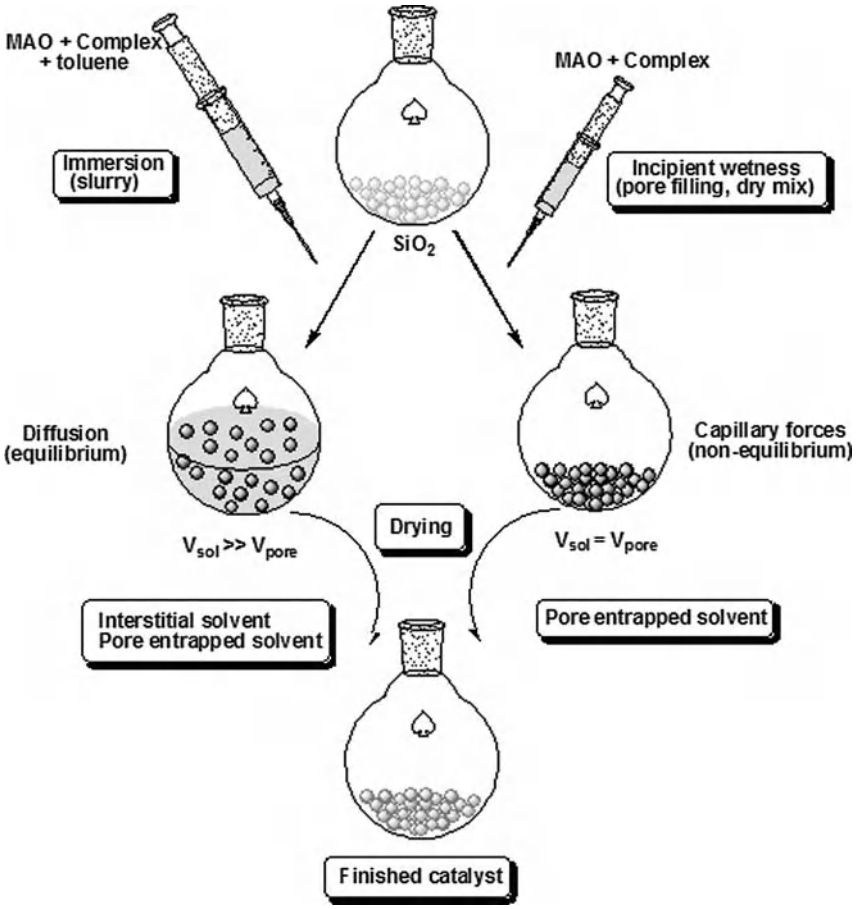

Figure 4.19 Schematic representation of various impregnation regimes [16].

and/or the transitions between the states during filling or drying, may need to be considered.

At this point it is prudent to mention the amount of residual hydrocarbon (typically toluene) which is left in the final catalyst, and some of the consequences. The porous supports and substrates discussed above are absorbent materials which can absorb substantial amounts of solvent while appearing to be dry. A careful understanding of the drying process of the final catalysts is required, as variations of time, temperature, inert gas flow rate, vacuum – or a combination of all these – may lead to substantially different hydrocarbon residue contents (from ~30 to ~1 wt.% catalyst). As the hydrocarbon is an inert material, it can be seen that the productivity (kg polymer g^{-1} catalyst) may be seriously affected by high hydrocarbon contents. Another factor in the drying processes that must be considered is the amount and rate of energy that can be introduced, which is frequently either complex- or catalyst-dependent.

4.3.4
A Summary of Catalyst Preparations

As might be imagined from the illustrative examples provided above, there is an almost infinite number of combinations of synthetic procedures, silica supports, reagent ratios/loadings and modifications that are available for a single precatalyst complex. Again, it should be borne in mind that commercial immobilized single-catalysts are designed to create a desired polymer resin in a certain dictated process. Therefore, an acceptable balance of several factors such as productivity, operability in the desired processes, kinetic profile and polymer morphology is needed, and although catalyst productivity is important, it is not the sole consideration. However, it is pertinent to remember the old saying that, "there is more than one way to skin a cat", and keep in mind that different processes may demand a different balance of the above factors to achieve a commercially viable catalyst for the same target resin, not forgetting proprietary technologies.

What hopefully is clear is that there is no standard procedure that suits all cases, and a substantial amount of thoughtful, well-designed systematic experimental work and research (FTO studies, etc.) is required when searching for a beneficial protocol to produce a commercially viable, immobilized, single-site catalyst.

4.4
Pitfalls in the Generation of Single-Site Polymer Material

As mentioned in Section 4.1, one of the advantages of homogeneous single-site α-olefin polymerization catalysts is the ability to rationally improve and tailor the polymerization performance and resultant resins. Several polymer products produced by such single-site catalysts, via either homogeneous or immobilized forms, have been commercially available for more than 10 years. However, throughout this chapter there have been numerous examples where a supported catalyst

derived from a combination of the precatalyst, MAO and silica dramatically alters the catalyst performance and resultant polymer resin, when compared to the corresponding unsupported system. It may, therefore, represent much more of a challenge to rationally tailor the microstructure of the polymer resin. It is also difficult to characterize the supported species, especially when the heterogeneous nature of the catalysts and the "black box" that is MAO are taken into consideration.

Ironically, more often than not it is the resultant polymer resin that has allowed a better understanding of the actual active site(s) at work. Busico eloquently proposed that the microstructure of the polymer chain could be considered as a "nano-tape" recording of what has occurred at an active site during propagation [63]. A variety of complementary analytic and spectroscopic techniques must be employed to study the polymer resin and the active species that produced it. Often, a basic analysis of molecular weight, MWD and melting temperatures is not sufficient to fully understand what is happening in the system. For example, the chemical composition distribution of a copolymer of ethylene and higher α-olefins (propene, 1-butene, 1-hexene or 1-octene) is one means of gaining useful information about the nature of the active site, and this is commonly determined through techniques such as temperature-rising elution fractionation (TREF) or crystallization temperature fractionation (CRYSTAF).

4.4.1 The Polymerization Experiment

Having stated that an analysis of the polymer resin is a useful technique for studying the effect that different immobilization techniques and starting materials have on a catalyst, it is important to bear in mind that a rigorous understanding and control of the polymerization experiment itself is essential, as artifacts of polymerization may lead to misinterpretation of the data generated from polymer analysis. Predominantly, laboratory/bench-scale polymerizations are carried out in batch or semi-batch reactors, where all reagents except the monomer are added in one batch, typically at the start of the polymerization. The monomer is then usually added on-demand to maintain a constant pressure. This is notably different to the continuous industrial particle-forming processes used to produce PE and PP, where the monomer, comonomer(s), H_2, catalyst and diluent or carrier gas are added continuously at controlled ratios.

Laboratory/bench scale reactors operating in a batch/semi-batch mode may have a considerable drift in the concentration ratios of the monomer/comonomer/chain-termination agent (hydrogen). Drifts in the concentration of hydrogen are particularly acute with some supported single-site catalysts (e.g., metallocenes) due to their high hydrogen response, and this can result in significant changes in the reactant composition during the course of the polymerization. Blom et al. made several reports highlighting the dramatic consequence of hydrogen drift on the molecular weight MWD of homo-polyethylene produced with various supported metallocenes [64–66]. The consequences of hydrogen drift on MWD, due to varying

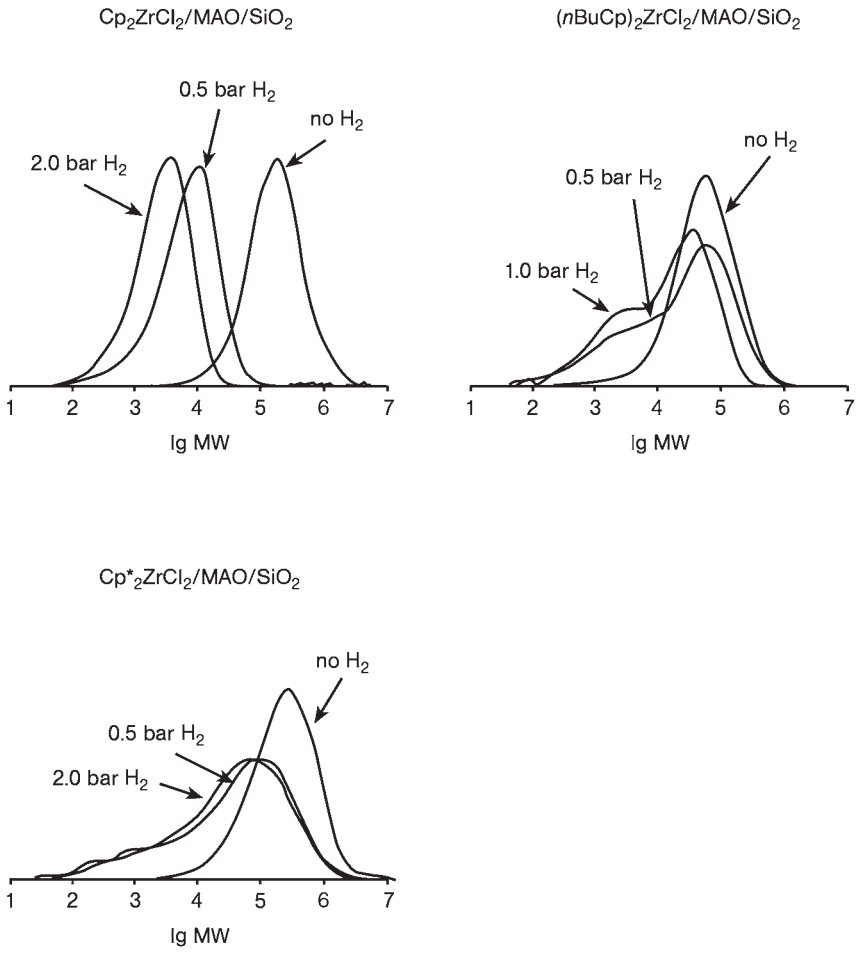

Figure 4.20 Consequences of drift in hydrogen concentration during a batch polymerization. (Reproduced with permission from Ref. [65]; © 2001 Wiley-VCH.)

reactivities of the metallocenes towards hydrogen and under the same conditions, are illustrated in Figure 4.20 [66].

The choice of diluent is as an important factor that can affect the final polymer properties. Commercial particle-forming processes use liquid monomer, fluidizing gas streams, or aliphatic hydrocarbons as diluents. Aromatic solvents such as toluene are not used in these processes. The solubility of MAO and single-site precatalyst/cocatalyst combinations is also much greater in toluene than in aliphatic hydrocarbons, which can lead to the appearance of multiple active sites, resulting from the homogeneous and heterogeneous polymerization of the same complex. In addition, commercial processes operate at the highest possible temperature for maximum efficiency, and at these elevated temperatures diluent-

induced swelling or solubility of the polyolefin particles produced becomes an important consideration, particularly for slurry-phase processes. The presence, type and amount of scavenger may also have a dramatic effect on the polymer and the polymerization rate [67].

4.4.2 Multiple Sites and Product Quality

4.4.2.1 Catalyst Homogeneity

Catalyst homogeneity in a heterogeneous, silica-supported catalyst may seem like a contradiction in terms. On the scale of the active complex, there will always be a considerable inhomogeneity in the "local" environment of the active sites, as a consequence of the heterogeneous nature of the initial support material. The variation in surface chemistry, area and pore size, shape and volume distributions that exist on a silica support can all be mirrored in the final catalyst. In addition, cross-contamination with a Ziegler or Cr catalyst may also affect the homogeneity of a catalyst. All of the above can have consequences for single-site catalysts and the polymer resins they produce.

The homogeneous distribution of active sites across the final catalyst particle is an important factor, irrespective of the chosen combination of procedures and starting reagents. A heterogeneous distribution of active sites across a particle can arise for various reasons, and the consequences are manifested in the polymerization process and the final polymer product.

A common method employed to provide an idea of the catalyst homogeneity on a microscopic scale is that of scanning electron microscopy/energy-dispersive X-ray (SEM-EDX) mapping of cross-sections of a catalyst particle. Silica and aluminum are the elements commonly mapped, as the active metals in question are typically too low in concentration to be accurately mapped. As a result, the assumption is that an active site can only exist in the presence of the aluminum-containing cocatalyst. Ideally, a homogeneous distribution of active sites throughout the catalyst particle is preferable to aid good morphological replication during polymerization.

The SEM-EDX micrograms of a catalyst with a large inter- and intra-particle variation in the distribution of active sites are shown in Figure 4.21. It can be seen that there are areas in the aluminum map with a high (red), moderate (green) or low (blue) loading of aluminum. When compared to the silica map, there are also areas where the aluminum has not impregnated the silica. Such distributions typically occur when poor mixing and/or a rapid addition of the MAO or MAO/ complex are employed.

By treating each individual catalyst particle as an individual "micro-scale polymerization plant" operating under the same global polymerization conditions, it can be seen that there is a large variation in the loading of active material from one catalyst particle to another, as well as particle size distribution, and that this results in "micro-plants" of varying capacities and "feedstock demands" (heat and mass balances) [14]. As a result of this, each catalyst particle could have a unique

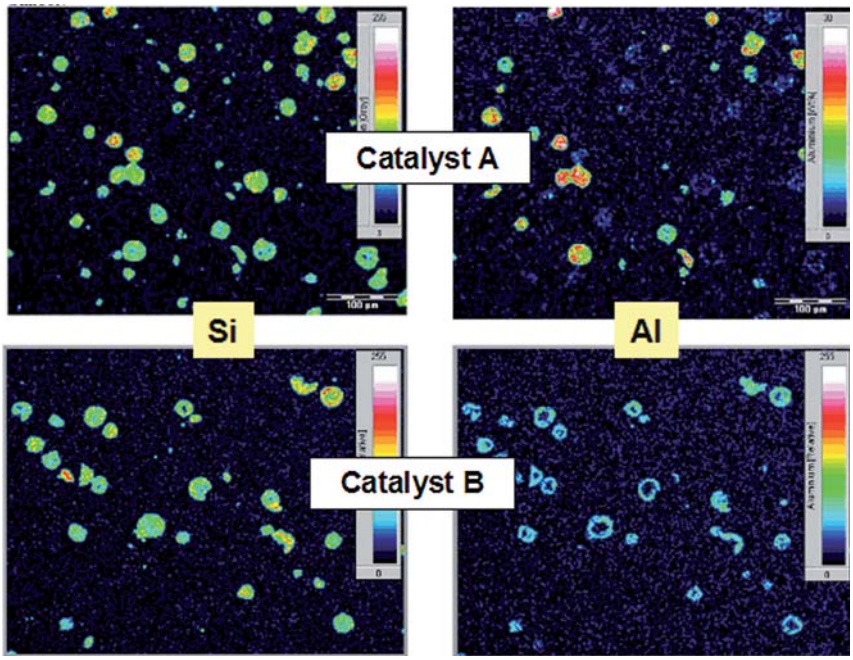

Figure 4.21 Scanning electron microscopy/energy-dispersive X-ray (SEM-EDX) images of a polymerization catalyst with inhomogeneous impregnation of active sites (Al) across the catalyst sample (catalyst A) and catalyst particle (catalyst B). (Reproduced with permission from Borealis Polymers.)

kinetic profile due to differing catalyst fragmentation or localized heat generation/dissipation behavior, particularly at start-up.

High loadings that result in localized overheating may be problematic, particularly in processes where heat transfer is less efficient, as the growing polymer particle may soften and form agglomerated particles, or even foul the reactor. Alternatively, or in addition, localized heating may cause catalyst deactivation or the production of polymer materials differing from the target resin in terms of molecular weight, tacticity or chain branching (short or long). In addition, catalyst particles with high loadings may not have the active sites firmly fixed to the support, and so may be prone to leaching and hence fouling under certain polymerization conditions. A combination of all of these factors may lead to the formation of polymer resins with more "multi-site" characteristics.

The core-shell distributions of aluminum atoms – and hence active sites – on a catalyst particle are another common form of catalyst inhomogeneity. The SEM-EDX micrograms of such a catalyst are illustrated in Figure 4.21. The aluminum resides at the surface of the catalyst particle, whilst the inner core remains unimpregnated, resulting in an inactive inner core. Core-shell distributions are generated as a result of deficiencies in either the synthetic strategies or the silica support.

Typical synthetic deficiencies arise from either an insufficient amount of MAO or MAO/precatalyst being contacted with silica, and/or an inadequate contact time which hinders the diffusion/migration of the reagents into the inner core, prior to drying or filtration. In the case where drying of the silica/MAO slurry is applied, there is an increased chance that active material is precipitated or becomes loosely associated to the surface of the support. Such material has an increased chance of leaching from the catalyst particle or polymerizing in an homogeneous phase. The absence of active material in the inner-core of the catalyst particle results in polymerization occurring at the outer surface. Little to no fragmentation occurs, and as a result the polymer particle formed has a void at its center. Due to the presence of hollow particles, the polymer produced has a low bulk density which can in turn affect plant throughput. In addition, large silica particles remain inside the hollow particle, and hence also in the polymer product (Figure 4.22).

The silica support material will always remain embedded in the polymer product, and the amount and particle size of these residues may have a strong influence on the final polymer. Commercial systems typically operate at productivities above 5 kg polymer g^{-1} catalyst, which results in less than 200 ppm (ash content) of the support material in the final polymer product. Ideally, these residues should be very small fragments, distributed homogeneously throughout the polymer matrix. The very small fragments (10–100 nm) characteristically consist of agglomerates of "primary particles" (1–10 nm), and are typically governed by the preparation procedure of the support [13]. Catalyst inhomogeneity, however, can cause a deviation from the ideal world, as described above. Carrier particles containing very low or no loading of the active material cause the appearance of relatively large silica fragments (silica gels) in the final polymer product. It should also be noted that

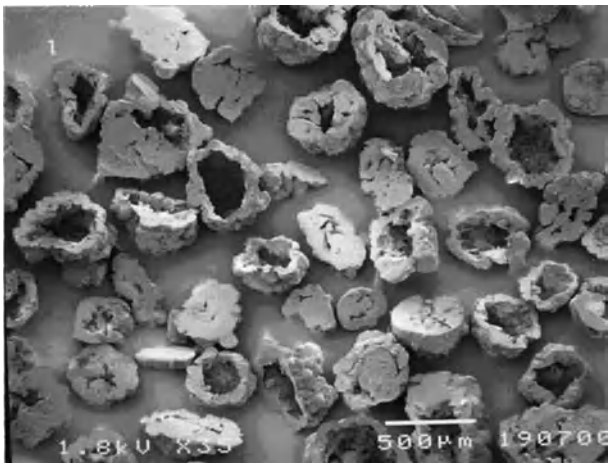

Figure 4.22 Scanning electron microscopy image of hollow polymer particles formed with a catalyst that had a core-shell distribution of active species. (Reproduced with permission from Borealis Polymers.)

silica gels can be formed by partial poisoning or deactivation of the catalyst during catalyst preparation, transportation, storage and transfer [68]. Impurities in the feedstock can also result in an increased occurrence of fouling, along with a loss in activity [68–70]. The presence and amount of silica gels in a polymer may be particularly crucial for the final polymer product application. For example, silica gels can seriously affect both the esthetic appearance and mechanical strength of film products. As an example, Figure 4.23 demonstrates how the presence of a "large" silica gel in a film can damage its integrity [16].

The cross-contamination of a single-site catalyst or its polymer resins with Ziegler- or Cr-based catalyst components or resins, during any part of the preparation, transportation, transfer, polymerization or processing, may result in the appearance of silica and/or polymer gels in the final product [69]. If the two catalyst systems are incompatible, any detrimental reaction between the two may lead to a partial poisoning, resulting in catalyst residues. However, cross-contamination usually results in the appearance of polymeric gels in the final product. This occurs due to the fact that single-site catalysts have drastically different reactivity ratios for molecular weight regulators or comonomers when compared to Ziegler–Natta- and Cr-based catalysts. Typically, a Ziegler–Natta or Cr catalyst operating under polymerization conditions suited for single-site catalysts will produce a polymer resin with a higher density and molecular weight. As a result, the polymer resins produced by the Ziegler or Cr catalysts may be immiscible with the bulk polymer phase produced by the single-site catalyst, and so appear as polymeric gels in the final product [69]. It should also be noted that polymer gels have been claimed to result from incomplete deactivation of the single-site catalyst following the polymerization reaction.

The results of various studies have also suggested that the pore size of a support can affect the activity and nature of the immobilized active sites. Sano et al. reported a segregation of MAO into different MAO species, and thus proposed

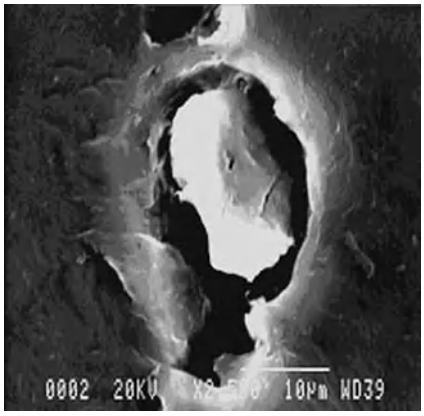

Figure 4.23 Scanning electron microscopy image of a catalyst residue in a polyethylene film. (Reproduced with permission from Borealis Polymers [16].)

that the pore size influenced the nature of the catalytic sites [71]. The effect of pore size on the resultant polymer was also studied by Wanke and coworkers [72], who identified a strong influence of the pore size of the support on gas-phase ethylene polymerization rates, as well as 1-hexene incorporation rates, for catalysts prepared by the impregnation of mesoporous molecular sieves with a range of narrow pore sizes (2.5 to 20 nm) with MAO and $^{n\mathrm{Bu}}Cp_2ZrCl_2$. The ethylene polymerization rates and 1-hexene incorporation rates decreased and increased, respectively, with increasing pore volume. A TREF analysis of the products indicated the presence of multiple types of active site, with the type and ratio being dependent on the pore size of the various supports.

4.4.2.2 Influencing the Coordination Sphere of the Active Sites

The decomposition or alteration of the active metal coordination sphere to form inactive or differing surface species can lead to a lowering of the activity of the catalyst, or the emergence of multiple distinct active sites. This in turn may lead to a broadening of molecular weight and chemical composition distribution, whether it be comonomer, stereo- or regio-selectivity. Collins et al. noted that the absorption of $Et(Ind)_2ZrCl_2$ onto silica afforded appreciable amounts of bis(indenyl)-ethane in the grafting solvent [73]. Such decomposition was believed to derive from the reaction of the metallocene framework with one or more surface silanol groups, though surprisingly no decomposition was reported with $Et(Ind\text{-}H_4)_2ZrCl_2$. The decomposition of a metallocene coordination sphere has also been proposed to explain the inactivity of silica-supported systems derived from *rac*-$MeO_2Si(Ind)_2ZrCl_2$ and di[(1′*S*,2′*R*, 5′*S*)-menthoxy]silylene-bis[1(*R*,*R*)-(+)-indenyl]zirconium dichloride [74].

The choice of synthetic strategies plays a crucial role in determining the type of catalyst formed. For example, Sacchi and coworkers reported that Ind_2ZrCl_2, which produces atactic PP under homogeneous conditions, produced moderately isotactic PP when grafted onto silica first prior to contact with MAO. In addition, an exceptionally broad MWD was observed. These authors attributed the increased isospecificity to decomposition of the metallocene coordination sphere and conversion to an isospecific form. Interestingly, elemental analysis of the SiO_2/Ind_2ZrCl_2 indicated that all the Cl at least has been reacted away [75]. In comparison, Janiak and Rieger reported that Ind_2ZrCl_2 activated by MAO/SiO_2 and in solution resulted in waxy atactic PP in both cases. Presumably, pretreatment of the silica with MAO resulted in a more homogeneous-like behavior [76]. A similar effect was reported by Kaminsky and coworkers on contacting $Et(Ind)_2ZrCl_2$ with silica previously dried *in vacuo* at 100 °C [77]. The grafted catalytic system, when contacted with MAO, afforded isotactic PP resins with high molecular weight and increased stereoregularity, when compared with the corresponding homogeneous system, whereas precontacting the silica with MAO prior to the addition of the metallocene afforded PP resins similar to those produced by the homogeneous systems. However, Sacchi et al. contacted $Et(Ind)_2ZrCl_2$ and Ind_2ZrCl_2 with silica, using virtually the same grafting procedure as Kaminsky. In their case, the resins produced by the supported systems were similar to those produced by the homogeneous system [75].

The picture becomes even more confusing when a comparison is made of ethylene/propylene copolymerization studies on $Et(Ind)_2ZrCl_2$, contacted with MAO/SiO_2. Chien and He studied the influence of Al/Zr ratio in the copolymerization of ethylene and propylene and concluded that, under their conditions, the polymerization behavior of the supported catalyst system showed that the silica does not change the chemistry of the precatalyst because the bonding is mediated by MAO. It should be noted, however, that this proposal was based on limited polymer analysis [78]. Ethylene and propylene copolymerization as a function of aluminum to metal ratio with the same complex, supported in a similar manner, was also studied by Dos Santos and coworkers [38]. The group found that the MWDs of the resins were relatively narrow (M_w/M_n = 2.1–2.4), and that they possessed similar molecular weights (50 000–67 000 Da). However, an analysis of the differential scanning calorimetry (DSC) thermogram and ^{13}C NMR spectra showed that low Al : Zr ratios produced a higher propylene incorporation, similar to the homogeneous system. Further analysis also revealed a heterogeneous chemical composition distribution. These authors proposed that the broad chemical composition distribution (CCD) may have originated from active species unequally activated by different alkyl aluminum cocatalysts and/or the steric influence of the support surface.

A unimodal MWD, yet broad or even bimodal CCD, has also been reported by Soares and coworkers. This group studied the poly(ethylene-*co*-1-hexene) resulting from Cp_2HfCl_2 supported on MAO-pretreated silica [79]. Although the MWDs of the sample were reported to be relatively narrow (2.1–3.0) and unimodal, the method of immobilization significantly altered the CCD of the resultant resins. The data in Figure 4.24 show that there is a wide difference in the CCD of the polymers produced; support preparations with MAO/silica and SMAO appeared to produce poly(ethylene-*co*-1-hexene) with a bimodal CCD, whereas non-pretreated silica yielded relatively unimodal polymers. Crystalline analysis fractionation (CRYSTAF) of a copolymer prepared using MAO/silica yielded fractions with very similar molecular weights, despite very different CCDs. This was tentatively linked to a partial reaction of Si–OH groups with MAO. It should be noted that all of the polymerizations were carried out under the same aluminum to hafnium ratio (Al : Hf = 800), although due to the difference in the support material there may have been different ratios of free TMAL in the system.

Multimodal sites have also been proposed by Muhle and coworkers, who studied supported metallocenes in the gas-phase polymerization of ethylene/1-hexene. A combined TREF and gel-permeation chromatography (GPC) analysis led these authors to propose a three-site model [80]. Similarly, a two-site model was proposed by Soga and coworkers to explain the two types of poly(ethylene-*co*-1-hexene) observed [81]. Perhaps the most pronounced example of the effect that a synthetic strategy may have on stereo-control is seen when $Me_2Si(Flu)(Cp)ZrCl_2$ is precontacted with silica prior to activation by MAO. In the absence of silica, the homogeneous precatalyst produces syndiotactic PP, whereas in the presence of silica isotactic PP is formed [82].

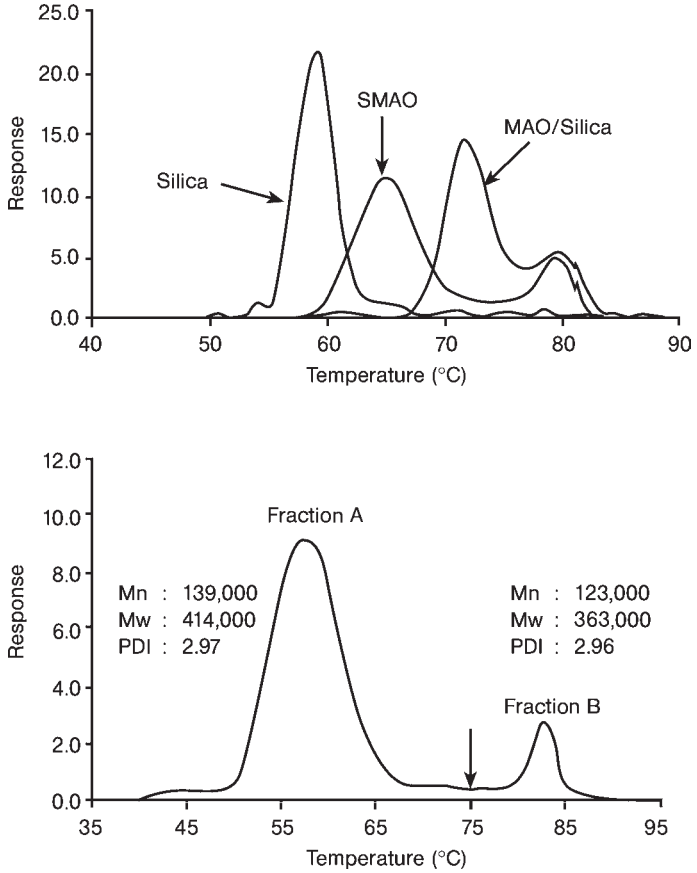

Figure 4.24 Polymer resin with unimodal molecular weight distribution and a bimodal chemical composition distribution. (Reproduced with permission from Ref. [79]; © 1999 Wiley-VCH.)

4.4.2.3 **Mass Transport Limitations**

Heterogeneity in the chemical composition of polymer resins resulting from a supported single-site catalyst has also been attributed to mass-transfer resistance. The latter is believed to be caused by the introduction of a support in the system, or different active sites with different local environments. Ray and coworkers illustrated the possibility of diffusion-controlled reactions and a broadening of MWDs, as a result of large radial concentration gradients in the growing polymer particle for traditional heterogeneous catalysts. Hoel and coworkers developed an ethylene–propylene copolymerization model dedicated to explaining an unexpectedly broad CCD when using supported single-site catalysts [83]. Based on experimental and theoretical results, these authors concluded that the breadth of the

CCD was a consequence of monomer mass transport limitation during the growth of the polymer particle.

Diffusion limitation has also been proposed by Fink to explain the formation of copolymers having a broad compositional distribution in ethylene/1-hexene copolymerization with *rac*-Me_2Si(2-Me-4-PhInd)$_2ZrCl_2$ immobilized on SiO_2/MAO [84]. Both, homo- and copolymerization of ethylene took place, explained by the formation of a copolymer envelope around the particle whereby the envelope acted as a filter to restrict diffusion of the larger monomer (1-hexene), resulted in ethylene homopolymerization in the inner reaches of the particle. Studies conducted by Chadwick et al. on the effects of 1-hexene comonomer on PE particle growth and CCD, resulting from Et(Ind)$_2ZrCl_2$/MAO impregnation of silica, supported the "filter model" [85].

An extensive and detailed study was reported by Kaminsky and coworkers on the polymerization of propylene using Me_2Si(2-Me-4-(1-Napth)Ind)$_2ZrCl_2$ as a precatalyst in conjunction with MAO or MAO/SiO_2 [86], and in various polymerization processes, such as toluene slurry, bulk monomer and gas phase (NaCl and PE mechanical stirred-fluidized bed). For all of the polymerization procedures used, the melting points of the polymer resins were seen to decrease with an increase of polymerization temperature and, once again, the homogeneous system yielded resins with higher melting points.

Figure 4.25 shows, graphically, the molecular weights which for homogeneous systems (1) and (2) are five- to 10-fold higher than their heterogeneous counterparts. In addition, a decrease in the melting points of the products afforded by the heterogeneous processes was observed. This was explained by the increased amounts of 2,1 misinsertion of propene units, due to lower monomer concentrations at the active site. This lower monomer concentration was also proposed to account for the relatively low molecular weights of the resins. Kaminsky's group then postulated that if misinsertions are propagated by the lack of monomer at the active site, then chain-termination reactions will appear more often.

Mülhaupt et al. investigated and compared the isoselective polymerization of propylene using a supported catalyst SiO_2/MAO/Me_2Si(2-Me-Benz[e]Ind)$_2ZrCl_2$ and the corresponding homogeneous system in a slurry [87]. Attention was centered on the influence of monomer concentration, the polymerization medium, temperature and scavenger type on the polymerization kinetics and PP properties. The results showed that heterogenization of the metallocene led to a significant decrease in activity when compared to the homogeneous system, and that the molecular weights and melting points of the resins produced were heavily dependent on the choice of medium and scavenger. Interestingly, the molecular weight decreased with increasing temperature for the homogeneous system, but hardly changed for the heterogeneous catalyst, while the MWD was narrow for both systems. The dependence of the resin melting temperature on polymerization temperature was also different for the homogeneous and heterogeneous systems. With increased polymerization temperatures, the melting points of the resins resulting from the homogeneous system decreased, whereas the opposite was seen for the resin derived from the heterogeneous system. A further analysis of the

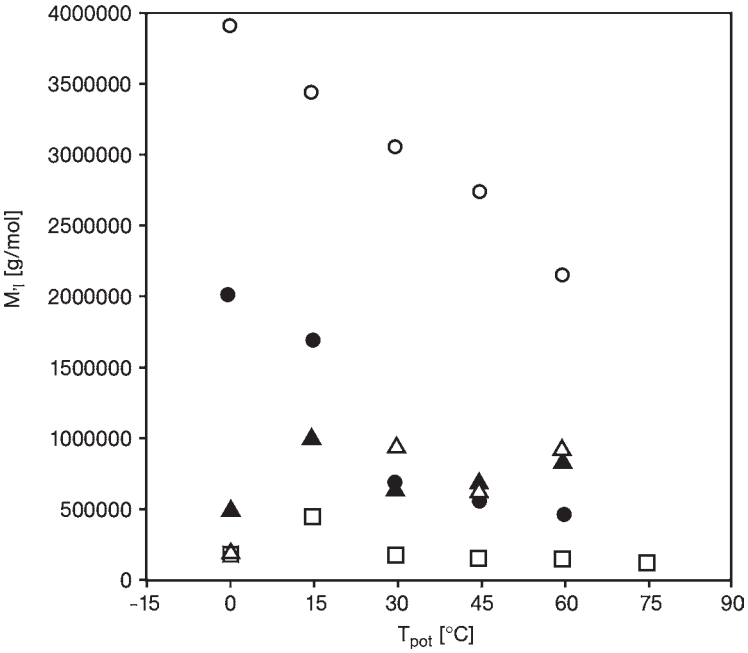

Figure 4.25 Viscosimetric average molar masses of polypropylenes afforded by procedure: (1) ●, homogeneous in toluene slurry; (2) ○, homogeneous in bulk propylene; (3) △, supported in bulk propylene; (4) ▲, supported in toluene slurry; (5) □, supported gas-phase in NaCl bed. (Reproduced with permission from Ref. [86]; © 2001 Wiley-VCH.)

resin revealed that the systems possessed different stereo- and regio-selectivity responses to polymerization temperatures. A lack of mass- and heat-transfer in the heterogeneous system was proposed to account for the different behavior of the two systems. Tailoring the immobilization procedure may help improve matters, and Fritze and coworkers used triethylaluminum (TEA) and triisobutylaluminum (TIBA) treatments to "pacify" silica supports before immobilizing a solution of *rac*-$Me_2Si(2\text{-}Me\text{-}4\text{-}PhInd)_2ZrCl_2$ and MAO. These groups found that such pretreatment yielded polymer resins with fewer stereo- and regio-errors, a higher melting point but similar molecular weights and MWDs when compared to the unpacified system [88]. Presumably, pacification of the silica support prior to contact causes a buffering of any unwanted steric or electronic interactions exerted by the support, allowing an environment similar to that of a homogeneous polymerization.

The immobilization of highly sensitive catalyst systems, such as those based on Brookhart's α-diimine-based nickel complexes, is extremely difficult – though not impossible – to achieve [89]. Brookhart complexes can produce a wide range of PE resins with branched (short- and long-chain) or linear microstructures [90]. The

properties of the resin are highly dependent on the steric environment around the active site and the polymerization conditions, such as ethylene concentration and reaction temperature.

Soares and coworkers studied the *in-situ* immobilization of (1,4-bis(2,6-diisopropylphenyl)acenaphthylene diimine nickel(II) dibromide onto MAO/SiO_2, comparing the polymer microstructure and morphology to those of its homogeneously produced counterpart [91]. The homogeneous system produces a polymer with a higher degree of short-chain branches (SCB) than the supported systems, whilst the effect of polymerization temperature on the total SCB content is greater for the supported system. Morphology studies showed that, at polymerization temperatures above 60 °C, two types of macroscopically distinct PE phases were easily identified. Increased polymerization temperatures also led to resins with broader to even bimodal CRYSTAF profiles. The authors considered three theories to explain the observed heterogeneity: (i) the presence of two or more distinct active sites resulting from chemical heterogeneity of the MAO/SiO_2 surface; (ii) the presence of supported and "leached" species (although the latter was not considered likely); and (iii) mass- and/or heat-transfer effects which resulted in varying local conditions. Either situation could affect the selectivity of the nickel catalyst with regard to its dependence on temperature and monomer concentration. However, the group speculated that the mechanism of polymer precipitation around the support surface might be responsible for the differences observed in the frequency of chain walking between the heterogeneous and homogeneous systems. Polymer crystallization on the support was thought to reduce the mobility of the growing polymer chain and consequently to lower the frequency of chain walking. As a result, the supported catalyst produced a polymer with fewer branches than the homogeneous counterpart. At high temperatures, a high degree of SCB occurred which resulted in a polymer that was soluble in the reaction medium; this minimized the effect of hindered chain mobility and resulted in polymer resins similar to those obtained with the homogeneous catalyst.

Zhu and coworkers compared the polymer resin produced by the same complex in homogeneous and heterogeneous conditions (MMAO/SiO_2) [92]. Likewise, it was found that, for a range of conditions, the supported catalyst system typically produced less short-chain branching than its homogeneous counterpart, indicating a lower rate of chain walking. In addition, depending on the polymerization conditions, the supported catalyst produced resins with bimodal thermograms (Figure 4.26). The authors proposed that the chain populations were most likely produced from two types of active site, resulting from supported and "leached" catalysts. The leached catalyst produced polymer similar to that of the homogeneous system, whereas the strong steric effects exerted by the support on the supported catalyst resulted in a lower rate of chain walking and hence fewer chain branches. The bimodality in the melt behavior was not reflected in the MWD, which indicated that the two active sites possessed similar chain-transfer/termination rates relative to chain propagation. Once again, the presence of multiple active sites could not be seen from an analysis of the MWD alone.

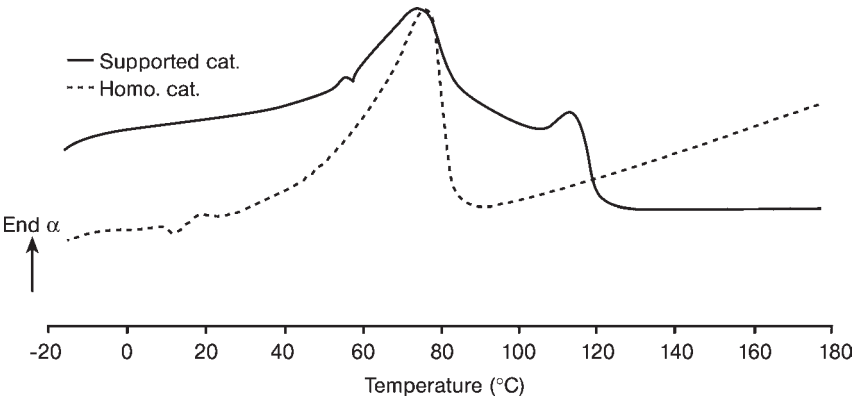

Figure 4.26 Differential scanning calorimetry thermograms for polyethylene produced with homogeneous and supported Brookhart catalyst. (Reproduced with permission from Ref. [92]; © 2001 Wiley-VCH.)

4.5 Conclusions

To some extent, the discussion on the factors that affect silica-supported, MAO-activated, single-site catalysts and the polymer resin that they produce is rather similar to the "Nature versus Nurture" debate, used to explain the physical and behavioral traits of human beings. As such, how a catalyst system produces a polymer resin is always dictated by a combination of its "genetic" dispositions (precatalyst ancillary ligand structure, etc.), the environment (local chemical and physical environment) in which it resides, and its past history.

In this chapter we have briefly described supported single-site catalysts derived from a combination of silica, MAO and a precatalyst complex which, whilst being a major technology, is only one type of system. In addition, we have discussed some of the commercial requirements, reagents, a multitude of synthetic procedures, and the consequent pitfalls for such catalysts. Hopefully, it will be appreciated just how complex such endeavors are, and how the description of supported, single-site catalysts as "drop-in" technologies somewhat trivializes an extremely challenging process.

References

1 D.S. Breslow, N.R. Newburg, *J. Am. Chem. Soc.* 1957, *79*, 5072.

2 G. Natta, P. Pino, G. Mazzanti, U. Giannini, *J. Am. Chem. Soc.* 1957, *79*, 2975.

3 K.H. Reichert, K.R. Meyer, *Makromol. Chem.* 1973, *169*, 163.

4 W.P. Long, D.S. Breslow, *Liebigs Ann. Chem.* 1975, 463.

5 W. Kaminsky, H. Sinn, *Liebigs Ann. Chem.* 1975, 424.

6 H. Sinn, W. Kaminsky, H.-J. Vollmer, R. Woldt, *Angew. Chem.* 1980, *92*, 396.

7 J.R. Severn, J.C. Chadwick, R. Duchateau, N. Friederichs, *Chem. Rev.* 2005, *105*, 4073, and references therein.

8 G.G. Hlatky, *Chem. Rev.* 2000, *100*, 1347.

9 Additives which aid reactor operability are commonly used in commercial processes. However, their effect will not be discussed further. Examples of such additives can be found in: A.K. Agapiou, C.-I. Kuo, D.M. Glowczwski, S.K. Ackerman U.S. Patent 6,608,153, 2003.

10 T.F. McKenna, J.B.P. Soares, *Chem. Eng. Sci.* 2001, *56*, 3931, and references therein.

11 A. Di Martino, G. Weickert, F. Sidoroff, T.L. McKenna, *Macromol. React. Eng.* 2007, *1*, 338.

12 (a) Z. Grof, J. Kosek, M. Marek, *Ind. Eng. Chem. Res.* 2005, *44*, 2389; (b) Z. Grof, J. Kosek, M. Marek, *AIChE J.* 2005, *51*, 2048.

13 (a) G. Fink, B. Steinmetz, J. Zechlin, C. Przybyla, B. Tesche, *Chem. Rev.* 2000, *100*, 1377; (b) A. Alexiadis, C. Andes, D. Ferrari, F. Sorber, K. Hauschild, M. Bochmann, G. Fink, *Macromol. Mater. Eng.* 2004, *289*, 457.

14 L.L. Böhm, *Angew. Chem. Int. Ed.* 2003, *42*, 5010.

15 (a) R.K. Iler (Ed.), *Colloid Chemistry of Silica and Silicates*, Cornell University Press, Ithaca, NY, 1955; (b) R.K. Iler (Ed.), *The Chemistry of Silica*, Wiley, New York, 1979; (c) W.A. Welsh, D.M. Chapman, *Ullmann's Encyclopedia of Industrial Chemistry*, A23: *Silica*, Chapter 5, 2007.

16 S.B. Fredriksen, A. Iveland, J. Lindroos, *Single-site catalyst design*. Oral presentation at EuropaCat V, Limerick, 2001.

17 Extracted from patent literature, in particular Ref. [46].

18 J. Trébosc, J.W. Wiench, S. Huh, V.S.-Y. Lin, M. Pruski, *J. Am. Chem. Soc.* 2005, *127*, 3057.

19 T. Tsutsui, Y.K. Yoshitsugu, K. Yamamoto, European Patent 516,458, 1997.

20 J.-N. Pédeutour, K. Radhakrisknan, H. Cramail, A. Deffieux, *Macromol. Rapid Commun.* 2001, *22*, 1095.

21 E. Zurek, T. Ziegler, *Prog. Polym. Sci.* 2004, *29*, 107.

22 L. Negureanu, R.W. Hall, L.G. Butler, L.A. Simeral, *J. Am. Chem. Soc.* 2006, *128*, 16818.

23 K. Radhakrisknan, H. Cramail, A. Deffieux, P. François, A. Momtaz, *Macromol. Rapid Commun.* 2002, *23*, 829.

24 D.W. Imhoff, L.S. Simeral, S.A. Sangokoya, J.H. Peel, *Organometallics* 1998, *17*, 1941.

25 D.E. Babuskin, N.V. Semikolenova, V.N. Panchenko, A.P. Sobolev, V.A. Zakharov, E.P. Talsi, *Macromol. Chem. Phys.* 1997, *198*, 3845.

26 E.W. Hansen, R. Blom, P.O. Kvernberg, *Macromol. Chem. Phys.* 2001, *202*, 2880.

27 D.E. Babuskin, H.-H. Brintzinger, *J. Am. Chem. Soc.* 2002, *124*, 12869.

28 M. Linnolahti, J.R. Severn, T.A. Pakkanen, *Angew. Chem. Int. Ed.* 2006, *45*, 331.

29 J. Stellbrink, A. Niu, J. Allgaier, D. Richter, B.W. Koenig, R. Hartmann, G.W. Coates, L.J. Fetters, *Macromolecules* 2007, *40*, 4972.

30 M. Bochmann, *J. Organomet. Chem.* 2004, *689*, 3982.

31 U. Wiesser, F. Schaper, H.-H. Brintzinger, *Macromol. Symp.* 2006, *236*, 63.

32 D.E. Babuskin, C. Naundorf, H.-H. Brintzinger, *Dalton Trans.* 2006, 4539.

33 M.E. Bartram, T.A. Michalske, J.W. Rogers, *J. Phys. Chem.* 1991, *95*, 4453.

34 S. Scott, T.L. Church, D.H. Hguyen, E.A. Mader, J. Moran, *Top. Catal.* 2005, *34*, 109.

35 T. Tao, G.E. Maciel, *J. Am. Chem. Soc.* 2000, *122*, 3118.

36 J. Li, J.A. DiVerdi, G.E. Maciel, *J. Am. Chem. Soc.* 2006, *128*, 17093.

37 E.P. Talsi, N.V. Semikolenova, V.N. Panchenko, A.P. Sobolev, D.E. Babushkin, A.A. Shubin, V.A. Zakharov, *J. Mol. Catal. A* 1999, *139*, 131.

38 M.C. Haag, C. Krug, J. Dupont, G.B. Galland, J.H.Z. dos Santos, T. Uozumi, T. Sano, K. Soga, *J. Mol. Catal. A* 2001, *169*, 275.

39 M. Chang, PCT Patent Appl. 96/04318, 1996.

40 M.O. Jelelowo, U.S. Patent 5,468,702, 1995.

41 M. Chang, U.S. Patent 5,629,253, 1997.

42 J.H.Z. dos Santos, C. Krug, M.B. da Rosa, F.C. Stedile, J. Dupont, M. de C. Forte, *J. Mol. Catal. A* 1999, *139*, 199.

43 R. Guimarães, F.C. Stedile, J.H.Z. dos Santos, *J. Mol. Catal. A* 2003, *206*, 353.

44 H.C. Welborn, U.S. Patent 4,808,561, 1989.
45 T. Takahashi, U.S. Patent 5,026,797, 1991.
46 A. Razavi, G.L.G. Debras, U.S. Patent 5,719,241, 1998.
47 W.J. Gauthier, J. Tian, D. Rauscher, S. Henry, U.S. Patent Appl. 2003/0236365, 2003.
48 G.B. Jacobsen, P.L. Wauteraerts, L. Spencer, U.S. Patent 6,043,180, 2000.
49 N.L. Krzystowczyk, S.P. Diefenbach, E.A. Burt, U.S. Patent 5,739,368, 1998.
50 R.H.A.M. Meijers, M.F.H. Van Tol, M. Kranenburg, U.S. Patent 6,383,968, 2002.
51 P.P.M. Hoang, D. Jeremic, J.R. Kearns, I.M. Coulter, R.D. Donaldson, U.S. Patent 6,340,771, 2002.
52 K. Soga, T. Shiono, H.J. Kim, *Makromol. Chem.* 1993, *194*, 3499.
53 C. Chao, W. Pratchayawutthirat, P. Praserthdam, T. Shiono, G.L. Rempel, *Macromol. Rapid Commun.* 2002, *23*, 672.
54 B. Jongsomjit, P. Kaewkrajang, S.E. Wanke, P. Praserthdam, *Catal. Lett.* 2004, *94*, 205.
55 X. Gao, P.S. Chisholm, R.D. Donaldson, I. McKay, PCT Patent Appl. 03/025027, 2003.
56 T.J. Burkhardt, M. Murata, W.B. Brandley, U.S. Patent 5,240,894, 1993.
57 W. Spaleck, F. Küber, A. Winter, J. Rohrmann, B. Bachmann, M. Antberg, V. Dolle, F.E. Paulus, *Organometallics* 1994, *13*, 954.
58 V. Fraajie, B. Bachmann, A. Winter, European Patent Appl. 780,402, 1997.
59 N. Paczkowski, A. Winter, F. Langhauser, U.S. Patent 7,169,864, 2006.
60 A. Speca, PCT Int. Pat. 00/12565, 2000.
61 K. Kallio, O. Andell, H. Knuuttila, U. Palmqvist, U.S. Patent 6,291,611, 2001.
62 G.A. Vaughan, A.N. Speca, P. Brant, J.A.M. Canich, U.S. Patent 5,863,853, 1999.
63 V. Busico, R. Cipullo, *Prog. Polym. Sci.* 2001, *26*, 443.
64 R. Blom, I.M. Dahl, *Macromol. Chem. Phys.* 2001, *202*, 719.
65 A. Andersen, R. Blom, I.M. Dahl, *Macromol. Chem. Phys.* 2001, *202*, 726.
66 R. Blom, O. Swang, R.H. Heyn, *Macromol. Chem. Phys.* 2002, *203*, 381.
67 B. Kou, K.B. McAuley, C.C. Hsu, D.W. Bacon, K.Z. Yao, *Ind. Eng. Chem. Res.* 2005, *44*, 2443.
68 K. Kallio, J. Maaranen, E. Kokko, V. Ojanpera, European Patent Appl. 1,785,435, 2007.
69 R. Nicasy, F.E. Gemoets, P.J. Schouterdan, J.F. Vandun, P.C.T. Int. Appl. 0,316,362, 2003.
70 R.S. Eisinger, D.P. Zilker, J.L. Swecker, U.S. Patent 6,987,152, 2006.
71 T. Sano, H. Hagimoto, S. Sumiya, Y. Naito, Y. Oumi, T. Uozumi, K. Soga, *Microporous Mesoporous Mater.* 2001, *44*, 557.
72 P. Kumkaev, L. Wu, P. Praserthdam, S.E. Wanke, *Polymer* 2003, *44*, 4791.
73 S. Collins, W.M. Kelly, D.A. Holden, *Macromolecules* 1992, *25*, 1780.
74 Y.-X. Chen, M.D. Rausch, J.C.W. Chien, *J. Polym. Sci., Polym. Chem.* 1995, *33*, 2093.
75 M.C. Sacchi, D. Zucchi, I. Tritto, P. Locatelli, *Macromol. Rapid Commun.* 1995, *16*, 581.
76 C. Janiak, B. Rieger, *Angew. Makromol. Chem.* 1994, *215*, 47.
77 W. Kaminsky, F. Renner, *Makromol. Chem. Rapid Commun.* 1993, *14*, 239.
78 J.C.W. Chien, D. He, *J. Polym. Sci., Polym. Chem.* 1991, *29*,1585.
79 J.D. Kim, J.B.P. Soares, *Macromol. Rapid Commun.* 1999, *20*, 347.
80 W. Kaminsky, *Macromol. Symp.* 1995, *89*, 203.
81 M.E. Muhle, in: *Proceedings of MetCon 98*, Houston, June 1998. Available at The Catalyst Group, P.O. Box 637, Spring House, PA 19477.
82 K. Soga, T. Uozumi, T. Arai, S. Nakamura, *Macromol. Rapid Commun.* 1995, *16*, 379.
83 E. Hoel, C. Cozewith, G.D. Bryne, *AIChE J.* 1994, *40*, 1669.
84 C. Prybyla, B. Tesche, G. Fink, *Macromol. Rapid Commun.* 1999, *20*, 328.
85 M. Smit, X. Zheng, R. Brüll, J. Loos, J.C. Chadwick, C.E. Koning, *J. Polym. Sci., Polym. Chem.* 2006, *44*, 2883.
86 D. Arrowsmith, W. Kaminsky, A. Laban, U. Weingarten, *Macromol. Chem. Phys.* 2001, *202*, 2161.
87 S. Jüngling, S. Koltzenburg, R. Mülhaupt, *J. Polym. Sci., Polym. Chem.* 1997, *35*, 1.
88 C. Fritze, B. Bachmann, F. Küber, U.S. Patent 6,271,164, 2001.

89 H.S. Schrekker, V. Kotov, P. Preishuber-Pflugl, P. White, M. Brookhart, *Macromolecules* 2006, *39*, 6341.

90 S.D. Ittel, L.K. Johnson, M. Brookhart, *Chem. Rev.* 2000, *100*, 1169.

91 L.C. Simon, H. Patel, J.B.P. Soares, R.F. de Souza, *Macromol. Chem. Phys.* 2001, *202*, 3237.

92 F. AlObaidi, Z. Ye, S. Zhu, *Macromol. Chem. Phys.* 2003, *204*, 1653.

5
Perfluoroaryl Group 13 Activated Catalysts on Inorganic Oxides

Gregory G. Hlatky and Michael W. Lynch

5.1
Introduction

Single-site olefin polymerization catalysts – especially metallocene catalysts – have been recognized for almost as long as their Ziegler–Natta counterparts. The extraordinary advances in single-site catalysis have derived partly from the elaboration of metal complex structures in order to influence catalyst activity and molecular characteristics. Another spur to their development has been the development of cocatalysts that not only enhance the activity of these systems but have also advanced our understanding of the catalytic process and the nature of the active, polymerizing sites.

Methylalumoxane (MAO), which is formed from the reaction of $AlMe_3$ with stoichiometric amounts of water, has been the major cocatalyst for single-site catalysts. The action of MAO on metallocenes was postulated to be alkylation combined with anion abstraction to generate a cationic polymerizing species $[Cp'_2MMe]^+$. Indeed, extensive investigations have been made into the development of stable formulations that are soluble in aliphatic hydrocarbons. Nonetheless, MAO remains an enigmatic material which must be used in considerable excess for adequate catalyst performance.

The discovery of fluoroaryl-based activators such as $[R_3NH][B(C_6F_5)_4]$ [1], $[Ph_3C][B(C_6F_5)_4]$ [2] and $B(C_6F_5)_3$ [3] led to catalysts which were not only comprehensively characterizable as to their ionic character (Scheme 5.1) but also had activities comparable to those of their MAO-activated counterpart, despite requiring only a stoichiometric quantity of the cocatalyst [4].

The enormous capital costs of a commercial polyolefin plant, and the nature of the incumbent conventional polymerization catalysts, mean that the catalyst must be formulated to operate efficiently in an existing facility. Heterogeneous (two-phase) catalysts are needed in slurry, bulk-monomer or gas-phase processes, where the polymer is insoluble in the reaction medium. Such catalysts must produce morphologically uniform polymer particles of high bulk density which do not adhere to the interior of the reactor, do not fragment to form fines, and polymerize monomers to form a polymer product at high activity. A further technical

Tailor-Made Polymers. Via Immobilization of Alpha-Olefin Polymerization Catalysts.
Edited by John R. Severn and John C. Chadwick

ISBN: 978-3-527-31782-0

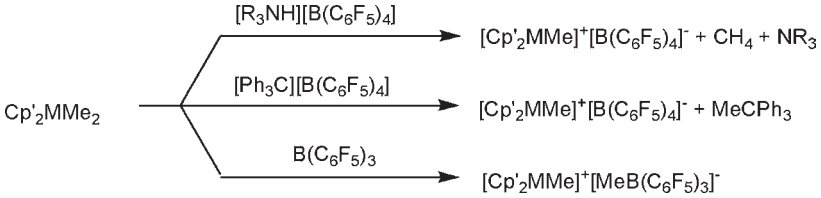

Scheme 5.1 Reactions of metallocene dimethyls with ionizing agents.

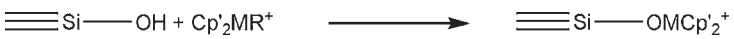

Scheme 5.2 Reaction of metallocenium cation with surface hydroxyl groups.

challenge is to support the catalyst while maintaining the desirable properties (e.g., molecular weight, molecular weight distribution (MWD), comonomer incorporation, stereoregularity) that must be imparted to the polymer product.

In recent years, the immobilization of single-site catalysts firmly on support materials has been the subject of extensive industrial research [5]. Metal oxides, principally silica, have been used because of their low cost, high surface area and pore volume, and ready availability in a variety of particle sizes and desirable morphologies. Perfluoroaryl-activated single-site catalysts have been successfully supported on inorganic oxides to produce catalysts which operate smoothly in almost all polyolefin processes.

5.2
Supported Perfluoroarylborate Catalysts

The support of single-site catalysts activated by non-aluminum agents – principally borate anions such as $[B(C_6F_5)_4]^-$ or $B(C_6F_5)_3$ – is far more problematic than alumoxane-based analogues. These systems are highly prone to deactivation by adventitious impurities. Even silica treated at 800 °C has surface hydroxyl groups in sufficient concentration to render a $[Cp_2ZrMe][B(C_6F_5)_4]$ catalyst inactive (Scheme 5.2).

Alumina or silica treated with alkylaluminums do not form active catalysts when reacted with Cp'_2MMe_2 complexes, but Cp'_2MMe_2-$[Ct][B(C_6F_5)_4]$ held on these supports are very active for olefin polymerization [6]. The supported catalysts can be used in slurry, bulk-monomer, or gas-phase processes [7]. Partially or fully hydroxylated supports can also be passivated by treatment with butyllithium or butylethylmagnesium, followed by reaction with BrC_6F_5 [8] or by reacting silica with NH_4F [9], hexamethyldisilazane [10] or chlorosilanes [11]. Not only bis(cyclopentadienyl) complexes were amenable to heterogenization by this method but also "constrained-geometry catalyst" (CGC) complexes such as $Me_2Si(N\text{-}t\text{-}Bu)(C_5Me_4)TiMe_2$ [12].

The early studies on supported perfluoroaryl catalysts used the dimethyl derivatives of the complexes as reactants. This involves an additional preparative step,

but one which is not always successful for some complexes. Matsumoto simplified this by generating Group IV metal catalysts from the halides, co-supporting on a variety of inorganic supports bis(cyclopentadienyl)-, mono(cyclopentadienyl)-, and cyclopentadienyl-free zirconium chlorides with ferricinium or dimethylanilinium tetrakis(pentafluorophenyl)borate (Scheme 5.3; Table 5.1) [13]. Triisobutylaluminum can be added in the support step or added to the reactor with the catalyst as the alkylating agent.

This method has proven generally useful for a wide array of metal complexes, including phosphinimine complexes of titanium [14], boratabenzene complexes of zirconium [15], chelating amido [16] and pyridyl-amide [17] complexes of hafnium, chromium compounds [18], and nickel bis(imide) complexes [19]. Tetrakis(pentafluorophenyl)borates have been the primary anionic salts used, but other ionic perfluoroaryl activators have been successfully employed, including perfluoroarylaluminates such as $[Ph_3C][HOAl(C_6F_5)_3]$ [20], the dianionic alkylsilane-bridged salt $[R_3NH]_2[(C_6F_5)_3BC_6F_4OSiMe_2CH_2CH_2Me_2SiOC_6F_4B(C_6F_5)_3]$ [21], and "extended" anionic complexes made through the reaction of $B(C_6F_5)_3$ with

Scheme 5.3 Formation of metallocene cations from metallocene dichlorides and alkylaluminums.

Table 5.1 Supported zirconium catalysts activated by trialkylaluminums and borate salts.

Metal complex	*Activator*	*Support*	*Pre- or post-support activation by Al(i-Bu)$_3$*	*Monomer*	*Activity (g mmol^{-1} Zr h^{-1})*
Cp_2ZrCl_2	$[HNMe_2Ph][B(C_6F_5)_4]$	Silica	Pre- and post-support	Ethylene	69 300
Cp_2ZrMe_2	$[HNMe_2Ph][B(C_6F_5)_4]$	Silica	Post-support	Ethylene	67 300
Cp_2ZrMe_2	$[HNMe_2Ph][B(C_6F_5)_4]$	Silica	None	Ethylene	14 000
Cp_2ZrCl_2	$[HNMe_2Ph][B(C_6F_5)_4]$	Alumina	Pre- and post-support	Ethylene	59 300
$CpZrMe_3$	$[Cp_2Fe][B(C_6F_5)_4]$	Silica	Post-support	Ethylene	78 600
$CpZrMe_3$	$[Cp_2Fe][B(C_6F_5)_4]$	Silica	None	Ethylene	13 300
$CpZrCl_3$	$[HNMe_2Ph][B(C_6F_5)_4]$	Silica	Post-support	Ethylene	65 300
$CpZrCl_3$	$[HNMe_2Ph][B(C_6F_5)_4]$	Alumina	Post-support	Ethylene-1-octene	30 300
$Zr(CH_2Ph)_4$	$[HNMe_2Ph][B(C_6F_5)_4]$	Silica	Post-support	Ethylene	74 000
$Zr(CH_2Ph)_4$	$[HNMe_2Ph][B(C_6F_5)_4]$	Silica	None	Ethylene	127
$ZrCl_4$	$[HNMe_2Ph][B(C_6F_5)_4]$	Silica	Post-support	Ethylene	653
$ZrCl_4$	$[HNMe_2Ph][B(C_6F_5)_4]$	Alumina	Post-support	Ethylene-1-octene	767
$Et(Ind)_2ZrCl_2$	$[HNMe_2Ph][B(C_6F_5)_4]$	Silica	Post-support	Propylene	1600
$Me_2C(Cp)(Flu)ZrCl_2$	$[HNMe_2Ph][B(C_6F_5)_4]$	Silica	Post-support	Propylene	1000

pentafluorophenol or $[HNMe(C_{18-22}H_{37-45})][B(C_6F_5)_3(C_6H_4OH)]$ in the presence of an aniline base [22].

Simple alkylaluminums such as $AlEt_3$ and $Al(i\text{-}Bu)_3$ are customarily used as the alkylating component, but other agents can be utilized. Metallocene dichlorides reacted with MAO are supported and prepolymerized before contacting with $[HNMe_2Ph][B(C_6F_5)_4]$; the final activities are low without the boron component [23]. Butylethylmagnesium and even butyllithium have been used successfully as alkylating agents to produce catalysts with activities comparable to those when $Al(n\text{-}C_6H_{13})_3$ was used [24]. Grignard reagents such as MeMgBr have been used to prealkylate the dichloride complex, followed by reaction with borate salt and deposition on silica [25]. Kristen and coworkers added stoichiometric or substoichiometric amounts of NMe_2Ph to an $(n\text{-}BuCp)_2ZrCl_2$-$[HNMe_2Ph][B(C_6F_5)_4]$-silica combination alkylated by butyloctylmagnesium, and identified an increase in activity over the aniline-free catalyst [26].

While the usual method of preparing supported single-site catalysts is to combine the metal component and activator on a support, another means of activation is to combine a separately supported metal component and activator. For example, $Me_2C(Cp)(Flu)ZrX_2$ (X = Cl, Me) on silica is combined in liquid propylene with separately supported $[Ph_3C][B(C_6F_5)_4]$ as the sole component of another fraction of carrier [27]. The reactor walls are not fouled by the syndiotactic polypropylene (PP) produced therefrom, indicating that the catalyst is physiadsorbed onto the silica and not leached, even though the metal component was not co-supported.

One of the great concerns in supported catalysts is to maintain good morphology and a narrow particle size distribution in the resin produced. Especially in slurry polymerizations, there is a possibility of leaching a soluble catalyst into the reaction medium, leading to poor particle regularity and fouling. Covalent fixing of the metal component to the support has been one means explored to avoid this outcome [5], but in these cases the beneficial effect of choice of substituent on the ligand is lost. Another means of ensuring that the ionic catalyst formed from the metal component and the activator in non-alumoxane systems is not leached from the support has been to covalently bind the *activator* instead of the metal complex to the support material.

Turner postulated, but did not specifically exemplify, the use of a partially hydroxylated silica surface to bind a polyfluorinated tetraphenylborate anion bearing a reactive group (Scheme 5.4) [28]; the essence of this concept was later put into practice by investigators at Dow and Nippon Polyolefins. For example, partially hydroxylated silica reacts with $[HNMe_2Ph][(C_6F_5)_3B(C_6F_4RCl)]$ (RCl = $SiCl_3$, $SiMe_2Cl$, $(CH_2)_8SiMe_2Cl$) to form a surface-bound activator for Cp'_2ZrCl_2-$Al(i\text{-}Bu)_3$ systems with an improved control of fines (Scheme 5.5) [29].

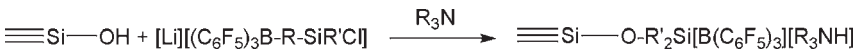

Scheme 5.4 Formation of surface-supported ionic activators from ionic tris(polyfluorophenyl) complexes.

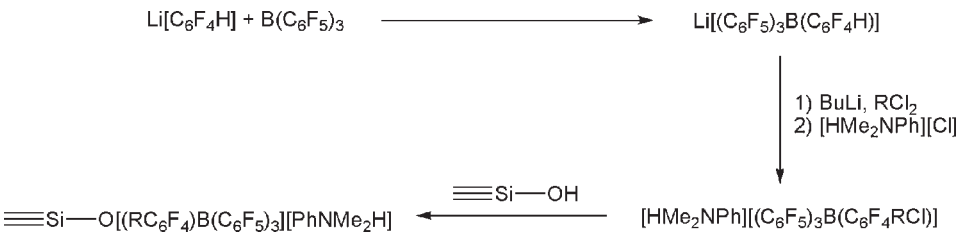

Scheme 5.5 Formation of surface-supported ionic activators from ionic tetrakis(polyfluorophenyl) complexes.

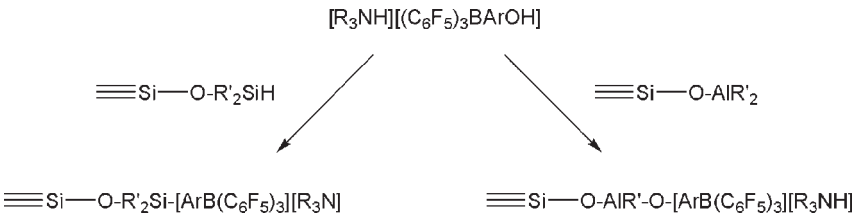

Scheme 5.6 Formation of surface-supported ionic activators from an ionic hydroxylated borate complex.

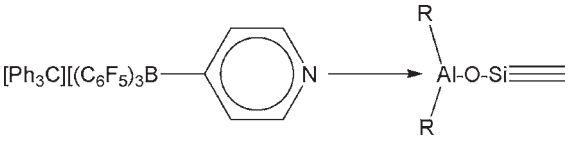

Scheme 5.7 Covalently tethered borate activator.

The reaction of silane-modified silicas with $[R_3NH][(C_6F_5)_3B\text{-Ar-OH}]$ salts (Ar = phenyl, biphenyl, naphthyl) also afford supported activators for $Me_2Si(C_5Me_4)(N\text{-}t\text{-Bu})TiMe_2$ complexes in slurry polymerization processes [30]. The same ammonium salts may be reacted with AlR_3-treated silicas and used as activators for $Me_2Si(C_5Me_4)(N\text{-}t\text{-Bu})Ti(\eta^4\text{-diene})$ complexes (Scheme 5.6) [31] or tridentate iron diimines [32]. A hydrocarbon-soluble hydroxylated borate anion where $[R_3NH]^+ = [NHMe(C_{18-22}H_{37-45})_2]^+$ was treated with triethylaluminum prior to adding the mixture to the silica support [33].

Another approach to immobilizing the borate anion is through Lewis acid/base interactions instead of covalent tethering. Holtcamp prepared $[Ph_3C][(C_6F_5)_3B(4\text{-}C_6F_4N)]$, used with alkylaluminum-treated silica as a cocatalyst for metallocenes (Scheme 5.7) [34].

The borate anion, supposedly non-coordinating, may also have an influence on the course of polymerization. Fixing the cationic portion of the activator to the surface gives even greater degrees of freedom in the choice of both the metal component and anion. Carnahan and Neithamer reacted 3-hydroxy-*N,N*-dimethylanilinium tetrakis(pentafluorophenyl)borate to alkylaluminum-treated silica to form an activator for $Me_2Si(N\text{-}t\text{-Bu})(C_5Me_4)Ti(1,3\text{-pentadiene})$ [35]. Okuda

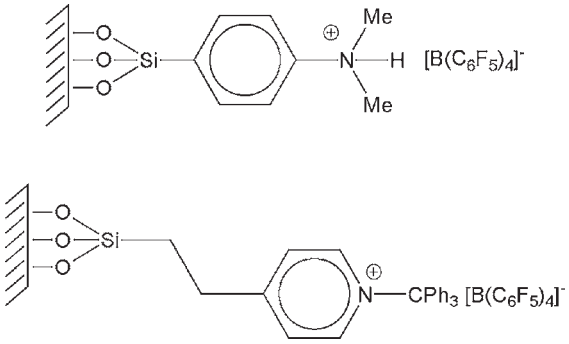

Scheme 5.8 Tethered cations for tetrakis(pentafluorophenyl)borate anions.

and coworkers allowed pyridylethylsilane-modified silica to react with $[Ph_3C][B(C_6F_5)_4]$ and subsequently with $Me_2Si(N\text{-}t\text{-}Bu)(C_5Me_4)TiX_2$ (X = Me, benzyl, Cl) [36]; similarly, a tethered anilinium salt of $[B(C_6F_5)_4]^-$ was successfully used with metallocene dichlorides and alkylaluminums to generate active catalysts [37] (Scheme 5.8). The Lewis bases formed in the reaction with the metal complex are labile donors toward the metal cations generated, and good catalyst activities are observed.

5.3 Supported Perfluoroarylborane and Perfluoroarylalane Catalysts

Like their ionic counterparts, non-ionic perfluorophenylborane and perfluoroarylalanes such as $B(C_6F_5)_3$ have been reacted with metallocenes [38] or CGC complexes such as $Me_2Si(C_5Me_4)(N\text{-}t\text{-}Bu)TiMe_2$ [39] and supported on alkylaluminum-treated silica to generate active catalysts for slurry or gas-phase polymerization. Moreover, the alkylaluminum used is not necessarily a simple trialkylaluminum, such as $AlEt_3$, but may be MAO [40].

The normal method of catalyst preparation is to combine the metal component and the borane and to deposit the mixture on the support. However, in one study the $AlMe_3$-treated silica and alumina was impregnated with metallocene and then activated with solutions of borane and borate cocatalysts. As a result, active catalysts were obtained, although the MWDs obtained tended to be broad [41]. Metallocene and CGC dimethyl and diene complexes supported on $AlEt_3$-treated silica and activated by $B(C_6F_5)_3$ similarly showed excellent performance, although omitting the borate component led to a complete loss of activity [42]. $B(C_6F_5)_3$ reacts with either trialkylaluminums [43] or MAO [44] to form perfluorophenylalanes and perfluorophenylalumoxanes (Scheme 5.9), which function as cocatalysts with CGC complexes when supported on silica. $Al(C_6F_5)_3$ is less stable than $B(C_6F_5)_3$ to surface hydroxyl groups, losing C_6F_5H and forming the surface-bound aluminum species $\equiv Si\text{–}O\text{–}Al(C_6F_5)_2$ [45]. The bis(pentafluoropheny)alanes are still potent activators for metallocene dimethyl complexes.

Scheme 5.9 Pentaflurophenyl exchange with alkylaluminums and methylalumoxane.

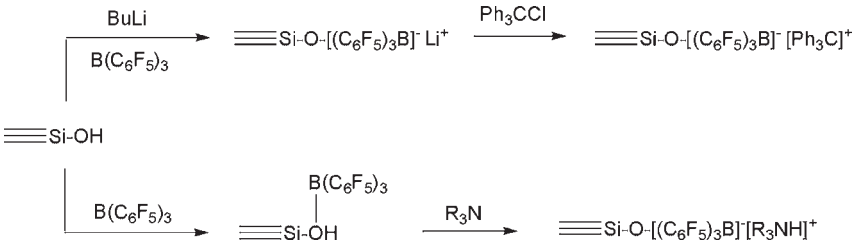

Scheme 5.10 Formation of surface-supported ionic activators from tris(pentafluorophenyl)borane.

The surface hydroxyl groups of silica and alumina can be used in the reaction of neutral bis- and tris(pentafluorophenyl)boranes to form supported ionic activators. $B(C_6F_5)_3$ acts as a Lewis acid towards the surface hydroxyl groups of silica, affording a Brønsted acid capable of reacting with Cp'_2ZrMe_2 procatalysts. Ammonium salts, which also function as ionic activators, are formed on reaction with tertiary amines [46]. Ward and Carnahan deprotonated the hydroxyl groups with butyllithium prior to reaction with $B(C_6F_5)_3$; metathesis of the lithium salt with Ph_3CCl generates the supported trityl complex (Scheme 5.10) [47]. The trityl salt $[\equiv Si–O–B(C_6F_5)_3][Ph_3C]$ can be formed even more simply from $[\equiv Si–O(H)–B(C_6F_5)_3]$ and Ph_3CCl [48]. The order of addition can be altered; for example, reacting partially dehydroxylated silica first with NMe_2Ph, then with $B(C_6F_5)_3$ followed by $Me_2Si(2\text{-methylindenyl})_2ZrMe_2/AlMe_3$ produces an active catalyst for propylene polymerization [49].

The activity of catalysts with tethered $B(C_6F_5)_3$ can also be impressive. The zeolite MCM-41 similarly treated with $B(C_6F_5)_3$, $PhNMe_2$ and $Cp_2ZrCl_2/AlMe_3$ functions as a propylene oligomerization catalyst with activity almost equal to that of the homogeneous system [50]. By using this technique, propylene is polymerized by $Me_2Si(2\text{-methyl-4-phenylindenyl})_2ZrMe_2$ with activities as high as 8600 g PP g^{-1} catalyst, with narrow polydispersity [51]. No anionic component remains in the polymer, which makes these catalysts especially useful when preparing resins for electrical applications [52].

An examination of the surface-supported activator $[\equiv Si–O–B(C_6F_5)_3][HNEt_2Ph]$ using infrared (IR) spectroscopy shows that not only is the unperturbed ammonium salt formed but also a secondary species, with hydrogen bonding between the ammonium salt and residual surface hydroxyl groups; the concentration of this secondary species increases with decreasing calcination temperature [53]. The results of combined IR and solid-state ^{13}C NMR studies have indicated that the surface-bound ammonium salt reacts cleanly with $(C_5Me_5)ZrMe_3$, releas-

ing one equivalent of methane to form [≡Si–O–$B(C_6F_5)_3$][$(C_5Me_5)Zr^+Me_2 \cdot HNEt_2Ph$] [54].

The interaction of $B(C_6F_5)_3$ with partially dehydroxylated silica appears only to cap a fraction of the hydroxyl groups on the surface [55]. In the absence of further scavenging agent such as triisobutylaluminum or silane [56], the catalyst activity is low. Surface hydroxyls may be partially capped before the addition of $B(C_6F_5)_3$ with alkylaluminums [57] or $HB(C_6F_5)_2$ [58], though sufficient hydroxyls remain for complexation with $B(C_6F_5)_3$.

Collins and coworkers examined the adsorption of $B(C_6F_5)_3$, $HB(C_6F_5)_2$ and $ClB(C_6F_5)_2$ with partially dehydroxylated silicas, and found that while only about 10% of hydroxyl groups reacted with $B(C_6F_5)_3$, 70–80% were capped by the bis(perfluorophenyl)boranes [59]. The surface-bonded bis(pentafluorophenyl)bora ne ≡Si–O–$B(C_6F_5)_2$ is an efficient activator for Me_2Si(2-methylindenyl)$HfMe_2$ in propylene polymerization [60]. Research investigations conducted at Basell have led to another method for the fixing of neutral triarylborane activators to silica surfaces by reacting $HB(C_6F_5)_2$ with silica modified by vinyltriethoxysilane (Scheme 5.11) or substituted tris(polyfluorophenyl)boranes with partially dehydroxylated silica (Scheme 5.12). The supported neutral activators can also be quaternized by reaction with $Li(C_6F_5)$ [61].

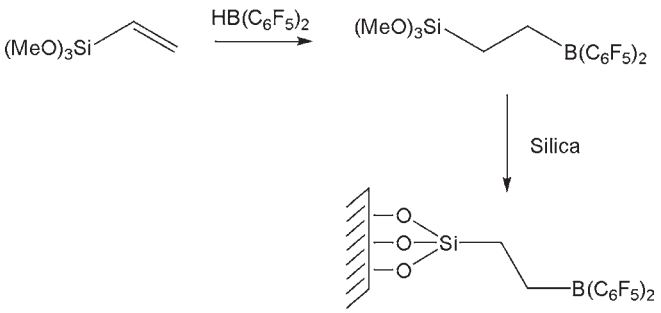

Scheme 5.11 Formation of tethered neutral borane activator.

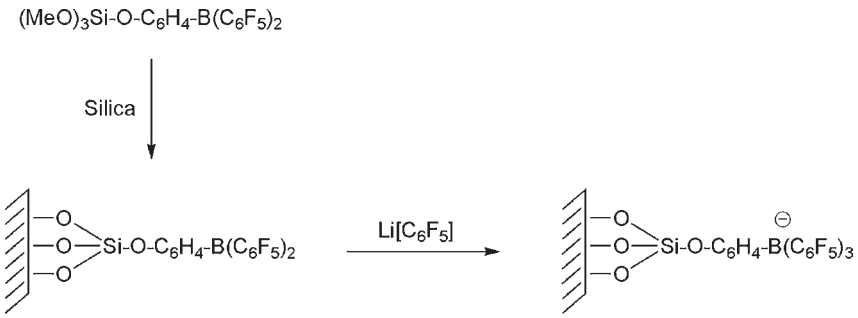

Scheme 5.12 Quaternization of a tethered neutral borane activator with lithium pentafluorophenyl.

Collins created a model for the surface reaction of perfluoroarylboranes with silica by reacting $XB(C_6F_5)_2$ (X = H, Cl) with a silsesquioxane (Scheme 5.13) [62]. As with the silica-supported heterogeneous catalysts, the model system with Cp_2ZrMe_2 is inactive unless a scavenger ($MeAl(BHT)_2$) and monomer are present. The $[Cp_2ZrMe]^+$ cation formed from the reaction of Cp_2ZrMe_2 with the silsesquioxane-supported borane is unstable with respect to decay, losing two equivalents of $MeB(C_6F_5)_2$ and forming Cp_2ZrO- species.

Recently, perfluorophenylboroxy-containing supported catalysts have been increasingly studied. $C_6F_5B(OH)_2$ reacts with two equivalents of $AlMe_3$ to form $C_6F_5B(OAlMe_2)_2$; when supported on $AlMe_3$-treated silica, this functions as a cocatalyst with metallocene complexes [63]. Either this or $((C_6F_5)_2BO)_2AlR$ (R = Me, *i*-Bu) can be used with Lewis base to form surface-supported anilinium boralumoxates (Scheme 5.14) [64]. The anhydride $(C_6F_5)_2B–O–B(C_6F_5)_2$, formed from

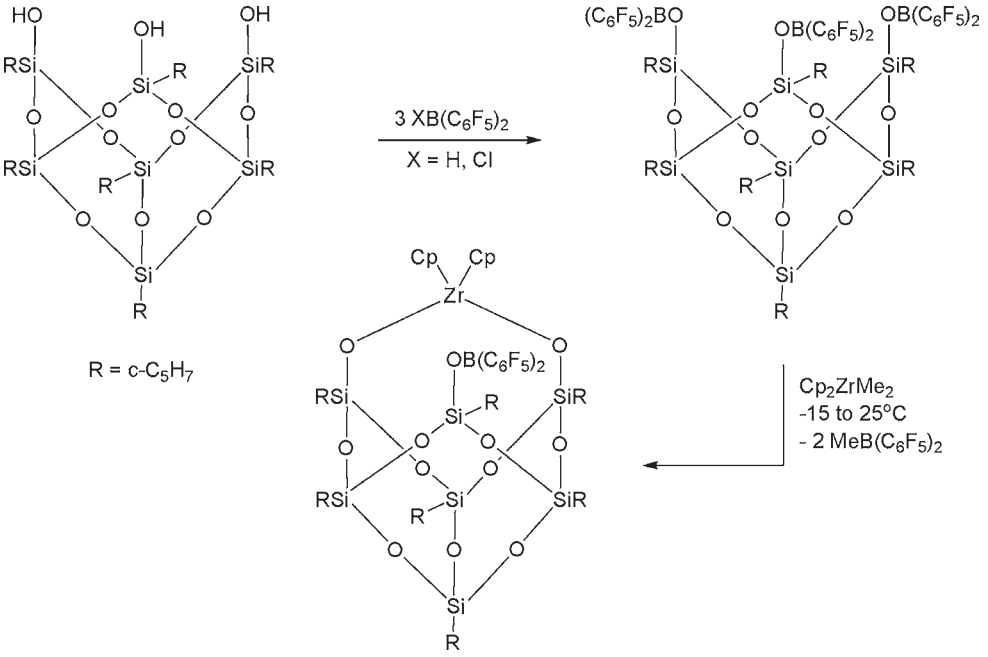

Scheme 5.13 Formation of silsesquioxane-supported borane activator and its reaction with Cp_2ZrMe_2.

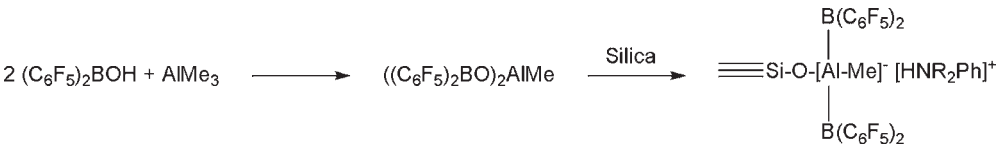

Scheme 5.14 Formation of a surface-supported ionic aluminoborate activator.

bis(pentafluorophenyl)borinic acid, supported on silica in the presence of Lewis base, also activates Me_2Si(2-methyl-4-phenylindenyl)$ZrCl_2/AlMe_3$ [65]. The boralumoxane $((C_6F_5)_2BO)_3Al$, formed from $AlMe_3$ and three equivalents of bis(perfluorophenyl)borinic acid, can be used in similar manner [66].

5.4 Conclusions

Perfluorophenylboron-based activators were originally intended for the creation of model systems to explore the nature of the active site in single-site polymerization catalysts. Nonetheless, these materials impart remarkable activities, indeed as high as those of their MAO-cocatalyzed counterparts, to the catalysts in which they are used, despite being present in stoichiometric ratios. In recent years, many research investigations, conducted notably within industrial laboratories, have led to these systems becoming commercially viable following their immobilization onto inorganic oxide carriers. In this way, they have become compatible with commercial polymerization processes that require insoluble and morphologically uniform catalysts to create polymers with properties similar to those produced by their homogeneous counterparts.

References

1 H.W. Turner, G.G. Hlatky, R.R. Eckman, U.S. Patent 5,198,401, 1993.
2 J.A. Ewen, M.J. Elder, U.S. Patent 5,387,568, 1995.
3 (a) X. Yang, C.L. Stern, T.J. Marks, *J. Am. Chem. Soc.* 1991, *113*, 3623; (b) J.A. Ewen, M.J. Elder, U.S. Patent 5,561,092, 1996.
4 E.Y.-X. Chen, T.J. Marks, *Chem. Rev.* 2000, *100*, 1391.
5 (a) G.G. Hlatky, *Chem. Rev.* 2000, *100*, 1347; (b) J.R. Severn, J.C. Chadwick, R. Duchateau, N. Friedrichs, *Chem. Rev.* 2005, *105*, 4073.
6 G.G. Hlatky, D.J. Upton, H.W. Turner, PCT Int. Appl. 91/09982, 1991.
7 G.G. Hlatky, D.J. Upton, *Macromolecules* 1996, *24*, 8019.
8 D.G. Ward, U.S. Patent 5,885,924, 1999.
9 K. Inatomi, K. Inahara, A. Yano, M. Sato, European Patent Appl. 628,574, 1994.
10 C.C. Meverden, M.W. Lynch, U.S. Patent 6,762,255, 2004.
11 T. Inatomi, F. Takahashi, A. Yano, M. Sato, M. Jpn. Laid-Open Appl. 08/109216, 1996.
12 D.J. Upton, J.M. Canich, G.G. Hlatky, H.W. Turner, PCT Int. Appl. 94/03506, 1994.
13 J. Matsumoto, U.S. Patent 5,444,134, 1995.
14 D.W. Stephan, J.C. Stewart, D.G. Harrison, European Patent Appl. 890,581, 1999.
15 S. Wang, U.S. Patent 6,291,386, 2001.
16 S.-C. Kao, P.A. Khokhani, U.S. Patent 6,852,659, 2005.
17 J.N. Colter, III, J.W. Van Egmond, L.J. Fouts, Jr., R.B. Painter, P.C. Vosejpka, U. S. Patent 7,115,689, 2006.
18 (a) M. Kristen, G. Hauck, PCT Int. Appl. 2001/077186, 2001; (b) C. Nenu, B. Weckhuysen, P. Bodart, European Patent Appl. 1,564,198, 2005.
19 L.S. Moody, P.B. Mackenzie, C.M. Killian, G.G. Lavoie, J.A. Ponasik, Jr., T.W. Smith, J.C. Pearson, A.G.M. Barrett, U.S. Patent 6,579,823, 2003.

20 M.W. Holtcamp, PCT Int. Appl. 2002/018452, 2002.
21 M.W. Holtcamp, U.S. Patent 6,632,770, 2003.
22 B.S. Kimberley, S. Mastroianni, M.J. Taylor, PCT Int. Appl. WO 2005/016980, 2005.
23 F. Takahashi, A. Yano, European Patent Appl. 619,326, 1994.
24 (a) J. Lynch, D. Fischer, H.-H. Görtz, G. Schweier, U.S. Patent 6,326,444, 2001; (b) J. Lynch, D. Fischer, H.-H. Görtz, G. Schweier, U.S. Patent 6,433,110, 2002.
25 C. Fritze, H. Bohnen, F. Küber, U.S. Patent 6,177,376, 2001.
26 M. Kristen, H. Gregorius, U. Rief, U.S. Patent 6,433,111, 2002.
27 N. Inoe, M. Jinno, T. Shiomura, Jpn. Laid-Open Appl. 05/155926, 1993.
28 H.W. Turner, U.S. Patent 5,427,991, 1995.
29 S. Hinokuma, S. Miyake, M. Ono, S. Inazawa, U.S. Patent 5,869,723, 1999.
30 E.M. Carnahan, M.J. Carney, D.R. Neithamer, P.N. Nickias, K.-Y. Shih, L. Spencer, U.S. Patent 6,087,293, 2000.
31 G.B. Jacobsen, P. Wijkens, J.T.B.H. Jastrzebski, G. Van Koten, U.S. Patent 5,834,393, 1998.
32 K.-Y. Shih, U.S. Patent 6,184,171, 2001.
33 G.B. Jacobsen, T.J.P. Stevens, P. Loix, U.S. Patent 5,783,512, 1998.
34 M.W. Holtcamp, U. S. Patent 6,147,173, 2000.
35 E.M. Carnahan, D.R. Neithamer, PCT Int. Appl. 2001/058969, 2001.
36 K. Musikabhumma, T.P. Spaniol, J. Okuda, *J. Mol. Catal.* 2004, *208*, 73.
37 T. Kaneko, M. Sato, U.S. Patent 5,807,938, 1998.
38 D. Fischer, F. Langhauser, J. Kerth, G. Schweier, J. Lynch, H.-H. Görtz, European Patent Appl. 700,935, 1996.
39 R.D. Swindoll, B.A. Story, B.W.S. Kolthammer, K.P. Peil, D.R. Wilson, J.C. Stevens, U.S. Patent 6,538,080, 2003.
40 B.W.S. Kolthammer, J.C. Tracy, R.S. Cardwell, R.K. Rosen, U.S. Patent 5,763,547, 1998.
41 H. Knuuttila, K. Kallio, O. Andell, U.S. Patent 6,506,858, 2003.
42 K.P. Peil, D.R. Wilson, U.S. Patent 6,479,599, 2002.
43 E.M. Carnahan, G.B. Jacobsen, U.S. Patent 6,475,945, 2002.
44 E.M. Carnahan, G.B. Jacobsen, E.Y. Chen, J.C. Stevens, U.S. Patent 6,696,379, 2004.
45 (a) M.W. Holtcamp, C.-T. Lue, PCT Int. Appl. 2000/04058, 2000; (b) L.G. McCullough, M.W. Holtcamp, U.S. Patent Appl. 2004/0102312, 2004.
46 J.F. Walzer, Jr., U.S. Patent 5,643,847, 1997.
47 D.G. Ward, E.M. Carnahan, U.S. Patent 5,939,347, 1999.
48 S. Charoenchaidet, S. Chavadej, E. Gulari, *J. Polym. Sci. Polym. Chem.* 2002, *40*, 3240.
49 H. Bohnen, C. Fritze, U.S. Patent 7,202,190, 2007.
50 M. Kwanten, B.A.M. Carrière, P.J. Grobet, P.A. Jacobs, *Chem. Commun.* 2003, 1508.
51 J.C. Vizzini, R.K. Chudgar, U.S. Patent 6,143,686, 2000.
52 (a) P. Brant, U.S. Patent 6,562,920, 2003; (b) P. Brant, U.S. Patent 6,590,055, 2003.
53 V.N. Panchenko, I.G. Danilova, V.A. Zakaharov, E.A. Paukshtis, *J. Mol. Catal. A* 2005, *225*, 271.
54 N. Millot, C.C. Santini, A. Baudouin, J.-M. Basset, *Chem. Commun.* 2003, 2034.
55 S. Charoenchaidet, S. Chavadej, E. Gulari, *J. Mol. Catal. A* 2002, *185*, 167.
56 (a) M. Chang, PCT Int. Appl. WO 2001/36499, 2001; (b) M. Chang, U.S. Patent 6,395,847, 2002.
57 S. Charoenchaidet, S. Chavadej, E. Gulari, *Macromol. Rapid Commun.* 2002, *23*, 426.
58 G. Rodriguez, A.N. Speca, M.C. Kuchta, D. H. McConville, T.J. Burkhardt, U.S. Patent Appl. US2005/0159299, 2005.
59 J. Tian, S. Wang, Y. Feng, J. Li, S. Collins, *J. Mol. Catal. A* 1999, *144*, 137.
60 G. Rodriguez, PCT Int. Appl. 2000/04059, 2000.
61 C. Fritze, F. Küber, H. Bohnen, U.S. Patent 6,329,313, 2001.
62 R.A. Metcalfe, D.I. Kreller, J. Tian, H. Kim, N.J. Taylor, J.F. Corrigan, S. Collins, *Organometallics* 2002, *21*, 1719.
63 (a) H. Bohnen, C. Fritze, U.S. Patent 6,500,908, 2002; (b) M.W. Lynch, C.C. Meverden, S. Nagy, K.L. Neal-Hawkins, U.S. Patent 6,759,361, 2004.
64 (a) H. Bohnen, C. Fritze, U.S. Patent 6,482,902, 2002; (b) H. Bohnen, M. Göres, C. Fritze, U.S. Patent 6,576,723, 2003;

(c) R. Kratzer, C. Fritze, J. Schottek, U.S. Patent 6,953,829, 2005; (d) R. Kratzer, V. Fraaije, U.S. Patent Appl. US2005/0272596, 2005; (e) R. Kratzer, U.S. Patent Appl. US2006/0105905, 2006; (f) R. Kratzer, PCT Int. Appl. WO2004/007570, 2004.

65 J. Schottek, C. Fritze, H. Bohnen, P. Becker, PCT Int. Appl. WO2000/20466, 2000.

66 T. Sell, J. Schottek, N.S. Paczkowki, A. Winter, PCT Int. Appl. WO2006/124231, 2006.

6
Catalysts Supported on Magnesium Chloride

John C. Chadwick

6.1
Introduction

As outlined in Chapter 2, the successful development of high-activity Ziegler–Natta catalysts for the production of polyolefins has been, and continues to be, based on the use of magnesium chloride supports. It is therefore somewhat surprising that, as noted by Hlatky [1] in 2000, magnesium chloride has been studied far less extensively than silica as a carrier for single-site catalysts. However, recently there has been a notable increase in the number of research investigations on single-site catalyst immobilization and activation using $MgCl_2$-based systems [2]. This interest stems partly from the use of methods for controlling the particle size, porosity and morphology of $MgCl_2$ supports, previously developed for Ziegler–Natta catalysts. Such supports may also have the advantage of easier fragmentation than is generally the case with silica supports, thereby facilitating polymer particle growth during polymerization [3, 4].

It has now been demonstrated that high polymerization activity can be achieved with a broad range of early- and late-transition metal catalysts immobilized on $MgCl_2$, using simple aluminum alkyl cocatalysts (see Section 6.5). In this chapter, details of catalyst activation with $MgCl_2$ in the absence of cocatalyst are first described (Section 6.2), followed by discussions on the use of $MgCl_2$ supports in combination with methylaluminoxane (MAO) and borate activators (Sections 6.3 and 6.4, respectively).

6.2
Magnesium Chloride as Activator

In certain cases, magnesium chloride can function as a catalyst activator even in the absence of any additional cocatalyst, as a result of its Lewis acidity. This has been reported by Marks, who showed that $MgCl_2$ was able to activate $(C_5Me_5)_2ThMe_2$ by the abstraction of a methide anion, generating a catalytically active actinide center $[(C_5Me_5)_2ThMe]^+$, as illustrated in Figure 6.1 [5]. The formation of $Mg–CH_3$

Tailor-Made Polymers. Via Immobilization of Alpha-Olefin Polymerization Catalysts.
Edited by John R. Severn and John C. Chadwick

ISBN: 978-3-527-31782-0

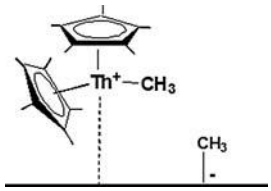

Figure 6.1 Generation of catalytically active species by CH_3^- transfer to a Lewis acidic surface site on $MgCl_2$ (data from Ref. [5]).

species and the insertion of ethylene into the Th–CH_3 bond was demonstrated using ^{13}C cross-polarization/magic angle spinning (CP/MAS) NMR spectroscopy, which also revealed that approximately 50% of the Th in this system was catalytically active [6].

The presence of surface acidic sites in magnesium chloride (which have been suggested as possible sites for $TiCl_4$ adsorption in a Ziegler–Natta catalyst) has been demonstrated for $MgCl_2$ prepared by the reaction of magnesium with excess *n*-BuCl in refluxing heptane [7]. Indeed, the concentration of surface acidic sites in this material was found to be much higher than that in a sample of ball-milled $MgCl_2$. The surface acidic site concentration in the chemically synthesized support corresponded to the amounts of titanium and iron catalysts that could effectively be immobilized on it [8]. However, the surface acidic site concentration of approximately 170 $\mu mol\,g^{-1}$ reported for this support may not necessarily correspond to the proportion of surface acidic sites able to activate a single-site catalyst by alkide abstraction.

An obvious limitation of the use of magnesium chloride in the absence of any further cocatalyst or activator is that, aside from lacking the beneficial effect of an aluminum alkyl as a scavenger of impurities in polymerization systems, this approach requires the use of transition metal alkyls rather than the more commonly used chlorides. Thus, much more attention has been paid to the possible use of magnesium chloride in combination with various cocatalysts and activators, as described in the following sections.

6.3
Magnesium Chloride/Methylaluminoxane

Taking into account the widespread development and utilization of silica/MAO-based systems for the immobilization of metallocenes and other single-site catalysts, it is not surprising that a variety of efforts have been made to use $MgCl_2$-immobilized catalysts together with MAO as cocatalyst, or to immobilize the aluminoxane itself on a magnesium chloride support.

An early example of the use of MAO as cocatalyst in ethylene polymerization with $MgCl_2$-supported metallocenes involved a support prepared by the reaction of $MgBu_2$ with *t*BuCl in the presence of di*iso*amyl ether in hexane, followed by

treatment with Cp_2ZrCl_2 [9]. This support had a spheroidal morphology with narrow particle size distribution; a narrow molecular weight distribution (MWD) polyethylene (PE) was obtained, indicating retention of the single-site characteristics of the zirconocene. A related patent describes the treatment of the support with *n*BuOH prior to contact with the metallocene [10]. Catalyst supports prepared by the reaction of $MgBu_2$ with *t*BuCl in the absence of an electron donor have also been described [11]. The resulting $MgCl_2$ was treated with a toluene solution of $(n\text{BuCp})_2ZrCl_2$ and MAO to give a catalyst used with $AlEt_3$ in ethylene polymerization. The activities obtained were significantly higher than those of comparative examples in which a SiO_2 support was used.

The preparation and use of supports obtained by partial dealcoholation of adducts of $MgCl_2$ and ethanol having spherical particle morphology has also been described [12]. The reaction of these supports with an aluminum alkyl gives rise to the formation of products having a composition $MgCl_2/AlEt_n(OEt)_{3-n}$ (this is described in more detail in Section 6.5). A spherical catalyst prepared by partial dealcoholation of $MgCl_2 \cdot 3EtOH$, followed by reaction with Al*i*Bu_3 and subsequent impregnation with a toluene solution containing the reaction product of *rac*-$Et(Ind)_2ZrCl_2$ and Al*i*Bu_3, was used together with MAO in ethylene polymerization in hexane slurry at 75 °C, giving a yield of 2 kg PE g^{-1} catalyst. A further example of heterogenization of a zirconocene on a $MgCl_2$-derived support is the reaction of $MgCl_2 \cdot n$EtOH with $AlEt_3$ and treatment of the product with $(n\text{-BuCp})_2ZrCl_2$ to give an immobilized catalyst used in ethylene polymerization in combination with MAO [13]. Relatively low activities (up to 158 kg mol^{-1} bar^{-1} h^{-1}) were reported. A Basell patent application describes the reaction of $MgCl_2 \cdot 2.5EtOH$ with MAO in toluene, followed by treatment of the product with *rac*-$Me_2Si(2\text{-Me-BenzInd})_2ZrCl_2$ and MAO [14]. This catalyst was used in propylene polymerization at 65 °C (liquid monomer, containing Al*i*Bu_3), giving isotactic polypropylene (PP) having a spherical particle morphology and narrow MWD (M_w/M_n = 2.0) in a yield of 0.4 kg g^{-1} catalyst. The preparation and use of an adduct of magnesium chloride and ethanol is also described in a recent Equistar patent application [15]. Here, $MgCl_2 \cdot 2.5EtOH$ was treated first with MAO and then with a mixture of MAO and a zirconocene complex containing an indenoindolyl ligand. The resulting catalyst had higher ethylene polymerization activity than was obtained using either anhydrous magnesium chloride or calcined SiO_2 as support material.

$MgCl_2$-based supports having relatively high contents of MAO have been obtained by the dealcoholation of a spherical adduct $MgCl_2 \cdot 2.6EtOH$ at 250 °C, followed by treatment with a solution of MAO in toluene and a crosslinking agent such as glycol, glycerol, or triethanolamine [16]. The incorporation of the crosslinking agent increased the Al content in the support up to around 12 wt.%. These $MgCl_2$/MAO supports were mixed with *rac*-$Et(Ind)_2ZrCl_2$ and used in ethylene polymerization, giving a spherical polyethylene morphology and activities of up to 2320 kg mol^{-1} bar^{-1} h^{-1} at 80 °C, about three-fold higher than the activity obtained with a support containing 3.8 wt.% Al prepared without a crosslinking agent.

Hydrated magnesium chloride, $MgCl_2.nH_2O$, has also been used as a support precursor for the immobilization of MAO and a zirconocene, after calcining at

200 °C [17]. It is likely that $Mg(OH)_nCl_{2-n}$ is formed during the calcination step, thus facilitating chemical tethering of MAO to the support.

Solid $MgCl_2 \cdot n$ROH supports have also been prepared by dissolving $MgCl_2$ in excess ethanol or methanol, adding decane, and then heating under vacuum to effect partial removal of the alcohol and precipitation of the support [18]. Such supports were reacted with aluminum alkyls and then treated with Cp_2ZrCl_2 or *rac*-$Et(Ind)_2ZrCl_2$ to give immobilized catalysts which were used together with MAO in ethylene/1-hexene copolymerization. The activity was found to be enhanced by the presence of the comonomer, as has been observed with many other heterogeneous catalysts, with activities of up to 3400 $kg\,mol^{-1}\,bar^{-1}\,h^{-1}$ being obtained. It was also observed that the MWDs obtained with these systems were broader than those obtained with Cp_2ZrCl_2/MAO under homogeneous polymerization conditions. The preparation of hybrid Ziegler–Natta/metallocene catalysts was also investigated, incorporating $TiCl_4$ together with the zirconocene [19–21].

Magnesium chloride has also been used together with silica for the immobilization of metallocene catalysts. One approach followed involved the impregnation of calcined silica with a solution of $MgCl_2$ and Cp_2TiCl_2 or Cp_2ZrCl_2 in tetrahydrofuran (THF). The immobilized catalysts were used in ethylene polymerization, with MAO as cocatalyst [22]. These systems gave higher activities and narrower polymer MWDs than were obtained in the absence of magnesium chloride. The $SiO_2/MgCl_2/Cp_2ZrCl_2$–MAO system was also active in producing polymer at high temperature (110 °C), in contrast to the homogeneous system Cp_2ZrCl_2–MAO, which produced only oligomers at this temperature.

A further example of the use of THF in support preparation is the ball-milling of a solid adduct of composition $MgCl_2 \cdot 2$THF with $AlEt_2Cl$ in toluene, followed by milling with Cp_2ZrCl_2 to give a catalyst which was used in ethylene polymerization together with MAO [23]. The results indicated that partial heterogenization of the metallocene could be obtained in this way, although this was not the case when AlR_3 or MAO was used in place of $AlEt_2Cl$. A more complete heterogenization was achieved by first ball-milling $MgCl_2 \cdot 2$THF and $AlEt_2Cl$ in hexane and then washing with hexane. The product, $MgCl_2 \cdot THF \cdot 0.34AlEt_2Cl$, was ball-milled with Cp_2ZrCl_2 in a mixture of hexane and toluene and washed with these solvents to remove non-immobilized zirconocene [24]. In ethylene polymerization at 50 °C, the polymer yield increased linearly with time, giving an activity of around 2400 $kg\,mol^{-1}\,bar^{-1}\,h^{-1}$. An increase in the polyethylene molecular weight with increasing polymerization time was also observed, and a narrow MWD (M_w/M_n = 2.4) was reported.

Catalysts prepared by contacting an aluminum alkyl with the product of ball-milling $MgCl_2 \cdot 2$THF with Cp_2ZrCl_2 have been used with MAO in ethylene/1-hexene copolymerization [25]. The activities were approximately five-fold lower than was obtained in a homogeneous polymerization with Cp_2ZrCl_2/MAO, the highest activity being obtained using MAO in both in the catalyst support treatment and as cocatalyst. The copolymer molecular weights were relatively low, in the range of 13 000 to 53 000, and decreased with increasing 1-hexene concentration. The MWDs (M_w/M_n = 2.5–4.5) were broader than those obtained in homo-

geneous polymerization, and differential scanning calorimetry (DSC) studies of the copolymers indicated a non-uniform chemical composition distribution (CCD). A subsequent report described the use of catalysts obtained by the treatment of $MgCl_2 \cdot 2THF$ with Al*i*Bu_3 and then ball-milling with various metallocenes [26]; in this way, catalysts containing 0.06 to 0.27 wt.% Zr were obtained. Again, using MAO as cocatalyst, the highest activity in ethylene homopolymerization (6400 kg $mol^{-1}\,bar^{-1}\,h^{-1}$) was obtained with $(i\text{PrCp})_2ZrCl_2$, while $(Me_5Cp)_2ZrCl_2$ gave the highest activity (6800 kg $mol^{-1}\,bar^{-1}\,h^{-1}$) in ethylene/1-hexene copolymerization, but with a low comonomer incorporation. The highest hexene incorporation was obtained with $(t\text{BuCp})_2ZrCl_2$. Cp_2ZrCl_2 gave activities of 6000 and 4400 kg $mol^{-1}\,bar^{-1}\,h^{-1}$ in homopolymerization and copolymerization, respectively, both of which were significantly higher than the activities of 400 to 800 kg $mol^{-1}\,bar^{-1}\,h^{-1}$ obtained with Cp_2TiCl_2. The latter catalyst gave significantly broader MWDs than were obtained with the zirconocenes. In all cases, comonomer incorporation with the immobilized catalysts was lower than in homogeneous polymerization. The compositional heterogeneity of copolymers synthesized in this way has been investigated by a DSC fractionation technique involving stepwise isothermal segregation [27]. A comparison of copolymers prepared with homogeneous and immobilized zirconocenes revealed broader composition distributions for the heterogeneous systems, which gave additional melting peaks in the high-temperature region, corresponding to fractions with very low comonomer contents.

6.4 Magnesium Chloride/Borate

Relatively few examples have been reported of the use of a magnesium chloride support in combination with borate activators. In this case, the main challenge is to develop an effective method for effective coordination or tethering of the activator on the support. A recent example of such an approach was the synthesis and use of the borate $[Ph_3C][B(C_6F_5)_3(C_6H_4NMe_2)]$ [28]. Here, use is made of the ability of the amine to coordinate strongly to magnesium chloride, leading to immobilization of the borate activator. Impregnation of a chemically activated $MgCl_2$ support with this borate, followed by treatment with a toluene solution of the product of reacting *rac*-$Me_2Si(1\text{-indenyl})_2ZrCl_2$ with Al*i*Bu_3, gave an immobilized catalyst used in ethylene and propylene homopolymerization and in ethylene/1-butene copolymerization. An ethylene polymerization activity of approximately 1700 kg $mol^{-1}\,bar^{-1}\,h^{-1}$ was obtained at 60 °C, without reactor fouling.

Another example of the preparation and use of a $MgCl_2$-supported borate activator is the reaction of $[HNEt_3][B(C_6F_5)_3(C_6H_4\text{-}4\text{-}OH)]$ with a support of type $MgCl_2/AlEt_n(OEt)_{3-n}$, obtained by the reaction of $AlEt_3$ with an adduct of magnesium chloride and ethanol [29]. This borate has previously been used in combination with silica supports pretreated with MAO or AlR_3, with the aim of tethering the borate to the support material via reaction of the Si–O–Al–R moiety with the active

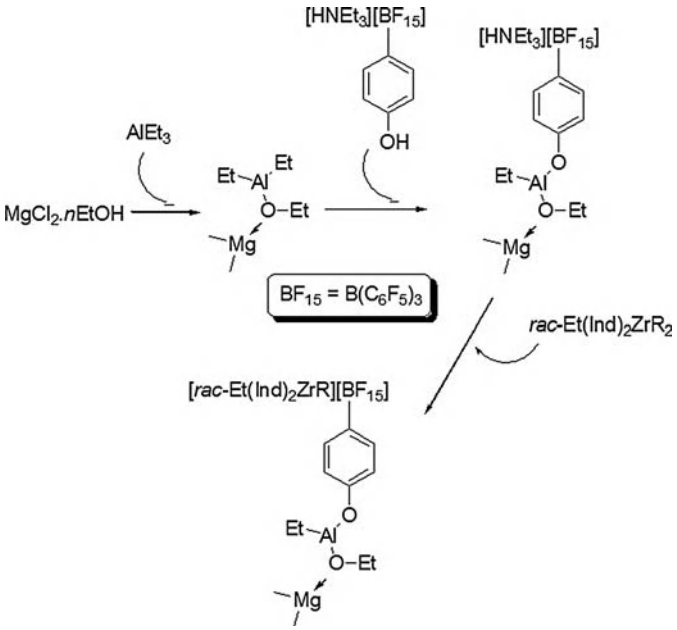

Figure 6.2 Immobilization of a borate-activated metallocene on a $MgCl_2$-based support [29].

hydrogen of the borate [30]. In the case of the $MgCl_2$-supported system, the aim was to immobilize the borate by reaction with an aluminum alkyl which is itself immobilized via the formation of coordinatively bridged species of type Mg–O(Et)–Al. The approach is illustrated in Figure 6.2. The use of the immobilized borate together with *rac*-$Me_2Si(1\text{-indenyl})_2ZrCl_2$ and $AliBu_3$ resulted in an activity of about 1000 kg mol^{-1} bar^{-1} h^{-1} in ethylene polymerization at 50 °C. A comparative experiment using a silica support gave a much lower activity, ascribed to the more difficult support fragmentation in the case of silica. The polymers prepared with the $MgCl_2$-based support were free-flowing powders with a spheroidal particle morphology.

The immobilization of a borate activator on a magnesium chloride support has also been carried out via physical impregnation [29]. This approach follows a method previously reported for the impregnation of $AlEt_3$-pretreated silica with $[Ph_3C][B(C_6F_5)_4]$ or $[HNMe_2Ph][B(C_6F_5)_4]$, making use of the relatively poor solubility of these borates in aliphatic hydrocarbon solvents, compared with their solubility in toluene [31]. The impregnation of a $MgCl_2/AlEt_n(OEt)_{3-n}$ support with a solution of the borate in toluene, followed by solvent removal and then contact with Cp_2ZrCl_2 or *rac*-$Me_2Si(2\text{-MeInd})_2ZrCl_2$ before polymerization, gave a very porous polyethylene particle morphology. In the case of propylene polymerization, catalyst leaching from the support was observed, the particle morphology being inferior to that obtained with chemically tethered borate [29].

Other examples of the use of magnesium chloride in combination with a borate activator are to be found in the patent literature. In one case, $MgCl_2$ was ball-milled with $[Ph_3C][B(C_6F_5)_4]$ and then contacted with the product of mixing *i*Pr(Cp)(Flu)$ZrCl_2$ and $AlEt_3$ to produce a catalyst giving syndiotactic PP [32]. In another case, $MgCl_2$ was mixed with Cp_2ZrCl_2, Al*i*Bu_3 and $[HNMe_2Ph][B(C_6F_5)_4$ and ball-milled in toluene to give a catalyst used in ethylene polymerization [33].

6.5
Magnesium Chloride/Aluminum Alkyl

The use of magnesium chloride in combination with a simple aluminum alkyl cocatalyst such as $AlEt_3$ or Al*i*Bu_3 has the desirable advantage of avoiding the use of a more expensive and more complicated aluminoxane or borate activator. It has been shown that an increasingly wide range of early- and late-transition metal catalysts can be activated in this way. Late-transition metal catalysts such as bis(imino)pyridyl iron complexes are readily activated by aluminum trialkyls even when unsupported, whereas with many early-transition metal complexes the magnesium chloride support plays an important role in the catalyst activation process. Examples of the immobilization and activation of early- and late-transition metal complexes, respectively, using $MgCl_2$-based supports and aluminum alkyls such as AlR_3, are described in the following subsections.

6.5.1
Early-Transition Metal Complexes

As indicated in Section 6.2, an important feature of magnesium chloride as a support material for single-site catalysts is the presence of Lewis acidic centers, which can enable catalyst activation without the use of MAO or borates. An example of this was the use of highly dispersed magnesium chloride, prepared by reaction of $MgCl_2 \cdot n AlEt_3$ with CCl_4 [34]. Treatment of the support with a toluene solution of *rac*-$Me_2Si(Ind)_2ZrCl_2$ for 1 h at 50 °C, followed by washing with heptane, gave an immobilized catalyst containing 0.2 wt.% Zr. With Al*i*Bu_3 as cocatalyst, an ethylene polymerization activity of 1155 kg mol^{-1} bar^{-1} h^{-1} was obtained at 80 °C, which was similar to activities obtained using a SiO_2/MAO support but much lower than obtained in homogeneous polymerization using MAO as cocatalyst. The $MgCl_2$-supported zirconocene was found to be relatively insensitive to chain transfer with hydrogen [34] and, in contrast to the SiO_2-supported catalyst, did not exhibit a comonomer activation effect in ethylene/1-hexene copolymerization [35].

An early report of the immobilization of a zirconocene using $MgCl_2$ involved ball-milling of a mixture of the anhydrous support and *rac*-Et(IndH4)$_2ZrCl_2$, to give a catalyst containing 20 μmol Zr g^{-1} [36]. The catalyst was active in propylene polymerization, with $AlMe_3$ or $AlEt_3$ as cocatalyst, although the activity was about

an order of magnitude less than that obtained in homogeneous polymerization using MAO. Isotactic PP with M_w/M_n of 4–5 was obtained, indicating the presence of non-uniform active species. A key role of the $MgCl_2$ support in the formation of active species was inferred from the fact that no activity was obtained with the systems *rac*-Et(IndH4)$_2ZrCl_2$–$AlMe_3$ or SiO_2/*rac*-Et(IndH4)$_2ZrCl_2$–$AlMe_3$. A subsequent report described the use of the same support for the immobilization of *i*Pr(Cp)(Flu)$ZrCl_2$ and Cp_2ZrCl_2, giving syndiotactic and atactic PP, respectively [37]. A linear increase in polymer yield with increasing polymerization time indicated very high stability for the system $MgCl_2$/*rac*-Et(IndH4)$_2ZrCl_2$–$AlMe_3$ [38]. Ethylene/propylene and ethylene/1-hexene copolymerization with the catalyst system $MgCl_2$/*rac*-Et(IndH4)$_2ZrCl_2$–AlR_3 resulted in mixtures of copolymers and polyethylene when Al*i*Bu_3 was used, whereas $AlMe_3$ gave random copolymers [39].

An important advantage of the use of magnesium chloride as a support for single-site catalyst immobilization is that this very often leads to very stable catalytic activity, preventing the rapid decay in activity that is often observed in olefin polymerization with homogeneous systems. An illustration of this was the stable activity obtained with a precipitated catalyst obtained by the addition of hexane to a solution of $MgCl_2$ and Cp_2TiCl_2 in THF [40]. Ethylene polymerization was carried out in xylene at 40 °C, with $AliBu_3$ as cocatalyst, giving an activity of 2.5 kg mol^{-1} bar^{-1} h^{-1}.

Magnesium chloride supports can also be prepared *in situ*, for example by the reaction of $MgBu_2$ with $AlEt_2Cl$, which generates $MgCl_2$ and AlR_3 [41]. Reaction in toluene resulted in a quasi-colloidal mixture containing finely dispersed magnesium chloride, which was used for the activation of Cp_2ZrCl_2 and other metallocenes in ethylene homopolymerization and ethylene/1-hexene copolymerization, giving activities which were five- to ten-fold lower than those obtained with MAO. Relatively broad MWDs were obtained (M_w/M_n = 10–15), although the copolymers had relatively narrow composition distributions. A mechanism of active center formation similar to that described by Marks [5] was proposed, whereby the $MgCl_2$ support abstracts R^- from the species formed by alkylation of the zirconocene.

The above approaches suffer the disadvantage of a lack of control over the particle morphology of the support. Recently, increased attention has been paid to the utilization and extension of approaches used in the development of controlled-morphology supports for Ziegler–Natta catalysts. One of these, developed by Basell and its predecessor companies, involves the production of almost perfectly spherical supports having controlled particle size by the cooling of emulsions of molten $MgCl_2 \cdot n$ROH adducts in paraffin oil [42]. In Ziegler–Natta catalyst production, these supports are reacted with $TiCl_4$ and other components. As indicated in Section 6.3, porous support materials may be prepared by the partial dealcoholation of a $MgCl_2 \cdot 3$EtOH adduct, followed by reaction with AlR_3 or MAO [12]. Similar supports have now been used for the immobilization of a range of early- and late-transition metal catalysts, as described below. A different approach – the roots of which are apparent in Ziegler–Natta catalyst patents filed by Mitsui [43] – involves the use of a solution of a 1:3 adduct of $MgCl_2$ and 2-ethyl-1-hexanol

in decane. Activation of the Ti-based bis(phenoxy-imine) complex **1**, one of a series of "FI" catalysts developed by Mitsui, was carried out by first contacting this solution with Al*i*Bu$_3$ to give MgCl$_2$/Al*i*Bu$_n$(OR)$_{3-n}$, after which the catalyst was added [44]. This support preparation and catalyst activation/immobilization was carried out *in situ* in the polymerization reactor, in toluene. Ethylene polymerization at 50 °C gave an activity of approximately 4000 kg mol^{-1} bar^{-1} h^{-1}, which was approximately 80% of the activity obtained under homogeneous conditions using MAO, and a well-defined polymer particle morphology was obtained. It was suggested that the effectiveness of the MgCl$_2$-based activator was related to the presence in the bis(phenoxy-imine) complex of O and N heteroatoms capable of electronic interaction with the support. Narrow MWDs were obtained (M_w/M_n = 2.4–2.7), indicating the presence of a single active species. A further indication for single-site catalysis was the narrow chemical composition distribution of an ethylene–propylene copolymer prepared with this catalyst system.

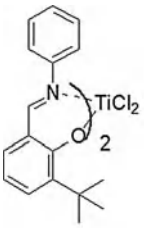

1

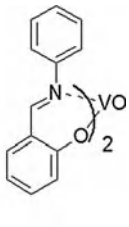

2

The use of supports obtained by reaction of AlR$_3$ with MgCl$_2$/2-ethylhexanol was subsequently extended to the activation of zirconium- and vanadium-based bis(phenoxy-imine) complexes [45–47]. The vanadium complex **2** was used in ethylene polymerization in combination with MgCl$_2$/AlEt$_n$(OR)$_{3-n}$, AlEt$_2$Cl and ethyl trichloroacetate. Stable polymerization kinetics were obtained at both 50 and 75 °C, whereas with VOCl$_3$ an increase in polymerization temperature led to rapid decay and a decrease in productivity. With complex **2**, an activity of 65 100 kg mol^{-1} bar^{-1} h^{-1} was obtained at 75 °C. An ethylene/propylene copolymerization gave an amorphous copolymer with relatively broad MWD (M_w/M_n = 4.7), with gel-permeation chromatography/infrared spectroscopy (GPC-IR) revealing that the propylene content was highest in the high-molecular-weight fraction of the copolymer [45]. Particularly high activities were obtained with bis(phenoxy-imine) zirconium complexes, the highest being an activity of 202 000 kg mol^{-1} bar^{-1} h^{-1} with complex **3** used with MgCl$_2$/Al*i*Bu$_n$(OR)$_{3-n}$ at 50 °C [45]. This activity was higher than that obtained when MAO was used as cocatalyst with complex **3**, and the polymer molecular weight (M_v) was estimated to exceed 5×10^6 Da. The MWD of this polymer could not be determined, but another zirconium bis(phenoxy-imine) complex catalyst (**4**) gave a broad MWD with M_w/M_n = 13.2. It was demonstrated that a spheroidal PE morphology, with a particle size around 100 µm, could be obtained via this approach [46]. Living polymerization has also been demonstrated

with an FI catalyst immobilized and activated using $MgCl_2/AliBu_n(OR)_{3-n}$ [48]. In this case, the fluorinated bis(phenoxy-imine) Ti complex **5** was used to polymerize propylene to syndiotactic PP. Use of the $MgCl_2/AlR'_n(OR)_{3-n}$ activator/supports for olefin polymerization catalysts has recently been reviewed by Fujita and coworkers [49].

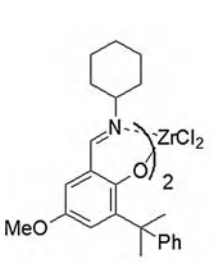

3

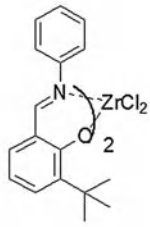

4

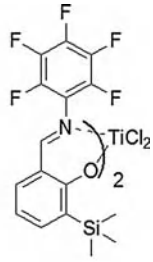

5

Supports obtained by reacting an aluminum trialkyl with solid $MgCl_2$/ethanol adducts having a spherical particle morphology have been shown to be effective for the immobilization and activation of a wide range of early-transition metal catalysts, including titanium-, vanadium-, and chromium-based systems [50–54]. The reaction of AlR_3 with $MgCl_2$/EtOH adducts having an EtOH/$MgCl_2$ molar ratio in the range 1.1 to 2.8 gave supports of composition $MgCl_2/AlR_n(OEt)_{3-n}$. The amount of residual alkylaluminum ethoxide in the solid support was greater with $AlEt_3$ than when $AliBu_3$ was used, and increased with increasing ethanol content in the $MgCl_2$/EtOH adduct [50]. In ethylene polymerizations carried out with Cp_2TiCl_2 on these supports, using $AliBu_3$ as cocatalyst/scavenger, the catalyst activity was observed to increase as the loading of catalyst on the support decreased. Immobilization was carried out simply by contacting the support with a solution of the catalyst in toluene; complete discoloration of the solution indicated quantitative uptake of catalyst by the support. Activities at 50 °C ranged from about 600 kg mol^{-1} bar^{-1} h^{-1} with Cp_2TiCl_2 to 7000–8000 kg mol^{-1} bar^{-1} h^{-1} with $CpTiCl_3$ and related complexes [51]. A narrow MWD was obtained, with M_w/M_n in the range 2–3. In comparison, an experiment with $TiCl_4$ gave an activity of more than 25 000 kg mol^{-1} bar^{-1} h^{-1}, but a broader MWD (M_w/M_n = 4.1), which was indicative of a Ziegler–Natta rather than a single-site catalyst system. Very stable polymerization kinetics were obtained in all of these polymerizations, which also resulted in polymers with a spherical particle morphology with no evidence of reactor fouling. Scanning electron microscopy images of typical polymers are shown in Figure 6.3.

The use of a support of composition $MgCl_2 \cdot 0.24AlEt_{2.3}(OEt)_{0.7}$ for the immobilization and activation of the vanadium(III) amidinate complexes **6** and **7** resulted in significantly higher activities (1500–3100 kg mol^{-1} bar^{-1} h^{-1} at 50 °C) than had previously been obtained in homogeneous polymerization [52]. This was ascribed

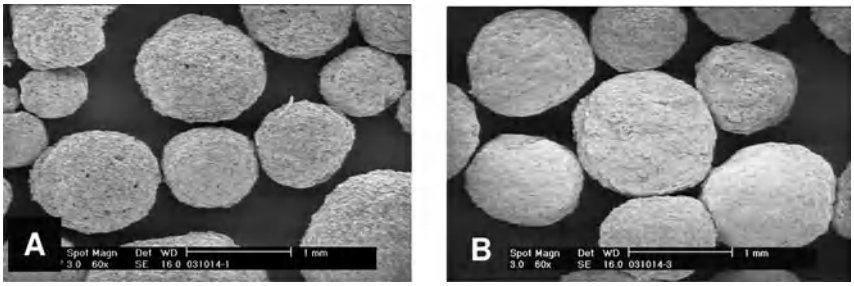

Figure 6.3 Scanning electron microscopy images of polyethylene prepared using catalysts immobilized on a $MgCl_2/AlEt_n(OEt)_{3-n}$ support. (a) [(*t*BuCp)$TiCl_3$]; (b) $TiCl_4$ [51].

to the stabilizing effect of the support, avoiding the rapid decay typically obtained in homogeneous systems. Polyethylene with a narrow MWD (M_w/M_n = 2.0) was obtained, indicating the retention of single-site catalyst behavior.

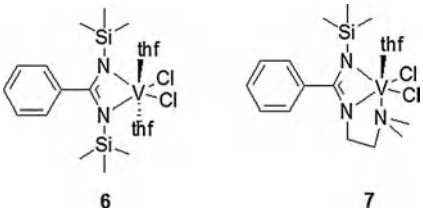

It is well known that heterogeneous, Phillips-type catalysts based on CrO_3/SiO_2 produce high-density PE with a broad MWD, as a result of the presence of a range of different active species [55]. Recently, what appears to be the first example of a high-activity, heterogeneous, chromium-based catalyst system exhibiting genuinely single-site behavior in ethylene polymerization has been reported [53]. Supports of type $MgCl_2/AlR_n(OEt)_{3-n}$, obtained by the reaction of various aluminum trialkyls with an adduct $MgCl_2 \cdot 1.1EtOH$, were used for the immobilization of the half-sandwich Cr(III) complex **8**, first synthesized by Jolly and coworkers [56, 57]. At 50 °C, using Al*i*Bu_3 as cocatalyst/scavenger, polymerization activities in the range 1900 to 2700 kg mol^{-1} bar^{-1} h^{-1} were obtained, comparable to activities obtained under homogeneous conditions with MAO as cocatalyst. Furthermore, the $MgCl_2$-immobilized catalysts gave a high molecular weight (1.3–1.6 × 10^6 Da) and very narrow MWD (M_w/M_n = 1.8–1.9). Confirmation of the narrow MWD, resulting from single-site catalysis, was obtained by investigation of the melt rheological properties of the polymers [53]. The shear frequency dependence of two polymers prepared with complex **8** immobilized on $MgCl_2/AlR_n(OEt)_{3-n}$ supports, compared to that of a polymer prepared with immobilized $TiCl_4$, is shown graphically in

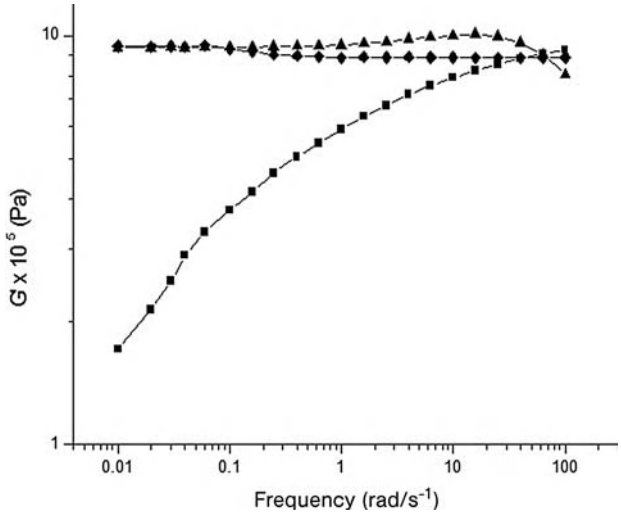

Figure 6.4 Shear frequency dependence of the storage modulus of (◆ and ▲) polyethylene ($\overline{M}_w/\overline{M}_n$ = 1.8–1.9) prepared using an immobilized Cr catalyst, compared to (■) a reference polymer having $\overline{M}_w/\overline{M}_n$ = 4.1 [53].

Figure 6.4. The constant storage modulus of the Cr-derived PEs over the entire frequency range is typical for narrow (Schulz–Flory) distribution polymers.

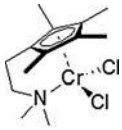

8

6.5.2 Late-Transition Metal Complexes

Recently, there has been increasing interest in late-transition metal catalysts for olefin polymerization, following the discovery by Brookhart and coworkers of aryl-substituted α-diimine nickel(II) complexes able to polymerize ethylene to give polyolefins with substantial chain branching [58–60]. Subsequently, the Brookhart and Gibson groups discovered, independently, that bis(imino)pyridyl iron(II) complexes can be activated with MAO to afford highly active catalysts for ethylene polymerization, giving essentially linear PE [61–63]. Both, the nickel and the iron complexes have now been successfully immobilized and activated on magnesium chloride supports.

Immobilization of the nickel diimine complexes **9** to **12** on a spherical support of composition $MgCl_2 \cdot 0.24AlEt_{2.3}(OEt)_{0.7}$, prepared by the reaction of $AlEt_3$ with $MgCl_2 \cdot 2.1EtOH$, followed by ethylene polymerization at 50 °C in the presence of Al*i*Bu$_3$, gave activities of up to about 7000 kg mol^{-1} bar^{-1} h^{-1} [64]. The activities were significantly higher than those previously reported for homogeneous polymeriza-

tion, or for nickel diimine complexes immobilized on silica [65, 66]. The highest degrees of branching in the resulting PEs were obtained with complexes **9** and **11**, induced by the presence of the isopropyl substituents in the *ortho* positions of the aryl rings. Narrow MWDs were obtained (M_w/M_n = 2.1–2.9), and the polymers were obtained in the form of free-flowing powders with a spherical particle morphology.

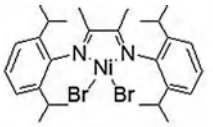

9

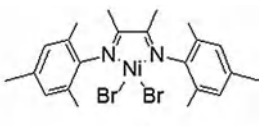

10

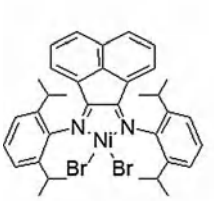

11

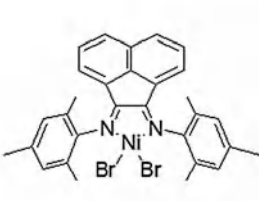

12

Similar supports have been used for the preparation of immobilized bis(imino)pyridyl iron(II) complexes such as **13** [67]. Relatively high iron loadings (0.3–1.5 wt.%) resulted in productivities of up to 10 kg PE g^{-1} in 1 h at 70 °C, using $AlEt_3$ as cocatalyst. Uniform impregnation of the catalyst on the support was evident from energy dispersive X-ray (EDX) analysis of a particle cross-section, and a spherical polymer particle morphology was obtained. The polymers had a relatively broad MWD (M_w/M_n > 10), but in contrast to homogeneous polymerization with this catalyst the distribution was not bimodal. A somewhat narrower MWD (M_w/M_n = 4–8) was obtained with complex **14**, in which the isopropyl substituents provide more steric bulk around the central metal atom [68]. Supports derived from the reaction of aluminum alkyls with adducts of $MgCl_2$ and 2-ethylhexanol have also been used for the immobilization and activation of iron catalysts [69].

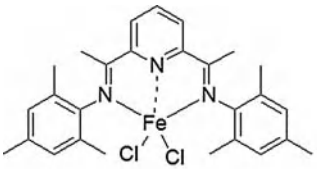

13

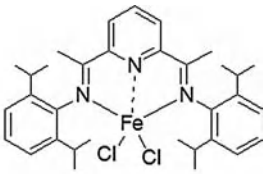

14

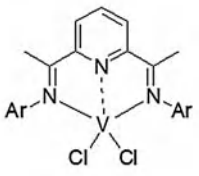

15

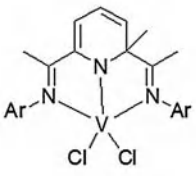

16

Supports obtained by the extensive thermal dealcoholation of a $MgCl_2$/ethanol adduct have been used for the immobilization of both iron and nickel complexes [70]. The thermal treatment of an adduct $MgCl_2 \cdot 2.56EtOH$ at 170 °C resulted in a decrease in ethanol content from 55.5 to 2.2 wt.%. The resulting support was used, without prior treatment with an aluminum alkyl, for the immobilization of **13**. Ethylene polymerization at 70 °C, with $AlEt_3$ as cocatalyst, resulted in an activity of around 11 200 kg mol^{-1} bar^{-1} h^{-1}. A stable polymerization activity, and also a high polymer bulk density (0.39 g mL^{-1}) was obtained, attributed to an even distribution of active species throughout the porous, dealcoholated support.

The broad polyethylene MWDs obtained with bis(imino)pyridyl iron catalysts indicate that neither the homogeneous nor the immobilized systems are single-site. In the case of homogeneous polymerization, evidence has been presented for the presence of highly reactive but unstable active centers producing a low-molecular-weight polymer fraction, as well as less active but more stable species producing a higher-molecular-weight polymer [71]. For bis(imino)pyridyl complexes on supports of type $MgCl_2/AlR_n(OEt)_{3-n}$, it has been shown that the PE molecular weight and MWD are heavily dependent on the nature of the transition metal [72]. For example, iron-based catalysts give polymers with MWDs ranging from 3 to 12, depending on the substituents in the bis(imino)pyridyl ligand, which also influence the polymer molecular weight. Generally, molecular weights obtained with the immobilized iron catalysts are somewhat higher than those reported for homogeneous polymerization. However, very different results were obtained with the bis(imino)pyridyl vanadium complex **15**. This complex, when immobilized on a $MgCl_2/AlEt_n(OEt)_{3-n}$ support and activated using either $AlEt_3$ or $Al\mathit{i}Bu_3$, gave much higher molecular weights than had been obtained under homogeneous conditions. Moreover, a Schulz–Flory MWD ($M_w/M_n = 2$) was obtained, and the narrow distribution, arising from a single active species, was confirmed by rheology [72]. The precursor for the active species in this system is likely to originate via alkylation of the pyridine ring, leading to a decrease in the metal coordination number and the formation of the species **16** [73].

Iron catalysts have also been immobilized on highly dispersed, activated $MgCl_2$, prepared by reaction of magnesium with excess *n*-butyl chloride in refluxing heptane [8]. Stable kinetics were observed in ethylene polymerizations carried out at 70 or 80 °C, using trialkylaluminum cocatalysts. Activities were in the range 5000 to 17 000 kg mol^{-1} bar^{-1} h^{-1}, and it was noted that the maximum amount of the iron complex **17** that could be immobilized was approximately 150 μmol g^{-1}, similar to the amount of $TiCl_4$ that could be adsorbed onto the same support. This suggested that $TiCl_4$ and $LFeCl_2$ complexes interact with the same surface sites on $MgCl_2$.

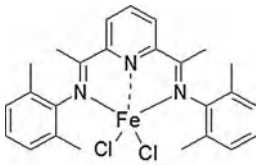

17

An unusual feature of $MgCl_2$-supported iron catalysts is their increased activity for ethylene polymerization in the presence of hydrogen, in contrast to what is observed, for example, with $MgCl_2/TiCl_4$-based systems [8]. It has been proposed that this results from the reactivation via chain transfer of dormant sites resulting from 2,1-insertion of vinyl-terminated oligomers into the polymer chain [74, 75], or from the hydrogenolysis of π-allyl species formed after coordination of a vinyl-terminated oligomer (or α-olefin) to the active center [76]. The latter mechanism is supported by the fact that the hydrogenolysis step is not accompanied by chain transfer, in line with the low sensitivity of bis(imino)pyridyl iron catalysts to chain transfer with hydrogen. The effect of hydrogen on catalyst activity and polymer molecular weight is dependent on the steric bulk of the bis(imino)pyridyl ligand; an overall increase in molecular weight on addition of hydrogen is obtained with catalysts containing relatively little steric bulk, as a result of decreased formation of vinyl-terminated oligomers [77]. This can be explained by deactivation of oligomer-forming active species and/or by the conversion of oligomers to polymers via hydrogenolysis of oligomeric π-allyl intermediate species. The decreased presence of vinyl-terminated oligomers therefore leads to less dormant site formation and greater activity at polymer-producing sites. However, the overall effect of hydrogen on polymer molecular weight with iron-based catalysts is relatively small when compared to the effectiveness of hydrogen as a chain-transfer agent in polymerization with, for example catalysts of type $MgCl_2/TiCl_4$. The dominant chain-transfer mechanism in iron-catalyzed polymerization is β-hydrogen elimination to give a vinyl-terminated chain, but chain transfer with $AlEt_3$ has also been reported to occur in ethylene polymerization at 80 °C [78]. In this case, complex **14** was used together with a support prepared by the *in-situ* reaction of MgEtBu with ethylaluminum sesquichloride.

The determination of the number of active centers (C*) in silica-, alumina- or $MgCl_2$-supported iron catalysts has resulted in values mostly in the range of 2 to 4% of the total iron present, whereas in homogeneous polymerization C* was in the range 16 to 41% [74, 75]. It was also noted that the nature of the support had little effect on the propagation rate constant, and it was concluded that the support was not a direct constituent of the active sites, but was instrumental in active-site stabilization, thereby preventing decay in catalyst activity.

Magnesium chloride can also be used for the immobilization of two or more different catalysts on a single support. Significant increases in the activity of heterogeneous, $MgCl_2$-supported catalysts have been obtained by the incorporation of a nickel diimine into an iron-, chromium-, or titanium-based catalyst system [79]. The increases in activity were ascribed to the nickel-catalyzed formation of branched polyethylene, reducing the monomer diffusion limitation inherent in ethylene homopolymerization with heterogeneous catalysts and thereby increasing the productivity of the main, linear PE-producing catalyst component. The coimmobilization of different catalyst components on $MgCl_2/AlEt_n(OEt)_{3-n}$ supports has also been applied for the preparation of bimodal polyethylene [80, 81]. The combination of the iron and chromium complexes **18** and **19**, giving molecular weights of around 100 000 Da and >1 000 000 Da, respectively, has been used

for the synthesis of intimately mixed blends of high- and low-molecular weight polyethylene [80]. Investigation of the melt rheological and crystallization behavior of these polymers has revealed that shear-induced orientation of the high-molecular-weight component results in partial crystallization even at a temperature as high as 137 °C, leading to a shish-kebab crystalline structure in the final polymer.

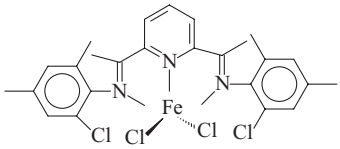

18

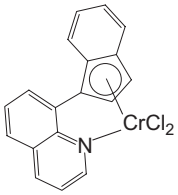

19

6.6 Conclusions

The use of magnesium chloride-based supports for the immobilization of single-site catalysts is a topic that is rapidly growing in importance, not least due to the utilization of supports having controlled particle size, morphology and porosity, previously developed for the production of Ziegler–Natta catalysts. Immobilized catalysts may be obtained which display stable kinetics during polymerization, thus preventing the rapid decay in activity often observed in homogeneous polymerization. In some cases, activities can be achieved which are substantially higher than those obtained in MAO-activated polymerization under homogeneous conditions. A further advantage of $MgCl_2$ supports is that the immobilized catalysts can, in many cases, be used together with simple aluminum trialkyls, thus avoiding the requirement for MAO or a borate activator.

The mechanistic aspects of single-site immobilization and activation using $MgCl_2$-based supports are, as yet, not fully resolved, and will differ according to the nature of the transition metal catalyst. In the case of metallocenes and related early-transition metal complexes, it is probable that Lewis acidic sites on the support surface will participate in the formation of cationic active species. On the other hand, this will be less important for late-transition catalysts such as bis(imino)pyridyl iron complexes, which can be activated by simple aluminum alkyls such as $AlEt_3$ or $Al\mathit{i}Bu_3$. Further advances in the development and use of magnesium chloride as a support for the immobilization and activation of many more early- and late-transition metal polymerization catalysts can be expected.

References

1 G.G. Hlatky, *Chem. Rev.* 2000, *100*, 1347–1376.
2 J.R. Severn, J.C. Chadwick, R. Duchateau, N. Friederichs, *Chem. Rev.* 2005, *105*, 4073–4147.
3 T.F. McKenna, J.B.P. Soares, *Chem. Eng. Sci.* 2001, *56*, 3931–3949.
4 M. Abboud, P. Denifl, K.-H. Reichert, *J. Appl. Polym. Sci.* 2005, *98*, 2191–2200.
5 T.J. Marks, *Acc. Chem. Res.* 1992, *25*, 57–65.
6 W.C. Finch, R.D. Gillespie, D. Hedden, T.J. Marks, *J. Am. Chem. Soc.* 1990, *112*, 6221–6232.
7 V.A. Zakharov, E.A. Paukshtis, T.B. Mikenas, A.M. Volodin, E.N. Vitus, A.G. Potapov, *Macromol. Symp.* 1995, *89*, 55–61.
8 T.B. Mikenas, V.A. Zakharov, L.G. Echevskaya, M.A. Matsko, *J. Polym. Sci.: Part A: Polym. Chem.* 2005, *43*, 2128–2133.
9 J.-C. Bailly, P. Bres, C. Chabrand, E. Daire, U.S. Patent 5106804, 1990.
10 J.-C. Bailly, C.J. Chabrand, European Patent 435514, 1990.
11 Z. Lin, Int. Patent WO 99/21898, 1998.
12 M. Sacchetti, S. Pasquali, G. Govoni, U.S. Patent 5698487, 1995.
13 (a) F.D. Silveira, M.C. Forte, J.H.Z. Santos, F.C. Stedile, J.J. Zacca, *Polim.: Cienc. Technol.* 2000, *10*, 42–48; (b) F.D. Silveira, M.C. Forte, J.H.Z. Santos, F.C. Stedile, J.J. Zacca, *Chem. Abstr.* 2000, *133*, 164382.
14 C. Süling, W. Spaether, N. Hüsgen, J. Rösch, J. Wulff-Döring, W. Bidell, Int. Patent WO 01/46271, 2000.
15 S. Wang, D.D. Klendworth, M.K. Reinking, U.S. Patent 6967231, 2004.
16 Z. Guan, Y. Zheng, S. Jiao, *J. Mol. Catal. A: Chemistry* 2002, *188*, 123–131.
17 S. Kamiyama, T. Takemori, M. Iijima, Y. Hane, S. Yamamoto, U.S. Patent 6455647, 2002.
18 H.S. Cho, W.Y. Lee, *J. Mol. Catal. A: Chemistry* 2003, *191*, 155–165.
19 H.C. Cho, J.S. Chung, J.H. Han, Y.G. Ko, W.Y. Lee, *J. Appl. Polym. Sci.* 1998, *70*, 1707–1715.
20 Y.G. Ko, H.S. Cho, K.H. Choi, W.H. Lee, *Korean J. Chem. Eng.* 1999, *16*, 562–570.
21 H.S. Cho, W.Y. Lee, *Korean J. Chem. Eng.* 2002, *19*, 557–563.
22 S. Sensarma, S. Sivaram, *Polym. Int.* 2002, *51*, 417–423.
23 W. Ochędzan-Siodłak, M. Nowakowska, *Eur. Polym. J.* 2004, *40*, 839–846.
24 W. Ochędzan-Siodłak, M. Nowakowska, *Eur. Polym. J.* 2005, *41*, 941–947.
25 K. Czaja, M. Białek, A. Utrata, *J. Polym. Sci.: Part A: Polym. Chem.* 2004, *42*, 2512–2519.
26 M. Białek, K. Czaja, A. Reszka, *J. Polym. Sci.: Part A: Polym. Chem.* 2005, *43*, 5562–5570.
27 M. Białek, K. Czaja, B. Sacher-Majewska, *Thermochim. Acta* 2005, *429*, 149–154.
28 V. Busico, M. Guardasole, R. Cipullo, L. Resconi, G. Morini, Int. Patent WO 2004/078804, 2004.
29 M. Smit, J.R. Severn, X. Zheng, J. Loos, J.C. Chadwick, *J. Appl. Polym. Sci.* 2006, *99*, 986–993.
30 G.B. Jacobsen, P. Wijkens, J.T.B.H. Jastrzebski, G. van Koten, U.S. Patent 5834393, 1998.
31 G.G. Hlatky, D.J. Upton, *Macromolecules* 1996, *29*, 8019–8020.
32 R. Sugimoto, T. Asanuma, T. Iwatani, K. Takeuchi, O. Uchida, European Patent 500944, 1991.
33 J. Matsumoto, European Patent 522581, 1991.
34 L.G. Echevskaya, V.A. Zakharov, N.V. Semikolenova, T.B. Mikenas, A.P. Sobolev, *Polym. Sci., Ser. A* 2001, *43*, 220–227.
35 (a) L.G. Echevskaya, V.A. Zakharov, N.V. Semikolenova, T.B. Mikenas, *Polimery* 2001, *46*, 40–43; (b) L.G. Echevskaya, V.A. Zakharov, N.V. Semikolenova, T.B. Mikenas, *Chem. Abstr.* 2001, *135*, 137742.
36 M. Kaminaka, K. Soga, *Makromol. Chem. Rapid Commun.* 1991, *12*, 367–372.
37 M. Kaminaka, K. Soga, *Polymer* 1992, *33*, 1105–1107.
38 K. Soga, M. Kaminaka, *Makromol. Chem.* 1993, *194*, 1745–1755.
39 K. Soga, M. Kaminaka, *Macromol. Chem. Phys.* 1994, *195*, 1369–1379.
40 G. Satyanarayana, S. Sivaram, *Macromolecules* 1993, *26*, 4712–4714.
41 Y.V. Kissin, T.E. Nowlin, R.I. Mink, A.J. Brandolini, *Macromolecules* 2000, *33*, 4599–4601.

42 M. Ferraris, F. Rosati, S. Parodi, E. Giannetti, G. Motroni, E. Albizzati, U.S. Patent 4399054, 1983.

43 (a) European Patent 37291, 1981; (b) N. Kashiwa, A. Toyota, Chem. Abstr. 1982, 96, 20579.

44 Y. Nakayama, H. Bando, Y. Sonobe, H. Kaneko, N. Kashiwa, T. Fujita, *J. Catal.* 2003, *215*, 171–175.

45 Y. Nakayama, H. Bando, Y. Sonobe, T. Fujita, *J. Mol. Catal. A: Chemistry* 2004, *213*, 141–150.

46 Y. Nakayama, H. Bando, Y. Sonobe, T. Fujita, *Bull. Chem. Soc. Japan* 2004, *77*, 617–625.

47 Y. Nakayama, H. Bando, Y. Sonobe, Y. Suzuki, T. Fujita, *Chem. Lett. (Japan)* 2003, *32*, 766–767.

48 Y. Nakayama, J. Saito, H. Bando, T. Fujita, *Macromol. Chem. Phys.* 2005, *206*, 1847–1852.

49 Y. Nakayama, J. Saito, H. Bando, T. Fujita, *Chem. Eur. J.* 2006, *12*, 7546–7556.

50 J.R. Severn, J.C. Chadwick, *Macromol. Rapid Commun.* 2004, *25*, 1024–1028.

51 J.R. Severn, J.C. Chadwick, *Macromol. Chem. Phys.* 2004, *205*, 1987–1994.

52 J.R. Severn, R. Duchateau, J.C. Chadwick, *Polymer Int.* 2005, *54*, 837–841.

53 J.R. Severn, N. Kukalyekar, S. Rastogi, J. C. Chadwick, *Macromol. Rapid Commun.* 2005, *26*, 150–154.

54 (a) J.R. Severn, J.C. Chadwick, Int. Patent WO 2005/077989, 2005; (b) J.R. Severn, J.C. Chadwick, 2005/092935, 2005.

55 M.P. McDaniel, C.H. Leigh, S.M. Wharry, *J. Catal.* 1989, *120*, 170–181.

56 R. Emrich, O. Heinemann, P.W. Jolly, C. Krüger, G.P.J. Verhovnik, *Organometallics* 1997, *16*, 1511–1513.

57 A. Döring, J. Göhre, P.W. Jolly, B. Kryger, J. Rust, G.P.J. Verhovnik, *Organometallics* 2000, *19*, 388–402.

58 L.K. Johnson, C.M. Killian, M. Brookhart, *J. Am. Chem. Soc.* 1995, *117*, 6414–6415.

59 S.D. Ittel, L.K. Johnson, M. Brookhart, *Chem. Rev.* 2000, *100*, 1169–1203.

60 V.C. Gibson, S.K. Spitzmesser, *Chem. Rev.* 2003, *103*, 283–315.

61 B.L. Small, M. Brookhart, A.M.A. Bennett, *J. Am. Chem. Soc.* 1998, *120*, 4049–4050.

62 G.J.P. Britovsek, V.C. Gibson, B.S. Kimberley, P.J. Maddox, S.J. McTavish, G.A. Solan, A.J.P. White, D.J. Williams, *Chem. Commun.* 1998, 849–850.

63 G.J.P. Britovsek, M. Bruce, V.C. Gibson, B. S. Kimberley, P.J. Maddox, S. Mastroianni, S.J. McTavish, C. Redshaw, G.A. Solan, S. Strömberg, A.J.P. White, D.J. Williams, *J. Am. Chem. Soc.* 1999, *121*, 8728–8740.

64 J.R. Severn, J.C. Chadwick, V. Van Axel Castelli, *Macromolecules* 2004, *37*, 6258–6259.

65 R.J. Maldanis, J.S. Wood, A. Chandrasekaran, M.D. Rausch, J.C.W. Chien, *J. Organometal. Chem.* 2002, *645*, 158–167.

66 P. Preishuber-Pflugl, M. Brookhart, *Macromolecules* 2002, *35*, 6074–6076.

67 R. Huang, D. Liu, S. Wang, B. Mao, *Macromol. Chem. Phys.* 2004, *205*, 966–972.

68 R. Huang, D. Liu, S. Wang, B. Mao, *J. Mol. Catal. A: Chemistry* 2005, *233*, 91–97.

69 Y. Nakayama, H. Kaneko, H. Bandoh, Y. Sonobe, J. Saito, S. Kojoh, M. Mitani, Y. Suzuki, S. Matsui, N. Kashiwa, T. Fujita, European Patent 1238989, 2002.

70 R. Xu, D. Liu, S. Wang, B. Mao, *Macromol. Chem. Phys.* 2006, *207*, 779–786.

71 A.A. Barabanov, G.D. Bukatov, V.A. Zakharov, N.V. Semikolenova, L.G. Echevskaja, M.A. Matsko, *Macromol. Chem. Phys.* 2005, *206*, 2292–2298.

72 R. Huang, N. Kukalyekar, C.E. Koning, J.C. Chadwick, *J. Mol. Catal. A: Chemistry* 2006, *260*, 135–143.

73 D. Reardon, F. Conan, S. Gambarotta, G. Yap, Q. Wang, *J. Am. Chem. Soc.* 1999, *121*, 9318–9325.

74 V.A. Zakharov, N.V. Semikolenova, T.B. Mikenas, A.A. Barabanov, G.D. Bukatov, L.G. Echevskaya, M.A. Mats'ko, *Kinet. Catal.* 2006, *47*, 303–309.

75 A.A. Barabanov, G.D. Bukatov, V.A. Zakharov, N.V. Semikolenova, T.B. Mikenas, L.G. Echevskaya, M.A. Mats'ko, *Macromol. Chem. Phys.* 2006, *207*, 1368–1375.

76 T.B. Mikenas, V.A. Zakharov, L.G. Echevskaya, M.A. Mats'ko, *J. Polym. Sci.: Part A: Polym. Chem.* 2007, *45*, 5057–5066.

77 R. Huang, C.E. Koning, J.C. Chadwick, *J. Polym. Sci.: Part A: Polym. Chem.* 2007, *45*, 4054–4061.
78 R. Ohnishi, T. Konakazawa, J. Amano, T. Fujimura, *Polym. Bull.* 2006, *56*, 1–8.
79 R. Huang, C.E. Koning, J.C. Chadwick, *Macromolecules* 2007, *40*, 3021–3029.
80 N. Kukalyekar, L. Balzano, J.C. Chadwick, S. Rastogi, *PMSE Preprints* 2007, *96*, 840–841.
81 S. Mihan, F. Fantinel, Int. Patent WO 2007/042252, 2007.

7
Metallocene Activation by Solid Acids

Max P. McDaniel, Michael D. Jensen, Kumindini Jayaratne, Kathy S. Collins, Elizabeth A. Benham, Neal D. McDaniel, P. K. Das, Joel L. Martin, Qing Yang, Mathew G. Thorn, and Albert P. Masino

7.1
Introduction

This chapter describes investigations which were conducted at Phillips Petroleum (later Chevron-Phillips Chemical) and started during the mid-1990s, the aim being to develop new platforms for the activation of metallocene catalysts [1]. The intent was to replace the more common (and expensive) methylaluminoxane (MAO) or fluoro-organoborate compounds. MAO is generally thought to function as a Lewis acid, helping to ionize – or at least to polarize – the metallocene compound. In addition, if the metallocene is present as the dihalide, MAO also serves to alkylate the transition metal.

Based on information obtained via the hydrocarbon-processing literature, a wide assortment of solid oxides are known to exhibit surface acidity. In fact, the acidic sites on some of these materials have been found to be so strong that they are referred to as "solid super-acids" [2–4]. Some of these oxides may also be made to achieve the high porosities necessarily for polymerization catalysts, which gives rise to the question of whether they could serve as effective metallocene activators, providing the acid function. Presumably, a less-expensive metal alkyl could also be added to alkylate the metallocene if the dihalide form were to be used, for example as shown in Scheme 7.1.

A number of attempts to activate metallocene by partially dehydroxylated alumina were reported during the early 1990s by Soga and Kaminaka [5–8]. However, the activity observed was very low, and the present authors' investigations have subsequently confirmed this. Although alumina may be quite porous, it is not usually known for its high surface acidity, and this may account for its poor performance as an activator. Thus, the decision was taken to explore the question further by preparing and testing other highly porous acidic materials. A brief summary of the results obtained is provided in this chapter.

Tailor-Made Polymers. Via Immobilization of Alpha-Olefin Polymerization Catalysts.
Edited by John R. Severn and John C. Chadwick

ISBN: 978-3-527-31782-0

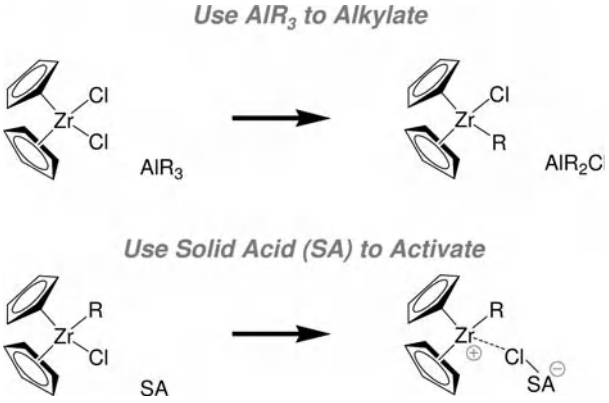

Scheme 7.1

7.2 Experimental

7.2.1 Solid Acid Preparation

In general, standard, commercially available, polymerization-grade oxide supports were used in these studies. The silica used (from W.R. Grace; grade 952) had a surface area of approximately $300\,m^2\,g^{-1}$ and a pore volume of ca. $1.6\,mL\,g^{-1}$; the alumina used (from Akzo; Ketjen grade B) had a surface area, after calcining, of ca. $400\,m^2\,g^{-1}$ and a pore volume of ca. $1.5\,mL\,g^{-1}$. The silica–alumina (from W.R. Grace, grade MS13-110) contained 13% alumina, and provided a surface area of ca. $450\,m^2\,g^{-1}$ and a pore volume of ca. $1.1\,mL\,g^{-1}$.

Often, these materials were treated with other compounds to provide the solid acid. This was usually accomplished simply by impregnating the additional salt in an aqueous solution into the commercial oxide to incipient wetness, followed by drying at 110 °C. Some chloriding and fluoriding treatments were performed during the calcining step. In this technique, perfluorohexane (for fluoride) or carbon tetrachloride (for chloride) were injected into the gas stream where they evaporated and were carried up into the calcining tube to contact the solid oxide at 600 °C.

In order to calcine the resulting support, ca. 10 g was placed in a 4.5-cm quartz tube fitted with a sintered quartz disk at the bottom. With the solid oxide powder supported on the disk, air or nitrogen (which had been dried by it being passed through a 13× molecular sieve column) was blown up through the disk at a linear rate of ca. $0.05\,m^3\,h^{-1}$. Using an electric furnace, the temperature of the quartz tube was then raised at $400\,°C\,h^{-1}$ to the indicated temperature (e.g., 600 °C). On reaching this temperature, the oxide powder was allowed to fluidize for 3 h in the dry

air or nitrogen, and then collected and stored under dry nitrogen (to protect it against atmospheric exposure) until used for testing.

7.2.2 Polymerization

Activity tests were conducted in a 2.2-L steel reactor equipped with a marine stirrer running at 400 r.p.m. The reactor was surrounded by a steel jacket containing circulating water, the temperature of which was controlled electronically using steam and water heat-exchangers such that the reactor temperature was maintained at ±0.5 °C during the reaction.

Unless otherwise stated, a small amount (0.01–0.1 g) of the solid acid support was first charged under nitrogen to the dry reactor. A 2.0-mL aliquot of a toluene solution containing 0.5 wt.% metallocene was added, followed by 600 mL of isobutane liquid. Next, 1.0 mL of a 1 M solution of the metal alkyl cocatalyst in heptane was added, followed by a further 600 mL of isobutane. The reactor was heated to a specified temperature (generally 90 °C), and finally ethylene was added to the reactor to equal a fixed pressure (generally ca. 40 bar).

The reaction mixture was stirred for ca. 1 h; as the ethylene was consumed, additional ethylene was metered in to maintain the pressure, and this provided an indication of the activity. After the allotted time, the ethylene flow was stopped and the reactor depressurized and opened to recover a granular polymer powder. In all cases the reactor was clean with no indication of any wall scale, coating, or other forms of fouling. The polymer powder was removed and weighed, and activity calculated as kilograms of polymer produced per gram solid acid component charged, per hour.

As might be expected, the activity obtained from the solid acid varied with the choice of metallocene. Thus, two common unbridged metallocenes were chosen as a standard to test the activity of solid acids in these studies, namely bis(cyclopentadienyl)zirconium dichloride and bis(*n*-butylcyclopentadienyl)zirconium dichloride (both from the Crompton Company). Activity also varied with the choice of cocatalyst; for these studies, triethylaluminum (TEA; from Akzo Co.) was used as the standard test reagent. The conditions were chosen for simplicity, and did not necessarily represent the highest activity that could be achieved.

The amount of each catalyst ingredient used was set such that the limiting reagent was always the solid acid component, rather than the metallocene or the metal alkyl cocatalyst. This enabled an accurate comparison to be made of the efficiencies of the various solid acids, although in other studies (or in a commercial operation) a different approach might be chosen.

The ethylene used (polymerization grade; from Union Carbide Corporation) was further purified before use by passage through a column of 6-mm beads of Alcoa A201 alumina, activated at 250 °C in nitrogen. Isobutane (polymerization grade, from Phillips Petroleum Co., Borger, Texas) was further purified by distillation, passed through Alcoa A201 alumina (as for ethylene), and activated at 250 °C in nitrogen.

7.2.3
Acidity Measurements

An *in-situ* Fourier transform infrared (FTIR) method was developed to measure acidity using pyridine as the probe molecule, which allowed for the quantification of both Brønsted and Lewis acid sites. The samples were pressed into self-supporting pellets and placed in the IR cell, which was evacuated to $<10^{-4}$ torr. The solid acid samples were pretreated by heating *in vacuo* before being exposed to pyridine vapor. Absorption measurements were taken at 1545 cm^{-1} for the Brønsted sites, and at 1447 cm^{-1} and 1597 cm^{-1} for the Lewis sites. Molar extinction coefficients were obtained from published sources [9] and further normalized using the weight of the sample as its geometric area. The IR spectra were recorded using a Nicolet Avatar 360 FTIR instrument fitted with a custom cell.

When placed in the instrument, each pressed sample was heated to a designated pretreatment temperature which was maintained for 30 min to remove residual moisture. The sample was then cooled to 170 °C *in vacuo* and a background spectrum obtained at 170 °C on the oxide itself. At 170 °C, pyridine vapor was introduced into the evacuated cell by opening a valve to the headspace of a reservoir containing liquid pyridine at 25 °C. This contact was maintained for 20 min. The cell was then re-evacuated at 170 °C for 30 min. Prior testing had established that all physisorbed pyridine could be removed from such oxides at this temperature. A spectrum was then obtained at 150 °C on the remaining chemisorbed pyridine. Adsorption on Brønsted sites identified the pyridinium ion, which could be distinguished spectroscopically from pyridine coordinated to a Lewis site.

7.3
Results and Discussion

7.3.1
Simple Oxides

The results of testing some simple, high-porosity solid oxides are listed in Table 7.1. Each was calcined at 600 °C to partially dehydroxylate the surface and to develop acidity where possible. To test the activity of each oxide, bis(*n*-butylcyclopentadienyl)zirconium dichloride and triethylaluminum cocatalyst were used in excess. As might be expected, silica, which is not known to develop either Lewis or Brønsted acidity, provided no activity whatsoever. Although further experiments were conducted with silica at other calcining temperatures, the results obtained were similar. On the other hand, alumina – which is known to exhibit some Lewis acidity after calcination – did provide some very low, but observable, activity. However, such activity (ca. 50 g of polymer per gram alumina per hour) was barely discernible under the test conditions, and would be completely unacceptable for commercial applications.

Table 7.1 Activity of simple oxide carriers without added anion.

*Solid oxide**	*Activity (gPE g^{-1} h^{-1})*
Silica	0
Alumina	50
Silica–Alumina	260
Silica–Zirconia	230
Silic–Titania	100
Alumina–Boria-Zirconia	300

* Calcined at 600 °C, tested with (n-butylCp)$_2$ZrCl_2 + $AlEt_3$.

Mixed oxides are often observed to develop greater acidity than either of the parent oxides, and silica–alumina is a well-known example of this. In agreement with this reasoning, the data in Table 7.1 show that the activity of silica–alumina was higher that that of pure alumina. The commercial silica–alumina used provided an activity of up to 75 g g^{-1} h^{-1}, while an activity up to 260 g g^{-1} h^{-1} was obtained from a special silica–alumina prepared by the co-gelation of sodium aluminate and sodium silicate. The calcination temperature was varied, but the optimum was approximately 600 °C. Although silica–aluminas provide an improvement over silica or alumina alone, it should be noted that these activities are still very low and would need to be at least an order of magnitude higher before being considered for commercial use.

Silica–zirconia is another mixed oxide known to develop high acidity. The silica–zirconia listed in Table 7.1 contained 10 wt.% Zr, and was prepared by the partial hydrolysis of tetraethyl silicate, followed by reaction with zirconium tetrapropoxide and alkaline hydrolysis. At 600 °C this material yielded an activity of ca. 230 g g^{-1} h^{-1}, but less activity was obtained at lower or higher calcining temperatures. Similarly, silica–titania yielded only ca. 100 g g^{-1} h^{-1}. The highest activity obtained from any mixed oxide was 300 g g^{-1} h^{-1}; this material, which was prepared by co-gelation of 10 molar parts each of boria and alumina and one part zirconia, had a surface area of almost 500 m^2 g^{-1} and a pore volume of ca. 0.9 mL g^{-1}. Once again, the optimum calcining temperature was about 600 °C. Despite the widespread use of silica–alumina and related materials as acid-cracking catalysts, none of these materials performed very well for metallocene activation.

7.3.2 Silica with Added Anion

These same simple oxides, however, were capable of developing high activity when treated also with an electron-withdrawing anion. The wide range of results obtained by adding various anions to silica are listed in Table 7.2. The addition of anion can be accomplished before the calcining step, during the calcining step, and in some cases after the calcining step (if performed anhydrously). However, for suc-

Table 7.2 Activity of silica treated with electron-withdrawing anions.

Solid acid[a]	*Activity (gPE g^{-1} h^{-1})*
Silica + F	0
Silica + Cl	0
Silica + SO_4	0
Silica + BF_4	1140
Silica + Al + BF_4	2310
Silica + TiF_6	156
Silica + ZrF_6	670

a Calcined at 600 °C, tested with (*n*-butylCp)$_2$ZrCl$_2$ + AlEt$_3$.

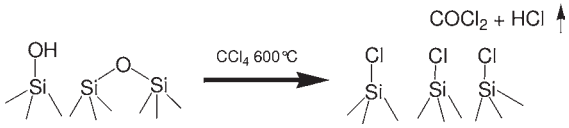

Scheme 7.2

cessful treatment, two conditions must be observed: (i) the oxide must contain a metal ion capable of Lewis acidity; and (ii) the anion must be thermally stable at the temperature of treatment, and afterwards.

7.3.2.1 **Fluoride Treatment**

The first three examples in Table 7.2 illustrate the effect of adding an electron-withdrawing anion to silica. In the first case, the silica was impregnated with an aqueous solution of ammonium bifluoride (3.5 mmol F g^{-1} SiO_2), followed by drying, and then calcining at 400 °C. During the calcining step ammonia is released and fluoride remains on the silica surface. The low temperature of only 400 °C was used because high levels of fluoride can promote sintering of the silica during calcining. Although higher and lower calcining temperatures, and levels of fluoride, were tested, all yielded the same null result. This material was incapable of activating metallocenes because it does not contain a Lewis acidic metal ion.

7.3.2.2 **Chloride Treatment**

The silica was also treated with chloride, as described previously [10]. A sample of silica was calcined at 600 °C in nitrogen, into which 2.36 mmol g^{-1} of carbon tetrachloride was injected. This treatment removes surface silanols (and even some siloxane groups) by replacing them with chloride (see Scheme 7.2). Again, however, this material was unable to activate metallocene, presumably due to the lack of a sufficiently Lewis acidic metal ion in or on the support.

7.3.2.3 Sulfate Treatment

In order to treat the silica with sulfate, an aqueous solution of sulfuric acid containing 2.5 mmol H_2SO_4 per gram silica was impregnated onto the silica. This was then dried and calcined at 300 °C, 400 °C, and 500 °C. Although, surprisingly, the silica retained a respectable amount of sulfate after the calcining steps (1.03, 0.85, and 0.22 mmol $SO_4\,g^{-1}$, respectively), none of the samples was able to activate metallocene.

7.3.2.4 Anions Containing a Lewis Acid Metal

Many different salts have been used to fluoride-treat the surface of silica, including materials containing a Lewis acidic metal [11–13]. In another series of experiments, silica was impregnated with ammonium fluoroborate (or even fluoroboric acid) as the fluoride source. The data (sample 4) in Table 7.2 show that a respectable activity developed, as boron is a Lewis acidic metal. This is not to say that the BF_4 ion necessarily survives the calcining step intact, as in many cases it most likely does not. Rather, the boron probably becomes attached to the silica matrix and the fluoride may redistribute, leaving an exposed, strongly Lewis acidic boron site. An activity of 1140 $g\,g^{-1}\,h^{-1}$ was achieved from silica treated with fluoroborate.

The amount of NH_4BF_4 impregnated was varied from 0.3 to 3 mmol g^{-1}, while the calcining temperature ranged between 200 °C and 700 °C. Again, high levels of fluoride (or BF_4 in this case) promoted sintering of the silica surface, especially at high calcining temperatures. This is clear from the data in Figure 7.1; it should be noted that the surface area falls sharply with temperature, indicating the onset of sintering. As the BF_4 loading was increased, sintering was observed at progres-

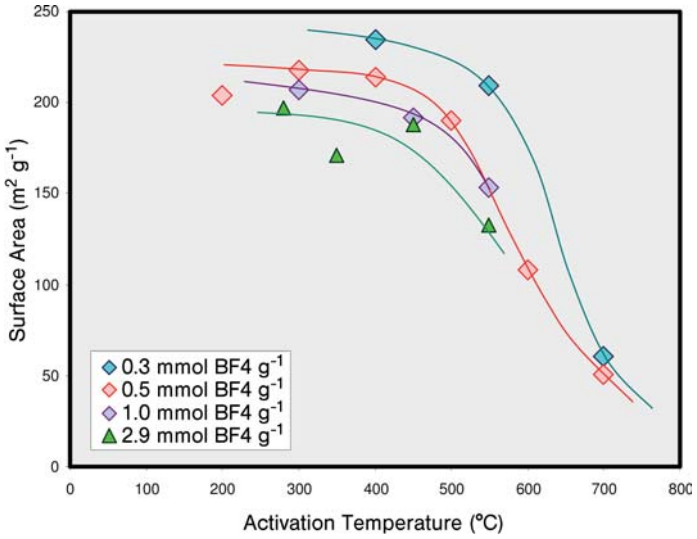

Figure 7.1 NH_4BF_4 on silica promotes sintering.

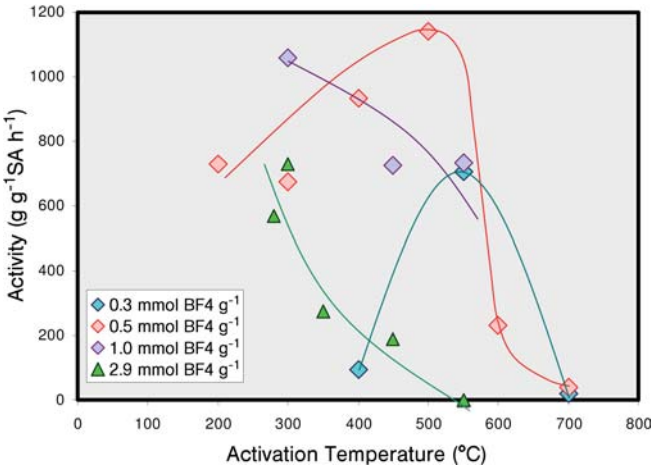

Figure 7.2 Activity from silica treated with NH_4BF_4.

sively lower temperatures. The activity observed from these samples is plotted in Figure 7.2, again under the same testing conditions described above. The observed activity is a compromise between two opposing effects: increasing the temperature or BF_4 loading improves activity, until the sintering point is reached. Thus, the activity usually goes through a maximum. The highest activity was observed at the relatively low BF_4 loading of 0.5 mmol g^{-1} and the relatively high calcining temperature of 500 °C.

In two more experiments, the silica was impregnated with 2 mmol g^{-1} each of aluminum nitrate and HBF_4, followed by calcining at 550 °C. An example is shown in Table 7.2, where the activity exceeded 2300 g g^{-1} h^{-1} activity, despite a high degree of sintering. The surface area had fallen to 172 m^2 g^{-1}, which again emphasized the need for a Lewis acidic metal to be present. The electron-withdrawing anion most likely amplifies this natural acidity.

Finally, the last two examples in Table 7.2 illustrate the addition of other fluoride-containing anions that include yet other Lewis acidic metals. Ammonium hexafluorotitanate was impregnated from aqueous solution onto the silica at 0.5 mmol g^{-1}. Calcining at between temperatures of 250 °C and 550 °C produced activities of ca. 150 g g^{-1} h^{-1}. Ammonium hexafluorozirconate was more effective, with the same amount producing 670 g g^{-1} h^{-1} after calcining at only 250 °C. In general, higher temperatures were less effective.

7.3.3
Alumina with Added Anion

Unlike the silica carriers, when alumina is used as a support it already contains an abundance of Lewis acidic metal ions, in the form of Al^{3+}. Therefore, the addition of an electron-withdrawing anion to alumina produced a respectable ability

Table 7.3 Activity of alumina carriers treated with electron-withdrawing anions.

Solid acid[a]	*Activity (gPE g^{-1} h^{-1})*
Alumina + F	1250
Alumina + Cl	2800
Alumina + Br	225
Alumina + PO_4	500
Alumina + Triflate	1800
Alumina + SO_4	2600

a Calcined at 600 °C, tested with $(n\text{-butylCp})_2ZrCl_2$ + $AlEt_3$.

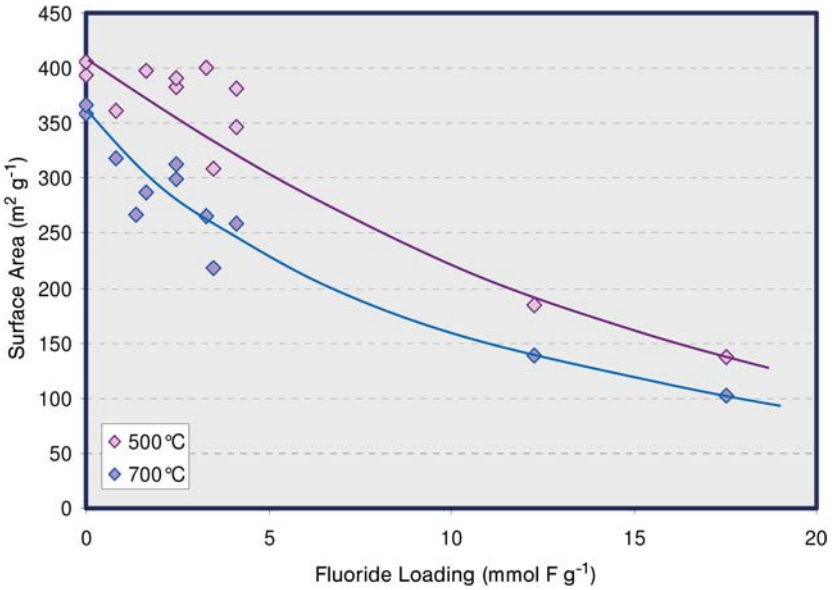

Figure 7.3 Virgin alumina was treated NH_4HF_2, then calcined as shown.

to activate metallocenes (see Table 7.3). In some cases the anion was added before calcining, but in other cases during or after calcining.

7.3.3.1 Fluoride Treatment

Fluoride may be easily added to the alumina through impregnation of an aqueous solution of HF, or an ammonium salt such as NH_4HF_2 or NH_4F. Adding approximately 3.5 mmol F g^{-1} in this way, followed by calcination at 600 °C, produced about 1250 g polyethylene (PE) g h^{-1} of activity. The activity obtained from fluorided alumina was dependent on the fluoride loading and also the calcining temperature, this being partly due to a tendency for fluoride to reduce the surface area of the alumina support. The samples in Figure 7.3 were the alumina was impregnated

with varying amounts of NH_4HF_2, then calcined at 500 °C or 700 °C. The fluoride addition caused a significant decrease in surface area, even at the lowest temperatures. Thus, its effect on alumina differs somewhat from that on silica, where it acts as a flux to promote thermal sintering. It also appears that, on alumina, the formation of Al–F bonds may affect the support structure.

One way of mitigating the destructive effect of fluoride is to calcine the alumina support at 600 °C, prior to fluoride addition. This converts the support structure from the hydrated bohemite form (AlOOH) to the crystalline gamma-Al_2O_3. The latter structure appears to be more resistant to attack by fluoride and other agents. The effect on surface area when a 600 °C-calcined alumina was treated with various amounts of fluoride, and then re-calcined at various temperatures, is shown in Figure 7.4. Acomparison of the data in Figures 7.3 and 7.4 indicates how much more resistant the "precalcined" support is to both fluoride and temperature.

Even with a stabilized surface area, the activity of fluorided alumina varied significantly with fluoride loading and calcining temperature. A low fluoride loading usually favored higher calcining temperatures, and vice-versa. An example of this trend is shown in Figure 7.5, where precalcined alumina was treated with various loadings of fluoride and then calcined at different temperatures. Activity often went through a peak with increasing temperature. Because much of this behavior cannot be attributed to changes in surface area, this suggests that if the fluoride level or temperature become too high, it can impair the required acid site density.

Many different fluoriding methods and compounds were found to be successful in developing the ability of alumina to activate metallocenes. For example other water-soluble fluoride salts such as NH_4SiF_6, NH_4PF_6 or $(NH_4)_2ZrF_6$ can be impreg-

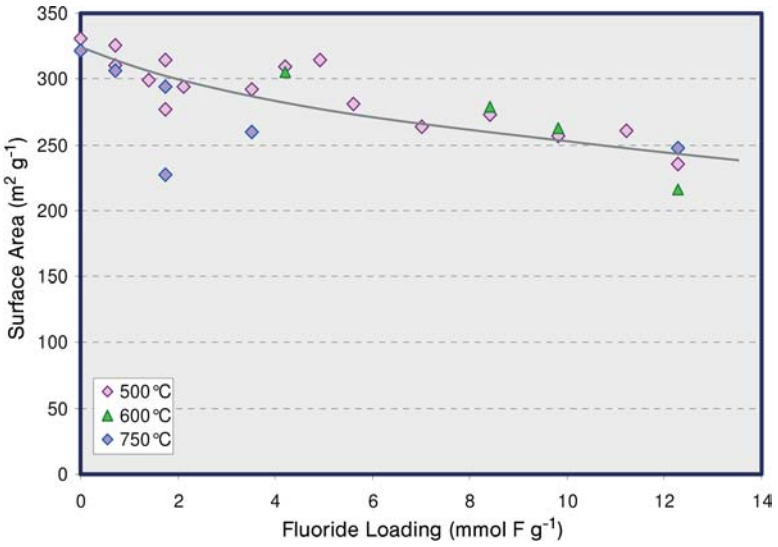

Figure 7.4 Alumina, calcined at 600 °C, was treated with NH_4HF_2, then calcined again.

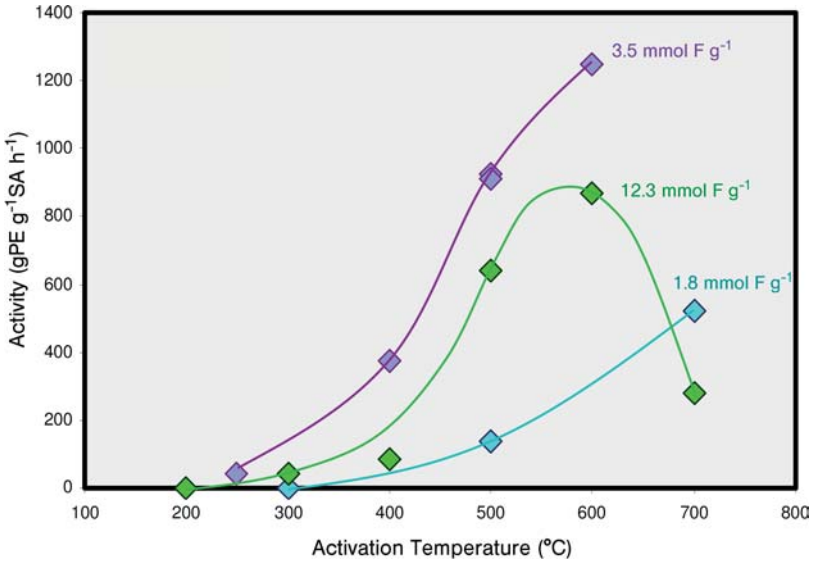

Figure 7.5 Alumina, 600 °C, treated with NH_4HF_2, then calcined as shown.

nated, with similar results. In other cases the acid was used, such as HF. Fluorided alumina is known to retain adsorbed ammonia even up to 500 °C [14]. However, after calcining at 600 °C no difference was noted in the performance of HF versus the ammonium salts. In other experiments, these compounds were simply dry-mixed and calcined together in a fluidized bed. The fluoride salt decomposes and releases fluoride-containing vapors. A fluoro-organic compound, such as perfluorohexane, was also vaporized into the gas stream during the final calcination at 600 °C. This was similarly effective as inorganic fluoride at treating the support, and produced some of the best activity observed.

7.3.3.2 Chloride Treatment

Another anion that greatly improved the activity of alumina support was chloride. The support could be easily treated with carbon tetrachloride vapor at 400–600 °C, as described above, to leave a deposit of surface chloride. When added in this way, chloride replaces all hydroxyls on the alumina surface; this removes all Brønsted acidity while the residual chloride enhances the Lewis acidity. Up to about 2 mmol g^{-1} of CCl_4 was quite effective, and had no effect on the surface area. However, the addition of more CCl_4 caused evaporation of the alumina as $AlCl_3$ vapor, and a loss of activity. Chloriding treatments other than CCl_4 were also found to be effective, including HCl gas, or vaporized $SiCl_4$, $SOCl_2$, $TiCl_4$, $ZrCl_4$, and $AlCl_3$.

Pure anhydrous $AlCl_3$ was also tested as the activator. Although known to be a strong Lewis acid, $AlCl_3$ exhibited no activity under these conditions when tested as a metallocene activator. As $AlEt_3$ cocatalyst was added to the reactor, it is possible that an exchange of ligands might have occurred. Anhydrous $AlCl_3$ was also depos-

ited onto a calcined alumina, using a dichloromethane solution. After evaporation on a hot plate, the support gave almost no activity with the test metallocene. When the material was then heated in a nitrogen carrier at 250 °C for 30 min, and re-tested, the activity was increased and reached over 400 $g\,g^{-1}\,h^{-1}$. Further heating in nitrogen up to 400 °C did not improve the activity, which suggests that a redistribution of the chloride had occurred during the heat treatment to produce the active acidic surface species.

$AlEt_2Cl$, $AlEtCl_2$, and $Al_2Et_3Cl_3$ were also impregnated onto alumina that had been calcined at 600 °C. When reacting with surface hydroxyls, these alkyls should leave known acidic surface species, such as that shown in Scheme 7.3. However, this treatment did not result in any improvement in activity over that exhibited by the base alumina. This indicates that the high activity observed from chlorided alumina probably does not derive from such species. When the $AlEtCl_2$-treated alumina was further heat-treated to 200 °C, a marked increase in activity was observed, suggesting a redistribution of surface chloride.

One consequence of using $TiCl_4$ or $ZrCl_4$ as a chloriding agent is that Ti or Zr halides are left behind. These may then be activated by the $AlEt_3$ cocatalyst to yield low Ziegler-type activity. This becomes apparent in the polymer as a high-molecular-weight component, sometimes with a very slight high-molecular-weight tail, imposed on the otherwise narrow molecular weight distribution (MWD).

7.3.3.3 **Bromide Treatment**

The alumina support can also be treated with bromide ion [15], and this also increases its activity. The bromide compound is most easily vaporized into the gas stream during calcining at 400–600 °C, either as HBr gas or as a bromide-containing organic. An example is shown in Table 7.3, where bromoform was injected at 600 °C. Even elemental Br_2 can be used if it is injected in the presence of a reducing atmosphere such as carbon monoxide (Scheme 7.4) [15]. Bromide seemed to be less effective than chloride or fluoride for the activation of metallocenes.

7.3.3.4 **Phosphate Treatment**

A further anion, phosphate, may be added to alumina in a number of ways, including impregnating a phosphate salt, or by vaporizing P_2O_5 or a phosphorus-

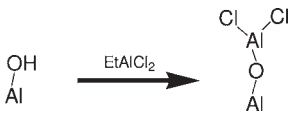

Scheme 7.3

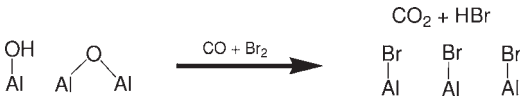

Scheme 7.4

containing compound into the gas stream during calcining. The simplest method is to impregnate H_3PO_4 onto the alumina before calcining. The alumina and phosphate components can even be co-gelled together as an amorphous aluminophosphate, as is commonly done for the Phillips chromium catalyst [16, 17]. These materials retain acidity and a high surface area even at high calcining temperatures. The example in Table 7.3 was co-gelled, in which the P/Al molar ratio was 0.2. This produced an activity of ca. $500\,g\,g^{-1}\,h^{-1}$ after being calcined at 750 °C. Other materials having more phosphate, or calcined at lower temperatures, were less effective.

7.3.3.5 **Triflate Treatment**

Adding trifluoromethyl sulfonic acid (triflic acid) or ammonium triflate to the alumina, followed by calcining, might also enhance surface acidity and thus activity. Unless the calcining step is performed at low temperatures, however, decomposition of surface triflate into surface fluoride is possible. Therefore, for clarity it is preferable to calcine the alumina first, followed by deposition of triflic acid at low temperatures. For example, in one experiment the alumina was first calcined at 600 °C, and then treated with triflic acid vapor at 230 °C; this sample exhibited activity of $200\,g\,g^{-1}\,h^{-1}$. Yet, when treated in nitrogen at 400 °C, the activity increased to $1000\,g\,g^{-1}\,h^{-1}$, and when further heated in nitrogen to 600 °C it produced $1800\,g\,g^{-1}\,h^{-1}$. Details of this sample are listed in Table 7.3. In this case, decomposition to surface fluoride is conceivable, but the sample actually displayed considerably higher activity than the best fluoride-treated alumina.

7.3.3.6 **Sulfate Treatment**

Another electron-withdrawing anion that enhanced the acidity of alumina, and consequently its activity, was sulfate. Again, this can be incorporated onto the alumina surface in several ways, but the simplest method is to impregnate the alumina with an aqueous solution of $(NH_4)_2SO_4$, NH_4HSO_4, or H_2SO_4, followed by calcination. Many metal sulfates, such as $Al_2(SO_4)_3$, produce similar results. The ammonium salts may even be dry-mixed with the alumina and the two calcined together. As the temperature is raised, the sulfate salt decomposes, releasing H_2SO_4 or SO_3 vapor which can then react with the alumina. Likewise, gaseous SO_3 may be introduced into the calcining atmosphere.

When alumina is treated with ammonium sulfate and then calcined, the ammonium ion is released fairly quickly. This effect is shown graphically in Figure 7.6, which shows the proportion of ammonium ions surviving calcination at various temperatures on an alumina that was originally treated with ca. $3.5\,mmol\,g^{-1}$ ammonium sulfate. By about 500 °C, almost all of the ammonium ion has been removed, whereas the large majority of the sulfate ion remained on the support up to about 550 °C. Only above that temperature did sulfate begin to evaporate (as SO_2 and O_2). At higher sulfate loadings, more of the sulfate evaporated off at 600 °C and higher, although at lower temperatures the alumina could hold more of the sulfate.

Sulfate is a useful anion because, unlike fluoride or chloride, it seems to have almost no effect on the porosity of the alumina. One indication of this, the surface area, is shown in Figure 7.6. In this series, alumina was impregnated with 3 mmol g^{-1} ammonium sulfate, and then calcined at various temperatures. Compared to an alumina containing no sulfate, the surface area was unchanged. Neither was there much change in surface area as the temperature was raised. By 900 °C, however, the usual sintering process began and the surface area declined normally. Thus, the porosity of the sulfated alumina was very similar to the untreated alumina, and sulfate did not promote sintering.

The data in Figure 7.7 show the activities of various sulfated alumina samples. Alumina was impregnated with ammonium sulfate in an amount equal to

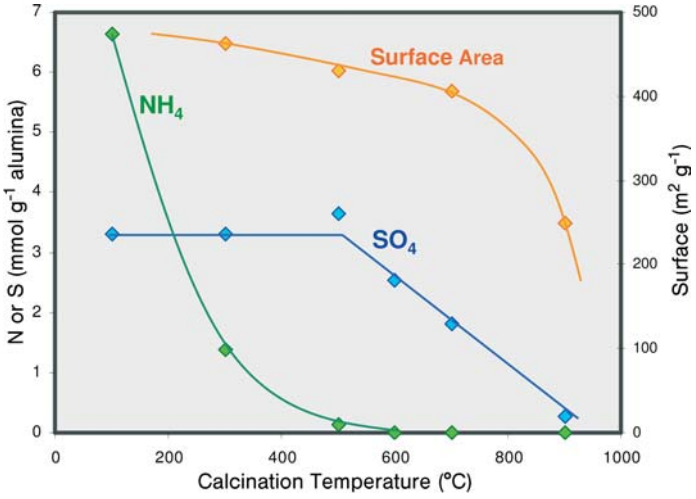

Figure 7.6 Alumina impregnated with $(NH_4)_2SO_4$ then calcined.

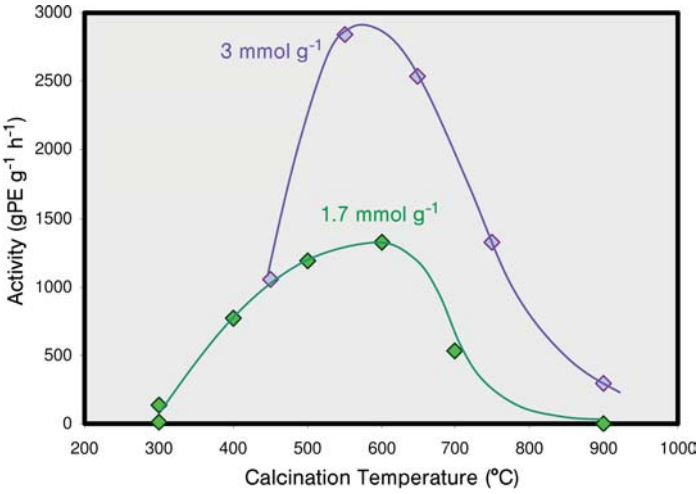

Figure 7.7 Activity of sulfated alumina as function of calcining temperature.

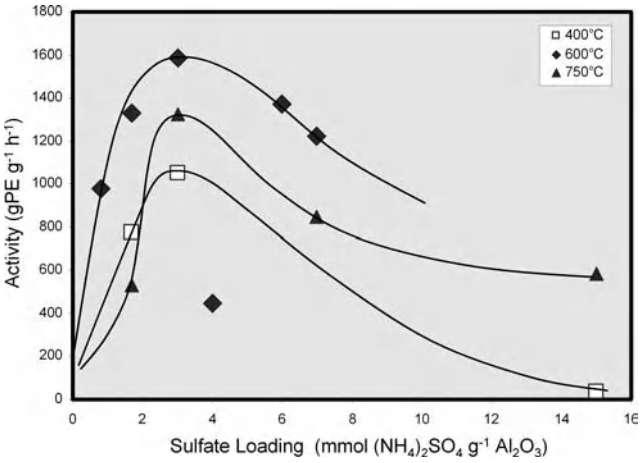

Figure 7.8 Activity of alumina impregnated with $(NH_4)_2SO_4$.

1.7 mmol g^{-1} or 3 mmol g^{-1}, and then calcined at various temperatures between 300 °C and 900 °C. In general, the activity passed through an impressive maximum at around 500–600 °C. It is easy to imagine the acidity increasing with dehydration as the temperature is raised. However, at about 600 °C the support began to lose sulfate through evaporation, which may account for the decreasing activity above about 600 °C. This finding would be in agreement with the fact that the higher loading seems to provide better activity in this series.

In fact, the optimum sulfate loading was usually found to be approximately 3 mmol g^{-1}, regardless of the calcination temperature. The data in Figure 7.8 show the activity of another series of samples in which the loading was varied, as well as the calcining temperature. Three groups were examined, calcined respectively at 400 °C, 600 °C, and 750 °C. In each case activity went through a maximum at ca. 3 mmol SO_4 g^{-1}. Again, it is easy to understand that, up to a point, acidity would at first increase with loading, but presumably above that point the surface is saturated in that excess sulfate does not increase acidity, and beyond that point the additional mass from the sulfate actually dilutes the activity or clogs the pores.

7.3.4
Silica–Alumina with Added Anions

The amorphous mixed oxides of silica and alumina already contain a higher degree of acidity than either parent. This acidity also seems to be amplified by adding an electron-withdrawing anion. Once again, the results obtained were highly dependent on which anion was used, and the best anions for alumina were not necessarily preferred for silica–alumina. A summary of these varied responses is listed in Table 7.4.

Table 7.4 Activity of silica–alumina carriers treated with electron withdrawing anions.

Solid acid	*Activity (gPE g^{-1} h^{-1})*
Silica–Alumina + F	18 000
Silica–Alumina + SO_4	100
Silica–Alumina + Cl	2 200
Silica–Alumina + $(CF_3CO)_2O$	3 200
Silica–Alumina + Triflate	12 000

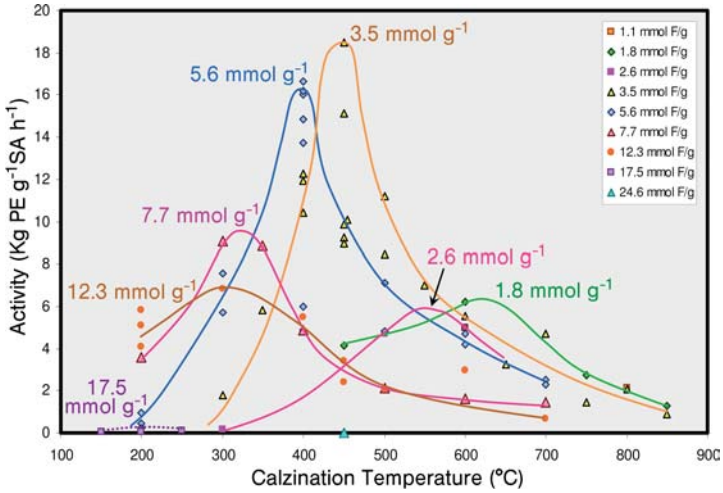

Figure 7.9 Activity of silica-alumina treated with NH_4HF_2.

7.3.4.1 **Fluoride Treatment**

One of the best anions tested with silica–alumina was fluoride, and activities of over 10 000 g g^{-1} h^{-1} became routine with this recipe. Many different fluoriding treatments were found to be effective, including NH_4HF_2, NH_4F, HF, $(NH_4)_2SiF_6$, $(NH_4)_2ZrF_6$, NH_4BF_4, HBF_4, NH_4PF_6, and TiF_4. In addition, the fluoride could be added as a fluorocarbon gas during the calcination step, as described above. As expected, potassium fluoride was ineffective as it does not increase acidity. When the fluoriding treatment contained other metals such as Ti or Zr, it was clear from the polymer that some of the activity came from the impregnated metal itself independently of the metallocene. Usually, these materials produced polymer having a high molecular tail.

The data in Figure 7.9 show the activities from silica–aluminas treated with differing amounts of ammonium bifluoride. The behavior seen here was also very typical of that seen from the other fluoriding treatments. For each fluoride loading, the activity rises with activation temperature up to some maximum, but then

declines at higher temperatures. The optimum calcining temperature varied with fluoride loading: higher fluoride levels caused a decrease in the optimum temperature. It is easy to understand why the activity would increase with higher temperature, as the degree of acidity depends on the temperature, as hydroxyls are removed to generate Lewis acidity.

However, it is a little more difficult to understand why the activity declines at higher temperatures. It is at first tempting to speculate that higher temperatures and fluoride loadings accelerate sintering, which decreases the activity. Such behavior is well known to occur on silica [18, 19]. In Figure 7.10, the surface areas from the samples tested in Figure 7.9 are displayed graphically, and show that there is indeed a loss of surface area with increasing fluoride and temperature. However, the onset of sintering does not usually coincide with the activity peak in Figure 7.9.

Therefore, an alternative process must be in operation. One possibility is that much of the activity comes mainly from Brønsted acid sites, and that while some fluoride generates Brønsted acidity, too much fluoride can displace these —OH sites. The data in Figure 7.11 show the results of IR spectroscopy obtained from these fluorided silica–alumina activators as a function of loading and temperature. The band at 1450 cm^{-1} is derived from the adsorption of NH_3 onto Brønsted sites, and is therefore taken as a measure of Brønsted acid groups on the surface [20, 21]. After exposure to NH_3 gas, the sample is evacuated and the IR spectrum taken. It can be seen in the figure that the number of Brønsted sites rises with fluoride level at each temperature, peaks, and then declines with further addition of fluoride. The number of Brønsted sites also decreased with temperature, no doubt due to their condensation.

Yet another possible explanation is a rearrangement of ligands to produce fewer coordinatively unsaturated Al^{3+} ions. It is possible, for example, that the alumina

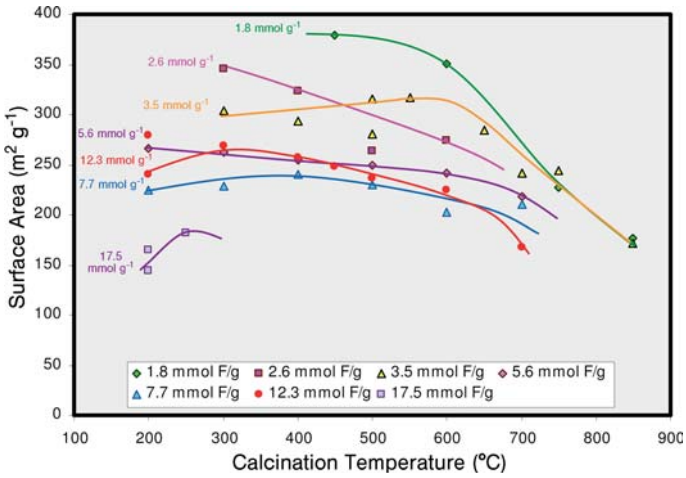

Figure 7.10 Surface area of silica-alumina treated with NH_4HF_2.

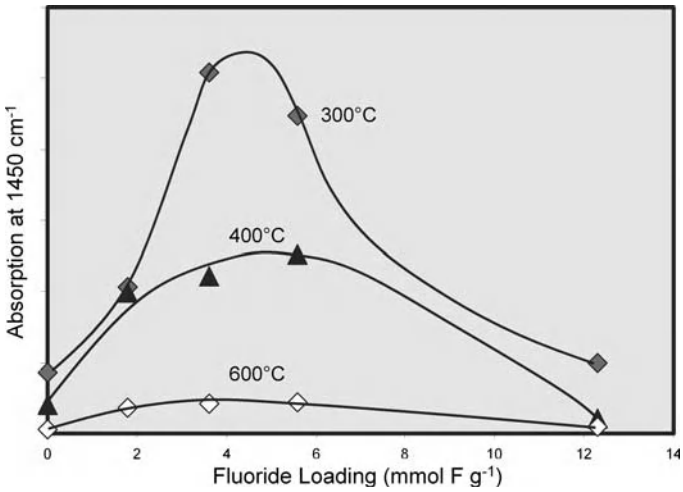

Figure 7.11 Bronsted acidity on fluorided silica-alumina.

phase of this catalyst, which most likely adsorbs the most of the fluoride, might be sintering somewhat independently of the overall silica matrix. In order to appreciate the amount of fluoride being added to these supports, it should be considered that the support in this study, MS13-110, contains 13% alumina, which corresponds to 2.5 mmol g^{-1} of Al. Thus, in most of these experiments there is sufficient fluoride present to provide at least one F per Al in the support. At higher loadings there is more than enough F present to convert all the alumina into AlF_3.

It was also considered that a rising activity with calcining temperature might be due to the desorption of residual NH_3 from the ammonium fluoride salts. However, similar plots made with hydrofluoric acid instead of ammonium fluoride salts produced similar curves and no higher activity.

Of all the peak activities, a different one for each fluoride loading, the highest seems to occur at about 3.5 mmol F g^{-1} and about 450 °C calcining, with activities of almost 20 000 g g^{-1} h^{-1} often being obtained. This value probably represents the best compromise between fluoride loading, dehydration, and sintering (local and overall). Such high activities from fluorided silica–alumina contrast with the results described above from fluorided alumina. The aluminum ions in silica–alumina are mostly in tetrahedral coordination, whereas those on alumina exist in both tetrahedral and octahedral configuration, but mostly octahedral. It is possible that the active site requires tetrahedral Al, and this is why silica–alumina is superior to alumina.

7.3.4.2 **Triflic Acid Treatment**

Trifluoromethanesulfonic acid (triflic acid) was also used to promote the acidity of silica–alumina. Several different procedures were used, and the observed activity is plotted in Figure 7.12 as a function of calcining temperature. For example,

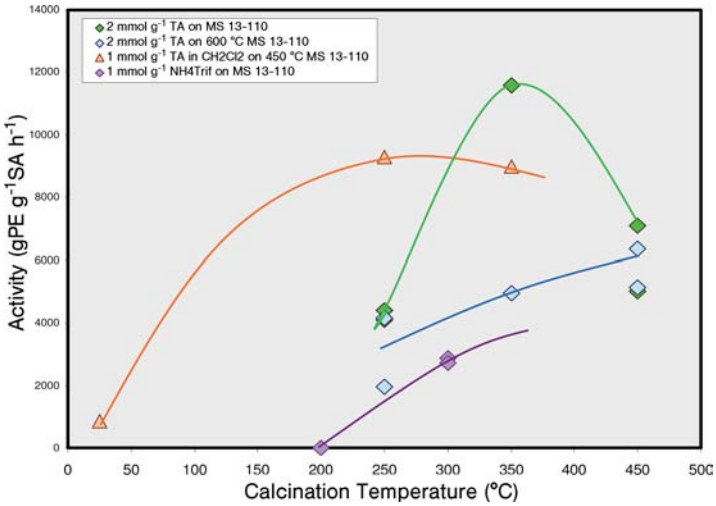

Figure 7.12 Activity of silica-alumina treated with triflic acid (TA).

in one series of experiments 2 mmol g^{-1} triflic acid was impregnated from aqueous solution onto silica–alumina, which was then calcined at various temperatures. Even the lowest calcining temperature, 250 °C, provided high activity, at 4000–4500 g g^{-1} h^{-1}. At that temperature the sample almost certainly contains intact triflate, and the activity must be ascribed to the triflic acid. Calcining in nitrogen at 350 °C provided almost 12 000 g g^{-1} h^{-1} and, again, it is likely that much of the triflic acid existed intact on the support. After calcining at 450 °C in nitrogen the activity was 4000–7100 g g^{-1} h^{-1}. As the temperature is raised, at some point decomposition of the triflate into fluoride is possible which, as shown above, also produced high activity.

In another series of experiments aqueous triflic acid was impregnated onto 600 °C precalcined silica–alumina. Drying in nitrogen at 250 °C provided up to 4200 g g^{-1} h^{-1}, while calcining at 350 °C and then 450 °C increased activity up to 6400 g g^{-1} h^{-1}, although decomposition to fluoride may have occurred.

Anhydrous triflic acid in dichloromethane (DCM) solution was also impregnated onto precalcined silica–alumina. Simply drying the sample on a hot plate did not provide an active catalyst, which suggests that perhaps the DCM was not completely removed. Drying in nitrogen at 250 °C raised the activity to 9300 g g^{-1} h^{-1}, while further drying at 350 °C brought the activity back down to approximately 6000 g g^{-1} h^{-1}. Ammonium triflate on silica–alumina also provided an activity of 3000 g g^{-1} h^{-1} when calcined at 300 °C.

7.3.4.3 Treatment with Other Anions

Although weaker in electron-withdrawing power, the trifluoroacetate anion was also tested. Silica–alumina, predried at 250 °C or 600 °C, was treated with trifluoroacetic anhydride (TFAA) vapor in a nitrogen carrier at 200 or 250 °C, and tested

for polymerization activity with the test metallocene. Such low temperatures were chosen for the TFAA treatment in an effort to avoid its decomposition. Clearly, at higher temperatures the TFAA would simply be another source of fluoride. These experiments generated some respectable activity, even above $3000\,g\,g^{-1}\,h^{-1}$.

Silica–alumina was also treated with chloriding agents at 600 °C, as described above, and this increased the activity to $2200\,g\,g^{-1}\,h^{-1}$. Although respectable, this activity was not comparable to the results with fluoride, triflate and trifluoroacetate. Whilst the reason for this unexpected result is not entirely clear, it is possible that with so little alumina present some may have been lost as $AlCl_3$ vapor during the treatment.

Surprisingly, adding sulfate to silica–alumina, at between 0.2 and $1.7\,mmol\,g^{-1}$, produced little enhancement in the activity.

7.3.5
Other Mixed Oxides with Added Anion

Although less commonly used for industrial applications, other acidic mixed oxides of silica were also tested. For example, silica–titania and silica–zirconia behaved much like silica–alumina in many respects, with high activities being obtained after treatment with fluoride or triflate, but not with sulfate (see Table 7.5). The aluminophosphates, where P_2O_5 is considered as a minority oxide with alumina, behaved more like aluminas, but were more acidic. Thus, fluoride, chloride, and even sulfate, were effective at low P : Al ratios. At high P : Al ratios, however, the results were more similar to silica or silica–alumina, and chloride or sulfate was less effective.

7.3.6
Combining Multiple Anions or Lewis Acidic Metals

On many occasions improvements in activity can be obtained by combining two different anions or two different Lewis acidic metals on one support. Possibly, this

Table 7.5 Activity of other mixed-oxide carriers treated with electron-withdrawing anions.

Solid acid	*Activity ($gPE\,g^{-1}\,h^{-1}$)*
Silica–Titania + F	2800
Silica–Zirconia + F	4400
Silica–Zirconia + Cl	1700
AIPO (P/Al = 0.4) + F	2200
AIPO (P/Al = 0.2) + F	2800
AIPO (P/Al = 0.8) + Cl	500

increases the polarity of metal oxide surface bonds, thereby increasing acidity. One strong example is the combination of fluoride and chloride on alumina (see Table 7.6). Fluorided alumina provided an activity of ca. 1200 $g\,g^{-1}\,h^{-1}$, while chlorided alumina provided up to 2000 $g\,g^{-1}\,h^{-1}$. However, when the alumina was first fluorided and then chlorided, an activity of up to 6320 $g\,g^{-1}\,h^{-1}$ was obtained, and this was repeated in may different experiments.

Similar results can be obtained by adding a second Lewis acidic metal to alumina, and a particularly good example for this purpose is zinc. Results obtained by impregnating 1.5 $mmol\,g^{-1}$ zinc nitrate onto the alumina before the final calcining and haliding treatment are listed in Table 7.7. Two paired experiments were conducted, one series fluorided (by treatment with perfluorohexane at 600 °C) and the other series chlorided (by treatment with CCl_4 vapor at 600 °C). In both cases, the presence of zinc greatly increased the activity obtained, by two- to eight-fold. However, zinc chloride on silica provided little or no activity, which suggests that zinc chloride itself is not responsible for the increase in activity. Neither did zinc, when added to silica–alumina, have the same effect, and therefore the enhancement must result from the incorporation of zinc into the alumina lattice. Again, this suggests that the added zinc may help to polarize the surface oxide bonds, which increases acidity. It may also increase the fraction of surface aluminum that exists in the tetrahedral configuration.

The optimum zinc loading was in the range of 1.5 to 2 $mmol\,g^{-1}$. This is shown in Figure 7.13 for a series of Zn/alumina samples treated with carbon tetrachloride at 600 °C. Presumably, an adequate surface concentration is reached at ca.

Table 7.6 Activity improvements are often obtained by combining multiple electron withdrawing anions.

Treatment	*Calcined (°C)*	*Activity ($g\,g^{-1}\,h^{-1}$)*
Fluorided alumina	600	1200
Chlorided alumina	600	1800
Fluorided then chlorided alumina	600	6320

Table 7.7 Activity improvements are often obtained on alumina by adding a second Lewis acidic metal ion.

Treatment	*Calcined (°C)*	*Activity ($g\,g^{-1}\,h^{-1}$)*
Fluorided alumina	600	1 200
Fluorided Zn/alumina	600	2 560
Chlorided alumina	600	1 800
Chlorided Zn/alumina	600	14 240

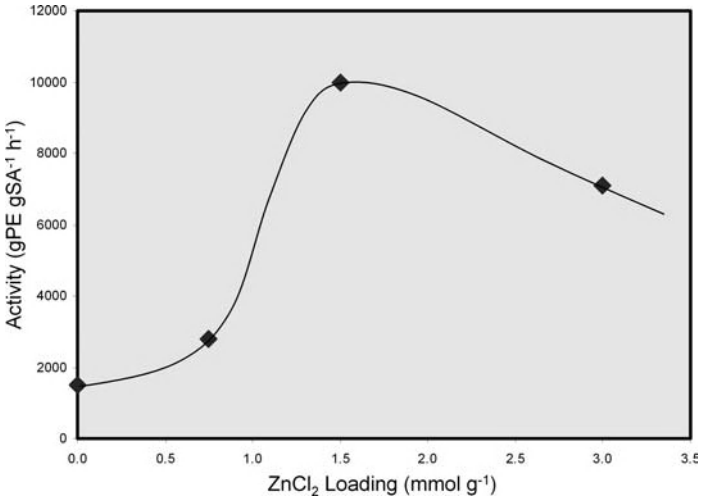

Figure 7.13 Activity of chlorided alumina as a function of zinc loading.

1.5 mmol g^{-1}, and higher levels only tend to hinder access through pores. The optimum calcining temperature was again found to be about 600 °C.

This raises the question of which Lewis acidic metal is activating the metallocene, that is, whether the improved activity is due to the added zinc or to an enhancement of the original Al^{+3} ions on the alumina. Actually, the phenomenon is not restricted to zinc but seems to be more universal. A list of activities obtained by chloriding, at 600 °C, aluminas treated with 1–2 mmol g^{-1} of a number of other metal ions is provided in Table 7.8. It is clear from these data that, although quite effective, zinc is not the only metal capable of enhancing activity. In general, the effective metals seem to be compatible with the alumina surface and possess some Lewis acidity of their own in the oxide state. Other particularly effective metal ions included Ag, Sn, V, and Cu. That so many different metal ions are capable of enhancing activity suggests that their effect is one of perturbing or polarizing the alumina surface, or converting Al^{+3} into the tetrahedral form, and that the active metal may still be aluminum in all these examples.

7.4 Metallocene Choice

The diverse levels of activity displayed by these solid acids are undoubtedly a combination of many influences. For example, the surface area and porosity of the support after treatment have already been cited above as important variables, as they are for supported Ziegler- and Phillips-type catalysts. Other characteristics include the acid site density, the type of acid site, the acid strength, and the choice of metallocene. The leaving group abstraction or "ionization" mechanism can be understood as an acid–base reaction in which the metallocene is the base. Therefore, just as the acid strength of the activator is important, so too is the basicity of

Table 7.8 Enhanced activity from second Lewis acidic metal ion.

Added metal ion	*Activity ($g\,g^{-1}\,h^{-1}$)*
None	1800
Zn	14237
Sn	6859
Ag	5159
Nb	2036
Ni	3690
W	3286
Mo	4512
V	6023
Cu	4669
Sb	2272
Ti	3936
Zr	1484
Ga	3115
Mn	1507
Mg	166
Fe	563
Cr	1217
La	1059
Nd	1158
Co	727

the metallocene. The hardness or softness of the activator and metallocene may also play a role in determining the degree of their interaction. These considerations may explain why different test metallocenes can sometimes yield very different results. Even the ranking order of a series of solid acids can depend on the choice of metallocene, perhaps reflecting the highest occupied molecular orbital-lowest unoccupied molecular orbital (HOMO-LUMO) pairing of each component.

For example, sulfated alumina is known to contain strongly acidic functionality, even "superacid" sites, whereas MAO is probably less acidic, followed by weakly acidic ordinary trialkylaluminum compounds. In the present authors' experience, certain metallocenes (e.g., unbridged (mono- or dialkylCp)$_2$$ZrCl_2$ compounds) are more easily activated than others (e.g., certain tightly bridged, unsubstituted-fluorenyl-containing metallocenes). Thus, the activity measured can vary considerably with the choice of metallocene, and metallocenes that are more difficult to ionize generally require stronger solid acids for activation.

7.5 Participation by Aluminum Alkyl

All of the above tests were conducted in the presence of an alkylaluminum cocatalyst. This compound, although necessary as an alkylating agent when the dihalide

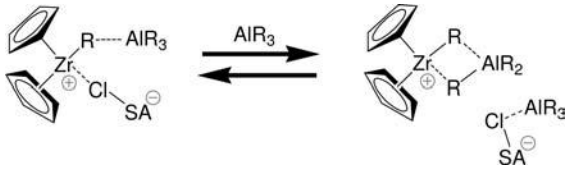

Scheme 7.5

metallocenes are used, actually plays a much greater role in the formation of the catalyst. In fact, there is considerable evidence that it actually becomes part of the active site and influences many of the catalyst characteristics. For example, the simplest way to illustrate the importance of the alkylaluminum cocatalyst is to omit it from the recipe, and to use the dialkyl metallocene (Cp_2ZrR_2) instead. Although some activity is often seen (i.e., even in the absence of added alkylaluminum cocatalyst), that activity is always greatly diminished. Furthermore, changes in the resultant polymer are also often seen, including higher molecular weight and/or higher levels of long-chain branching.

Another indication that the alkylaluminum becomes an integral part of the active site is the fact that different aluminum alkyls produce a wide variety of responses. For example, three similar cocatalysts – trimethylaluminum, triethylaluminum, and tri-isobutylaluminum – can yield very different activities from the same metallocene and solid acid. One possible explanation is that the aluminum alkyl helps to solvate and separate the ion pair (metallocene cation and solid acid anion), perhaps through bridging structures such as that illustrated in Scheme 7.5.

7.6 Brønsted versus Lewis Acidity

Many of the solid acids studied here contain both Brønsted and Lewis acidity, and in fact are better known for their Brønsted acidity. This raises the question as to which type of acidity participates in the activation of metallocenes. At least three mechanisms of activation can be imagined (see Scheme 7.6) utilizing both Lewis and Brønsted acidity:

- A simple coordinatively unsaturated Lewis acidic metal abstracts a ligand, probably chloride, from the metallocene.
- The metallocene reacts with a Brønsted site, losing a ligand, probably alkyl.
- The Brønsted site may react with alkylaluminum to form a Lewis site, which then goes on to activate metallocene by ligand abstraction.

In Scheme 7.6 it is assumed that the metallocene has already been partially alkylated by reaction with the alkylaluminum cocatalyst.

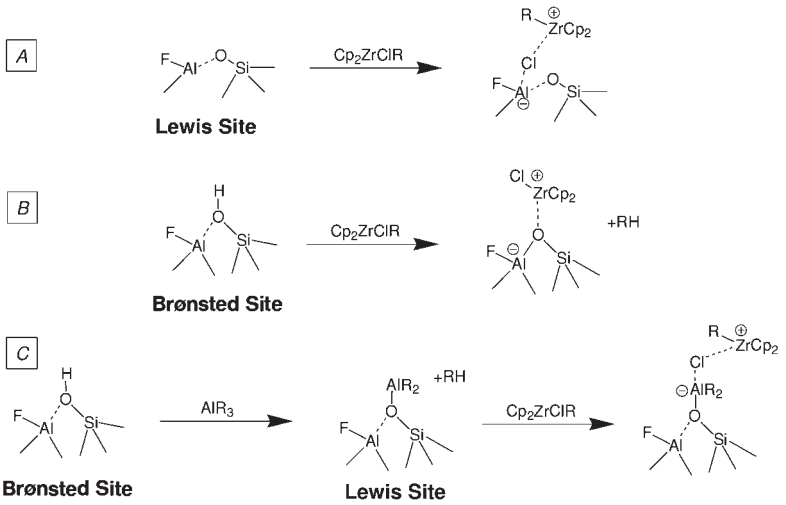

Scheme 7.6 Possible mechanisms of metallocene activation.

There is reason to believe that all three of these mechanisms contribute to the observed overall activity, and that the relative contribution of each can vary widely depending on the solid acid, and the method of catalyst preparation. For example, on some solid acids, such as those treated with a chloriding agent at high temperature, all of the acidity is Lewis, which implies the activation of metallocene as shown in Scheme 7.6, route A. The chlorided zinc–alumina, which exhibited excellent activity, is one example of this.

On the other extreme, solid acids known for their Brønsted acidity, such as sulfated alumina calcined at low temperatures, can be treated with the metallocene dialkyl species in the absence of an alklyaluminum cocatalyst, which would most likely lead to the species in Scheme 7.6, route B. Marks has reported one example of this experiment [22], and the results of the present authors' own similar experiments agree with these findings, in that activity was very poor. In addition, such catalysts tend to produce quite different polymers, distinguished by high molecular weight and viscosity, when compared to other preparations. In fact, similarities between such catalysts and Ballard-type catalysts are noteworthy.

However, if the same dialkyl metallocene and sulfated alumina are combined in the presence of an alkylaluminum cocatalyst, then the activity is increased, sometimes by orders of magnitude. This in itself is consistent with participation of the mechanism in Scheme 7.6 route C, but the point can be made even more directly. The result now depends on the order of contact. If the solid acid is first treated with the alkylaluminum cocatalyst, and then with the metallocene, very high activity is obtained. In contrast, if the solid acid is first contacted with the metallocene, and then with the cocatalyst, the activity is usually poor and the polymer is sometimes altered by the presence of a high-molecular-weight, highly viscous component. These results indicate a competition between routes B and C

of Scheme 7.6. In fact, when the solid acid is first treated with alkylaluminum, then no Brønsted acidity should remain.

7.7
Polymer Molecular Weight Distribution

When these solid acids were used to activate simple unbridged metallocenes, such as the bis(*n*-butylcyclopentadienyl)zirconium dichloride used as a test reagent in these studies, the polymer MWD was usually very narrow, with M_w/M_n approaching 2.0. This is the typical "single-site" distribution, and it indicates that the heterogeneity of the oxide surface does not exert a major influence on the active sites. In other words, the oxide surface does not seem to be part of the inner coordination sphere of the zirconium. Likewise, when these simple metallocenes are activated by vastly different solid acid or MAO activators, little or no difference is observed in the molecular weight of the polymer produced. This is another indication that the activator in these systems is relatively "non-coordinating". Most likely, the substituted cyclopentadienyl rings dominate the Zr coordination sphere on these metallocenes.

This behavior is in contrast to many other oxide-supported catalysts, such as Ballard- and Phillips-type catalysts, where the heterogeneity of the oxide surface is indeed reflected in a broad polymer MWD [19]. Figure 7.14 contrasts the MWD of polymer from a metallocene [$(n\text{-buCp})_2ZrCl_2$)] and a Ballard catalyst [$ZrBenzyl_4$], both activated by the same sulfated alumina support. One provides a narrow "single-site" MWD, while the other provides an exceedingly broad MWD. Intermediate between these two extremes is the polymer derived from a half-sandwich zirconium complex (only one Cp ring), and again activated by the same solid acid.

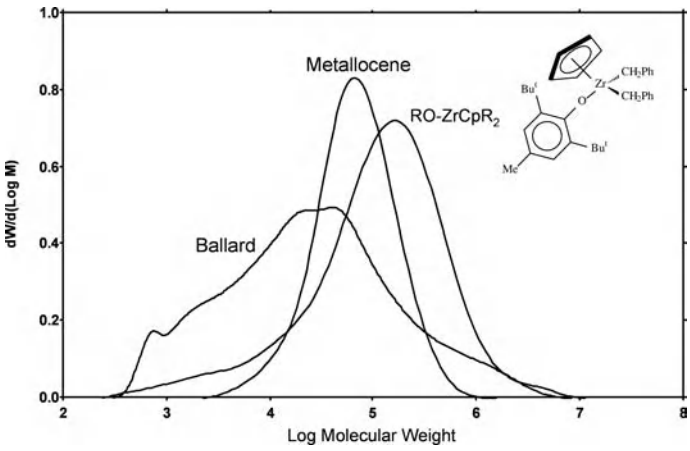

Figure 7.14 MW distribution from three Zr compounds activated by the same SA.

While single-site polymer distributions are common (even normal) from these solid acid activators, there are still times when subtle variations in MWD can be observed, depending on the solid acid or catalyst preparation. One example of this, as noted above, is the reaction of the metallocene with a Brønsted site (as suggested in Scheme 7.6 route B). The oxo-Zr species resulting from this reaction seems to produce a much higher molecular weight polymer than from other species. Under normal conditions the contribution from this pathway is minor, and little or no broadening in the MWD may be noted. However, the difference becomes quite visible when steps are taken to maximize the formation of this species.

One way to do this is to add a metallocene dialkyl, in the absence of alkylaluminum cocatalyst, to a solid acid containing a high concentration of Brønsted acidity. An extremely high-molecular-weight and viscous polymer is obtained. An example of this is provided in Figure 7.15, where bis(indenyl) zirconium dibenzyl was contacted with a sulfated alumina. In a contrasting case in Figure 7.15, the solid acid was first treated with alkylaluminum, to remove Brønsted sites before contact with the metallocene. This should minimize formation of the oxo-Zr species. The result was a narrow, much lower MWD. In yet another case (see Figure 7.15), the solid acid was first treated with metallocene to maximize the oxo-Zr species, but the alkylaluminum cocatalyst was still used later in the reactor. Here, in the presence of cocatalyst, the contribution from Brønsted sites can be seen as a minor high-molecular-weight component that accompanies the more normal single-site polymer. Presumably the high-molecular-weight, Brønsted-derived component is obtained from the formation of an oxo-Zr species (as shown in route B of Scheme 7.6). Attack on the metallocene rings by the strong Brønsted acid is also conceivable, but evidence for such decomposition has not been found [22].

Yet another way to influence the MWD by the solid acid activator is by the incorporation of a second active metal into the solid acid. Several examples of this

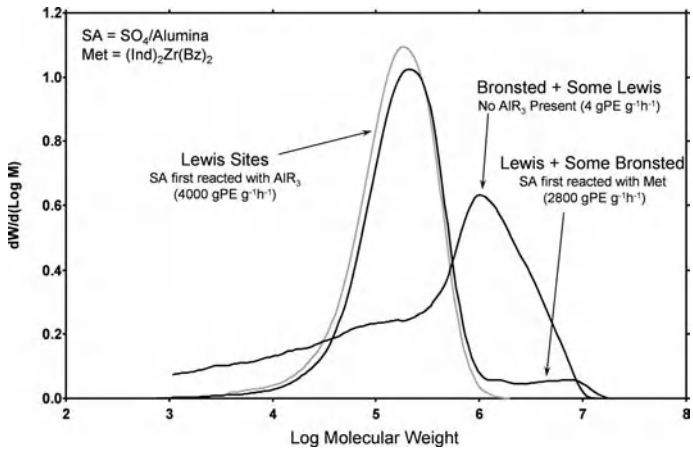

Figure 7.15 MW distribution from Bronsted vs. Lewis sites.

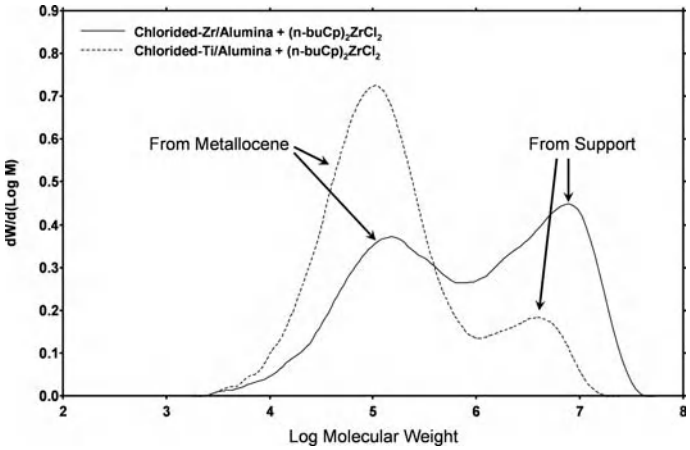

Figure 7.16 MW distribution containing contribution from two sources.

have been described, such as fluoride-treatment of silica–alumina by impregnation with ammonium hexafluorozirconate or ammonium hexafluorotitanate. Similarly, $ZrCl_4$ or $TiCl_4$ can be used to apply chloride to alumina, and chromium can be added to any of these oxide carriers. In all of these cases the added transition metal is activated by the cocatalyst and produces its own polymer contribution, quite independent of the metallocene contribution. Often, this affords a linear, high-molecular-weight tail, or even bimodal MWD. One example is shown in Figure 7.16, where two mixed oxides of Al and Zr, and of Al and Ti, were chlorided and used as a solid acid activator. It should be noted that there is a contribution to the polymer from both the metallocene and the solid acid.

7.8 Leaching of the Metallocene

One of the difficulties of commercializing metallocene catalysts for use in slurry-phase polymerization is leaching of the metallocene from the support and into the polymerization solvent. Polymer produced in the solvent, instead of on the support, tends to foul the reactor by coating the heat-transfer surfaces, and for this reason much of the patent literature has focused on ways to bond the metallocene chemically to an inert support (usually silica). Another alternative approach has been to support the MAO activator (normally liquid) onto a silica or other oxide surface, although it is sometimes difficult to maintain the MAO on the silica under reaction conditions. On occasion, the leaching of a MAO–metallocene complex still occurs if the correct precautions are not taken, and this will result in reactor fouling.

As there are no soluble ionizing species, such considerations do not apply to the solid acid activators discussed here. Although metallocene can be added to the catalyst, or even to the reactor, as a hydrocarbon solution, it is not activated until it has been adsorbed onto the solid acid surface. Thus, only adsorbed (ionized)

metallocene produces polymer. The activating acid sites form an integral part of the oxide surface, and cannot be leached into a hydrocarbon solution. The activated metallocene is always held by electrical attraction to the solid acid; therefore, the catalyst remains a solid, the polymer precipitates on the solid particle, and fouling is intrinsically avoided.

7.9 Characterization of Active Sites

7.9.1 Adsorption of Pyridine

In an attempt to gather more information on the nature of the acid sites responsible for metallocene activation on these oxide surfaces, an *in-situ* FTIR method was developed. Here, pyridine was employed as the probe molecule, which allowed for the quantification of both Brønsted and Lewis acid sites (Scheme 7.7) [9]. Each solid acid was exposed to pyridine vapor at 170 °C, and the amount adsorbed onto the Brønsted and Lewis sites determined.

The results of these experiments are shown in Table 7.9 for a number of different solid acid activators. In every case, the Lewis acid site density is higher than

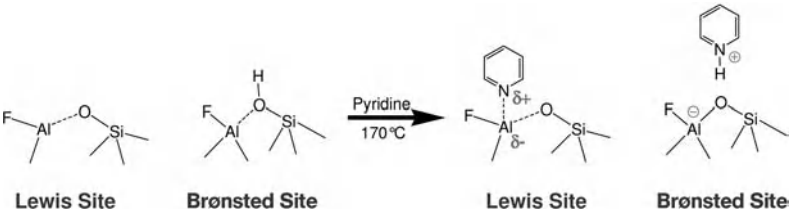

Scheme 7.7 Acidity by pyridine absorption.

Table 7.9 FTIR acidity determinations by pyridine adsorption.

Sample description	*Pretreatment temperature (°C)*	*Brønsted (mmol g^{-1})*	*Lewis (mmol g^{-1})*	*Polymerization Activity*
Silica–alumina (MS13-110)	450	0.050	0.124	<10
Alumina	550	0	0.349	<10
Sulfated alumina (alumina + 1.7 mmol g^{-1} H_2SO_4)	550	0.154	0.289	2000
Fluorided silica–alumina (MS13-110 + 1.75 mmol g^{-1} NH_4HF_2)	450	0.159	0.121	15000
Fluorided silica–alumina (MS13-110 + 1 mmol g^{-1} HF)	450	0.067	0.104	1500
Chlorided Zn/alumina (CCl_4 600 °C)	600	0	0.275	8000

the Brønsted site density. Both, Lewis and Brønsted sites have been considered to be potential sites for metallocene activation, and many of these solid acids contained both types of acidity. However, it is clear that on chlorided Zn/alumina the activation of metallocene must occur at a Lewis site, as there are no Brønsted sites on that solid acid. Likewise, the alumina sample did not exhibit Brønsted acidity – not because of a lack of hydroxyls, but because they were apparently basic (or at least not acidic). However, when sulfate was added to the alumina, followed by calcination, substantial Brønsted activity did develop. The addition of fluoride to silica–alumina also seems to have caused a significant increase in Brønsted acidity.

Details of the polymerization activity obtained from each solid acid are also listed in Table 7.9, for comparison. It is difficult to correlate the observed activity with either the measured Brønsted or Lewis acidity. Those solid acid samples containing the largest Brønsted or Lewis acid density are not necessarily the most active, perhaps because pyridine is too strong a base for these experiments, and measures more sites than are actually involved in metallocene activation. The pyridine adsorption on Brønsted sites was almost irreversible; once treated with pyridine, heating the sample even to temperatures where pyridine begins to decompose failed to cause its release to any great extent. This was true for all samples containing Brønsted sites. In contrast, Lewis sites released their adsorbed pyridine fairly easily, with most being removed by 200 °C, and this was true of all the samples tested.

7.9.2 Adsorption of Metallocene

A titration of fluorided silica–alumina was also conducted using metallocene as the base over a wide range. Activity measurements were then taken at each metallocene loading. The metallocene used in this test was simple zirconocene dichloride, and the cocatalyst was 1 mL of 1 M triethylaluminum. In Figure 7.17, the solid acid (SA) activity results (in kg PE produced g^{-1} SA h^{-1}) are plotted against the metallocene : SA ratio. Initially, the SA activity increases with rising metallocene loading, but at some point the activity stops rising, indicating that the SA has become saturated with metallocene. The activity then turns down at very high metallocene loadings. The reason for this is not clear at present, but it has been suggested that the free metallocene in solution begins to bind with the activated metallocene, and thus interferes with its activity. Another possibility is that overloading the support blocks pore openings, causing poor activity. This trend has often been seen for chromia and other inert dopants on Cr/silica catalysts.

The saturation loading occurs at about 2 μmol metallocene g^{-1} SA. This is a very small number in comparison to the values obtained from the pyridine measurements, and explains why no correlation was possible with Brønsted or Lewis site density as measured by pyridine. Apparently, only a small percentage of these acid sites serve to activate metallocenes. Of course higher activities can be obtained from bulkier metallocenes, but the saturation loading remains very low for this

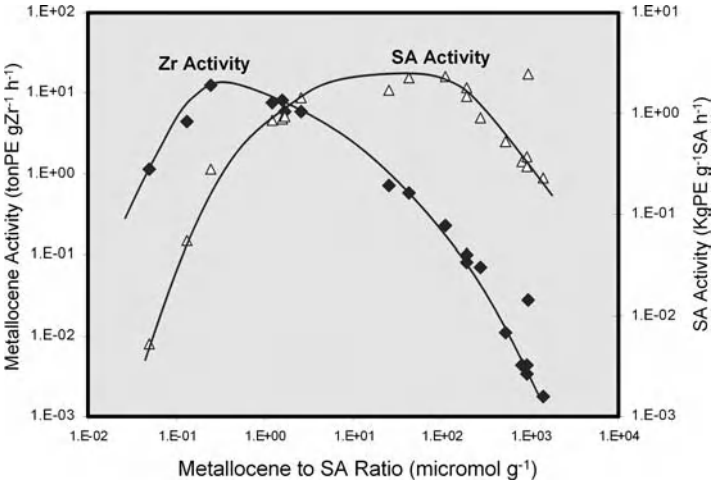

Figure 7.17 Influence of metallocene loading on activity.

solid acid. The saturation loading can vary considerably, however, with the choice of solid acid.

The observed saturation loading effect does not occur because the large metallocene molecule really does cover all of the available surface, forming a "monolayer". Simply dividing the available surface area by the cross-sectional area of a metallocene indicates that complete spatial coverage should occur at about a 1000-fold higher loading. Therefore, the acidic sites in question seem to be very special.

Metallocene adsorption onto fluorided silica–alumina was also measured by observing the loss in ultraviolet (UV) signal from toluene solutions. Several metallocenes were investigated, including zirconocene dichloride. The data in Figure 7.18 show the adsorption curves obtained as metallocene was added to a toluene solution containing fluorided silica–alumina. The adsorption of zirconocene dichloride was almost 100-fold smaller than the maximum allowed by spatial coverage, but was still over 10-fold larger than the saturation loading implied by polymerization behavior.

Also shown in Figure 7.18 is the adsorption of $(Cp)_2Zr(Me)_2$ onto fluorided silica–alumina. Although the polymerization activity of this material was no different from $(Cp)_2ZrCl_2$ in these tests, it adsorbed onto the fluorided silica–alumina in much larger amounts than the corresponding dichloride. Adsorption of the dimethyl compound even begins to approach the theoretical maximum spatial coverage. Possibly, the dimethyl compound may also react with oxide surface bonds.

If an excess of triethylaluminum cocatalyst is included in the metallocene solution, then the solid acid adsorbs much less metallocene. An example is shown in Figure 7.19 using bis(*n*-butylcyclopentadienyl)zirconium dichloride. In fact, the adsorption number was so small that it begins to approach the saturation loading

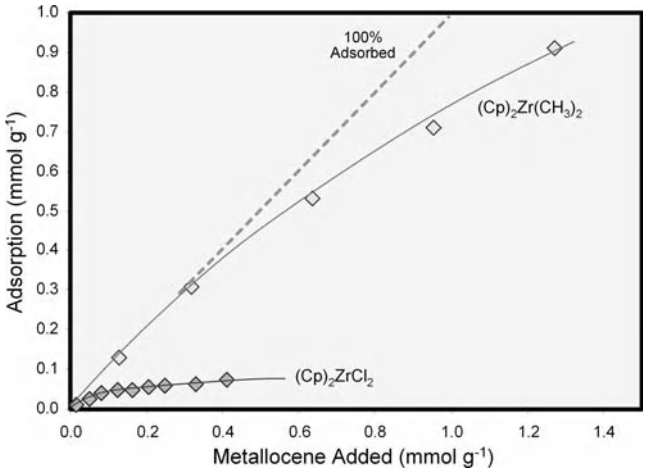

Figure 7.18 Adsorption of metallocene on fluorided silica-alumina.

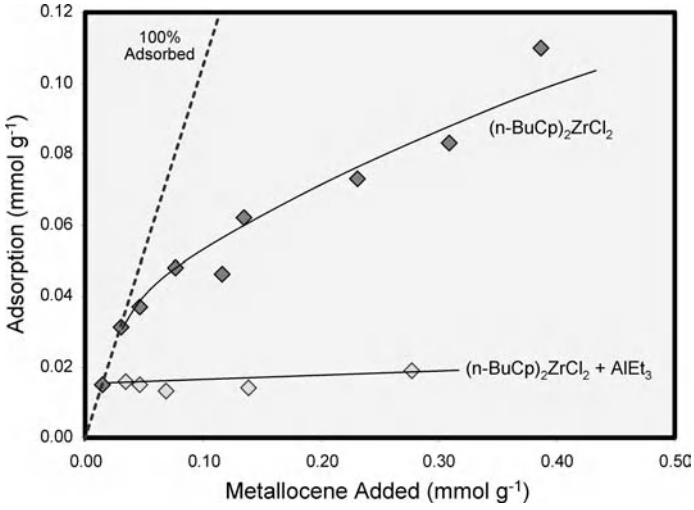

Figure 7.19 Adsorption of metallocene on fluorided silica-alumina.

observed from polymerization. This suggests that the alkylaluminum occupies sites that might otherwise adsorb metallocene.

This saturation loading in Figure 7.17 serves as an upper bound on the number of active sites. If all metallocene at this loading is active, then the active site density can be no higher than $2\,\mu mol\,g^{-1}$. The data in Figure 7.17 also show the metallocene activity (in tons PE produced g^{-1} $Zr\,h^{-1}$) plotted against metallocene loading. Maximum activity is reached at a much lower loading ($0.2\,\mu mol\,g^{-1}$ SA), after which the metallocene activity begins to decrease at higher loadings. These two plots resemble similar plots made from Cr/silica, and this same

behavior has been noted [18, 23, 24]. The usual explanation for this behavior is that, initially, Cr is adsorbed by the support very efficiently to yield active sites. At higher Cr loadings, however, increasingly fewer of the Cr species adsorbed are actually turned into active Cr sites. As the adsorption becomes progressively less efficient the Cr activity turns down, even though the overall catalyst activity is still rising.

One method of estimating the active site concentration is to determine the maximum activity of the metallocene at low loadings, to assume that all of the Zr is active at these low loadings, and then to determine the average activity per site. Even though this particular metallocene is not noted for high activity, the data in Figure 7.17 indicate that at very low metallocene loadings the activity of each site is no less than about 12 tons PE g^{-1} Zr h^{-1}. This is a lower limit because it assumes that every Zr initially added is active. If that is not the case, then the activity per site is even higher. The peak activity per gram of sold acid was about 2.5 kg PE g^{-1} SA h^{-1}. Dividing this maximum solid acid activity by the maximum Zr activity indicates a maximum active site concentration of about 2 μmol g^{-1} SA. This represents an upper limit, because it assumes a lower limit on the activity per site. If each site is actually more active, then it follows that there must be fewer sites. It is also interesting that 12 tons PE g^{-1} Zr h^{-1} represents a turnover frequency of 11 000 ethylene molecules incorporated per second per site.

7.9.3
Adsorption of Ether

Since pyridine was concluded to be too strong a base, several solid oxides were exposed to a weaker base, diethyl ether, in another series of experiments. Presumably, adding a Lewis base to the solid acid could neutralize some of the Lewis (but not Brønsted) acidity, which could reduce the polymerization activity. In these experiments several solid acids were exposed to a large excess of ether vapor at between 25 and 200 °C as 1 mL of diethyl ether was evaporated into a stream of N_2 flowing through the sample. The sample was then flushed with nitrogen for increasing times and temperatures to remove successively more ether. Each sample was then tested for polymerization activity; the results obtained are shown in Table 7.10.

The first series of solid acids to be treated were fluorided silica–aluminas, calcined at 450 °C. Ether had little or no effect on the activity of these materials. However, when treated with ether at 25 °C, followed by 30 min of N_2 flushing at the same temperature, the solid acid adsorbed 0.21 mmol of ether per gram of solid acid, and only about 11% of the activity was lost. (In fact, in some repeat runs no activity was lost.) Flushing this sample at 100 °C restored all of the lost activity, suggesting that the ether does not bind to sites at 100 °C. Prolonged flushing at 25 °C also restored the activity. The calcination temperature was varied from 350 °C to 550 °C to determine if this might change the participation by Lewis versus Brønsted sites. However, neither the sample calcined at 350 °C nor that calcined at 550 °C was affected by exposure to ether.

Table 7.10 Neutralizing Lewis acidity by exposure to diethyl ether.

Solid acid	*Ether vapor treatment (°C)*	*N_2 flush*	*Ether adsorbed (mmol g^{-1})*	*Polymerization activity loss (%)*
Fluorided silica–alumina	25	30 min/25 °C	0.21	0–11
Fluorided silica–alumina	100	30 min/100 °C		0
Fluorided silica–alumina	200	30 min/200 °C		0
Fluorided silica–alumina	25	12 h/25 °C	0.02	0
Chlorided Zn/alumina	25	30 min/25 °C	0.38	100
Chlorided Zn/alumina	165	30 min/165 °C		99
Sulfated alumina, 1.5 mmol g^{-1} 650 °C	25	1 h/25 °C	0.36	77
Sulfated alumina, 1.5 mmol g^{-1} 450 °C	25	12 h/25 °C	0.32	68
Sulfated alumina, 4 mmol g^{-1} 400 °C	25	12 h/25 °C	0.92	0

Table 7.11 Summary of adsorption results on fluorided silica–alumina.

Method of measurement	*Adsorption (mmol g^{-1})*
Brønsted acidity by pyridine	0.159
Lewis acidity by pyridine	0.121
Cp_2ZrCl_2 adsorption	~0.06
$Cp_2Zr(CH_3)_2$ adsorption	~1
Cp_2ZrCl_2 adsorption + $AlEt_3$	~0.015
Lewis acidity by ether	0.21
Active site density by polymerization	<0.002

The adsorption numbers obtained by different methods using fluorided silica–alumina are summarized in Table 7.11. The polymerization behavior still implies a much smaller number of active sites than any of the other adsorption measurements.

The lack of sensitivity of fluorided silica–alumina to ether vapor can be explained in perhaps two ways. First, ether should have little or no effect on Brønsted acidity, and it could therefore be postulated that most of the activity on this solid acid derives from Brønsted rather than Lewis sites. The parallel loss of Brønsted acidity and polymerization activity with high fluoride loading in Figures 7.9 and 7.11 might also suggest this explanation. A second possibility is that the Lewis sites on

this solid acid are too weak to hold the ether in the reactor at 90 °C in the presence the triethylaluminum cocatalyst, which is also a weak Lewis acid. If true, however, the Lewis sites must still be acidic enough to activate the metallocene, which the $AlEt_3$ cocatalyst will not do.

The second series in Table 7.10 incorporated the same experiment, but using a chlorided zinc–alumina activator. This solid acid is expected to contain strong Lewis but no Brønsted acidity, because the 600 °C chloriding step should remove all surface —OH groups. This was confirmed by the pyridine adsorption in Table 7.9. This solid acid adsorbed 0.38 mmol ether per gram, which completely killed the polymerization activity. Even flushing at 165 °C failed to restore any of the activity. This behavior was consistent with activation by strong Lewis acidity only.

The third solid acid tested in Table 7.10 was sulfated alumina, which is known for very strong Brønsted and Lewis acidities. In the first run an effort was made to maximize the Lewis component, and a high dehydration temperature was chosen, at 650 °C. This solid acid adsorbed 0.36 mmol ether when exposed at 25 °C, and lost about 77% of its activity. This also was consistent with activation by primarily Lewis acidity. In the second run in the series, the calcining temperature was lowered to 450 °C in an effort to shift the composition slightly away from Lewis and more toward Brønsted sites. This sample adsorbed slightly less ether (0.32 mmol g^{-1}), and lost a little less activity (68%). Clearly, most of the activity was still coming from Lewis sites. Finally, in the third run the sulfate loading was greatly increased, while the calcining temperature remained low to avoid evaporation of sulfate. This might be expected to produce still more Brønsted acidity. The extra sulfate lowered the overall activity by about 65%, but that activity was unaffected by ether, which might be interpreted as a stronger contribution from Brønsted sites. However, it also adsorbed a large amount of ether, which was puzzling. This support is known to be a strong adsorbent for organics, and perhaps this adsorption does not reflect the Lewis acidity used for metallocene activation.

7.9.4
Adsorption of Carbon Monoxide

Although not known as a sigma-type Lewis base, CO was also tested as an adsorbent for some solid acid activators. In no case was any loss of activity noticed from exposure to CO. Although CO is a strong poison for the activated metallocene when introduced into the reactor, it apparently has little or no affinity for the solid acid itself.

7.9.5
Adsorption of Water Vapor

The experiment described above with ether vapor was repeated using water vapor, which is a much stronger base. Samples of sulfated alumina were exposed to known amounts of water vapor at 25 °C, and then tested for polymerization. Expo-

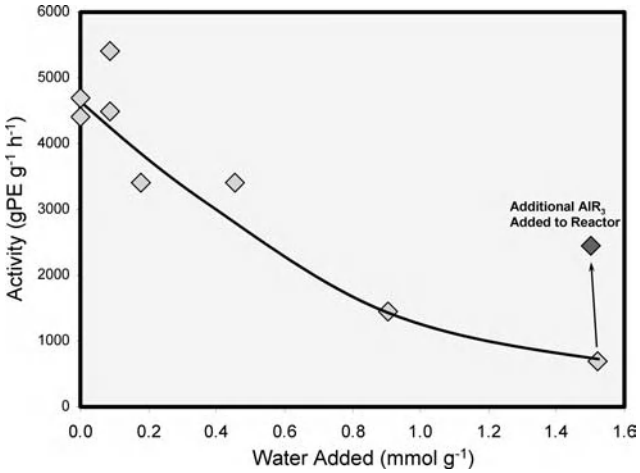

Figure 7.20 Poisoning of sulfated alumina by moisture.

sure to water did lower the activity (see Figure 7.20); almost 2 mmol g^{-1} was required to completely kill the activity. This lack of sensitivity to water might be due in part to the fact that hydration of Lewis sites leads to Brønsted sites, which can still activate metallocene. However, another explanation is indicated by the raised point ("Additional AlR_3 added to reactor") in Figure 7.20. After most of the activity had been lost from exposure to water, the amount of trialkylaluminum cocatalyst added to the reactor was then doubled and a large part of the lost activity was restored. This suggests that the water was also reacting with the cocatalyst in the reactor, depleting its concentration. When more cocatalyst was added, activity was restored. Thus, water – unlike the other adsorbents studied – can be considered as a reversible interaction. As expected, some restoration of activity could also be attributed to the *in-situ* formation of aluminoxane, for some cocatalysts, like $Al(CH_3)_3$ or $Al(i\text{-}Bu)_3$.

7.10
Clay as an Activator

During the mid-1990s it was discovered by the research group at Mitsubishi that certain natural layered minerals, or clays, could be calcined and used to activate metallocenes [25–32]. This activity was attributed to the natural acidity of clays, which were used as early cracking catalysts before the evolution of silica–aluminas and then zeolites for this purpose. If true, this conclusion would be a discontinuity from the present authors' results with many other types of similarly acidic silica–aluminas and unpromoted acidic mixed oxides described in this chapter. In an effort to understand which clay sites are responsible for this apparently anomalous acidic behavior, these materials were studied and the results obtained were com-

pared with solid acids, as described above. As expected, tests with clays revealed that results vary widely depending on the choice of clay, although some were indeed capable, without chemical modification, of activating the test metallocene to achieve quite respectable activities.

The Japanese patents define their activators as a "layered clay mineral", with an emphasis on the layered nature of the support. X-ray diffraction patterns provide strong and sharp lines from this ordered layering. The structure usually consists of sheets of silica and other mixed metal oxides which give rise to negative charges in the interior of the sheet. These negative charges are balanced by metal cations held between the sheets by electrical attraction. Unlike typical ion-exchanged silicas, these negative charges in the interior of the sheet tend to be separated by a significant distance from their balancing positive charges between the layers. Because of the extremely high aspect ratio of the sheets, which can extend for hundreds of nanometers, almost all of the surface area of these layered minerals resides on the faces of these sheets.

Therefore, it seems strange that in some reports the activity of these layered minerals was attributed to acid sites along the edges of the sheets, as the edge surfaces would constitute only a tiny fraction of the total surface area. Such high activity might be expected to require more working surface than the sheet edges provide.

Furthermore, the good activity of some clays is in contrast to results obtained with other simple amorphous mixed oxides, which are well known for high acidity but where significant metallocene activity was not attainable in the absence of an electron-withdrawing anion. Some of the best clays for metallocene activation are silicate materials that are not distinguished for high acidity compared to the many amorphous mixed oxides that were tested in this study, without success.

Likewise, these layered minerals responded quite differently to calcination. Their ability to activate metallocene required little more than drying at 110–150 °C, but this disappeared at slightly higher calcining temperatures. For example, some of the best materials reached peak activity at only 250–300 °C, and most of this was lost by 400 °C or 450 °C, where changes began to occur to the layered structure.

Another apparent contradiction was the observation by Japanese research groups (and subsequently confirmed by the present authors) that the activity can be highly influenced by ion exchanging the natural inter-layer cations with other metal cations [31]. It is difficult to see how such a procedure would affect acid sites on the edges of the sheets; neither does acid-exchanging these materials usually provide the best activity.

Therefore, it would seem that the operative mechanism of metallocene activation occurring on the layered materials is significantly different from the amorphous mixed oxides, and their unusual structure must play a role. One possible explanation is that it is not the acidity that is primarily responsible for the ability of these layered materials to activate metallocenes. Instead, the activity may come through the ability of clay to conduct ion exchange between the metallocene and the inter-layer cations. Unlike surface cations on the amorphous oxides, positive cations spaced between the sheets of clay are unusually isolated because they

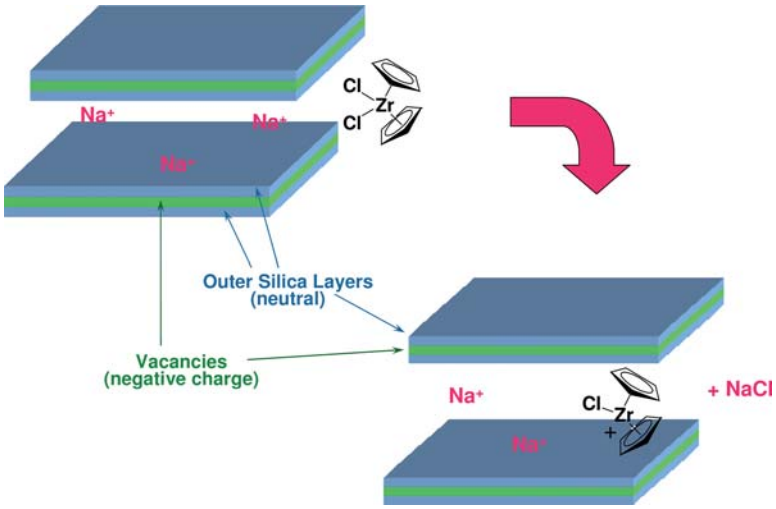

Figure 7.21 Possible mechanism of metallocene activation on clays.

balance negative charges within the *interior* of the sheets. Thus, the cation is uniquely separated from its balancing anion by an "insulating layer" of silica. It is conceivable that metallocenes are activated by this separation, perhaps by ion exchange, as illustrated in Figure 7.21, where sodium chloride is formed. Such ion exchange might then allow the clay anion and the metallocene cation, both of which might be considered as the "soft" ions, to combine, and also the "hard" sodium and chloride ions to associate with each other. The high concentration of interstitial cations, and/or the irreversible nature of the ligand exchange, could help explain the robust activity in comparison to simple acidic, amorphous, mixed oxides.

7.11
Zeolites as Metallocene Activators

Another class of crystalline aluminosilicate materials which *are* distinguished for high acidity are the zeolites. Several of these materials were evaluated with the test metallocene, but in no case was any significant activity observed. This may be attributed, in most cases, to the extremely low pore volume of most zeolites, which rule them out as polymerization catalyst supports. The low pore volume imparts high strength to the zeolite matrix, which then cannot be fractured during polymerization in the usual way needed to generate activity. In some experiments an attempt was made deliberately to break up these zeolites by prolonged, high-energy sonication. However, these samples provided only about 10–20 $g\,g^{-1}\,h^{-1}$ activity. Some higher pore volume, or mesoporous zeolites, do exist which can attain pore diameters up to 100 Å, but even these materials were found not to be

significantly active, consistent with other non-doped, mixed oxides tested in these studies.

7.12 Conclusions

Acidity develops on high surface area solid oxides when they are calcined to remove adsorbed moisture. A diverse assortment of solid acids has been found capable of activating metallocenes, presumably by halide or alkyl abstraction, or at least polarization. Evidence suggests that both Brønsted and Lewis acid sites contribute to this ability, although the role of Brønsted sites is perhaps more complicated. Attempts to maximize the contribution of direct activation by Brønsted sites (Scheme 7.6, route B) usually did not result in high activity. Rather, indirect activation by Brønsted sites (Scheme 7.6, route C) seems likely to contribute more to the activity on many solid acids.

Surprisingly, simple or mixed solid oxides, which are well known for high acidity, were not very effective as metallocene activators unless they were also promoted with an electron-withdrawing anion. This suggests that an element of "superacidity" may indeed be needed, perhaps to fortify or modify the Lewis sites. Likewise, the Brønsted sites may require high acidity when participating indirectly through reaction with alkylaluminum cocatalyst (Scheme 7.6, route C). In comparison, the Lewis sites on MAO are not usually considered to be so strongly acidic.

A major additional enhancement in activity can sometimes be obtained by combining multiple Lewis acidic metal ions and/or promoter anions. Such combinations are thought to further polarize the surface, thereby enhancing acidity.

Even though these solid acids contain an abundance of acidic sites, and can adsorb a large amount of metallocene, the number of activated metallocenes responsible for the observed high activity seems exceedingly low. This suggests that a very few acid sites possess some unusual properties. It may also explain why the unpromoted oxides, which are usually known for their Brønsted acidity, fail to develop high activity. It is currently unclear, however, just what these special site attributes might be. The presence of an alkylaluminum cocatalyst no doubt changes the surface character significantly, and greatly reduces the amount of metallocene adsorbed. Indeed, the cocatalyst is thought to play much wider role than just alkylation, as it may also participate in the site or help to solvate the activated metallocene–anion pair.

In most cases, polymers having a "single-site" MWD were obtained, suggesting that the oxide surface does not participate directly in the coordination sphere of the zirconium. An exception occurred apparently when the Brønsted contribution by route B in Scheme 7.6 was emphasized. These catalysts tended to produce some very high-molecular-weight polymers, either alone, or as a second component. The resemblance of these catalysts to Ballard catalysts was noted, in both cases participation by the oxide surface to the coordination sphere seemed likely.

References

1 A.M. Sukhadia, G.D. Jerdee, K.R. Frey, M.D. Jensen, M.P. McDaniel, Y. Yu, *64th Annual Technical Conference – Society of Plastics Engineers*, 2006, pp. 558–565.

2 K. Tanabe, M. Misono, Y. Ono, H. Hattori, in: B. Delmon, J.T. Yates (Eds.), *New Solid Acids and Bases, Their Catalytic Properties, Studies in Surface Science and Catalysis*, Volume 41, Elsevier, Tokyo, 1989.

3 A. Corma, H. Garcıa, *Chem. Rev*. 2003, *103*, 4307–4365.

4 A. Corma, *Chem. Rev*. 1995, *95*, 559–614.

5 M. Kaminaka, K. Soga, *Makromol. Chem. Rapid Commun*. 1991, *12*, 367–372.

6 K. Soga, M. Kaminaka, *Macromol. Chem. Rapid Commun*. 1992, *13*, 221–224.

7 K. Soga, M. Kaminaka, *Makromol. Chem*. 1993, *194*, 1745–1755.

8 K. Soga, M. Kaminaka, *Macromol. Chem. Phys*. 1994, *195*, 1369–1379.

9 C.A. Emeis, *J. Catal*. 1993, *141*, 347–354.

10 M.P. McDaniel, *J. Phys. Chem*. 1981, *85*, 532.

11 M.P. McDaniel, *J. Catal*. 1982, *76*, 37.

12 J.P. Hogan, U.S. Patent 3,130,188, issued to Phillips Petroleum, April 21, 1964.

13 L.R. Kallenbach, U.S. Patent 3,445,367, assigned to Phillips Petroleum Co., Filed November 1965, issued May, 1969.

14 A.N. Webb, *Ind. Eng. Chem*. 1957, *49*, 261.

15 M.P. McDaniel, *J. Phys. Chem*. 1981, *85*, 537.

16 T.T.P Cheung, K.W. Willcox, M.P. McDaniel, M.M. Johnson, *J. Catal*. 1986, *102*, 10–20.

17 P.J. DesLauriers, M.P. McDaniel, D.C. Rohlfing, R.K. Krishnaswamy, S.J. Secora, E.A. Benham, P.L. Maeger, A.R. Wolfe, A.M. Sukhadia, W.B. Beaulieu, *Polym. Eng. Sci*. 2005, *45*, 1203–1213.

18 M.P. McDaniel, *Adv. Catal*. 1985, *33*, 47–98.

19 M.P. McDaniel, Ethylene polymerization by the Phillips Chromium Catalysts, in: G. Ertl, H. Knozinger, F. Schuth, J. Weitkamp (Eds.), *Handbook of Heterogeneous Catalysis*, 2nd edn, 2007, Chapter 15.1, Wiley-VCH Verlag, Weinheim, Germany.

20 H. Kosslick, H. Landmesser, R. Fricke, *J. Chem. Soc., Faraday Trans*. 1997, *93*, 1849–1854.

21 E.L. Lee, I.E. Wachs, Nature of surface acidic sites in mixed metal oxide catalysts. Abstracts of Papers, 228th ACS National Meeting, Philadelphia, PA, United States, August 22–26, 2004.

22 C.P. Nicholas, H. Ahn, T.J. Marks, *J. Am. Chem. Soc*. 2003, *125*, 4325–4331.

23 M.P. McDaniel, D.C. Rohlfing, E.A. Benham, *Polym. React. Eng*. 2003, *11*, 105–135.

24 J.P. Hogan, *J. Polym. Sci., Part A-1* 1970, *8*, 2637.

25 Y. Suga, Y. Maruyama, E. Isobe, T. Suzuki, F. Shimizu, U.S. Patent 5,308,811, Assigned to Mitsubishi Kasei Corporation, Tokyo, Japan, May 3, 1994.

26 Y. Suga, Y. Uehara, Y. Maruyama, E. Isobe, Y. Ishihama, T. Sagae, U.S. Patent 5,928,982, Assigned to Mitsubishi Chemical Corporation, Tokyo, Japan, July 27, 1999.

27 Y. Suga, Y. Uehara, Y. Maruyama, E. Isobe, Y. Ishihama, T. Sagae, U.S. Patent 5,973,084, Assigned to Mitsubishi Chemical Corporation, Tokyo, Japan, October 26, 1999.

28 T. Sugano, K. Yamamoto, U.S. Patent 5,942,459, Assigned to Mitsubishi Chemical Corporation, Tokyo-To, Japan, August 24, 1999.

29 Y. Suga, E. Isobe, T. Suzuki, K. Fujioka, T. Fujita, Y. Ishihama, T. Sagae, S. Go, Y. Uehara, *MetCon 1999*, "Polymers in Transition", June 9–10, 1999, Houston, Texas.

30 Y. Ishihama, K. Takahashi, T. Sugano, Y. Kashiwagi, Yokohama Research Center, Yumito Uehara, *MetCon 2001*, May 17, 2001, Houston, Texas.

31 T. Takashashi, H. Nakano, U. Hideshi, T. Tayano, T. Sugano, *Polym. Preprints* 2002, *43*, 1259.

32 H. Nakano, T. Tayano, H. Uchino, T. Takahashi, U.S. Patent 6,531,552, assigned to Japan Polychem Corporation (Tokyo, JP), March 11, 2003.

8
Supported Multicomponent Single-Site α-Olefin Polymerization Catalysts

Nic Friederichs, Nourdin Ghalit, and Wei Xu

8.1
Introduction

Soon after the discovery of highly active metallocenes and other single-site catalysts for olefin polymerizations, much research effort – both in academia and in industry – was directed towards the understanding of, and control over, basic catalyst performance such as activity, stereo- and regio-regularity, comonomer incorporation, and attainable molar mass. All of these seminal studies resulted in an enormous and versatile toolbox of countless combinations of transition metals, ligands, activators, scavengers and support materials. Almost as a natural extension of this control over the behavior of discrete catalyst systems, the application of multicomponent systems is increasingly being explored, and might even become one of the most important areas for the commercial application of metallocene and post-metallocene catalysts. The research targets for such multicomponent systems, which may be mixed single-site catalysts or combinations of Ziegler- or Phillips-type catalysts with discrete single-site catalysts, are directed either towards cooperative effects of the different components ("concurrent tandem catalysis") or towards the concurrent effects of the individual components [1]. The majority of these developments can be found in the area of polyethylene, and examples of concurrent tandem catalysis are predominantly developments in the area of *in-situ* comonomer synthesis for the production of branched polyethylene from a single ethylene feedstock. Examples in the area of the concurrent action of individual components are mostly dealing with the *in-situ* formation of polymer alloys, resulting in broadened or multimodal molar mass distribution (MMD) and, in the case of copolymerization, accompanied by a tunable comonomer distribution. Recently, several reviews have dealt with the topic of binary or multicomponent catalysis, strongly focused on homogeneous systems [1, 2], whereas in this chapter the aim is to focus on the application of *supported* multicomponent catalyst systems.

Tailor-Made Polymers. Via Immobilization of Alpha-Olefin Polymerization Catalysts.
Edited by John R. Severn and John C. Chadwick

ISBN: 978-3-527-31782-0

8.2
Supported Catalysts for Concurrent Tandem Oligomerization/Copolymerization

A major part of the commercially produced polyolefins involves copolymers of ethylene and α-olefins such as linear low-density polyethylene (LLDPE), plastomers and elastomers, using comonomers such as propene, 1-butene, 1-hexene, or 1-octene. Apart from propene, production of the higher α-olefins is carried out in dedicated plants. 1-Butene can be prepared via the dimerization of ethylene, whereas the majority of the higher α-olefins is produced via the oligomerization of ethylene using aluminum alkyls-based Ziegler chemistry (the "Aufbau" reaction), nickel-based catalysts ("SHOP" process) or, alternatively, via syngas-based Fisher–Tropsch chemistry. Although recently several selective oligomerization catalysts for the synthesis of 1-hexene and 1-octene have been reported, most of the currently employed processes lead to a mixture of different α-olefins [3]. Hence, the crude product must be distilled, after which the purified α-olefin is transported to the polyolefin plant in order to undergo its fate as comonomer. As polyolefin producers often have to purchase the comonomers from external suppliers, the exploration of catalysts capable of producing the comonomer *in-situ* during the polymerization, based on concurrent tandem catalysis using a single ethylene feedstock (see Scheme 8.1) seems an attractive development.

A classical example was reported by Beach and Kissin using $Ti(O^iPr)_4/AlEt_3$ and $TiCl_4/MgCl_2$, where the $Ti(O^iPr)_4/AlEt_3$ component oligomerizes ethylene to predominately 1-butene, whilst the $TiCl_4/MgCl_2$ component co-incorporates ethylene and the oligomers into short-chain branched polyethylene resins [4]. Also within the class of conventional Phillips-type catalysts, *in-situ* comonomer production has been described by treating Cr-oxide-based Phillips catalysts with an organochromium compound such as $Cr_4[CH_2Si(CH_3)_3]_8$ [5a], or with organic modifiers such as pyrrole derivatives [5b] or triethylboron [5c]. Examples of homogeneous tandem

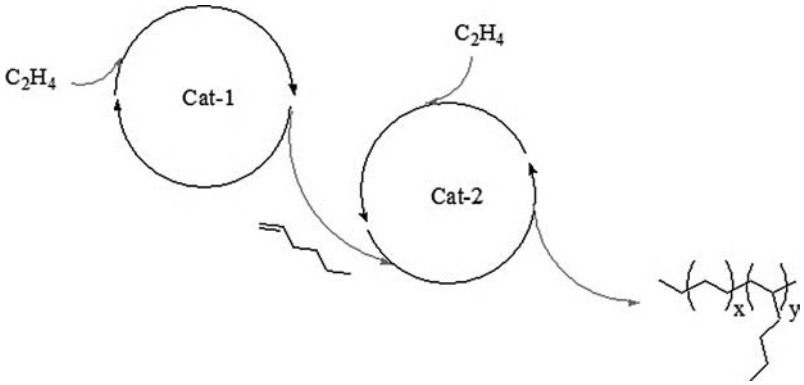

Scheme 8.1 Schematic representation of concurrent tandem catalysis in the case of *in-situ* 1-hexene generation by catalyst 1 (Cat-1) and subsequent copolymerization with ethylene by catalyst 2 (Cat-2).

catalysts yielding short-chain branched polyethylene (PE) resins also include single-component chromic 2-ethylhexanoate activated by poly(isobutylaluminum oxide) [5d] or titanium [6] systems.

The vast majority of reported tandem catalysis for concurrent oligomerization/polymerization deals with unsupported catalyst components, such as the binary systems developed by Bianchini et al. [7], Zhu et al. [8], Fink et al. [9], and the triple-component system reported by Bazan et al. [10]. These unsupported systems are ideally suited to demonstrate the concept of concurrent tandem catalysis, and several reviews have recently been published which cover these developments [1, 2].

At present however, relatively few examples of *supported* concurrent tandem oligomerization/copolymerization systems containing a discrete oligomerization catalyst exist. And indeed, the requirement for (co-) supporting the oligomerization catalyst together with the polymerization catalyst is not that obvious. The heterogenization of single-site polymerization catalysts is predominantly driven by the need for good powder morphology in particle-forming polymerization processes, which is not obvious for an *in-situ*-applied oligomerization catalyst. In contrast, separate feeding of the oligomerization and polymerization catalysts would be advantageous with respect to the flexibility of adjusting the comonomer production and hence concentration in the reactor in order to control polymer crystallinity. However, co-supporting both types of catalysts on the other hand might be able to deliver interesting behavior due to so-called "proximity effects", while bimolecular deactivation pathways can also be suppressed through immobilization.

An early example has been provided by Fink and coworkers, who obtained branched PE from ethylene feedstock only, by combining the SHOP-type nickel catalyst, $Ph_2PCH_2CH(Ph)ONi(Ph).P(Ph)_3$, for the *in-situ* ethylene oligomerization with an alkylaluminum-free heterogeneous Ziegler catalyst based on MgH_2/α-$TiCl_3/Cp_2TiCl_2$ [9]. The unusual Ziegler catalyst was required since the SHOP-type catalyst was deactivated by alkylaluminum compounds. One drawback of the applied Ziegler catalyst was that, besides copolymerization also isomerization of the *in-situ*-produced oligomers took place. Additionally, Ostoja-Starzewski et al. combined for example the nickel ylide compound $NiPh(Ph_2PCHCPhO)(Ph_3P)$ with a chromium on silica catalyst to obtain branched PE [11].

Alternatively, Okuda et al. reported a tandem catalyst system in which the oligomerization catalyst, pyridyl-2,6-diisopropylphenylimine nickel dibromide, is left in the homogeneous phase, whilst a methylaluminoxane (MAO) preactivated constrained geometry copolymerization catalyst is immobilized on a pyridylethylsilane-modified silica support [12]. The individual nickel catalyst, activated by modified MAO (MMAO), is able to produce methyl branched 1- and 2-olefins with an average molar mass of 447 g mol^{-1} and a 2-olefin oligomer to 1-olefin oligomer molar ratio of 6.9. Analysis of the PE produced with the Ni/Ti tandem catalyst based on a *tert-butyl*amido constrained geometry copolymerization catalyst revealed the incorporation of the 1-olefin oligomer into the PE backbone. However, an analysis of the polymer resins made via the Ni/Ti tandem catalyst based on a *methyl*amido constrained geometry copolymerization catalyst unexpectedly indi-

cated that only methyl-branches were present in the copolymer, which led the group to propose an elaborate multicomponent mechanism to explain this unexpected behavior.

Combinations using bis(imino)pyridyl iron oligomerization catalysts and a plurality of other polymerization catalysts, including Ziegler systems, have also been reported [13] For example, the research group at DuPont reported the co-impregnation of a bis(imino)pyridyl iron catalyst capable of oligomerizing ethylene together with the polymerization catalyst $Me_2C(Cp)(Flu)ZrCl_2$ onto MAO-modified silica to produce PEs with branches of up to about 30 ethylene units [13a–c].

Bis(imino)pyridyl iron oligomerization catalysts have also been utilized in the homogeneous phase in combination with supported catalysts based on *rac*-Et(1-Ind)$_2ZrCl_2$/MAO/montmorillonite to form an *in-situ* copolymerization catalyst. Increased Fe/Zr ratios led to an increase in chain branching, accompanied by an increase in the residual unreacted olefinic oligomer in the final product [14a]. The same group recently published data on the combination of a bis(imino)pyridyl iron oligomerization catalyst with a $TiCl_4/MgCl_2$ Ziegler catalyst [14b]. The branches in the obtained PE were predominantly ethyl and butyl, indicating 1-butene and 1-hexene incorporation, respectively. Branches longer then hexyl were also shown to be present.

Casagrande et al. recently reported on the tandem action of a tris-pyrazolylborate nickel oligomerization catalyst [$Tp^{Ms}NiCl$, Tp^{Ms} = HB(3-mesityl-pyrazolyl)$_3^-$] and Cp_2ZrCl_2, co-supported on MAO/SiO_2 [15]. The melting point of the polyethylene was decreased upon increasing the amount of nickel catalysts, indicative of copolymerization. This group also demonstrated the possibility for *in-situ* co-supporting of the precatalysts on MAO/SiO_2, which could be interesting from the viewpoint of flexibility in a continuous polymerization process.

Several considerations need to be taken into account when developing such supported tandem systems for concurrent oligomerization/polymerization. First – and perhaps most obviously – the oligomerization and polymerization catalyst should be compatible, at least to some extent. Whereas this requirement seems very straightforward, it is not uncommon that for example Ziegler systems and single-site catalyst display a combined catalyst activity that is well below the simple sum of the activities observed when using the individual components. Second, the oligomerization catalyst should not be susceptible to hydrogenolysis in case hydrogen is used as a chain-transfer agent in the olefin polymerization. Hydrogenolysis of the transition metal–carbon bond results in the corresponding transition metal hydride and a saturated hydrocarbon. In case the oligomerization catalyst is also susceptible to hydrogenolysis, the quite expensive production of alkanes from ethylene feedstock can be envisaged. Additionally, it is not uncommon – especially in ethylene polymerizations – that hydrogen causes a significant decrease in the activity of the polymerization catalyst, in particular when a single-site catalyst is used. Third, the selectivity of the oligomerization catalyst should be high, and its performance should be robust. For example, in case a substantial fraction of higher α-olefins or internal olefins is produced, these less-reactive or inert products might accumulate in a continuous commercial process. Also, a possible excessive isom-

erization of olefinic oligomers upon adding additional catalyst components should be avoided. A final point of attention deals with the heat of reaction per mass of copolymer. Due to the highly exothermic polymerization, heat removal in polyolefin plants is a crucial step. The additional heat of oligomerization due to the *in-situ* oligomerization, which traditionally is liberated at the external comonomer production plant, must now be removed during the concurrent oligomerization/copolymerization. This means that per mass unit of produced branched PE, more heat will be liberated in the polymerization reactor in the case of *in-situ* oligomerization compared to the use of off-line produced comonomer. Of course, this issue will become more relevant for copolymers containing high amounts of comonomer, and as long as the plant bottleneck is not due to heat removal, this is not an issue.

All the above-described requirements and considerations create challenging targets for the chemists and engineers with respect to the development of viable *in-situ* oligomerization catalysts and might, to a large extent, explain why this seemingly elegant technology is not yet applied commercially.

8.3 Concurrent Tandem Catalysis for Increased Levels of Long-Chain Branching (LCB)

Single-site catalysts typically produce linear, narrow MMD PEs, often accompanied by improved mechanical properties compared to conventional Ziegler products. However, the processing of these polymers is generally considered to be more difficult, especially when compared to grades with broader MMD or LCB-containing low-density polyethylene (LDPE). Additionally, as LDPE is produced using radical initiators at very high pressures and temperatures with the accompanying mechanical requirements, it is not surprising that there always has been interest to produce "LDPE-like" materials in low-pressure PE processes, and one approach is to use polymerization catalysts that are able to generate LCB.

The influence of LCB on polymer melt behavior has long been recognized [16]. At comparable molar mass, the zero shear viscosity of LCB-containing polymers is higher compared to their linear counterparts, and both shear sensitivity and melt stability can be improved significantly. An important limitation in the usefulness of literature data is the determination of LCB, both qualitatively and especially quantitatively. In order for a long chain branch to display a significant impact on rheological behavior, its length should be at least twice the critical molar mass for entanglement which, in the case of PE, corresponds to branch lengths well above 100 carbon atoms [16b]. Already at less than one LCB per 10^4 to 10^5 carbon atoms there is a significant rheological effect [16c], and several methods have been described in order to determine the amount of LCB using for example ^{13}C-NMR, size-exclusion chromatography (SEC) using viscosity detectors, or multi-angle laser light scattering and rheological techniques [17]. However, there is still no generally accepted analytical procedure available, and the reported numbers for LCB content should be treated with great care.

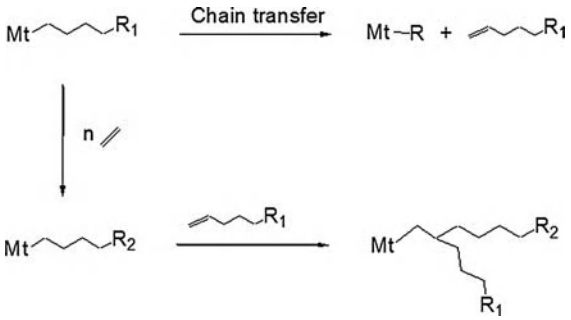

Scheme 8.2 Schematic representation for the postulated mechanism for *in-situ* long-chain branching formation, where Mt is the active transition metal and R, R_1 and R_2 are alkyl groups.

The generally accepted mechanism behind the catalytic formation of LCB is that vinyl-terminated polymer chains, formed after the termination of chain growth via β-hydrogen abstraction, behave as long-chain α-olefinic comonomers or so-called *macromonomers* or *macromers*. The incorporation of such a macromer back into another growing chain leads to the formation of LCB, as depicted in Scheme 8.2.

Based on this hypothesis, it can be reasoned that a LCB-generating catalyst should have a high ability to incorporate long-chain α-olefins, and that the termination of chain growth should preferably result in vinyl-terminated polymer chains. In order to increase the content of LCB in high-molar-mass polymers, a dilemma can be envisaged for single-component systems because, at a given polymer concentration on a mass basis, a high molar concentration of vinyl-terminated macromers will be reached in case of low-molar-mass polymers. Alternatively, whilst a low monomer to macromer ratio will favor macromer incorporation, a low monomer concentration is not beneficial for catalyst yield, and in some cases can even limit the attainable molar mass. One way to overcome this is the use of multicomponent systems, aiming at concurrent tandem catalysis by making use of a dual system consisting of a macromer-producing catalyst and a macromer-incorporating catalyst in order to obtain a better balance between LCB content, overall molar mass, and catalyst yield. The reaction scheme is very similar to that depicted in Scheme 8.1, except that instead of hexene-1 now a macromer is produced. This principle of dual catalysts also has been used by Soares et al. to enhance LCB levels in PEs derived from a solution process [18a–e].

Although the formation of LCB via *un*supported single-site catalysts has long been known from the studies of research groups at Mitsui [18f] and especially Dow [18g], the investigators at Union Carbide (Karol et al.) were among the first to report that significant levels of LCB are also present in certain gas-phase *m*LLDPEs. As the vinyl moiety of a macromer must be reincorporated in order to generate chain branching, it may be argued intuitively that LCB formation would be favored in solution-based processes due to the enhanced mobility of the

dissolved polymer chains. However, according to Karol and colleagues, the formation of LCB in gas-phase polymerization is enhanced because the reactive vinyl moiety of the terminated polymer chains remains in the vicinity of the catalytic site due to the restricted mobility of the crystallized polymer chains, thereby creating a high local concentration near the active center [19].

Since that time, many patent applications have appeared dealing with LCB- containing PE using single-component catalysts precursors; multicomponent systems have also been reported capable of enhancing the amount of LCB. For example, a gas-phase process for producing PE containing LCB is described using the *in-situ* heterogenization of a bridged metallocenes/MAO mixture [19b]. Possible combinations of catalysts include the bridged metallocenes (as shown in Figure 8.1). Although both catalysts individually generate low levels of LCB, enhanced branching can be achieved by using these metallocenes as a binary mixture. Catalyst A produces lower molar mass vinyl-terminated polymer chains, serving to increase the concentration of the macromers to be incorporated by metallocene B (Table 8.1).

The difference in molar mass as produced by these catalysts is clearly illustrated by the melt flow rates (which are inversely proportional to the molar mass) produced by catalyst A and B alone (see examples 5 and 6 in Table 8.1). Using such a binary catalyst mixture, especially with these different molar masses, will cause broadening of the MMD in case the macromer is not fully reincorporated.

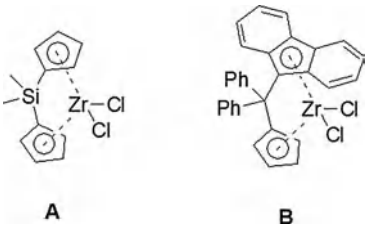

Figure 8.1 Metallocene components for dual-site catalyst for enhanced long-chain branching. (Some examples from this patent application are shown in Table 8.1.)

Table 8.1 Selected examples of long-chain branching containing linear low-density polyethylenes (LLDPEs) [19b].

Example no.	*Cat A:cat B*	*Melt flow rate ($°C\,min^{-1}$)*	*MMD*	*Density ($kg\,m^{-3}$)*	*LCB/1000C*
5	1:0	400	5.1	945	0.2
6	0:1	0.6[a]	3.5	928	0.7
2	3:1	0.6	12	940	0.9
3	5:1	4.1	10	940	2.0

a Hydrogen added as melt index regulator.
MMD, molar mass distribution; LCB, long-chain branching.

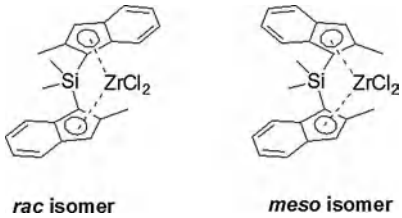

Figure 8.2 *rac/meso* combination as a multicomponent catalyst system.

Another binary catalyst system deals with a mixture of the *rac* and *meso* isomers of dimethylsilylbis(2-methylindenyl)zirconium dichloride [20] (Figure 8.2). With this binary system, LCB-containing LLDPE with a MMD >3 was obtained from a gas-phase reactor.

Killian and colleagues co-impregnated a nickel-based catalyst and a bis-indenyl zirconocene copolymerization catalyst onto MAO-modified silica with the aim of obtaining long-chain branched PE [21].

A binary catalyst system containing a Ziegler catalyst and an unsubstituted metallocene compound has also been described for obtaining LCB-containing bimodal PE [22]. The inventors claim the presence of LCB based on the measured activation energy of flow of 38 kJ mol^{-1}, which is somewhat higher than the reported value of 26–35 kJ mol^{-1} for linear PEs, but well below the value of ≥55 kJ mol^{-1} for LDPE [17h,i].

8.4 Supported Multicomponent Catalysts for Bimodal/Multimodal MMD Polyethylene

Currently, bimodal PE is one of the fastest growing high-volume polyolefins. For example, bimodal high-density PE (bimodal HDPE) typically constitutes a fraction of a relatively high molar mass (HMM) PE which contains a few mass percent of comonomer, and a fraction of relatively low molar mass (LMM) ethylene homopolymer in a single resin. The MMD is rather broad and displays either multiple discrete components, or at least a substantial broadening. The HMM part of the resin results in enhanced tensile strength, impact strength, puncture resistance, environmental stress crack resistance and toughness, whereas the LMM serves to improve the processability and is responsible for the stiffness of the material. So, by combining a HMM PE with a LMM PE, excellent physical properties and good processability can be achieved. Such bimodal resins find application in pipes, blow-molding, and thin-film applications. Similarly, bimodal LLDPE can be produced in order to tune polymer properties.

The traditional process for the production of bimodal resins is a cascade process, using a conventional Ziegler catalyst [23], and in most cases just one catalyst formulation is needed for the entire product range. In general, in the first reactor a high hydrogen to ethylene ratio is used, resulting in a relatively LMM, highly crystalline homopolymer. After an intermediate hydrogen removal step, the still

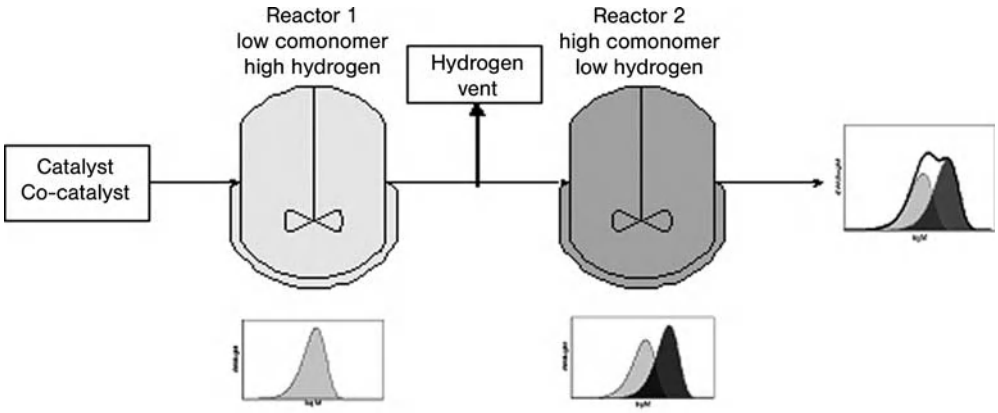

Figure 8.3 Schematic diagram of a cascade continuous stirred-tank reactor process for bimodal polyethylene.

active catalyst, embedded in the homopolymer, is transferred to a second reactor, where a much lower hydrogen to ethylene ratio and a comonomer such as butene-1 or hexene-1 are applied. The overall result is that virtually every powder granule is an intimate blend of polymers, or polymer alloy, and displays a bimodal MMD having the comonomer placed in the HMM part of the polymer. A schematic representation of a typical cascade process is depicted in Figure 8.3. Several cascade processes have been developed, including for example multiple continuous stirred-tank reactors (CSTRs), slurry-loop reactors, gas-phase reactors or hybrid polymerization technologies [24].

The development of multicomponent catalysts aims at the production of such bimodal polymers from a single reactor, preferably gas-phase as this is one of the most cost-effective processes today. The main driver for this development is the decrease in investment costs for a single gas-phase reactor compared to a staged process, especially compared to a diluent-based cascade process. Also, operational costs may be lower because multiple reactors are considered to be more complex as they use different settings for the reactors, require an intermediate flash step, and need recycling of the diluents [25].

It is generally accepted that the HMM and LMM polymer should be intimately mixed to obtain good product properties. When aiming at multicomponent concurrent catalysis, such efficient mixing can be obtained via a solution-based polymerization process, or by supporting the different catalysts on a single carrier. Most application developments involve the latter strategy, as gas-phase and slurry process are commercially the most frequently applied and have less technological restrictions with respect to processing very HMM polymers. In addition, multicomponent mixtures can be used for broadening of the MMD of single-site catalyst–based resins instead of targeting at discrete bimodal distributions [26].

Different olefin polymerization catalysts can be combined in order to obtain multicomponent catalyst systems. Although such catalysts based solely on traditional Ziegler- or Phillips-type catalysts have long been reported in the patent lit-

Table 8.2 Mixed catalyst combinations for broadened or bimodal polyethylene.

Catalyst combinations	*Z/N or Cr + SSC*	*SSC + SSC*
Descriptions	Z/N produces HMM and SSC produces LMM	One SSC produces HMM with high comonomer incorporation; the other produces LMM with low comonomer incorporation
Includes	Z/N-metallocene, Z/N-LTM, Z/N-chromocene, Cr-metallocene, Cr-LTM, Cr-chromocene,	Metallocene-metallocene, metallocene-LTM, metallocene-chromocene

Cr: chromium-based catalysts including Cr oxides and silylchromates; LTM: late transition metal-based catalysts; Metallocene: transition metal complex with at least one cyclopentadienyl type ligand; SSC: single-site catalysts (metallocene and LTM are explicitly mentioned due to their abundance); Z/N: Ziegler–Natta-type catalysts based on Group III–VB metals.

erature [27], these systems are not ideal as it is difficult to exclude the comonomer from being incorporated into the LMM part of the MMD, while at the same time being incorporated in the HMM part. In order to tackle this last shortcoming, many polyolefin producers are investigating the use of mixed catalysts with at least one single-site catalyst component as this allows a better tailoring of the catalyst behavior. Frequently encountered combinations are listed in Table 8.2, and are discussed in the following section.

8.4.1
Mixed Ziegler or Phillips and Single-Site Polymerization Catalysts

Hybrid catalysts derived from a heterogeneous Ziegler- or Phillips-type catalyst and a single-site catalyst component represent some of the most interesting examples of binary catalysis. Indeed, they have demonstrated that the interface of what some consider to be rival technologies can lead to considerable benefits with regard to the final polymer product. In general, the Ziegler- or Phillips-type catalyst components are applied to produce the HMM fraction that provides the greater toughness performance of the polymer, whereas the single-site component gives the LMM, which provides the lubrication needed to process the resin. As early as 1986, Welborn reported the use of a supported binary catalyst containing a metallocene such as Cp_2ZrCl_2 and a Ziegler component such as $TiCl_4$ or $(^nBuO)_2TiCl_2$, co-impregnated on silica to obtain a bimodal PE from a single reactor [28]. One advantage of this catalyst concept is that the design of a catalyst component which produces a LMM ethylene homopolymer in the presence of comonomer and small amounts of hydrogen is likely to be more successful based on a discrete component compared to the still highly empirical modification of Ziegler catalysts.

The most frequently used synthetic sequence is to support the Ziegler component on silica, followed by the metallocene components. For example, a Ziegler catalyst component is synthesized by contacting $MgBu_2$/butanol-modified silica with $TiCl_4$. The solid catalyst is subsequently impregnated with a solution of MAO/metallocene, often using the "incipient wetness" technique [29]. The resulting catalysts are highly active and produce resins with broad or bimodal MMDs. Several modifications on this general procedure have been reported; for example, it has been suggested that the metallocene component might be supported before the Ziegler catalyst component [30], and instead of using the metallocene complex, a cyclopentadienyl-based ligand such as indene was added to a Zr- or Hf-containing Ziegler component to form a hybrid catalyst [31].

Usually, the metallocene component is activated by MAO which is introduced in the solid support material. Although MAO (or the residual trimethylaluminum in it) also activates the Ziegler component to some extent, it is mostly an external aluminumalkyl, such as trimethylaluminum (TMA), triethylaluminum (TEAL) or triisobutylaluminum (TiBA), that is used as a cocatalyst during polymerization to optimize catalyst yield. An interesting concept was developed at Mobil and subsequently Exxon-Mobil, which involved non-supported MAO or *in-situ*-generated MAO by reacting TMA with water in the reactor to activate the metallocene catalyst [22, 32]. By altering the cocatalyst composition, the relative contribution of the HMM and LMM catalyst components can be adjusted without reformulating the multicomponent catalyst.

A variety of single-site catalysts has been used in such bimetallic systems. By far the most popular and abundant are the well-known metallocenes, including for example $(^nBuCp)_2ZrCl_2$, ethylene-bis[1-indenyl]zirconium dichloride [33], and also unsubstituted metallocenes [32b]. Shamshoum et al. found that the addition of a titanocene [34a] or even cyclopentadienyl ligands at a Ti/Cp molar ratio of 2 [34b] to a Ziegler catalyst could be used to broaden the MMD of the resins and improve the catalyst's hydrogen response. In addition, the use of samarocenes [35] and self-immobilizing single-site catalysts [36] is reported to be suitable in multicomponent formulations. Recently, metallocene catalysts having fluoride instead of the commonly encountered chloride as σ ligands were reported to result in increased efficiency of the multicomponent system [37].

Modification of the Ziegler component is also frequently encountered. For example, the butanol can be replaced by an aldehyde [38] or other carbonyl-containing groups in order to increase the MMD of the HMM component. When the Bu_2Mg/1-butanol/$TiCl_4$ system was precontacted with aluminum alkyls (in particular with aluminumalkylchlorides), the resulting bimetallic catalyst displayed higher productivity [39].

The calcination temperature of the initial silica support was also found to be of great importance in terms of catalyst activity, with a calcination temperature of 600 to 800 °C leading to the most active systems [40]. Besides silica-supported hybrid catalyst systems, several reports on $MgCl_2$-supported systems have also been published. For example, Maozhu et al. prepared such a supported system by dissolving $MgCl_2$ in a solution consisting of ethanol, tributyl phosphate and

epichlorohydrin, followed by the addition of $TiCl_4$ to obtain, after work-up, a solid that is subsequently impregnated with a mixture of MAO and a metallocene [41]. Alternatively, a method was developed for immobilizing a metallocene and a Ziegler component, using polymeric supports [42].

Combinations of Ziegler catalysts with phosphinimide-containing titanium compounds [43] or bis(imino)pyridyl-based iron catalyst [44] have also been described. The advantage of the iron-based catalysts is their frequently encountered reluctance against the incorporation of higher α-olefins, which makes them excellent candidates for a multicomponent formulation.

The so-called Phillips-type catalysts include a silica-supported chromium oxide catalyst and a silylchromate-on-silica catalyst. It is well known that ethylene polymers having a broad MMD can be obtained using these catalysts [45a,b], especially when chromium oxide is present on aluminophosphate-based supports [45c] or titanated silica-aluminophosphate supports [45d]. A dual-site polymerization catalyst system containing a chromium oxide catalyst and a chromocene compound has been reported to give polymers with a bimodal or broad MMD [46]. Follestad et al. reported a dual-site catalyst for PE based on chromium oxide and a metallocene catalyst [47]. A multicomponent catalytic system containing a metallocene, a discrete ionic activator such as $(C_6H_5)_3C^+B(C_6H_5)_4^-$, and a Phillips-type chromium compound has also been reported by Lhost and Zandona [48].

As mentioned above, optimal product performance requires the comonomer to be incorporated into the HMM part of the bimodal PE, but this is difficult to achieve with conventional Ziegler or Phillips catalysts in a single reactor. The combination of these conventional catalysts with at least one single-site catalyst might bring about this desired characteristic, and might be able to mimic products from a cascade process. However, in case the single-site component is used to produce the LMM part, the distribution of the comonomer in the HMM part of the product still reflects the typical distribution for Ziegler- or Phillips-type products, namely a decrease in comonomer content upon increasing molar mass (Figure 8.4, left).

Alternatively, the application of a well-considered cocktail of single-site catalysts should, in principle, be able to achieve a truly "reversed" comonomer distribution (Figure 8.4, right), which could give such systems an advantage in product properties compared to conventional Ziegler cascade products.

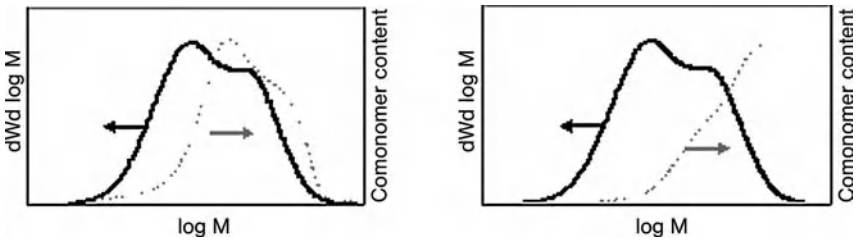

Figure 8.4 Schematic representations of a bimodal polyethylene having (left) a typical Ziegler comonomer distribution, or (right) a "reversed" comonomer distribution.

8.4.2 Mixed Single-Site Catalysts

As the number of discrete catalyst components is already unimaginably huge and still increasing, the well of possible combinations of different components is seemingly inexhaustible. Hence, many reports involving the immobilization of two or more different single-site catalysts on the same support have been disclosed, and still keep emerging. By carefully choosing different single-site catalyst components and the accompanying process conditions, such a multicomponent catalyst should, in principle, be capable of producing any desired polymer composition such as breadth of the MMD and absence of LMM waxes, and also provide a means to control the comonomer distribution. Quite fortunately for the popular concept of "rational polymer design", the choice of different compounds in a multicomponent formulation can often be based on the performance of the individual catalysts, although adverse or synergistic effects are not unprecedented. So, based on an initial screening of the single components and determining for example their performance in copolymerization and their hydrogen response, a preselection of candidates for a multicomponent formulation can be performed. The most commonly encountered design principles are that the components must produce different molar mass polymers, and also have different copolymerization abilities, of course at desirable catalyst activity.

As a result, reports dealing with the immobilization of different single-site catalyst components have spread across the entire spectrum of transition metals and ligands, including for example combinations of metallocenes and constrained geometry-type catalysts, hafnium- and zirconium-based metallocenes, zirconocenes bearing modified ligands for producing either HMM or LMM polymers, combining bridged and unbridged metallocenes. Additionally, discrete precatalysts based on iron or nickel have also been included in the multicomponent formulations [44, 49–58].

For example, Soares et al. reported the synthesis of intimate blends of PE resins in which the MMD and chemical composition could be controlled by the combination of $Et(Ind)_2ZrCl_2/Cp_2HfCl_2$ or $Et(Ind)_2ZrCl_2/Me_2SiCp^*N(^tBu)TiCl_2$ supported on MAO-modified silica [59a]. In the latter system, the ability of the precatalyst to co-incorporate the comonomer led to resins with varying chemical compositions. Polyethylene resins produced with the supported $Et(Ind)_2ZrCl_2/Cp_2HfCl_2$ system possessed monomodal or bimodal molar mass distributions, with HMM or LMM shoulders, depending upon polymerization variables such as hydrogen concentration. The hafnocene component is more responsive to hydrogen than $Et(Ind)_2ZrCl_2$, and polymerization at high hydrogen concentrations therefore yielded a polymer resin possessing a LMM, hafnocene-polymerized fraction, and a HMM, $Et(Ind)_2ZrCl_2$-polymerized fraction, whilst the reverse is observed in the absence of hydrogen [59b].

Dos Santos et al. prepared a series of supported catalysts by combining $(^nBuCp)_2ZrCl_2$ and Cp_2ZrCl_2 sequentially grafted onto silica in different ratios (1 : 1 and 1 : 3) and immobilization order. All of these systems were shown to be active

in ethylene homopolymerization having methylaluminoxane as the cocatalyst. Catalyst activity was shown to depend on the metallocene nature, but not on the addition order. The highest activity was achieved with a $Cp_2ZrCl_2/(^nBuCp)_2ZrCl_2$ (1 : 3) catalyst system (ca. 4.26 kg PE $mmol^{-1}$ Zr h^{-1}). In spite of bearing two catalyst centers, no clear bimodality was observed in the resulting polymers [60].

The research team at ExxonMobil reported a multi-metallocene (three or more) catalyst system, comprising metallocenes having at least two substituents on each Cp ring [61], including isomeric mixtures of $(MeEtCp)_2ZrCl_2$, $(Me^nPrCp)_2ZrCl_2$ or $(Me^nBuCp)_2ZrCl_2$. The resulting multicomponent systems were able to produce PEs with broadened MMDs and narrow composition distributions, and displaying properties resembling long-chain branched LDPE, including its renowned processability.

Besides targeting at broadened MMD, control over the compositional distribution in comonomer-containing PEs is also frequently reported for mixed metallocenes. A multicomponent catalyst system described as the combination of "a poor comonomer incorporating metallocene catalyst and a good comonomer incorporating metallocene catalyst" has been used to produce polymers with bimodal composition distributions [62]. Using $(Ind)_2ZrCl_2$ as a reference point, several examples of good and poor comonomer incorporators have been revealed. Poor comonomer incorporators are, for example, siloxane-bridged bis-1-indenyl zirconocenes which, due to the relatively long bridging moiety, are sterically crowded at the active center, resulting in poor incorporation of longer chain α-olefins, similar to an earlier report by Herrmann, Rohrmann and colleagues for $-(CH_3)_2SiCH_2CH_2Si(CH_3)_2-$ bridged bis-1-indenyl zirconocenes [63]. Good comonomer incorporators include sterically more open systems such as the Me_2Si-bridged bis-1-indenyl zirconocenes. A binary catalyst system based on a comonomer-selective metallocene using a 2-indenyl bridged metallocene and another bridged metallocene, has been reported to produce multi-modal polymers [64].

In addition to metallocenes, post-metallocenes in combination with other types of olefin polymerization catalysts can also be used to produce bimodal PEs (using the same principle as described above), and several such systems have been reported. For example, mixed transition metal olefin polymerization catalyst systems comprising late transition metal catalyst systems, for example bidentate diimine nickel or tridentate bis(imino)pyridyl iron compounds, have been reported [44]. A combined supported catalyst system with one metallocene or constrained geometry catalyst and one non-metallocene bidentate transition metal compound or tridentate transition metal compound (e.g., a bis(imino)pyridyl iron catalyst) with a spray-dried silica/clay agglomerate support-activator has been used to produce polymers having a broad MMD with good polymer morphology [65]. A mixed catalyst system consisting of a hafnocene-based catalyst component which is suitable for producing the HMM fraction of the polyolefin and a bis(imino)pyridyl iron complex which is suitable for producing the LMM fraction of the polyolefin with little comonomer incorporation, has been outlined by Razavi [66].

Titanium compounds bearing phosphinimine ligands have also been described as useful for the production of broad MMD polymers. For example,

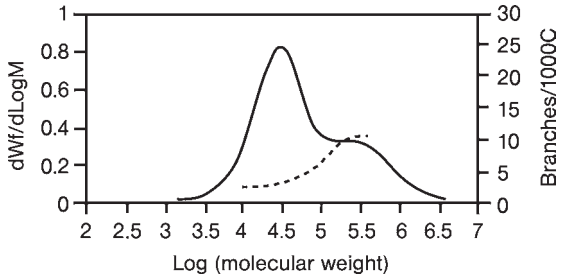

Figure 8.5 Gel-permeation chromatography-Fourier transform infrared trace of a ethylene–hexene polymer, showing a reversed comonomer content distribution.

(Ind)(^{t}BuP=N)$TiCl_2$ has been combined with (Cp)(^{t}BuP=N)$TiCl_2$, (^{n}BuCp)$_2ZrCl_2$ or $(CH_3)_2Si$(Cp*)(N^{t}Bu)$TiCl_2$ on MAO/SiO_2 in order to obtain multicomponent catalysts for PE, and it was reported that the resulting catalyst systems have desirable hydrogen responses [43]. The research groups at Innovene and Nova Chemicals each reported the preparation of copolymers having a reverse comonomer distribution in a single reactor by using a polymerization catalyst system comprising a physical mixture of supported single-site catalysts, containing a constrained geometry-type titanium catalyst and a phosphinimide-Cp titanium-based catalyst (Figure 8.5) [67]. Additionally, discrete transition metal compounds bearing nitrogen chelates [68] or bisphenolates [69] have been combined with other single-site catalysts to produce resins with a broadened MMD.

The above examples describing the use of a binary metallocene system to produce reactor-blended PE resins have all been activated by MAO or perfluoroborane or borate-based activators. Oshima and Takaoki have recently described the use of a novel support/activator to immobilize binary metallocene systems. The support/activator was initially synthesized by contacting $ZnEt_2$ with a half-equivalent of C_6F_5OH, followed after some time by one equivalent of H_2O in THF. The product from the reaction was then contacted with silica to form a support/activator which was capable of effectively activating a tri-isobutyl-aluminum (TIBA)–contacted binary solution of *rac*-Et(Ind)$_2HfCl_2$ and (BuCp)$_2ZrCl_2$ [70]. Furthermore, it has been reported that, by using a mixture of different cocatalysts, a single precatalyst can be used to produce resins with a broader MMD. When a single metallocene catalyst was activated with a mixture of two cocatalysts, as for example MAO and $B(C_6F_5)_3$, the resulting system gave rise to polyolefins having broad, bimodal or multimodal MMDs [71]. Silica gel with a different pore radius is reported to be useful as a support to provide a polyolefin having a broad or bimodal MMD [72]. Additionally, binary systems that consist of a combination of metallocenes supported on separate carriers [73] or with one component unsupported have been reported [74].

An alternative and interesting approach towards a catalyst system containing multiple active sites is the use of heterobinuclear catalysts. A number of reports have appeared dealing with unsupported binuclear systems [75], often with intrigu-

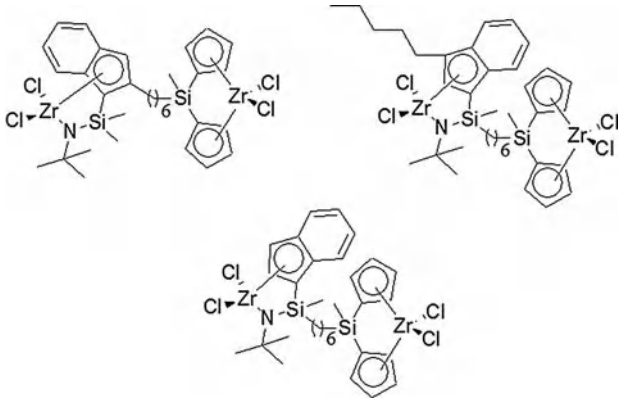

Figure 8.6 Heterobinuclear catalysts containing constrained geometry and metallocene moieties [76a]. Details of several similar multinuclear metallocene catalyst systems containing at least two different central metal atoms have been published [77].

ing results due to so-called "proximity effects", but only a few are available on analogous supported systems. Alt and coworkers used heterobinuclear ansa zirconocene complexes containing a half-sandwich and a metallocene moiety (Figure 8.6) [76]. After activation with MAO, these catalysts produce PEs with bimodal MMDs in homogeneous polymerizations, as well as in heterogeneous polymerizations using silica support. The binuclear catalyst produced a different resin as compared to a 1:1 mixture of the corresponding mononuclear catalysts, which was suggested by the authors to have resulted from the enforced separation of the active centers in the binuclear systems.

8.4.3
Challenges in Operating Dual Catalysts for Bimodal Polyethylene in a Single Reactor

Although the prospect of using a dual-site catalyst in single reactor technology is very attractive, the commercial application on an industrial scale remains a clear challenge. Such challenges are related to the sophisticated composition of bimodal products, which is illustrated graphically in Figure 8.7.

Typical important formulation parameters for a bimodal product include the overall molar mass, comonomer content, breadth of the individual components and the overall MMD, and especially the split [which is defined as the mass fraction of the LMM part in the total product, e.g., m1/(m1 + m2)]. In a cascade process, the split can be elegantly controlled for example via adjustment of the partial ethylene pressure in the individual reactors, thereby controlling catalyst productivity per stage which subsequently translates into a precise control over bimodality. This flexibility of a cascade process allows one to use a single Ziegler catalyst formulation for producing several bimodal grades which differ in the above-described product parameters, aiming at specific end-use applications.

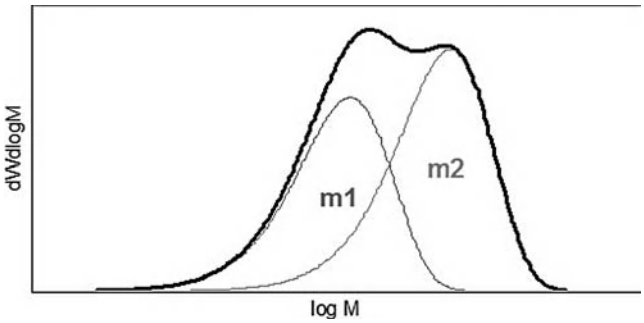

Figure 8.7 A schematic size-exclusion chromatography trace of a bimodal polymer. See text for details.

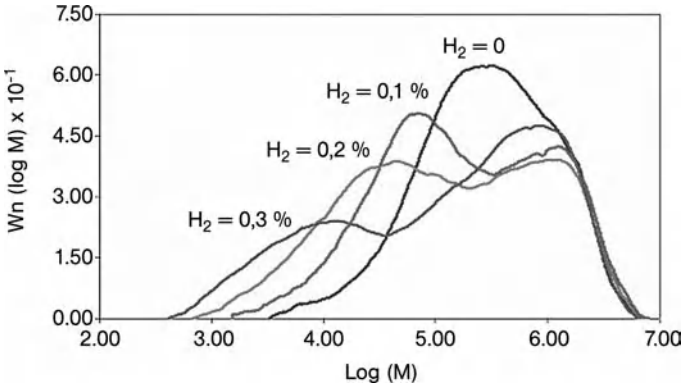

Figure 8.8 Size-exclusion chromatography traces of Ziegler/metallocene combinations using different levels of hydrogen percentage in the ethylene feed to the headspace of a gas/liquid semi-batch reactor.

In a multicomponent catalyst formulation however, the base split is determined via the productivity, and hence loading, of the individual components. So, the formulation of a multicomponent catalyst must be carefully tuned to produce the products with the desired molar mass, comonomer incorporation, split and breadth of the MMD. However, in case the catalyst components have very different kinetics, it can be envisaged that the split is dependent on the polymerization conditions, such as the monomer pressure, hydrogen concentration, cocatalyst, poisons, temperature, and residence time. An illustrative example has been obtained in the present authors' laboratories using a silica-supported Ziegler/metallocene combination, where the applied metallocene component is much more sensitive to hydrogen compared to the Ziegler component, both with respect to the attainable molar mass and productivity. As a result, both the overall molar mass as well as the split of the resulting polymer are dependent on the applied hydrogen feed (Figure 8.8). As different kinetics are quite common in Ziegler/metallocene com-

binations, much effort has been expended into the research after independent molar mass and split control. For example, Nowlin et al. reported a method for the regulation of the bimodal product split made in a single reactor. A supported bimetallic catalyst system and a make-up feed consisting of one of the catalyst components constitute the catalyst system in this method [78]. The make-up catalyst, consisting of a single catalyst component, is added in a proportion necessary to make-up the deficiencies in the amounts of the HMM or LMM components. The type of make-up catalyst added depends on whether an increase in the HMM or LMM component is sought. While this method can be used to control the split, it has a possible drawback as the resin produced may contain particles consisting of only one component, causing a possible heterogeneity in the resin which can subsequently degrade film appearance and performance. As an apparent extension to the above method, the split can also be controlled by a make-up catalyst through in-line mixing with the supported bimetallic catalyst. The method combines a supported catalyst in slurry with a catalyst component in solution to form the completed bimetallic catalyst composition before being introduced into the polymerization reactor to control the properties of the bimodal polymer products [79]. The activities of the metallocene and non-metallocene portions can also be controlled by adjusting the ratio of organoaluminum and methylaluminoxane cocatalyst. The method allows the adjustment of polyolefin properties on a real-time basis, as the polyolefin is forming [80]. Nemzek et al. also reported the use of one unsupported metallocene with one supported metallocene for a better control in gas-phase polymerization. When the supported metallocene is different from the unsupported metallocene, broad MMD polymers can be obtained. Such a system also takes advantage of the high activity of the unsupported catalyst and the stability of a supported catalyst [81].

Water and/or carbon dioxide can also be used for regulation of the bimodal product split made in a single reactor. The mass fraction of the HMM component decreases with the addition of small amounts of water or carbon dioxide, possibly through reaction with the applied cocatalyst TMA to generate additional alumoxanes, which favors the relative contribution of the metallocene compound. This method allows the split to be adjusted in the reactor, without reformulating the bimetallic catalyst [82]. Other examples of split control agents include alcohols, ethers, amines, and oxygen [83]. A different approach is based on using two bicomponent catalysts, each having a HMM component and a LMM component, but in a different ratio [84]. In this way, the possible production of particles containing only HMM or LMM is avoided. Further, this system is substantially less sensitive to perturbations in catalyst feed rates or feed ratios.

The developments in the area of multicomponent systems for bimodal PE, especially for the Ziegler/metallocene hybrids and mixed metallocene systems, have resulted in systems that are on the brink of commercialization. However, as the products from this emerging technology must compete with the existing, highly sophisticated and well-accepted bimodal polymers, the breakthrough appears to be currently on a par with the rate of penetration of metallocene products in other high-volume polyolefin segments. As the catalyst costs for a multi-

component system will exceed the costs for a base Ziegler system, some resistance against such commercial implementation is inevitable. On the other hand, as mentioned above, a major motive for using this technology is the reduced investment cost of a single gas-phase reactor versus a cascade process. Perhaps in due time, as new PE capacity must be installed in order to meet the increasing demand for bimodal resins, this multicomponent technology might come to rival the existing technologies for the production of bimodal PE.

8.5 Multicomponent Catalysts for Polypropylene

Multicomponent catalysis has also been utilized in propylene (PP) polymerization. As in the case of bimodal PE, the combinations of a Ziegler–Natta catalyst with a metallocene catalyst as well as two or more different metallocenes have been explored. However, very few reports have dealt with *supported* multicomponent systems. As the stereochemistry using single-site catalysts can be varied, several possible combinations can be applied.

Reactor blends of metallocene *i*PP and Ziegler–Natta-based *i*PP have been produced via sequential semi-batch polymerizations by Eisen et al. These authors used combinations of *rac*-ethylene[1-Ind]$_2$ZrCl$_2$ or *rac*-Me$_2$Si[1-Ind]$_2$ZrCl$_2$ with a MgCl$_2$-supported Ziegler–Natta catalyst [85]. The unsupported MAO preactivated metallocene and the Ziegler–Natta components were sequentially added to the reactor before adding propylene, and the PP obtained consisted of a mixture of a fine powder and beads. According to the authors, the metallocene PP adsorbed partially on the surface of the growing PP particles from the Ziegler–Natta component. Dong et al. applied a combined Ziegler–Natta/metallocene system in a two-stage process for the production of HiPP [86]. The metallocene was kept latent during the first stage, but then activated during the second stage, for example by adding a suitable cocatalyst. Lee et al. treated a MgCl$_2$/TiCl$_4$/di-isobutylphthalate Ziegler–Natta catalyst with *rac*-Et(Ind)$_2$ZrCl$_2$ [87]. The activity of the hybrid catalyst in propylene polymerizations was much lower compared to the base Ziegler–Natta catalyst. Surprisingly, the isospecificity (II, %) was as high as 96.8%, even in the absence of an external donor, and appeared to be similar to the value reported earlier by Soga had when treating Ziegler–Natta catalysts with Cp$_2$TiMe$_2$ [88]. The same group also reported *in-situ* iPP reactor blends using a sequential addition of the same combination of catalysts [87b].

Reddy and Shamshoum reported the synthesis of resins consisting of an intimate blend of iso- and syndiotactic PP from a mixed suspension of an isospecific Ziegler–Natta catalyst and the solid reaction product of Me$_2$C(Cp)(Flu)ZrCl$_2$/MAO [89]. Reactor blends of iPP and amorphous PP, using the combined action of a Ziegler–Natta catalysts and a late transition metal catalyst such as bis(imino)nickel systems, have also been reported [44a].

Reactor blends of PP have also been achieved with binary metallocene systems. Many mixed, non-supported metallocene systems that produce PP having a broad

MMD have been reported, but this is beyond the scope of this chapter [90]. However, supporting these systems seems to be a straightforward extension of these developments. Speca and McAplin have outlined some of the merits of using mixed metallocenes for iPP [91a], by illustrating that differences in the hydrogen and ethylene responses of the individual metallocenes cause, for example, the MMD also to respond on different hydrogen or ethylene levels. Whereas, narrow MMD m-iPP may have some specific advantages in certain applications, m-iPP prepared using mixed metallocenes might fit better into the broad application window of conventional ZN-iPP. Binary catalysts for obtaining reactor blends of isotactic PPs with broadened MMD have been prepared by the consecutive impregnation of $Me_2Si(H_4\text{-}Ind)_2ZrCl_2$ and $Me_2Si(2\text{-}Me\text{-}Ind)_2ZrCl_2$ onto MAO-modified silica [91b]. Mehta et al. reported an isotactic PP product with broad or bimodal MMD using a dual metallocene catalyst system supported on MAO/SiO_2 in a staged process [92]. The conditions applied in the staged reactors differed with respect to temperature and/or ethylene content, and the procedure resulted in a blend of at least four different polymers which differed in molar mass and/or ethylene content.

Reactor blends of syndiotactic PP with broadened MMD have been formed by the co-impregnation of $Ph_2C(Cp)(Flu)ZrCl_2$ and $Me_2C(Cp)(2,7\text{-}^tBu_2\text{-}Flu)ZrCl_2$ [93]. A dual supported metallocene catalyst for sPP is reported to increase the activity over that for a single supported metallocene catalyst, and to produce sPP having a relatively broad MMD [93b].

In addition, the preparation of sPP/iPP reactor blends from a mixture of a stereorigid isospecific metallocene and a stereorigid syndiospecific metallocene on MAO/SiO_2, have been described by Fink et al. [94], by Shamshoum et al. [95], and by Marques et al. [96]. The latter group also reported a binary system based on $Ph_2C(Flu)(Cp)ZrCl_2$ and $Me_2Si(2\text{-}Me\text{-}4Ph\text{-}Ind)_2ZrCl_2$ co-supported on MAO/SiO_2. They concluded from differential scanning calorimetry (DSC) evaluation of the polymers made with the individual catalysts and with the binary system, that possible stereoblock formation had occurred (*vide infra*).

Blends of iso- and atactic PP have also been reported with supported binary metallocene systems based on $Cp_2ZrCl_2/Me_2Si(Ind)_2ZrCl_2$ [97] and *rac*-$Et(Ind)_2ZrCl_2$/$Et(Flu)_2ZrCl_2$ or *rac*-$Me_2Si(Ind)_2ZrCl_2/Et(Flu)_2ZrCl_2$ [98]. Similarly, reactor blends of isotactic and elastomeric PP have been reported using a system synthesized by the impregnation of a $Et(Ind)_2ZrCl_2$/MAO solution onto $Zr(CH_2{}^tBu)_4/Al_2O_3$ [99].

An interesting development in the area of PP has been reported by Zhu et al. Via the combined action of an unsupported a-specific bis(imino)pyridyl iron catalyst and the iso-specific *rac*-$Me_2Si(2\text{-}MeBenz[e]Ind)_2ZrCl_2$, these authors obtained a polymer consisting of an iPP backbone with aPP branches [100]. However, in order to obtain a branched PP, it was necessary to introduce the bis(imino)pyridyl iron catalyst first, followed by the zirconocene, being more of a staged process, whereas simultaneous addition of the components did not produce branched PP. The authors hypothesized that the iPP produced by the zirconocene, encapsulates the catalyst and forms a type of diffusion barrier for the aPP produced by the iron catalyst. Another example of *in-situ* versus *ex-situ* grafting is described by Dekmezian et al. [101], who observed better grafting efficiencies when using a consecutive

procedure, which was subsequently rationalized by modeling the concentration of macromers in both procedures.

8.6 Multicomponent Catalysts for Block Copolymers

An intriguing application of multicomponent catalysis involves the synthesis of block copolymers. In the case of PP, stereoblock copolymers of isotactic and atactic PP might be accessible via epimerization or isomerization of the active cationic species of discrete catalysts [102]. This might be a special theme in the area of multicomponent catalysis, as the single component catalyst precursor displays for example either *rac/rac* or *rac/meso* isomerization. Besides this approach, the use of reversible chain-transfer reactions using multicomponent catalysts may also lead to block copolymer formation.

Chien and colleagues postulated alkylaluminum-mediated chain transfer as one of the possible explanations for the presence of stereoblock PP when they used a mixture of *rac*-$Me_2Si[1\text{-ind}]_2ZrCl_2$ and ethylene-$[9\text{-Flu}]_2ZrCl_2$ co-supported on SiO_2 [103a], and similarly in an unsupported system consisting of a mixture of $Ph_2C(Cp)(Flu)ZrCl_2$ and *rac*-$Et(1\text{-Ind})_2ZrCl_2$ [103b]. Fink and coworkers co-supported the syndiospecific *i*-Pr[FluCp]$ZrCl_2$ and the isospecific *rac*-$Me_2Si[1\text{-Ind}]_2ZrCl_2$ on MAO/SiO_2 [94]. This group obtained a blend consisting of sPP, iPP and stereoblock PP. The stereoblock formation was proposed to be mediated by chain transfer via aluminum. It was concluded, therefore, that simultaneous impregnation of the different metallocenes was more effective in generating stereoblocks than was consecutive impregnation. Brintzinger et al. have shown that stereoblock PP is attainable via a mixture of different unsupported metallocenes using aluminum-mediated chain shuttling [104]; the same group also showed that the rate of chain transfer to aluminum and the back transfer from aluminum to a metallocene cation depends on the steric environment of the metallocene and aluminum compounds. The catalytic preparation of PE-based block copolymers has recently been published by a research team from Dow [105]. By making use of two different unsupported catalysts which differ in their copolymerization characteristics, such as a zirconium bis(phenoxyimine) catalyst and a hafnium pyridylamide catalyst, combined with a chain-shuttling agent such as $Zn(C_2H_5)_2$, block copolymers containing both hard, crystalline PE and soft, amorphous ethene-*co*-1-octene blocks could be produced. The system was optimized using high-throughput techniques, resulting in a narrow MMD block copolymer, without residual homopolymers.

8.7 Conclusions

The application of a single-site catalyst containing multicomponent catalysts remains a highly versatile tool for the tailoring of polymer properties. Indeed, such

a system might be capable of delivering economically attractive alternatives to existing processes as well new concepts for polyolefins that are unattainable via conventional techniques. Although the commercialization of these systems currently seems to be moving at a similar pace to the penetration of metallocenes in existing polyolefin markets, there is a strong probability that this technology will, in time, escape from the laboratory to large-scale production. In particular, recent examples in the area of block copolymers illustrate that the application of multicomponent catalysts is likely to lead to new concepts and products. Moreover, it proves – once again – that the future for innovative developments in the area of polyolefins remains very bright.

References

1 J.-C. Wasilke, S.J. Obrey, R.T. Baker, G. C. Bazan, *Chem. Rev.* 2005, *105*, 1001.

2 (a) M. Frediani, P. Piel, W. Kaminsky, C. Bianchini, L. Rosi, *Macromol. Symp.* 2006, *236*, 124; (b) C. Bianchini, H. Miller, F. Ciardelli, Combinations of transition metal catalysts for reactor blending, in: F. Ciardelli, S. Penczek (Eds.), *Modification and Blending of Synthetic and Natural Macromolecules*, Kluwer Academic Publishers, The Netherlands, 2004, p. 15; (c) R.F. de Souza, O.L. Casagrande, *Macromol. Rapid. Commun.* 2001, *22*, 1293.

3 See for example: (a) J.T. Dixon, M.J. Green, F.M. Hess, D.H. Morgan, *J. Organomet. Chem.* 2004, *689*, 3641 and references therein; (b) M.J. Overett, K. Blann, A. Bollmann, J.T. Dixon, D. Haasbroek, E. Killian, H. Maumela, D. S. McGuinness, D.H. Morgan, *J. Am. Chem. Soc.* 2005, *127*, 10723; (c) *European Chemical News* 2004, *31 May-6 June*, 16–18.

4 (a) D.L. Beach, Y.V. Kissin, *J. Pol. Sci: Pol. Chem. Ed.* 1984, *22*, 3027; (b) Y.V. Kissin, D.L. Beach, *J. Pol. Sci., Part A: Pol. Chem.* 1986, *24*, 1069.

5 (a) E.A. Benham, P.D. Smith, M.P. McDaniel, *Polym. Eng. Sci. 1988*, 28, 1469; (b) T.M. Pettijohn, W.K. Reagen, S.J. Martin, U.S. Patent 5331070, 1992; (c) E.A. Benham, M.P. McDaniel, R. McElvain, R.O. Schneider, U.S. Patent 5071927, 1990; (d) R.M. Manyik, W.E. Walker, T.P. Wilson, U.S. Patent 3300458, 1963.

6 C. Pellecchia, D. Pappalardo, G.-J. Gruter, *Macromolecules* 1999, *32*, 4491.

7 C. Bianchini, M. Frediani, G. Giambastiani, W. Kaminsky, A. Meli, E. Passaglia, *Macromol. Rapid Commun.* 2005, *26*, 1218.

8 Z. Ye, F. Al Obaidi, S. Zhu, *Macromol. Rapid Commun.* 2004, *25*, 647.

9 C. Denger, U. Haase, G. Fink, *Makromol. Chem., Rapid Commun.* 1991, *12*, 697.

10 (a) Z.J.A. Komon, G.M. Diamond, M.K. Leclerc, V. Murphy, M. Okazaki, G.C. Bazan, *J. Am. Chem. Soc.* 2002, *124*, 15280; (b) Z.J.A. Komon, X. Bu, G.C. Bazan, *J. Am. Chem. Soc.* 2000, *122*, 1830.

11 (a) K-H.A. Ostoja-Starzewski, J. Witte, H. Bartl, K.-H. Reichert, G. Vasiliou, U.S. Patent 5616529, 1986; (b) K.A. Ostoja Starzewski, J. Witte, K.H. Reichert, G. Vasiliou, Linear and branched polyethylenes by new coordination catalysts, in: W. Kaminsky, H. Sinn (Eds.), *Transition Metals and Organometallics as Catalysts for Olefin Polymerization*, Proceedings of an International Symposium Hamburg/ FRG, Springer-Verlag, Heidelberg, 1988, p. 349.

12 K. Musikabhumma, T.P. Spaniol, J. Okuda, *J. Pol. Sci., Part A: Pol. Chem.* 2003, *41*, 528.

13 (a) A.M.A. Bennett, E.B. Coughlin, J.D. Citron, L. Wang, WO9950318, 1999; (b) Z. Guan, L. Wang, WO01/23444, 1999; (c) L. Wang, M. Spinu, J.D. Citron, WO01/23443, 1999; (d) P.J. Maddox, S.J. Partington, WO0055216, 2000.

14 (a) Z. Zhang, C. Guo, Y. Ke, Y. Hu, *J. Appl. Pol. Sci*. 2004, *94*, 1690; (b) Z. Lu, Z. Zhang, Y. Li, C. Wu, Y. Hu, *J. Appl. Pol. Sci*. 2006, *99*, 2898.

15 M.C.A. Kuhn, J.L. da Silva, A.C.A. Casagrande, R.S. Mauler, O.L. Casagrande, *Macromol. Chem. Phys.* 2006, *207*, 827.

16 See for example: (a) W.W. Greassley, *Acc. Chem. Res*. 1977, *10*, 332; (b) P.M. Wood-Adams, J.M. Dealy, A.W. deGroot, G.D. Redwine, *Macromolecules* 2000, *33*, 7489 and references therein; (c) J.M. Carella, *Macromolecules* 1996, *29*, 8280.

17 (a) E. Kolodka, W.-J. Wang, P.A. Charpentier, S. Zhu, A.E. Hamielec, *Polymer* 2000, *41*, 3985; (b) D. Yan, W.-J. Wang, S. Zhu, *Polymer* 1999, *40*, 1737; (c) P.M. Wood-Adams, *J. Rheol*. 2001, *45*, 203; (d) P.J. Doerpinghaus, D.G. Baird, *J. Rheol*. 2003, *47*, 717; (e) D.J. Read, T.C.B. McLeish, *Macromolecules* 2001, *34*, 1928; (f) J. Janzen, R.H. Colby, *J. Mol. Struct.* 1999, *485–486*, 569; (g) Y. Yu, P.J. DesLauriers, D.C. Rohlfing, *Polymer* 2005, *46*, 5165; (h) S.G. Hatzikiriakos, *Pol. Eng. Sci*. 2000, *40*, 2279; (i) A. Mamberg, E. Kokko, P. Lehmus, B. Löfgren, J.K. Seppälä, *Macromolecules* 1998, *31*, 8448; (j) Especially in the patent literature, one often encounters the ratio of two melt-indices measured at different loadings, such as I_{10}/I_2 or I_{21}/I_2 to indicate the combined effect of breadth of the MMD and LCB.

18 (a) D. Beigzadeh, J.B.P. Soares, *Macromol. Rapid Commun*. 1999, *20*, 541; (b) D. Beigzadeh, J.B.P. Soares, T. A. Duever, *Macromol. Symp*. 2001, *173*, 179; (c) D. Beigzadeh, J.B.P. Soares, A. E. Hamielec, *J. Appl. Polym. Sci*. 1999, *71*, 1753; (d) K.-J. Chu, J.B.P. Soares, A. Penlidis, *Macromol. Chem. Phys*. 2000, *201*(*3*), 340; (e) J.B.P. Soares, J.D. Kim, *J. Polym. Sci., Part A: Polym. Chem.* 2000, *38*(*9*), 1408; (f) N. Kashiwa, Feature of metallocene-catalyzed polyolefins, in: K. Soga, M. Terano (Eds.), *Catalyst Design for Tailor-Made Polyolefins*, Elsevier Publishers, 1994, p. 381; (g) S.-Y. Lai, J.R. Wilson, G.W. Knight, J.C. Stevens, P.-W.S. Chum, U. S. Patent 5272236, 1991.

19 (a) F.J. Karol, S.-C. Kao, E.P. Wasserman, Z. Yu, in: W. Kaminsky (Ed.), *Metalorganic Catalysts for Synthesis and Polymerization*, Springer 1999, p. 629; (b) F.J. Karol, E.P. Wasserman, S.-C. Kao, R. C. Brady, European Patent 0659773, 1994.

20 (a) T. Chen, G.N. Foster, D.-C. Lee, R.H. Vogel, S.J. Kurtz, L.H. Gross, S.H. Wasserman, European Patent 0743327, 1996; (b) P.C. Shista, E.P. Wasserman, S. J. Karol, European Patent 1217013, 1996.

21 C.M. Killian, P.B. Mackenzie, G.G. Lavoie, J.A. Ponasik, L.S. Moody, U.S. Patent 6620896, 1999.

22 R.I. Mink, T.E. Nowlin, S.D. Schregenberger, K.G. Schurzky, P.P. Shirodkar, U.S. Patent 6420298, 1999.

23 See for example: F.P. Alt, L.L. Böhm, H. F. Enderle, J. Berthold, *Macromol. Symp.* 2001, *163*, 135.

24 (a) See for example for combined slurry-gas phase: A. Ahvenainen, K. Sarantila, H. Andtsiö, J. Takakarhu, A. Palmroos, WO9212182, 1991; (b) gas-phase-gas-phase: K.H. Lee, F.J. Karol, S.B. Samuels, U.S. Patent 5149739, 1991; (c) W. Michie, A.C. Neubauer, B.A. Cobler, C.E. Baker, WO2004101674, 2004; (d) slurry-slurry: see also Ref. [23]; T. Tanaka, A. Marakami, O. Kishiro, N. Gohko, European Patent 0057352, 1982.

25 H.T. Liu, C.R. Davey, P.P. Shirodkar, *Macromol. Symp*. 2003, *195*, 309.

26 H.C. Welborn, U.S. Patent 5183867, 1991.

27 (a) F. Masi, S. Malquori, L. Barazzoni, C. Ferrero, A. Moalli, F. Menconi, R. Invernizzi, N. Zandona, A. Altomare, F. Ciardelli, *Makromol. Chem. Suppl*. 1989, *15*, 147; (b) G. Mashio, C. Bruni, L. De Tullio, F. Ciardelli, *Macromol. Chem. Phys*. 1998, *199*, 415; (c) V. Graves, U.S. Patent 4562170, 1984; (d) T.J. Pullukat, R.E. Hoff, *Catal. Rev.–Sci. Eng*. 1999, *41*(*3&4*), 289; (e) C. Bianchini, H. Miller, F. Ciardelli, Combinations of transition metal catalysts for reactor blending, in: F. Ciardelli, S. Penczek (Eds.), *Modification and Blending of Synthetic and Natural Macromolecules*, Kluwer Academic Publishers, The Netherlands, 2004, p. 15;

28 H. C. Welborn, U.S. Patent 4701432, 1986.

29 (a) R.I. Mink, Y.V. Kissin, T.E. Nowlin, P.P. Shirodkar, G.O. Tsien, S.D. Schregenberger, U.S. Patent 6740617, 2002; (b) F.Y. Lo, T.E. Nowlin, P.P. Shirodkar, U.S. Patent 5032562, 1989; (c) R.I. Mink, T.E. Nowlin, S.D. Schregenberger, P.P. Shirodkar, G.O. Tsien, U.S. Patent 5614456, 1994.

30 W.J. Sartain, P.A. Hooks, K.M. Lindstrom, S.L. Ellis, D.D. Klendworth, A.P. Masino, R.W. Fries, T.A. Pastrick, U.S. Patent 6395669, 2000.

31 R.C. Job, W.T. Reichle, U.S. Patent 6444605, 1999.

32 Y.V. Kissin, R.I. Mink, T.E. Nowlin, U.S. Patent 6001766, 1997.

33 (a) F.Y. Lo, R.I. Mink, T.E. Nowlin, S.D. Schregenberger, P.P. Shirodkar, WO99/03899, 1998; (b) R.I. Mink, T.E. Nowlin, K.G. Schurzky, K. Dackson, S. D. Schregenberger, P.P. Shirodkar, WO03/022890, 2002.

34 (a) E.S. Shamshoum, L. Haspeslagh, H. Chen, U.S. Patent 6730751, 2002; (b) G. Debras, L. Peters, European Patent 0952164, 1998.

35 D.M. Brown, European Patent 1101777, 2000.

36 I.R. Little, J.P. McNally, U.S. Patent 5747405, 1998.

37 C.I. Kuo, L.G. McCullough, P.P. Shirodkar, F.D. Ehrman, P.C. Shannon, R.L. Santana, S.K. Ackerman, D.G. O'Neil, U.S. Patent US6875828, 2003.

38 R.I. Mink, T.E. Nowlin, P.P. Shirodkar, G.M. Diamond, D.B. Barry, C. Wang, H.A. Fruitwala, S.C. Ong, WO0244222, 2001.

39 S.C. Kao, M.D. Awe, WO2004060864, 2003.

40 R.I. Mink, T.E. Nowlin, K.G. Schurzky, R.L. Santana, P.P. Shirodkar, WO2003047752, 2002.

41 J. Maozhu, L. Yuexiang, R. Peng, H. Shen, M. Yin, Z. Ma, C. Xie, Y. Sun, B. Zhu, B. Xing, U.S. Patent 6387839, 1999.

42 (a) H. Orass, A.A. Moman, A. Abu-raqabah, A. Al-Nezari, European Patent 1302480, 2001; (b) H. Orass, A. Moman, A. Abu-raqabah, U.S. Patent 6403520, 2000.

43 I. McKay, A. Ciupa, B.C. Hall, U.S. Patent 6486273, 2001.

44 (a) J.A.M. Canich, G.A. Vaughan, P.T. Matsunaga, D.E. Gindelberger, T.D. Shaffer, K.R. Squire, U.S. Patent 6194341, 1997; (b) B.S. Kimberley, D. Pratt, WO9946304, 1999.

45 (a) J.P. Hogan, *Appl. Indust. Catal.* 1983, *1*, 149; (b) M.P. McDaniel, *Adv. Catal.* 1985, *133*, 47; (c) P.J. DesLauriers, M.P. McDaniel, D.C. Rohlfing, R.K. Krsihnaswamy, S.J. Secore, E.A. Benham, P.L. Maeger, A.R. Wolfe, A.M. Sukhadia, B.B. Beaulieu, *Pol. Eng. Sci.* 2005, *45*(*9*), 1203; (d) G.L. Debras, U.S. Patent 2002002109, 2001.

46 (a) J.J. Bergmeister, U.S. Patent 5527867, 1995; (b) J.J. Bergmeister, U.S. Patent 5543376, 1995; (c) J.J. Bergmeister, S.E. Kufeld, M.P. McDaniel, U.S. Patent 5648439, 1995; (d) J.J. Bergmeister, S.E. Kufeld, M.P. McDaniel, U.S. Patent 5624877, 1995.

47 (a) A. Follestad, V. Almquist, E. Ommundsen, T. Dreng, WO9940131, 1999; (b) A. Follestad, V. Almquist, U. Palmqvist, H. Hokkanen, WO9940126, 1999.

48 O. Lhost, N. Zandona, U.S. Patent 6013595, 1996.

49 For the combination of a titanocene and a zirconocene, each having different olefin polymerization termination rate constants in the presence of hydrogen. P. M. Stricklen, U.S. Patent 5064797, 1990.

50 For the combination of a bridged fluorenyl-containing metallocene and an unbridged metallocene using boroxine treated MAO supports. M.B. Welch, R.L. Geerts, S.J. Palackal, T.M. Pettijohn, U.S. Patent 5594078, 1994.

51 For the combination of a supported mixture containing hydrogenated indenyl or fluorenyl metallocenes see: (a) A. Razavi, U.S. Patent 5914289, 1997; (b) A. Razavi, U.S. Patent 6225428, 1999.

52 For the combination of a high MFR metallocene combined with a low MFR metallocene see: D.J. Crowther, J.F. Szul, U.S. Patent 20040132933, 2003.

53 For the combination of dimethylsilyl bridged bis-indenyl zirconocene dichlorides where one zirconocene contains saturated indenyls and one contains unsaturated indenyls see: A.H. Dekmezian, N.A. Merrill, U.S. Patent 20040220360, 2003.

54 (a) For the combination of bridged and unbridged metallocenes, see: A. Razavi, G.L.G. Debras, U.S. Patent 6541413, 1995; (b) For the combination of one bridged indenoindolyl complex and one unbridged indenoindolyl complex system, see: S. Wang, WO2004113397, 2004.

55 For the combination of $Me_2Si(Cp^*)(MeCp)ZrCl_2$ and $Me_2Si(Ind)_2ZrCl_2$, see: C.-T. Lue, D.J. Crowther, U.S. Patent 6207606, 2001.

56 For the combination of Cp_2NbCl_2 and $(BuCp)_2ZrCl_2$ see: J.H.Z. Dos Santos, A. E. Gerbase, K.C. Rodenbusch, G.P. Pires, M. Martinelli, J. Bichinho, *J. Mol. Catal. A: Chem.* 2002, *184*, 167.

57 For the combination of $(BuCp)_2ZrCl_2$/ Cp_2ZrCl_2 see: F. Silveria, S.R. Loureiro, G. de Galland, F.C. Stedile, J.H. Dos Santos, T. Teranishi, *J. Mol. Catal. A: Chem.* 2003, *206*, 398.

58 (a) For the combination of a high-MFR metallocene (a cyclic bridged metallocene) and a low-MFR metallocene (a bridged metallocene), see D.J. Crowther, J.F. Szui, U.S. Patent 2004/132933, 2004; (b) For the combination of isomers of $(MeRCp)_2ZrCl_2$, see R.L. Bamberger, M. O. Jejelowo, U.S. Patent 6136930, 2000.

59 (a) J.D. Kim, J.B.P. Soares, *J. Polym. Sci., Polym. Chem.* 2000, *38*, 1427; (b) J. D. Kim, J.B.P. Soares, G.L. Rempel, *Macromol. Rapid. Commun.* 1998, *19*, 197.

60 F. Silveira, S.R. Loureiro, G.B. de Galland, F.C. Stedile, J.H.Z. Dos Santos, T. Teranishi, *J. Mol. Catal. A: Chem.* 2003, *206*(*1–2*), 389.

61 R.L. Bamberger, M.O. Jejelowo, U.S. Patent 6608000, 2000.

62 G.A. Vaughan, J.F. Szul, M.G. Mckee, J.M. Farley, C.T. Lue, S.C. Kao, WO2003008468, 2002.

63 (a) W.A. Hermann, J. Rohrmann, E. Herdtweck, W. Spaleck, A. Winter, *Angew. Chem. Int. Ed. Engl.* 1989, *28*(*11*), 1511; (b) W.A. Hermann, J. Rohrmann, E. Herdtweck, W. Spaleck, A. Winter, *Angew. Chem.* 1989, *101*, 1536.

64 W. Xu, H. Al-Shammari, S. Palackal, A. Abu-Raqabah, European Patent 1574525, 2004.

65 K.Y. Shih, U.S. Patent 6686306, 2002.

66 A. Razavi, WO2004029101, 2003.

67 G.B. Jacobsen, D. Jeremic, S. Mastroianni, I.D. Mckay, WO2006054048, 2005.

68 (a) D.R. Loveday, D.H. McConville, J.F. Szul, K.A. Erickson, S. Mawson, T.H. Kwack, F.J. Karol, D.J. Schreck, U.S. Patent 6841631, 2003; (b) D.R. Loveday, D.H. McConville, J.F. Szul, K.A. Erickson, S. Mawson, T.H. Kwack, F.J. Karol, D.J. Schreck, U.S. Patent 6274684, 1999.

69 R. Blom, K.J. Jens, A. Follestad, O.B. Ryan, WO02060963, 2002.

70 H. Oshima, K. Takaoki, U.S. Patent 20030060579, 2003.

71 W.M. Vega, A. Munoz-Escalona, European Patent 0719797, 1995.

72 L.J. Rekers, R.D. Laib, U.S. Patent 5321105, 1993.

73 T.T. Wenzel, D.J. Schreck, U.S. Patent 2002119890, 2001.

74 T.L. Nemzek, F.J. Karol, S.-C. Kao, R.C. Brady, U.S. Patent 6069213, 1997.

75 Examples of unsupported hetero binuclear systems are: (a) T. Ushioda, M.L.H. Green, J. Haggit, X. Yan, *J. Organomet. Chem.* 1996, *518*, 155; (b) X. Yan, A. Chernega, M.L.H. Green, J. Sanders, J. Souter, T. Usioda, *J. Mol. Catal. A: Chemistry* 1998, *128*, 119; (c) G.M. Diamond, A.N. Chernega, P. Mountford, M.L.H. Green, *J. Chem. Soc., Dalton Trans.* 1996, 921; (d) J. Wang, H. Li, N. Guo, L. Li, C.L. Stern, T.J. Marks, *Organometallics* 2004, *23*, 5112; (e) H. Li, C.L. Stern, T.J. Marks, *Macromolecules* 2005, *38*, 9015 and references therein; (f) J. Kuwabara, D. Takeuchi, K. Osakada, *Chem. Commun.* 2006, *36*, 3815.

76 (a) H.G. Alt, R. Ernst, I.K. Böhmer, *J. Organomet. Chem.* 2002, *658*, 259; (b) H. G. Alt, R. Ernst, *J. Mol. Catal. A: Chemistry* 2003, *195*, 11.

77 (a) M.W. Holtcamp, L.G. McCullough, WO03027131, 2002; (b) J.C. Tsai, K.-K. Liu, S.H. Chan, S.J. Wang, M.J. Young, U.S. Patent 6297392, 1997; (c) R.B. Wilson, Jr., WO9920637, 1998.

78 T.E. Nowlin, S.D. Schregenberger, P.P. Shirodkar, G.O. Tsien, WO9607478, 1995.

79 S. Mawson, S.-C. Kao, T.H. Kwalk, T.R. Lynn, D.H. McConville, M.G. Mckee, J. F. Szul, K.A. Terry, T.T. Wenzel, M.G. Goode, J.H. Oskam, R.J. Jorgensen, R. H. Vogel, U.S. Patent 2004254312, 2004.

80 R.I. Mink, T.E. Nowlin, K.G. Schurzky, K. Dackson, S.D. Schregenberger, P.P. Shirodkar, U.S. Patent 2004242808, 2002.

81 T.L. Nemzek, F.J. Karol, S.-C. Kao, WO9931147, 1998.

82 R.I. Mink, T.E. Nowlin, S.D. Schregenberger, P.P. Shirodkar, G.O. Tsien, WO9609328, 1995.

83 F.D. Ehrman, P.P. Shirodkar, M.B. Davis, D.P.J.R. Zilker, P.C. Shannon, U.S. Patent 2005085600, 2003.

84 M.W. Tilston, V. Maheshwari, M.B. Davis, WO0224768, 2001.

85 (a) A. Lisovskii, M. Shuster, M. Gishvoliner, G. Lidor, M.S. Eisen, *J. Pol. Sci., Part A: Pol. Chem.* 1998, *36*, 3063; (b) A. Lisovskii, M. Shuster, M. Gishvoliner, G. Lidor, M.S. Eisen, *Appl. Organomet. Chem.* 1998, *12*, 401.

86 J. Dong, Z. Han, J. Liu, D. Wang, WO2006047913, 2005.

87 (a) T.O. Ahn, S.C. Hong, W.S. Huh, Y. C. Lee, D.H. Lee, *Pol. Eng. Sci.* 1999, *39*(7), 1257; (b) T.O. Ahn, S.C. Hong, J. H. Kim, D.-H. Lee, *J. Appl. Pol. Sci.* 1998, *67*, 2213.

88 (a) K. Soga, T. Uozumi, T. Shiono, *Makromol. Chem., Rapid Commun.* 1989, *10*, 293; (b) K. Soga, T. Uozumi, H. Yanagihara, *Makromol. Chem.* 1989, *190*, 31.

89 B.R. Reddy, E.S. Shamshoum, U.S. Patent 5804524, 1993.

90 (a) For example, two different chiral, stereo-rigid metallocene catalysts: J.A. Ewen, U.S. Patent 4975403, 1988; (b) For the production of syndiotactic polyolefins having a broad molecular mass distribution: A. Winter, V. Dolle, W. Spaleck, U.S. Patent 5587501, 1995; (c) For the production of polypropylene having a broad molecular mass distribution using ansa bridged bis-indenyl systems, see: A. Winter, V. Dolle, W. Spaleck, U.S. Patent 5350817, 1994; (d) A. Winter, W. Spaleck, B. Bachmann, U.S. Patent 6150481, 1997.

91 (a) A.N. Speca, J.J. McAlpin, Mixed metallocenes for designer polymers, in: G.M. Benedikt, B.L. Goodall (Eds.), *Metallocene Catalyzed Polymers*, Plastic Design Library, New York, 1998, p. 73; (b) A.N. Speca, J.L. Brinen, J.J. McAlpin, U.S. Patent 5786291, 1997.

92 (a) A.K. Mehta, M.C. Chen, J.J. McAlpin, A.N. Speca, K. Tormaschy, C.Y. Lin, U.S. Patent 6576306, 2001; (b) A.K. Mehta, M. C. Chen, J.J. McAlpin, A.N. Speca, K. Tormaschy, C.Y. Lin, U.S. Patent 6583227, 2001.

93 (a) E.S. Shamshoum, C.G. Bauch, U.S. Patent 5847059, 1996; (b) E.S. Shamshoum, C.G. Bauch, European Patent 0849286, 1997.

94 C. Przybyla, G. Fink, *Acta Polym.* 1999, *50*, 77.

95 (a) E. Shamshoum, M. Lopez, T. Harris, S. Kim, European Patent 0870779, 1998; (b) E.S. Shamshoum, M. Lopez, T.G. Harris, S. Kim, U.S. Patent 6362125, 2000.

96 (a) M. Marques, C.C. Pombo, R.A. Silva, A. Conte, *J. Pol. Sci., Part A: Pol. Chem.* 2002, *40*, 2979; (b) M. Marques, A. Conte, *J. Appl. Pol. Sci.* 2006, *99*, 628.

97 M.F.V. Marques, C.C. Pombo, R.A. Silva, A. Conte, *Eur. Pol. J.* 2003, *39*, 561.

98 J.C.W. Chien, Y. Iwamoto, M.D. Rausch, W. Wedler, H.H. Winter, *Macromolecules* 1997, *30*, 3447.

99 E. Ernst, J. Reussner, W. Neissl, European Patent 0695765, 1994.

100 Z. Ye, S. Zhu, *J. Pol. Sci., Part A: Pol. Chem.* 2003, *41*, 1152.

101 A.H. Dekmezian, J.B. Soares, P. Jiang, C. A. Garcia-Franco, W. Weng, H. Fruitwala, T. Sun, D.M. Sarzotti, *Macromolecules* 2002, *35*, 9586.

102 See for example: (a) G.W. Coates, *Chem. Rev.* 2000, *100*, 1223; (b) G.W. Coates, R. M. Waymouth, *Science* 1995, *267*, 217; (c) F.J. Gomez, R.M. Waymouth, *Science* 2002, *295*, 635; (d) V. Busico, R. Cipullo, A.L. Segre, G. Talarico, M. Vacatello, V. Van Axel Castelli, *Macromolecules* 2001, *34*, 8412; (e) V. Busico, R. Cipullo, W.P. Kretschmer, G. Talarico, M. Vacatello, V. Van Axel Castelli, *Angew. Chem. Int. Ed.* 2002, *41*, 505; (f) V. Busico, R. Cipullo, W.P. Kretschmer, G. Talarico, M. Vacatello, V. Van Axel Castelli, *Angew. Chem.* 2002, *114*, 523.

103 (a) J.C.W. Chien, Y. Iwamoto, M.D. Ruasch, W. Wedler, H.H. Winter, *Macromolecules* 1997, *30*, 3447; (b) J. C.W. Chien, Y. Iwamoto, M.D. Rausch, *J. Pol. Sci., Part A: Pol. Chem*. 1999, *37*, 2439.

104 S. Lieber, H.-H. Brintzinger, *Macromolecules* 2000, *33*, 9192.

105 (a) D.J. Arriola, E.M. Carnahan, P.D. Hustad, R.L. Kuhlman, T.T. Wenzel, *Science* 2006, *312*, 714; (b) D.J. Arriola, A.E.M. Carnahan, Y.W. Cheung, D.D. Devore, D.D. Graf, P.D. Hustad, R.L. Kuhlman, P.S.C. Li, B.C. Poon, G. Roof, J.C. Stevens, P.J. Stirn, T.T. Wenzel, WO2005090427, 2005.

9
Tethering Olefin Polymerization Catalysts and Cocatalysts to Inorganic Oxides

Jason C. Hicks and Christopher W. Jones

9.1
Introduction

Tethering olefin polymerization precatalysts to solid supports is perhaps the most versatile approach to construct heterogeneous precatalysts. Current tethering methodologies take into account the effects of the support material (usually silica or alumina), the length of the tether from the surface, the spacing between tethered sites, the type of reactive molecule used to tether to the surface (usually alkoxysilanes or chlorosilanes), and the type of ligand bound to the surface. In particular, tethering has attracted attention due to the possibility, in principle, to completely prevent catalyst leaching in slurry-phase processes. Additionally, the presence of fixed tethers can, in principle, be used to construct very well-defined, single-site supported complexes that are amenable to structural characterization, ultimately yielding molecular level structure–property relationships.

The two main routes used to tether olefin polymerization precatalysts are either: (i) building the precatalyst off of the surface using a stepwise approach; or (ii) tethering a preformed precatalyst directly to the surface [1]. The disadvantage with the first method involves the amount of tedious, and often non-stoichiometric steps required to form the precatalyst on the surface, as well as the possible formation of deactivated precatalysts through interaction with the support material. The second approach requires the synthesis of a pure homogeneous precatalyst that has the capability of being grafted onto the surface. Very often, the formation of a pure tetherable precatalyst is not trivial, as the synthetic and purification procedures are quite extensive and economically unfavorable. This immobilization method can also produce multiple types of sites due to the interaction between the metal and the surface during the grafting step, especially when using early transition metals. The characterization of these synthesized materials can also be very difficult, as metal-center characterization techniques either provide limited data (e.g., UV-Visible spectroscopy) or most often require detailed *in-situ* experimental investigations (e.g., extended X-ray absorption fine structure, EXAFS).

Tailor-Made Polymers. Via Immobilization of Alpha-Olefin Polymerization Catalysts.
Edited by John R. Severn and John C. Chadwick

ISBN: 978-3-527-31782-0

This chapter focuses on the advances in tethering precatalysts and cocatalysts, and on the formation of model compounds of such systems, highlighting recent reports from the open and patent literature.

9.2
Surface-Tethered Precatalysts

9.2.1
Surface-Tethered Metallocene Precatalysts

The first literature reports of tethered olefin polymerization precatalysts were made by Soga and colleagues [2–5], who built silica-tethered indenyl ligands by first reacting the silica with $SiCl_4$, followed by the addition of a lithium salt of indene [3]. This afforded an indenyl ligand bound to the surface that was deprotonated by the addition of *n*-butyllithium and subsequently metallated with $ZrCl_4 \cdot 2THF$ (Scheme 9.1). The resulting tethered zirconium precatalyst was activated by either methylaluminoxane (MAO) or triisobutylaluminum (TIBA) for the production of isotactic polypropylene (PP). However, when this catalytic system was used, both isotactic and atactic PP were formed. The authors suggested that a detailed characterization of the tethered zirconium precatalyst was needed to better understand why the multiple types of precatalyst were formed on the silica support. In a separate publication, this method was used to tether neodymocene precatalysts for the polymerization of ethylene [4]. As reported, the neodymocene precatalysts were activated with an alkylating agent (such as TIBA, trimethylaluminum, BuMgEt, *n*BuLi, MeLi, or MAO) to produce catalytic activities up to 90 kg PE mol^{-1} Nd h^{-1}). However, the polydispersity of the polyethylene was quite broad, with M_w/M_n values ranging from 2 to 17.

Soga and coworkers also reported a method to immobilize olefin polymerization precatalysts on 3-aminopropyl-modified silica surfaces for the copolymerization of ethylene and 1-octene [5]. The tethered precatalyst was synthesized by first reacting 3-aminopropyltrimethoxysilane to the silica surface. Subsequently, the precatalyst (Cp^*TiCl_3) was added to react with the amine functionalities. As a comparison, the authors synthesized a heterogeneous precatalyst by reacting Cp^*TiCl_3 directly to the silica surface. Leaching with MAO was tested with both methods, showing that a greater fraction of the complex was lost on the Cp^*TiCl_3-SiO_2 support com-

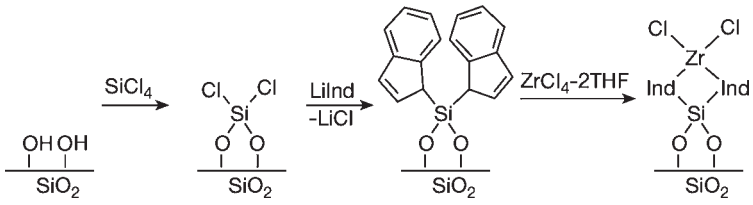

Scheme 9.1

pared to the Cp*$TiCl_3$/NH_2-SiO_2 support, with 5.4 and 1.7 mol.%, respectively. However, in both cases only trace amounts of polyethylene (PE) were recovered from a polymerization experiment using the leached components. Nevertheless, the authors reported that MAO can more easily break Ti–O bonds with the surface than Ti–N bonds, due to the amount of titanium leached. By using the Cp*$TiCl_3$/NH_2-SiO_2 precatalyst, a greater amount of octene was incorporated into the copolymer. However, the polymers produced were more amorphous than the somewhat crystalline copolymers produced when Cp*$TiCl_3$-SiO_2 was used.

Pakkanen and coworkers employed a strategy involving a surface reaction with a silane coupling agent to construct α-olefin polymerization precatalysts from the surface of silica [6]. The method involved reaction of $Cp(CH_2)_3Si(OEt)_3$, in the gas phase, with the surface silanols or siloxane bridges on the silica surface, as determined by Fourier transform infrared (FTIR) and ^{13}C cross-polarization/magic angle sample (CP/MAS) nuclear magnetic resonance (NMR) spectroscopies. The surface-bound cyclopentadiene species were activated by reaction of *n*BuLi to form the deprotonated cyclopentadienyl ligand (LiCp) for the metal precatalyst (Scheme 9.2). By reaction of $CpZrCl_3$ with the surface LiCp groups, a tethered precatalyst was created which produced PE with a relatively narrow polydispersity index (PDI) when activated by MAO (Al/Zr 1500 or 2000) [7]. As a comparison, $CpZrCl_3$ was reacted directly to the silica surface and activated with MAO to form PE. It was determined that surface pretreatment with the Cp moiety provided a better support material to form the tethered precatalyst, as the activity of the control material was much lower. However, multiple types of site were expected to exist on the silica surface due to the interaction of *n*BuLi with unreacted Si–OEt groups. This reac-

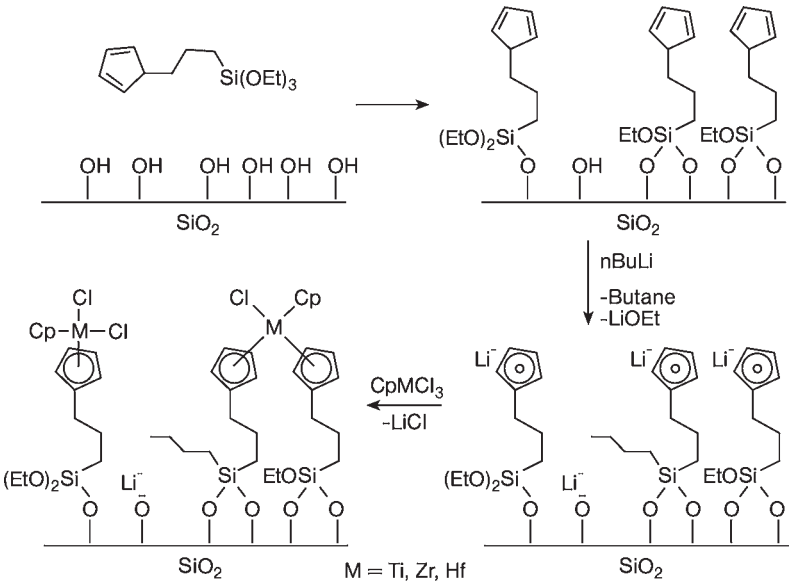

Scheme 9.2

tion was suggested to yield LiOEt and Si–Bu surface groups. Thus, the LiOEt can react with the $CpZrCl_3$ to form $CpZr(OEt)Cl_2$ which can interact with surface silanols to evolve EtOH or HCl. The authors did not comment on leaching of the metal precatalyst in this study.

In separate reports, Pakkanen and coworkers immobilized $ZrCl_4(THF)_2$, $HfCl_4(THF)_2$, $CpHfCl_3$, $CpTiCl_3$, $[\eta^5\text{-}C_5(CH_3)_5]TiCl_3$, $[\eta^5\text{-}C_5(CH_3)_5]ZrCl_3$, $[\eta^5\text{-}C_5(CH_3)_5]HfCl_3$ and $CrCl_3(THF)_3$ on Cp-modified silica [8, 9]. The support materials were characterized with FTIR, ^{13}C and ^{29}Si solid-state NMR spectroscopies; however, characterization of the metal center was absent. The $CpHfCl_3$-supported precatalyst performed similarly to the $CpZrCl_3$-supported precatalyst previously discussed. However, when activated by MAO, the major products from $CpTiCl_3$ and $CrCl_3(THF)_3$ with ethylene present were *n*-butene and other oligomers. In this case, the homogeneous catalyst, $[CpCrMe(\mu\text{-}Cl)]_2$/MAO produced PE, but oligomers were also present. When $[\eta^5\text{-}C_5(CH_3)_5]TiCl_3$, $[\eta^5\text{-}C_5(CH_3)_5]ZrCl_3$ and $[\eta^5\text{-}C_5(CH_3)_5]HfCl_3$ were supported and activated with MAO, very low activities, per metal center, were observed for the formation of PE, and the PDIs of the PE produced were also very broad. Additional studies indicated that leaching occurs for these types of supported precatalyst with MAO [9].

By using a similar strategy, Pakkanen and coworkers eliminated the use of the harsh organolithium agent by using a zirconium or titanium amide complex $[Zr(NMe_2)_4$ or $Ti(NMe_2)_4]$ to bind to the Cp-modified silica surface (Scheme 9.3) [10]. When the metal amide complex was used, one step in the modification was eliminated. The polymerization activity of the titanium-based precatalysts when activated by MAO was comparable to the homogeneous control, $(CH_3)_3SiCpTi[N(CH_3)_2]_3$, for production of linear high-density PE. However, the activity of the catalyst was greatly dependent on the Al/Ti ratio. For instance, Al/Ti ratios of 4000 produced an order of magnitude increase in catalytic activity compared to Al/Ti ratios of 1000. The authors did not comment on the leaching of the metal precatalyst from the surface with the addition of MAO.

Bortolussi et al. patented a method to immobilize Group IV metal precatalysts by first contacting a silica surface with *n*BuLi and subsequently reacting 6,6-dimethylfulvene to the surface (Scheme 9.4) [11]. The result is a supported cyclopentadienyl ring that can be used to tether $ZrCl_4 \cdot 2THF$ to produce the supported metal. Subsequently, an additional reaction with cyclopentadienyllithium pro-

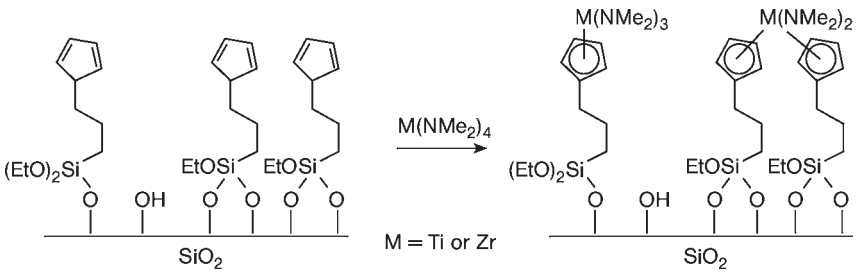

Scheme 9.3

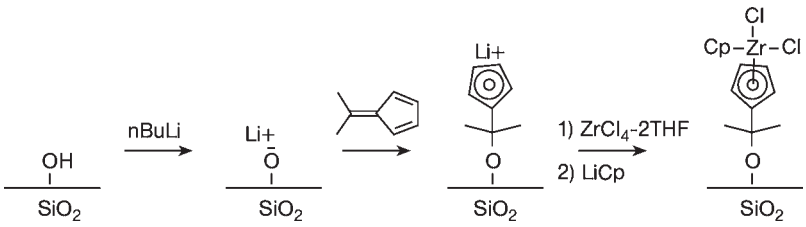

Scheme 9.4

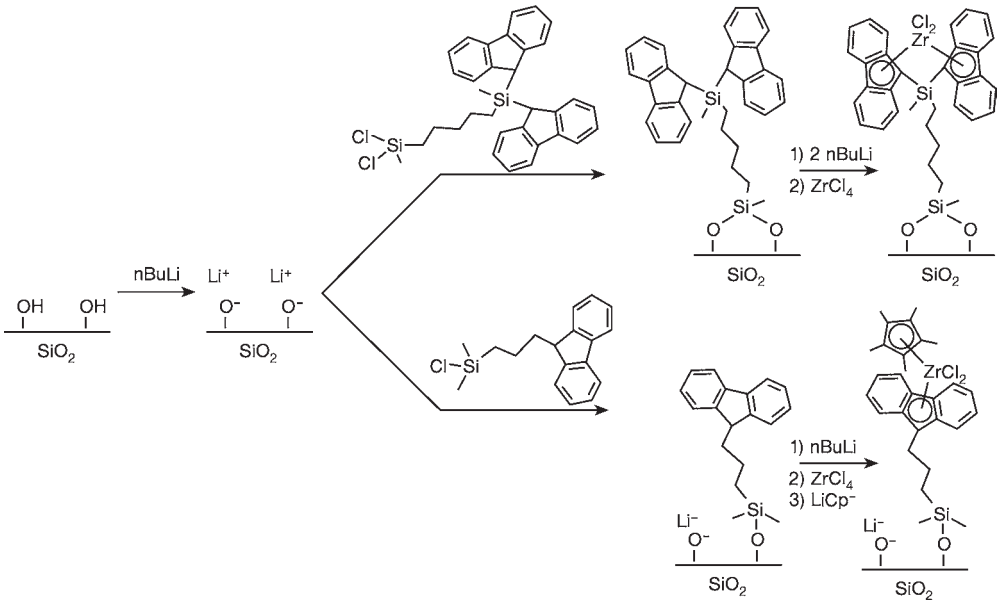

Scheme 9.5

duces the tethered metallocene precatalyst. When TIBA and *N,N*-dimethylaluminum tetra(pentafluorophenyl)borate were added as activators, the supported zirconocene was able to produce polyethylene with a productivity of 3580 g PE g^{-1} catalyst.

Alt and coworkers synthesized immobilized mono- and bis-fluorenyl zirconocene precatalysts on polysiloxane micro gels and silica (Scheme 9.5) [12]. These authors synthesized the fluorenyl-based precatalysts on silica by first immobilizing a fluorenyl-based chlorosilane on temperature-pretreated (600 °C) silica. The addition of *n*BuLi resulted in a deprotonated ligand for metalation with either Cp*$ZrCl_3$ or $ZrCl_4$. When activated by MAO, the silica-based zirconium catalysts produced PE with higher molecular weights and reduced reactor fouling compared to the homogeneous catalysts. However, the activities of the silica-based catalysts were much less than the homogeneous catalysts.

Lee and Oh tethered bis(cyclopentadienyl)zirconium dichloride complexes having acid-labile acetal, ketal, or *tert*-butyl ether substituents on the Cp ligand

through reaction of the Cp substituents and a dehydroxylated silica surface (heated at 800 °C for 15 h under vacuum) [13]. The methodology used in this study involved reaction of the ether functional group to the dehydroxylated silica surface in order to tether the cyclopentadienyl ligand (Scheme 9.6). However, leaching was hypothesized with this method. The immobilized precatalyst containing the *tert*-butyl ether substituent on the Cp group produced PE, with the addition of MAO, having activities of 6.8×10^5 g PE mol^{-1} Zr h^{-1} bar^{-1}.

Herrmann and coworkers reported the immobilization of $CpZr(NMe_2)_3$ precatalysts on $Si(Ind)(CH_3)_2Cl$ and 1,1,1,3,3,3-hexamethyldisilazane (HMDS)-modified silica surfaces [14]. The HMDS was added after the $Si(Ind)(CH_3)_2Cl$ to reduce possible side reactions with the transition metal and the silica support by capping surface silanols. From the report, the authors indicated that capping of the silanols produces a support material with mainly monografted complexes, which produces a less-active catalyst due to the deactivation by leaching with lower polydispersities for the polymerization of ethylene when activated by MAO. When the precatalyst was produced with silanols present (without addition of HMDS), more bigrafted precatalysts were formed (with the metal bonded to the indenyl ligand and the surface silanols) which produced more stable, but less-active catalysts when activated by MAO for ethylene polymerization (Scheme 9.7). Thus, Herrmann and coworkers determined that HMDS is important to prevent side reactions of the precatalyst in order to produce "single-site" polymerization precatalysts. However, the stability of the precatalysts using the capping method is a major disadvantage. Other reports by Lee and coworkers are available on the immobilization of $Cp(Ind)ZrCl_2$ tethered precatalysts for the polymerization of ethylene [15, 16]. In these reports, the cyclopentadiene ligand was tethered to the surface using either hexamethyltrisiloxane or pentamethylene spacers (Scheme 9.8). Afterwards, *n*BuLi and $IndZrCl_3$ were added to produce the tethered precatalyst. The ethylene polymerization results showed that the homogeneous $Cp(Ind)ZrCl_2$ was over four-fold more active than the corresponding tethered versions, when activated by modified-methylaluminoxane (MMAO) at 40 °C. At 70 °C the activities were almost as large as those produced from $Cp(Ind)ZrCl_2$, although leaching of the zirconium from the surface was not investigated.

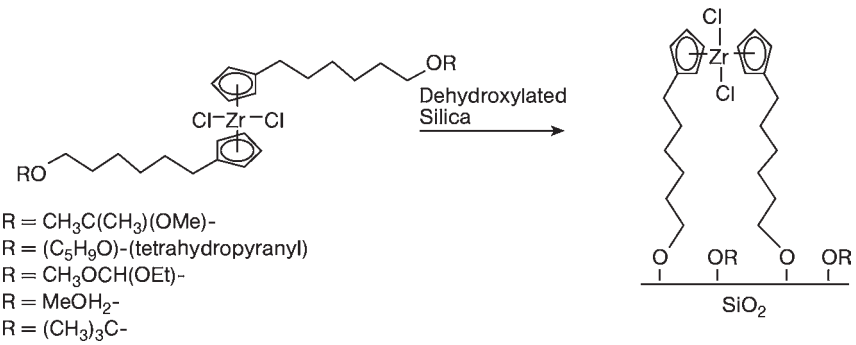

Scheme 9.6

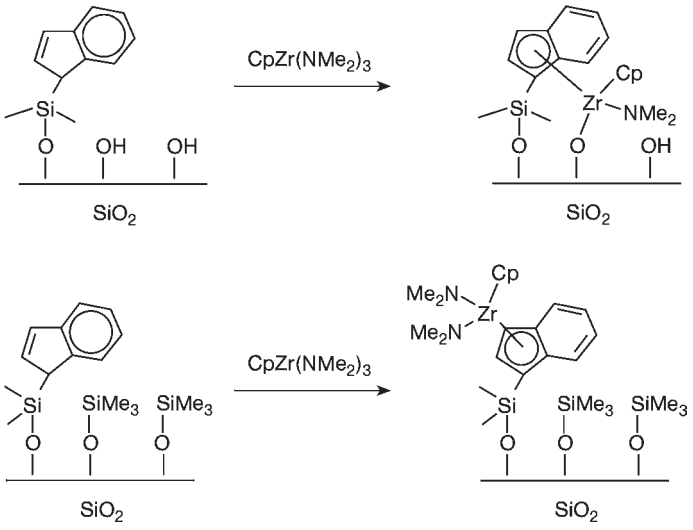

Scheme 9.7

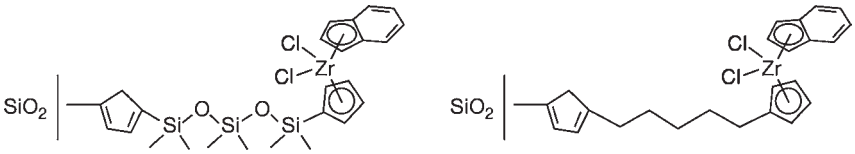

Scheme 9.8

Suzuki and coworkers used a method to covalently tether isospecific ansa-zirconocene catalysts on silica for the polymerization of propylene [17]. The authors immobilized three types of zirconocene precatalyst: (i) formation of an ansa-zirconocene with a chlorosilane functionality to react with surface silanols; (ii) pretreatment of the silica surface with Me_3SiCl before addition of the ansa-zirconocene with a chlorosilane functionality; and (iii) reaction of the surface silanols with $Me_2(Cl)Si(CH{=}CH_2)$, and used these olefins to couple with the ansa-zirconocene via a hydroboration technique. As indicated from the report, the order of better to worst activity for the various techniques, when activated by MAO, was (iii) > (ii) > (i).

Collins and coworkers used hydrosilylation chemistry to tether various zirconocenes to the silica surface (Scheme 9.9) [18]. In these studies, two different synthetic strategies were employed: (i) treating silica with Me_2SiHCl and then a zirconocene with a $(CH_2{=}CH)SiMe$ bridge; or (ii) treating silica with $Me_2(Cl)Si{-}R$ (where R is an alkyl chain with a terminating olefin), and coupling this supported olefin to a synthesized ansa-metallocene complex containing a silicon hydride. As reported, various supported precatalysts can be formed with either indenyl or cyclopentadienyl ligands with various tethering lengths from the silica surface to the metallocene center. The longer the length of the tether, the more active the catalyst (when activated by MAO for polymerization of propylene). However,

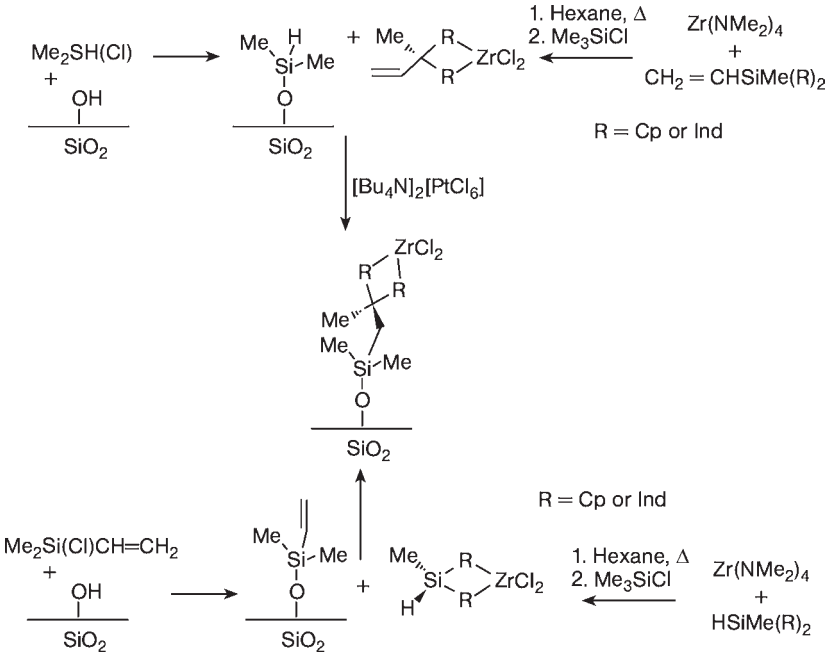

Scheme 9.9

leaching of the catalysts by MAO was determined at elevated temperatures (up to 50% leached at 70 °C), but leaching was minimized to ca. 10% when lower temperatures were employed.

9.2.2
Surface-Tethered Constrained-Geometry Precatalysts

As mentioned above, Soga and coworkers used an aminopropylsilyl-modified silica support as a coupling group for Cp*$TiCl_3$ precatalysts [5]. Based on these findings, Pakkanen and coworkers developed a methodology to support constrained-geometry catalysts by using aminopropyl-modified silica as a coupling group to the cyclopentadienyl ligand (Scheme 9.10) [19, 20]. The first report from Pakkanen and coworkers involved deprotonation of the amines on the silica with *n*BuLi [20]. Subsequently, either $Me_2Si(C_5Me_4H)Cl$ or $MeHSi(C_5Me_4H)Cl$ was added, which formed LiCl as a side product. The materials were characterized by ^{1}H, ^{13}C and ^{29}Si solid-state NMR, as well as FTIR spectroscopies.

The results indicated that *n*BuLi not only deprotonates the amines, but also reacts with siloxane bridges and unreacted ethoxy groups from the aminosilane coupling agent. In order to prevent the side reaction associated with *n*BuLi, the authors attempted the reaction of either $Me_2Si(C_5Me_4H)Cl$ or $Me(H)Si(C_5Me_4H)Cl$ directly with the amine groups on the silica surface [19]. However, when using this method the HCl formed not only interacted with the amine groups to form a

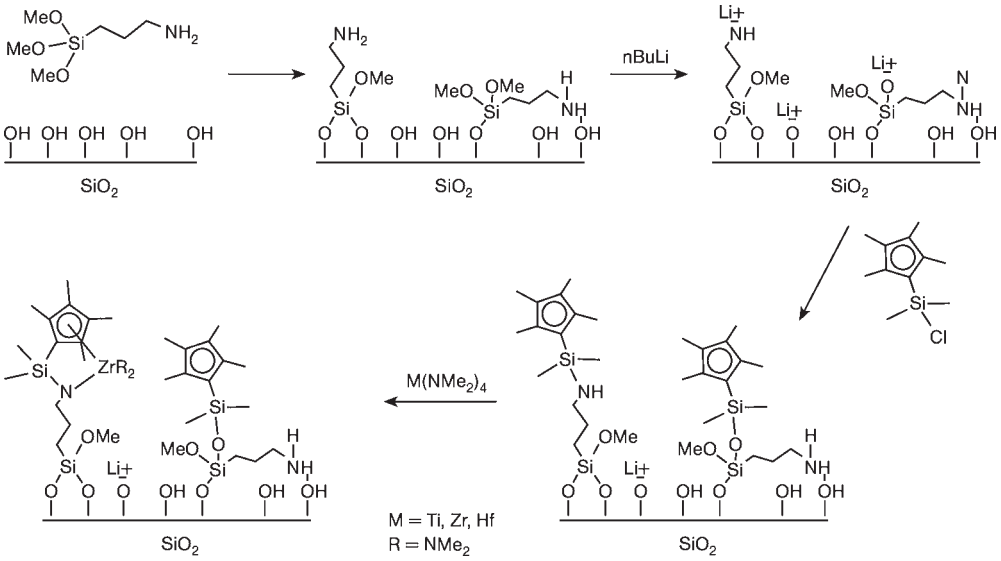

Scheme 9.10

protonated salt, but the results also indicated cleavage of the Cp–Si bond. Due to such cleavage, Pakkanen and coworkers synthesized immobilized Zr-, Hf-, and Ti-inspired constrained-geometry catalysts (CGCs) by using the *n*BuLi treatment of the aminopropyl-modified silica for the addition of $Me_2Si(C_5Me_4H)Cl$ or $Me(H)Si(C_5Me_4H)Cl$ [21–23]. All three Group IV metal CGCs were compared for ethylene polymerization when attached to $Me_2Si(C_5Me_4H)Cl$-modified aminosilica [21]. When the tethered CGC precatalysts were activated by MAO for the polymerization of ethylene, the activities of the metal were better for Zr-CGC and Hf-CGC rather than for Ti-CGC. In fact, very little PE was recovered when the heterogeneous (Cp*)Ti-CGC was used. However, the heterogeneous Zr-CGC was over twice as active as the Hf analogue. The Ti-CGC was thought to be inferior due to the formation of a multisited material, with some inactive metal centers, which was much less active than either the Zr or Hf versions. However, the authors did not compare the tethered CGCs to the homogeneous analogue [21]. Nor were the structures of the immobilized CGCs verified in the report, which led to speculation for the reasons of metal-center deactivation. When $Zr(NMe_2)_4$ was added to $Me_2Si(C_5Me_4H)Cl$- or $Me(H)Si(C_5Me_4H)Cl$-modified aminosilica, only 33% and 23% of the amine sites, respectively, were loaded with Zr atoms [23]. By comparison, when $Hf(NMe_2)_4$ was added to $Me_2Si(C_5Me_4H)Cl$- or $Me(H)Si(C_5Me_4H)Cl$-modified aminosilica, only 24% and 21% of the amine sites, respectively, were loaded with Hf atoms [22]. Although the synthesis of various tethered gave materials useful for the polymerization of ethylene, much of the surface was not used by the metal atoms. Thus, in order to obtain single-site catalysts using this methodology, the metal/amine ratio should be much closer to 1.0.

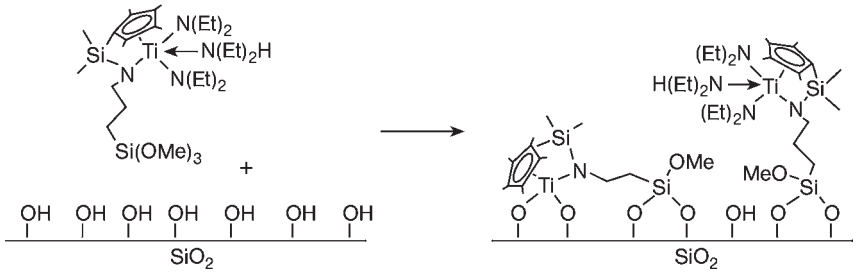

Scheme 9.11

Eisen and coworkers developed a method to produce a homogeneous, tetherable titanium constrained-geometry catalyst for applications in the field of heterogeneous olefin polymerizations (Scheme 9.11) [24]. The pretethered homogeneous species showed fairly high activity for the polymerization of ethylene, when activated by MAO. However, once immobilized on either SiO_2 or Al_2O_3, the activities decreased for ethylene polymerizations. The advantages of this method, compared to other grafting methods described above, are the following: (i) the amine to metal ratio is 1.0; (ii) the lack of *n*BuLi treatment prevents the creation of multiple types of sites via action of this reagent; (iii) the reaction between the surface of the support and the alkoxy silane groups on the complex evolves methanol which does not remove the Cp ligands from the metal center, but still allows for attachment with the support material; and (iv) the tethered CGC involves a one-step reaction between the immobilizable homogenous titanium constrained-geometry precatalyst and the support material. Although this method has many advantages, the main disadvantage involves the interaction between the Ti-CGC and the surface silanols through an amine elimination reaction. This interaction caused a decrease in activity due to a creation of fraction of presumably inactive sites formed on the surface [24].

Jones and coworkers employed a method to create "site-isolation" on silica by using an amine protection/deprotection strategy to space the amine groups before the metal precatalyst was added (Scheme 9.12) [25–27]. Multiple surface manipulations were used to achieve amine-separation on the surface, including: (i) synthesis of the protected aminopropylalkoxysilane with either a trityl or benzyl group; (ii) reaction of the protected amine to the silica surface; (iii) capping silanols with HMDS to reduce the possibility of amine–silanol interactions as well as metal–silanol interactions; (iv) hydrolysis of the protecting group with HCl(aq)/MeOH to form the "spaced" amine groups on the surface; and (v) a final capping step with HMDS to cap silanols possibly formed during the final hydrolysis step. The protection/deprotection materials were characterized by FT Raman spectroscopy [26–28], ^{13}C and ^{29}Si CP/MAS NMR [26, 27], potentiometric titration [27], thermogravimetric analysis (TGA) [26–28], steady-state/lifetime fluorescence spectroscopy [27, 28], and X-ray diffraction (XRD) [27], which together indicated that the protecting groups are cleaved in virtually quantitative yield without destruction of the mesoporous oxide framework.

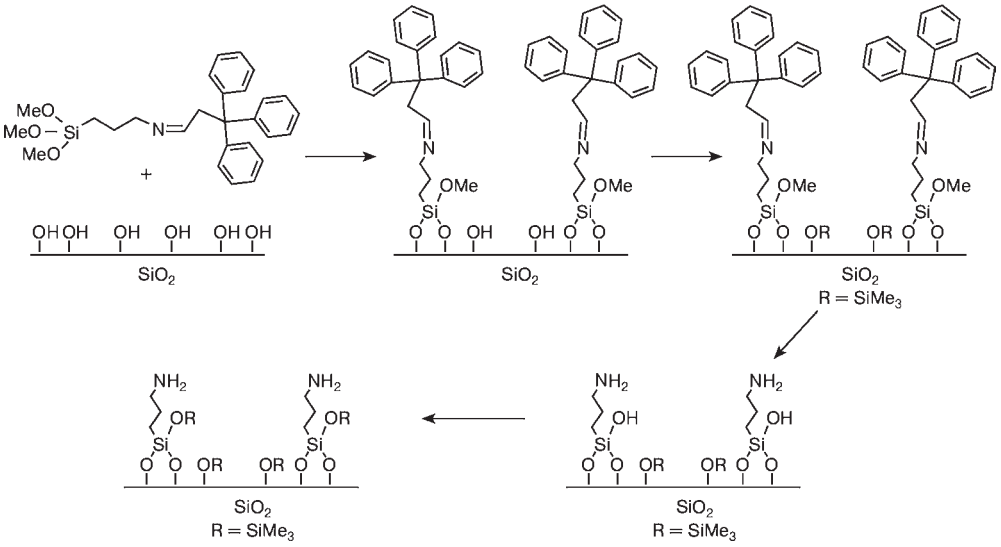

Scheme 9.12

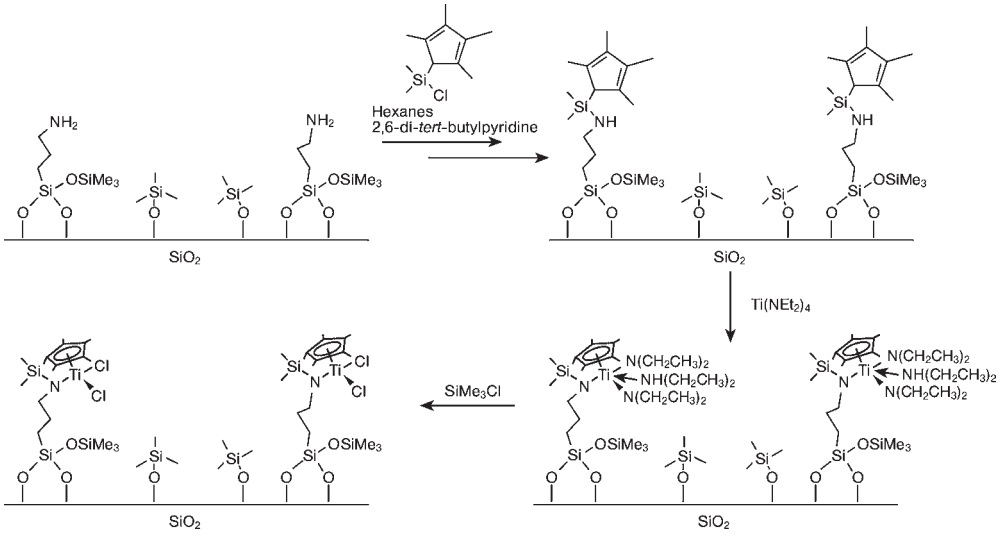

Scheme 9.13

McKittrick and Jones employed the trityl-protection/deprotection strategy for the formation of "site-isolated" Group IV CGC-inspired complexes on mesoporous SBA-15 (Scheme 9.13) [29–32]. Using the protocol to synthesize trityl-spaced amines on the silica surface, the authors added $Me_2(Cl)Si(C_5Me_4)$ along with 2,6-di-*tert*-butylpyridine as a proton sponge to trap the HCl evolved. By addition of

$Ti(NEt_2)_4$ and exchange of the diethylamino-ligands for Cl-groups (with Me_3SiCl), a trityl-spaced titanium CGC inspired complex was formed on the surface for use as a heterogeneous olefin polymerization precatalyst. The tethered CGC was activated with either MAO or the combination of tris(pentafluorphenyl)borane [33] and a trialkylaluminum complex (TMA or TIBA). As reported, when using the trityl-protection/deprotection strategy to produce "site-isolated" amine sites on SBA-15, virtually quantitative addition of the Ti complex to the amine sites can be achieved (nearly 1 for the Ti/N ratio). As evidenced by the reported data, using the trityl-protection/deprotection method, the productivity of the titanium GCG, when activated by an alkylaluminum/borane cocatalyst, was approximately five-fold greater than using a preformed CGC complex reacted directly to silica [24], and 10- to 15-fold greater than using the traditional route of synthesizing supported CGC sites on unprotected aminosilicas [19–23] for the polymerization of ethylene [29]. The same authors also determined that using a traditional approach [19] to produce tethered CGC-inspired catalysts (when activated by an alkylaluminum/borane cocatalyst) produces an inactive catalyst for the copolymerization of ethylene-norbornene [31]. However, if the "spacing" protocol of the aminosilica is employed, the incorporation of both norbornene and ethylene is seen in the polymer, thus improving the properties of the tethered organometallic catalysts through spatial separation.

The aforementioned studies performed on tethered Group IV olefin polymerization precatalysts were mainly focused on different methods to tether various metal complexes to the solid support. However, leaching experiments of such tethered precatalysts were generally absent in most reports. It is commonly asserted that tethering the precatalyst can combine the polymerization properties of both traditional heterogeneous and homogeneous catalysts, with a special advantage being preventing reactor fouling. Although these goals have been emphasized in many research investigations, leaching experiments and the molecular-scale characterization of the metal are absent in many cases. If more were known about the "true" catalytic sites on the surface, a possible implementation in industrial-scale reactors might be accomplished as more efficient catalysts could be synthesized.

9.2.3
Tethering Late Transition Metal Precatalysts

Although not as common as Group IV metal precatalysts for olefin polymerizations, late transition metal precatalysts, such as Ni(II), Fe(II) and Co(II) complexes, have received increasing attention due to their ability to produce, in some cases, branched PE.

Mendez Llatas and coworkers reported the synthesis of α-diimines tethered to a silica support using either one or two trimethylsiloxypropyl groups combined with surface silanols (Scheme 9.14) [34]. The resulting tethered α-diimine was metallated with a dibromo(dimethoxyethane)nickel(II) complex to produce the

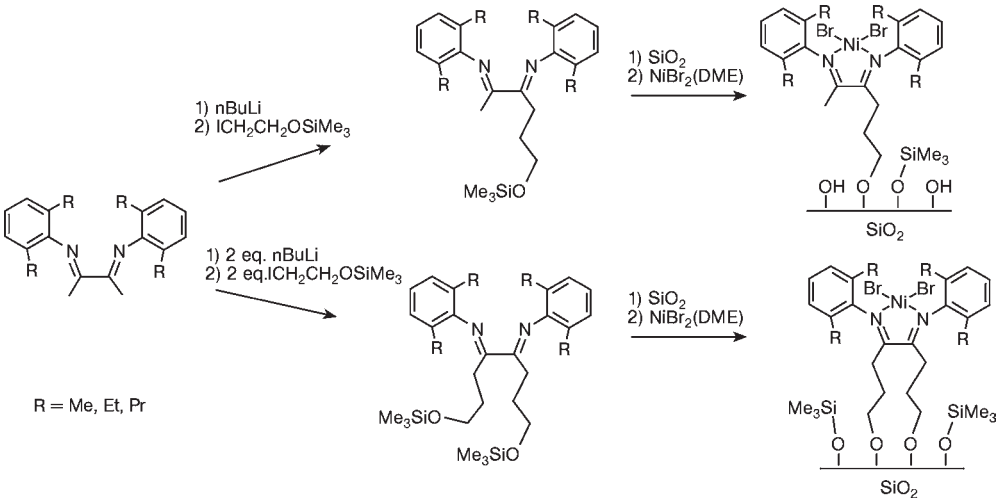

Scheme 9.14

tethered Ni(II) precatalyst. However, as reported, only 40–80% of the tethered ligands were metallated [based on inductively coupled plasma (ICP) analysis]. The precatalysts were activated with MAO to produce branched PE with productivities ranging between 10 and 100 kg PE mol^{-1} Ni bar^{-1} h^{-1}.

Brookhart and coworkers have synthesized Ni(II) α-diimine complexes with a hydroxyl functionality to tether to trimethylaluminum-passivated silica [35–37]. Once tethered, the Ni(II) precatalyst can be activated with ethylaluminum sesquichloride or methylaluminum dichloride to produce PE, with productivities of 375 kg PE g^{-1} Ni h^{-1} and PDIs of between 3 and 4 using an Al/Ni ratio of 700 [35]. More recently, Schrekker et al. optimized the tethered Ni(II) α-diimine precatalysts for the polymerization of ethylene by monitoring the affects of ethylene pressure, Ni(II) loading, temperature, and calcination temperature of the silica [36]. The results indicated the optimum conditions for this system to be an ethylene pressure of 50 bar, a reaction temperature of 80 °C, a 3 wt.% Ni(II) loading, and a silica calcination temperature of 500 °C.

Herrmann and coworkers reported the synthesis of tethered bis(imino)pyridyliron(II) complexes on $SiMe_2H$-modified silica via hydrosilation using different spacer lengths (allylic, butenylic, and pentenylic spacers) between the metal center and the silica support [38]. As indicated in that report, the tethered Fe(II) complexes may be activated with MAO or MMAO to produce catalysts with higher activities at 80 °C than their homogeneous analogues. In addition, as the spacer length increased from the allyl-modified catalyst to the butenyl- or pentenyl-modified catalyst, the productivity increased without observation of reactor fouling. These results were very similar to the "site-isolation" effects of CGC-inspired complexes previously discussed [29–32]. However, a disadvantage was that no propylene could be polymerized with these tethered Fe(II) catalysts.

Kim and coworkers employed a different route to tether bis(imino)pyridyl-iron(II) and -cobalt (II) complexes on silica by synthesizing a complex with the immobilizable ethoxysilyl- or allylic linker at the para position on the central pyridyl ring to immobilize directly to the silica surface or to a 1,1,3,3-tetramethyldisilazane-modified silica surface, respectively (Scheme 9.15) [39, 40]. In one report, a nine-step synthesis was described which produced a tethered Fe(II) or Co(II) precatalyst that, when activated by MAO, showed a 100-fold decrease in activity compared to the homogeneous analogues [39]. In a subsequent report, Kim and coworkers suggested that the decrease in activity from the homogeneous to the heterogeneous catalysts was primarily due to the reduced number of active centers from the diffusion limitations of MAO within the pores of the silica gel [40].

Recently, Zheng et al. reported a method to tether bis(imino)pyridyl iron(II) precatalysts on silica with one or two reactive linkers in order to increase the precatalyst loading on the support (Scheme 9.16) [41]. The authors tethered the bis(imino)pyridyl ligand and then added $FeCl_2 \cdot 4H_2O$ as the metal source to obtain loadings four times greater than reported previously [38–40]. When activated by MMAO, productivities of approximately 1000 kg PE mol^{-1} Fe bar^{-1} h^{-1} were observed. Again, the tethered versions produced catalysts with much less activity than the corresponding homogeneous analogue. However, the tethered precatalysts exhibited long lifetimes and produced polymers with higher molecular weights than did the homogeneous complexes.

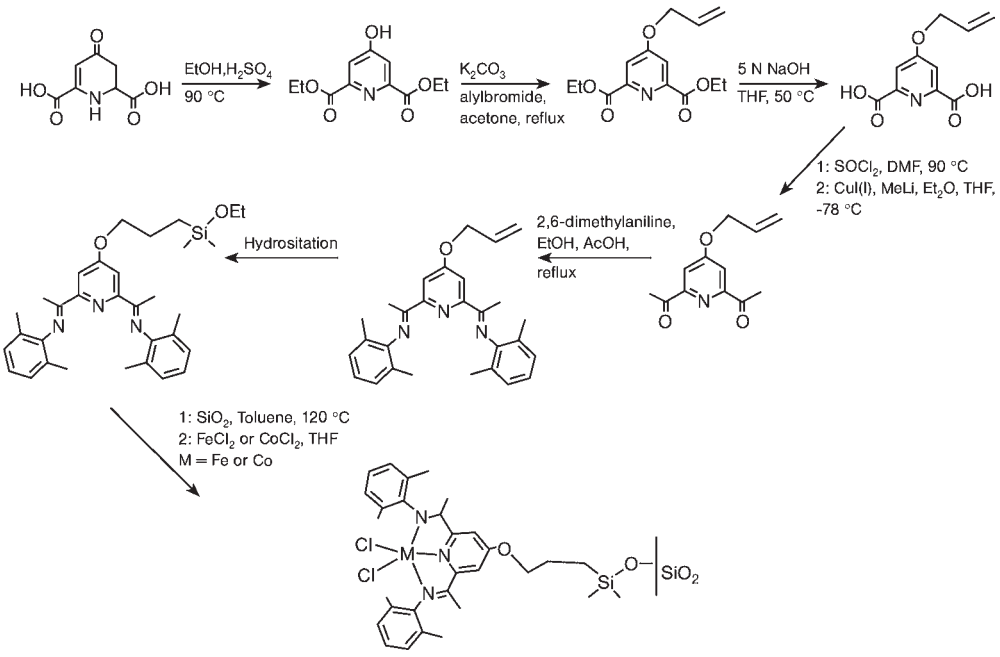

Scheme 9.15

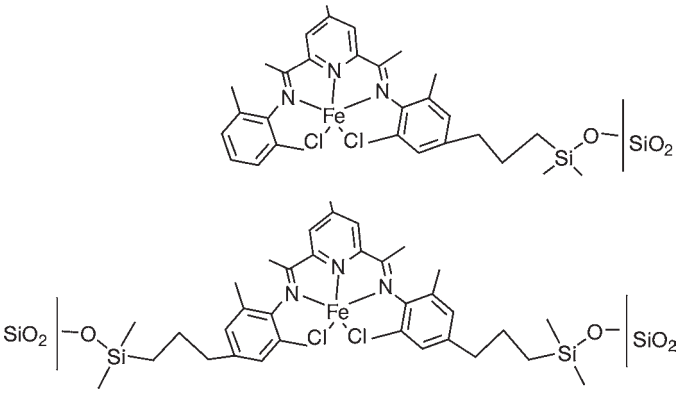

Scheme 9.16

Research into the tethering of late transition metal olefin polymerization precatalysts has led to the possibility of implementing this technology into an industrial-scale slurry-phase reactor as "drop-in" technology [36]. However, the key disadvantages with many tethered late transition metal precatalysts are: (i) the relatively low loading on the support; (ii) the reactor fouling caused from leaching; and (iii) the substantial decrease in activity when the metal is tethered compared to the homogeneous analogue. The synthesis of such catalysts also requires many steps, which are economically unfavorable, as well as time-consuming.

9.3
Tethering Cocatalysts

Tethering cocatalysts on the support is a more versatile method to produce heterogeneous olefin polymerization catalysts, as various precatalysts can be used with a single tethered cocatalyst support. As the predominant source of most of these investigations is in the patent literature, it is sometimes difficult to determine the exact claim or synthesis procedure used with these tethered cocatalysts. For example, findings in this field were first reported by Turner, whereby various borane cocatalysts were allegedly tethered to silica [42]. However, the patent reports only the synthesis of poly(styrene), poly(p-methylstyrene), and poly(vinylbenzene) -supported boranes, and so will not be discussed at this point. Likewise, Fritze et al. reported the synthesis of tethered boranes on silica using either chlorosilane or ethoxysilane reactive substituents [43]. However, as deduced from the patent, the silica-tethered boranes were not used as cocatalysts for olefin polymerizations. Instead, a homogeneous CGC (dimethylsilanediylbis(2-methyl-indenyl)zirconium dimethyl) was mixed with the homogeneous borane cocatalyst, which led to the productivities reported. Alternatively, Hinkouma and coworkers reported the synthesis of silica-tethered borates by using surface-reactive chlorosilane linkers [44]. In these patents, multiple types of tethered borate were synthesized and used

as cocatalysts for the activation of metallocenes with triisobutylaluminum present.

Further studies in this area were reported by Carnahan and coworkers [45, 46], whereby the tetherable borane cocatalysts were created with a protic (mainly an alcohol) substituent that is reactive with passivated silica (passivated with either a trialkylaluminum and/or a silane with Si–H groups; see Scheme 9.17). As evidenced by diffuse reflectance infrared Fourier transform spectroscopy (DRIFTS), the Si–H bond was noticeable around 2178 cm^{-1} when $PhSiH_3$ was reacted with the silica surface (which evolved hydrogen gas during the reaction). After $[NHMe_2Ph]^+[(C_6F_5)_3B(C_6H_4\text{-p-OH})]$- had been added, which also resulted in the evolution of hydrogen gas, the Si–H peak was found at 2190 cm^{-1} from the DRIFTS spectra. In addition, the methyl groups in the anilinium counterion were seen at 48.5 ppm in the ^{13}C CP/MAS spectrum, indicating reaction of the borate with the surface. The authors reported using 200 mg of the silica-tethered anilinium borate complex to activate 10 mg (31 mmol) of a titanium CGC to produce 7.14 g of PE after 10 min at 75 °C [45]. The PDI of the PE was determined as 2.47.

Other reports involved the synthesis of tethered cocatalysts (such as borates) via a method using protic substituents from the boron center that react with either MAO- or trialkylaluminum-passivated silica surfaces (Scheme 9.18) [47]. For example,

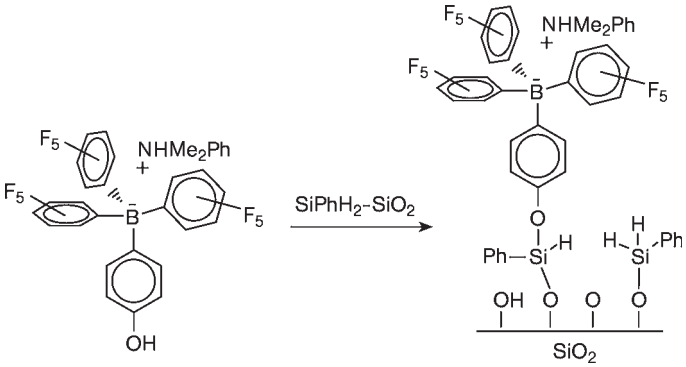

Scheme 9.17

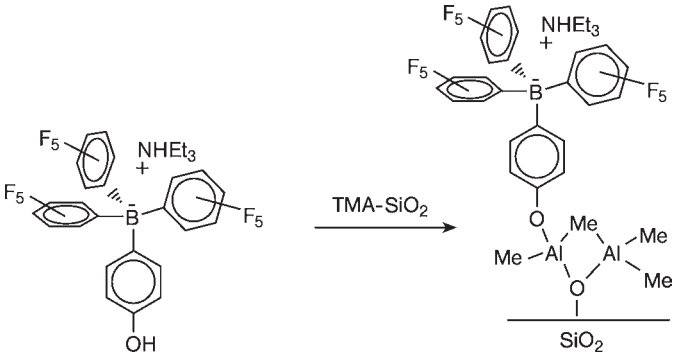

Scheme 9.18

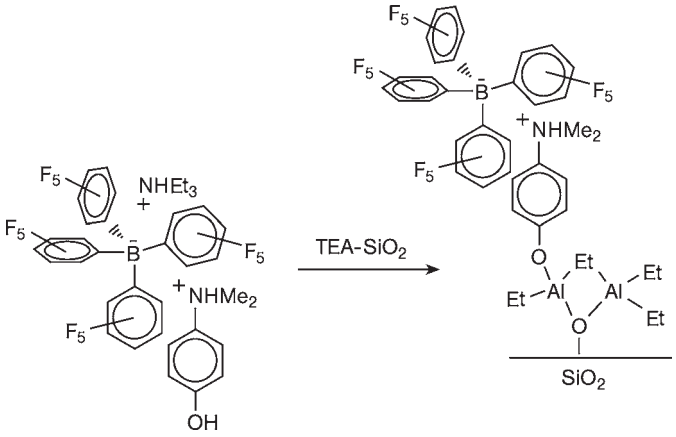

Scheme 9.19

triethylammonium tris(pentafluorophenyl)(4-hydroxyphenyl)borate was reacted with an alkylaluminum-passivated silica material to activate [(*tert*-butylamido)(dimethyl)(tetramethyl-η^5-cyclopentadienyl)silane] dimethyl titanium using a slurry polymerization reaction of ethylene or the copolymerization of ethylene/1-octene and ethylene/1-butene. The resulting tethered cocatalyst was efficient enough to produce very active titanium catalysts for the various olefin homo- and copolymerizations. Another method reported by Jacobsen and coworkers involved the synthesis of $[(p\text{-}HOC_6H_4)B(C_6F_5)_3][NHMe(C_{18-22}H_{37-45})_2]$, which was reacted with triethylaluminum and the titanium precatalyst before reaction with triethylaluminum-passivated silica [48]. The borate synthesized with the long-chain ammonium salt was found to be two orders of magnitude more soluble in toluene than the triethylammonium version.

Other methods to create tethered borates have been reported in which the reaction between the cocatalyst and the surface occurs with a hydroxyl functionality from the ammonium salt, $[HOC_6H_4NMe_2H]^+[B(C_6F_5)_4]^-$ (Scheme 9.19), with trialkylaluminum-passivated silica [49], or by tethering the ammonium salt directly on silica [50], using $Me_2NC_6H_4Si(OMe)_3$, and then reacting lithium tetra(fluorophenyl) borate after the amine is protonated with HCl.

In the majority of these inventions, a trialkylaluminum-passivated silica material was the basis of the tethered cocatalyst. It is very difficult to deduce from the patents the exact nature of the immobilized cocatalysts, where often 3-coordinate aluminium is shown, as trialkylaluminums tend to form 4-coordinate interactions with the surface [51]. Thus, the structure of the tethered groups is unknown in many cases when using a trialkylaluminum-passivated silica surface.

9.4 Molecular Models

As mentioned above, it is difficult to synthesize tethered precatalysts due to the multiple types of side reactions that are possible. Very few reports have focused

on the interaction between the metal and the surface, on how the surface affects the catalyst's performance during polymerization, or even the stability of the precatalyst on the surface. One way to attempt to explain these interactions is by modeling the reactions using silsesquioxanes, homogeneous model compounds, or flat surfaces, to replicate the interactions of tethered precatalysts on silica particles. The use of such model compounds might help to optimize tethered precatalyst systems by understanding how each step affects the resulting precatalyst.

Silsesquioxanes have been used by Duchateau and coworkers as model compounds for chemically tethered olefin polymerization catalysts (Scheme 9.20) [52, 53]. Initially, Severn et al. studied the synthesis of (c-C_5H_9)$_7Si_8O_{12}CH_2$Flu(H) via two different methods. The first method involved the reaction between (c-C_5H_9)$_7Si_7O_9(OH)_3$ with $(EtO)_3SiCH_2$-9-Flu(H). In addition, a two-step reaction was studied by first reacting (c-C_5H_9)$_7Si_7O_9(OH)_3$ with Cl_3SiCH_2Cl (with triethylamine present in excess) and subsequently reacting fluorenyllithium. From this study, it was apparent that the silylether reaction with the silsesquioxane was much slower than the two-step reaction. However, the two-step reaction involved the formation of ammonium salts that must be removed from the support if a porous silica material is used. It was also determined that the electron-withdrawing nature of the silsesquioxane produced a tethered fluorenyl complex with more acidity than Me-9-Flu(H), indicating that an electronic effect is noticeable with a methylene spacer between the silsesquioxane and the fluorenyl ligand. In a later report, the authors determined that if the linker between the fluorenyl ligand and the silsesquioxane is changed, the ability to lithiate the fluorenyl complex is greatly hampered [53]. For example, if the ligand is bound directly to the silsesquioxane

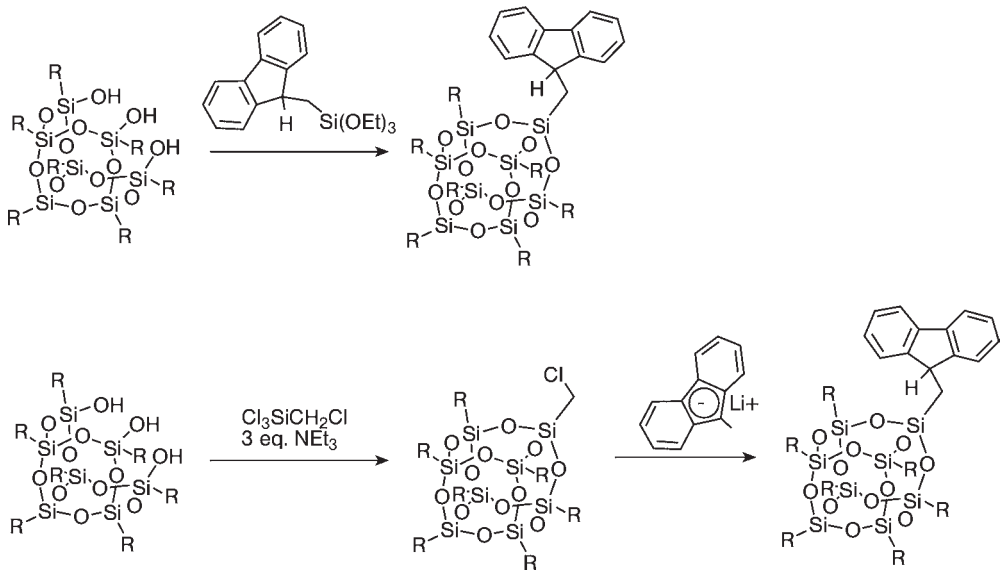

Scheme 9.20

without a spacer, there were multiple side products that were not identified. However, if a methyl- or propyl-spacer was used, then formation of the fluorenyl anion was accomplished. Another key finding using this model system was the reaction between $(c\text{-}C_5H_9)_7Si_7O_9(OH)_3$ and $Cp''[FluCH_2Si(OEt)Me_2]ZrCl_2$ resulted in the formation of the corner-capped silsesquioxane with $ZrCp''$ and the loss of a fluorenyl group [53]. Thus, as silica has many surface silanols it is likely that the reaction between a preformed metal complex and the surface would result in a similar effect, which was suggested to be a possible side reaction in the tethered CGC studies conducted by Eisen and colleagues [24].

Another model complex reported in the literature involves the formation of polysiloxane-bridged dinuclear metallocenes (Scheme 9.21) [15, 54]. These reports focus on the steric and electronic effects of the length of the polysiloxane bridge between the metal centers. From the experimental results, it is evident that as the metallocenes are spaced further away, the activity of the catalyst increases; however, the molecular weight of the resulting PE decreases. It was determined that if the catalytic active sites are close together, the activity decreases due to the limited access of the monomer, while the molecular weight increases due to a reduction of the β-hydrogen elimination pathway. It is interesting to compare these results with the site-isolated constrained-geometry inspired investigations conducted by McKittrick and colleagues [29, 31, 32]. In the latter studies, the activity corresponded well with the model compounds reported by using polysiloxane bridges. For example, although as the precatalysts were separated the activities were seen to increase, the only difference was in the molecular weights of the PE produced from densely loaded CGCs on silica. In fact, the molecular weights actually decreased as the distance between the metal center decreased. This was considered most likely to have resulted from the difficulty in creating uniform single-site precatalysts on silica surfaces. Thus, model compounds may serve as important new avenues for the study of supported olefin polymerization catalysts, although much additional investigation is needed before these systems can be reliably used to optimize tethered precatalytic systems.

Recently, the tethering of bis(imino)pyridyl iron(II) olefin polymerization precatalysts on a flat surface has been reported as a model support [55]. For example, Han et al. used multiple surface reactions to tether these precatalysts on a Si(100) wafer, and X-ray photoelectron spectroscopy was then used to determine the loading of the ligand and iron(II) precatalysts, which was virtually quantitative.

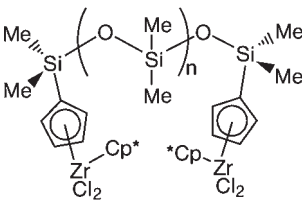

n = 1, 2, or 3

Scheme 9.21

Scanning electron microscopy was subsequently used to image the PE films after polymerization, and this showed the formation of PE "islands" caused by the PE shrinking when it was removed from the toluene solution. This is the first report of a tethered homogeneous olefin polymerization precatalyst on a flat surface.

9.5 Conclusions

As mentioned above, a successful tethered precatalyst must possess the properties of both heterogeneous and homogeneous precatalysts. The existing literature mainly describes the various strategies available to tether either Group IV or late transition metal precatalysts to supports, with these new precatalysts being screened for polymerization activity and selectivity. It is often suggested that the motivation to design catalysts in this manner is to prevent reactor fouling and to control the polymer's morphology. However, traditional heterogeneous precatalysts, with physisorbed or chemisorbed organometallic catalysts on oxide or other surfaces, can perform similarly, quite often with lower catalyst-related costs. Thus, the question might be asked – why tether the precatalyst when traditional heterogeneous precatalysts function satisfactorily?

Hence, the real motivation for tethering precatalysts to oxide surfaces must revolve around the possibility of: (i) completely preventing leaching in slurry-phase processes; and/or (ii) developing truly well-defined, single-site catalysts that are amenable to detailed structural characterization. Unfortunately, it is exceedingly rare for research groups to probe catalyst leaching or to characterize the structure and bonding of the metal center in tethered precatalysts, and consequently this area of investigation will continue to stagnate until efforts are expanded beyond the simple "synthesize and test" paradigm.

This analysis may suggest that tethering precatalysts is solely for academics, as the procedure is very tedious and expensive. However, the combined advantages of tethering precatalysts may outweigh the increased catalyst costs and arduous synthetic steps in some applications, such as slurry-phase polymerization. Indeed, in principle, correctly designed tethered precatalysts could combine the benefits of homogeneous and traditional heterogeneous olefin polymerization precatalysts by: (i) preventing reactor fouling; (ii) preventing metal–metal deactivation, as seen in homogeneous systems; (iii) enhancing molecular weights; (iv) controlling the polymer morphology; (v) reducing cocatalyst requirements; and (vi) forming a stable complex on the surface to prevent metal leaching in slurry-phase reactions.

In this chapter, recent advances in the tethering of either Group IV or late transition metal precatalysts, as well as tethered olefin polymerization cocatalysts, have been briefly outlined. However, based on the published or patented literature, many further investigations must be conducted with regards to the formation of single-site olefin polymerization precatalysts on solid supports. In particular, emphasis must be placed on the complete characterization of the supported prec-

atalysts and catalysts, coupled with the generation of molecular-level structure–property relationships for these materials.

References

1 (a) J.C.W. Chien, *Top. Catal.* 1999, *7*, 23; (b) E.Y.-X. Chen, T.J. Marks, *Chem. Rev.* 2000, *100*, 1391; (c) G.G. Hlatky, *Chem. Rev.* 2000, *100*, 1347; (d) J.R. Severn, J.C. Chadwick, R. Duchateau, N. Friederichs, *Chem. Rev.* 2005, *105*, 4073.

2 (a) K. Soga, H.J. Kim, T. Shiono, *Macromol. Chem. Phys.* 1994, *195*, 3347; (b) K. Soga, T. Arai, H. Nozawa, T. Uozumi, *Macromol. Symp.* 1995, *97*, 53; (c) K. Soga, *Macromol. Symp.* 1995, *89*, 249; (d) K. Soga, *Macromol. Symp.* 1996, *101*, 281; (e) J.H.Z. dos Santos, H.T. Ban, T. Teranishi, T. Uozumi, T. Sano, K. Soga, *J. Mol. Catal. A* 2000, *158*, 541; (f) J.H.Z. dos Santos, H.T. Ban, T. Teranishi, T. Uozumi, T. Sano, K. Soga, *Appl. Catal. A* 2001, *220*, 287; (g) J.H.Z. dos Santos, T. Uozumi, T. Teranishi, T. Sano, K. Soga, *Polymer* 2001, *42*, 4517.

3 K. Soga, H.J. Kim, T. Shiono, *Macromol. Rapid Commun.* 1994, *15*, 139.

4 J. Jin, T. Uozumi, K. Soga, *Macromol. Rapid Commun.* 1995, *16*, 317.

5 T. Uozumi, T. Toneri, K. Soga, T. Shiono, *Macromol. Rapid Commun.* 1997, *18*, 9.

6 (a) E.I. Iiskola, S. Timonen, T.T. Pakkanen, O. Harkki, P. Lehmus, J.V. Seppala, *Macromolecules* 1997, *30*, 2853; (b) E.I. Iiskola, S. Timonen, T.T. Pakkanen, O. Harkki, J.V. Seppala, *Appl. Surf. Sci.* 1997, *121*, 372.

7 H. Sinn, W. Kaminsky, H.J. Vollmer, R. Woldt, *Chem. Int. Ed.* 1980, *19*, 390.

8 A.M. Uusitalo, T.T. Pakkanen, E.I. Iiskola, *J. Mol. Catal. A* 2000, *156*, 181.

9 A.M. Uusitalo, T.T. Pakkanen, E.I. Iiskola, *J. Mol. Catal. A* 2002, *177*, 179.

10 (a) S. Timonen, T.T. Pakkanen, E.I. Iiskola, *J. Mol. Catal. A* 1999, *148*, 235; (b) S. Timonen, T.T. Pakkanen, E.I. Iiskola, *J. Organomet. Chem.* 1999, *582*, 273.

11 F. Bortolussi, C. Boisson, R. Spitz, J. Malinge, J.-P. Broyer, U.S. Patent Appl. 2004/0147692, 2004.

12 H.G. Alt, P. Schertl, A. Koppl, *J. Organomet. Chem.* 1998, *568*, 263.

13 B.Y. Lee, J.S. Oh, *Macromolecules* 2000, *33*, 3194.

14 H. Schneider, G.T. Puchta, F.A.R. Kaul, G. Raudaschl-Sieber, F. Lefebvre, G. Saggio, D. Mihalios, W.A. Herrmann, J.M. Basset, *J. Mol. Catal. A* 2001, *170*, 127.

15 D.-H. Lee, K.-B. Yoon, E.-H. Lee, S.-K. Noh, G.-G. Byun, C.-S. Lee, *Macromol. Rapid Commun.* 1995, *16*, 265.

16 D.-H. Lee, K.-B. Yoon, S.-K. Noh, *Macromol. Rapid Commun.* 1997, *18*, 427.

17 (a) N. Suzuki, H. Asami, T. Nakamura, T. Huhn, A. Fukuoka, M. Ichikawa, M. Saburi, Y. Wakatsuki, *Chem. Lett.* 1999, 341; (b) N. Suzuki, J. Yu, N. Shioda, H. Asami, T. Nakamura, T. Huhn, A. Fukuoka, M. Ichikawa, M. Saburi, Y. Wakatsuki, *Appl. Catal. A* 2002, *224*, 63.

18 J. Tian, Y. Soo-Ko, R. Metcalfe, Y.D. Feng, S. Collins, *Macromolecules* 2001, *34*, 3120.

19 H. Juvaste, E.I. Iiskola, T.T. Pakkanen, *J. Mol. Catal. A* 1999, *150*, 1.

20 H. Juvaste, E.I. Iiskola, T.T. Pakkanen, *J. Organomet. Chem.* 1999, *587*, 38.

21 H. Juvaste, T.T. Pakkanen, E.I. Iiskola, *Organometallics* 2000, *19*, 4834.

22 H. Juvaste, T.T. Pakkanen, E.I. Iiskola, *J. Organomet. Chem.* 2000, *606*, 169.

23 H. Juvaste, T.T. Pakkanen, E.I. Iiskola, *Organometallics* 2000, *19*, 1729.

24 M. Galan-Fereres, T. Koch, E. Hey-Hawkins, M.S. Eisen, *J. Organomet. Chem.* 1999, *580*, 145.

25 V.N. Zaitsev, V.V. Skopenko, Y.V. Kholin, N.D. Konskaya, S.A. Mernyi, *Zh. Obshch. Khim.* 1995, *65*, 529.

26 M.W. McKittrick, C.W. Jones, *Chem. Mater.* 2003, *15*, 1132.

27 J.C. Hicks, C.W. Jones, *Langmuir* 2006, *22*, 2676.

28 J.C. Hicks, R. Dabestani, A.C. Buchanan, III, C.W. Jones, *Chem. Mater.* 2006, *18*, 5022.

29 (a) M.W. McKittrick, C.W. Jones, *J. Am. Chem. Soc.* 2004, *126*, 3052; (b) M.W.

McKittrick, C.W. Jones, *J. Catal.* 2004, *227*, 186.
30 (a) K.Q. Yu, M.W. McKittrick, C.W. Jones, *Organometallics* 2004, *23*, 4089; (b) C.W. Jones, M.W. McKittrick, J.V. Nguyen, K.Q. Yu, *Top. Catal.* 2005, *34*, 67.
31 M.W. McKittrick, C.W. Jones, *Chem. Mater.* 2005, *17*, 4758.
32 M.W. McKittrick, K.Q. Yu, C.W. Jones, *J. Mol. Catal. A* 2005, *237*, 26.
33 (a) A.G. Massey, A.J. Park, *J. Organomet. Chem.* 1964, *2*, 245; (b) J.A. Ewen, M.J. Elder, European Patent Appl. 0,427,697, 1991; (c) J.A. Ewen, M.J. Elder, U.S. Patent. 5,561,092, 1996; (d) X. Yang, C.L. Stern, T.J. Marks, *J. Am. Chem. Soc.* 1991, *113*, 3623; (e) X. Yang, C.L. Stern, T.J. Marks, *J. Am. Chem. Soc.* 1994, *116*, 10015.
34 L. Mendez Llatas, A. Munoz-Escalona Lafuente, J. Campora Perez, E. Carmona Guzman, M. Lopez Reyes, European Patent Appl. 1,134,225, 2000.
35 P. Preishuber-Pflugl, M. Brookhart, *Macromolecules* 2002, *35*, 6074.
36 H.S. Schrekker, V. Kotov, P. Preishuber-Pflugl, P. White, M. Brookhart, *Macromolecules* 2006, *39*, 6341.
37 P. Preishuber-Pflugl, Patent PCT WO02079276, 2002.
38 F.A.R. Kaul, G.T. Puchta, H. Schneider, F. Bielert, D. Mihalios, W.A. Herrmann, *Organometallics* 2002, *21*, 74.
39 I. Kim, B.H. Han, C.-S. Ha, J.-K. Kim, H. Suh, *Macromolecules* 2003, *36*, 6689.
40 I. Kim, B.H. Han, J.S. Kim, C.-S. Ha, *Catal. Lett.* 2005, *101*, 249.
41 Z. Zheng, J. Liu, Y. Li, *J. Catal.* 2005, *234*, 101.
42 H.W. Turner, U.S. Patent 5,427,991, 1995.
43 C. Fritze, F. Kuber, H. Bohnen, U.S. Patent 6,329,313, 2001.
44 (a) S. Hinkouma, S. Miyake, M. Ono, S. Inazawa, U.S. Patent 5,869,723, 1999; (b) S. Ishigaki, S. Hinkouma, European Patent Appl. 1,359,166, 2003; (c) S. Ishigaki, S. Hinkouma, PCT Int. Pat. Appl. 03/035708, 2003.
45 E.M. Carnahan, M.J. Carney, D.R. Neithamer, P.N. Nickias, K.-Y. Shih, L. Spencer, PCT Int. Appl. 97/19959, 1997.
46 (a) E.M. Carnahan, D.R. Neithamer, R.B. Shankar, PCT Int. Appl. 00/63262, 2000; (b) K.-Y. Shih, U.S. Patent 6,184,171, 2001.
47 (a) G.B. Jacobsen, F. Matsushita, L. Spencer, P.L. Wauteraerts, U.S. Patent 2001/0039320, 2001; (b) G.B. Jacobsen, P. Wijkens, J.T.B.H. Jastrezebski, G. van Koten, U.S. Patent 5,834,393, 1998.
48 G.B. Jacobsen, T.J.P. Stevens, H.H. Loix, U.S. Patent 6,271,165, 2001.
49 E.M. Carnahan, D.R. Neithamer, PCT Int. Appl. 01/58969, 2001.
50 T. Kaneko, M. Sato, U.S. Patent 5,807,938, 1998.
51 S.L. Scott, T.L. Church, D.H. Nguyen, E.A. Mader, J. Moran, *Top. Catal.* 2005, *34*, 109.
52 J.R. Severn, R. Duchateau, R.A. van Santen, D.D. Ellis, A.L. Spek, *Organometallics* 2002, *21*, 4.
53 J.R. Severn, R. Duchateau, R.A. van Santen, D.D. Ellis, A.L. Spek, G.P.A. Yap, *Dalton Trans.* 2003, 2293.
54 (a) S.-K. Noh, G.-G. Byun, C.-S. Lee, D.-H. Lee, K.-B. Yoon, K.S. Kang, *J. Organomet. Chem.* 1996, *518*, 1; (b) S.-K. Noh, S. Kim, J. Kim, D.-H. Lee, K.-B. Yoon, H.-B. Lee, S.W. Lee, W.S. Huh, *J. Polym. Sci., Part A: Polym. Chem.* 1997, *35*, 3717; (c) S.-K. Noh, J. Kim, J. Jung, C.S. Ra, D.-H. Lee, H.-B. Lee, S.W. Lee, W.S. Huh, *J. Organomet. Chem.* 1999, *580*, 90; (d) G. Tian, B. Wang, S. Xu, X. Zhou, B. Liang, L. Zhao, F. Zou, Y. Li, *Macromol. Chem. Phys.* 2002, *203*, 31.
55 W. Han, C. Muller, D. Vogt, J.W. Niemantsverdriet, P.C. Thune, *Macromol. Rapid Commun.* 2006, *27*, 279.

10
Polymerization with the Single-Site Catalyst Confined within the Nanospace of Mesoporous Materials or Clays

Young Soo Ko and Seong Ihl Woo

10.1
Introduction

Since its first development by the Mobil research group during the early 1990s [1], MCM-41 and other mesoporous materials have been extensively studied in the areas of catalysis and materials science; in addition, related research has extended to nanotechnology due to the fact that both the pore structure and size can be controlled on a molecular level. Hence, today these mesoporous materials face the era of nanotechnology, and now represent a new field of materials science and catalysis; as a consequence, mesoporous materials are now often referred to as nanoporous materials [2].

Traditionally, due to their large surface areas, porous materials have been applied as catalysts, as adsorbents, and also as supports for catalysts. They are grouped into three different materials categories according to the pore size, whether microporous, mesoporous, or macroporous. Zeolites and other molecular sieves with po diameters <1 nm belong to the microporous materials, and selective adsorption, cracking and reforming reactions may be carried out with their characteristic solid acid sites.

In 1992, the Mobil research group reported the first mesoporous materials, known as the M41S family [1], and showed these to contain a regular pore structure similar to that of honeycomb, with pore diameters in the nanometer range. Furthermore, it was claimed the pore diameter could be precisely controlled from 1 nm to 30 nm, and this in turn resulted in the start of a new era of synthesizing and developing new types of mesoporous material (see Figure 10.1) [1]. During the past decade, many research groups worldwide have focused on, and reported the synthesis of, new structures of mesoporous materials. Due to its characteristic pore nanostructure, the application of such materials in the area of catalyst and materials science has also been greatly boosted.

Ko and colleagues were the first to explore the concept of immobilization of a single-site catalyst on mesoporous material, MCM-41, which resulted in propylene polymerization (see Figure 10.2) [3]. This in turn ignited enormous academic and commercial interest in the effect of the nanoenvironment on polymerization

Tailor-Made Polymers. Via Immobilization of Alpha-Olefin Polymerization Catalysts.
Edited by John R. Severn and John C. Chadwick

ISBN: 978-3-527-31782-0

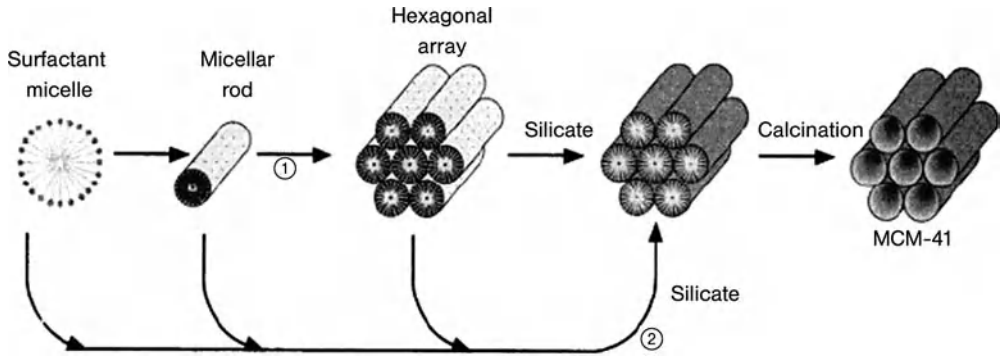

Figure 10.1 The proposed mechanism for the synthesis of mesoporous material, MCM-41, and its hexagonal pore structure [1].

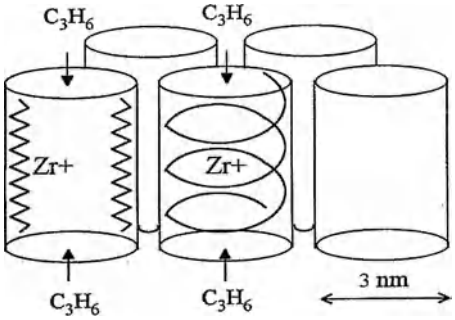

Figure 10.2 Conceptual confinement of single-site catalyst and growth of polyolefin chain inside the regular cylindrical nanopores of MCM-41 arranged hexagonally [3].

mechanisms and the structures of the resultant polymers, not only in the polyolefin catalyst field but also in nanomaterials science. Since the first report of MCM-41, many research groups have provided interesting results in the form of articles and patents.

Similar to mesoporous materials, mineral clays have also been employed for the immobilization of single-site catalysts as supports, on the basis of both commercial and academic importance. Besides serving as supports, clays are closely linked to the preparation of nanocomposites of major commercial interest. The preparation of nanocomposites via *in-situ* polymerization was seen as a way by which nanocomposites could be produced with complete intercalation of the layers in clays. This point proceeded to attract many investigations in the area of immobilization of single-site catalysts on clays which are not only relatively inexpensive supports but also serve as a nano-gallery for other applications in the nanocomposite field.

The aim of this chapter is to discuss how research into the immobilization of single-site catalysts approached the concept of nanotechnology with mesoporous

materials and clays with regular pore structures and sizes. In addition, efforts to confine single-site catalysts within the nanospace of mesoporous materials and clays will be discussed, and results on the polymerization mechanism and structures of the resultant polymers reviewed.

10.2
Single-Site Catalyst Confined within the Nanopores of Mesoporous Materials

10.2.1
Ethylene Polymerization

10.2.1.1 Extrusion Polymerization within the Pore

Observations of the traditional metallocene catalyst entrapped inside the pores of MCM-41 have been reported since the late 1990s, not only for olefin polymerizations but also for extrusion polymerization [3]. For example, crystalline nanofibers of linear polyethylene (PE) having a high molecular weight were reported to polymerize inside the nanopore of MCM-41. This represented a new approach within mesoporous silica with the Cp_2Ti-MCM-41 catalyst system, and was of major interest in the application area of nanopolymer technology. The nanopore and regular pore structures of MCM-41 provide the opportunity to control the orientation of PE during the polymerization process. During the polymer extrusion process, the propagation of polymerization was shown to proceed along the nano-cylindrical pore, with the assumption that the pore structure was maintained despite volume expansion of the resulting polymer inside the cylindrical pore. Hence, the PE was seen to be produced as a fiber which, according to scanning electron microscopy (SEM) and small-angle X-ray scattering analysis, consisted of extended-chain crystals (Figure 10.3).

Ye et al. investigated in detail the fibrous morphology of nascent PE using SEM, and suggested that the microfibers had diameters of between 1 and 30 μm that in turn consisted of extended-chain nanofibrils with diameters of approximately 60 nm (Figure 10.4; Scheme 10.1). Furthermore, the nanofibrils were parallel-packed into individual microfibers [5].

Recently, a similar result was obtained for the fibrous morphology of PE produced in the nanopores of MCM-41. Here, the nanofibers and floccules were seen as the major morphological units, which coalesced into aggregates and bundles, while the single fiber had diameters of between 80 and 100 nm (Figure 10.5) [6]

SBA-15 also showed the same chain-extrusion polymerization behavior according to Dong's report [6]. This research group prepared nano-PE fibers and floccules using the SBA-15-supported Cp_2ZrCl_2 catalytic system. The diameter of a single nanofiber was reported to be range from 120 to 200 nm, and was larger than the above-described nanofiber. SBA-15 is known to have a pore diameter which is 6–12 nm larger than that of MCM-41 [7].

Turunen and colleagues also reported the fibrous morphology of PE produced using MCM-41-supported Cp_2TiCl_2 [8], but assigned the additional peak from the differential scanning calorimetry (DSC) endotherm curve and the extra reflections

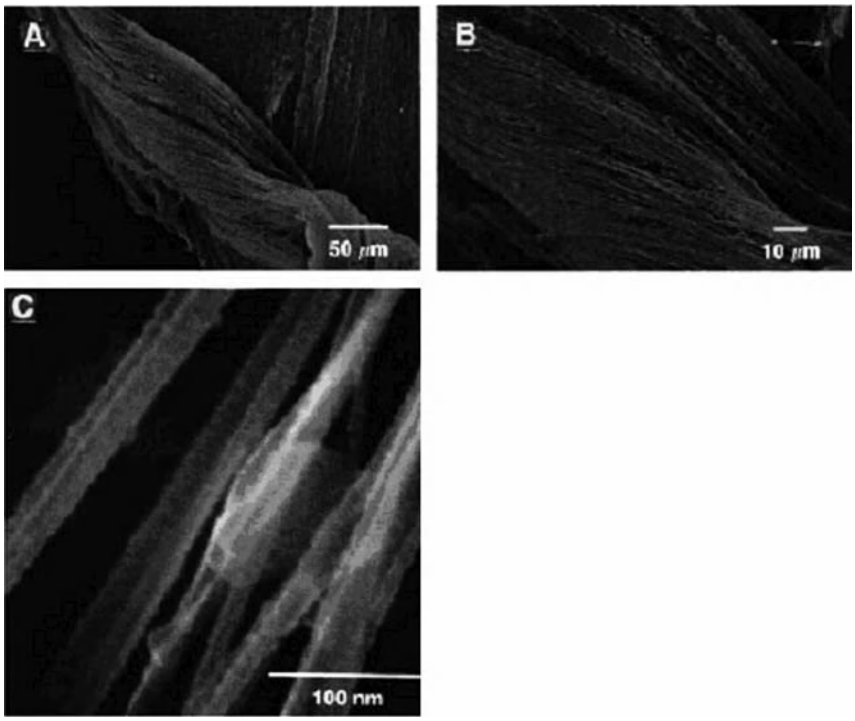

Figure 10.3 (A–C) Scanning electron microscopy images of freeze-dried polyethylene at three different magnifications [4].

in the powder X-ray diffraction (XRD) data of the PE to the aluminum residue, but not to the extended PE chain, as claimed by Aida et al. [4].

All of the above studies on extrusion polymerization were performed at very low productivity, which suggested that a slow or low polymerization rate would be necessary in order to maintain the cylindrical nanopore structure during the polymerization.

10.2.1.2 **Al-MCM-41**

Siliceous MCM-41, as described above, consists of silicon and oxygen atoms, but may also contain other metal substituents, such as aluminum. MCM-41 has been also examined for the confinement of single-site catalysts. For example, Rahiala et al. compared the results of ethylene polymerization with Cp_2ZrCl_2 inside the silica, MCM-41 and Al-modified MCM-41 [9]. By following the concept of extrusion polymerization, several results with a similar concept were reported, with the greatest amount of Cp_2ZrCl_2 being attached to Al-modified MCM-41 (Si/Al = 32), together with the most reactive sites for the attachment of metallocene catalyst in the preparation. ^{13}C-Cross-polarization/magic angle sample (CP/MAS) nuclear magnetic resonance (NMR) studies revealed that Cp_2ZrCl_2 is anchored to the

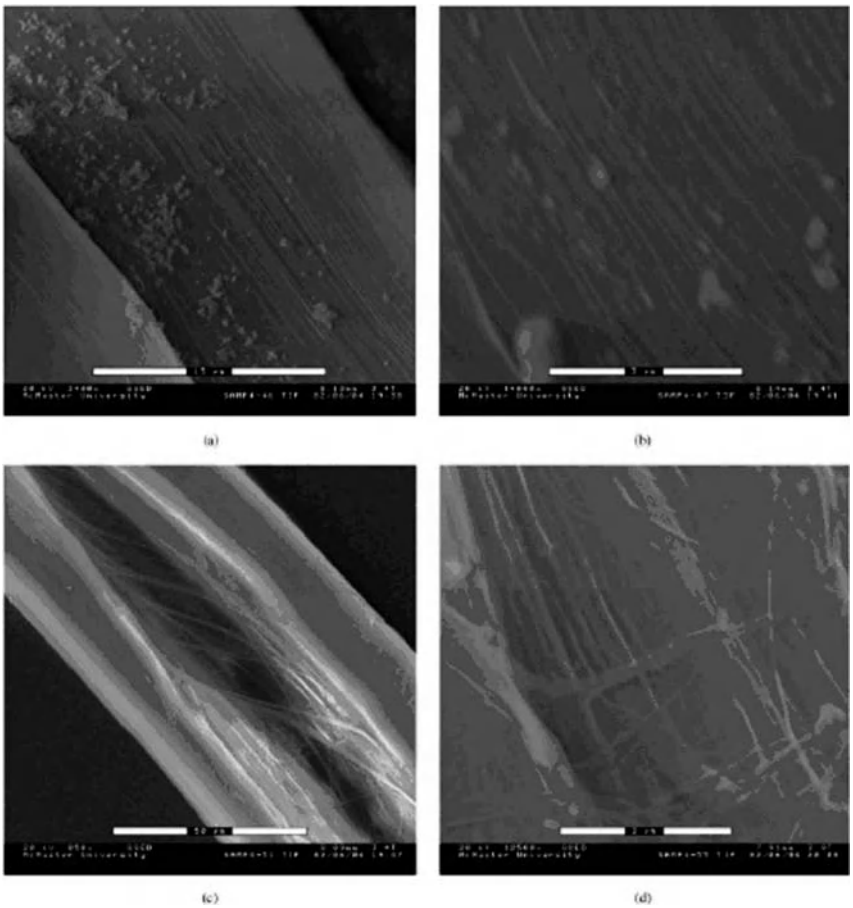

Figure 10.4 (a,b) Scanning electron microscopy (SEM) images of the polyethylene microfiber structure at two different magnifications, showing nanofibrils. (c,d) SEM images of the cleaved position of the microfiber at two different magnifications, also showing nanofibrils [5].

support surface, with the highest activity in ethylene polymerization being demonstrated with Al-MCM-41.

Lee et al. also reported a comparison of the supports MCM-41 and Al-MCM-41 [10], and found that Cp_2ZrCl_2 on Al-MCM-41 without methylaluminoxane (MAO) showed a comparable activity with homogeneous ethylene polymerization, while immobilizing MAO with Cp_2ZrCl_2 increased the activity drastically. The presence of Al in the framework of MCM-41 provided the Lewis acid sites, but the higher content of Al caused irregularity in the regular and cylindrical pore structures. In the report by Lee et al. [10], although the contents of metallocene adsorbed onto the surface were not mentioned, the higher activity could be explained on the basis

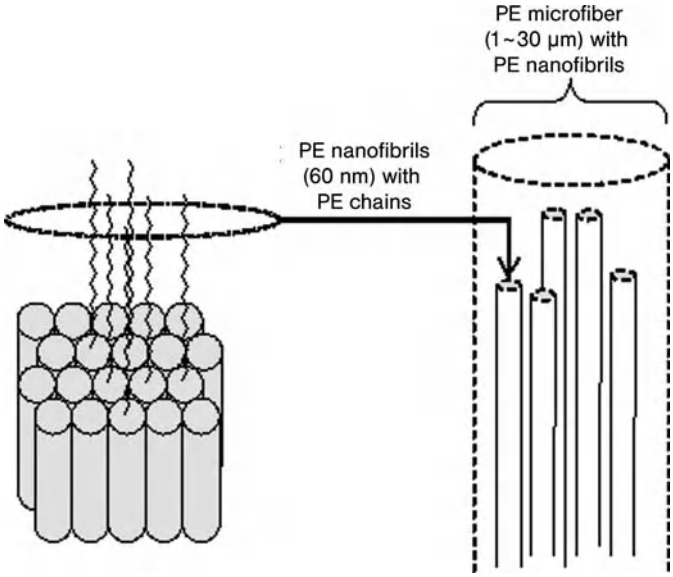

Scheme 10.1 The formation of extended polyethylene (PE) nanofibrils inside the nano-cylindrical pores; the PE microfibers consisted of PE nanofibrils.

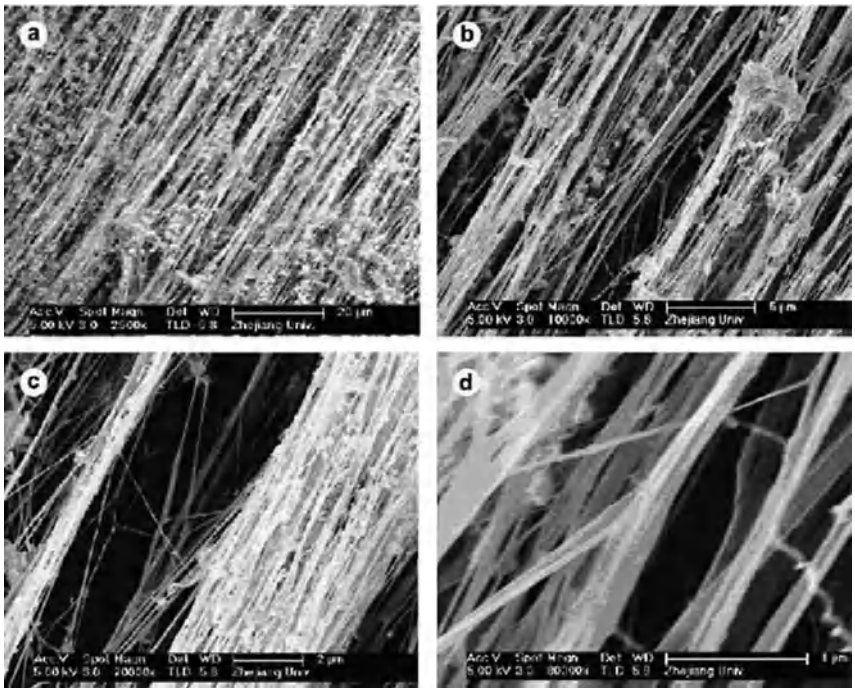

Figure 10.5 Scanning electron microscopy images of the polyethylene fiber sample. (a) Parallel aggregates of polyethylene fibers with floccules among them. (b–d) Increasingly magnified views of image (a); see scale bars for magnification factors [6].

of results reported by Rahiala et al. [9], which claimed that the presence of Al enhanced the degree of metallocene adsorption on the surface. Lee and colleagues [10] also reported that the activity of metallocenes within the nanopore was affected by the bulkiness of the ligands in metallocenes, and was high with a less-bulky ligand.

10.2.1.3 Shape-Selective Polymerization in the Nanopore

The effect of pore size and structure on the propagation of polymerization was investigated, and results suggested the presence of a shape-selective polymerization mechanism within the pore's nanospace [11]. The copolymerization of ethylene and either propylene or 1-octadecene was carried out with support from ^{13}C-NMR studies on the polymer microstructure, and also of kinetic studies. The smaller molecular size of propylene resulted in only a small difference between the homogeneous copolymerization and copolymerization within the nanospace. In contrast, a larger size of comonomer, namely 1-octadecene, showed a clear difference in copolymerization behavior and the microstructure of the resulting copolymer between the homogeneous and nanospace polymerizations (Figure 10.6). Due to the lesser mobility of 1-octadecene in the nanospace, its incorporation into the polymer chain was decreased drastically, although the kinetics of polymerization did not change, regardless of the presence of 1-octadecene (see Figure 10.7). Although the insertion of 1-octadecene into the metal resulted in the active site [P-1-octadecene–Cat] (where P is the polymer chain, and Cat is the catalyst) in the pore of MCM-41, it proved difficult to insert another octadecene into this active

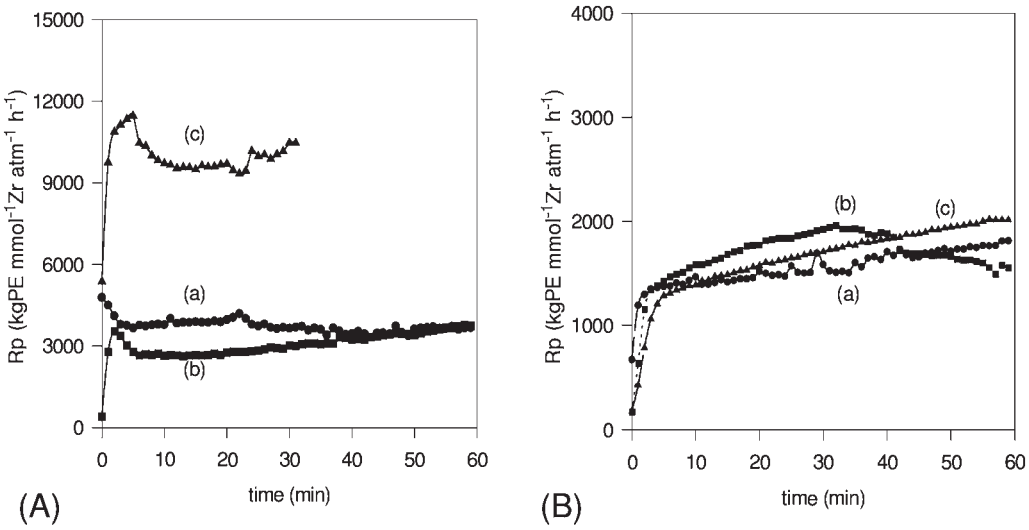

Figure 10.6 Comparison of profiles of monomer consumption rate in ethylene-1-octadecene copolymerization catalyzed with (A) homogeneous $Et(ind)_2ZrCl_2$ and (B) MCM-41/MAO/$Et(ind)_2ZrCl_2$. Polymerization conditions: Temperature = 50 °C; Pressure = 1.2 atmos.; Al/Zr ratio = 1000; C_{18}/C_2 molar ratio = (a) 0.0, (b) 0.5, (c) 1.0 [11].

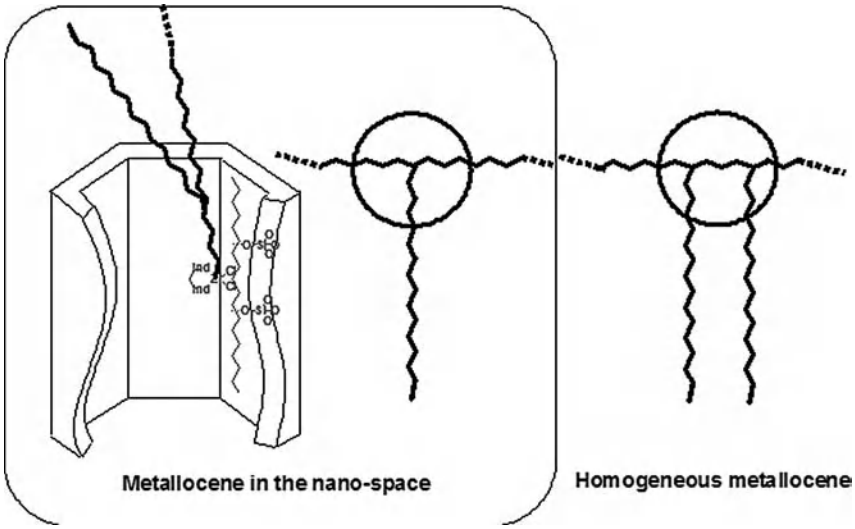

Figure 10.7 A plausible scheme for the growth of ethylene-1-octadecene copolymers inside the nanopore of MCM-41, and in a homogeneous state.

site due to steric hindrance. It is likely that the conformation of the growing chain end [P-1-octadecene–Cat] would also slow down the insertion rate, thus abolishing the comonomer enhancement effect. These observations may provide evidence for steric hindrance of the regular and nanopore structure of MCM-41 on stereoregularity and polymerization.

10.2.1.4 **The Effect of Pore Diameter on Polymerization**

Pore diameters in the range of 2.6 nm to 25 nm were studied by Kumkaew et al. to investigate the effect on activity and other polymerization behaviors [12]. The activities of the supported catalyst prepared with mesoporous materials having pore diameters of 2.6 and 5.8 nm were higher than those with larger pore diameters. It was shown that the pore diameter of supports did not significantly affect either the polydispersity or kinetic profile. Previously, Sano et al. reported the details of several investigations on the adsorptive separation of MAO using different pore diameters of MCM-41 [13–15]. The concept of adsorptive separation was based on that the fact that different pore diameters of MCM-41 could separate various MAO molecules, depending on the size or length of the MAO.

In the case of ethylene polymerization, MCM-41 with a diameter of 25 Å had the highest activity among other MCM-41s with pore diameters less than 300 Å [13]. $Et(Ind)_2ZrCl_2$ was used for the propylene polymerization with the concept of adsorptive separation, whereupon the isotacticity was seen to be influenced by pore diameter. The increase in isotacticity when MAO was confined within the nanopore of MCM-41 explained why MAO might have at least two different structures [14, 15]. Here, the authors considered mainly the separation of MAO in the nano-

pore and the effect of separated MAO on polymerization, and not the effect of the actual pore diameter on the nature of the active species of single-site catalysts.

10.2.1.5 Tethering of Single-Site Catalyst within the Nanopore of MCM-41

Many studies have been conducted on the tethering of single-site catalysts on the surface of silica for the purposes of olefin polymerization [16]. As for the silica-supported single-site catalyst, the concept of tethering a single-site catalyst has also been applied to mesoporous materials.

A constrained-geometry catalyst (CGC) was tethered to the nanopore surface of MCM-41 which had been treated and functionalized by *p*-aminophenyltrimethoxysilane. The amine group of *p*-aminophenyltrimethoxysilane played a role in tethering between the CGC and the surface of the mesoporous material. The influence of the pore nanospace was considered secondary to distinguishing it from the influence of ligands of single-site catalysts on polymerization mechanisms and behaviors. In other words, the nanospace of the mesoporous material may influence the polymer structures as ligands of the single-site catalyst. The higher degree of crystallinity for PE produced from small-pore mesoporous materials suggested that the nanospace had restricted the conformation and location of polymer chains. This may in turn lead to a greater tendency towards the formation of a higher crystalline polymer compared to the non-nanospace environment [17].

10.2.1.6 *In-situ* Synthesis of CGC on the Surface of SBA-15

Further attempts to support a single-site CGC inside the nanopore of SBA-15 were made by McKittrick et al. [18–22]. It is of interest that the assembly of CGCs on aminosilica surfaces using two different metallation protocols had been attempted. In the case of silica supports, the *in-situ* synthesis of single-site catalysts was first attempted during the early 1980s, but did not attract any commercial interest for further applications due to the low activity (per gram catalyst, rather than per mole of metal). The same group [18–21] developed methods to synthesize CGC catalysts on the surfaces, although before catalyst synthesis the surface of SBA-15 was functionalized with amine, and showed isolated and uniform amine sites on the surface. The concept of constructing isolated amine sites was eventually realized by using the molecular patterning technique, based on the fact that a tritylimine ([3-(trimethoxysilanyl)propyl]-(3,3,3-triphenylpropylidene)amine) patterning agent could be located on the surface at a certain distance from other amines due to spatial occupation by the tritylimine group [22].

Following amine functionalization of the surface, two different methods were used to prepare the CGC catalyst on the surface: (i) the amine elimination route; and (ii) the Royo method [22] (Scheme 10.2). An amine elimination reaction was chosen as a second step for the catalyst synthesis (see Scheme 10.3). In addition, the synthesis of silica-supported zirconium CGC catalyst was prepared via the Royo method (see Scheme 10.4). The research group claimed that the CGC catalysts were successfully synthesized and active for both the homo- and copolymerization of ethylene. Moreover, the molecular patterning technique was seen to be effective for the preparation of a more productive supported catalyst [18–21].

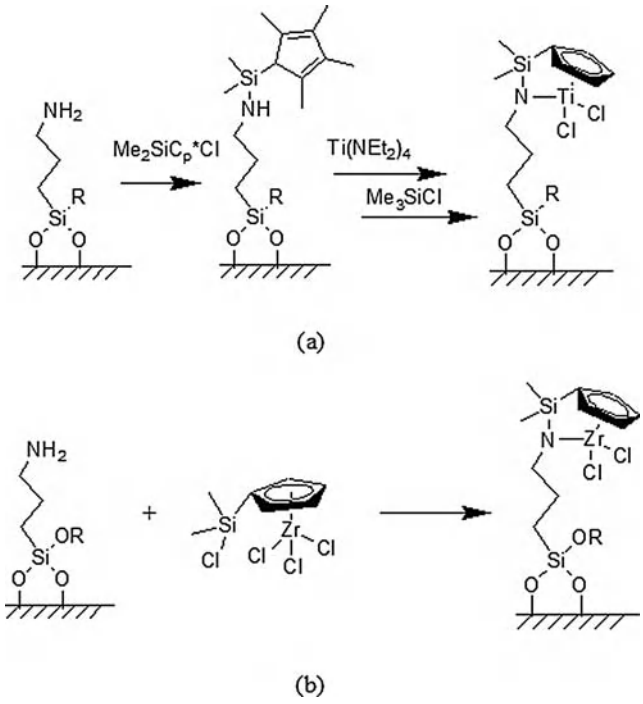

Scheme 10.2 (a) The amine route elimination route; (b) the Royo method [36].

10.2.2
Propylene Polymerization

As noted in Section 10.1, Ko et al. [3] were the first to report the details of PP polymerization with a single-site catalyst, $Et(Ind)_2ZrCl_2$, inside the nanopore of MCM-41. These authors showed that the single-site complex located within the nanoenvironment resulted in a higher stereoregularity, melting point and molecular weight compared to the homogeneous catalyst. The reason for these findings were explained by the fact that the small, regular and cylindrical pores of MCM-41 suppress the formation of inactive binuclear complexes between metallocene and metallocene, and this results in stable active sites and a high activity in propylene polymerization [3].

Tudor and O'Hare conducted a related study by placing metallocene inside the nanopore of MCM-41, but focused rather on the morphology of the resulting PP [23]. Their results showed that PP produced by the MCM-41-derived catalyst consisted of spherulite particles, with a distinct shell and core morphology, exhibiting high isotacticity and a high melting point.

Likewise, in a study conducted by Kaminsky et al., *i*-Pr(Cp)(Flu)$ZrCl_2$ was supported on the surface of MCM-41 for syndiotactic propylene polymerization. The results coincided with those above, and meant that a higher syndiotacticity and

higher melting point could be achieved with the prepared MCM-41-supported catalyst in comparison to the homogeneous catalyst [24].

O'Hare [25] continued his studies on the grafting of a PP–metallocene complex onto the surface of MCM-41, SBA-15 and MCM-48, and using disordered mesoporous phase rather than a silica-supported form. In the case of ethylene polymerization, a very high molecular weight with low dispersity was revealed when $Me_2Si(Ind)_2ZrCl_2$ was grafted onto the surface (in fact one methyl of Si was propyl group bonded to silicon on the surface), together with a higher isotacticity for propylene polymerization [25].

Various metal-containing MCM-41s (Metal MCM-41) were prepared with the expectation that the generated strong Lewis acid sites could activate the metallocene catalyst. When Ti, Zr, Hf and Mn were used, the result was an isotactic propylene polymerization with a broad molecular weight distribution (MWD) in the range of about 3.0 to 4.0 [26].

Sano et al. [13–15] employed MCM-41 to characterize MAO molecules based on the phenomenon of the adsorptive separation of MAO molecules in the nanopore of MCM-41 [6–8], and concluded that two types of active species were present in the *rac*-$Et(Ind)_2ZrCl_2$/MAO system.

10.3
Single-Site Catalyst Confined within the Nanogalleries of Mineral Clays

The physical and thermal properties of polyolefins have been improved by the addition of inorganic materials such as silica, glass fiber, clay, and other inorganic materials. In these polyolefin–inorganic material composites, the polymer and additives are not dispersed homogeneously in a nanoscale range; rather, the challenge is to disperse the inorganic materials into the polyolefin matrix on the nanoscale. Polyolefin nanocomposites represent a class of hybrid materials composed of an organic polyolefin matrix embedded with inorganic particles at the nanoscale range. It has been noted that the addition of a small fraction of mineral clay to a nanocomposite leads to dramatic improvements in properties such as a higher heat-distortion temperature, enhanced flame resistance, increased modulus, better barrier properties, decreased thermal expansion coefficient, and altered electronic and optical properties [27].

Mineral clays such as montmorillonite (MMT), hectorite, hydrotalcitite, smectite, mica and kaolin have been studied as inorganic supports for the implementation of single-site catalysts into slurry- and gas-phase polyolefin processes. Polyolefins are non-polar in nature, and cannot easily be intercalated into the lattices of the polar clay. Instead, the best approach to obtain a nanocomposite is to perform *in-situ* polymerization of an olefin with a single-site catalyst that had been included in the clay galleries. Then, as the polymerization progresses inside the clay galleries and the polymer chain mass increases, the layers are gradually pushed apart and eventually become exfoliated and dispersed within the growing polyolefin matrix.

Mineral clays, also known as a layered silicates, have a stacked structure of 1 nm-thick sheets, with variable distances between them depending on the types of silicate. Silicate sheets consist mainly of silicon and oxygen atoms, together with a small number of aluminum, magnesium and other metal ions. MMT, saponite and mainly hectorite have been used for the preparation of nanocomposites because of their intercalation abilities. Their crystalline structure (see Figure 10.8) [28] consists of a two-dimensional layer obtained by blending two tetrahedral silica laminae with metal atoms (i.e., Mg for talc, Al for mica) to form a corresponding octahedral metal oxide lamina.

In order to prepare a mineral clay-supported single-site catalyst, similar methods as are used for silica-supported catalysts have been employed. Clays such as MMT and hectorite contain a moderate surface negative charge that is balanced electrically with the cation located inside the galleries between layers [28], thus making the clays hydrophilic. Hence, a certain degree of pretreatment is required to create an organophilic surface before any further immobilization of single-site catalysts can be carried out. Modified organophilic clay can be intercalated by *in-situ* polymerization of the olefin with single-site catalysts supported within the clay galleries and using a cocatalyst of MAO or other alkylaluminum.

In one approach to clay preparation [29, 30], the clays were pretreated with cocatalyst MAO or alkylaluminum, and a single-site catalyst was added to initiate the olefin polymerization. Jerome and colleagues [29] used non-modified MMT and hectorite, which were first treated with MAO before being contacted by a CGC [*tert*-butylamido)dimethyl(tetramethyl-η^5-cyclopentadienyl)silane titanium dimethyl]. The production of a very high-molecular-weight PE was reported, without using any chain-transfer agent. The mechanical strength of the PE was reported not to be excellent, and not to be influenced by the nature and content of the silicate. Jeong et al. [30] investigated the effect of water and acidity of the clay in ethylene polymerization with MMT K-10 (MMT-10) and Kunipia F reacted by partial hydrolysis of trimethylaluminum (TMA). The research groups at Mitsubishi [31] and Idemitsu [32], and also of Weiss and colleagues [33] have each

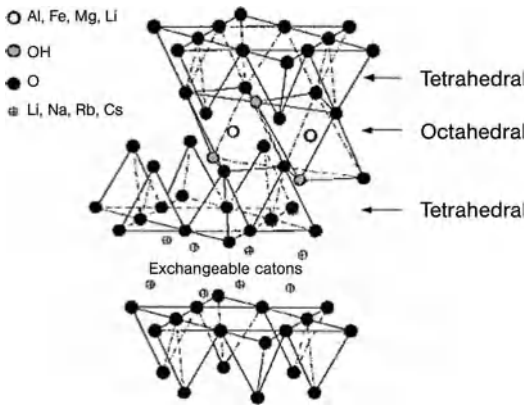

Figure 10.8 The structure of 2:1 phyllosilicates [28].

conducted extensive studies on the pretreatment of the clay surface with an alkylaluminum prior to contact with a solution of single-site catalyst and alkylaluminum.

Sun et al. [34] reported that the organo-clay precursors were prepared with amine compounds and ion-exchanging clays. The organically modified clay powder was mixed with hydrolytic scavengers and a highly isotactic single-site propylene polymerization catalyst. This was then contacted with propylene monomer, resulting in the PP nanocomposite with a high activity and improved mechanical properties. Bergman et al. [35] intercalated a cationic palladium-based Brookhart catalyst, [{2,6-*i*-$Pr_2C_6H_3N$=C(Me)C(Me)=NC_6H_3-*i*-Pr_2-2,6}$Pd(CH_2)_3CO_2Me$] [$B(C_6H_3(CF_3)_2$-3,5)$_4$], into the spaces of fluorohectorite, changing the white organoclay into an orange-brown product (Scheme 10.3). Perfluoroborates were then used as an activator to initiate polymerization with ethylene, the result being a rubbery polyethylene/clay nanocomposite.

A different approach for the preparation of PE nanocomposites, using the MMT/silica hybrid (MMT-Si)-supported catalyst, was reported by Wei and colleagues [36]. As shown in Scheme 10.4, Na-MMT was pretreated with cetyltrimethylammonium bromide (CTAB), which allowed the entry of tetraethyl orthosilicate

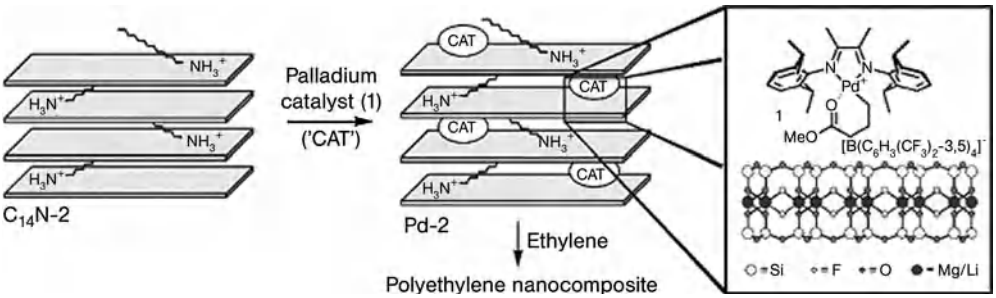

Scheme 10.3 Cationic palladium-based Brookhart catalyst-intercalating silicate fluorohectorite [35].

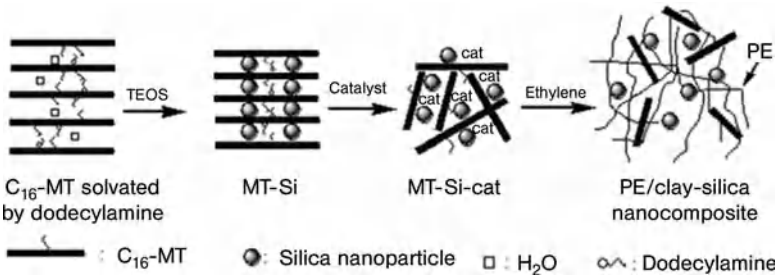

Scheme 10.4 Conceptual illustration of mechanism for formation of montmorillonite silica (MMT-Si) hybrid and the PE/MMT-Si nanocomposites [36].

(TEOS) and its deposition between the galleries of the clay. By using this method it was possible to form a new hybrid support, MMT-Si. Cp_2ZrCl_2/MAO was then allowed to fix onto the MMT-Si surface using a common method. Following ethylene polymerization, two types of nanofiller (clay layers and silica nanoparticles) were dispersed concurrently in the PE matrix, and in this way PE/clay–silica nanocomposites were obtained.

Wang et al. reported the *in-situ* polymerization of ethylene by intercalating MMT with zirconocene and MAO. Attempts were made to place the single-site catalyst between the galleries of pristine MMT by the reaction of MMT with MAO and $(n\text{-BuCp})_2ZrCl_2$/MAO [37]. The intercalated catalyst Zr-MMT-MAO showed a different XRD spectrum from that of MMT, which suggested that it corresponded to the size of MAO with the single-site catalyst. High-molecular-weight and high-melting PE were obtained using the MMT-supported single-site catalyst.

10.4 Summary

In recent years, significant attention has been paid to polyolefins due to their commercial importance with regards to a wide variety of applications, coupled with future expectations that they may replace many conventional materials. During the same period, and as outlined elsewhere in this book, many studies have been conducted to determine the commercial applications of single-site catalysts and the drop-in technology for present-day polyolefin processes. In addition, one of the most recent trends in advanced materials science is that mesoporous materials should expanded the material sciences to the nanoscale range.

Confining single-site catalysts to the nanospace of mesoporous materials represents a combination of commercially and academically important areas. During the past 10 years, numerous research investigations have been undertaken to examine the effects of confinement within the nanospace of mesoporous materials, thereby opening new routes to control the molecular structure of the resultant polyolefins. The production of polyolefin nanocomposites has long been an area requiring improvements in the methods of preparation and in the properties of the final products. *In-situ* polymerization with single-site catalysts within the nanogalleries of mineral clays has provided a major opportunity to produce polyolefin nanocomposites more efficiently than by using conventional compounding methods, and also to enhance the mechanical properties of the final products based on significant improvements in the efficiency of exfoliation.

Today, materials science and engineering continue to seek new and advanced materials (carbon nanotubes is an excellent example) that may serve as supports for single-site catalysts. It is especially exciting that these new procedures may lead to the production of revolutionary polyolefin materials.

References

1 C.T. Kresge, M.E. Leonowicz, W.J. Roth, J.C. Vartuli, J.S. Beck, *Nature* 1992, *359*, 710–712.

2 IUPAC Manual of Symbols and Terminology, Appendix 2, Part 1, Colloid and Surface Chemistry, *Pure Appl. Chem.* 1972, *31*, 578.

3 Y.S. Ko, T.K. Han, J.W. Park, S.I. Woo, *Macromol. Rapid Commun.* 1996, *17*, 749–758.

4 K. Kakeyama, J. Tamazawa, T. Aida, *Science* 1999, *285*, 2113–2115.

5 Z. Ye, S. Zu, W. Wang, H. Alsyouri, Y.S. Lin, *J. Polym. Sci. Part A: Polym. Chem.* 2003, *41*, 2433–2443.

6 X. Dong, L. Wang, W. Wang, H. Yu, J. Wang, T. Chen, Z. Zhao, *Eur. Polym. J.* 2005, *41*, 797–803.

7 X. Dong, L. Wang, W. Wang, G. Jiang, Y. Chen, Z. Zhao, J. Wang, *Macromol. Mater. Eng.* 2005, *290*, 31–37.

8 J.P.J. Turunen, M. Haukka, T.T. Pakkanen, *J. Appl. Polym. Sci.* 2004, *93*, 1812–1815.

9 H. Rahiala, I. Beurroies, T. Eklund, K. Hakala, R. Gougeon, P. Trens, J.B. Rosenholm, *J. Catal.* 1999, *188*, 14–23.

10 K.-S. Lee, C.-G. Oh, J.-H., Yim, S.-K. Ihm, *J. Mol. Catal. A: Chemistry* 2000, *159*, 301–308.

11 Y.S. Ko, S.I. Woo, *Macromol. Chem. Phys.* 2001, *202*, 739–744.

12 P. Kumkaew, S.E. Wanke, P. Parserthadam, C. Danumah, S. Kaliaguine, *J. Appl. Polym. Sci.* 2003, *87*, 1161–1177.

13 T. Sano, K. Doi, H. Hagimoto, Z. Wang, T. Uozumi, K. Soga, *Chem. Commun.* 1999, *8*, 733–734.

14 T. Sano, H. Hagimoto, J. Jin, Y. Oumi, T. Uozumi, K. Soga, *Macromol. Rapid. Commun.* 2000, *21*, 1191–1195.

15 T. Sano, H. Hagimoto, S. Sumiya, Y. Naito, Y. Oumi, T. Uozumi, K. Soga, *Macropor. Mesopor. Mater.* 2001, *44–45*, 557–564.

16 J.R. Severn, J.C. Chadwick, R. Duchateau, N. Friedrichs, *Chem. Rev.* 2005, *105*, 4073–4147.

17 S.L. Burkett, S. Soukasene, K.L. Milton, R. Welch, A.J. Little, R.M. Kasi, E.B. Coughlin, *Chem. Mater.* 2005, *17*, 2712–2723.

18 M.W. McKittrick, K. Yu, C.W. Jones, *J. Mol. Catal. A: Chemistry* 2005, *237*, 26–35.

19 M.W. McKittrick, C.W. Jones, *J. Catal.* 2004, *227*, 186–201.

20 K. Yu, M.W. McKittrick, K. Yu, C.W. Jones, *Organometallics* 2004, *23*, 4089–4096.

21 M.W. McKittrick, K. Yu, C.W. Jones, *J. Am. Chem. Soc.* 2004, *126*, 3052–3053.

22 M.W. McKittrick, K. Yu, C.W. Jones, *Chem. Mater.* 2003, *15*, 1132–1139.

23 J. Tudor, D. O'Hare, *Chem. Commun.* 1997, 603–604.

24 W. Kaminsky, C. Strubel, H. Lechert, D. Genske, S.I. Woo, *Macromol. Rapid Commun.* 2000, *21*, 909–912.

25 C.J. Miller, D. O'Hare, *Chem. Commun.* 2004, 1710–1711.

26 T. Sano, Y. Oumi, *Catal. Surv. Asia* 2004, *8*, 295–304.

27 M. Zanetti, S. Lomakin, G. Camino, *Macromol. Mater. Eng.* 2000, *279*, 1–9.

28 E.P. Giannelis, R. Krishinamooriti, E. Manias, *Adv. Polym. Sci.* 1999, *118*, 108–147.

29 M. Alexandre, P. Dubois, T. Sun, J.M. Garces, R. Jerome, *Polymer* 2003, *43*, 2123–2132.

30 D.W. Jeong, D.S. Hong, H.Y. Cho, S.I. Woo, *J. Mol. Catal. A: Chemistry* 2003, *206*, 205–211.

31 (a) Y. Suga, Y. Uehara, Y. Maruyama, E. Isobe, Y. Ishihama, T. Sagae, U.S. Patent 5,928,982, 1999; (b) Y. Suga, Y. Uehara, Y. Maruyama, E. Isobe, Y. Ishihama, T. Sagae, U.S. Patent 5,973,084, 1999; (c) N. Kusaka, H. Kurokawa, Y. Uehara, Jpn Laid-Open Appl. 09/324008, 1997; (c) T. Sagae, Y. Uehara, European Patent Appl. 874,006, 1998; (d) T. Sugano, T. Suzuki, H. Shoda, T. Aoshima, E. Isobe, Y. Maryuma, M. Kashimato, S. Nishimura, N. Iwama, S. Nayakawa, T. Kato, S. Sieber, Y. Suga, European Patent Appl. 846,696, 1998.

32 (a) F. Okuda, H. Sato, M. Kuramoto, European Patent Appl. 1,054,021, 2000; (b) H. Sato, M. Kuramoto, European Patent Appl. 1,026,176, 2000.

33 K. Weiss, C. Wirth-Pfeifer, M. Hofmann, S. Botzenhardt, H. Lang, K. Bruning, E. Meichel, *J. Mol. Catal. A: Chemistry* 2002, *143*, 182–183.
34 T. Sun, J.M. Garces, *Adv. Mater.* 2002, *14*, 128–130.
35 J.S. Bergman, H. Chen, E.P. Giannelis, M.G. Thomas, G.W. Coates, *Chem. Commun.* 1999, 2179–2180.
36 L. Wei, T. Tang, B. Huang, *J. Polym. Sci. Part A: Polym. Chem.* 2004, *42*, 941–949.
37 Q. Wang, Z. Zhou, L. Song, H. Xu, L. Wang, *J. Polym. Sci. A: Polym. Chem.* 2004, *42*, 38–43.

11
Polymeric Supported Catalysts

Markus Klapper and Gerhard Fink

11.1
Introduction

Towards the end of the year 2005, J. R. Severn, J. C. Chadwick, R. Duchateau, and N. Friederichs published a review article [1] entitled: "Bound but not gagged – Immobilizing Single-Site α-Olefin Polymerization Catalysts". This review was comprehensive and detailed, and covered almost all of the relevant subject areas (approximately 1000 literature references). Here, Severn and colleagues' review chapter, "Polymeric Supports" has been further supplemented with more recent reports which have been made up until July 2007.

Metallocenes immobilized on solid support materials have been successfully introduced in industry as polymerization catalysts for the production of new, application-oriented polymer materials. Industrial polymerization processes, which are carried out either as a slurry process in liquid propene or as a gas-phase process, require that catalysts are in form of solid grains or pellets; soluble metallocene catalysts must therefore be supported on a solid carrier (so-called drop-in catalysts).

An additional objective of the heterogenization process was, on the one hand, to preserve the advantages of homogeneous metallocenes, such as the high activity, narrow molecular weight distributions, stereospecificity, and uniform comonomer incorporation. On the other hand, the intention was to combine these features with the properties of supported-catalyst technologies, such as controlled particle growth – thus forming morphologically uniform polymer particles of the desired size and shape which mirror the starting catalyst particles but which are at least 20 times their size – as well as a high bulk density, without any reactor fouling.

While inorganic supports such as silica or $MgCl_2$ are well established in industrial polymerization, organic materials are considered somehow as "exotic" supports. However, they offer certain advantages over the established supports as one is able to control the size of the support and the interaction with catalysts over wide ranges. In addition, the shape of the support can vary, as linear polymers, loose networks or single or aggregated nanoparticles have all been described. This

Tailor-Made Polymers. Via Immobilization of Alpha-Olefin Polymerization Catalysts.
Edited by John R. Severn and John C. Chadwick

ISBN: 978-3-527-31782-0

allows for easy tuning of the polymerization behavior by the control of loading, immobilization and activation of the catalyst. The behavior of the support, such as fragmentation, can also be adjusted.

The recent most prominent examples of investigated organic supports such as polysiloxanes, polyolefins, polystyrene based resins and latex particles will be discussed in the following sections.

11.2 Polysiloxanes

11.2.1 Supported Precatalysts

Tethered polysiloxane-supported catalysts have been prepared by the hydrolysis or cohydrolysis of a silyl chloride- or silyl ethoxide-containing ancillary ligand. The ancillary ligands, bridged by a dichlorosilyl-moiety, Cl_2SiCp' (Cp′ = C_5Me_4, Ind and Flu), were hydrolyzed or cohydrolyzed with a dihydroxy-functionalized linker by Soga et al. to produce a series of tethered ligands. When ligand systems were deprotonated and reacted with $ZrCl_4$, heterogeneous precatalysts were produced (Scheme 11.1) [2].

The stoichiometric quantities of reagents (Cp′/*n*BuLi/Zr = 2 : 2 : 1) employed to synthesize the supported precatalyst should have led to a quantitative conversion. However, the extent of zirconium incorporation in the final catalyst varied greatly between the supports (1 to 75%, based on one Zr to two Cp′). This observation indicates that a considerable amount of the inner portion of these supports is

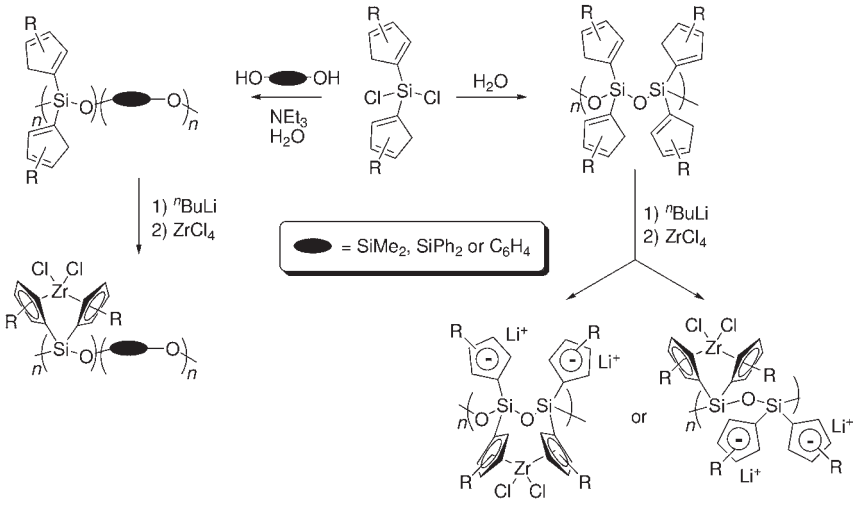

Scheme 11.1 Synthesis of polysiloxane-supported metallocene precatalysts.

inaccessible to at least one or all of the reagents. As a consequence, catalyst/support fragmentation may be seriously hindered, resulting in adverse polymer particle morphologies. The Soga group also established that the supported precatalysts constructed from the homogeneous hydrolysis of $Cl_2SiCp'_2$ outperformed those obtained when $Cl_2SiCp'_2$ was reacted with a dihydroxy-containing complex. Additionally, relatively good activities were observed for the methylaluminoxane (MAO)-activated indenyl- and fluorenyl-containing precatalyst, while the tetramethylcyclo-pentadienyl-containing precatalyst showed surprisingly poor activity in ethylene polymerization. This series of polysiloxane-supported zirconocene precatalysts was also employed in ethylene-*co*-1-octene and propylene polymerization, using MAO as a cocatalyst.

Salt metathesis reactions between $Cl_2Si(Ind)_2$ and *p*-dilithiophenyl or *p*-dilithiodiphenyl have also been used to form supported metallocenes. The *p*-(silylene)phenylene-supported precatalysts have been used in the homopolymerization of ethylene and propylene. In the case of propylene polymerization, an enhancement in catalyst stability, stereoselectivity, and regioselectivity was observed when compared to the corresponding mononuclear and dinuclear catalysts, $Ph_2Si(Ind)_2ZrCl_2$ and $C_6H_4(SiPh(Ind)_2ZrCl_2)_2$, respectively. However, broad molecular weight distributions were observed for polypropylene ($M_w/M_n = 2.9–4.5$) and especially polyethylene ($M_w/M_n = 4.4–8.5$) [3].

Dos Santos and coworkers have utilized the cohydrolysis reaction of bisindenyldiethoxysilane ($Ind_2Si(OEt)_2$) with tetraethoxysilane, (TEOS, $Si(OEt)_4$), (ratio of indene to TEOS 1:3–5) to form indene-containing xerogels. The latter can be converted to a supported metallocene, following lithiation and metathesis with $ZrCl_4 \cdot 2THF$ [4]. In a similar way, Deffieux and coworkers have produced an indene-modified silica support via reaction of bisindenyldichlorosilane, Me_2SiCl_2, $(ClMe_2Si)_2O$, and TEOS under a non-hydrolytic sol–gel process. The supports, once metallated, were found to be active in the polymerization of ethylene, again producing resins with high polydispersities ($M_w/M_n = 3.1–127$) [5].

Metallocenes tethered to a polysiloxane through the cyclopentadienyl ligand have been assembled by Böhm et al., via hydrosilylation of $(CH_2{=}CH–L–Cp')_2ZrCl_2$ (L = $(CH_2)_2$ or CH_2SiMe_2, Cp′ = Cp or Ind) with polymethylhydrogensiloxane in the presence of chloroplatinic acid, forming a crosslinked polysiloxane (Scheme 11.2) [6].

Polymethylhydrogensiloxane-*co*-dimethylsiloxane has also been used by Nagy and Tyrell to construct a tethered metallocene. In this case, the silane functions of the polymer were brominated and reacted with LiCp to form a tethered cyclopentadiene, which could be converted into a zirconocene complex (Scheme 11.3) [7]. The groups have also used other polysiloxane copolymers to form immobilized precatalysts. The reaction of 1,5-diamino-2-methyl-pentane with 1,5-dichlorohexamethyltrisiloxane formed a copolymer material whose amine functions could be lithiated and reacted with $CpZrCl_3$ (Scheme 11.4). The resultant tethered precatalyst, when used in combination with MAO, effectively polymerized ethylene [8].

Polysiloxanes derived from the hydrolysis of chloro- or alkoxy-silanes leave polymeric materials with hydroxyl groups that require capping, usually with a silane

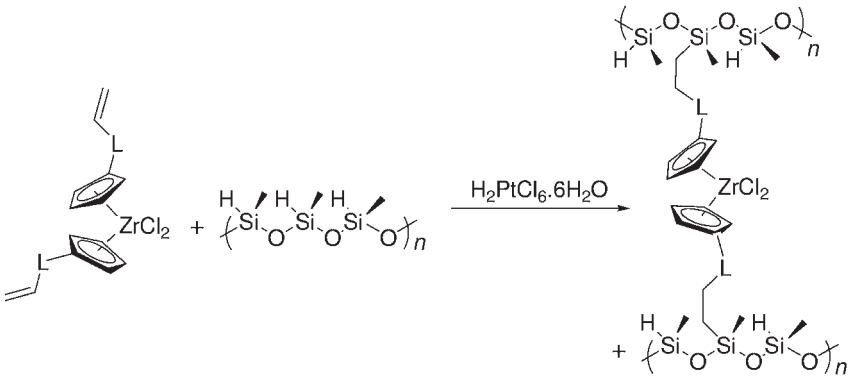

Scheme 11.2 Hydrosilation as a synthetic route to polysiloxane-tethered metallocene precatalysts.

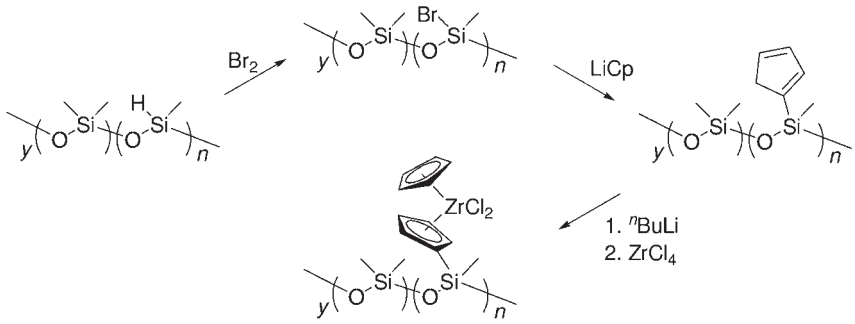

Scheme 11.3

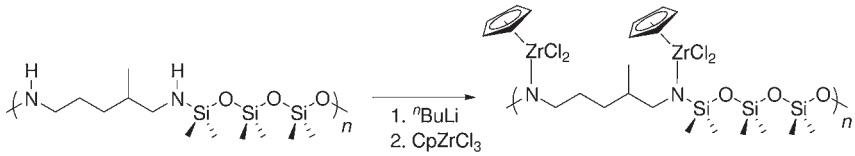

Scheme 11.4

complex (hexamethyldisilazane, HMDS, or $ClSiR_3$) [2, 3, 5]. Alt and coworkers took advantage of these functional groups to tether an *ansa*-bridged difluorene ligand [9]. The hydroxyl groups of polymethylsiloxane microgels were end-capped with $HOSiMe_2(CH_2)_6SiMe(Flu)_2$ (Scheme 11.5). Deprotonation and subsequent metathesis with $ZrCl_4$ afforded a supported metallocene capable of producing a moderately active catalyst species (up to 1.44 kg PE g^{-1} Zr h^{-1}) in conjunction with MAO.

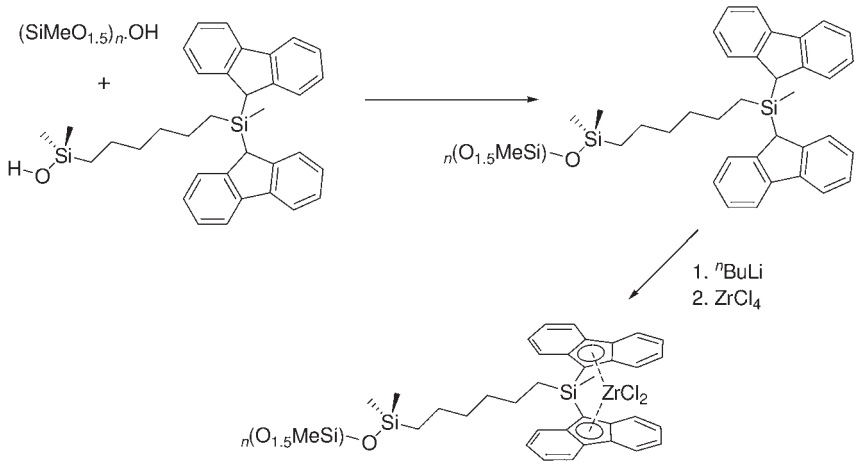

Scheme 11.5

11.2.2 Supported Cocatalysts

The polymethylsiloxane microgels have been modified to facilitate the *in-situ* generation and immobilization of the ubiquitous cocatalyst MAO. The surface of the microgels are partially pacified with $Me_2(Oct)Si(OEt)$, $Me_2SiH(OEt)$, or $Me_2SiH(OEt)$, the latter being subsequently used to hydrosilylate octene to form the finished support. The remaining hydroxyl groups on the supports are "pacified" with hexamethyldisilazane. The modified polymethylsiloxane can then be treated with trimethylaluminum (TMA), followed by an appropriate amount of water (at –78 °C!), to form MAO-like structures on the surface of the support. The supports pacified via hydrosilylation with octene proved to be the most effective substrate in comparative polymerization experiments with a metallocene precatalyst [10]. The supported cocatalysts could also be employed to activate late transition metal catalysts [11, 12].

The efficiency of the supported cocatalysts, in combination with different precatalysts, was found to depend strongly on the TMA/H_2O ratio used in the *in-situ* generation of MAO. No one ratio of TMA/H_2O was found to be ideal for all precatalysts [11]. As a result, each precatalyst needed a specific supported MAO microgel, the TMA/H_2O ratio of which had been optimized to achieve maximum activity. The optimized systems did, however, prove to be comparable to some commercially available silica-supported MAOs [13].

The presence of reactive groups within a supported system, and their effect on catalyst performance and resultant polymer products, must be borne in mind. Clearly, the deactivation of the active species by such groups is of utmost importance, but additional consideration should be given to their ability to undergo

chain-transfer reactions with the active species before, and especially during, polymerization. If such reactions were to take place, then the effect on the molecular weight capabilities of a system may need to be assessed. Hydrosilane-containing compounds (RR′R″Si–H) are one such example, and these have been extensively reported by Marks and coworkers to be efficient chain-transfer agents for homogeneous and heterogeneous single-site α-olefin polymerization catalysts [14]. In fact, polysiloxanes such as polymethylhydrosiloxane have themselves been used as chain-transfer agents for single-site catalysts, immobilized on porous polyethylene particles [15]. The addition of a polysiloxane modifier to the system was also reported to increase catalyst activity in ethylene-*co*-α-olefin polymerization.

Not only molecular weight capabilities are affected with such chain-transfer agents. In the case of hydrosilane-containing compounds, the silane functionality (RR′R″Si-H) is transferred to the growing polyolefin chain, thus leading to a polyolefin with either a functional end group or a block polyolefin-*co*-polysiloxane polymer.

Bergbreiter et al. [16] used polysiloxanes as soluble inorganic polymer supports for organocatalysts (Scheme 11.6), and demonstrated that liquid/liquid separations are a viable way to recover/re-use polysiloxane-bound catalysts after a monophasic reaction. Silica supports which have had their surface modified with titanium oxide were prepared and coated with poly(methyloctylsiloxane) by Collins et al. [17]. Subsequently, immobilization of the polysiloxane was induced by thermal treatment or microwave radiation.

Recently, Rauscher and Gauthier [18] supported stereospecific metallocene/alkylaluminoxane catalysts on a particulate polyorganosilsesquioxane comprising spheroidal particles having an average diameter with the range of 0.3 to 20 μm. This polyorganosilsesquioxane support is characterized by a crosslinked structure (see Structure 1) in which the siloxane bond extends three-dimensionally, and by a relatively low surface area of less than $100\,m^2\,g^{-1}$.

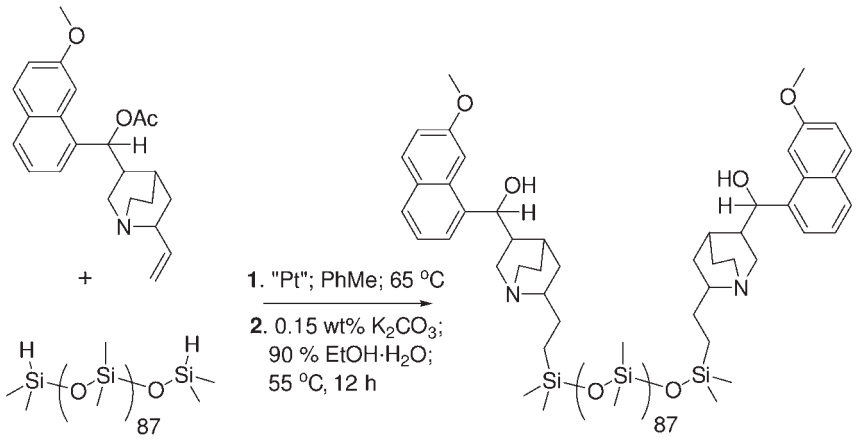

Scheme 11.6

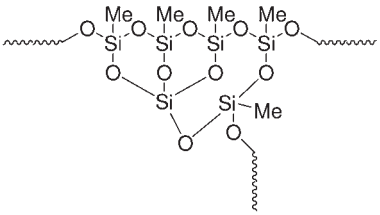

Structure 1

As indicated by the structural formula, the polymethylsilsesquioxane support has methyl functional groups (Si–CH_3) which can react with MAO and thus be involved in anchoring some portion of the MAO to the siloxane support:

$$\text{Me-Al(Me)-O-(Al(Me)-O-)}_n\text{-Al(Me)}_2 + \text{[Si]-Me} \rightarrow$$
$$\text{[Si]-O-Al(Me)-O-)}_n\text{-Al(Me)}_2 + \text{AlMe}_3.$$

Finally, the supported metallocene component can take the form of a single metallocene or two or more metallocenes which are cosupported on the polyorganosilsesquioxane.

11.3 Polystyrene

Many organic supports are based on polystyrene-related polymers. Therefore, this group of carriers should be divided into three different types, namely (i) linear polystyrene chains; (ii) resins and porous networks; and (iii) surface-functionalized nanoparticles.

11.3.1 Metallocene Functionalized Linear Polystyrene

The first case discussed is that of linear polystyrene chains functionalized in various ways to immobilize the catalyst via covalent or non-covalent bonding. In most cases, either a presynthesized metallocene catalyst was directly attached to the backbone [19, 20], or the catalysts were synthesized in several polymer analogous steps on the polystyrene chain. The polystyrene was functionalized with ligands such as cyclopentadienyl or fluorenyl, after which the metallocene was generated by a reaction with half-sandwiches of a zirconocene [15, 21].

The cyclopentadienyl units were in some cases only partially transferred into the catalysts, and free cyclopentadienyl units were used for a reversible network formation by Diels–Alder reaction (Scheme 11.7). It was proposed that this was made possible by the reaction heat and the mechanical stress created by the formed polyolefin. This method had already been described in 1999 [21], but was again revisited by Wang et al. who generated a well-defined linear polystyrene with

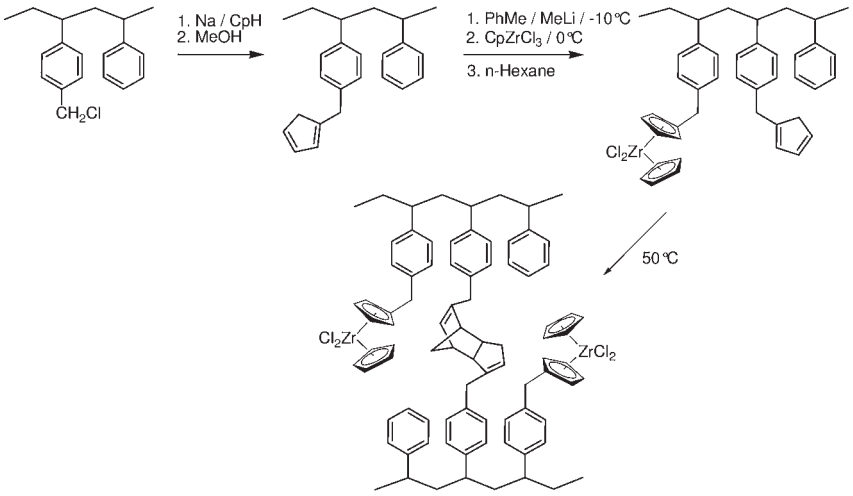

Scheme 11.7 Cyclopentadienyl functionalized polystyrene for supporting metallocenes and for reversible crosslinking.

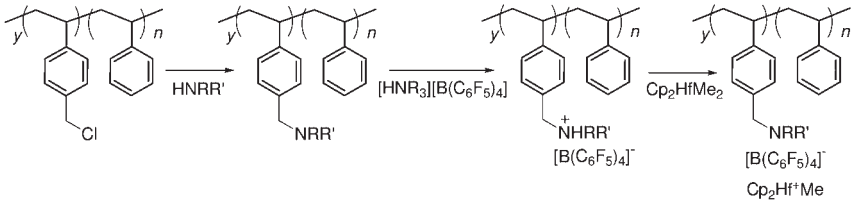

Scheme 11.8 Borate-activated metallocenes supported on Merryfield resins.

cyclopentadienyl groups [22] and studied the influence of the reversibility of network on the olefin polymerization. All of the polystyrene-supported metallocene catalysts showed high activity and stability in olefin polymerization.

As this strategy requires for each catalyst a specific synthesis, the approach is not very flexible and hampers any rapid systematic investigation of the catalysts.

11.3.2
Metallocene Inside Polystyrene Resins

The second approach considers polystyrene resins with different crosslinking densities. For example, ammonium-substituted Merryfield resins were used for the immobilization of catalysts by the interaction with borate-activated hafnium or zirconium complexes (Scheme 11.8) [23].

However, the activities which could be attributed to the very dense network formed by the resin were low. The pores are most likely very rapidly filled with

the formed polyolefin, and polymerization proceeds mainly on the surface. Fragmentation in such Merryfield resins does not occur, this being demonstrated by optical scanning confocal microscopy [24].

In an approach which is based on the chemistry published by Soga [19] and Müllen et al. [21], supported Cp derivatives were prepared by reacting the halogen-functionalized resins with an excess of sodium 1,2,3,4-tetramethyl-1,3 cyclopentadienide [25]. In a second step, the metallocene is formed by metallation with a moncyclopentadienyl metal trichloride. The authors claimed in their preliminary polymerization results that the supported metallocene catalysts derived from Merrifield resins showed reasonable activities (150 kg PE mol^{-1} Zr h^{-1} bar^{-1}) under extremely mild conditions (1 bar, Al/Zr = 1000), with no catalyst leaching. Furthermore, field emission-scanning electron microscopy (FE-SEM) analysis of the resultant PE products indicated that polymerization with Merrifield-supported catalysts occurred only at the surface of these resins. Altering the catalyst particle surface area/volume ratio has been shown to significantly improve the activity of these catalysts.

A very extensive study of imido titanium complexes supported on amino-functionalized polystyrene was presented by Mountford et al. [26]. Therein, systematically different titanium-based catalysts using triazacyclic ligands were investigated in solution and supported on organic resins (see Structure 2). The solid phase-supported catalysts were either linked via the macrocycle or the imido ligand to a 1% crosslinked polystyrene support. The supported catalysts showed almost no activity in ethylene polymerization, which was similarly observed by Nielson, who also found a negligible activity for supported $Ti(NR)Cl_2$ (tmeda) [27]. It was assumed that, due to the limited swelling of the resins, the accessibility of the catalyst drastically decreases the polymerization rate. Remarkably, an increase of activity after supporting catalysts was found by Gibson for imido vanadium complexes, and this was explained by the suppressing of bimolecular catalyst deactivation processes [28].

Therefore, many attempts were made to use a support with less crosslinked polystyrene networks. The ethylene (co)polymerization with metallocene catalysts encapsulated in gel-type poly(styrene-*co*-divinylbenzene) beads was described by Hong et al. [29]. In this approach, weakly crosslinked poly(styrene-*co*-divinylbenzene) beads (PS beads) were used as a carrier to encapsulate metallocene catalysts through a simple swelling–shrinking procedure. The catalytic

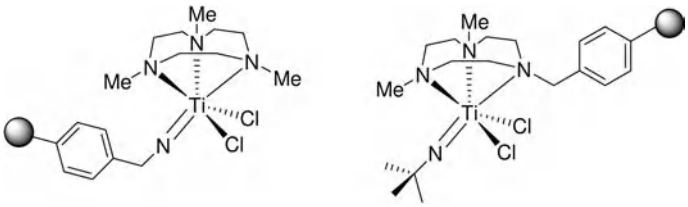

Structure 2 Imido titanium complexes supported on amino-functionalized polystyrene.

species were distributed homogeneously in the PS bead particle. The catalyst exhibited high and stable ethylene polymerization and ethylene/1-hexene copolymerization activity, affording uniform spherical polymer particles (1 mm). The polymerization rate profiles exhibited slow initiation and stable increases in polymerization activity with time.

Tang et al. described a catalyst system obtained from porous polystyrene beads-supported Cp_2ZrCl_2 which was tested for ethylene polymerization with methylaluminoxane as a cocatalyst [30]. By comparison, the porous supported catalyst maintained a higher activity and produced polyethylene with a better morphology than the corresponding solid-supported catalyst. The differences between activities of the catalysts and morphologies of the products were explained by the fragmentation processes of the support, as frequently observed with the inorganic supported Ziegler–Natta catalysts. Investigation into the distribution of polystyrene in the polyethylene revealed the fact that the porous polystyrene-supported catalyst had undergone fragmentation during polymerization. In addition, Tang et al. prepared macroporous and modified macroporous poly(styrene-*co*-methyl methacrylate-*co*-divinylbenzene) particles [31] (m-PS and mm-PS) supported Cp_2ZrCl_2 which were applied to ethylene polymerization using MAO as a cocatalyst. The influences of the swelling response of the support particles on the catalyst loading capabilities of the supports, as well as on the activities of the supported catalysts, were studied. It was shown that the Zr loadings of the supports and the activities of the supported catalysts increased with the swelling extent of the support particles. The m-PS or mm-PS supported catalysts exhibited very high activities when the support particles were well swollen, whereas those catalysts devoid of swelling treatment gave much lower activities. Investigation on the distribution of the supports in the polyethylene by transmission electron microscopy (TEM) indicated that the swelling of the support particles allowed the fragmentation of the catalyst particles. In contrast, the fragmentation of the support particles with poor swelling was hindered during ethylene polymerization (Figure 11.1).

Soga extended this concept to networks containing 2% vinylpyridine, and was able to immobilize $[Cp_2ZrMe]^+[B(C_6F_5)]_4]^-$. The catalysts showed activities above 1000 kg PE mol^{-1} Zr h^{-1}, although the bulk densities were rather low (>0.18 g L^{-1}) [32].

11.3.3
Metallocene Supported on Polystyrene Nanoparticles

The third concept uses polystyrene nanoparticles prepared by emulsion processes. While in the previous case for fragmentation, covalent bonds must be broken (which is not always very likely), more promising and more versatile is the use of physically crosslinked organic nanoparticles. Such particles can easily be obtained by using mini-emulsion or emulsion polymerization. The use of suitable emulsifiers [e.g., Lutensols, pyridine, polyethylene oxide (PEO)] allows for tailoring of the nucleophilicity of the surface for immobilization of the catalysts [33]. Latex particles based on polystyrene seem to be one of the best candidates for such supports.

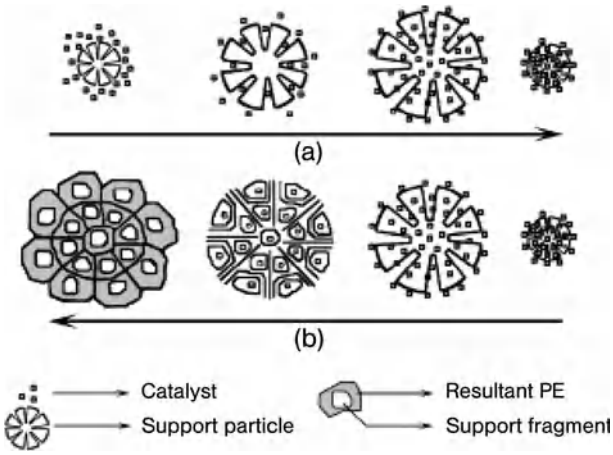

Figure 11.1 (a) Preparation of the supported metallocene catalyst via swelling–shrinking of the support particles. (b) Fragmentation of the catalyst particle in ethylene polymerization through the swelling response of the support particle. (Reproduced with permission from Ref. [31]; © 2007, Elsevier.)

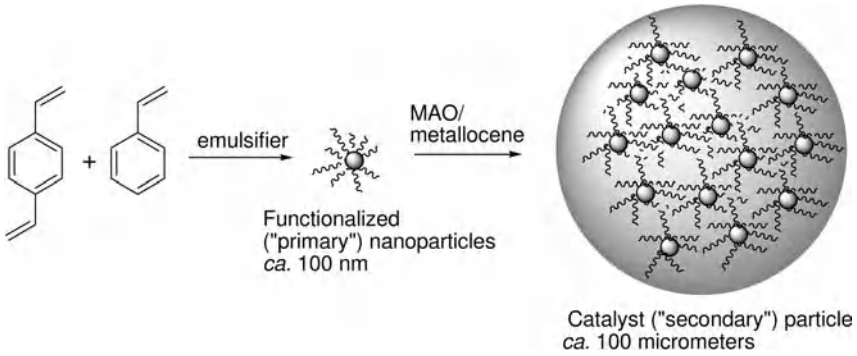

Figure 11.2 Polyethylene oxide (PEO)-functionalized nanoparticles as support for metallocenes: synthesis and supporting process.

Carriers based on polystyrenes containing methoxy groups or PEO chains, which allow for an immobilization of active MAO/metallocene complexes through non-covalent bonding with nucleophilic groups, were reported [21, 34]. These catalysts show high activities and productivities, and formed distinct polymer particles with high bulk density (~400 g L^{-1}). This concept was developed further, by applying polystyrene-based nanoparticles functionalized with PEO chains on the surface acting as catalyst carriers [35]. In this concept, the uniform and well-defined carrier particles (80–300 nm) were reversibly aggregated by interaction of the PEO chains with the MAO/zirconocene clusters (Figure 11.2). It was proposed that, during polymerization, the catalysts are completely and homogeneously fragmented within the final product down to the initial nanosized particles of the support, due

to formation of the polyolefins between the latex particles. Such fragmentation, as has been proven for silica-based supports, is considered essential for the control of morphology in polyolefin polymerization.

Such organic supports formed from latex particles were applicable not only to the metallocenes but also to post-metallocene complexes (catalysts with heteroatoms as electron-donating ligands such as the titanium complexes bis[*N*-(3-*t*-butyl-salicylidene) cycloheptylaminato]titanium(IV) dichloride (FI-catalysts) [36, 37]. These complexes are known for their capability to synthesize ultra-high-molecular-weight polyethylene (UHMWPE). It was shown that such supports, which are surface-functionalized with pyridyl groups, gave excellent polymerization results for titanium complexes (see Structure 3; FI-catalysts). The supports are readily accessible by the synthesis of pyridine-containing latex particles by copolymerization of styrene and vinylpyridine [32, 38]. As the vinylpyridine is hydrophilic, the particles are easily available via a self-stabilizing emulsion. It can be assumed that the vinylpyridine remains on the surface of the latex particles and is, together with the PEO chains, capable of completely adsorbing the titanium catalyst.

Molecular weights (M_w) of polyethylene in excess of $7 \times 10^6\,g \cdot mol^{-1}$ were achieved in a MAO-activated polymerization with a long-term stability of the catalytic system. Even after 5 h, no decrease in activity was measured, which clearly indicated that the nucleophilic centers did not interact with the catalysts to promote side reactions such as deactivation or transfer. Remarkably, the pyridyl groups were essential for this supporting process as they not only immobilized the catalyst, but also acted as selective scavengers for trimethylaluminum (TMA). TMA – which is a byproduct in all commercially available MAOs and would here decompose the titanium complex – was removed by reaction with the pyridyl groups [36].

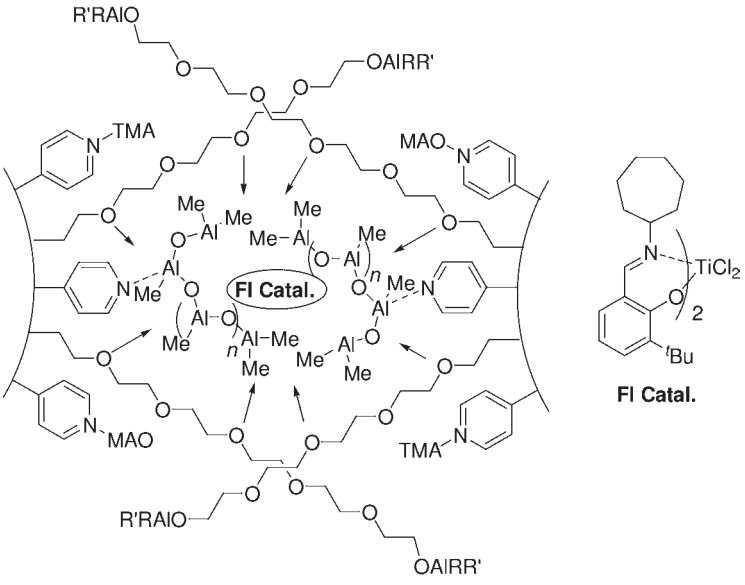

Structure 3: immobilization of the FI-catalyst/MAO-complex.

Not only latex particles with long PEO chains were investigated, but also those with just hydroxyl groups. Gels of the copolymers of styrene, hydroxyl isopropenylstyrene and a Cp-functionalized styrene were successfully used as supports for the metallocenes. In these copolymers the hydroxyl groups act as binding sites to the MAO/metallocene complex ($Me_2Si(2\text{-}MeBenzInd)_2ZrCl_2$), while the Cp units are again used as a reversible crosslinker (via Diels–Alder reaction) to allow fragmentation of the support. The activities of these systems are rather high (6300 kg PP mol^{-1} Zr h^{-1} bar^{-1} and 100 kg PE mol^{-1} Zr h^{-1} bar^{-1}) [39].

Wanke et al. also used hydroxyl functionalized particles, whereby the particles were created by the copolymerization of hydroxyethylmethacrylate, styrene and divinylbenzene [40]. These authors systematically varied the pore radius of the supports (from 2 to 5–8.5 nm, as obtained by BET measurements), and investigated the influence on the polymerization behavior of $(n\text{-}BuCp)_2ZrCl_2$. All product particles showed a very special onion-type structure, although they had very high bulk densities (0.23 to 0.49 g L^{-1}). Furthermore, the influences of activation and aluminum content on comonomer incorporation was extensively described, and a clear comonomer effect observed.

As an alternative to latex particles, microgel particles have been applied as supports for catalysts. In particular, star-like polystyrenes with PEO-functionalized arms have been designed and used as organic supports for a tridentate bis(imino)pyridinyl iron catalyst toward ethylene polymerization. Similar to the above-described nanoparticles, common aluminum-based activators (MAO or TMA) are immobilized via nucleophilic interactions with the ethylene oxide units at the periphery of each arm [41]. A second strategy is based on the synthesis of star-like polystyrene with arms ended either by a benzaphenone or a benzoic acid function [42]. Indeed, the reaction of TMA with these functional microgels leads to the *in-situ* formation of alkoxide aluminum-based species at the periphery of the star-like microgels (Figure 11.3). All of these functional polystyrene microgels have been used as supports to immobilize and activate the $MeDIP(2,6\text{-}iPrPh)(2)FeCl_2$ catalyst towards ethylene polymerization. Based on such organic support, high catalytic activities and polyethylene beads of spherical morphology, constituted of polyethylene chains of monomodal molar mass distribution have been obtained.

Despite it being shown in initial studies that polymeric supports are applicable carriers for catalysts in olefin polymerization, many open questions remained to be answered in order to fully understand the role of organic supports and to consider an industrial application. When discussing such systems, most authors describe only the polymerization behavior, such as activity and productivity, whereas morphology control is mainly discussed only phenomenologically. In particular, proving fragmentation of the support turned out to be a major challenge, such that an extensive comparison between the different types of structures has been performed in only a very few cases.

In particular, the aspect of fragmentation of a support, which has been proven to be essential for silica- or $MgCl_2$-supported catalysts systems [43], is often neglected in the case of organic supports. One reason for this might be that electron microscopy, which can be easily applied for silica-supported catalysts due to the higher contrast between support and polyolefin, is not very practicable for the

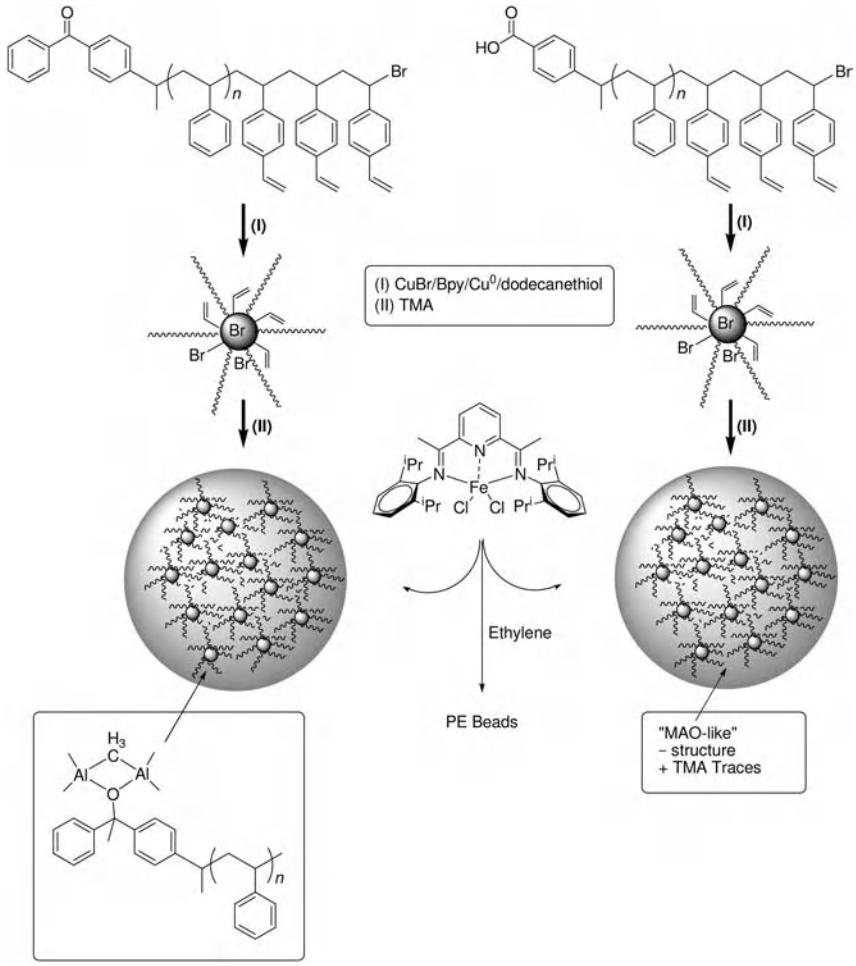

Figure 11.3 Synthesis of benzophenone and benzoic acid functionalized polystyrene microgels by atom transfer radical polymerization (ATRP), and the immobilization of the catalytic complex [42].

visualization of a highly diluted organic support within an organic polyolefin matrix. During recent years, it has been shown successfully that modern optical methods allow for a very rapid study of the behavior of supported metallocene catalysts. By using videomicroscopy [44], several polymeric supports functionalized with cyclopentadiene (CP) units or PEO and polypropylene oxide (PPO) chains and loaded with a metallocene, have been studied simultaneously. This method allowed a direct comparison of the different catalysts under identical conditions in a single experiment. In addition, by this experiment, more detailed information of the behavior of the supports could be obtained by studying the growth kinetics of single grains [45].

As a second investigative technique, laser scanning confocal fluorescence microscopy (LSCFM) [46] was applied. By using dye-labeled supports, LSCFM can be used as a very rapid means of studying the fragmentation of supports. This is demonstrated by three-dimensional (3-D) images which show the distribution of the different support fragments in the polyethylene product particles (Figure 11.4) [24a].

Whilst the kinetics and morphology of inorganic supports have been widely investigated, systematic reports for organic materials are rare, or even absent. Metallocenes were immobilized on silica and also on two organic supports, namely polystyrene latex particles and a polystyrene resin, which were stained with fluorescent perylene dyes. All supported catalysts showed different activities in ethylene polymerization under the same reaction conditions. The recording of fluorescence images of the polyolefin product beads at different polymerization times, using LSCFM, led to the identification of several different fragmentation processes for the catalyst. While almost no fragmentation of the micrometer-sized polystyrene resins was observed, supports based on aggregated latex particles fragmented throughout the bead from the outset, corresponding to the multi-grain model established for Ziegler-type catalysts [47]. For the silica particles, fragmentation which started from the outer spheres to the core was detected, thus confirming in a rapid and very simple manner the layer-by-layer model developed by electron microscopy studies.

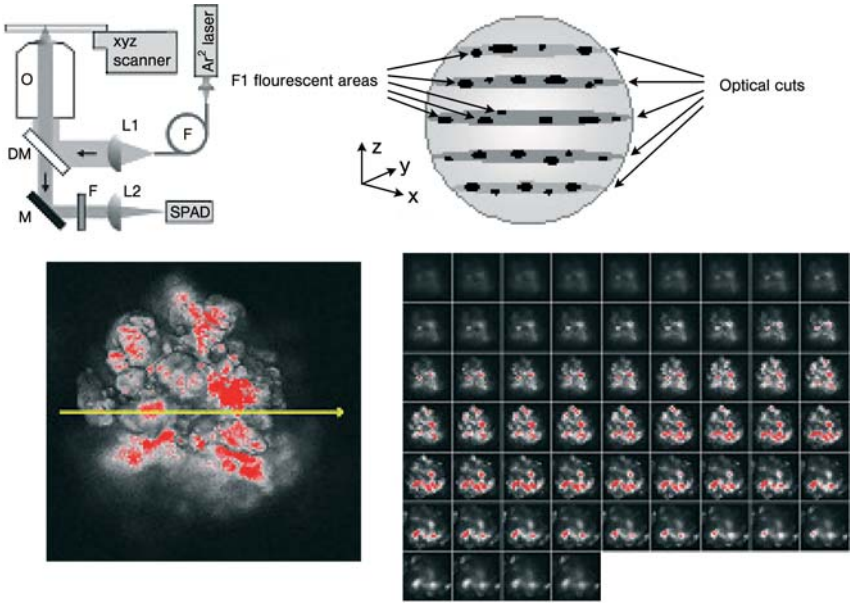

Figure 11.4 Schematic description of laser scanning confocal fluorescence microscopy (LSCFM) and example of the catalyst distribution in a polyethylene particle after 15 min of polymerization.

11.4
Dendrimers

While nanoparticles typically have diameters in the range of 30 to 200 nm, dendrimers are typically one order of magnitude smaller. This makes them very attractive carriers for metallocenes as they can be considered as particles; however, the surface area is much higher than in the case of latex particles, although the number of contributions is very limited. An overview of this topic was provided by Helms and Frechet [48]. Due to the high reactivity and sensitivity of the catalysts, only inert dendrimers may be used as carriers, and therefore the structures are limited to carbosilanes or polyphenylenes. Similar to the above-described polystyrene systems, the catalyst here is also immobilized by pentafluorophenylborates which are covalently attached to the core moieties of G0–G2 generations of a carbosilane (Scheme 11.9) [49].

Likewise, different polyphenylene dendrimers were reported and functionalized with Cp_2ZrCl_2 in the periphery; this catalyst system was activated by MAO. Although very high activities were reported for both systems, it must be considered that even if these systems were to be supported, the polymerization behavior would

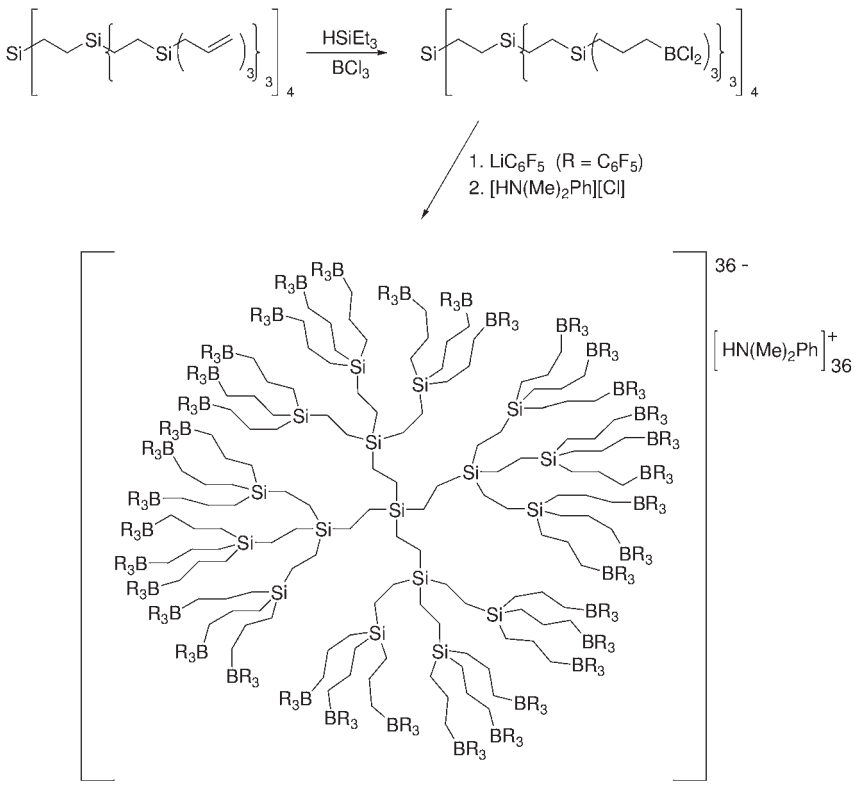

Scheme 11.9 The synthesis of the polyanionic carbosilane dendrimers.

most likely be more comparable to a solution polymerization than to a polymerization in suspension. Therefore, limitation of the polymerization rate due to diffusion processes, and fragmentation of the support can be neglected. On the other hand, it became clear that the control of morphology could not be achieved, as only "fluffy" material could be obtained (see Structure 4). Partially molten material indicates the presence of an exothermic reaction due to the very high activities in these systems.

It was possible to improve the catalyst behavior of the dendrimers simply by adopting the concept of crosslinking via non-covalent interactions between PEO chains on the surface to dendrimers [50]. By mixing MAO and metallocene ($Me_2Si(2MeBenzInd)_2ZrCl_2$) with polyphenylene dendrimers functionalized with

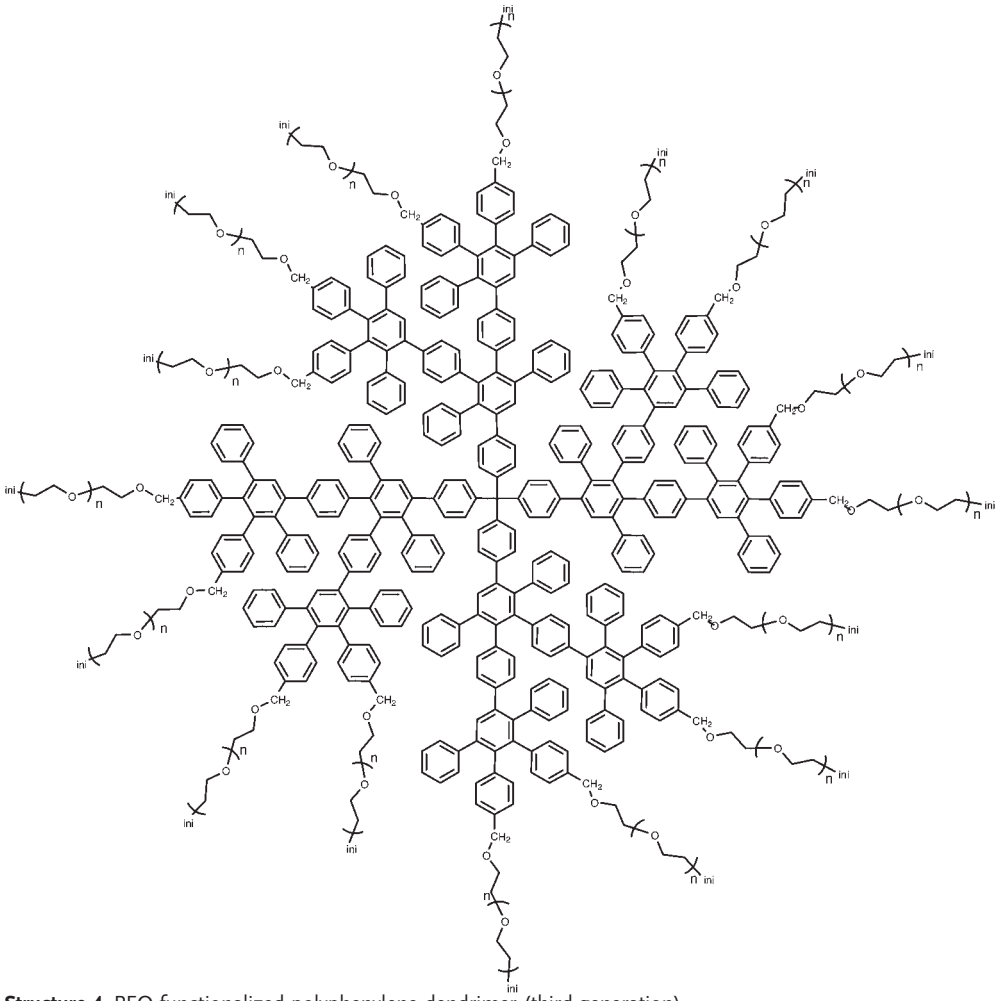

Structure 4 PEO-functionalized polyphenylene dendrimer (third-generation).

PEO chains, fragmentable aggregates of the dendrimers became accessible. These systems showed excellent activities (1100 kg PE mol^{-1} Zr h^{-1} bar^{-1}) and morphology control, as indicated by the formation of spherical particles [51].

In practical terms, such structures are synthetically very demanding and too expensive for general use in technical processes. However, they may serve as model compounds for the immobilization of catalysts and for fragmentation studies.

11.5 Polyolefins

Porous polyolefins have proven themselves to be suitable support materials for the immobilization of single-site α-olefin polymerization catalysts. Like polystyrene, porous unfunctionalized polyolefins may swell in some hydrocarbon solvents, such as toluene, at elevated temperatures. Therefore, the encapsulation of a single-site system by swelling and shrinking of the porous polyolefin support can be achieved in much the same way as the above-mentioned polystyrene systems [29]. It should be noted here that the loading mechanism for this procedure is one of physisorption of the metallocene to the support. As a result, the amount of catalyst loading for a specific system may vary greatly, depending on the steric and electronic nature of the species. Nonetheless, these systems have been reported to produce heterogeneous PE- [52–54], PP- [53, 55], or 1,2-polybutadiene-supported [56] catalysts suitable for use in either gas-phase or slurry-phase polymerization processes, despite concerns that leaching of the catalyst species in a liquid medium or monomer may prevent the application of these supported catalysts in slurry-phase processes. Fait et al. immobilized a C_2-symmetric metallocene system onto porous polyethylene and polypropylene supports [54].

Expanding the application of polyolefin materials via incorporation of polar functionalities has developed into an area of intense research activity, and has led to the development of various functional polyolefin resins with graft or block structures [57]. As a result, many porous functionalized polyolefin support materials, capable of fixing a high loading of metallocene/MAO catalysts, have become accessible. One such support material is maleic anhydride-grafted polypropylene, which has been used by Sunaga and coworkers to immobilize MAO [58]. Several PP-supported MAO systems with differing MAO loadings, depending on the extent of maleic anhydride grafting, were prepared and used as supported activators for various metallocene precatalysts in the polymerization of propylene. Recently, polar functionalized polypropylene-supported catalysts with higher catalyst loading capabilities than the corresponding unfunctionalized support have also been reported [59]. In this disclosure, porous polypropylene containing hydroxyl functionalities was synthesized by copolymerizing propylene with 5-hexenyl-9-BBN, using a fourth-generation $MgCl_2$-supported Ziegler–Natta catalyst [60]. Treatment of the resulting polymer with H_2O_2/NaOH afforded a spherical hydroxyl-containing *i*PP resin which, when slurried in toluene and contacted

consecutively with MAO and zirconocene dichloride, formed an immobilized catalyst with a high catalyst loading. The supported catalyst was used to polymerize ethylene in toluene at 50 °C, and was claimed to possess "relatively high productivities" (32 g PE g^{-1} catalyst h^{-1} bar^{-1}), and to produce PE resin with a better morphology than those supported on unfunctionalized PP. The scanning electron micrographs, however, clearly show ruptured and hollow particle morphology. Again, the use of toluene as a polymerization diluent may have been the root of such poor morphology for the unfunctionalized support. As mentioned above, the encapsulation of a metallocene/MAO system with a porous unfunctionalized polypropylene support is achieved by swelling and shrinking the polymer [53–55]. It would, therefore, be futile to polymerize under conditions where the polymer support is reswollen, allowing the catalyst to leach out. High-density polythylene (HDPE) has also been treated with CO_2 plasma to create a surface carboxylic acid function that can be used to support a metallocene/MAO catalyst [61].

11.6 Carbon Nanotubes

Carbon nanotubes (CNTs), like graphite, diamond and fullerenes, represent another allotropic modification of the element carbon. The structure conforms to a rolled-up monoatomic layer of graphite (graphene) forming a hollow cylinder with a diameter of a few nanometers and a length of some micrometers. In principle, there is a distinction between multi-walled nanotubes (MWNTs) and single-walled nanotubes (SWNTs). Since their discovery [62], CNTs have attracted intense attention as a result of their unique properties, such as extremely high mechanical strength and high electrical and thermal conductivities [63]. In olefin polymerization catalysis, CNTs have been introduced during recent few years as catalyst supports or/and as polymer fillers.

Wang et al. [64] describes, in a study on ethylene polymerization catalyzed by a Cp_2ZrCl_2/carbon nanotube MAO-pretreated system, the effects of the structure of a pristine CNT and an open-ended CNT on the activity of the catalyst, and the resultant polyethylene morphology. It is important in this context to recognize in which way the CNTs are prepared, as the materials are different and this may affect the location of the active sites and consequently the morphology of the resultant polymer. The multi-walled CNTs in the studies reported by Wang et al. (but provided by Professor Xiaobin Zhang) were synthesized by using the cobalt-catalyzed decomposition of acetylene, while the open-ended CNTs were obtained by refluxing CNTs in nitric acid at 120 °C for 4 h [65]. In the presence of nitric acid, the cap of the CNTs can be opened at the defect sites to shorten the CNT length and introduce hydroxylic functional groups (Scheme 11.10; from Ref. [64]).

The pore sizes of these CNTs were determined by nitrogen adsorption/desorption measurements. The S_{BET} surface area, pore volume and average pore diameter were found to be 133.9 $m^2 g^{-1}$, 1.25 $cm^3 g^{-1}$, and 37.3 nm, respectively.

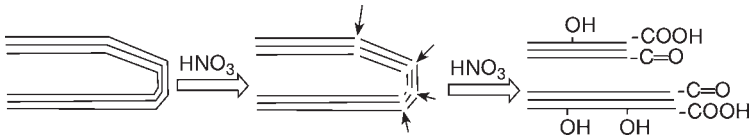

Scheme 11.10 Opening of defect site to form functional carbon nanotubes. (Reproduced from Ref. [64]; © 2006 Elsevier.)

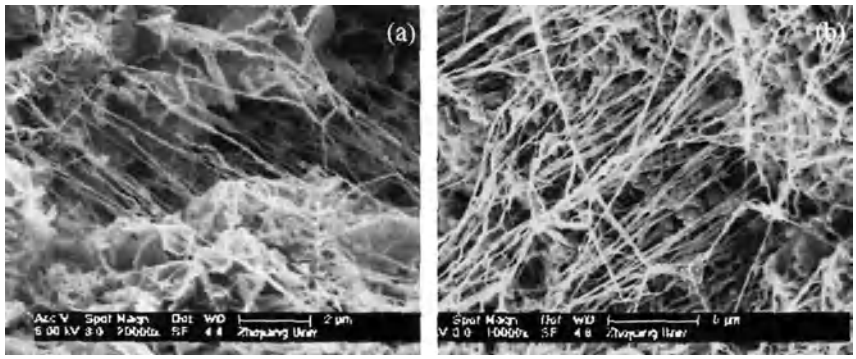

Figure 11.5 (a,b) Scanning electron microscopy images of polyethylenes prepared by pristine CNT-supported Cp_2ZrCl_2/MAO catalysts. (Reproduced from Ref. [64]; © 2006 Elsevier.)

The SEM images (Figure 11.5a and b) of polyethylenes prepared by pristine CNT-supported Cp_2ZrCl_2/MAO catalysts at different polymerization temperatures {[Al]/[Zr] = 3000; (a) = 50 °C, (b) = 60 °C} demonstrated the effect of the CNTs on polyethylene morphology. The pristine CNTs are long and slender fibers and capped at each end, so that the Cp_2ZrCl_2 could not disperse into the pores and adsorb only onto the surface of the CNTs.

The resultant polyethylene encapsulates the surface of the CNTs and produces fiber morphology. The possible formation process of this nano-polyethylene fibers is shown in Figure 11.6 [64].

The SEM images (Figure 11.7a and b) [64] of the polyethylene prepared by open-ended CNTs supported Cp_2ZrCl_2/MAO catalysts {[Al]/[Zr] = 3000; (a) = 50 °C, (b) = 60 °C} demonstrate mainly fractional morphology, this being the result of a change in the structure of the CNTs. Following treatment with nitric acid, the capped ends of the CNTs were opened, whereupon the catalysts were seen not only to be adsorbed onto the surface of the CNTs but also to be dispersed into the pores.

At 60 °C, the polymerization proceeds rapidly, and the hydraulic pressure of the growing polymer allows the CNTs to be broken up into fragments, and hence the polyethylene morphology resembles broken particles. Since at 50 °C the polymerization rate is slower, the hydraulic pressure of the formed polymer cannot break up the CNTs completely, and so some of the polyethylene pieces retain a fiber morphology. This proposed process is shown schematically in Figure 11.8 [64].

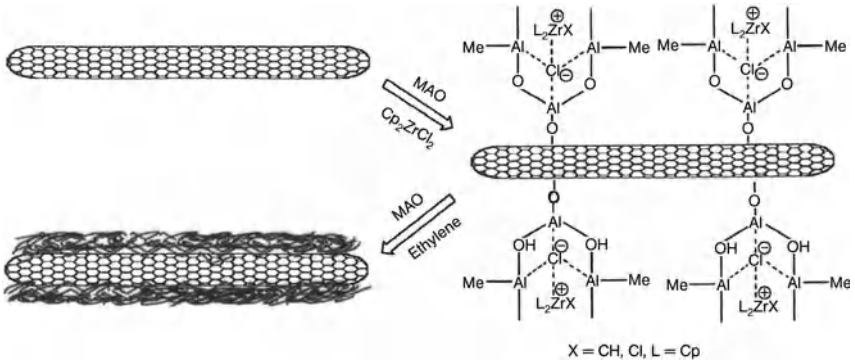

Figure 11.6 Proposed formation process for the generation of nano-polyethylene fibers. (Reproduced from Ref. [64]; © 2006 Elsevier.)

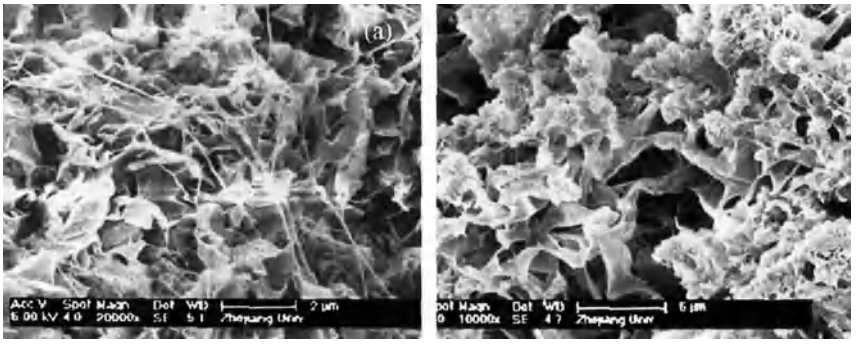

Figure 11.7 (a,b) Scanning electron microscopy images of polyethylene prepared by open-ended CNTs supported Cp_2ZrCl_2/MAO catalysts. (Reproduced from Ref. [64]; © 2006 Elsevier.)

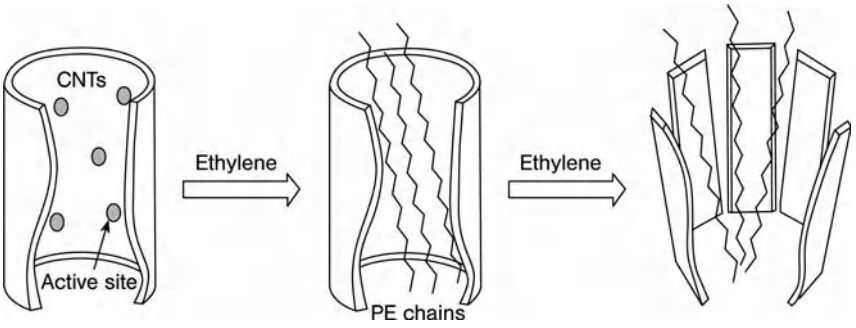

Figure 11.8 Proposed process for CNT fragmentation with retention of nano-fiber polyethylene morphology. (Reproduced from Ref. [64]; © 2006 Elsevier.)

The incorporation of MWNTs in polymers is envisaged to produce structural materials with dramatically improved modulus and strength. However, the preparation of nanocomposites with CNTs dispersed homogeneously within a polymer matrix is a technical challenge, as this type of one-dimensional nanofiller shows a trend to form aggregates owing to very strong and numerous π-π interactions, as well as a high density of entanglements [66]. Recently, Dubois et al. [67] reported an original method which relies upon the *in-situ* polymerization of ethylene catalyzed by a highly active metallocene/MAO complex which was anchored physicochemically (i.e., by electrostatic interaction) onto the CNT surface. As a result, the CNTs were homogeneously coated by the *in-situ*-grown polyethylene chains, leading ultimately to the destruction of the nanotube bunches. The method used is derived from the polymerization-filling technique (PFT) initially investigated in Ziegler–Natta polymerization [68], and more recently developed for metallocene catalysis applied to a broad range of microfillers such as kaolin, silica, wollastonite, and graphite [69].

The PFT, as applied to CNTs according to Dubois [67], is shown schematically in Figure 11.9.

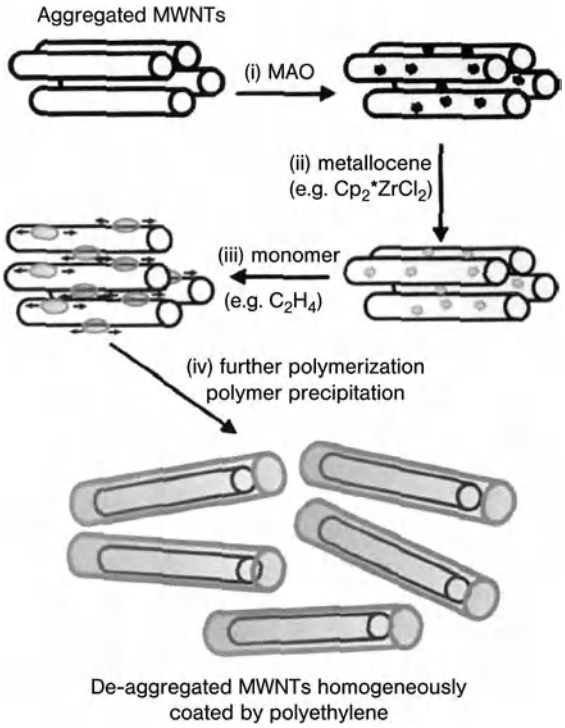

Figure 11.9 Polymerization filling technique as a means to deaggregate multi-walled carbon nanotubes (MWNTs). (Reproduced from Ref. [67]; © 2007, Royal Society of Chemistry.)

The purified MWNTs (Nanocyl® 3100; Nanocyl S.A., Sambreville, Belgium) used in the investigations of Dubois [66, 70] had an average diameter of 10 nm, with lengths ranging from ca. 0.1 μm to 10 μm. Depending on the cocatalyst employed (MAO or modified MAO-3A), the MWNTs were covered homogeneously or not, and showed either a relatively smooth or textured polymer coating present on the surface of individual, debundled nanotubes; that is, PE/MWNT nanohybrid "sausage"-like or "shish-kebab"-like structures, respectively. Thus, the type of coating morphology can be controlled by tuning the experimental conditions. As a result, the native CNT aggregates are isolated in comparison with the starting bundle-like associations. Such deaggregation of the nanotubes is desirable in order to obtain a truly nanocomposite structure with improved properties, and the results of Dubois et al. have shown that such PE-coated MWNTs, when melt-blended, may be dispersed homogeneously in various matrices, including high-density polyethylene [67] or ethylene-vinyl acetate copolymer [71].

In this context, Dubois et al. [70] achieved for the first time by the *in-situ* copolymerization of ethylene and 2-norbornene, a homogeneous surface coating of MWCNTs as catalyzed directly from the nanotube surface previously treated by the highly active metallocene-based complex-*rac*-Et(Ind)$_2$ZrCl$_2$/modified MAO-3A. This copolymerization reaction allows for the destruction of the native nanotube bundles which, upon further melt blending with an ethylene–vinyl acetate copolymer matrix (27 wt.% vinyl acetate), leads to high-performance polyolefinic nanocomposites. Depending on the experimental conditions used (e.g., ethylene pressure, solvent, feed norbornene concentration), the relative quantity of ethylene–norbornene copolymer can be tuned, as can the norbornene content incorporated along the polymer chain and, accordingly, the glass transition temperature [70].

In order to characterize the extent of ethylene–norbornene copolymer coating around the CNTs, TEM observations that contained 45 wt.% of copolymer were carried out. In Figure 11.10, MWNTs coated by *in-situ*-grown ethylene–norbornene

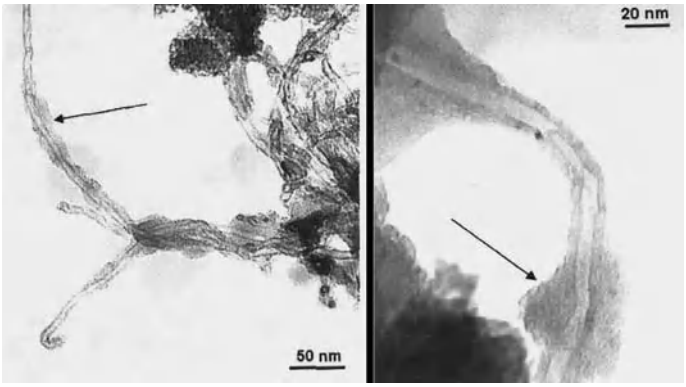

Figure 11.10 Transmission electron microscopy images of multi-walled carbon nanotubes (MWNTs) coated by *in-situ*-grown ethylene–norbornene copolymer. (Reproduced from Ref. [70]; © 2007, Wiley-VCH.)

copolymer are shown (highlighted by an arrow) [70], while MWNTs can also be observed relatively well separated from the starting highly entangled bundle-like associations, and covered by a rather homogeneous ethylene–norbornene copolymer layer (the coating average diameter is ca. 15 nm). The fine and homogeneous dispersion of a small amount of these coated CNTs (a few percent) in an ethylene–vinyl acetate copolymer model matrix, by somewhat conventional melt blending, caused a significant enhancement in the mechanical properties of the material [70].

Of interest, Funck and Kaminsky [72] have very recently reported on the possibility of polymerizing isotactic propylene from CNTs by also using a metallocene/MAO catalytic system and the PFT. In this study, the MAO cocatalyst proved to be covalently bound to the surface of oxidized CNTs, and this resulted in a better CNT/matrix interfacial adhesion (Figure 11.11) [72].

The figure shows hydroxyl or carboxyl groups present on the filler surface (tube edges) reacting with added MAO to form the heterogeneous cocatalyst. The MAO is now anchored, but still able to form an active complex with the metallocene. Therefore, the polymer is growing directly from the surface, and this leads to a good matrix adhesion. All thin straight and coiled MWCNTs used in these investigations (2 to 20 walls, average outer diameter 15 nm, length up to 50 μm) were supplied from Nanocyl S.A. The resultant nanocomposites had a filler content of 0.8 to 8 wt.%, and were investigated with respect to their morphology, crystallization and melting temperatures, and the half-time of crystallization (which decreases very rapidly depending on the rising filler content). All types of nanotubes were seen to act as nucleating agents, and this in turn increased the crystallization

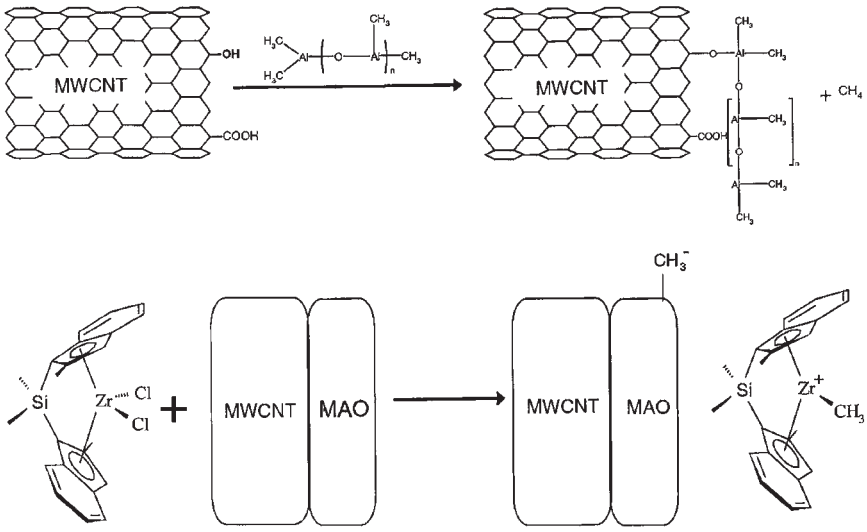

Figure 11.11 Methylaluminoxane (MAO) cocatalyst covalently bound to the surface of oxidized carbon nanotubes. (Reproduced from Ref. [72]; © 2007, Wiley-VCH.)

temperature, the rate constant of crystallization, and the dimension of the crystallite growth. In addition, coated MWCNTs were found to have a lower nucleating ability than did the non-covered nanotubes [72].

References

1 J.R. Severn, J.C. Chadwick, R. Duchateau, N. Friederichs, *Chem. Rev.* 2005, *105*, 4073.

2 (a) T. Arai, H.T. Ban, T. Uozumi, K. Soga, *J. Polym. Sci.: Polym. Chem.* 1998, *36*, 421; (b) K. Soga, H.T. Ban, T. Arai, T. Uozumi, *Macromol. Chem. Phys.* 1997, 198, 2779; (c) T. Arai, H.T. Ban, T. Uozumi, K. Soga, *Macromol. Chem. Phys.* 1997, *198*, 229; (d) K. Soga, T. Uozumi, T. Arai, DE19636233, *Chem. Abstr.* 1997, *126*, 277881; (e) K. Soga, T. Arai, B.T. Hoang, T. Uozumi, *Macromol. Rapid Commun.* 1995, *16*, 905.

3 H.T. Ban, T. Uozumi, T. Sano, K. Soga, *Macromol. Chem. Phys.* 1999, *200*, 1897.

4 (a) J.H.Z. dos Santos, H.T. Ban, et al., *Appl. Catal., A* 2001, *220*, 287; (b) J.H.Z. dos Santos, T. Uozumi, T. Teranishi, T. Sano, K. Soga, *Polymer* 2001, 42, 4517; (c) J.H.Z. dos Santos, H.T. Ban, et al., *J. Mol. Catal.: Chem.* 2000, *158*, 541.

5 C. Dever, A. Deffieux, H. Cramail, S. Mastroianni, *Macromol. Rapid Commun.* 2003, *24*, 883.

6 M. Antberg, L. Boehm, J. Rohrmann, DE3840772, *Chem. Abstr.* 1990, *115*, 208842.

7 S. Nagy, J.A. Tyrell, L.V. Cribbs, WO9745459, *Chem. Abstr.* 1997, *128*, 48616.

8 S. Nagy, J.A. Tyrell, L.V. Cribbs, WO9741157, *Chem. Abstr.* 1997, *128*, 4003.

9 H.G. Alt, P. Schertl, A. Koppl, *J. Organomet. Chem.* 1998, *568*, 263.

10 A. Koppl, H.G. Alt, R. Schmidt, *J. Organomet. Chem.* 1999, *577*, 351.

11 H. Alt, F. Baumann, J. Weis, A. Koppl, WO9914269, *Chem. Abstr.* 1999, *130*, 252799.

12 M. Helldorfer, H.G. Alt, J. Ebenhoch, *J. Appl. Polym. Sci.* 2002, *86*, 3021.

13 R. Schmidt, H.G. Alt, J. Ebenhoch, *J. Appl. Polym. Sci.* 2001, *80*, 281.

14 (a) H. Makio, K. Koo, T.J. Marks, *Macromolecules* 2001, *34*, 4676; (b) T.J. Marks, K. Koo, US6077919, *Chem. Abstr.* 2000, *133*, 59231; (c) K. Koo, T.J. Marks, *J. Am. Chem. Soc.* 1999, 121, 8791; (d) K. Koo, P.-F. Fu, T.J. Marks, *Macromolecules* 1999, *32*, 981; (e) K. Koo, T.J. Marks, *J. Am. Chem. Soc.* 1998, *120*, 4019; (f) T.J. Marks, P.-F. Fu, EP739910, *Chem. Abstr.* 1996, *125*, 329872.

15 K.E. Meyer, M.K. Reinking, US6642326, *Chem. Abstr.* 2003, *139*, 338344.

16 M.A. Grunlan, K.R. Regan, D.E. Bergbreiter, *Chem. Commun.* 2006, 1715.

17 D.A. Fonseca, K.E. Collins, C.H. Collins, *J. Chromatogr., A* 2004, *1030*, 209.

18 D.J. Rauscher, W.J. Gauthier, US7125937, *Chem. Abstr.* 2006, *145*, 124946.

19 S.C. Hong, H.T. Ban, N. Kishi, J.Z. Jin, T. Uozumi, K. Soga, *Macromol. Chem. Phys.* 1998, *199*, 1393.

20 S.C. Hong, T. Teranishi, K. Soga, *Polymer* 1998, *39*, 7153.

21 M. Stork, M. Koch, M. Klapper, K. Müllen, H. Gregorius, U. Rief, *Macromol. Rapid Commun.* 1999, *20*, 210.

22 W.Q. Wang, L. Wang, J.F. Wang, Z.L. Ma, J.J. Wang, *J. Appl. Polym. Sci.* 2005, *97*, 1632.

23 S.B. Roscoe, J.M.J. Frechet, J.F. Walzer, A.J. Dias, *Science* 1998, *280*, 270.

24 (a) Y.-J. Jang, C. Naundorf, M. Klapper, K. Müllen, *Macromol. Chem. Phys.* 2005, *206*, 2027; (b) Y.-J. Jang, K. Bieber, C. Naundorf, N. Nenov, M. Klapper, K. Müllen, D. Ferrari, S. Knoke, G. Fink, Optical methods to study the behavior of supported metallocene catalysts during olefin polymerisation, in *e-Polymers*, 2005, *13*.

25 A.S. Shearer, Y.R. de Miguel, E.A. Minich, D. Pochan, C. Jenny, *Inorg. Chem. Commun.* 2007, *10*, 262.

26 P.D. Bolton, N. Adams, E. Clot, A.R. Cowley, P.J. Wilson, M. Schroeder, P. Mountford, *Organometallics* 2006, *25*, 5549.

27 A.J. Nielson, M.W. Glenny, C.E.F. Rickard, *Dalton Trans*. 2001, 232.

28 M.C.W. Chan, K.C. Chew, C.I. Dalby, V.C. Gibson, A. Kohlmann, I.R. Little, W. Reed, *Chem. Commun*. 1998, 1673.

29 S.C. Hong, U. Rief, M.O. Kristen, *Macromol. Rapid Commun*. 2001, *22*, 1447.

30 Y.X. Qin, T. Tang, Z.F. Zhao, B.T. Huang, *J. Polym. Sci.: Polym. Chem*. 2003, *41*, 3313.

31 L.Y. Shi, Y.X. Qin, W.X. Cheng, H. Chen, T. Tang, *Polymer* 2007, *48*, 2481.

32 K. Musikabhumma, T. Uozumi, T. Sano, K. Soga, *Macromol. Rapid Commun*. 2000, *21*, 675.

33 M. Klapper, C.G. Clark, K. Müllen, *Polym. Int*. 2007, 56, in press (doi 10.1002/pi.2301).

34 M. Koch, M. Stork, M. Klapper, K. Müllen, H. Gregorius, *Macromolecules* 2000, *33*, 7713.

35 M. Koch, A. Falcou, N. Nenov, M. Klapper, K. Müllen, *Macromol. Rapid Commun*. 2001, *22*, 1455; (b) M. Klapper, Y.J. Jang, K. Bieber, T. Nemnich, N. Nenov, K. Müllen, *Macromol. Symp*. 2004, 213, 131.

36 C. Naundorf, S. Matsui, et al., *J. Polym. Sci.: Polym. Chem*. 2006, *44*, 3103.

37 M. Klapper, S. Nenov, T. Diesing, K. Müllen, *Macromol. Symp*. 2007, accepted.

38 F.H. Meng, G.Q. Yu, B.T. Huang, *J. Polym. Sci.: Polym. Chem*. 1999, *37*, 37.

39 M. Koch, M. Klapper, K. Müllen, *Organomet. Catal. Olefin Polym*. 2001, 396.

40 J.M. Zhou, N.H. Li, N.Y. Bu, D.T. Lynch, S.E. Wanke, *J. Appl. Polym. Sci*. 2003, *90*, 1319.

41 C. Bouilhac, E. Cloutet, A. Deffieux, D. Taton, H. Cramail, *Macromol. Chem. Phys*. 2007, *208*, 1349.

42 C. Bouilhac, H. Cramail, E. Cloutet, A. Deffieux, D. Taton, *J. Polym. Sci.: Polym. Chem*. 2006, *44*, 6997.

43 F. Langhauser, J. Kerth, M. Kersting, P. Kolle, D. Lilge, P. Müller, *Angew. Makromol. Chem*. 1994, *223*, 155.

44 (a) K. Zollner, K.H. Reichert, *Chem. Ing. Tech*. 2001, *73*, 849; (b) S. Knoke, D. Ferrari, B. Tesche, G. Fink, *Angew. Chem., Int. Ed*. 2003, 42, 5090.

45 M. Klapper, D. Fischer, Y.J. Jang, C. Naundorf, K. Müllen, *DECHEMA Monographien* 2004, *138*, 275.

46 K. Tsumoto, F. Luckel, K. Yoshikawa, *Biophys. Chem*. 2003, *106*, 23.

47 S. Knoke, F. Korber, G. Fink, B. Tesche, *Macromol. Chem. Phys*. 2003, *204*, 607.

48 B. Helms, J.M.J. Frechet, *Adv. Synth. Catal*. 2006, *348*, 1125.

49 M. Mager, S. Becke, H. Windisch, U. Denninger, *Angew. Chem., Int. Ed* 2001, *40*, 1898.

50 V. Atanasov, V. Sinigersky, M. Klapper, K. Müllen, *Macromolecules* 2005, *38*, 1672.

51 (a) M. Stork, U.M. Wiesler, M. Klapper, K. Müllen, *Polym. Mater. Sci. Eng*. 1999, *80*, 8; (b) N. Nenov, Ph-thesis, Polymer carriers for metallocene catalysts in heterogeneous olefin polymerisation, in: *MPI Polymerforschung*, Mainz, 2003.

52 K.E. Meyer, M.K. Reinking, WO2001036096, *Chem. Abstr*. 2001, *135*, 5981.

53 T. Sugano, JP08208733, *Chem. Abstr*. 1996, *125*, 276900.

54 (a) L. Resconi, E. Ciaccia, A. Fait, WO2004092230, *Chem. Abstr*. 2004, *141*, 380567; (b) M. Covezzi, A. Fait, WO2001044319, *Chem. Abstr*. 2001, *135*, 61744.

55 (a) R. Schlund, B. Rieger, EP518092, *Chem. Abstr*. 1992, *119*, 50091; (b) H.F. Herrmann, B. Bachmann, B. Hierholzer, W. Spaleck, EP563917, *Chem. Abstr*. 1993, *120*, 192572; (c) P. Francois, S. Bettonville, D. Marchand, EP1013676, *Chem. Abstr*. 2000, *133*, 59223; (d) J.-L. Costa, V. Laurent, P. Francois, D. Vercammen, EP627447, *Chem. Abstr*. 1994, *122*, 291760; (e) P. Francois, S. Bettonville, D. Marchand, EP1013677, *Chem. Abstr*. 2000, *133*, 74458; (f) T. Matsukawa, M. Nakano, M. Takahashi, JP10152516, *Chem. Abstr*. 1998, *129*, 82077.

56 Y.N. Bocharov, V.A. Kabanov, M.A. Martynova, V.G. Popov, V.I. Smentjuk, V.V. Federov, SU492298, *Chem. Abstr*. 1975, *84*, 60257.

57 (a) N.K. Boaen, M.A. Hillmyer, *Chem. Soc. Rev*. 2005, *34*, 267; (b) G. Moad, *Prog. Polym. Sci*. 1999, 24, 81; (c) T.C.M. Chung, *Functionalization of Polyolefins*, 2002.

58 T. Sunaga, Y. Ishii, T. Asanuma, EP773237, *Chem. Abstr*. 1997, *127*, 34628.

59 J. Liu, J.-Y. Dong, N. Cui, Y. Hu, *Macromolecules* 2004, *37*, 6275.

60 Similar boron-mediated transformations were previously used by Chung et al. to synthesize well-defined polyolefins with block or graft structures; (a) J.Y. Dong, E. Manias, T.C. Chung, *Macromolecules* 2002, *35*, 3439; (b) T.C. Chung, D. Rhubright, *Macromolecules* 1994, *27*, 1313; (c) T.C. Chung, D. Rhubright, G.J. Jiang, *Macromolecules* 1993, *26*, 3467.

61 N. Medard, J.-C. Soutif, I. Lado, C. Esteyries, F. Poncin-Epaillard, *Macromol. Chem. Phys.* 2001, *202*, 3606.

62 S. Iijima, *Nature* 1991, *354*, 56.

63 (a) M.M.J. Treacy, T.W. Ebbesen, J.M. Gibson, *Nature* 1996, *381*, 678; (b) E.W. Wong, P.E. Sheehan, C.M. Lieber, *Science* 1997, *277*, 1971; (c) P.M. Ajayan, *Chem. Rev.* 1999, *99*, 1787; (d) R.H. Baughman, A.A. Zakhidov, W.A. de Heer, *Science* 2002, *297*, 787.

64 X. Dong, L. Wang, T. Sun, J. Zhou, Q. Yang, *J. Mol. Catal.: Chem.* 2006, *255*, 10.

65 E. Dujardin, T.W. Ebbesen, A. Krishnan, M.M.J. Treacy, *Adv. Mater.* 1998, *10*, 611.

66 D. Bonduel, S. Bredeau, M. Alexandre, F. Monteverde, P. Dubois, *J. Mater. Chem.* 2007, *17*, 2359.

67 D. Bonduel, M. Mainil, M. Alexandre, F. Monteverde, P. Dubois, *Chem. Commun.* 2005, 781.

68 (a) L.A. Kostandov, N.S. Enikolopov, F.S. Dyachkovskij, L.A. Novokshonova, Y.A. Gavrilov, O. Kudinova, T.A. Maklakova, L.A. Akopyan, K.-M.A. Brikenshtejn, SU763379, *Chem. Abstr.* 1980, *94*, 4588; (b) E.G. Howard, Jr., US4097447, *Chem. Abstr.* 1978, *89*, 164489.

69 (a) W. Kaminsky, H. Zielonka, *Polym. Adv. Technol.* 1993, *4*, 415; (b) M. Alexandre, E. Martin, P. Dubois, M. Garcia-Marti, R. Jerome, *Macromol. Rapid Commun.* 2000, 21, 931; (c) M. Alexandre, E. Martin, P. Dubois, M.G. Marti, R. Jerome, *Chem. Mater.* 2001, *13*, 236; (d) M. Alexandre, M. Pluta, P. Dubois, R. Jerome, *Macromol. Chem. Phys.* 2001, *202*, 2239.

70 S. Bredeau, L. Boggioni, F. Bertini, I. Tritto, F. Monteverde, M. Alexandre, P. Dubois, *Macromol. Rapid Commun.* 2007, *28*, 822.

71 S. Peeterbroeck, B. Lepoittevin, E. Pollet, S. Benali, C. Broekaert, M. Alexandre, D. Bonduel, P. Viville, R. Lazzaroni, P. Dubois, *Polym. Eng. Sci.* 2006, *46*, 1022.

72 A. Funck, W. Kaminsky, *Composites Sci. Technol.* 2007, *67*, 906.

12
Self-immobilizing Catalysts for Olefin Polymerization

Helmut G. Alt and Christian Görl

12.1
General Aspects: Why Heterogenize Homogeneous Olefin Polymerization Catalysts?

The idea of designing catalysts that can produce their own support is very convincing, because a whole series of problems associated with the commercialization of a homogeneous catalyst can be solved:

- The advantages of homogeneous and heterogeneous catalysts can be combined because the polymerization process starts with a homogeneous catalyst that becomes heterogeneous by self-immobilization.
- The disadvantages of supports can be avoided, such as the fact that they may have a negative influence on the activity of the catalyst, for example when the catalyst has Lewis acidic properties and the support surface has Lewis basic properties. Such a situation is faced when metallocene or half-sandwich catalysts are supported on the widely used silica.
- The price of a support is not negligible. In order to fix 1 kg of a catalyst on a support at a concentration of 2%, 50 kg of support are necessary. Price-wise, 1 kg of a support such as silica may easily cost $US 10.
- As the catalyst and support remain in the produced polyolefin, a problem may be created when such products are burned or recycled thermally (e.g., with magnesium chloride as support).
- The "bleeding" problem of heterogeneous catalysts can be eliminated because the heterogeneous catalyst is a chemical compound and not a physically adsorbed species.
- Patent infringements can be avoided because many support materials are patented.

Tailor-Made Polymers. Via Immobilization of Alpha-Olefin Polymerization Catalysts.
Edited by John R. Severn and John C. Chadwick

ISBN: 978-3-527-31782-0

12.2
A New Approach: Self-immobilizing Catalysts – Let the Catalyst Produce its own Support

How can all of the disadvantages mentioned above be avoided? The answer is very simple: the catalyst should not only be a catalyst but also an olefin. When the catalyst has copolymerization potential it should be possible not only to polymerize a monomer such as ethylene but also to copolymerize a homogeneous catalyst molecule as soon as it is available in solution. As a consequence, a multinuclear network is formed and every metal center in this network maintains its potential to start a new polymerization. This is the moment when a homogeneous catalyst becomes heterogeneous, as shown in Scheme 12.1.

When the homogeneous catalyst precursor is activated with methylaluminoxane (MAO) in toluene, the yellow color of the dissolved catalyst precursor turns into dark red, although the solution remains completely homogeneous. As soon as an olefin such as ethylene is bubbled through the solution, a dark red precipitate is formed (Figure 12.1). This precipitate can be isolated by filtration, washed with toluene and pentane, dried, and stored for years without losing its catalytic properties. It is an active heterogeneous catalyst that can be applied as a so-called "drop-in" catalyst. Although it is not necessary to isolate the heterogeneous species, this is only a possible option that is recommended when the catalyst is to be stored for longer periods of time.

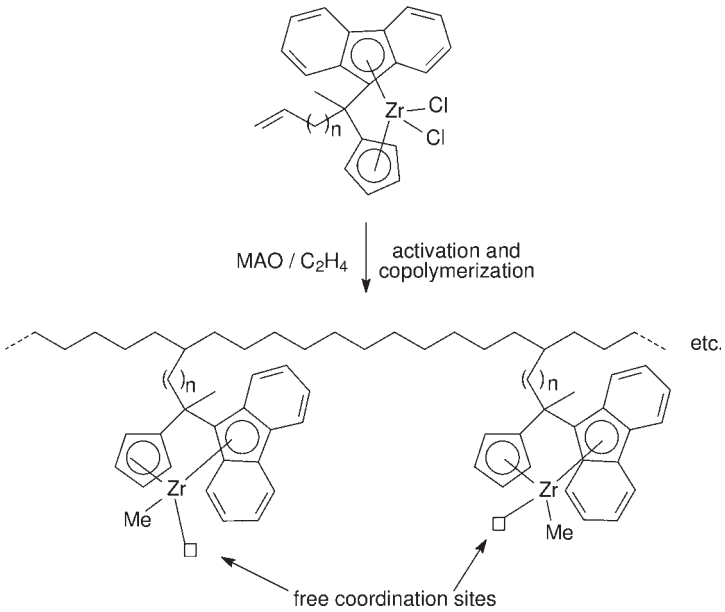

Scheme 12.1 Proposed mechanism for the "self-immobilization" of a homogeneous *ansa*-metallocene catalyst [1].

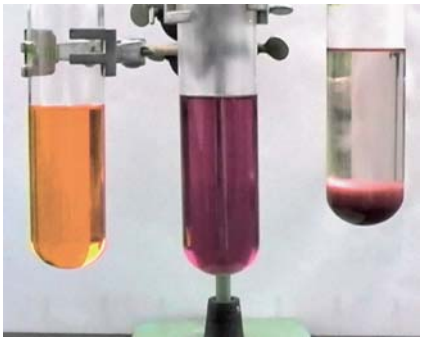

Figure 12.1 Self-immobilization of a homogeneous metallocene catalyst with ethylene in a Schlenk tube. Left: a solution of the catalyst precursor in toluene (yellow). Center: after activation with methylaluminoxane (red). Right: the precipitated self-immobilized catalyst (dark red) [2].

12.3 Self-immobilizing Metallocene Catalysts

12.3.1 Preparation of Various Alkenyl Functionalized Metallocene Complexes

Metallocene catalysts are very attractive because they offer many advantages compared to Ziegler–Natta or Phillips catalysts, and they already contribute to commercial processes. They show high activities or stereoselectivities when prochiral olefins such as propene are polymerized, they produce unique polyolefin materials with narrow molecular weight distributions (MWDs), and the resin properties can be designed with "structure–property" relationships in mind. Today, numerous reviews have been prepared dealing with the preparation, characterization and application of various metallocene catalysts [1–44]. Since 1990, the Alt group, at the University of Bayreuth, has synthesized more than 700 different metallocene complexes in order to study structure–property relationships empirically in order to produce tailored polyolefins [10, 15,16, 45–87]. Some of these superior resins are already available commercially, such as the linear low-density polyethylene (LLDPE) "mPact" (ChevronPhillips) or "Elite" (Dow) [88].

A major disadvantage, however, is the fact that heterogenization [89–91] of these homogeneous catalysts on a support such as silica can be accompanied by a drastic loss of activity, due to the fact that the actual catalyst is a strong Lewis acid, a cationic 14-electron species, and the support contains plenty of heteroatoms such as oxygen, behaving as Lewis bases (Scheme 12.2).

Another goal was to avoid all of these disadvantages and to combine the advantages of homogeneous and heterogeneous catalysts. In addition, it can be very disadvantageous when zirconium or hafnium are used as metals in these complexes because they are known for their strong oxophilicity.

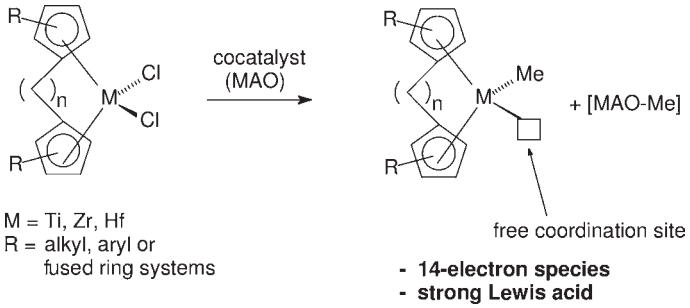

Scheme 12.2 Activation steps for a metallocene catalyst precursor [1].

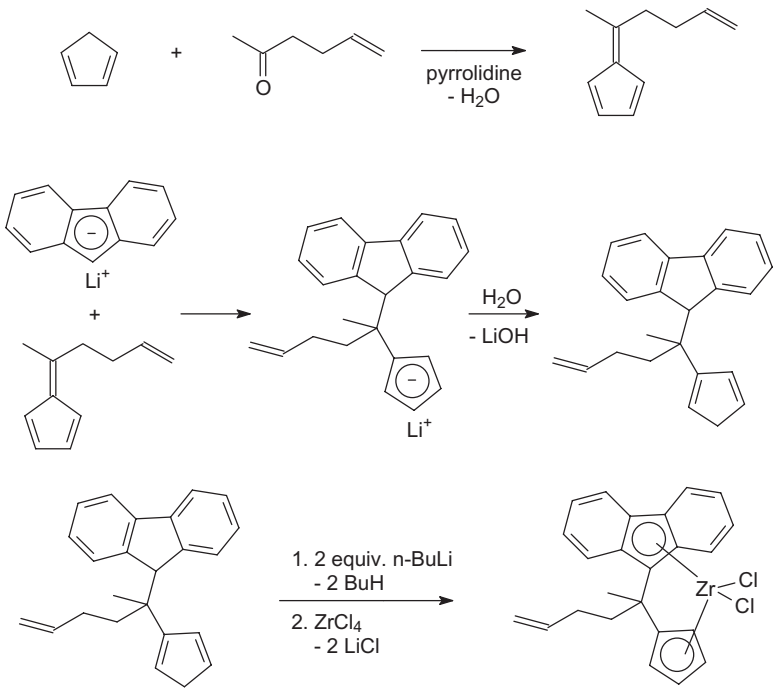

Scheme 12.3 Preparation of an *ansa*-metallocene complex containing an ω-alkenyl function in the bridge [61].

In order to functionalize metallocene compounds with an olefinic group, a variety of possibilities are feasible [61, 63, 64, 66, 69]. For example, one or more olefin functions containing substituents can be placed on the aromatic ligands (cyclopentadienyl, indenyl or fluorenyl). In the case of *ansa*-metallocene complexes, such substituents can also be placed as terminal groups on the bridging unit. The example shown in Scheme 12.3 illustrates the preparation of an *ansa*-cyclopentadienyl-fluorenyl metallocene complex containing an ω-alkenyl function in the bridge.

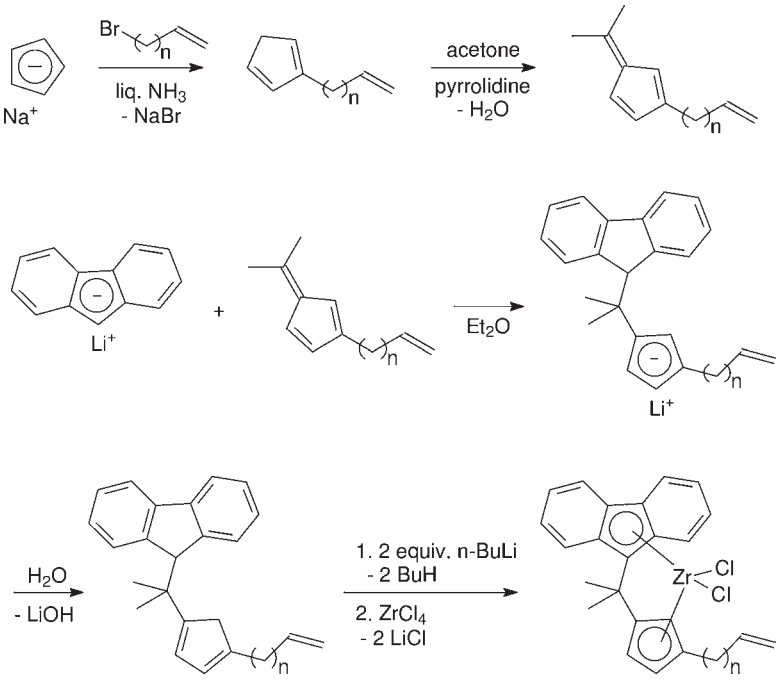

Scheme 12.4 Preparation of an *ansa*-metallocene complex with an ω-alkenyl function on the cyclopentadienyl ligand [61].

The introduction of ω-alkenyl groups into the bridging unit can also be accomplished using ω-alkenyl-substituted dichlorosilanes; these may be reacted with the sodium or lithium salts of cyclopentadiene, indene, and fluorene or their derivatives to yield silicon-bridged ligand precursors [48, 63, 65, 67].

In a similar manner, it is possible to fix an alkenyl function on an aromatic ligand such as a cyclopentadienyl, an indenyl or a fluorenyl ligand or their substituted derivatives (Scheme 12.4) [61].

The length of the spacer between the actual ligand and the olefin function has a very strong influence on the activities of such catalysts (the "dog on the leash" phenomenon) (Figure 12.2) [66, 72, 75].

While complexes containing internal alkenyl or alkynyl functions also have the potential to self-immobilization [61], complexes containing ω-alkynyl groups on their ligand frameworks do not react in the desired manner but rather yield black polyacetylene derivatives upon activation with alkyl aluminum compounds [61].

12.3.2
Metallacyclic Metallocene Complexes [32, 75, 92–131]

In nearly all cases metallocene catalyst precursors are applied as the corresponding dichloride compounds. Upon activation with methylaluminoxane (MAO) or other

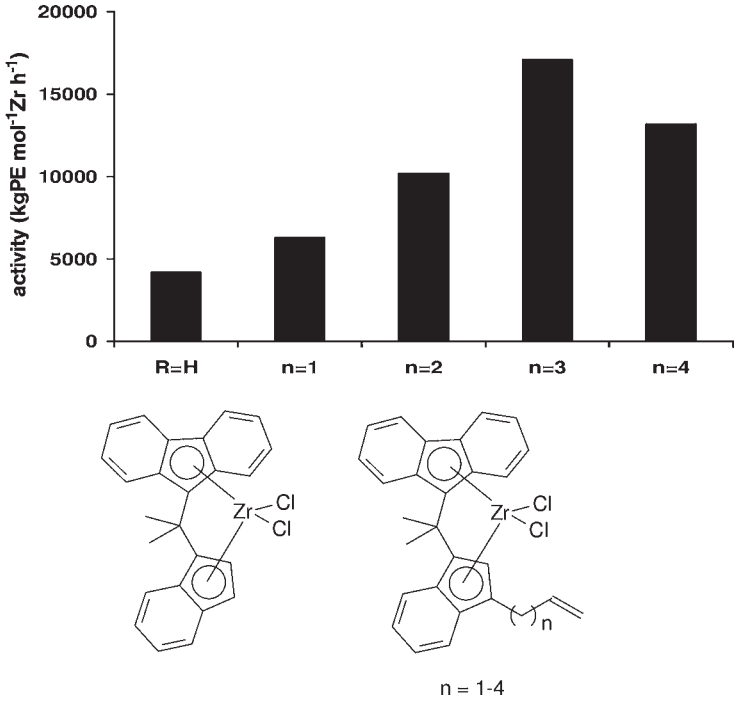

Figure 12.2 Influence on the ω-alkenyl chain length on the polymerization activities of some C_1-bridged fluorenyl-indenyl-zirconium complexes [66].

cocatalysts, both chloride ligands are substituted and a cationic metallocene monomethyl catalyst cation is formed; this is the actual catalyst. In this process, the halides are fixed on the MAO counteranions and remain in the produced polyolefin because the catalyst is neither recycled nor recovered. This fact has two consequences:

- As halides are Lewis bases they can interact with the catalyst cation, which is a strong Lewis acid, and thus reduce the activity of the corresponding catalyst. Another disadvantageous effect appears when such polyolefins are burned or thermally recycled.
- The formation of hydrogen halides can cause corrosion and pollution, especially in cases when metallocene dichlorides are activated with perfluorated boranes or borates.

In order to avoid all of these disadvantages, thermally stable metallacyclic metallocene complexes were synthesized that did not contain any halides [32, 75, 124–131]. In addition, these complexes had the potential for self-immobilization. The reaction shown in Scheme 12.5 describes the preparation of a metallacycle starting with the parent dichloride complex:

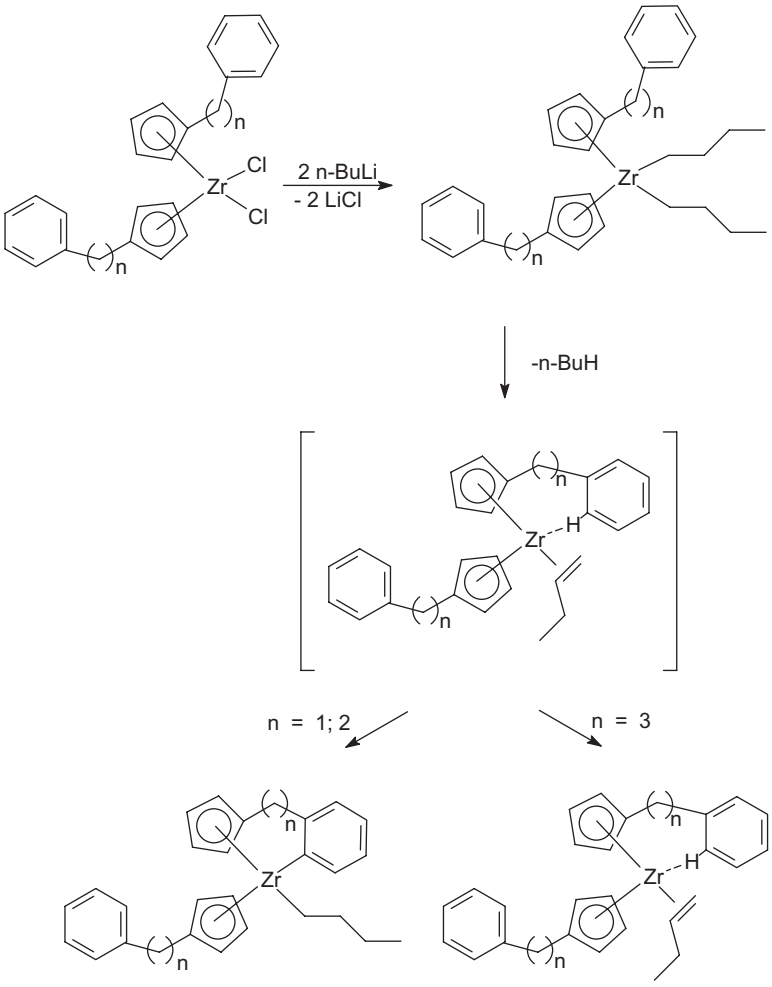

Scheme 12.5 Preparation of a metallacyclic metallocene complex by *ortho*-metallation of a phenyl substituent [32, 75, 125, 126].

Depending on the number of spacer carbon atoms and the end groups of substituents, differently structured metallacycles are accessible (Scheme 12.6) [2, 32, 66, 76, 126, 127].

Metallacyclic metallocene complexes can be activated with MAO and then be applied as catalysts for ethylene polymerization. In most cases they show higher activities than the parent metallocene dichloride complexes [125, 126, 128, 130], and they are self-immobilizing in solution [2]. In this respect, the mechanism in Scheme 12.7 is suggested:

As an alternative, a non-metallacyclic active species may also be discussed, whereby the butyl ligand is coordinated to the metal and the MAO anion is bonded to the *ortho*-position of the aromatic system (see Scheme 12.8) [1].

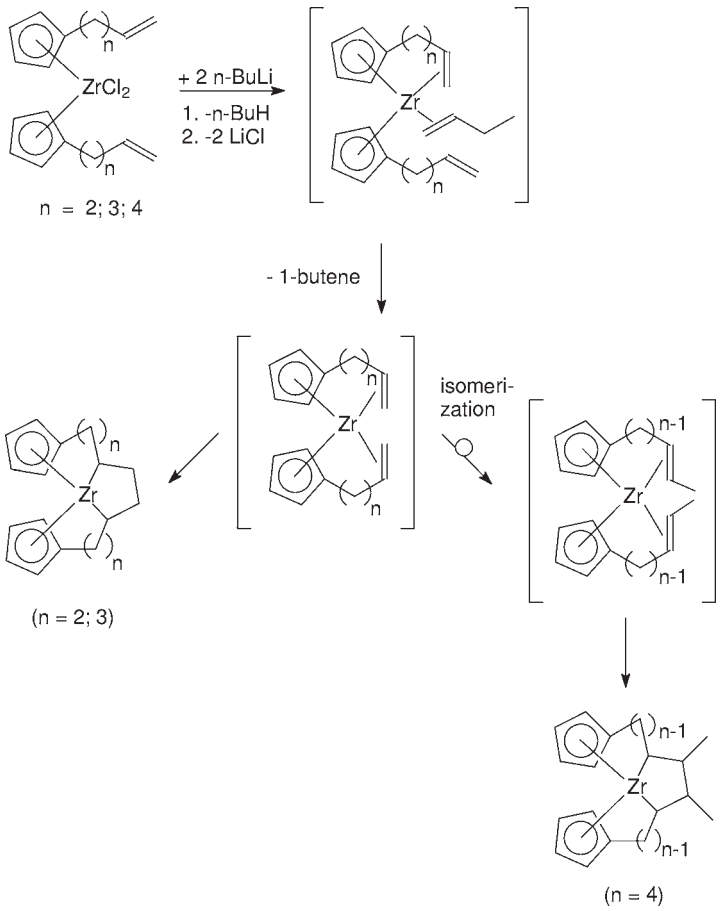

Scheme 12.6 Influence of the number n of spacer methylene groups onto the preparation of various metallacyclic complexes from their parent dichloride complexes [127]. For more theoretical details, see Refs. [100, 101].

In the case of non-aromatic metallacycles (Scheme 12.9):

Following activation of the metallacycle with MAO and formation of the cationic homogeneous catalyst, ethylene can coordinate to the metal and insert into the already existing metal–carbon-σ-bond. These steps can occur over and over again, in so doing "pumping up" the ring size until β-hydrogen elimination occurs forming an olefin function that can be used for copolymerization, and a metal hydride function that has the catalytic potential to start a new polymer chain. Ultimately, a heterogeneous multinuclear catalytic network is formed that does not contain any halide molecules when it is separated from the reaction solution by filtration. In most cases, the activity of such metallacyclic catalysts is considerably higher than that of the corresponding chlorine-containing parent complexes (Figure 12.3).

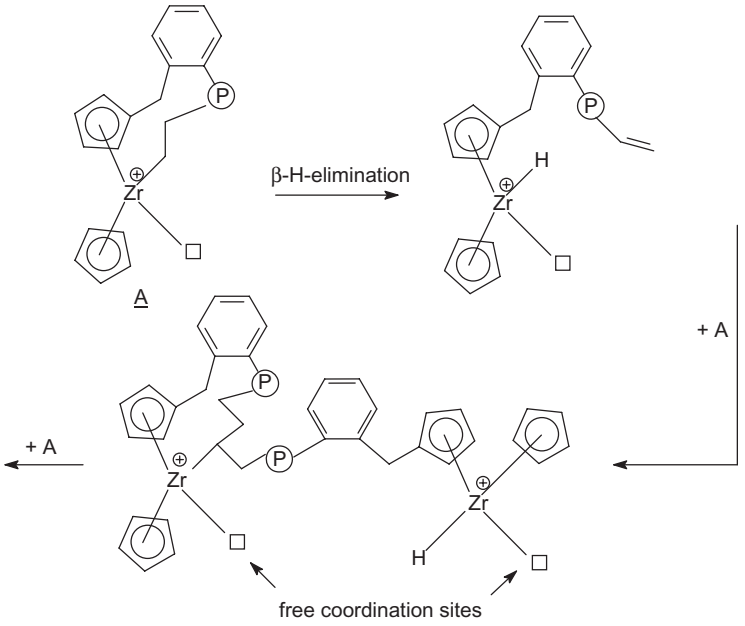

Scheme 12.7 Formation of a polynuclear heterogeneous catalyst network by self-induced β-hydrogen elimination and subsequent copolymerization [1].

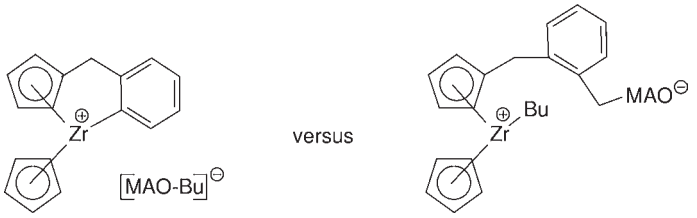

Scheme 12.8 The possibility of various active species.

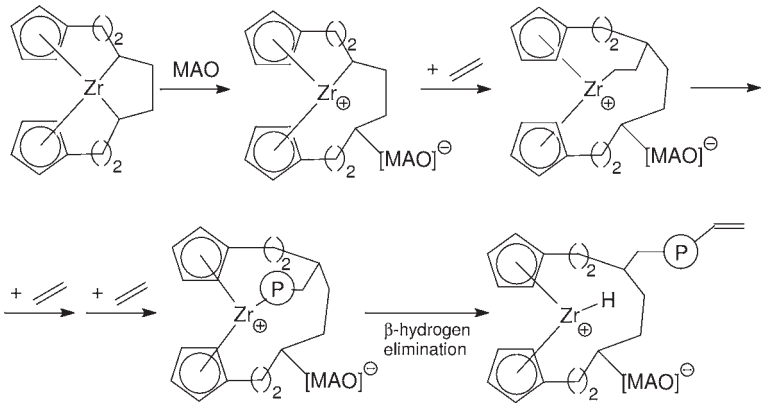

Scheme 12.9 Activated metallacycles as catalysts for ethylene polymerization [32].

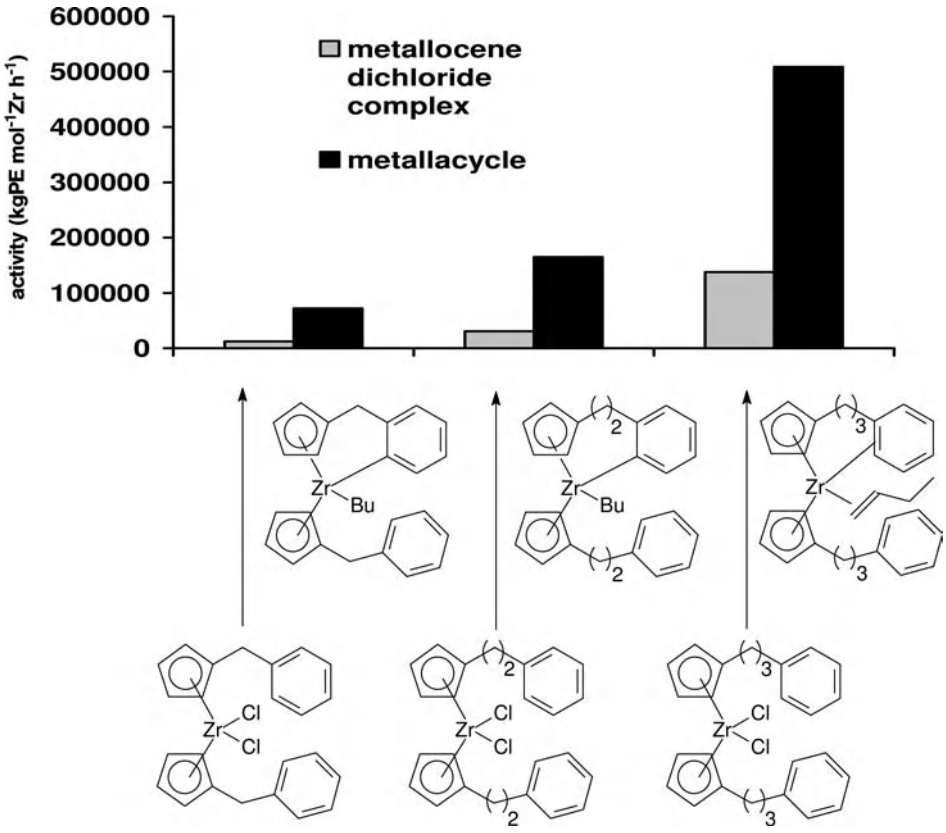

Figure 12.3 Comparison of activities in ethylene polymerization: parent complex versus metallacycle (60 °C, Al : Zr = 3000 : 1, pentane, 1 h, 10 bar ethylene) [126].

The differences between the molecular weights of the produced polyethylenes are quite small, although in most cases they are somewhat lower when formed by metallacyclic catalysts than by the corresponding parent complexes (Figure 12.4).

It cannot be excluded that the apparently lower molecular weights of the "metallacyclic" polyethylenes rather derive from branching effects.

12.4 Self-immobilizing Half-Sandwich Complexes

Although simple ω-alkenyl-substituted half-sandwich complexes such as (allylcyclopentadienyl)zirconium trichloride or (1-allylindenyl)zirconium trichloride have not been reported, details of the analogous titanium complexes have been published by the Alt group [80]. The corresponding catalysts showed only low activities

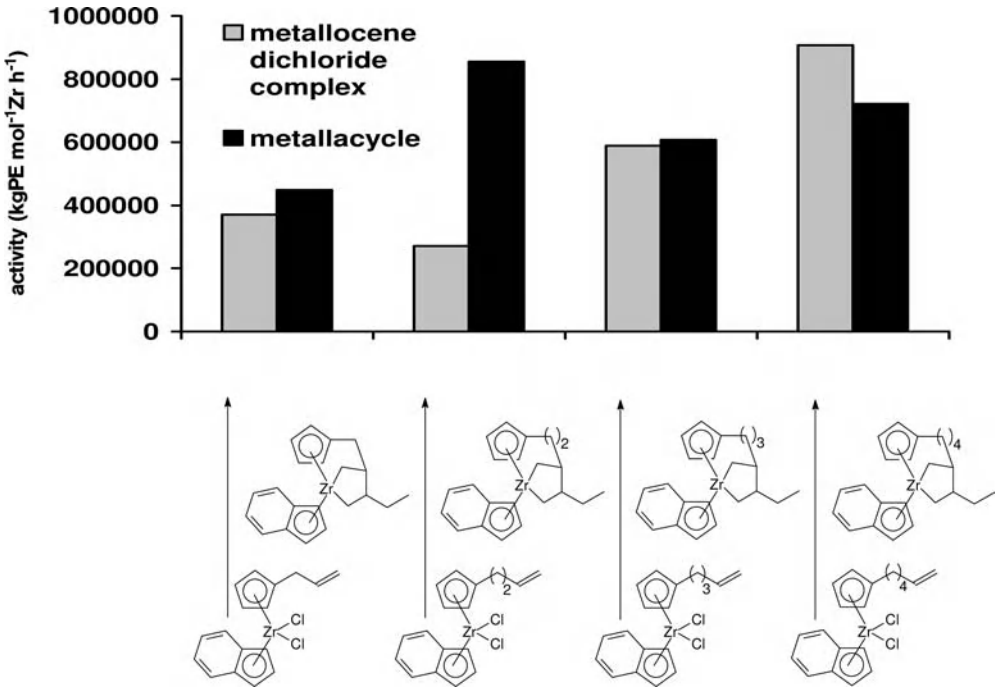

Figure 12.4 Comparison of molecular weights of polyethylenes produced with metallocene dichloride and metallacyclic metallocene derivatives [127].

in the polymerization of ethylene. Fixing the π-ligand, as it is realized in *ansa*-amido functionalized half-sandwich complexes (so-called "constrained geometry catalysts"; CGC), has a beneficial effect on the polymerization behavior. Complexes of this type [132–142] are very attractive olefin polymerization catalysts not only because of high activities but also because of their high copolymerization potential [138, 143–148] and their high thermal stabilities. Therefore, these complexes are excellent candidates as self-immobilizing catalysts. Scheme 12.10 illustrates the possible ways to functionalize such molecules and to perform analogous reactions, as in the case of metallocene complexes [138–140].

The synthesis of such complexes is straightforward because some reaction steps can be applied from the corresponding metallocene chemistry.

The prepolymerization of the activated catalyst with ethylene proceeds in a similar way: the olefin function of the catalyst is incorporated into the growing polymer chain via copolymerization, and the new active site in the "prepolymerized" polyethylene begins to grow its own polymer chain.

Indenylidene complexes have much higher activities than the corresponding cyclopentadienyl derivatives. This behavior is already known from metallocene catalysis [16], and one reason could be that the electron system of the indenyl ligand (potential ring slippage behavior) is more flexible than in the case of the

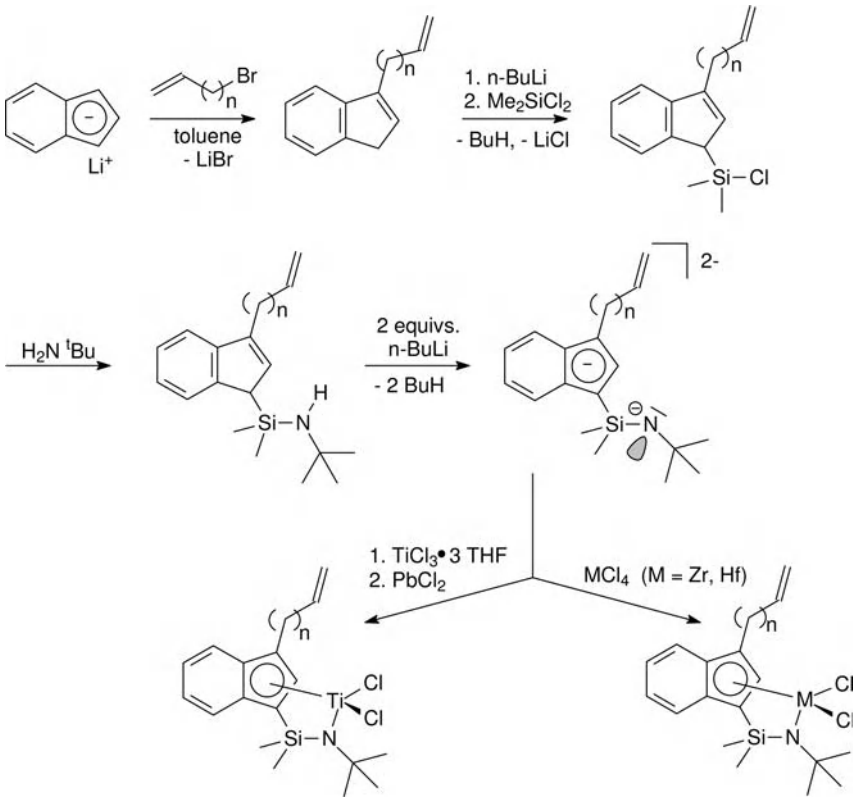

Scheme 12.10 Preparation of amido-functionalized half-sandwich complexes. Instead of indenyllithium, cyclopentadienylsodium may also be used [138–140].

cyclopentadienyl system. Another important parameter for the activity is the chain length of the substituent containing the ω-alkenyl group. A similar result has been observed with ω-alkenyl-functionalized metallocene complexes [66, 127, 129], and interpreted with the restricted mobility of the catalyst molecule that is fixed on the backbone of the polymer chain (the "dog on the leash" phenomenon) (Scheme 12.11).

The longer the chain, the better the activity of the corresponding zirconium catalyst (see Table 12.1, complexes 6–9) [138], while the activities of analogous titanium catalysts decrease with longer ω-alkenyl chain lengths (complexes 1–5). It is difficult to predict trends because small differences in the structure of the catalyst can induce a strong impact on the kinetics of the polymerization process. Hafnium catalysts of the amido-functionalized half-sandwich type generally show lower activities in ethylene polymerization than do analogous titanium or zirconium derivatives [137, 138].

Upon activation with MAO and pre-polymerization at low ethylene pressure, again a heterogeneous multinuclear catalyst is formed supported on its own poly-

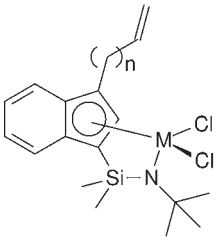

Complex	M	n
1	Ti	1
2	Ti	2
3	Ti	3
4	Ti	4
5	Ti	5
6	Zr	1
7	Zr	2
8	Zr	3
9	Zr	4
10	Hf	4

Scheme 12.11 Selected *ansa*-amido functionalized half-sandwich complexes [138–140].

Table 12.1 Polymerization data for selected amido-functionalized half-sandwich complexes.

Complex	*Activity (kg PE mmol^{-1} M h^{-1})*	*SEC*			*DSC*		
		M_w (g mol^{-1})	*M_n (g mol^{-1})*	*PD*	*T_m (°C)[a]*	*ΔH_m (J g^{-1})*	*α [b]*
1	1046	>1 100 000[c]	ND	ND	136.5	99.2	34.2
2	9421	>1 100 000	ND	ND	136.6	98.7	34.0
3	3607	695 300	ND	ND	141.5	126.5	43.6
4	3324	573 000	71 500	8.01	138.3	101.1	34.9
5	2246	1 207 000	203 500	5.93	ND	ND	ND
6	1961	875 800	228 800	3.29	138.8	125.3	43.2
7	2864	>1 100 000	ND	ND	141.5	138.5	47.6
8	1396	>1 100 000	ND	ND	139.2	108.5	37.4
9	4260	1 179 000	189 600	6.22	141.9	141.1	48.7
10	685	605 700	27 890	21.71	136.7	23.5	8.1

a The maximum of the melting peak at the second heating course of the DSC was selected as melting point.
b $\alpha = \Delta H_m/\Delta H_{m,0}$ with $/\Delta H_{m,0} = 290\,J\,g^{-1}$.
c New styragel HT6E-SEC-column; molecular weight too high.
DSC, differential scanning calorimetry; ND, not determined; SEC, size-exclusion chromatography.

ethylene. The catalyst can be separated from the solution, the excess MAO can be recycled (dynamic equilibrium), and the activated catalyst can be stored as a solid for many years without losing its activity.

A very special application is the use of diastereomeric *ansa*-half-sandwich catalysts. These produce bimodal polyolefin resins because there are two different catalysts operating in one system (Figure 12.5) [139].

In a similar way, metallacyclic half-sandwich complexes can be applied. These may be prepared in a one-pot reaction and then applied in a similar manner as in the case of the metallacyclic metallocene complexes (Scheme 12.12) [140].

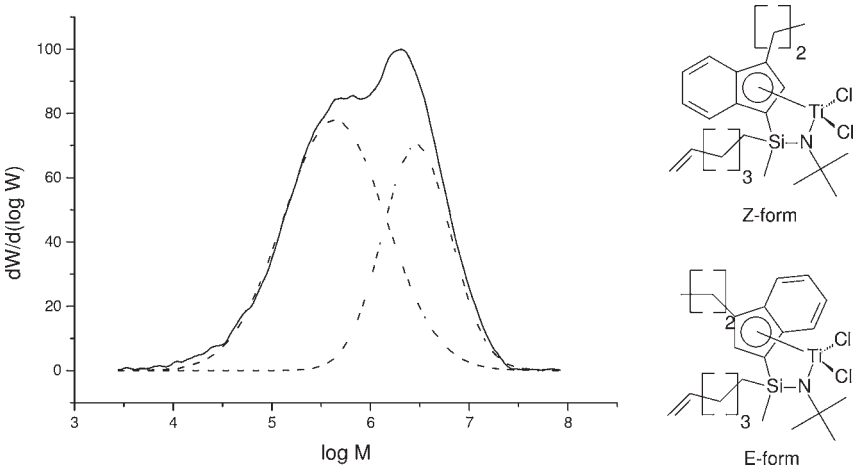

Figure 12.5 HT-SEC diagram of the polyethylene obtained from diastereomeric half-sandwich catalysts. Each of the diastereomers produces a specific polymer. The molecular weight distribution for both components of the polymer is indicated by dotted Gauss curves [139].

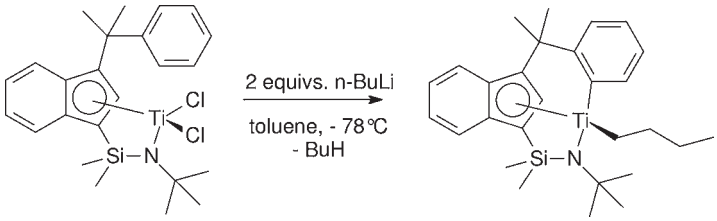

Scheme 12.12 Synthesis of a metallacyclic *ansa*-amido functionalized half-sandwich complex from its parent dichloride complex [140].

Insertion of the olefin into the metal–carbon-σ-bond increases the ring size until a β-hydrogen elimination leads to an olefin function in the polymer moiety and a metal hydride function on the active site that can start the growth of a new polymer chain.

12.5 Self-immobilizing Non-Metallocene Transition Metal Complexes

It was tempting to incorporate late transition metal complexes, for example of nickel or iron, into the self-immobilization process. During the past few years, bis(imino)pyridine complexes [149–152] have attracted much attention because they represent excellent olefin polymerization catalysts and they are not as sensi-

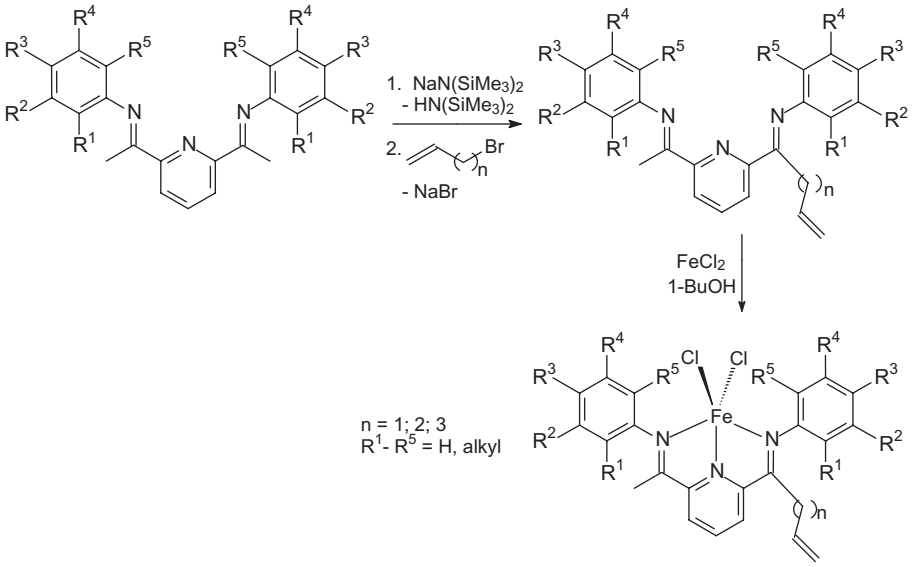

Scheme 12.13 Synthesis of bis(arylimino)pyridine iron complexes containing ω-alkenyl substituents at the iminoethyl moiety [158].

tive to heteroatoms [153–157] or Lewis bases as are the early transition metal complexes. A variety of complexes has been synthesized, but the self-immobilization potential did not always meet the expectations. Both, Herrmann et al. [158] and Jin et al. [159–164] have described two different approaches to prepare ω-alkenyl-substituted bis(arylimino)pyridine iron complexes (see Schemes 12.13 and 12.14):

The complexes shown in Scheme 12.13 were subjected to ethylene polymerization after activation with modified MAO (MMAO), but there was no clear proof of the incorporation of the pendant alkenyl function into the growing polymer chain. In contrast to metallocene catalysts, these self-immobilized iron catalysts are very unstable at room temperature and decompose within a few hours. In all cases, rapid catalyst deactivation was also observed with an increase in polymerization temperature. The resulting polyethylene resins showed very broad or bimodal MWDs [158].

In the second approach, ω-alkenyl-functionalized catalyst precursors (see Scheme 12.14) are copolymerized with styrene in a radical polymerization using 2,2′- azobisisobutyronitrile (AIBN) as an initiator [159–164]. The resulting polystyrene resins contain the immobilized iron complexes and serve as support materials.

The same approach was applied to other complex types which are known to be active in ethylene polymerization, including α-diimine nickel complexes [165, 166], salicylaldiminato nickel complexes [167–170], and bis(phenoxyimine) titanium and zirconium complexes [171,172] (see Scheme 12.15).

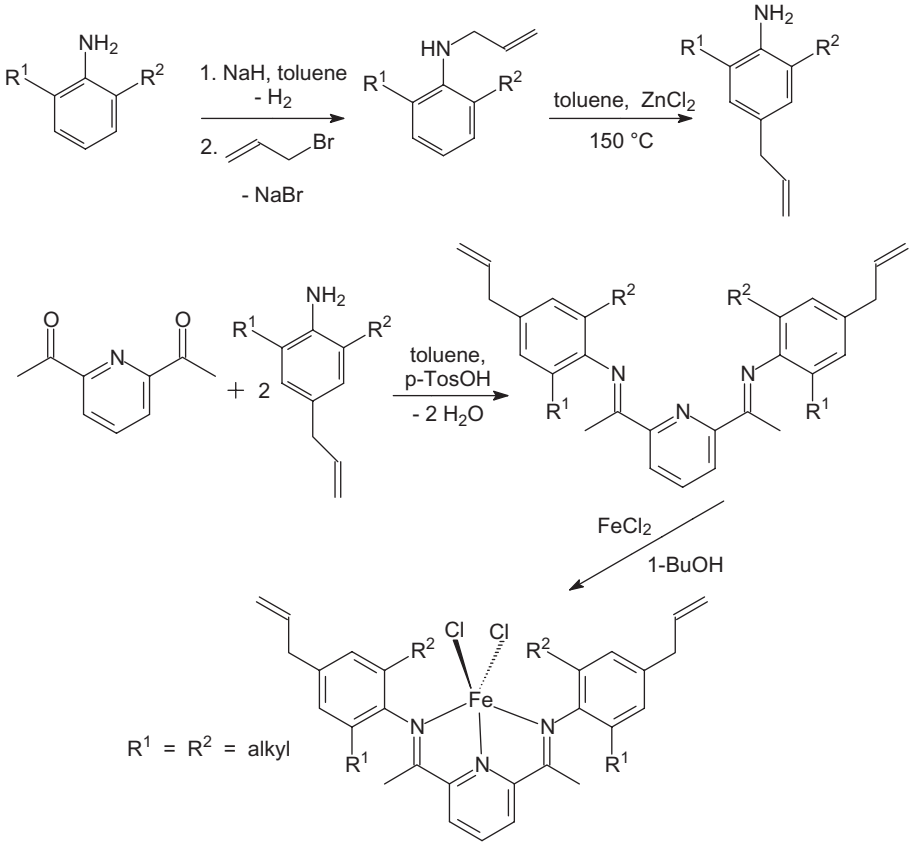

Scheme 12.14 Synthesis of bis(arylimino)pyridine iron complexes starting from diketopyridines and ω-alkenyl-substituted anilines [160, 162–164].

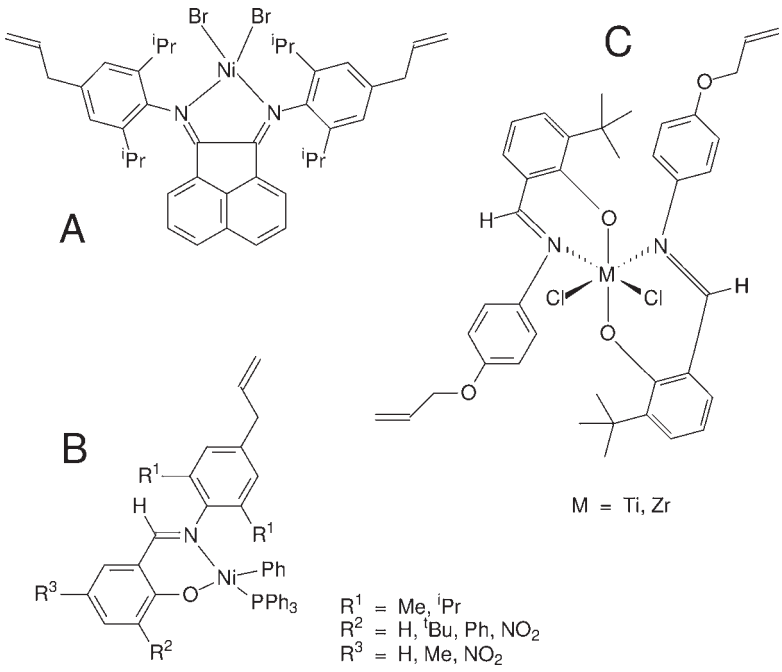

Scheme 12.15 ω-Alkenyl functionalized α-diimine nickel complexes (A), salicylaldiminato nickel complexes (B), and bis(phenoxyimine) titanium and zirconium complexes (C).

The disadvantage of this method is that additional reaction steps are involved for the preparation of the heterogeneous catalyst.

12.6 Self-immobilizing Cocatalysts

One disadvantage of all self-immobilizing catalysts is the fact that only this individual complex can perform the job, and it is not possible to transfer such potential to other complexes. Meanwhile, the worldwide pool of catalyst precursors that is currently available cannot be exploited with this method. The challenge, therefore, was to design the most frequently used cocatalyst MAO in such a way that it has self-immobilization potential. It should then be possible to apply any available catalyst precursor, without undergoing cumbersome syntheses. As the catalyst is a cationic species, a heterogeneous counteranion would fix the catalyst and provide a heterogeneous catalyst without any additional support. The solution to the problem must be widely applicable, cheap and elegant, and provide additional information about the active MAO species. An alkenyl-functionalized MAO would be ideal because it would be copolymerized with ethylene in the polymerization process.

Initially, the functionalization of MAO with an alkenyl group seemed extremely difficult, not only because the nature of the active MAO species is still unknown (because MAO consists of a dynamic equilibrium of a variety of different species [173–180] that cannot be separated), but also because of the high excess of MAO that is essential for a good activation. Early approaches to the partial hydrolysis of alkenyl dimethylaluminum in order to synthesize such species failed, and did not provide any useful results [181].

However, the solution to the problem was easier than might have been expected: "The enemy was beaten with its own weapons" [182]. First, a metallocene dichloride complex is treated with one or two equivalents of an ω-alkenylmagnesium halide (Grignard reagent) (Scheme 12.16).

As a result, mono- or disubstituted ω-alkenyl complexes are formed, but it is not necessary to isolate these products. The next step is the activation with MAO in solution, whereby one or both former ω-alkenyl ligands are substituted by methyl groups from the activating MAO species. At the same time, the alkenyl groups are transferred to this MAO unit, functionalizing it as an olefin so that it can be copolymerized with ethylene from an active site of another catalyst molecule. In the past few years it has become increasingly obvious that the active MAO species is a cage inside which are the monomeric trimethylaluminum molecules responsible for the various activation steps [174, 176, 181] (Scheme 12.17).

The heterogenized MAO cages are able to activate other metallocene di(alkenyl) complexes to produce a multinuclear heterogeneous catalyst system. Simple filtration after this pre-polymerization process allows the activated heterogeneous catalyst to be separated from excess MAO. As MAO represents a dynamic equilibrium it can be recycled. The major advantage of this method is the fact that, in principle,

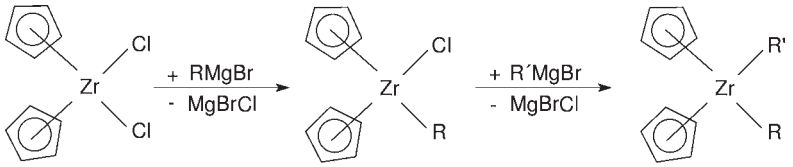

Scheme 12.16 Preparation of metallocene di(alkenyl) complexes [182].

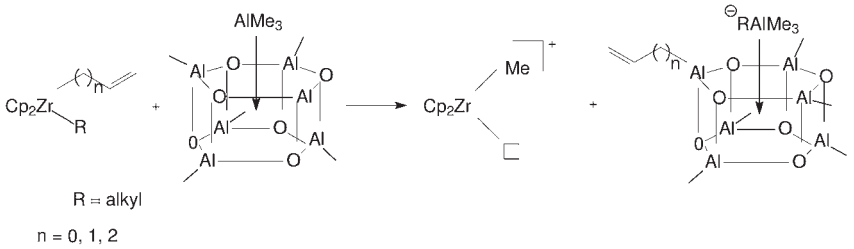

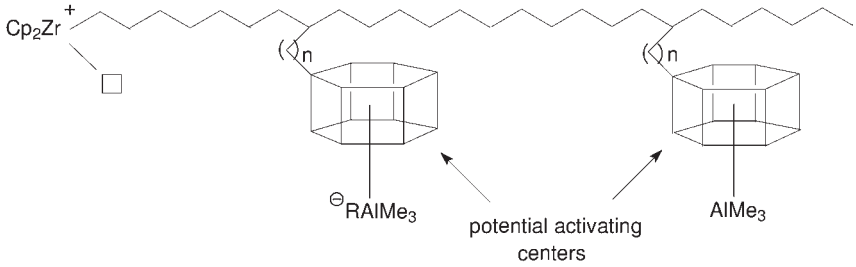

Scheme 12.17 Suggested mechanism for the copolymerization of alkenyl-functionalized MAO (simplified presentation) with ethylene [1].

all metallocene catalyst precursors are appropriate candidates for the method. A minor disadvantage is the occasional lower activity of the resulting catalysts compared to that of those obtained by conventional homogeneous methods.

References

1 H.G. Alt, *J. Chem. Soc., Dalton Trans.* 2005, 3271.

2 H.G. Alt, *J. Chem. Soc., Dalton Trans.* 1999, 1703.

3 D.S. Breslow, N.R. Newburg, *J. Am. Chem. Soc.* 1957, *59*, 5072.

4 H. Sinn, W. Kaminsky, H.J. Vollmer, *Angew. Chem.* 1980, *92*, 396.

5 F. Wild, L. Zsolnai, G. Huttner, H.-H. Brintzinger, *J. Organomet. Chem.* 1982, *232*, 233.
6 J.A. Ewen, L.R. Jones, A. Razavi, J.J. Ferrara, *J. Am. Chem. Soc.* 1988, *110*, 6255.
7 P.C. Möhring, N.J. Coville, *J. Organomet. Chem.* 1994, *479*, 1.
8 F. Küber, *ChiuZ* 1994, *28*, 197.
9 H.H. Brintzinger, D. Fischer, R. Mülhaupt, B. Rieger, R. Waymouth, *Angew. Chem.* 1995, *107*, 1255.
10 H.G. Alt, *Russ. Chem. Bull.* 1995, *44*, 1.
11 M. Bochmann, *J. Chem. Soc., Dalton Trans.* 1996, 255.
12 W. Kaminsky, M. Arndt, *Adv. Polym. Sci.* 1997, *127*, 143.
13 A. Razavi, L. Peters, L. Nafpliotis, *J. Mol. Catal. A: Chemistry* 1997, *115*, 129.
14 W. Kaminsky, *J. Chem. Soc., Dalton Trans.* 1998, 1413.
15 H.G. Alt, E. Samuel, *Chem. Soc. Rev.* 1998, *27*, 323.
16 H.G. Alt, A. Köppl, *Chem. Rev.* 2000, *100*, 1205.
17 L. Resconi, L. Cavallo, A. Fait, F. Piemontesi, *Chem. Rev.* 2000, *100*, 1253.
18 G.G. Hlatky, *Chem. Rev.* 2000, *100*, 1347.
19 G. Fink, B. Steinmetz, J. Zechlin, C. Przybyla, B. Tesche, *Chem. Rev.* 2000, *100*, 1377.
20 W. Kaminsky, A. Laban, *Appl. Catal. A: General* 2001, *222*, 47.
21 G. Schweier, H.H. Brintzinger, *Macromol. Symp.* 2001, *173*, 89.
22 H.G. Alt, *Synth. Methods Organomet. Inorg. Chem.* 2002, *10*, 167.
23 Y. Qian, J. Huang, M.D. Bala, *Curr. Top. Catal.* 2002, *3*, 103.
24 D.-H. Lee, S.K. Noh, *Curr. Trends Polymer Sci.* 2003, *8*, 223.
25 W. Wang, L. Wang, *J. Polym. Mater.* 2003, *20*, 1.
26 A. Razavi, V. Bellia, Y. De Brauwer, K. Hortmann, L. Peters, S. Sirole, S. van Belle, V. Marin, M. Lopez, *J. Organomet. Chem.* 2003, *684*, 206.
27 C. Bianchini, G. Giambastiani, *Chemtracts* 2003, *16*, 53.
28 M. Bochmann, *J. Organomet. Chem.* 2004, *689*, 3982.
29 W. Kaminsky, *J. Polym. Sci. A: Polym. Chem.* 2004, *42*, 3911.
30 A. Ostoja Starzewski, *Macromol. Symp.* 2004, *213*, 47.
31 N. Suzuki, *Topics Organomet. Chem.* 2005, *8*, 177.
32 H.G. Alt, E.H. Licht, A.I. Licht, K.J. Schneider, *Coord. Chem. Rev.* 2006, *250*, 2.
33 P.C. Möhring, N.J. Coville, *Coord. Chem. Rev.* 2006, *250*, 18.
34 G. Erker, G. Kehr, R. Fröhlich, *Coord. Chem. Rev.* 2006, *250*, 36.
35 W. Kaminsky, O. Sperber, R. Werner, *Coord. Chem. Rev.* 2006, *250*, 110.
36 S. Prashar, A. Antinolo, A. Otero, *Coord. Chem. Rev.* 2006, *250*, 133.
37 C. Janiak, *Coord. Chem. Rev.* 2006, *250*, 66.
38 C. Janiak, F. Blank, *Macromol. Symp.* 2006, *236*, 14.
39 W. Kaminsky, O. Sperber, R. Werner, *Coord. Chem. Rev.* 2006, *250*, 110.
40 S. Prashar, A. Antinolo, A. Otero, *Coord. Chem. Rev.* 2006, *250*, 133.
41 A. Razavi, U. Thewalt, *Coord. Chem. Rev.* 2006, *250*, 155.
42 C. Cobzaru, S. Hild, A. Boger, C. Troll, B. Rieger, *Coord. Chem. Rev.* 2006, *250*, 189.
43 I. Tritto, L. Boggioni, D.R. Ferro, *Coord. Chem. Rev.* 2006, *250*, 212.
44 B. Wang, *Coord. Chem. Rev.* 2006, *250*, 242.
45 H.G. Alt, W. Milius, S.J. Palackal, *J. Organomet. Chem.* 1994, *472*, 113.
46 K. Patsidis, H.G. Alt, *J. Organomet. Chem.* 1995, *501*, 31.
47 M.A. Schmid, H.G. Alt, W. Milius, *J. Organomet. Chem.* 1995, *501*, 101.
48 K. Patsidis, H.G. Alt, W. Milius, S.J. Palackal, *J. Organomet. Chem.* 1996, *509*, 63.
49 H.G. Alt, R. Zenk, *J. Organomet. Chem.* 1996, *512*, 51.
50 M.A. Schmid, H.G. Alt, W. Milius, *J. Organomet. Chem.* 1996, *514*, 45.
51 H.G. Alt, R. Zenk, W. Milius, *J. Organomet. Chem.* 1996, *514*, 257.
52 H.G. Alt, R. Zenk, *J. Organomet. Chem.* 1996, *518*, 7.
53 H.G. Alt, R. Zenk, *J. Organomet. Chem.* 1996, *522*, 39.
54 H.G. Alt, R. Zenk, *J. Organomet. Chem.* 1996, *522*, 177.
55 M.A. Schmid, H.G. Alt, W. Milius, *J. Organomet. Chem.* 1996, *525*, 9.

56 M.A. Schmid, H.G. Alt, W. Milius, *J. Organomet. Chem.* 1996, *525*, 15.
57 H.G. Alt, R. Zenk, *J. Organomet. Chem.* 1996, *526*, 295.
58 K. Patsidis, H.G. Alt, S.J. Palackal, G.R. Hawley, *Russ. Chem. Bull.* 1996, *45*, 2216.
59 H.G. Alt, S.J. Palackal, K. Patsidis, R. Zenk, M.A. Schmid, *Educ. Adv. Chem.* 1996, *2*, 21.
60 M.A. Schmid, H.G. Alt, W. Milius, *J. Organomet. Chem.* 1997, *541*, 3.
61 B. Peifer, M.B. Welch, H.G. Alt, *J. Organomet. Chem.* 1997, *544*, 115.
62 C. Schmid, H.G. Alt, W. Milius, *J. Organomet. Chem.* 1997, *544*, 139.
63 P. Schertl, H.G. Alt, *J. Organomet. Chem.* 1997, *545–546*, 553.
64 B. Peifer, W. Milius, H.G. Alt, *J. Organomet. Chem.* 1998, *553*, 205.
65 H.G. Alt, M. Jung, W. Milius, *J. Organomet. Chem.*, 1998, *558*, 111.
66 H.G. Alt, M. Jung, G. Kehr, *J. Organomet. Chem.* 1998, *562*, 153.
67 H.G. Alt, M. Jung, *J. Organomet. Chem.* 1998, *562*, 229.
68 H.G. Alt, K. Föttinger, W. Milius, *J. Organomet. Chem.* 1998, *564*, 109.
69 H.G. Alt, M. Jung, *J. Organomet. Chem.* 1998, *568*, 87.
70 H.G. Alt, M. Jung, *J. Organomet. Chem.* 1998, *568*, 127.
71 H.G. Alt, P. Schertl, A. Köppl, *J. Organomet. Chem.* 1998, *568*, 263.
72 H.G. Alt, M. Jung, *J. Organomet. Chem.* 1999, *580*, 1.
73 P. Schertl, H.G. Alt, *J. Organomet. Chem.* 1999, *582*, 328.
74 A. Köppl, A.I. Babel, H.G. Alt, *J. Mol. Catal. A: Chemistry* 2000, *153*, 109.
75 E.H. Licht, H.G. Alt, M.M. Karim, *J. Organomet. Chem.* 2000, *599*, 275.
76 E.H. Licht, H.G. Alt, M.M. Karim, *J. Mol. Catal. A: Chemistry* 2000, *159*, 273.
77 E.H. Licht, H.G. Alt, M.M. Karim, *J. Mol. Catal. A: Chemistry* 2000, *164*, 9.
78 R. Schmidt, H.G. Alt, *J. Organomet. Chem.* 2001, *621*, 304.
79 R. Schmidt, M. Deppner, H.G. Alt, *J. Mol. Catal. A: Chemistry* 2001, *172*, 43.
80 H.G. Alt, A. Weis, A. Reb, R. Ernst, *Inorg. Chim. Acta* 2003, *343*, 253.
81 H.G. Alt, R. Ernst, I. Böhmer, *J. Mol. Catal. A: Chemistry* 2003, *191*, 177.
82 H.G. Alt, R. Ernst, *J. Mol. Catal. A: Chemistry* 2003, *195*, 11.
83 H.G. Alt, R. Ernst, *Inorg. Chim. Acta* 2003, *350*, 1.
84 M. Deppner, R. Burger, H.G. Alt, *J. Organomet. Chem.* 2004, *689*, 1194.
85 H.G. Alt, R.W. Baker, M. Dakkak, M.A. Foulkes, M.O. Schilling, P. Turner, *J. Organomet. Chem.* 2004, *689*, 1965.
86 M. Deppner, R. Burger, M. Weiser, H.G. Alt, *J. Organomet. Chem.* 2005, *690*, 2861.
87 A. Kestel-Jakob, H.G. Alt, *Z. Naturforsch.* 2007, *62b*, 314.
88 H.G. Alt, *Macromol. Symp.* 2001, *173*, 65.
89 K. Soga, M. Kaminaka, *Macromol. Chem. Rapid Commun.* 1991, *12*, 367.
90 W. Kaminsky, F. Renner, *Macromol. Chem. Rapid Commun.* 1993, *14*, 239.
91 T. Takahashi, K. Yamamoto, K. Hirakawa, U.S. Patent No. 5474962, 1995.
92 P.C. Wailes, R.S.P. Couts, H. Weigold, *Organometallic Chemistry of Titanium, Zirconium and Hafnium*, Academic Press, New York, 1974.
93 E.H. Braye, W. Hübel, I. Caplier, *J. Am. Chem. Soc.* 1961, *83*, 4406.
94 G.W. Watt, F.O. Drummond, *J. Am. Chem. Soc.* 1970, *92*, 826.
95 J.X. Dermott, G.M. Whitesides, *J. Am. Chem. Soc.* 1974, *96*, 947.
96 H.G. Alt, M.D. Rausch, *J. Am. Chem. Soc.* 1974, *96*, 5936.
97 G. Fachinetti, C. Floriani, *J. Chem. Soc., Chem. Commun.* 1977, 66.
98 M.D. Rausch, W.H. Boon, H.G. Alt, *Ann. N. Y. Acad. Sci.* 1977, *295*, 103.
99 H.G. Alt, H.E. Engelhardt, M.D. Rausch, L.B. Kool, *J. Am. Chem. Soc.* 1985, *107*, 3717.
100 C.J. Rousset, D.R. Swanson, F. Lamaty, E. Negishi, *Tetrahedron Lett.* 1989, *30*, 5105.
101 E. Negishi, R.S. Miller, *J. Org. Chem.* 1989, *54*, 6014.
102 E. Negishi, S.J. Holmes, J.M. Tour, J.A. Miller, F.E. Cederbaum, D.R. Swanson, T. Takahashi, *J. Am. Chem. Soc.* 1989, *111*, 3336.
103 H.G. Alt, C.E. Denner, U. Thewalt, M.D. Rausch, *J. Organomet. Chem.* 1988, *356*, C83.
104 H.G. Alt, C.E. Denner, *J. Organomet. Chem.* 1989, *368*, C15.

105 H.G. Alt, C.E. Denner, *J. Organomet. Chem.* 1990, *390*, 53.
106 H.G. Alt, J.S. Han, *J. Organomet. Chem.* 1993, *456*, 89.
107 G. Erker, J. Wicher, K. Engel, F. Rosenfeldt, W. Dietrich, C. Krüger, *J. Am. Chem. Soc.* 1980, *102*, 6344.
108 G. Erker, J. Wicher, K. Engel, C. Krüger, *Chem. Ber.* 1982, *115*, 3300.
109 H. Yasuda, Y. Koshihara, K. Mashima, K. Nagasuna, K. Lee, A. Nakamura, *Organometallics* 1982, *1*, 388.
110 G. Erker, G. Kehr, R. Fröhlich, *J. Organomet. Chem.* 2004, *689*, 4305 and references therein.
111 V.V. Burlakov, A. Ohff, C. Lefeber, A. Tillack, W. Baumann, R. Kempe, U. Rosenthal, *Chem. Ber.* 1995, *128*, 967.
112 A. Tillack, W. Baumann, A. Ohff, C. Lefeber, A. Spannenberg, R. Kempe, U. Rosenthal, *J. Organomet. Chem.* 1996, *520*, 187.
113 D. Thomas, W. Baumann, A. Spannenberg, R. Kempe, U. Rosenthal, *Organometallics* 1998, *17*, 2096.
114 P.-M. Mellny, V.V. Burlakov, N. Peulecke, W. Baumann, A. Spannenberg, R. Kempe, V. Francke, U. Rosenthal, *J. Organomet. Chem.* 1999, *578*, 125.
115 V.V. Burlakov, P. Arndt, W. Baumann, A. Spannenberg, U. Rosenthal, *Organometallics* 2004, *23*, 4160.
116 U. Rosenthal, V.V. Burlakov, P. Arndt, W. Baumann, A. Spannenberg, V.B. Shur, *Eur. J. Inorg. Chem.* 2004, 4739.
117 V.V. Burlakov, M.A. Bach, M. Klahn, P. Arndt, W. Baumann, A. Spannenberg, U. Rosenthal, *Macromol. Symp.* 2006, *236*, 48.
118 M.R. Kesti, R.M. Waymouth, *Organometallics* 1992, *11*, 1095.
119 E. Negishi, T. Takahashi, *Acc. Chem. Res.* 1994, *27*, 124.
120 D.P. Lewis, R.J. Whitby, R.V.H. Jones, *Tetrahedron* 1995, *51*, 4541.
121 V.K. Dioumaev, J.V. Harrod, *Organometallics* 1997, *16*, 1452.
122 L.H. Doerrer, M.L.H. Green, D. Häußinger, J. Saßmannshausen, *J. Chem. Soc., Dalton Trans.* 1999, 2111.
123 T.H. Warren, G. Erker, R. Fröhlich, B. Wibbeling, *Organometallics* 2000, *19*, 127.
124 E.H. Licht, H.G. Alt, W. Milius, S. Abu-Orabi, *J. Organomet. Chem.* 1998, *560*, 69.
125 E.H. Licht, H.G. Alt, *J. Mol. Catal. A: Chemistry* 2000, *154*, 65.
126 E.H. Licht, H.G. Alt, *J. Organomet. Chem.* 2000, *599*, 261.
127 A.I. Licht, H.G. Alt, *J. Organomet. Chem.* 2003, *648*, 134.
128 A.I. Licht, H.G. Alt, *J. Organomet. Chem.* 2003, *684*, 91.
129 A.I. Licht, H.G. Alt, *J. Organomet. Chem.* 2003, *687*, 142.
130 A.I. Licht, H.G. Alt, *J. Organomet. Chem.* 2003, *688*, 254.
131 H.G. Alt, C.E. Denner, W. Milius, *Inorg. Chim. Acta* 2004, *357*, 1682.
132 J. Okuda, *Chem. Ber.* 1990, *123*, 1649.
133 J.A.M. Canich, U.S. Patent No. US 5026798, 1991.
134 A.K. Hughes, A. Meetsma, J.H. Teuben, *Organometallics* 1993, *12*, 1936.
135 W.J. Richter, T. Schmidt, *Nachr. Chem. Tech. Lab.* 1994, *42*, 138.
136 H.G. Alt, K. Föttinger, W. Milius, *J. Organomet. Chem.* 1998, *564*, 115.
137 H.G. Alt, K. Föttinger, W. Milius, *J. Organomet. Chem.* 1999, *572*, 21.
138 H.G. Alt, A. Reb, W. Milius, A. Weis, *J. Organomet. Chem.* 2001, *628*, 169.
139 A. Reb, H.G. Alt, *J. Mol. Catal. A: Chemistry* 2001, *174*, 35.
140 H.G. Alt, A. Reb, K. Kundu, *J. Organomet. Chem.* 2001, *628*, 211.
141 H.G. Alt, A. Reb, *J. Mol. Catal. A: Chemistry* 2001, *175*, 43.
142 H. Braunschweig, F.M. Breitling, *Coord. Chem. Rev.* 2006, *250*, 2691 and references therein.
143 K. Soga, J. Park, T. Shiono, *Polym. Commun.* 1991, *10*, 310.
144 C. Pellecchia, A. Proto, A. Zambelli, *Macromolecules* 1992, *25*, 4490.
145 P. Aaltonen, J. Seppälä, *Eur. Polym. J.* 1994, *30*, 683.
146 F.G. Sernetz, R. Mülhaupt, R.M. Waymouth, *Macromol. Chem. Phys.* 1996, *197*, 1071.
147 G. Xu, *Macromolecules* 1998, *31*, 2395.
148 M. Kamigaito, T.K. Lal, R.M. Waymouth, *J. Polym. Sci. A: Polym. Chem.* 2000, *38*, 4649.
149 B.L. Small, M. Brookhart, *J. Am. Chem. Soc.* 1998, *120*, 7143.

150 B.L. Small, M. Brookhart, A.M.A. Bennett, *J. Am. Chem. Soc.* 1998, *120*, 4049.

151 G.J.P. Britovsek, V.C. Gibson, B.S. Kimberley, P.J. Maddox, S.J. McTavish, G.A. Solan, A.J.P. White, D.J. Williams, *Chem. Commun.* 1998, 849.

152 G.J.P. Britovsek, V.C. Gibson, B.S. Kimberley, P.J. Maddox, S.J. McTavish, G.A. Solan, A.J.P. White, D.J. Williams, *J. Am. Chem. Soc.* 1999, *121*, 8728.

153 H.W. Boone, P.S. Athey, M.J. Mullins, D. Philipp, R. Muller, W.A. Goddard, *J. Am. Chem. Soc.* 2002, *124*, 8790.

154 L.S. Baugh, J.A. Sissano, *J. Polym. Sci. A: Polym. Chem.* 2002, *40*, 1633.

155 P.M. Castro, K. Lappalainen, M. Ahlgren, M. Leskelä, T. Repo, *J. Polym. Sci. A: Polym. Chem.* 2003, *41*, 1380.

156 P.M. Castro, M.P. Lankinen, *Macromol. Symp.* 2004, *213*, 199.

157 K. Yliheikkilä, K. Lappalainen, P.M. Castro, K. Ibrahim, A. Abu-Surrah, M. Leskelä, T. Repo, *Eur. Polym. J.* 2006, *42*, 92.

158 F.A.R. Kaul, G.T. Puchta, H. Schneider, F. Bielert, D. Mihalios, W.A. Herrmann, *Organometallics* 2002, *21*, 74.

159 C.-K. Liu, G.-X. Jin, *Gaodeng Xuexiao Huaxue Xuebao* 2001, *22*, 1233.

160 C.-K. Liu, G.-X. Jin, *Huaxue Xuebao (Acta Chimica Sinica)* 2002, *60*, 157.

161 G.-X. Jin, H. Zhu, C. Liu, G. Tang, Chinese Patent No. CN 1371923, 2002.

162 C. Liu, G.-X. Jin, *New J. Chem.* 2002, *26*, 1485.

163 G.X. Jin, D. Zhang, *J. Polym. Sci. A: Polym. Chem.* 2004, *42*, 1018.

164 J. Zhang, X. Wang, G.-X. Jin, *Coord. Chem. Rev.* 2006, *250*, 95.

165 D. Zhang, G.-X. Jin, *Appl. Catal. A: General* 2004, *262*, 13.

166 S. Guo, D. Zhang, G.-X. Jin, *Chin. Sci. Bull.* 2004, *49*, 249.

167 D. Zhang, G.-X. Jin, N.-H. Hu, *Chem. Commun.* 2002, 574.

168 D. Zhang, G.-X. Jin, N.-H. Hu, *Eur. J. Inorg. Chem.* 2003, 1570.

169 D. Zhang, G.-X. Jin, *Organometallics* 2003, *22*, 2851.

170 D. Zhang, G.-X. Jin, *Organometallics* 2004, *23*, 3270.

171 D. Zhang, G.-X. Jin, *Appl. Catal. A: Chemistry* 2004, *262*, 85.

172 Z.-J. Chen, D. Zhang, G.-X. Jin, *Wuji Huaxue Xuebao* 2005, *21*, 1775.

173 H. Sinn, W. Kaminsky, *Adv. Organomet. Chem.* 1980, *18*, 99.

174 H. Sinn, *Macromol. Chem., Macromol. Symp.* 1995, *97*, 27.

175 E. Zurek, T. Ziegler, *Prog. Polym. Sci.* 2004, *29*, 107.

176 M.R. Mason, J.M. Smith, S.G. Bott, A.R. Barron, *J. Am. Chem. Soc.* 1993, *115*, 4971.

177 C.J. Harlan, M.R. Mason, A.R. Barron, *Organometallics* 1994, *13*, 2957.

178 C.J. Harlan, S.G. Bott, A.R. Barron, *J. Am. Chem. Soc.* 1995, *117*, 6465.

179 A.R. Barron, *Macromol. Symp.* 1995, *97*, 15.

180 E.Y.-X. Chen, T.J. Marks, *Chem. Rev.* 2000, *100*, 1391.

181 H. Schumann, private communication.

182 C.E. Denner, H.G. Alt, *J. Appl. Polym. Sci.* 2003, *89*, 3379.

Index

Tailor-Made Polymers. Via Immobilization of Alpha-Olefin Polymerization Catalysts.
Edited by John R. Severn and John C. Chadwick

ISBN: 978-3-527-31782-0